



UNIVERSITÄT
DES
SAARLANDES



Self-Healing Polymer-based Nanocomposites using the Diels-Alder-reaction: Studies on the Influence of Composition on Self-Healing Properties

Sandra Schäfer

Dissertation
Fachrichtung Chemie
2018

Self-Healing Polymer-based Nanocomposites using the Diels-Alder-Reaction: Studies on the Influence of Composition on Self-Healing Properties



UNIVERSITÄT
DES
SAARLANDES

Dissertation

Zur Erlangung des Grades
des Doktors der Naturwissenschaften
der Naturwissenschaftlich-Technischen Fakultät
der Universität des Saarlandes

vorgelegt von

Sandra Schäfer

Saarbrücken 2018

Tag des Kolloquiums:	05.03.2019
Dekan:	Guido Kickelbick
Berichterstatter:	Guido Kickelbick Gerhard Wenz
Vorsitz:	Gregor Jung
Akademischer Mitarbeiter:	Bernd Morgenstern

Die vorliegende Arbeit wurde in der Zeit von April 2014 bis März 2018 im Fachbereich Anorganische Festkörperchemie bei Prof. Dr. Guido Kickelbick an der Universität des Saarlandes angefertigt.

Wissenschaft ist einer verbreiteten falschen Darstellung zufolge „das Wissen, das durch wiederholbare, kontrollierte Laborexperimente gewonnen wurde“. In Wirklichkeit ist sie etwas viel Umfassenderes: der Erwerb zuverlässiger Kenntnisse über die Welt. – Jared Mason Diamond aus „Arm und Reich. Die Schicksale menschlicher Gesellschaften.“

DANKSAGUNG

Mein besonderer Dank gilt Prof. Dr. Guido Kickelbick, der mir diese Arbeit auf einem spannenden und aktuellen Forschungsthema ermöglichte, sowie für seine Anregungen und Unterstützung. Prof. Dr. Gerhard Wenz danke ich für die wissenschaftliche Begleitung und die Zweitkorrektur dieser Arbeit.

Meiner langjährigen Laborpartnerin Christina Odenwald. danke ich für die gemeinsame Zeit im Labor, die konstruktiven Gespräche und Überlegungen, die gemeinsame Reise zur EuCheMS Konferenz nach Spanien. Meinem guten Freund Peter Zimmer aus Diplom-Zeiten für den gemeinsamen Weg und Austausch über diesen. Nils danke ich für die Hilfe bei UV/Vis-Messungen und die Verwirklichung der Kanutour als Arbeitsgruppenausflug. Christina Odenwald, Nils, Nina, Tom, Charlotte, Achim, Nadja, Patrick, Dennis Meier, Dennis Becker, Thomas, Jessica, Robert, Jonas, Christina Hein, Kristina Brix und Ralf danke ich für die kollegiale und freundliche Arbeitsatmosphäre. Nina und Nadja für die Durchführung der TEM-, Susanne Harling für die CHN-, Michael für Festkörper-NMR, Dennis Becker und Jessica für XRD-Messungen und Volker für die Einkristallstrukturanalysen. Susanne Limbach danke ich für die große Unterstützung bei organisatorischen Angelegenheiten. Meinem Forschungspraktikanten Dennis Becker und Bachelor Lucas danke ich für die Unterstützung im Labor. Christel danke ich für die Mithilfe bei Aufarbeitungen und Messungen, Sylvia und Hermann für die Herstellung maßgeschneiderter Arbeitsmaterialien und Stefan für die tatkräftige Unterstützung bei technischen Fragestellungen.

Meinen Eltern, Winfried und Petra Schäfer danke ich, dass sie mir diesen Werdegang ermöglicht haben und die Mut machenden Worte auf meinem Weg. Meinem Freund David danke ich für die immerwährende konstruktive Kritik und seine Ausgeglichenheit.

KURZZUSAMMENFASSUNG

SiO₂-Nanopartikel-Polymer-Grenzflächen wurden auf ihre Eignung als Diels-Alder (DA) reversible Vernetzungsstelle untersucht. Die Rolle des chemischen Aufbaus der Polymermatrix wurde gezeigt. Mehrere Millimeter große Schnitte konnten im Siloxan-basierten Nanokomposit nach Herstellung eines Kontaktes der Schnittflächen mittels CHCl₃ durch die DA-Reaktion geheilt werden.

Die Limitierung der Grenzflächenreaktivität wurde in einer Cofunktionalisierungsstudie untersucht. Dazu wurden Fe_xO_y-Nanopartikel mit einer Monolage an DA-alkylphosphonsäuren funktionalisiert. Ein drastischer Einbruch des Umsatzes wurde bei Verwendung der Maleimid-/Furan-Dodecylderivate anstelle von Maleimid/Methylfuran als angreifende Reagenzien beobachtet. Dieses Ergebnis weist darauf hin, dass aufgrund der Sterik nur ein minimaler Umsatz mit Polymerketten erzielt werden kann.

Daher wurden Dien und Dienophil statistisch in der Matrix verteilt, statt sie kumulativ an der Füllstoffoberfläche zu lokalisieren. Lineare Einkomponenten-Polymere, welche Dien, Dienophil und ein zusätzliches H-Brücken-Motiv enthalten, wurden über kontrollierte radikalische Polymerisationen hergestellt. Urea-Gruppen tragende Spherosilikate wurden in hohen Ausbeuten synthetisiert. Durch Mischen beider Komponenten wurden Hybridmaterialien mit zweifach intrinsisch reversiblen Netzwerken erhalten. Die H-Brücken halten Schnittflächen schon bei 30°C wieder zusammengehalten, wonach Schnitte im mm-Bereich über die DA Reaktion geheilt wurden.

ABSTRACT

SiO₂-nanoparticle-polymer-interfaces were tested according to their suitability as a DA - reversible crosslinking site. The role of the chemical composition of the polymer matrix was shown. Cuts of several millimeters could be healed within the siloxane-based nanocomposite, after reconnection of cut surfaces with the help of chloroform, by the DA reaction.

The limit of interface-reactivity was investigated in a cofunctionalization study. Therefore, Fe_xO_y nanoparticles were functionalized with a monolayer DA-alkyl phosphonic acids. A drastic drop in conversion was recorded, when the attacking reagents were dodecyl derivatives of maleimide and furan instead of maleimide/methylfuran. This result indicates, that due to the sterical situation created by the attacking reagent on the surface only a minimal conversion with polymer chains is possible

Therefore, diene and dienophile were distributed statistically within the matrix, instead of being located cumulative at the particle surface. Linear one-component polymers, consisting of diene, dienophile and one additional hydrogen bonding motive were synthesized using controlled radical polymerization techniques. Urea-group bearing spherosilicates were synthesized in high yields. By blending these both components, a hybrid material with double intrinsically reversible networks was received. The H bonds reconnect cut interfaces at 30°C, whereafter cuts in the mm-scale could be healed by the DA reaction.

ABBREVIATIONS

AIBN	azobisisobutyronitrile
ATR	attenuated total reflection
2M4F	DA polymer composed of bismaleimide crosslinking molecule (2M) and tetrafuran propionic acid crosslinking molecule (4F) (Figure 19, left)
3M4F	DA polymer composed of trismaleimide crosslinking molecule (3M) and and tetrafuran propionic acid crosslinking molecule (4F) (Scheme 9)
AMF	alternating magnetic field
APTES	(3-aminopropyl)triethoxysilane
ARGET ATRP	activators regenerated by electron transfer atom transfer radical polymerization
ATRP	atom transfer radical polymerization
BMA	butyl methacrylate
BMI	1,1'-(methylenedi-4,1-phenylene)bismaleimide
CHN	carbon, hydrogen, nitrogen elemental analysis
Cp	cyclopentadiene
CPDB	cyanoisopropyl dithiobenzoate
CRP	controlled radical polymerization
DA	Diels-Alder
DiCp	dicyclopentadiene
DMF	<i>N,N</i> -dimethylformamide
DSC	differential scanning calorimetry
DLS	dynamic light scattering
ESI-MS	electrospray ionization – mass spectrometry
FMA	furfuryl methacrylate
FPU	polyurethane functionalized with furan moieties
FRP	free radical polymerization
FTIR	Fourier-transform infrared spectroscopy
FUTES	furanundecenyl triethoxysilane
HEMA	2 -hydroxyethyl methacrylate

HMDS	hexamethyldisilazane
HMTETA	1,1,4,7,10,10-hexamethyltriethylenetetramine
HOMO	highest occupied molecular orbital
ICEMA	2-isocyanatoethyl methacrylate
LUMO	lowest unoccupied molecular orbital
MiMA	maleimidoalkyl methacrylate; alkyl = ethyl or propyl
MMA	methyl methacrylate
MPTES	maleimidopropyl triethoxysilane
MWCNT	multi-walled carbon nanotube
NMR	nuclear magnetic resonance
PABTC	(propionic acid)yl butyl trithiocarbonate
PET	polyethylene terephthalate
PDI	polydispersity index
PDMS	polydimethylsiloxane
PMDETA	<i>N,N,N',N'',N'''</i> -pentamethyldiethylenetriamine
POS	polyhedral oligomeric silicate, also called sphaerosilicates
POSS	polyhedral oligomeric silsesquioxane
PU	polyurethane
PVC	polyvinyl chloride
RAFT	reversible addition-fragmentation chain-transfer
rDA	retro Diels-Alder
TEM	transmission electron microscopy
TEOS	tetraethyl orthosilicate
TFA	trifluoroacetic acid
TGA	thermogravimetric analysis
TMI	meta-isopropenyl benzyl isocyanate
T _g	glass transition temperature
Upy	2-ureido-4-pyrimidone
UV/Vis	ultraviolet-visible spectroscopy

Content

1	INTRODUCTION	1
1.1	Plastics	1
1.2	The idea of artificial self-healing materials	3
1.3	Classification of self-healing polymer based materials	6
1.4	Intrinsic self-healing systems	8
1.4.1	Dynamic covalent bond chemistry	9
1.4.2	Diels-Alder based systems	11
1.4.3	Dynamic non-covalent bond chemistry	17
1.4.4	Hydrogen bond based systems	18
1.5	Combination of intrinsic healing interactions	20
1.6	Peculiarity of self-healing composites and hybrid materials compared to self-healing polymers	24
1.6.1	DA composites with physically incorporated filler - DA groups solely in the matrix	25
1.6.2	DA composites with DA groups on the filler-matrix interface	27
1.7	Analytical methods for the determination of reversibility and self-healing behavior	33
1.8	Inorganic filler and their surface adjustment for the incorporation into organic matrices	34
1.8.1	Silica nanoparticles and silane coupling agents	35
1.8.2	Silsesquioxanes and Spherosilicates	37
1.8.3	Metal oxides and phosphonic acid and acid ester coupling agents	42
1.9	Polymer Matrices for self-healing	46
1.9.1	Elastomeres - Siloxanes and their synthetic access	46
1.9.2	Thermoplastics and their synthetic access via Controlled Radical Polymerizations	49
1.10	Knowledge gaps in the known systems	58
2	RESEARCH GOALS	59
2.1	Objective	59
2.2	Concept	60
3	RESULTS AND DISCUSSION	62
3.1	Self-Healing Polymer Nanocomposites based on Diels-Alder-Reactions with Silica Nanoparticles: The Role of the Polymer Matrix	62
3.2	Diels-Alder Reactions on the Surface of Magnetite/Maghemite Nanoparticles: Application in Self-Healing Materials	77

3.3	Simple and High Yield Access to Octafunctional Azido, Amine and Urea Group bearing Cubic Spherosilicates	92
3.4	Double Reversible Network – Improvement of Self-Healing in Hybrid Materials via the Combination of Diels-Alder-Crosslinking and Hydrogen Bonds	100
4	SUMMARY AND OUTLOOK	114
5	REFERENCES	118
6	SUPPORTING INFORMATION	132
6.1	Self-Healing Polymer Nanocomposites based on Diels-Alder-Reactions with Silica Nanoparticles: The Role of the Polymer Matrix	132
6.2	Diels-Alder Reactions on Surface-Modified Magnetite/Maghemite Nanoparticles: Application in Self-Healing Nanocomposites	140
6.3	Simple and High Yield Access to Octafunctional Azido, Amine and Urea Group bearing Cubic Spherosilicates	199
6.4	Double Reversible Network – Improvement of Self-Healing in Hybrid Materials via the Combination of Diels-Alder-Crosslinking and Hydrogen Bonds	233

1 Introduction

1.1 Plastics

Plastics are distributed throughout the whole world and find widespread use in manifold applications, such as automotive, architecture, packages and clothing. The discovery of vulcanization of natural rubber by Goodyear around 1840 led to the first resin, called Ebonite, which was commercially used. In 1905, one of the first entirely synthetic plastics "Bakelite" was developed by Leo Hendrik Baekeland. The historical development of plastics is shown in Figure 1. In the late 1930's to early 1940's intensive research was done to develop polymeric materials with adjustable properties to produce new bulk materials. The major advantages, of this novel material class, are the low production costs, low energy consumption in the production and lightweight of the resulting materials. Polystyrene, polyvinyl chloride (PVC), polyethylene terephthalate (PET) and Nylon name only a few results of this era. The "Age of Plastics" began, when these products entered into objects of everyday life, in form of rubber tires, electric insulators, safety glasses, laundry baskets, shopping bags, nylon tights and many more.

The most special feature about plastics, which are classified in thermosets, thermoplastics and elastomers is, that they can be molded into any shape, while mechanical properties can be tailored.

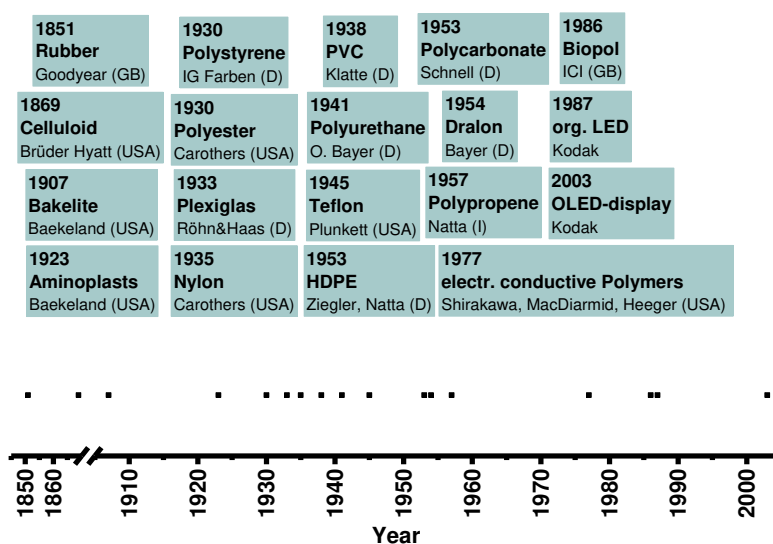


Figure 1: History of Plastics.[1]

Several Nobel Prizes in chemistry further highlight the role of this artificial material class because the prize is given to whom, who made the most important chemical discovery or improvement within the last years. In 1953, Hermann Staudinger received the prize for the discovery, that polymers are built of macromolecules, instead of the former common opinion that they are built of micelles. Ten years later, Karl Ziegler and Giulio Natta gained the prize

for the usage of metal organic catalysts in polymerizations of olefins, which lowered the necessary process pressure. In 1974 Paul Flory became a Nobel laureate for his theoretical and experimental work concerning the behavior of polymer chains in solution. In 2000, Hideki Shirakawa, Alan Heeger and Alan MacDiarmid received the prize for electrically conducting polymers.

In general, most plastics are made of fossil fuels (natural gas and crude oil), which once seemed to be a never ending raw material. The commercial industrial production of crude oil began around 1855. Crude oil, containing mostly a mixture of hydrocarbons, is produced by drilling a long hole into the earth, pumping it to the surface and bringing it to oil refinery to separate parts of other materials. In petrochemical plants, large hydrocarbons getting cracked into small ones, like aromatics, naphtha and olefins. These small monomers build the basis to synthesize resins or plastics by controlled polymerizations. Further modifications, like adding additives have to be done until plastic products can be molded, casted or drawn. However, due to an increased demand because of industrialization, the crude oil prices are rising (Figure 2). As a direct following product, the plastic prices strongly correlate with these prices (Figure 2). Also, the worldwide production of plastics increased from 10.000 t /year in 1930 to 380.000.000 t/year in 2017.^[2]

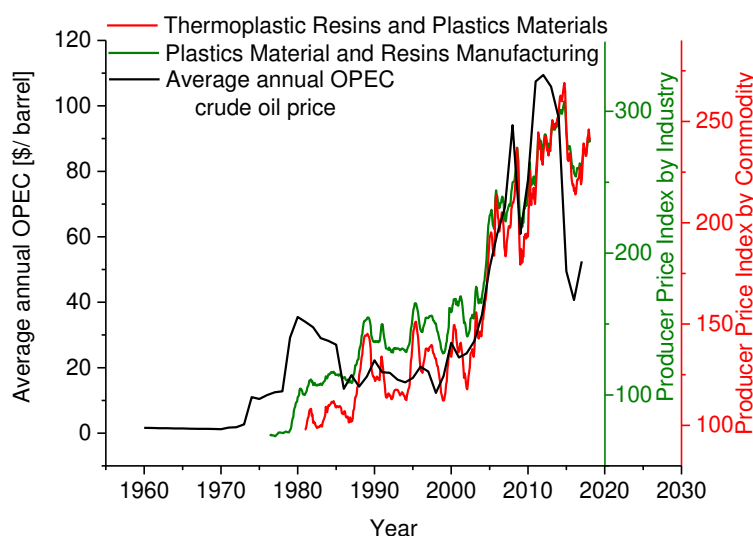


Figure 2: Correlation between Crude Oil price and Producer Price Index.[3, 4]

The era of plastics goes along with numerous environmental issues (Figure 3). Plastic nano and micro particles are distributed in the oceans. Marine animals and birds getting trapped in plastic waste or die because of plastic that fills their stomach. Around 10% of human waste is caused by plastic and it takes 400-1000 years to degrade. One attempt to reduce the problem, is recycling, especially of the one-way plastic. However, only 9% of ever worldwide produced plastics are actually recycled, because it is difficult to collect or sort the different types in a pure form. Since mixtures would lead to worse material properties, they are not suitable for industry.

FACTS ABOUT PLASTIC
4 % annual petroleum production converted directly into plastics
50 % of plastics for single-use disposable items
400 – 1000 years for plastics to degrade
9 % of all worldwide produced plastics recycled up to now
12% incinerated
79 % in landfills or environment
10 % of total human waste is plastics
10 million tons plastics end up in the oceans each year

Figure 3: Facts about the plastic problem.

Various researches propose the „Anthropocene“, as an epoch, which is significantly impacted by humans.^[5] One of its characteristics would be the deposition of human-caused technofossils, such as rainfalls of atomic bomb attempts and even the deposition of plastics. These all are indications, that it is worthwhile to rethink the human’s behavior and leave behind the time of one-way and throw-away materials.

Various approaches could help to realize this, like renewable and biodegradable raw materials or the increase of lifetime of plastic based products. Healable polymers provide a promising possibility to increase the useful lifetime of polymeric materials.

1.2 The idea of artificial self-healing materials

Inspired by the healing ability of natural organisms, scientists developed the wish to manufacture healable, artificial materials. The magnificent complex mechanisms, that nature uses to regain functionality, were developed as life forms evolved from single cell to amphibian and finally mammal life.^[6] For example, in skin healing, an inflammatory response induces the blood clotting followed by a proliferation in which new tissue is grown. In the remodeling process, collagen becomes realigned along tension lines. Although scars can remain, which lowers the performance of the tissue, the main functionality can be retrieved.

Encouraged by natural systems like the wound healing of skin, the general stages of healing for artificial materials were concluded (Figure 4).^[7] The damage should lead to an activation phase, followed by a transportation phase and as a final step the reparation phase.

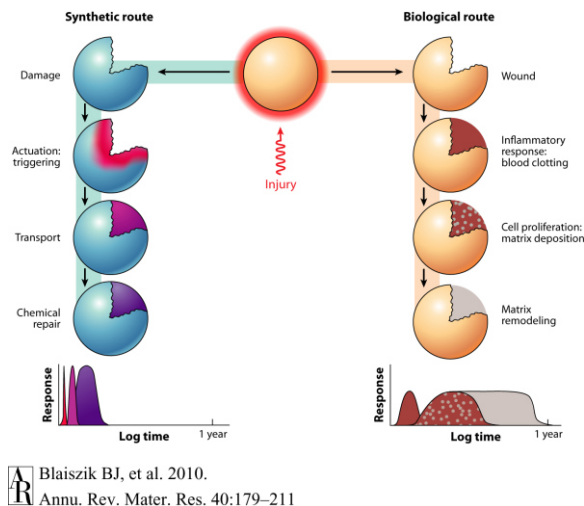


Figure 4: Synthetic route (left) and biological route to healing. Reprinted with permission from Ref. [7]. Copyright Annual Reviews, Inc.

However, the main difference between living organisms and synthetic materials is, that the former comprise a transportation system to deliver “healing agents” and fresh material components, while destroyed material is carried away. These complex mechanisms, involving precisely developed cells, perfected over millions of years of evolution, are difficult to mimic. Therefore, the healing mechanisms in synthetic materials had to be broken down to simplified procedures. Different healing approaches had to be developed according to the nature of the material. Metal, ceramics and polymers are the three basic categories.^[8]

Nowadays, most engineered materials are designed for damage prevention. In case of a failure, damage repair is done by replacement of the broken part. These materials would benefit from healable components. The incredible potential of continuous self-healing as a promising, safe, environmentally friendly and cost efficient principle for material constructions is already proved by the ancient romans. Amphitheatres, aqueducts, triumphal arches and impressive buildings like the Pantheon in Rome withstand about 2000 years now in an exceptionally good condition (Figure 5). The main component of these buildings consist of “opus caementitium”, a sort of concrete, made of gravel, sand, water, cement and volcanic ash. The healing principle is simple and highly efficient at the same time: when little cracks occur, they can be filled back, after rain or moisture dissolves parts of the concrete and the inorganic content (lime) newly solidifies within the crack upon drying.^[9, 10]



Figure 5: Roman Concrete is the first artificial Self-Healing material. Images: S.Schäfer.

Healing of artificial materials became a popular field in research with the beginning of 21. Century in the context of the aforementioned throw-away society and the plastic era. The number of publications by year containing the phrase “self-healing polymer” is continuously increasing (Figure 6).

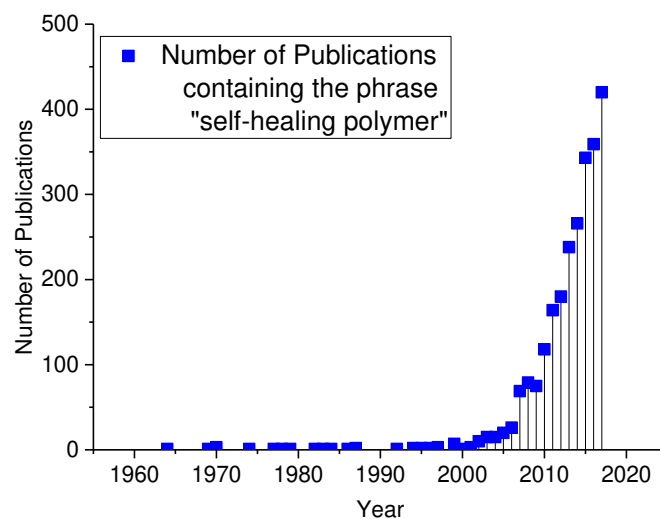


Figure 6: Increasing number of publications containing the phrase “self-healing polymer”.^[11]

The word “healing” is defined as “the process of making or becoming sound or healthy again”.^[12] In synthetic materials generally the restoration of only one property is regarded, which means that upon healing, not all properties are restored.^[13] In literature, most often mechanical properties, before and after healing are studied. The efficiency of the healing process (η) is measured by building the quotient of initial and healed property (Equitation 1).

$$\eta (\%) = \frac{K_{healed}}{K_{virgin}} \times 100 \quad (\text{Eq. 1})$$

The healing efficiency is commonly determined by mechanical tests, such as fracture test, fatigue test or tear test but also the surface smoothness can be regarded.^[14] The variety of tests is reasoned by the numerous different materials investigated in artificial self-healing. For this reason, a direct comparison of the healing efficiencies does only make sense, if similar materials are regarded.

The main goal of this interdisciplinary research is, to increase safety, extend longevity of the materials and enable a more sustainable and environmentally friendly handling of resources. Less raw materials and transportation would be necessary if materials heal efficiently and therefore the energy consumption in total would be lowered. Moreover, fatal accidents could be prevented, when fractures which cannot be easily detected in the beginning, heal before causing material failure.

It is worth mentioning, that the term "self-healing", which was established within the past 20 years is somehow irritating, as at least most of the intrinsic systems need a trigger, and therefore are not able to heal autonomously. The term "healable materials" would be more precise in this regard, but the term "self-healing" is originated from the biological models, which indeed do self-heal.

However, also living organisms do not heal autonomously, when taking into account that permanently energy is added to the system, e.g. by eating and drinking. The consumption of energy during healing is guaranteed because of the organization of the system, which means a negative entropy.^[13, 14] The occurring processes differ significantly according to the consistence of injured tissue.^[13] In soft skin an interpenetration of injured material from the damage interface with underlying virgin material is possible. Thus, an equalization of new and old material is possible. In hard bone, only surfaces can "reconnect", because the initial material is steady and cannot mix readily. According to the material, nature developed different healing strategies. In all cases, firstly, a fast process that fixes only rough structures begins, which is followed by prolonged mechanisms, to regain the original properties.

Based on this knowledge, scientists from different fields developed various healing mechanisms depending on the material type and studied the resulting properties.^[8, 14, 15] In this work, the focus lies on polymer based systems.

1.3 Classification of self-healing polymer based materials

Within self-healing polymeric systems, two categories can be distinguished:^[16] the autonomous and non-autonomous ones (Figure 7).

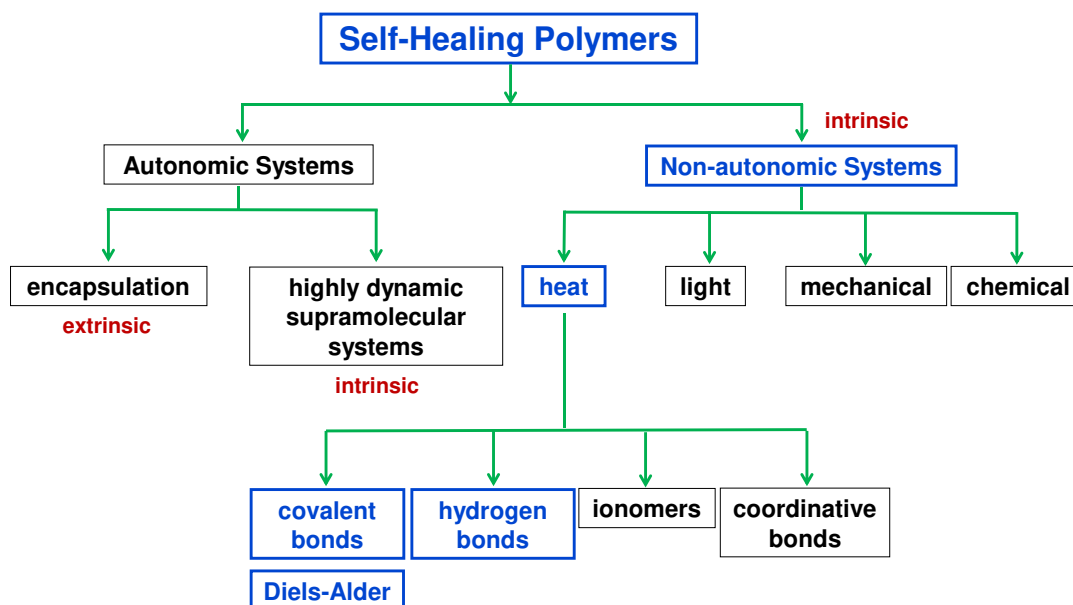
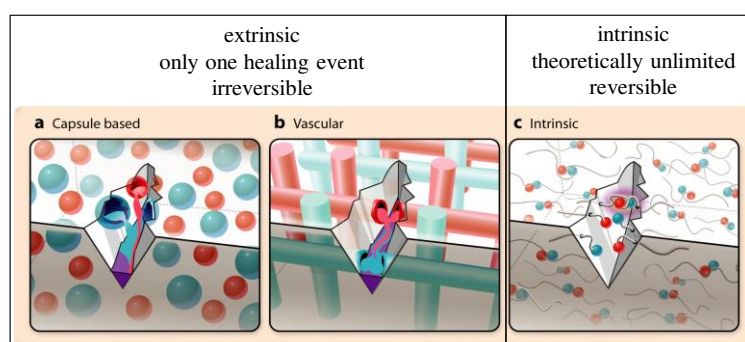


Figure 7: Classification of self-healing polymer based materials according to V.K. Thakur and M.R. Kessler.[16]

Non-autonomous systems, which are always intrinsic (Figure 7), need an energy input like heat, light, pressure or a chemical reagent, which is able to induce a chemical reaction or provide contact, so that the bulk properties of the material can be recovered. Intrinsic means, that the healing functionalities are incorporated homogeneously in the matrix on a molecular level (Figure 8). In particular, this can be found in systems, where chemical bonds alone are the key to healing. Reversible covalent bonds, hydrogen bonds, ionic bonds or coordinative bonds are suitable for this. These latent functionalities are commonly directly incorporated within the polymer matrix *via* copolymerization. In general, these reactions or interactions are theoretically fully reversible, which means that healing can take place at the same location in the material theoretically infinitely.



Blaiszik BJ, et al. 2010.
Annu. Rev. Mater. Res. 40:179–211

Figure 8: Extrinsic (left) vs. intrinsic (right) reprinted with permission from Blaiszik *et al.* Ref. [7]. Copyright Annual Reviews, Inc. Outer box added by Sandra Schäfer.

Autonomous systems can be both, intrinsic or extrinsic (Figure 7). Extrinsic means that capsules or tubes are incorporated in the matrix, which contain a healing agent (Figure 8). The healing agent normally consists of a mixture of monomers and catalyst, which is similar or the same as the matrix. One drawback is, that the healing can take place only once in the same region. The synthesis requires more steps, as the capsules or tubes and the matrix have to be synthesized separately and mixed afterwards.

Non-autonomous, intrinsic healing systems are the subject in this work and will be described in more detail in the following chapter.

1.4 Intrinsic self-healing systems

Intrinsic healing takes place at the molecular level, which specifies that healing occurs only at nanometer scale or below, when the proximity of reactants is given.^[13] All of these chemical healing processes are only possible if the crack interfaces are in contact. However, it has to be considered, that the reactions in bulk are slower than in solution, because they are hindered by the lowered possibility of reactive groups to come in close proximity. In hard materials, these conditions cannot be achieved because of the static surface, which makes heating or the addition of solvent necessary to provide the required proximity and mobility of reaction partners. In soft materials, the gap can be closed by pressing the surfaces of damaged area together.

The very basic intrinsic healing is the physical self-healing in thermoplastics, which is induced by a molecular movement and rearrangement of polymer chains above the glass transition temperature (T_g). De Gennes, Prager *et al.* and Wool *et al.* described this phenomenon theoretically in 1971 and 1981 respectively.^[17, 18, 19] De Gennes already mentioned dependency of healing time and the overall-mobility and diffusion and its relation to the molecular weight of one polymer molecule.^[17] Prager *et al.* pointed out the importance of the initial configurational distribution of the chains according to the healing time.^[18] Wool and O'Connor published the theory of five stages in crack healing in polymers: 1) surface rearrangement, 2) surface approach, 3) wetting, 4) diffusion, and 5) randomization.^[19] One basic approximation therefore is the reptation model, wherein one polymer chain is assumed as a tube (Figure 9), which can move by self-diffusion through the bulk material.

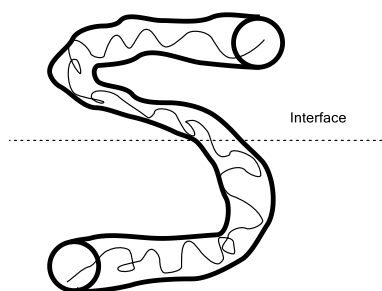


Figure 9: Polymer chain is diffusing as a tube according to reptation model within bulk.^[19]

Relations for strength, elongation to break, impact energy, and fracture parameters were obtained as a function of time, molecular weight, temperature, pressure, and processing conditions. Microscopy, spectroscopy, or scattering experiments were found to coincide with restoration of mechanical properties after crack closure.^[19]

First experimental results from Jud and Kausch on poly(methyl methacrylate) demonstrated the possibility of healing of thermoplastic material.^[20] In this early stage, they already described that the diffusion of whole molecular coils with a diameter of 20 nm is rather unlikely to occur. The diffusion of chain end segments seem to penetrate into the matrix to form physical linkages. Already in this early stage, the other option of healing in such a material, namely, the homolytic or heterolytic cleavage of covalent bonds due to mechanical stress, which leads to the formation of radicals, was identified almost not to contribute. Later studies further confirmed this, by cleavage through the use of radical reporter molecules, such as 2,2-diphenyl-1-picrylhydrazyl and pentamethylnitrosobenzene. These radicals are too reactive towards atmospheric oxygen and get immediately quenched before a recombination could occur.^[21]

In more recent studies specific reversible interactions were chosen to increase the ability to self-heal, improve the strength of the material, and to accelerate, consolidate and trigger the reversible processes. These interactions can be divided into non-covalent and covalent ones.^[16]

The non-covalent interactions comprise π - π -stacking,^[22, 23, 24, 25] hydrogen bonding,^[26, 27, 28, 29] ionic interactions,^[30, 31] and coordinative bonds.^[32, 33, 34, 35] Although they are weak, when regarded separately, the sum of many of these forces in total lead to a strong network. Most often, these interactions are incorporated in relatively soft materials, like hydrogels.^[36] Covalent interactions were designed using the Diels-Alder (DA) cycloaddition,^[37, 38] radical exchange,^[39, 40] dynamic urea bond,^[41] and trans-esterification.^[42, 43, 44] The covalent bonds are principally stronger than the non-covalent ones – and therefore the materials using this healing type can be harder. Within the evolution of living organisms, nature developed materials, which combine the advantages of the strong covalent and weaker reversible bonds.^[13]

1.4.1 Dynamic covalent bond chemistry

The intrinsic healing method based on dynamic covalent bond chemistry (Scheme 1) can be classified in three main categories: the condensation, exchange and addition type of equilibrium reactions,^[45] but the transitions are fluent (Figure 10). Each of these reactions is reversible under the addition of energy. The necessary energy input can be realized by irradiation, light, increase of temperature or the addition of chemicals. Temperature is most often employed as a trigger, because an increase in temperature assures a higher mobility of functional moieties, which is one essential condition for intrinsic healing.

Condensation**Exchange****Addition**

boronate ester

acylhydrazone

vitrimers

thiol-ene

Diels-Alder

oxime

metathesis

urea

Cycloaddition

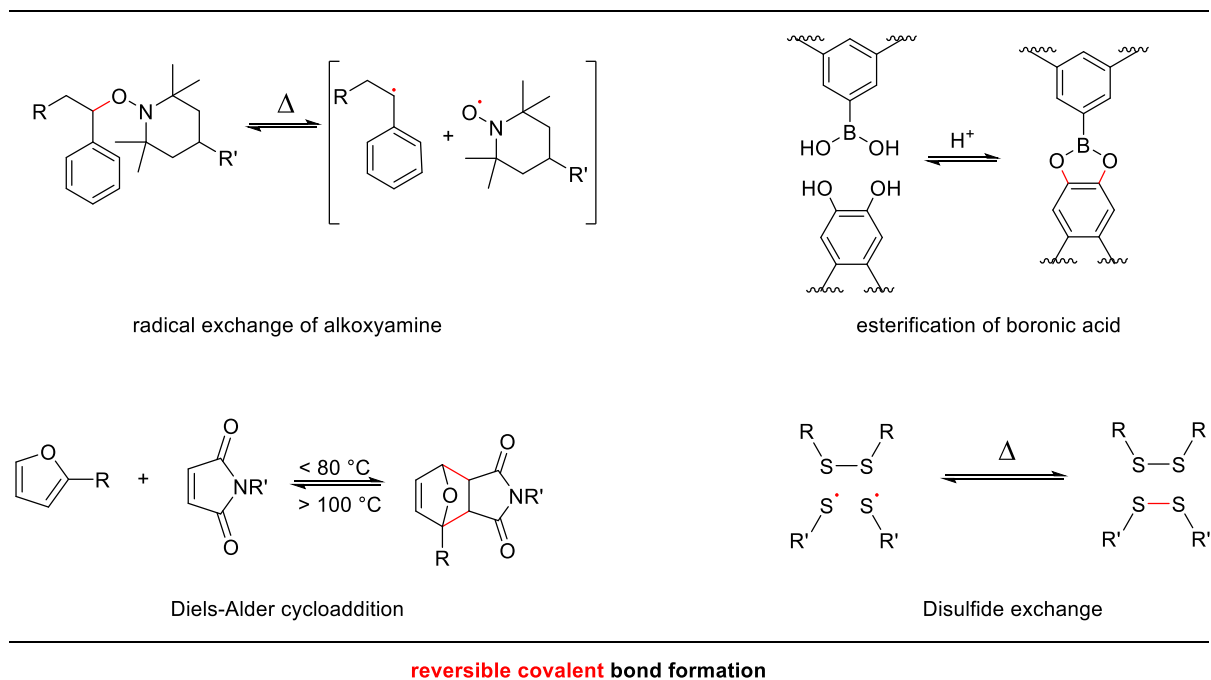
imine

siloxane

disulfide

Diarylbibenzofuranone

alkoxyamine

Figure 10: Intrinsic dynamic covalent bond chemistry. Adapted from Ref. [45].**Scheme 1:** Selected intrinsic reversible covalent interactions.

In the first type, the condensation reaction, two functional moieties react with each other under release of a third small molecule (e.g. water, alcohol). Lehn *et al.* investigated the acid catalyzed condensation of di(aldehyde) and di(acylhydrazines) to acylhydrazones under release of water.^[46, 47] The condensation of boronic acids with diols, such as catechol enables the formation of boronate esters, which is responsive to the pH value.^[48] Both condensation type reactions are commonly applied for the preparation of self-healing hydrogels having low mechanical strength.

In the second type, the exchange reactions, the reactive, isofunctional groups can switch or reshuffle their connections. Usually, the opening and closing of bonds proceed at the same time. Examples comprise imines^[49] and oximes,^[50] which are most often employed in hydrogels, disulfide bonds,^[40] which enable healing at low temperatures but these bonds are weak and thermally unstable at elevated temperatures, dynamic urea bonds,^[41] which can dissociate reversibly to isocyanate and an amine when bearing an appropriate bulky substituent, siloxane exchange,^[51, 52] which offers access to a low toxic material, which is chemically stable and can heal at ambient temperature, but has a low mechanical strength. Radical exchange in alkoxyamines^[53, 54, 55] enables the use of polymers with higher mechanical strength, but some of the systems are unstable towards O₂. Because of the high reactivity of

the NO radical, several side reactions occur, and elevated temperatures are required to shift the chemical equilibrium to the free radicals.^[55] Olefin metathesis^[56, 57] shuffles strong C-C double bonds by the application of transition metal catalysis.

In the third category, the addition reaction, two reactive molecules give one product without the formation of any byproduct. Examples in this category include various types of the DA reaction which is a [4+2] cycloaddition,^[38, 58] the [2+2] cycloaddition of coumarin and cinnamoyl groups and the [4+4] cycloaddition of anthracene. The cycloadditions involving $4n$ π -electrons always proceed photochemically, which leads to a problem with healing, because the penetration depth of light into the bulk material is limited.^[45] The Michael addition of thiol-ene systems offers access to reversible C-S bonds, but they are generally weaker, and the materials tend to degrade at higher temperatures.^[59, 60, 61]

Each of the mentioned reactions, which are known for intrinsic self-healing materials possesses its specific range for a possible application. The advantages and disadvantages have to be considered with respect to the desired properties. In Dahlke's review it was pointed out, that good healing efficiency with high mechanical strength at the same time is difficult to obtain.^[45] Intrinsic healing systems having the highest strength along with relatively short healing times contain the DA chemistry. The further increase of mechanical strength of intrinsic healing systems is still a challenging field of current research.

The DA chemistry probably represents the most versatile function for the generation of self-healing polymers because of the high tolerance of functional groups, the temperature range of application and the thermal trigger. According to that, the by far most often employed reaction is the thermoreversible [4+2] cycloaddition, namely the DA reaction. Many advantages, such as the formation of strong C-C bonds in high yields, the absence of side reactions, the orthogonality, which means the reaction has a high tolerance of functional groups, no need of further chemicals for association or dissociation, the temperature range, in which the reaction is thermoreversible, the versatile possibilities of chemical modification of required diene and dienophiles and the robustness (air stable, proceed in almost any medium). The diene and dienophile pair can be chosen according to the desired temperature range for the materials application. Also, the well-known DA chemistry makes this type of reaction an appropriate tool for the covalent connection of polymers to inorganic materials in composites.^[45] Compared to non-covalent bonds, the covalent ones are principally stronger - and therefore the materials using this healing type can have a higher mechanical strength. For these reasons, we chose to work with the DA reaction for the investigated approach and therefore only this type of dynamic covalent bonds will be discussed in more detail.

1.4.2 Diels-Alder based systems

The DA chemistry provides a unique access to strong covalent, thermally reversible carbon-carbon bonds within a suitable temperature range for polymers. As a click-reaction, the [4+2] cycloaddition between diene and dienophile, has a high thermodynamic driving force with an excellent selectivity for one single product and accordingly a high atom efficiency. Six π -electrons rearrange in a six-membered cyclic transition state by a positive overlap of the

highest occupied molecular orbital (HOMO) of the diene and the lowest unoccupied molecular orbital (LUMO) of the dienophile, in DA pairs with normal electron demand (Figure 11).^[62] This overlap is the precondition of the formation of the two new σ -bonds.

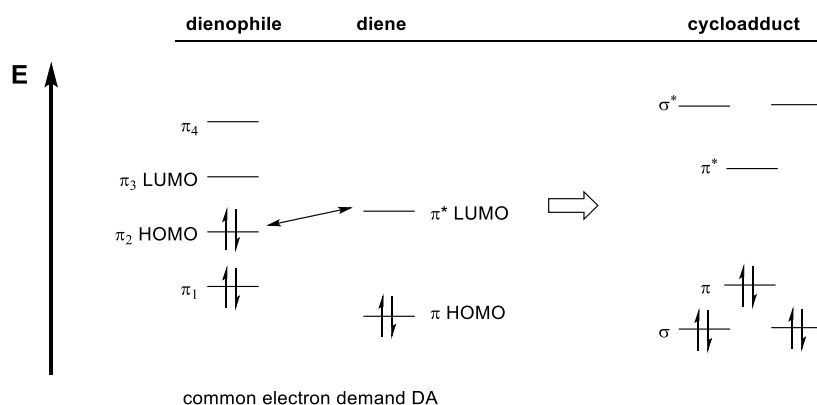


Figure 11: Interaction of HOMO diene and LUMO dienophile.^[62]

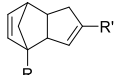
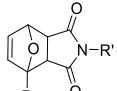
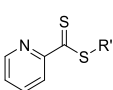
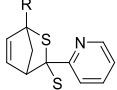
The chemical equilibrium state can be tailored by choosing the temperature according to Le Chatelier. To produce starting materials from the DA adduct, energy has to be added to the system by an increase in temperature. The probably most simple DA pair is 1,3-butadiene/ethylene, but the reaction proceeds rather slow and requires high temperatures for the back reaction. Accordingly, it has no meaning for material development. Better suitable are cyclic dienes, as the substituents on double bonds are trapped in the cis-conformation, and no rotation around the reacting bond is necessary.

The number of suitable DA pairs for materials applications is low, because of the specific temperature ranges and the time in which these pairs can be reversible switched from starting material to the product. Most DA pairs would show rather a degradation on thermal treatment than dissociation into the starting materials. Only three types of DA reaction match the condition to have a sufficiently low DA reaction enthalpy so that the dynamic equilibrium can be affected by heating without thermal degradation. The three suitable DA reactions are:

- a) the homoaddition of cyclopentadiene (Cp),
- b) the addition of two different heterocycles; e.g furan and maleimide
- c) the hetero-DA reaction, in which a six-membered heterocycle having a C-X (e.g. X=S) bond is built.

Their healing times and temperatures are depicted in Table 1.

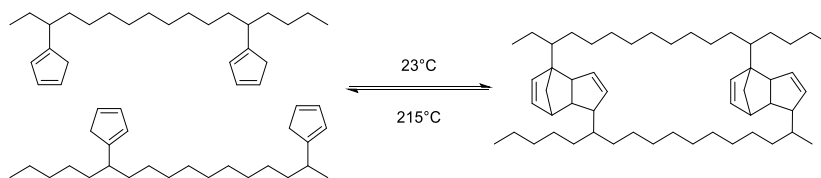
Table 1: The three suitable DA pairs and their healing times and temperatures.[63]

Diene	Dienophile	DA adduct	Conditions
			DA: 25-120°C rDA: >120°C time: hours to days
			DA: 80-120°C rDA: >120°C or > 180°C depending on R and R' time: hours to days
			DA: 25-80°C rDA: >80°C time: minutes catalyst TFA or ZnCl ₂

These three systems have in common, that the dienes are cyclic. Accordingly, the substituents on double bonds are trapped in the cis-conformation and no extra-rotation around the connecting σ -bond is necessary before the addition can proceed. By choosing stable dienes, such as the aromatic furan or producing less stable adducts, such as dicyclopentadiene (DiCp) or the pyridinyldithioformate, a low energy barrier for the equilibrium can be realized.

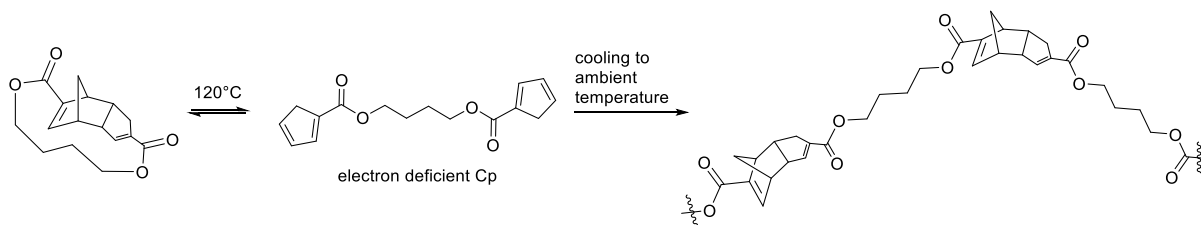
The most simple diene/dienophile pair are two cyclopentadienes, which can dimerize within hours at ambient temperatures. This molecule can act as both, diene and dienophile and also the DA adduct was found to react as dieneophile.^[64, 38, 65] The main driving force of this reaction, besides the formation of two new σ -bonds, is the reduction of ring strain in both Cp units. However, because cyclopentadiene tends to dimerize, crosslinking prior to shaping can occur. The required temperature for the cycloreversion is rather high since cracking of dicyclopentadiene affords a temperature of 170°C.^[66]

Already in 1961, Stille and Plummer investigated the polymerization of 1,n-bis(cyclopentadienes) alkanes by DA reaction, but they did not investigate the thermal reversibility of these systems.^[67] In 1979, Kennedy and Castner were the first who showed the thermal reversibility of a dicyclopentadienyl crosslinked system.^[68, 69] The polymers contained either terminal or randomly distributed pendant cyclopentadiene groups.^[69] The latter ones were able to undergo the DA and the reverse reaction at 170°C to afford remoldable polymers (Scheme 2).

**Scheme 2:** Reversible dicyclopentadiene crosslinked polymer.[69]

Remolding under maintenance of the same polymer properties was possible two times. In the third cycle, the polymer could no more adapt to the shape of the mold cavity, and the pieces did not coalesce. Kennedy and Castner gave no explanation, but later Bergman and Wudl

speculated that exposing the system multiple times to high reversal temperatures cause undesired decomposition of the material.^[38] Further, they stated in their review from 2008, that despite a few rather old reports, dicyclopentadiene (DiCp) DA systems have not been investigated for remoldable polymers until Wudl *et al.* came up with a new modification.^[70]

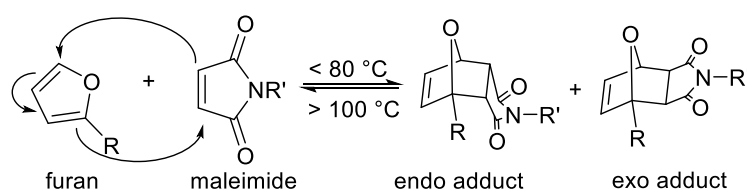


Scheme 3: Modified dicyclopentadiene crosslinked polymer with tremendously lowered rDA temperature.^[70]

In their work, they used a DiCp unit, which opens up to α,ω -bis(cyclopentadiene) monomer (Scheme 3). The DA adduct itself can undergo the DA reaction with nearby crosslinking monomers, leading to trimer formation. Either the double bond of norbornene or the cyclopentene bond can react as the dienophile. In the case of carboxylated cyclopentadienes, the less sterically hindered cyclopentene double bond undergoes the reaction. Incorporated in this network, the reverse DA reaction proceeds at 120-150°C instead of the required 170°C for the cracking of the pure DiCp molecule. Crosslinking proceeds by cooling to ambient temperature.

The required temperature in cyclopentadiene systems can be lowered to some extent, depending on the substituents attached to the ring.^[70] However, electron rich dienes and electron poor dienophiles exhibit a higher reactivity because of the electronical activation. Hence, the furan/maleimide pair is the most often employed in intrinsic healing systems (Scheme 3).^[71, 72, 73] The dienophile is activated by strongly electron withdrawing, conjugated C=O groups, while the diene is a π -excessive aromatic. Thus, the LUMO of dienophile is lower, and the HOMO of the diene is higher in energy, which allows a DA reaction between room temperature and 80°C, and the cycloreversion between 80 and 120°C.^[63]

Two stereo conformers (Scheme 4) of the furan/maleimide adduct are possible, the exo and the endo product. Although in prototype like DA reactions the endo isomer is favored, furan [4+2] cycloadducts provide a mixture of both isomers, depending on the reaction conditions.^[74] The slight kinetic preference of the endo product is diminished by the aromatic stabilization of the heterocyclic electron rich furan ring, which also allows the rDA reaction to proceed at lower temperatures. Furthermore, maleimide and furan allow for numerous chemical modifications, indicated by R and R' in Scheme 4.



Scheme 4: Diels Alder [4+2] cycloaddition equilibrium of maleimide and furan.

The maleimide ring can be substituted differently at the nitrogen atom. In most cases, the ring is synthesized starting from a suitable amine by adding maleic anhydride and a following ring closure by elimination of water. Appropriate reaction conditions are necessary in which the functional groups present in the molecule are tolerated and the undesired homopolymerization (radical addition to the double bond) of maleimide is not favored.^[75]

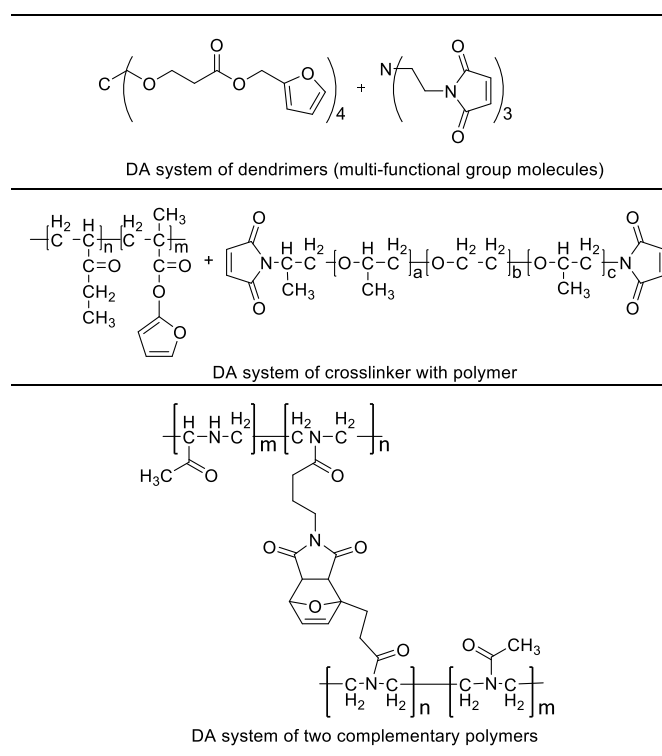
The heteroaromatic furan ring is generally already present in the starting molecule, as there are numerous commercial, natural precursors, such as furan, furfuryl alcohol, furfurylamine. For example, furan can be modified starting with a deprotonation^[76] followed by a reaction with alkyl halides.^[77] Furfuryl alcohol can be reacted e.g. with acid chlorides^[78] and furfurylamine can be converted with epoxides.^[79]

The DA product between maleimide and furan forms between room temperature and 80°C and the back reaction occurs above 120°C. For many polymer matrices, this is an ideal temperature range, as the T_g is below rDA temperature. A high mobility of chains and flexibility of functional DA groups can be guaranteed above T_g . Also, this temperature range allows usage of the material at ambient temperature and slightly above.

Although the DA reaction was already discovered in 1928 by Otto Diels and Kurt Alder^[80] and awarded with the Nobel Prize in 1950, the first attempts to use the furan/maleimide pair for thermoreversible crosslinking in polymers were made in 1966 by DuPont.^[81] The authors claimed the synthesis of various polymer backbones such as polyesters, polyurethanes, polyureas, polyimides and polyamides modified with furan, which could be thermally crosslinked by bis- or trismaleimides.^[81] The products were reported to show a unique post-formability and therefore could be used for gaskets or diaphragms. Moreover, the excellent suitability as an adhesive or coating was claimed with "the added advantage of being easily repaired by heating". In 1983, a patent of Minnesota Mining and Manufacturing Company described an "one-part solvent free thermosettable blocked prepolymer composition, containing a diene, together with chain extender, chain terminator and a dienophile" and point out the ability to cure into solidified adhesives or coatings.^[82]

Contrary to the patents, which normally come out because of an economic interest, in scientific literature, only few publications in the field of thermoreversible crosslinked DA polymers can be found until the early years of the 21. century. To the best of my knowledge, the first who described maleimide-group modified polystyrene, which was crosslinked with the difurylester of adipic acid, were Stevens and Jenkins in 1979.^[83] Saegusa *et al.* described the reversible gelation of polyoxazoline hydrogel by the DA reaction in 1990.^[84] This article was first cited in 1997 by Gandini and Belgacem, who collected the state of the art of furan-bearing polymers.^[85] Several early attempts were mentioned in this work, which comprise polymer backbones bearing furan as functional group being crosslinked with bismaleimides. Up to then, the term "self-healing" was not developed in this context. Probably the first, who brought the terms "self-healing" and "DA" in a context, were Wudl *et al.* in 2002.^[58] A multidiene (tetra-furan) and a multidienophile (tris-maleimide) were crosslinked to a polymeric material, which showed healing of a macroscopic cut and load displacement measurements showed a recovery of 57% of the initial strength. Since then, an increasing number of different strategies for optimization, like crosslinking of dendrimers (molecular multi-furans

with –maleimides),^[58, 86, 87, 88] crosslinkers with polymers^[89, 90, 91] and two complementary polymers have been tested (Scheme 5).^[84, 92]



Scheme 5: Various strategies using dendrimer, crosslinker, polymers and combinations of those for the design of DA self-healing polymers.^[58, 84, 89]

The polymers including various different backbones, such as methacrylates,^[93] polyurethanes,^[94, 95] epoxies,^[96] and siloxanes.^[97, 98] DA based self-healing materials have been intensively reviewed.^[38, 71, 72, 73] In general, a direct comparison of these systems is inappropriate, as they do not aim to solve one specific problem. Crosslinking densities are fundamentally different, when comparing multifunctional molecular crosslinker with modified polymers, which can have only a small percentage of DA functional groups. Materials properties vary according to the chosen main component, e.g. from elastomeric,^[97] to thermosetting^[99, 100] and hydrogels.^[101] But, they all have in common, the temperature range in which the furan/maleimide system is reversible and healing occurs, when damaged surfaces are in close proximity. In all systems a temporary local increase of mobility due to decrosslinking of the polymeric chains is a necessary healing condition.

The reaction of two cyclopentadienes requires several hours to days in bulk,^[63, 69] but their ability to undergo DA reaction under ambient temperature along with high temperatures required for the reverse reaction (>120 or >180°C) makes this pair less favorable for the design of new materials. The furan/maleimide pair also requires several hours to days in bulk, but are advantageous regarding the reaction temperatures. Almost no conversion of the pair is observed at ambient temperatures and accordingly a significant cycloaddition would require days to proceed.^[37] Temperatures between 60 and 80°C lead to reaction times of several hours.^[37] The reverse reaction can be started by heating the sample above 120°C.

Outstanding fast is the hetero-DA reaction of dithioesters and cyclopentadiene, which proceeds within minutes.^[102, 103, 104] The reaction can be further accelerated by the addition of a catalyst, such as trifluoroacetic acid (TFA)^[65, 105] or ZnCl_2 ^[106] which further decrease the electron density of diene by coordinating the S atoms. The reverse reaction of unstable 6-dihydro-2H-thiopyranes can be performed above 80°C within minutes.^[103, 107]

For example, in 2010 Barner-Kowollik *et al.* described a cyanodithioester/Cp pair, which is thermoreversible between 40-120°C within less than five minutes and without the need of a catalyst (Figure 12).^[108]

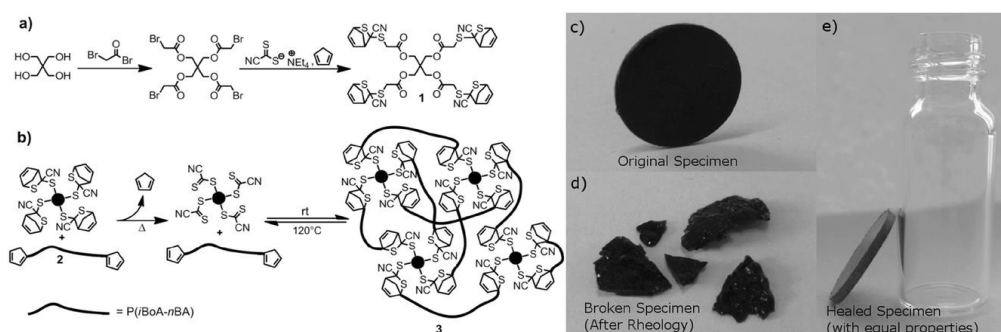


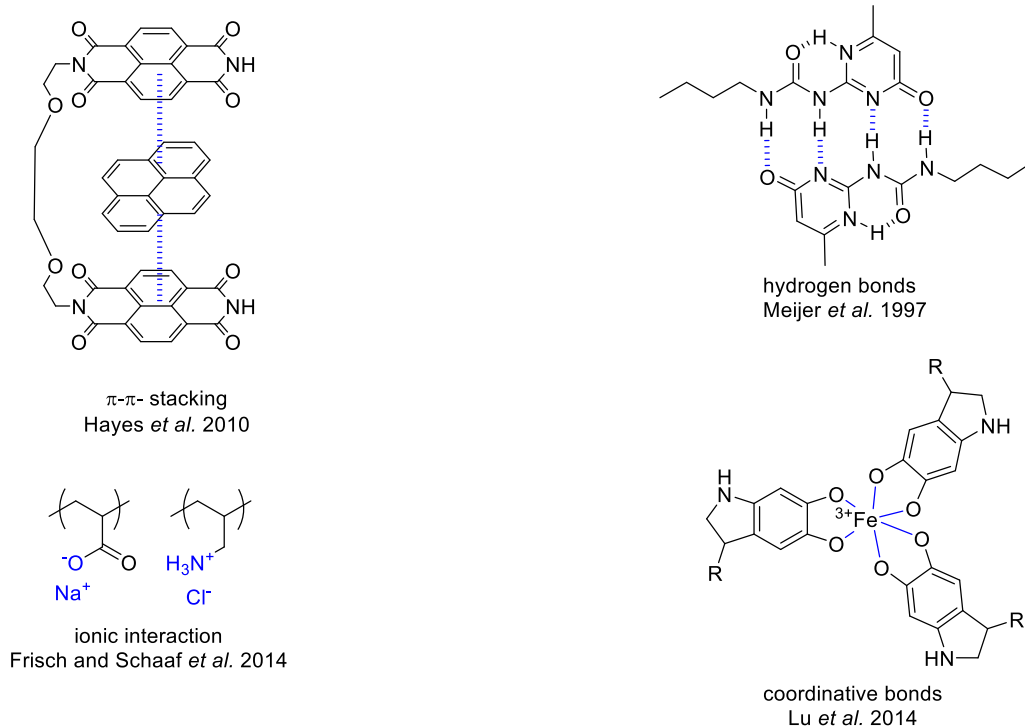
Figure 12: Cyanodithioester/Cp pair developed by Barner-Kowollik *et al.* Reprinted with permission from Ref. [108]. Copyright 2014 WILEY-VCH Verlag GmbH & Co. KGaA, Weinheim.

However, this fast reaction allows only for material usage in a small temperature range and the compounds are labile at elevated temperatures.^[65, 105, 108]

Hence, because of the high robustness and adequate temperature range, the furan/maleimide pair is probably the most interesting one for the design of self-healing materials.

1.4.3 Dynamic non-covalent bond chemistry

The non-covalent interactions, which are able to form dynamic supramolecular networks comprise π - π -stacking,^[22, 23, 24, 25] hydrogen bonds,^[26, 27, 28, 29] ionic interactions,^[30, 31] and coordinative bonds.^[32, 33, 34, 35] Examples for these interactions are depicted in Scheme 6. Although non-covalent forces are weak, when regarded separately, the sum of many of these forces in total lead to a strong network.



reversible non-covalent bond formation

Scheme 6: Intrinsic reversible non-covalent interactions.

These forces have an impact on strength, flow and viscosity and intrinsic polymer chain ordering of the modified polymer.^[35] Of particular interest is the generation of liberated supramolecular moieties at interfaces, after a damage occurred. Because of the weakness of these bonds compared to covalent bonds, the supramolecular ones will fail first. These unbonded moieties recombine spontaneously after damage to return to equilibrium, which leads to a rather fast healing.^[35]

Most often, these interactions are incorporated in relatively soft materials, like hydrogels,^[36] because the supramolecular forces can lower the chain mobility, which is crucial for the self-healing process. Therefore, the reasonable amount of incorporated supramolecular has to be considered for each material.

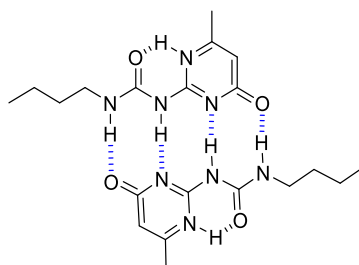
In this work, only hydrogen bonds were used as a second intrinsic reversible bond and accordingly, only this supramolecular force will be more intensively discussed.

1.4.4 Hydrogen bond based systems

The non-covalent, dynamic hydrogen bonds are another outstanding interaction for self-healing polymers, as they form spontaneously and autonomously at room temperature.^[109] They are in an equilibrated state, which means, that they immediately reconnect when cleaved within a bulk material.^[13] Therefore, a general requirement is a sufficiently soft matrix, to guarantee the required mobility for recombination by this weak interaction.

The weak bond energy of hydrogen bonds is between 0.2 - 40 kcal/mol,^[110] but collectively they form stable networks, like in the nucleobases within our DNA. In nature, hydrogen

bonds are the most often represented non-covalent interaction for the assembly healing of soft tissue. In literature, this strength is most intensively used for self-healing hydrogels, which are soft-solids or solid-like materials containing a large amount of water.^[111] These systems are mostly applied in biomedicine. When aiming for other applications e.g. in mechanical engineering, the main task is to realize high mechanical strength in combination with autonomous self-healing due to supramolecular forces.



2-ureido-4-pyrimidone (Upy)

Scheme 7: General Scheme Hydrogen bond interactions. Hydrogen bonds depicted in blue.

Already in 1997, Meijer *et al.* reported 2-ureido-4-pyrimidone (Upy) (Scheme 7), which is self-complementary with four hydrogen bonds, and employed it as an end group in reversible self-assembling polymers.^[26] It was the first example of a reversible hydrogen bond unit which realized the synthesis of linear supramolecular polymers due to a sufficiently high association constant.^[27] Due to cheaper and faster production, along with reduced energy consumption during processing and the improved recycling properties compared to conventional polymers, systems based on Upy units have been already commercialized in the company "SupraPolix".^[27]

Leibler *et al.* reported a self-healing rubber composed of a fatty di- and triacid diethylene triamine adduct, which is further reacted with urea.^[28] The product mixture consisting of oligomeric amidoethyl imidazolidone, di(amidoethyl) urea and diamido tetraethyl triurea self-assembles by directional hydrogen bond interactions. After damage, self-healing takes place at room temperature without any further action when the surfaces of the cut are brought back into contact. A dominant parameter for the quality of the healing is the time passed after the damage was done and contacting the split surfaces again, because after a certain waiting time, the number of available, non-associated groups decreases.

Through the combination of covalent and supramolecular interactions the mechanical performance of self-healing materials was improved.^[112, 113, 114, 115] Sijbesma *et al.* incorporated different ratios of covalent and UPy dimer crosslinks into polyester-polyurethanes, to create a mixture of covalent and non-covalent crosslinks.^[112] These materials showed simultaneously typical thermoset properties as well as some features of thermoplastic materials. The authors describe, that the UPy groups lead to a higher creep compliance below T_g , which means that mechanical tensions in the material can be relaxed again. Recovering from internal stresses thanks to UPy units is a type of completely autonomous healing. Guan *et al.* reported a free radically polymerized polystyrene backbone bearing amide functionalized brushes.^[114] This polymer collapses into a core-shell nanostructure, in which the polystyrene unit forms the

hard particle-like segment while the amide brushes form the dynamic reversible surrounding. This thermoplastic elastomer showed a high autonomous self-healing potential and reached between 75 and 90% recovery of extensibility after 24 h healing. In 2014, Picchioni *et al.* were probably the first who combined DA and hydrogen bonding moieties in one polymer. A furan, carbonyl and amine bearing polymer was crosslinked by bismaleimide. Thus, an increase of T_g from 100°C to 185°C was realized.^[116] As shown in these few examples, the synergistic combination of these two reversible intrinsic healing forces, namely the hydrogen bond and the DA reaction is promising for ongoing work.

1.5 Combination of intrinsic healing interactions

As mentioned before, during the evolution of living organisms, nature took the advantages of combining both, the strong covalent and weaker reversible bonds for the design of materials.^[13] For example, proteins are composed of unbranched amino acid chains, and their shape is caused by noncovalent interactions within this chain.^[117] Cysteine, which is part of many proteins, is able to form additional intramolecular reversible covalent disulfide bonds. This bond can be built under oxidative and cleaved under reductive conditions. The intramolecular disulfide bonds contribute to the physical and thermal stability of proteins.^[118] Despite this increase in stability, denaturation can be caused by temperature, pH or chemicals. The primary structure of the proteins often remains, and due to the reversible bonds, the initial functionality can be recovered.^[119]

Slowly, this double intrinsically reversible principle, developed by nature, begins to enter the field of artificial self-healing materials. Through the combination of covalent and supramolecular bonds, a molecular memory within the material can be achieved.^[120] The weaker supramolecular bonds are reversible under ambient conditions and reassemble spontaneously, while the robust covalent bonds can be triggered via various stimuli. In the following, several doubly intrinsic healing systems are presented.

Oxime exchange/Boronate ester bonds

Collins *et al.* synthesized a double dynamic self-healing hydrogel based on oxime and boronate ester bonds (Figure 13),^[121] by mixing glycerol ethoxylate tribenzaldehyde, tetraethylene glycol bishydroxylamine and 3,5-diformylphenylboronic acid. After addition of polyphenol or tannic acid, the boronate ester bonds formed. The increased crosslinking density compared to the pure oxime hydrogel led to a doubled strength of the material.

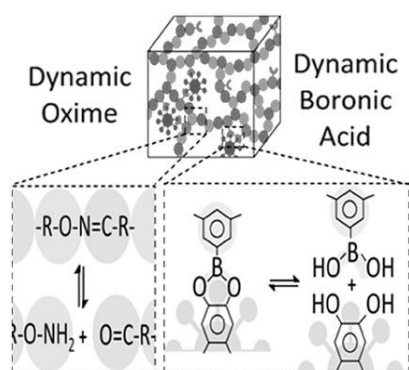


Figure 13: Double intrinsic reversible system by combination of oxime and boronic acid bonds. Reprinted with permission from Ref. [121]. Copyright 2017 WILEY-VCH Verlag GmbH & Co. KGaA, Weinheim.

The double intrinsic reversible gel was cut in two halves and pressed together physically to self-heal. After 3 h, the gel withstands pulling perpendicular to the cut. In a rheology experiment, stress was applied to the gel until the material failed. Ten minutes after stress relief, the storage modulus was fully recovered.

Boronate ester bonds /Disulfide bonds

Chen *et al.* developed quadruple-stimuli (temperature, pH, glucose, and redox-responsive) sensitive hydrogels based on boronate-catechol interactions between a disulfide-containing, boronic acid-based crosslinker, and a catechol-functionalized poly(*N*-isopropyl acrylamide) (Figure 14).^[122]

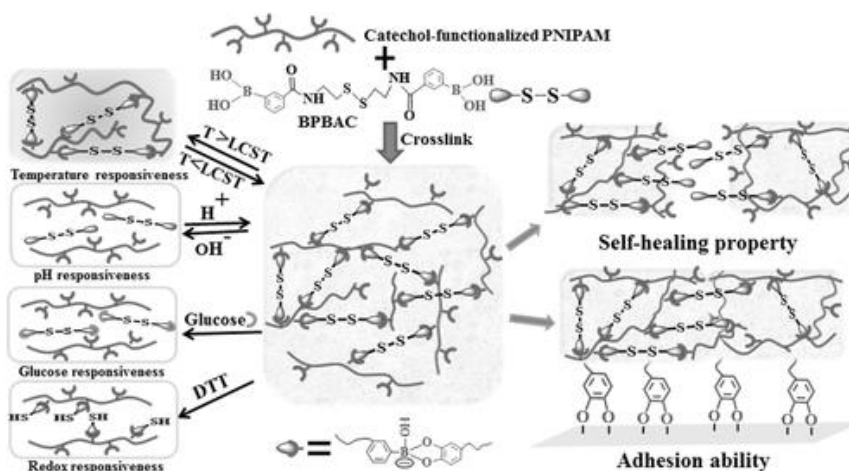


Figure 14: Quadruple intrinsic reversible system developed by Chen *et al.* bonds. Reprinted with permission from Ref. [122]. Copyright 2017 WILEY-VCH Verlag GmbH & Co. KGaA, Weinheim.

The hydrogel was able to heal after putting the pieces into contact for 5 min.

Disulfide bonds/Hydrogen bonds

In 2018, self-healing polyurethanes based on disulfide bonds and hydrogen bonds were described by Xiao and colleagues.^[123] Polyurethane networks were prepared by reacting polytetramethylene ether glycol, 3-isocyanatomethyl-3,5,5-trimethylcyclohexyl isocyanate and 2-hydroxyethyl disulfide in a common one-pot polymerization (Figure 15, left).

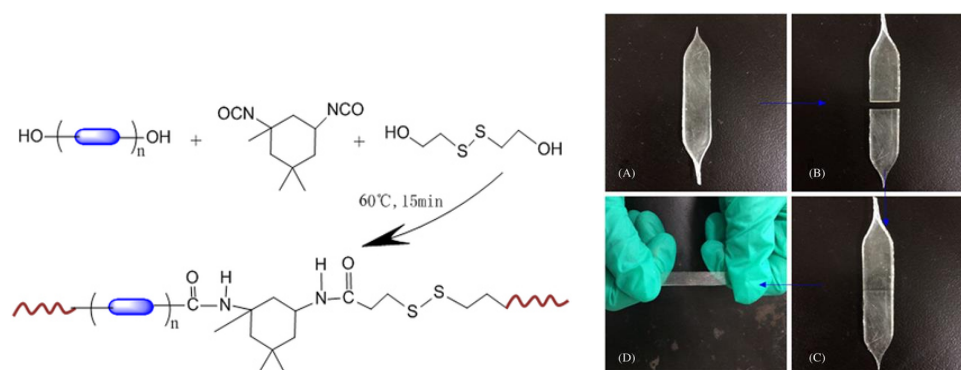


Figure 15: Left: Synthesis of polyurethane having disulfide and hydrogen bonds. Right: Healing of the specimen after cutting into two halves, reconnected at 12 h by contact at ambient conditions. Reprinted with permission from Ref. [123]. Copyright 2017 John Wiley & Sons, Ltd.

The specimen was cut into two halves, and after 12 h at 60°C, the healed sample could not be manually separated (Figure 15, right). In this material, a compromise between the mechanical stiffness and the healing capability has to be found. On the one hand, hydrogen bonds increase the stiffness, but on the other hand, they decrease the polymer segment movement which lowers the self-healing ability. Using a reference material, having no sulfide bonds, the authors determined a healing efficiency of around 46% solely by hydrogen bonds. The double reversible network can reach efficiencies of 100%.

Disulfide exchange/Acylhydrazone exchange

Deng et al. developed dual reversible, multi-responsive hydrogel based on acylhydrazone and disulfide exchange reactions (Figure 16).^[124] Both reactions are reversible upon a change in pH, acylhydrazone exchange in acidic conditions and disulfide exchange in basic ones.

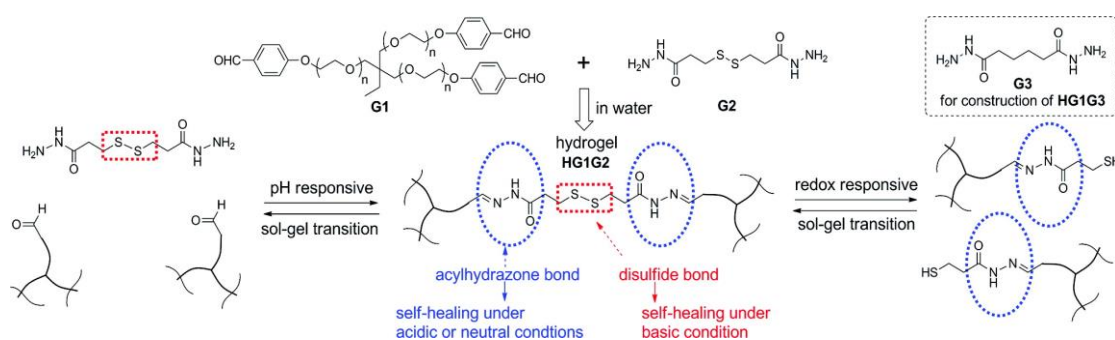


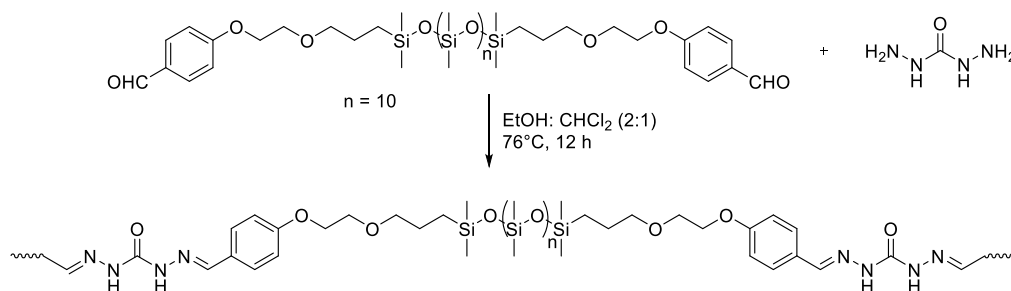
Figure 16: Synthesis of a dual responsive dynamic hydrogel by acylhydrazone and disulfide groups. Reprinted with permission from Reference [124]. Copyright 2012 American Chemical Society.

In a self-healing experiment, the cut samples were able to heal at room temperature in air saturated with moisture within 48 h under either acidic (acylhydrazone) or basic (disulfide) conditions. Under the addition of catalytic amounts aniline, the authors managed even to heal the hydrogel under neutral conditions, due to the acceleration of acylhydrazone exchange.

Acylhydrazone exchange/Hydrogen bonds

Lehn *et al.* combined hydrogen bonds with the acylhydrazone exchange. Oligo-dynamers connected by reversible covalent acylhydrazones are connected to supramolecular polymeric units through supramolecular hydrogen bonds.^[125] However, this study focused on the preparation of the material, and no self-healing experiment was conducted. The same group developed a similar double dynamic supramolecular polymer, having a sextuple hydrogen bond and the reversible acylhydrazone unit.^[126] Also in this study, no healing experiments were conducted.

Later, Lehn *et al.* developed double dynamic self-healing polymers using bis-iminocarbohydrazide motifs, having the opportunity to form hydrogen bonds and acylhydrazone linkages (Scheme 8).^[127] An α,ω -aldehyde group bearing polydimethylsiloxane (PDMS) was condensed with carbodihydrazide.



Scheme 8: Synthesis of a dynamic polymer by polycondensation of the monomeric bis-aldehyde and carbodihydrazide.^[127]

The synthesized polymer films could be healed under ambient conditions in a few hours without application of any additional pressure or load, and recovered 90% of its original strain. Despite this result, the authors mentioned, that probably mainly hydrogen bonds cause the healing behavior. A control experiment, in which an acid catalyst was added to accelerate the acylhydrazone exchange did not change the healing time.

DA reaction/hydrogen bonds

Probably the first who studied the combination of DA and hydrogen bonds was the group of Picchioni.^[116, 128] As a first attempt, aliphatic polyketones were modified with furan and primary amines, which were crosslinked with commercial bismaleimides. An increase in T_g was observed by the formation of hydrogen bonds. However, this system suffers from an irreversible side reaction between amine and carbonyl groups.^[116] In the following work of Picchiono *et al.* this problem was solved using OH groups instead of amines (Figure 17).^[128]

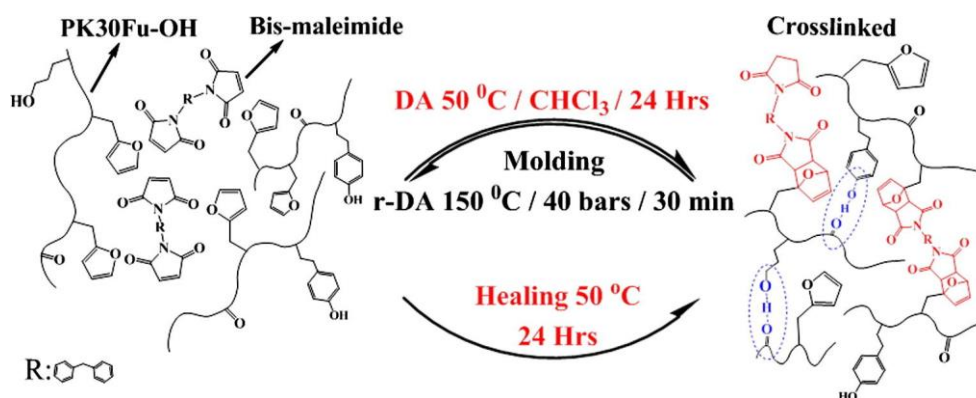


Figure 17: Double intrinsic healing system by DA chemistry and hydrogen bonds. Reprinted with permission from Ref. [128] Copyright 2016 Elsevier Ltd.

In 2017, Raquez *et al.* reported one-component DA based polyurethanes in three different compositions.^[129] In tensile tests, the best composition regained a tensile strength of 68% after reconnecting two cut pieces by a thermal treatment (30 min at 130°C and 24 h at 50°C). The authors emphasized that this recovery is superior compared to the majority of reported polymers.

The combination of several reversible principles can create the next generation of more complex self-healing materials. Up to now, all double reversible systems are only for pure matrices, mostly for hydrogels. To the best of my knowledge, none has been described for composites so far.

1.6 Peculiarity of self-healing composites and hybrid materials compared to self-healing polymers

Hybrid materials and nanocomposites are material classes, which commonly consist of an inorganic and an organic compound. In hybrid materials both components are blended on a molecular scale.^[130] In nanocomposites at least one of the components has at least one dimension of the order of nanometers,^[131] more particular in a size range of 1-100 nm.^[130] Both material classes exhibit properties, which are not achievable with conventional materials (Figure 18). For example, lightweight can be combined with high mechanical strength, as it is realized in carbon fiber reinforced plastics. In insulating polymers, electrical conductivity can be implemented by adding an appropriate filler.

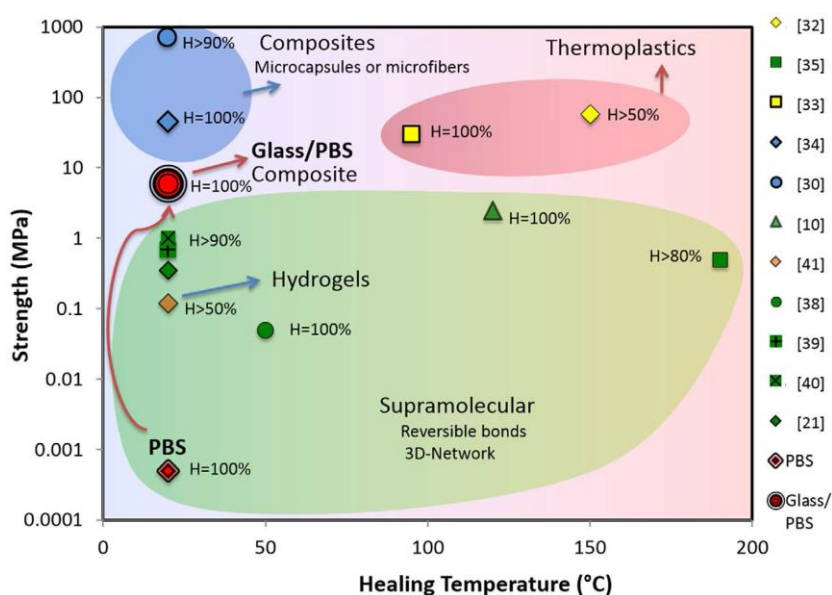


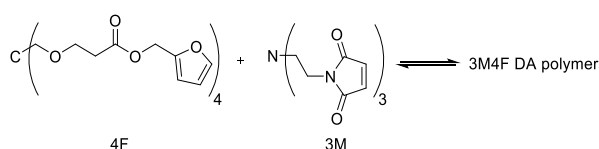
Figure 18: Strength vs. healing temperature for self-healing materials. Reprinted with permission from Ref. [132]. Copyright 2016, Macmillan Publishers Limited.

Self-healing polymer nanocomposite materials in general have been reviewed by Kessler *et al.*^[16] Recently, Arslan and Tasdelen reviewed polymer nanocomposites based on click chemistry reactions.^[133] Herein, the ones based on DA chemistry are summarized in two categories: DA composites with physically incorporated filler - DA groups solely in the matrix (Chapter 1.6.1) and DA composites with DA groups on the filler-matrix interface (Chapter 1.6.2).

1.6.1 DA composites with physically incorporated filler - DA groups solely in the matrix

The following examples for DA based composite materials comprise the ones, in which the healing event is caused solely in the matrix. Both diene and dienophile are located in the organic matrix, which surrounds fibers or coils of various materials, such as copper coils,^[134, 135] carbon fibers,^[136, 137] or glass fibers.^[138] Until now, it is not possible to heal the reinforcement itself.

Nemat-Nasser *et al.* incorporated straight and coiled copper wires in a DA healable polymer matrix reinforced with various fibers, which makes the material electrically conductive.^[134] The matrix is a DA polymer a polymer consisting of three maleimide and four furan groups per polymer (3M4F), composed of a trismaleimide crosslinking molecule (3M) and a tetra furan propionic acid crosslinking molecule (4F) (Scheme 9).



Wudl *et al.* 2002

Scheme 9: 3M4F developed by Wudl *et al.*[37, 88]

Originally, this matrix system was investigated by Wudl *et al.*^[37, 88] and behaves partly like a thermoplastic, because of the thermoreversible bonds and partly like a thermoset, because of the high crosslinking density. E-glass fibers impregnated with epoxy resin, Spectra (Honeywell UHMW polyethylene) fibers impregnated with vinyl ester resin or quartz fibers impregnated with cyanate ester resin, were used for the reinforcement of the material. The authors declare that all components contribute to the self-healing performance: the matrix with thermoreversible covalent bonds, the compression of the material by reinforcing fibers and the electrical and thermal conductivity of the copper wires. However, no self-healing tests were conducted, as the authors focus on the preparation of this three-component material. Similarly, Hahn *et al.* incorporated carbon fibers within a mixture of tetrafulan – bismaleimides, in which healing after delamination was carried out by electrical resistive heating.^[136] Again, the DA polymer, composed of a bismaleimide crosslinking molecule (2M) and tetrafulan propionic acid crosslinking molecule (4F) (2M4F) was investigated by Wudl *et al.*^[88] The corresponding monomers are depicted in Figure 19.

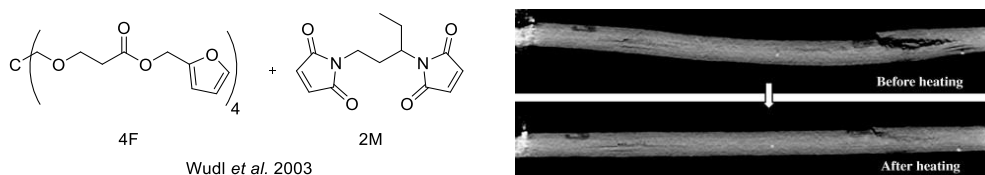


Figure 19: Left: Chemical structures of monomers to make 2M4F. Right: X-ray tomography of carbon fibers in damaged and healed composite. Reprinted with permission from Ref. [136]. Copyright 2010 Elsevier Ltd.

The damage in the material was caused by a three-point flexural test. Within this test, Hahn *et al.* tried not to break the carbon fibers, because the healing process is limited to the matrix. Electrical resistive heating with 1.2 A via silver coated carbon fiber was used to initiate the healing process. Temperatures of 100-110°C were caused in the middle of the specimen for various healing times (1, 2, 3 h), followed by cooling to room temperature. However, the authors mentioned, that although the damage of fibers visually almost disappeared, which was studied by X-ray tomography (Figure 19, right), the strength of composite could not be recovered once the fibers were broken. An average healing efficiency of 86%, measured by strain energy, was determined after 3 h of resistive heating.

Ghezzi *et al.* also investigated carbon fiber reinforced polymer (CFRP) laminates,^[137] using a same polymer matrix like Hahn *et al.* The thermo-mechanical properties of pure 2M4F, and the CFRPs were investigated and concluded and it turns out that the CFRPs have T_g 's around or above the pure polymer. Since the materials have a drop in stiffness around the T_g , the authors mentioned that it would be advantageous to adapt the healing temperature, so that a decrease in the material's performance during healing can be prevented. However, no healing experiments were shown for this system.

Palmese *et al.*^[138] developed a glass fiber reinforced epoxy-amine thermoset (Figure 20, left). The polymer is composed of three components. Phenyl glycidyl ether and furfuryl glycidyl ether are polymerized by the addition of 4,4'-methylene biscyclohexanamine. The furan bearing polymer matrix is capable to be crosslinked via a BMI-DMF (BMI = 1,1'-(methylenedi-

4,1-phenylene)bismaleimide; DMF = *N,N*-dimethylformamide) healing solution under slight pressure.

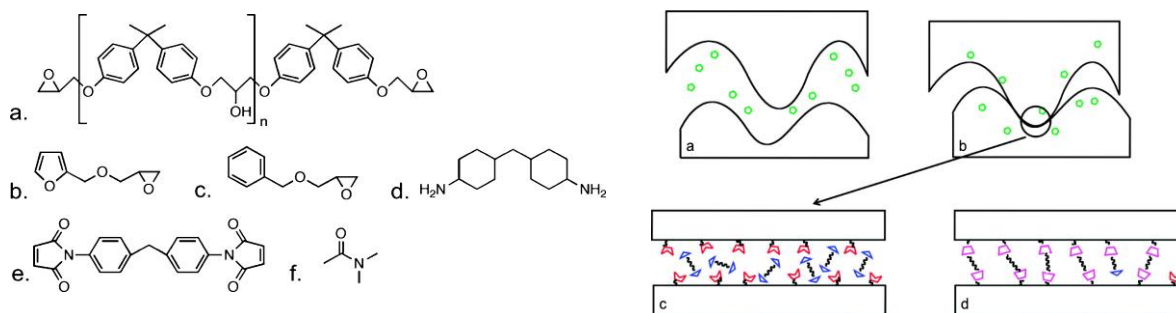


Figure 20: Left: Components for the synthesis of the epoxy-amine thermoset. Right: Proposed healing mechanism – first swelling by DMF, second covalent crosslinking by bismaleimide with furan bearing polymer. Reprinted with permission from Ref. [138]. Copyright (2010) American Chemical Society.

The schematic healing process is shown in Figure 20 on the right. Healing is caused by injection of the curing agent, which causes swelling of the polymer and thus the bismaleimide can contact the crack surfaces and react to the DA adduct. In double cantilever beam testing, mainly the resin-fiber interface failed, but the healing ability of the matrix led to 67% of recovered interfacial strength.

1.6.2 DA composites with DA groups on the filler-matrix interface

In the following, examples for DA based composite materials, the filler-matrix interface is the location where reversible crosslinking takes place. The diene or dienophile is attached to the inorganic surface, and the corresponding DA unit is located in the organic matrix, which surrounds the organically modified particles, fibers or nanosheets of various materials, such as glass fibers,^[139] or graphene oxide nanosheets^[140] or $\text{CaCu}_3\text{Ti}_4\text{O}_{12}$ nanoparticles.^[141] Until now, also in this approach, it is not possible to heal the reinforcement itself.

Based on DA chemistry, a glass fiber reinforced composite was synthesized by Palmese *et al.* (Figure 21).^[139] Maleimide surface-functionalized fibers were incorporated in a furan-modified epoxy-amine thermosetting material. The fibers were modified by attachment of (3-aminopropyl)triethoxysilane (APTES) on the surface, followed by a post-modification in a Michael addition of BMI (Scheme 10). Furan-functionalized polymers were prepared by adjusting the weight ratio of bisphenol A diglycidyl ether to furfuryl glycidyl ether and mixing these epoxy monomers with a stoichiometric quantity of the amine curing agent 4,4'-methylene biscyclohexylamine. Most tests were carried out in a 6:4 weight ratio of bisphenol A diglycidyl ether to furfuryl glycidyl ether. The reversible covalent bonding at the network-reinforcement interface led to 41% healing efficiency.

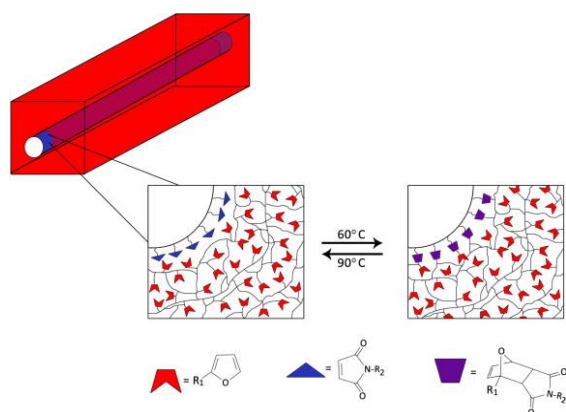
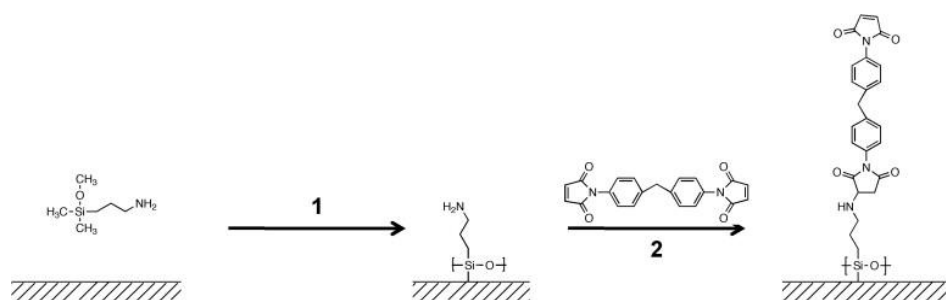
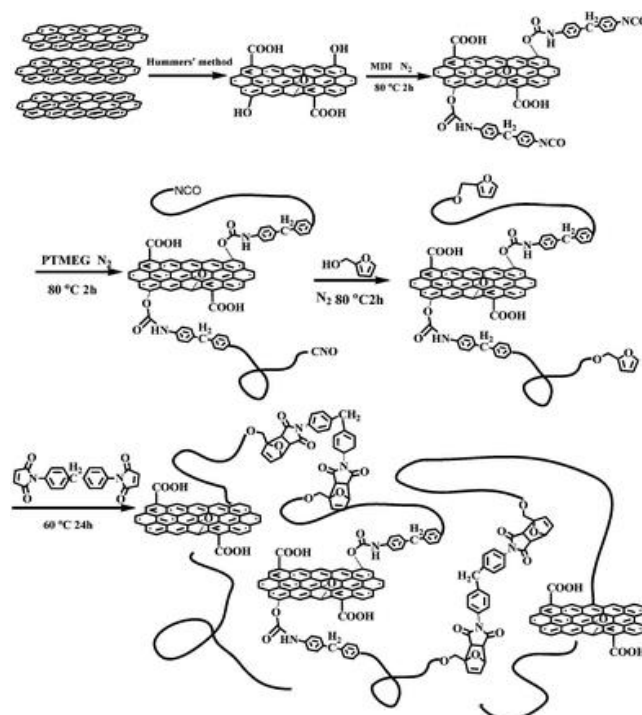


Figure 21: Schematic representation of the DA interface healing concept on glass fibers. Reprinted with permission from Ref. [139]. Copyright 2010 Elsevier Ltd.



Scheme 10: Modification of glass fibers by attachment of APTES followed by a Michael Addition of BMI. Reprinted with permission from Ref. [139]. Copyright 2010 Elsevier Ltd.

Wong *et al.* crosslinked furan-polyurethane modified graphene oxide sheets with BMI (Scheme 11).^[140] The polyurethane (PU) prepolymer was synthesized from graphene oxide, 4,4-diphenylmethane diisocyanate and poly(tetramethylene glycol) and terminated with furfuryl alcohol. The organic modification of graphene oxide sheets led to a homogenous distribution of the filler and a reinforcement of the material. The material's performance was tested in a scratch-healing test analyzed by atomic force microscope. After thermal treatment at 150°C for 4 h and 65°C for 24 h, a healing efficiency of 78% in average was obtained.



Scheme 11: Synthesis of furan-polyurethane modified graphene oxide sheets crosslinked by BMI. Reproduced from Ref. [140] with permission from The Royal Society of Chemistry. Copyright The Royal Society of Chemistry 2014.

Moreover, multi-walled carbon nanotubes (MWCNTs) represent a special case of interface connection via DA reaction.^[133] The surface of the carbon nanotube, which is characterized by sp^2 carbon-carbon bonds itself is suitable for the DA reaction, either with electron-deficient dienes (e.g. tetrazine)^[142] or with the electron-rich furan.^[143, 144] For example, Raquez *et al.* developed an electrically conductive poly(ester-urethane)-poly(ϵ -caprolactone) having the matrix connected to MWCNTs via DA chemistry and additionally DA crosslinks originating from the furan/maleimide pair within the matrix.^[144] This composite is able to heal macroscale damages by the Joule effect. Changes in local resistivity induce a local increase in temperature (ca. 110°C after 90 s), high enough for the rDA reaction. This increase led to healing within 3 min. In this special case, not the interface was the healing site, but there are also systems, requiring higher temperatures, in which the interface is the healing site.^[133] Usually, these systems require higher temperatures for rDA reaction than the ones based on the furan/maleimide pair.

Chujo *et al.* developed a hybrid material consisting of 20% furan modified polystyrene, which was reacted *in situ* with tetraethyl orthosilicate (TEOS) and a maleimidoalkoxysilane.^[145] Under appropriate conditions, a highly solvent resistant, homogeneous material was produced. The authors did not investigate the healing properties, but described a successful cleavage of DA bonds, which was evidenced by the liberation of the furan modified polystyrene by treatment in DMF at 130°C and occurrence of the endothermic signal of rDA in differential scanning calorimetry (DSC) measurements.

Kickelbick and Engel investigated pFMAcoBMA@SiO₂ (FMA = furfuryl methacrylate, BMA = butyl methacrylate) nanoparticles in a surface initiated atom transfer radical copolymerization (ATRP) of butyl and furfuryl(methacrylate) (Figure 22, left).^[146] After embedding these particles in the corresponding pMiMAcoBMA (MiMA = maleimidoalkyl methacrylate) and subsequent

crosslinking of the material, scratch healing tests showed the disappearance of the damage in the μm scale upon thermal treatment (Figure 22, right).

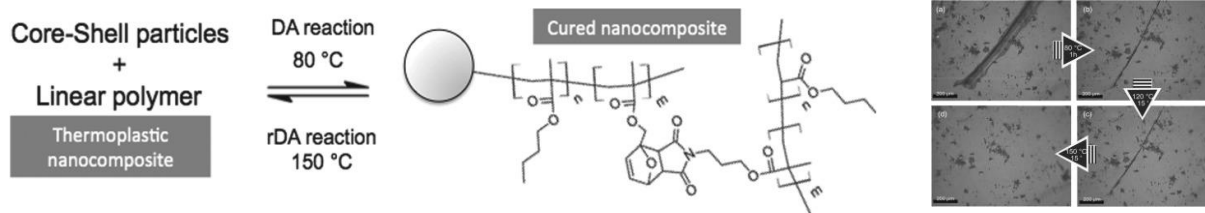


Figure 22: left: Nanocomposite of pFMAcoBMA grafted onto silica nanoparticles, crosslinked by deprotected pMiMAcoBMA; right: Optical microscope images of scratch healing test. Reproduced with permission from Ref. [146]. Copyright 2013 Society of Chemical Industry.

Liu *et al.* described an octamethyl methacrylate modified polymeric octahedral silsesquioxane (POSS), which was either reacted with furfurylamine in a DA reaction with the furan group or in a Michael addition with the amine group to afford a partially thermoreversible network.^[147] Scratched samples were treated at 160°C for 1 h to realize the rDA reaction and at 120°C for 12 h to re-crosslink. Although the material gained higher mobility due to the cleavage of DA adduct, which decreases the damage, due to the high brittleness (40% filler) of the material, no satisfying healing was obtained.

Lin *et al.* developed an octafuranfunctional silsesquioxane crosslinked with commercial BMI (Figure 23), which afforded a tough solid.^[79] Crosslinking proceeds predominantly within the first 4 h, as evidenced by ultraviolet-visible spectroscopy (UV/Vis). In a healing test, cracks disappeared upon treating at rDA temperature (150°C, 30 min), but heavy scratches remained because of material loss in this region and the lack of material transport within the short rDA temperature period. This observation again emphasizes the necessity of a close proximity of damaged edges in the application of intrinsic self-healing, since healing occurs on the molecular level.

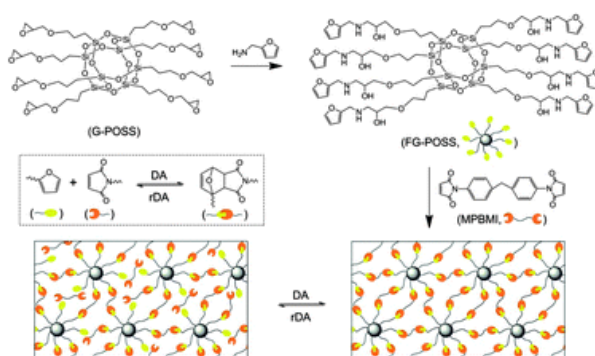


Figure 23: Synthesis of POSS nanocomposites using FuranPOSS crosslinked with BMI. Reproduced from Ref. [79] with permission of The Royal Society of Chemistry. Copyright The Royal Society of Chemistry 2013.

Based on the work of Lin *et al.*^[79], our group incorporated octafuran-functional spherosilicates, synthesized by hydrosilylation of octakis(hydridodimethylsiloxy)silsesquioxane, in BMI or in α,ω -maleimidodimethylsiloxane.^[148] In the first case, a hard glassy solid was obtained, while using the siloxane resulted in an elastomeric material. Both showed a high self-healing potential.

The BMI-containing system was able to heal scratches by treatment at 110°C for 10 min, which was evidenced by transmission light microscopy images. The PDMS containing system could be reshaped within 10 min at 100°C.

Later, Zelisko *et al.* also synthesized a hybrid material composed of octafuran-modified spherosilicate, namely octakis(furan-2-ylmethyl)-functionalized polyhedral oligomeric silsesquioxane, which was crosslinked with maleimidocarboxyphenylpentasiloxane-dimethylsiloxane copolymer.^[98] Two pieces of the cut specimen could be reconnected upon thermal treatment for 2 h at 110°C prior to 5 h at 50°C. Furthermore, the cyclability was evidenced with solid-state ¹H NMR (nuclear magnetic resonance) experiments along with DSC measurements.

Very recently, in June 2018, Singha *et al.* published a self-healing material composed of a polyurethanes, functionalized with furan groups (FPU) on each side of a linear polymer chain and monomaleimidoheptaisobutyl POSS. The components were linked in a DA reaction. Although this material is not actually crosslinked by DA, because the silsesquioxanes are mono-maleimide functional, the material showed scratch healing in μm scale after treatment of the samples at 130°C for 3 h and subsequent heating at 70°C for 15 h. Contrary, pure FPU did not show any healing performance. The amount of monomaleimidoheptaisobutyl POSS has to be sufficient (~ 12-36 mol%) to observe self-healing behavior.

Zhu and Xiong *et al.* developed a recoverable motion sensor using maleimide surface-modified CaCu₃Ti₄O₁₂ nanoparticles. These were embedden in a DA polymer build of the commercially available monomers BMI and 2,2'-(thiodimethylene)difuran (Figure 24).^[141] The surface modification was again realized by the attachment of APTES on the surface with a post-modification of the primary amine group.

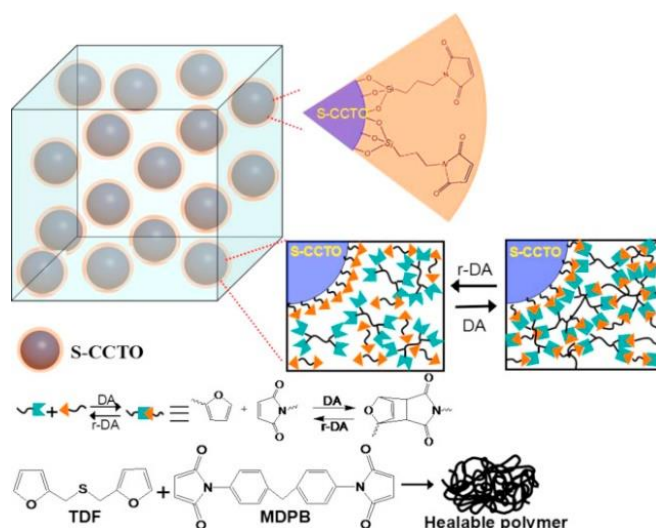


Figure 24: Maleimide functionalized CaCu₃Ti₄O₁₂ nanoparticles in DA polymer matrix. Reprinted with permission from Ref. [141]. Copyright 2015 Elsevier Ltd.

In this material, both, diene and dienophile, are simultaneously located in the matrix, and additionally the dienophile is attached on the inorganic surface. Thus, the healing process is less dependent from the successful crosslinking at the interface. The organic modification on CaCu₃Ti₄O₁₂ probably only assures a homogenous distribution, without having covalent

bonding at the interface. Nevertheless, the authors were able to restore up to 82% capacitance after the ten times cutting the material.

In general, in the field of self-healing materials, fewer studies have been conducted for nanocomposites and hybrid materials than on pure polymers. The incorporation of a filler makes the systems more complicated and is contradictory to the requirements for efficient self-healing. Fillers reduce the chain mobility, which is essential for healing. The increased T_g lowers the mobility of the functional groups, and moreover, the perfect miscibility has to be guaranteed between matrix and filler to ensure a homogenous distribution. The filler itself should not be damaged during crack formation or should be able to heal under the same conditions as the matrix. Fillers can be classified in the particle- and the fiber-type. Healing of fiber-reinforced composites is difficult since irreversible fiber breakage or fiber-matrix debond can occur. While fibers are often brittle and can easily break, particles are not affected by mechanical stress. Moreover, nanoparticles were found to diffuse to damaged interfaces.^[149, 150, 151, 152] In case of extrinsic healing systems, when nanospheres filled with a healing agent are incorporated, this can be advantageous because the healing agent would be directly transported to the crack. Contrary, in intrinsic systems this phenomenon can be undesired because it leads to an inhomogeneous distribution of the filler and consequently to inhomogeneous material properties. These considerations point out the complexity of the design of self-healing nanocomposites and hybrid materials. Nevertheless, using the technique of material combinations is highly promising, because it supports the economic and ecological idea of artificial self-healing materials. Less bulk material is needed to synthesize better or at least identical good materials compared to traditional materials and lower energy consumptions can be realized in the transportation sector because of the lightweight of these materials.

The field of self-healing nanocomposites based on intrinsic mechanisms or in particular on DA chemistry are way less investigated than the ones based on extrinsic healing mechanisms. For DA composites, or hybrid materials, different strategies can be followed. The DA groups can be located only in the matrix or on the filler-matrix interfaces. Adhesion of the reinforcement to the polymer matrix is essential for load transfer from the polymer matrix to the reinforcement material in fiber-reinforced composites. In hybrid materials, compared to nanocomposites, the sizes of filler and polymer chains are more similar, so that they provide a higher degree of crosslinking per inorganic content. Therefore, the strategy and thus the resulting materials always have to be adjusted to the specific demand given. Numerous inorganic fillers are possible, which allow incorporating additional functionality like magnetism, or conductivity. The fillers have to be tuned on their surface for a perfect interface match. Therefore, the fillers applied in the present work and their surface functionalization will be discussed in the following chapter (1.8) as well as possible organic matrices (1.9).

1.7 Analytical methods for the determination of reversibility and self-healing behavior

Plenty of common scientific measurement methods are suitable to follow the healing processes.

The observation of the reversibility of the DA healing reaction on a molecular scale can be realized using spectroscopic methods, such as NMR,^[79, 148] Fourier-transform infrared spectroscopy (FTIR),^[144] UV/Vis.^[79, 146] For example, in ¹H NMR, the peaks of unreacted furan and maleimide can be distinguished from the DA adduct.^[79, 148] By integration of these signals and measurements over time, reaction kinetics can be followed in solution. Although this method is a useful tool for the comparison of different model systems, it should be considered, that processes in bulk require more time, due to the limited mobility of the reacting species. Solid state NMR of either ¹³C^[37, 88] or the ¹H^[98] nucleus can help to overcome this disadvantage, but the recording of numerous measurements require a lot of time, since one measurement takes several hours. Accordingly, this method is better suited for a comparison of crosslinked and non-crosslinked state, but less for the investigation of a kinetic.

Contrary, attenuated total reflection (ATR-) FTIR and UV/Vis are very fast methods (one measurement is in the range of seconds) and can be measured on thin films of polymers, nanocomposites or hybrid materials.^[97] Following specific absorption bands over time, e.g. the maleimide ring deformation band around 695 cm⁻¹ or the H-C= band at 830 cm⁻¹ in IR^[144] and the absorption of maleimide around 300 nm in UV/Vis^[79, 146] reaction kinetics can be easily obtained.

Thermal analysis, especially DSC is a very useful tool to follow the endothermic rDA reaction within a bulk material.^[37, 79, 88, 97, 153] Depending on the DA pair, the signal can be found in the concerning temperature ranges. For the furan/maleimide adduct, the signal is visible in the range of 100 and 200°C, depending on the heating rate. Because the DA reaction is rather slow, usually this process cannot be observed. Also, the T_g is a valuable indicator because in a crosslinked material, the T_g should be significantly increased compared to the virgin material. Dynamic Mechanical Analysis (DMA)^[88, 100] and rheology^[144, 146] measurements also provide access to bulk properties. Storage Modulus (G'), Loss Modulus (G'') and T_g indicate the inherent structure properties in dependence of the temperature. When crosslinking takes place, an increase in G' is observed.^[144, 146] A repeatable intersection of G' and G'' indicates the reversible crosslinking by the DA reaction. In a crosslinked system, G' is higher than G'' and in an uncrosslinked system, the roles are exchanged. This observation results from the change of a solid-like behavior, when G' is higher than G'' and the fluid-like behavior when G'' is higher than G'. All methods mentioned so far can prove the reversibility of the DA reaction by doing the experiments in temperature cycles, or by reversion of the DA reaction, e.g. in an oven and perform the measurement cycle again.

Different imaging procedures, such as optical^[79, 146], atomic force^[153] or scanning electron^[37, 153] microscope images are commonly used to observe the actual healing process itself on a

fracture site. These tests are a valuable supplement, because the observation of the reversibility of a reaction does not automatically imply the ability to heal. In intrinsic healing systems, a contact in the nanometer or molecular scale of fracture surfaces is indispensable to observe healing. The condition is not always realized satisfactory, although the reversibility is given, e.g. when materials are too brittle or the material cannot flow upon heating.

Mechanical tests are the ones, which are important when mechanical properties shall be regained. Depending on the nature of the material, the fracture test, fatigue test or tear test can be made.^[14] The fracture strength of initial and healed material can be compared, which gives information on the healing efficiency (Chapter 1.2). Since the presented work focusses on the chemical aspects of healing and targets the deeper understanding on a molecular scale in self-healing nanocomposites, the mechanical methods will not be discussed in detail herein. The interested reader is referred to Reference 14. If properties different from mechanical ones, such as conductivity shall be regained the tests have always to be matched on the specific question given.

1.8 Inorganic filler and their surface adjustment for the incorporation into organic matrices

This chapter provides a brief introduction to the field of organically modified nanoparticles. The field of “nano-research” emerged in the last 30-40 years and is fast growing further.^[154] Numerous different materials such as metals, metal oxides, silica and carbon have been investigated in manifold nanostructural shapes. Compared to bulk material, an enormous surface to volume ratio and high surface areas per gram material are reached (Figure 25).

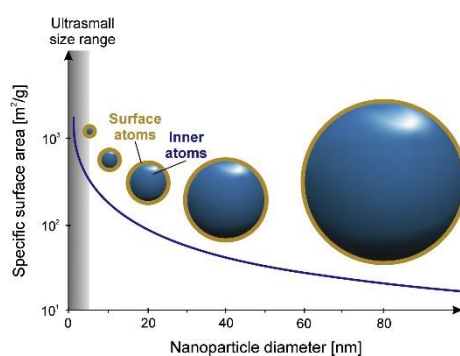
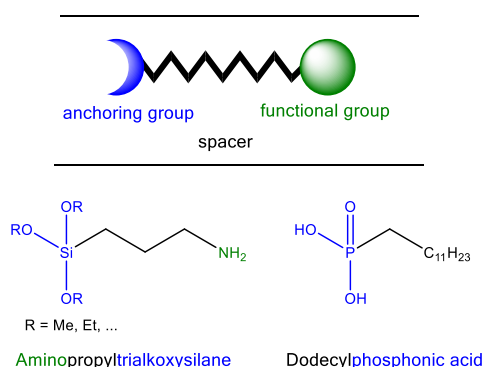


Figure 25: Surface to volume ratio of nanoparticles. Reprinted with permission from Ref. [155]. Copyright 2016 Elsevier Inc.

The energy of surface atoms is higher than the one in the inner material, because of the unfavorable thermodynamic state. In order to minimize surface tension, non-stabilized particles tend to aggregate. Because of these differences compared to bulk material novel properties are observed. The applications range from catalysis, medicine and sensing to energy storage and information technology. The most important point to obtain non-aggregated particles within colloidal dispersions or organic matrices is to focus on the

surface of inorganic nanoparticles. So called coupling agents provide the possibility to stabilize inorganic fillers and incorporate them into organic matrices.^[156]



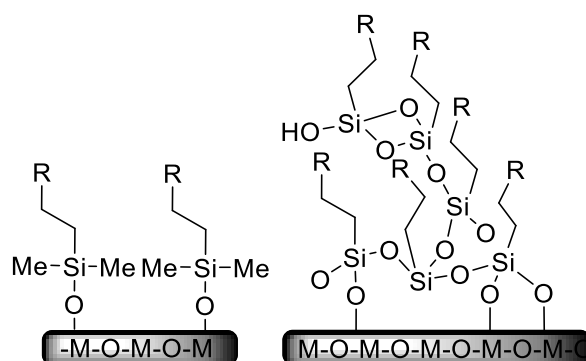
Scheme 12: General structure of coupling agents with selected examples.

Coupling agents consist of an anchor function, a spacer and eventually a functional group (Scheme 12). They are used to create a suitable transition from an inorganic filler, such as nanoparticles, to an organic matrix. For example, this can be realized by elements, forming stable X-C bonds on the one hand and stable X-O bonds on the other hand. For example, X can be silicon or phosphorus. Alkoxysilanes or phosphonic acids as anchoring groups realize this demand (Scheme 12). The synthesis of complex coupling agents can be challenging because the functional group and anchoring group has to tolerate each other. Also, the group that is introduced in the molecule first has to tolerate the reaction conditions necessary to build up the other group. The nanoparticles itself are most often synthesized in a wet chemical bottom-up approach, but also gas-phase or top-down methods are represented among others.

1.8.1 Silica nanoparticles and silane coupling agents

Silica nanoparticles are often synthesized in a bottom-up approach from TEOS, in the so-called Stöber-process.^[157] This reaction belongs to the field of sol-gel chemistry, which is characterized by the hydrolysis and condensation of alkoxy group bearing monomers (precursors) to colloidal solution (sol) or an integrated network (gel) consisting of either discrete particles or three dimensional polymers.^[158] The reaction times can be influenced by the choice of leaving group. For example, chlorosilanes and methoxysilanes provide shorter reaction times than the corresponding ethoxysilanes.

Surfaces of SiO₂ nanoparticles are commonly modified applying organoalkoxysilanes or chlorosilanes.^[156] Both are capable to form stable Si-O-Si bonds. While mono alkoxysilanes and chlorosilanes can form only monolayers, di- or trifunctional alkoxysilanes are able to undergo homocondensation or form networks and thus they are able to build multilayers (Scheme 13).^[156]



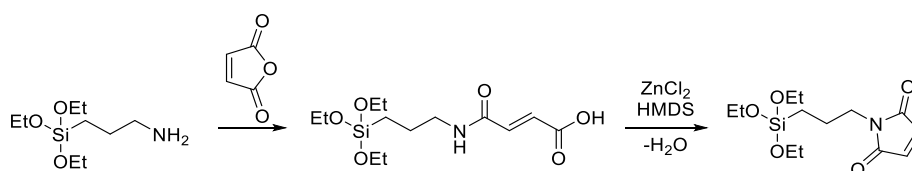
Scheme 13: Binding modes of monoalkoxy (left) and trialkoxysilane (right) to metal oxide. Formation of monolayer vs. multilayer according to reference [156].

Therefore, the surface modification using di- or tri alkoxy silanes has drawbacks in terms of reproducibility and hydrolytic stability.^[156] Nevertheless, silane coupling agents are intensively used to tailor various substrate surfaces to modify the polarity, bind ligands for catalysts or create chemically reactive surfaces.^[156]

Since the development of glass fiber reinforced resins around 1940, a huge requirement of coupling agents arose^[159] because these substances were able to overcome the drawback of debonding on the interfaces. A broad variety of silane coupling agents was explored since then and afforded manifold silane coupling agents. The interested reader is referred to reference 159.

The field of DA group bearing alkoxy silane coupling agents provides the additional feature of building up thermoreversible chemical bonds close to the organic/inorganic interface in materials or on surfaces of inorganic nanocontainers. In the first case, scientists are interested in rebonding, if delamination occurs and in the second case, they are interested in terms of drug delivery systems.

However, for the synthesis of maleimidoalkylalkoxysilanes only one general procedure is known (Scheme 14).^[160] Addition of maleic anhydride to the commercially available APTES at room temperature affords the maleamic acid intermediate. This open structure can be cyclized using ZnCl_2 and hexamethyldisilazane (HMDS) as a catalyst at elevated temperatures. This type of catalyst is necessary because of the hydrolytic instability of the alkoxy silane group.^[161]



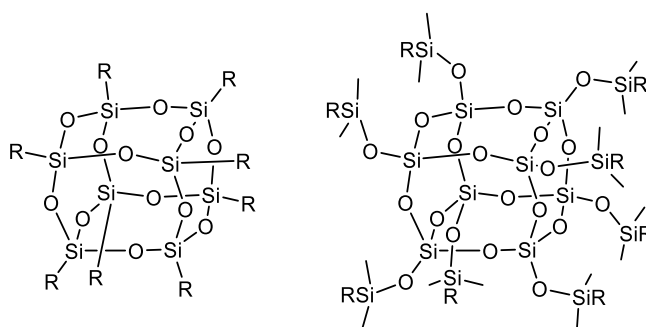
Scheme 14: Synthesis of maleimidopropyltriethoxysilane.

All following reports of the synthesis of this molecule used the same strategy with slight modifications.^[162, 163, 164, 165] Also, other spacer lengths (C4-C17) have been realized using the same method.^[166] Contrary, corresponding furan molecules were not reported in the literature. Another common method to attach DA functional groups on inorganic surfaces is

the usage of a post-modification. For the attachment of maleimide, a Michael Addition of bismaleimides is used.^[139] Therefore APTES is attached to the surface, and the amine group is used for further chemical conversion after the silane group has reacted, and thus the hydrolytic instability does not longer exist. Also, furan was attached in a post-modification beginning from APTES grafted to the silica surface and adding furfural to the amine-bearing surface.^[167] However, one disadvantage of this procedure is, that no precise control of the number of functional groups is possible. The procedure of post-modification will not be further discussed, because it does not actually imply the synthesis of maleimide or furan-silane coupling agents.

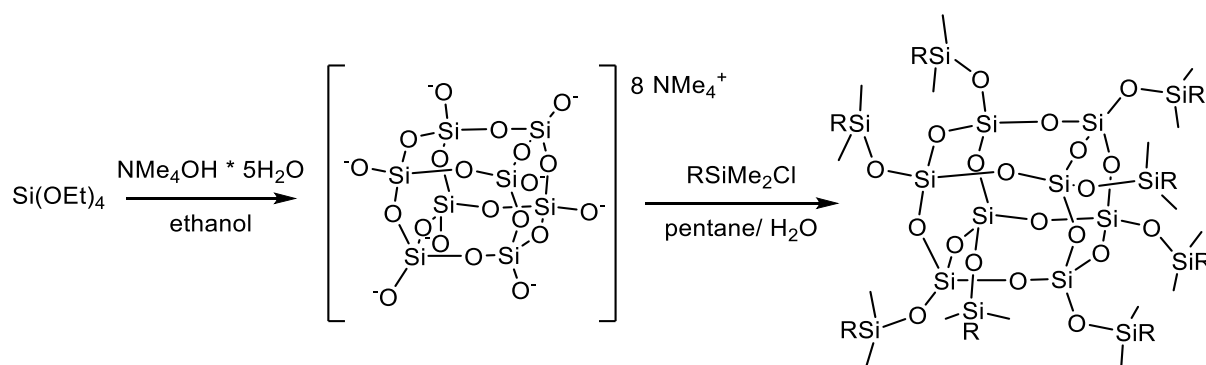
1.8.2 Silsesquioxanes and Spherosilicates

The smallest silica units are POSS^[168, 169] and the related polyhedral oligomeric silicate, also called spherosilicates (POS)^[170] Both are polycyclic oligomers, containing a core with the general formula $(R-SiO_{1.5})_n$ ($n = \text{even number, mostly } 8, 10, 12$). POSS directly bears an organic rest ($R = \text{alkyl, aryl, arylene}$) whereas POS bears $R = OSiMe_2R$ units at the corners.



Scheme 15: Examples for closed cage silsesquioxane (POSS) left and spherosilicate (POS) right.

These cubic molecules consist of a rigid, high symmetrical SiO_2 core have a core size of 0.54 nm for $n = 8$, and generally bear organic rests on each corner.^[170] The synthesis of silsesquioxanes is realized by catalytic homocondensation of organotrialkoxysilanes or hydrolyzed trichlorosilanes, to afford octa- vinyl-,^[171] hydrido-^[172] or methacrylate-^[173] silsesquioxanes to name only a few.^[170] However, these synthesis suffer from drawbacks, such as many byproducts due to incomplete condensed, e.g. ladder like or open cage structures, low yields (below 50%) and long reaction times. Contrary, spherosilicates made from TEOS using a bulky base to selectively form an octaanion can be synthesized in straightforward reactions and in high yields (Scheme 16).^[174, 175] In a nucleophilic substitution reaction, a variety of organic rests can be introduced by the addition of organo chlorosilanes.

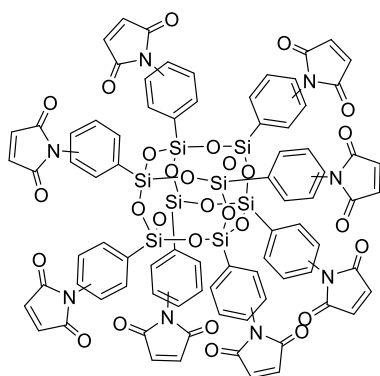


Scheme 16: Modification of spherosilicate octa anion (POS).

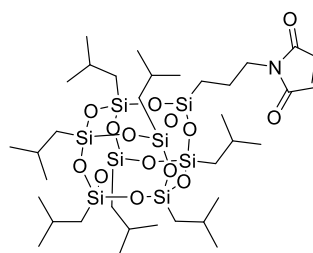
Adjusting the substituents at the corners, this type of nanocages can be incorporated into almost any conventional polymer by covalent attachment or by physical blending. These monodisperse inorganic-organic hybrid particles have the ability to improve material properties, regarding their fire resistance, lightweight, higher temperature use and increase of mechanical stability.^[168, 170]

DA group bearing spherosilicates and silsesquioxanes

DA functional group bearing spherosilicates and silsesquioxanes are rarely reported. Only two silica cubes bearing maleimide are known: octa(maleimido phenyl) silsesquioxane firstly synthesized by Laine *et al.* in 2001^[176] and mono(maleimido)hepta(isobutyl) silsesquioxane synthesized by Hybrid Plastics.^[177] The octa(maleimidophenyl) silsesquioxane was synthesized starting from phenyltrichlorosilane, which is condensed to octa(phenyl)silsesquioxane in water, using benzyltrimethylammonium hydroxide as a catalyst (Scheme 17). Treating this cube in fuming nitric acid led to octa(nitrophenyl) silsesquioxane, which was catalytically reduced using formic acid and triethylamine with Pd/C as catalyst. The octa(aminophenyl)silsesquioxane was treated with eight equivalents maleic acid to afford the intermediate maleamic acid POSS. Cyclization was conducted using acetic anhydride as a solvent and trimethylamine as a catalyst, affording 79% of the desired octa(maleimidophenyl) POSS.



Laine *et al.*

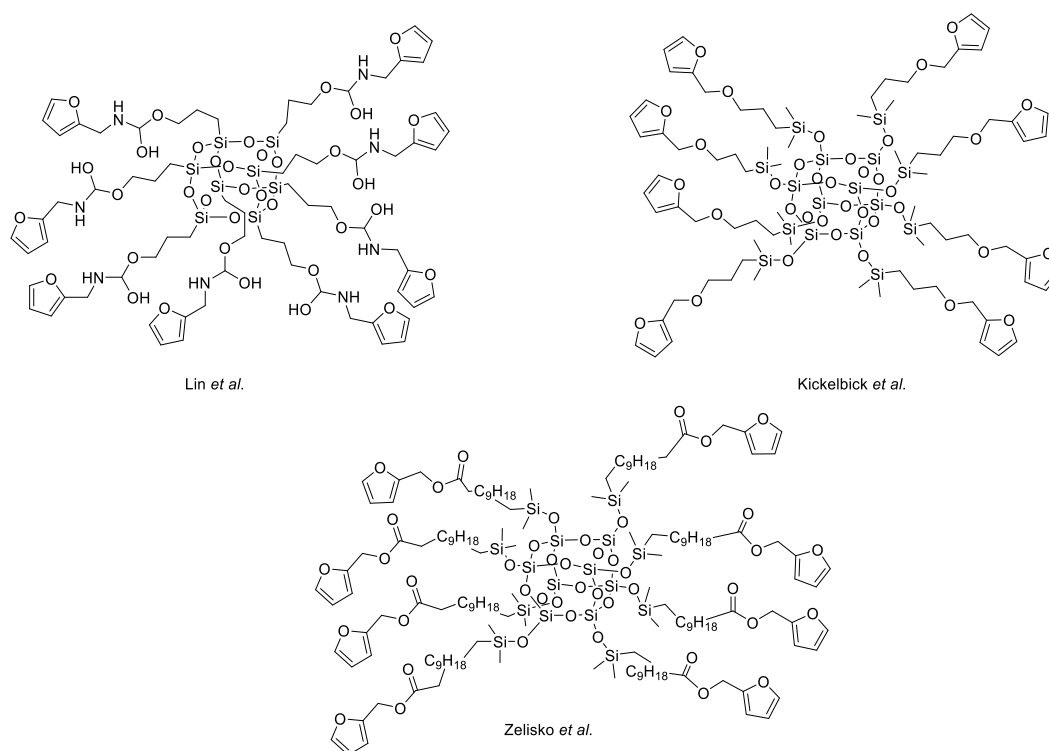


Hybrid Plastics, USA

Scheme 17: Two POSS molecules bearing maleimide moieties are known.[176, 177]

Mono(maleimido)hepta(isobutyl) silsesquioxane, which was synthesized by Hybrid Plastics, should be synthesized in a similar cyclization, starting from an (aminopropylheptaisobutyl) POS. Unfortunately, no information is given for that synthesis.

All of the three furan bearing silsesquioxanes and spherosilicates were already mentioned in chapter 1.6.2. The molecular structures, developed by Lin *et al.*, Kickelbick *et al.* and Zelisko *et al.* are depicted in Scheme 18.



Scheme 18: Three cubic molecules bearing furan moieties are known.[79, 98, 148]

Lin *et al.* used a commercially available octa(glycidyl) POSS and added a slight excess furfurylamine.^[79] After reacting the mixture 22 h at 60°C in DMF, the desired product was obtained (yield not given). Kickelbick *et al.* and Zelisko *et al.* used hydrosilylation reactions to afford the desired octafuran functional cubes.^[98, 148] The first mentioned group used octakis(hydridodimethylsiloxy)octasilsesquioxane and added 2-[(prop-2-en-1-yloxy)methyl] furan using platinum divinyltetramethyldisiloxane (Karstedt catalyst) in toluene. After stirring at 60°C for three days, the desired product was obtained in quantitative yield. Similarly, Zelisko *et al.* used octakis(dimethylsiloxy)-silsesquioxane and added furan-2-ylmethyl undec-10-enoate. The reaction mixture was refluxed in pentane, using the Karstedt catalyst. The desired product was obtained in 71% yield after work-up.

Hydrogen bond motif bearing spherosilicates and silsesquioxanes

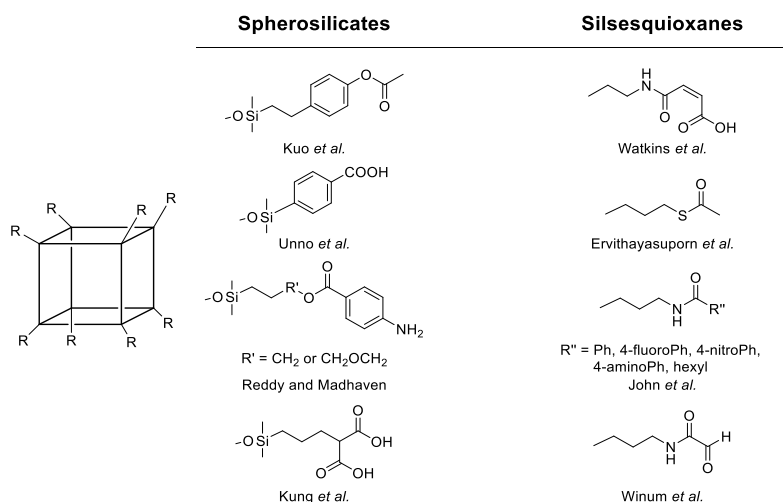
Several examples of spherosilicates and silsesquioxanes which are able to form hydrogen bonds have been reported. Only a few of them have been synthesized explicitly for the use in

hydrogen derived self-healing hybrid materials. Nevertheless, cubes bearing interesting motifs for this purpose are summarized in the following and depicted in Scheme 19.

In 2006 Kuo *et al.* synthesized octakis(acetostyrenedimethylsiloxy)octasilsesquioxane in a hydrosilylation reaction of octakis(hydridodimethylsiloxy)octasilsesquioxane and acetoxystyrene applying Karstedt's catalyst and received 93% yield.^[178] The product was incorporated in a phenolic resin. Hydrogen bonding between the phenolic O-H and the carbonyl group and siloxane groups of octakis(acetostyrenedimethylsiloxy)-octasilsesquioxane were shown by FTIR.

Unno *et al.* reported in 2008 the synthesis of octa(carboxyphenyl) spherosilicate.^[179] Starting from TEOS, an octaspherosilicate anion, coordinated by NMe_4^+ as counterion was converted with chloro(dimethyl)tolyl silane to afford octakis(dimethyl-(*p*-methylphenyl)silyl)silicate. This cube was brominated by *N*-bromosuccinimide to produce octakis(dimethyl(4-tribromomethylphenyl)-silyl)silicate in 85% yield. After hydrolyzation under treatment with AgNO_3 and formic acid afforded octa(carboxyphenyl) spherosilicate was achieved in 90% yield.

Reddy and Madhavan synthesized ester-amine-functionalized silsesquioxane starting from octakis(hydridodimethylsiloxy)octasilsesquioxane and performing hydrosilylation applying Karstedt's catalyst with either allyl 4-aminobenzoate or allyl(oxy)ethyl 4-aminobenzoate. They obtained 75 and 70% yield respectively.^[180] These cubes were incorporated in PU prepolymers. Although the cubes are not highly dispersive, hydrogen bonding in the hybrid films was observed.



Scheme 19: Cubes bearing interesting motifs for hydrogen bonding.

The group of Watkins built silsesquioxanes bearing maleamic acid or aminophenyl groups on all eight corners which are able to form hydrogen bonding with the poly(ethylene oxide).^[181] The aminophenyl cube was described before by Laine *et al.*^[176] No information on the preparation of the cubes of Watkins *et al.* can be given, as they were purchased by Hybrid Plastics. However, it can be assumed that the synthesis proceeds as previously mentioned for the octa(maleimidophenyl)silsesquioxane. Therefore, octa(nitrophenyl)silsesquioxane is catalytically reduced to octa(aminophenyl)silsesquioxane which can be treated with maleic

acid to afford the octa(maleamic acid)silsesquioxane. The maleamic acid unit, having two acceptors and two donor units, enabled to incorporate 80% silsesquioxane within poly(ethylene oxide). The amino unit, having only one donor site, the incorporation was limited to 40%.

Erwithayasuporn *et al.* synthesized an octafunctionalized thioacetate POSS derivative.^[182] Octakis(3-chloropropyl)octasilsesquioxane, which was synthesized as previously reported by co-condensation of 3-chloropropyltrimethoxysilane,^[183] was converted with a slight excess potassium thioacetate within 16 h at room temperature in DMF. The desired product was obtained as a colorless solid in 83% yield, and the authors were able to recrystallize the substance to perform single-crystal X-ray diffraction. The authors focused on the preparation and no experiments on incorporating this cube in materials is given.

Kung and coworkers synthesized a spherosilicate bearing eight malonic acid groups in one or two reaction steps respectively.^[184] Octakis(hydridodimethylsiloxy)octasilsesquioxane was reacted by hydrosilylation using Karstedt's catalyst with dibenzyl allylmalonate and gave 87% yield. The benzyl ester bonds were cleaved by treatment with H₂ under catalytic reduction over Pd/C after stirring for 7 h at ambient temperature and a yield of 97% was obtained. Treating this product with trivinylchlorosilane and diethylamine afforded the octa(allyl silyl ester) cube, which can be easily hydrolyzed in 85% yield. Moreover, octa(allyl silyl ester) cube can react intramolecularly by hydrosilylation or the arms can be crosslinked by treatment with 1,4-bis-dimethylsilylbenzene to afford core-shell nanospheres. The authors emphasize that the polyacids can be donor and acceptor in hydrogen bonding which can be interesting for crystal engineering or the use as building blocks for supramolecular structures.

John *et al.* described five octa(amido) group bearing POSSs, which were prepared by treatment of octa(aminopropyl) POSS-based salts (octaammonium salts, counterions: Cl⁻, CF₃SO₃⁻, CF₃COO⁻ with 45, 95 and 90% yield respectively) with 1.1 equivalents of acid chloride (benzoyl chloride and its 4-nitro- and 4-fluoro-derivatives as well as hexanoyl chloride) in DMF at 0°C and afforded yields around 95%.^[185] The 4-aminobenzoyloamide-POSS was obtained using zinc dust and concentrated hydrochloric acid for the reduction of 4-nitrobenzoyloamide POSS.

In 2017 Winum *et al.* reported the preparation of stable glyoxylic aldehyde bearing octa functional silsesquioxane, which can be obtained in multigram scale in three reaction steps in 83% yield.^[186] This cube can readily react with oxyamines or hydrazides to form oximes or acylhydrazones. Octa(glyoxylic aldehyde)silsesquioxane was synthesized starting from commercially available octa(3-aminopropyl)silsesquioxane hydrochloride in a peptide coupling reaction with protected serine Boc-L-Ser(OtBu)OH. Treating this compound with TFA cleaved the *tert*-butyloxycarbonyl protecting groups. Oxidative cleavage of intermediate amino alcohol using NaIO₄ (8.8 equiv.) gave the pure product in 94% yield by dialysis. As the authors are interested in bioconjugates, they did not discuss the hydrogen bonding aspects of this molecule.

The most of the synthesized cubes contain aryl units, which makes the organic arms attached to the silica core less flexible. Even more interesting for material development are those cubes, having flexible alkyl arms attached to the core. However, the cubes having alkyl arms

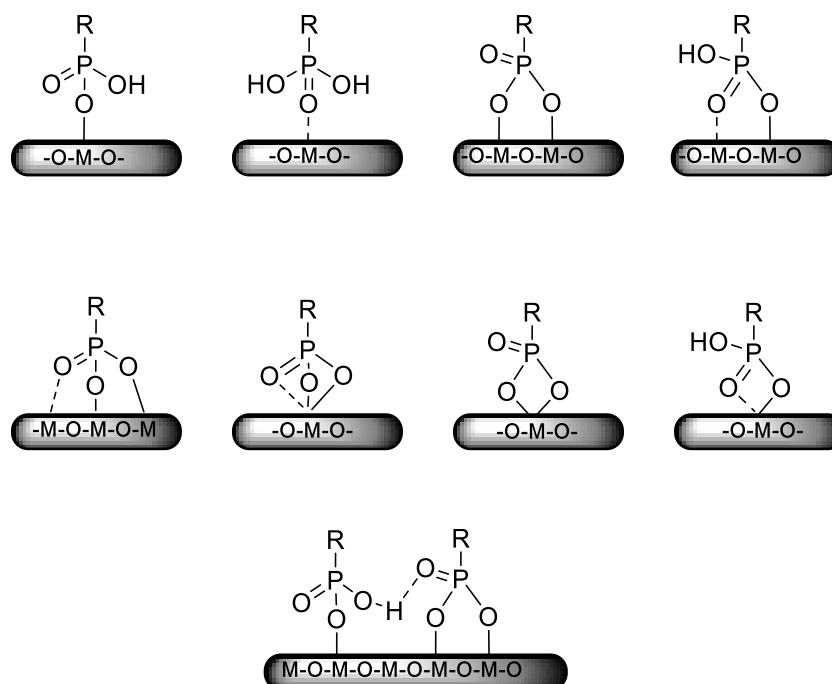
are limited to propyl chains. Longer chains would be interesting because they provide more flexible arms, more space and greater distribution of functional groups. Although, the urea motif would be a strong hydrogen bonding unit having two donors (N-H) and one acceptor (C=O), no cube bearing this functional group has been described so far.

1.8.3 Metal oxides and phosphonic acid and acid ester coupling agents

Another important type of nanoparticles are metal oxides.^[154, 187] They provide access to tailor manifold material properties, such as conductivity,^[188] antibacterial and cytotoxic,^[189] catalytic activity^[188] or magnetism.^[190] Various methods were developed to synthesize metal oxide nanoparticles like ZrO₂, HfO₂, TiO₂, ZnO, Al₂O₃ and Fe_xO_y. Manifold processes, reaching from chemical vapor deposition to milling processes, wet chemical processes, autoclave reactions amongst others, have been developed in the rather young field of nanoparticle research.^[187, 189, 191]

For example, magnetite (Fe₃O₄) can be produced in a precipitation from FeCl₂ and FeCl₃ by the addition of NaOH as a base at room temperature.^[192] High yields are obtained using this protocol, but careful adjustment of pH value is difficult and inhomogeneous sizes and shapes were reported. Also, these particles do not bear any stabilizer on their surface, hence they tend to aggregate. Sun *et al.* developed a thermal decomposition procedure of Fe(acac)₃ under the presense of stabilizing oleic acid, 1,2-hexadecanediol and oleylamine and received highly monodisperse iron oxide.^[190] Due to control experiments, the authors assumed that there should be a mix of oleic acid and amine on the particle surface. However, Klokkenberg *et al.* reported later, that oleic acid has a greater affinity to the iron oxide surface and the amine facilitates the bonding because of deprotonation of the carboxylic acid.^[193] This result agrees with the hard-soft acid–base principle. While the softer Fe²⁺ ion coordinates nitrogen and oxygen, the harder Fe³⁺ ion has a higher affinity to oxygen.^[194] Several methods reported, that superparamagnetic iron oxide nanoparticles have a magnetite core (Fe²⁺, Fe³⁺) and a maghemite shell (only Fe³⁺) at the surface.^[195, 196]

To organically modify iron oxide nanoparticles, several coupling agents, such as carboxylic acids, amines, catechols, phosphonic acids and silanes are possible. While carboxylates and amines bind primarily by coordinative and ionic interactions,^[197, 198] catecholates build a covalent bond with contributions of σ - and π -donor bonding^[194] and phosphonic acids or silanes are able to form more stable covalent bonds. Different substitution patterns in catechol derived anchoring groups can change the electronic situation that much in Fe^{2+/3+} that much, that a subsequent particle degradation can occur.^[194] Phosphonic acids are superior over silanes because they were found to be fast reacting under mild conditions and form stable M-O-P bonds, serving as a protective layer against oxidation.^[156, 199, 200] Only monolayers are formed because phosphonic acids and acid esters do not have the tendency to react intermolecularly and thus they have no ability to form networks, as it is the case for silanes.^[199] Scheme 20 shows the different possible binding modes according to reference 156.



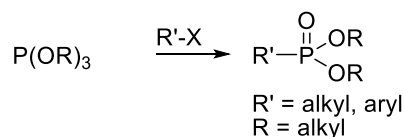
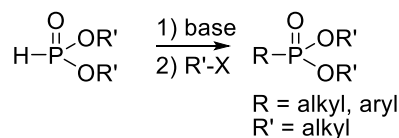
Scheme 20: Possible binding modes of phosphonate to metal oxide according to reference 156.

Mono-, bi- and tridentate binding, bridging and non-bridging binding modes to only one or to several metal atoms can occur. The P=O double bond can either coordinate to the surface or to a residual O-H group of a neighboring coupling agent via hydrogen bonds.^[201]

This class of coupling agents is of particular interest in the field of nanoparticle research, because the monolayers form quickly, are hydrolytically stable, the surface reactions can even be conducted in water (at least when the substrate tolerates it) and the M-O-P layer protects the substrate underneath.

Mefford *et al.* tested coupling agents concerning their exchange reaction against ¹⁴C radiolabeled carboxylic acid.^[202] The ¹⁴C radiolabeled carboxylic acid was bound on iron oxide nanoparticles and coupling agents, containing carboxylic acid, catechol, phosphonic acid or amine, were offered to the system for an exchange. Mefford *et al.* determined a binding hierarchy, in which catechol and phosphonic acids are superior over amine and carboxylic acid. All of the tested substances react readily with the iron oxide surface under ambient temperature.

Several techniques for the generation of P-C bonds were developed, but the Michaelis-Arbuzov and the Michaelis-Becker reaction are by far the most versatile and cheapest ones (Scheme 21).^[200, 203] In the Michaelis-Arbuzov reaction, a trialkyl phosphite is reacted with an organo halogenides and in the Michaelis-Becker reaction a dialkyl phosphites are reacted with a base to form the dialkyl phosphite salt, followed by the subsequent addition of an organo halogenide. In both cases, organo phosphonic acid esters are obtained.

Michaelis-Arbuzov Reaction**Michaelis-Becker Reaction**

Scheme 21: Two most common procedures to form P-C bonds: the Michaelis-Arbuzov and the Michaelis-Becker reaction.

The P-O-C bonds can be cleaved using either acid or base or by reaction with a halogen substituted trimethylsilane, followed by the addition of water, to afford the free acids.

Since organophosphonic acids are rather young compounds in the field of coupling agents, functional molecules are rarely reported.^[199] In one early report, Arbuzov *et al.* described the synthesis of furfurylphosphonic acid and the corresponding ethyl ester (Scheme 22).^[204] Furfuryl alcohol was converted with PBr₃ to obtain furfuryl bromide. In a Michaelis-Becker reaction, using Na as a base, the diethyl furfurylphosphonate was obtained in 56% yield.

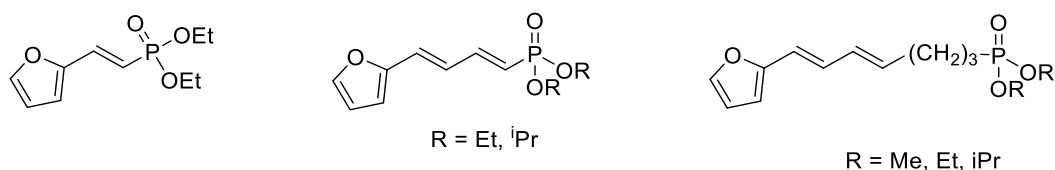


Arbuzov and Lugovkin, 1952

Scheme 22: First furan alkyl phosphonic acid synthesized by Arbuzov *et al.*^[204]

Hydrolysis in hydrochloric acid at 100-110°C led to a tar, but treating the ethyl ester with NaOH gave a residue, which could be extracted with ethanol to obtain the desired acid in 84% yield. These early authors reporting about such compounds were exclusively interested in the preparation of this compound.

Oh *et al.* reported the preparation of various 2-arylethenephosphonates (Scheme 23).^[205] In a reaction of α-lithio methylphosphonate with carbonyl compounds (such as furfural) followed by the addition of diethyl chlorophosphate yielded in bisphosphates, which could undergo an elimination by treatment with ^tBuOK. Diethyl (2-(furan-2-yl)vinyl)phosphonate was obtained in 80% yield.



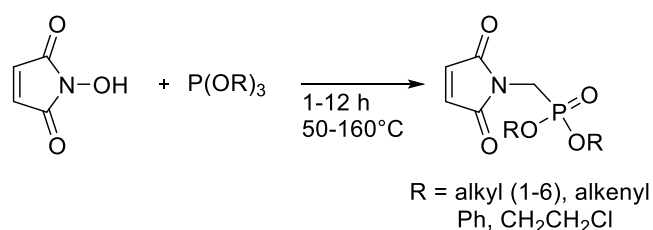
Oh *et al.* 1995

Chen *et al.* 2000

Scheme 23: 2-Arylethenephosphonates synthesized by Oh *et al.*^[205]

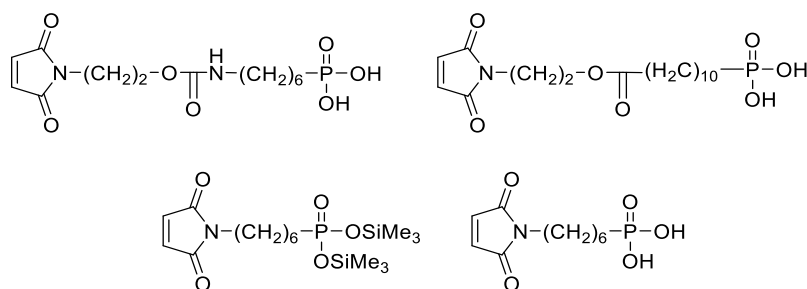
Chen *et al.* reported several unsaturated phosphonates bearing furan rings (Scheme 23).^[206] Dialkyl-4-(furan-2-yl)buta-1,3-dien-1-yl)phosphonate was synthesized by the Wittig-Horner reaction of bisphosponylmethane with 3-(furan-2-yl)propenal. Dialkyl-7-(furan-2-yl)hepta-4,6-dien-1-yl)phosphonate was synthesized using the Michaelis-Becker reaction of ω -bromodienes with sodium phosphite. Also, in this case, the authors focused solely on the synthesis of the organic substances.

Phosphonic acids or acid esters bearing the maleimide ring are even less described. Two US patents mentioned such compounds in 1975 and 1991.^[207, 208] Imidomethyl phosphonates were invented by Golborn and Duffy.^[207] These compounds were synthesized by reacting *N*-hydroxymethyl imides with trialkyl phosphites at elevated temperatures. The synthesis of the maleimide derivatives is depicted in Scheme 24. The invention targets the usage of these compounds as flame retardants for thermoplastic or thermosetting resins.



Scheme 24: Synthesis of maleimidomethyl phosphonates according to Golborn and Duffy.^[207]

Imai and Sorori reported a presensitized aluminium plate for the application in lithographic printing using maleimido phosphonate coupling agents (Scheme 25) to improve the adhesion between the substrate and the photodimerizable polymer.^[208]



Scheme 25: Synthesis of maleimido phosphonates with different spacers according to Imai and Sorori.^[208]

Unfortunately, although many molecular structures were given in their report, no information on the synthesis of the compounds is part of the patent.

Furan or maleimide bearing phosphonic acids or acid esters have been rarely reported so far, and to the best of my knowledge, they have not been used for the design of interfaces in self-healing materials.

1.9 Polymer Matrices for self-healing

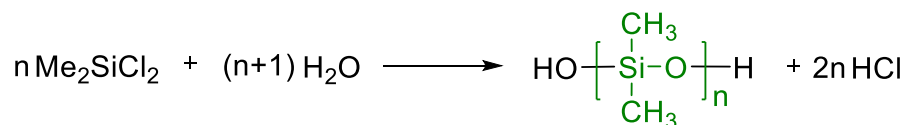
Polymers can be divided into three main categories, the thermoplastics, elastomers and thermosets, according to their properties, mainly based on their behavior which they show upon heating.^[209] This behavior depends on the crosslinking type on molecular scale. Thermoplastics generally have unbranched polymer chains, which can slide past each other when heated and makes them malleable at higher temperatures. Elastomers have a few, widely distributed crosslinks between the chains, which causes their softness and elasticity, but also that they are non-formable. Thermosets have plenty of the interchain crosslinks, which causes their hardness, but at the meantime the inflexibility of the chains. Therefore, this polymer class is non- malleable upon heating. Consequently, the two interesting matrices for self-healing polymer-based systems are elastomers and thermoplastics. In this work, siloxanes were used as elastomer and pBMAs as thermoplastic matrix, so that only a brief introduction in the synthetic access to these materials is given.

1.9.1 Elastomeres - Siloxanes and their synthetic access

Elastomers (acrylnitrile/butadiene/acrylate, acrylnitril/methyl methacrylat, isoprene-rubber, polyisobutylene, ...) are elastically malleable and have a T_g below the operating temperature.^[209] Upon mechanical stress, they transform into another shape, but re-shape upon relaxation. Commonly, organic elastomers are synthesized by free radical polymerizations (FRPs). In this work, the polydimethylsiloxanes $[\text{SiO}(\text{CH}_3)_2]_n$, which are elastic at low temperatures and viscoelastic at high temperatures, were employed for the design of self-healing materials.

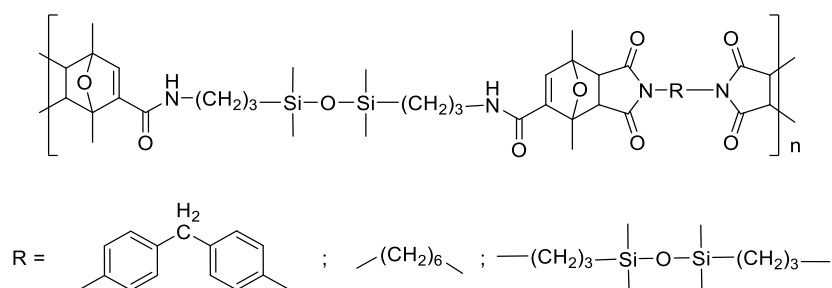
Polydimethylsiloxanes

Polydimethylsiloxanes are synthetically available by the reaction of dimethyldichlorosilane with water (Scheme 26).^[210, 211, 212] Polymers synthesized by this reaction are commonly OH-terminated, which gives the possibility to introduce various functional groups or chains on the α, ω – end.



Scheme 26: General synthetic access to PDMS.

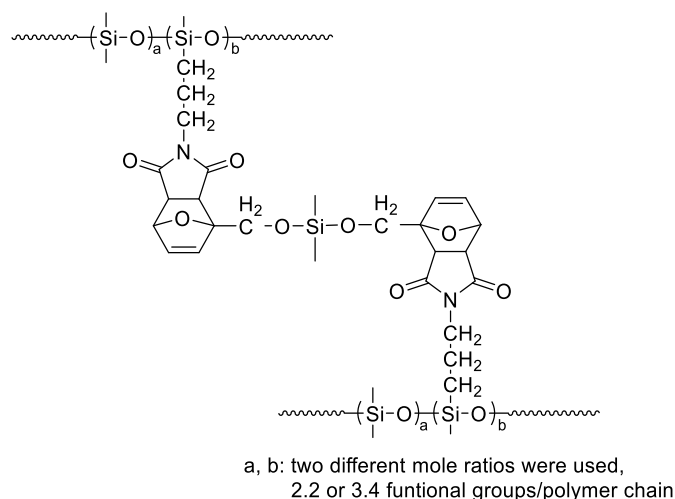
DA group bearing siloxanes are rarely reported. Already in 1986, Tesoro *et al.* described siloxane-containing bis(furans), which were crosslinked with three different bismaleimides (Scheme 27).^[213]



Scheme 27: Siloxane containing DA polymers synthesized from siloxane-bis(furans) and three different bismaleimides.[213]

The bismaleimides had either a hexyl-, methylene-4,1-phenylene- or a tetramethyldisiloxane linker. In this early time, the authors were not interested in self-healing properties of the material. The DA adduct was even destroyed by treatment with acetic acid under reflux to afford the phthalimide. Nevertheless, this work showed the possibility of functionalization and DA polymerization in bulk, when having siloxane backbones.

Gandini *et al.* developed a DA derived system using a low T_g (around -112°C) maleimidodimethylsiloxane copolymer as a dienophilic unit and bis(2-methoxyfuran)dimethylsilane as a crosslinker (Scheme 28).^[89] The siloxanes were synthesized from commercially available propylamine dimethylsiloxane in a two-step procedure by adding maleic anhydride and treating the intermediate maleamic acid with acetic anhydride and trimethylamine. The diene unit was prepared by nucleophilic substitution of furfuryl alcohol with dimethylsilyl dichloride.

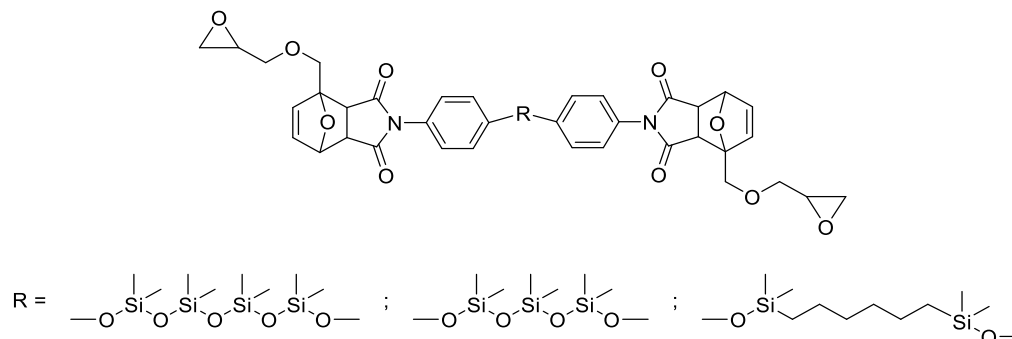


Scheme 28: DA crosslinked siloxane developed by Gandini *et al.*[89]

The network was formed in dichloromethane while stirring for three days at room temperature. The obtained gels were tested in thermal de-crosslinking (chlorobenzene, 80°C , 12 h) in the presence of an excess 2-methylfuran and an excellent reversibility of these systems was found.

Aubert *et al.* developed removable epoxy resins by the employment of three different bismaleimide siloxane crosslinkers, forming a DA product with furfuryl glycidyl ether (Scheme 29).^[214] The glycidyl ether function allows for covalent bonding to the epoxy resin. The

bismaleimide crosslinkers were synthesized reacting 4-hydroxyphenyl maleimide with 1,7-dichlorooctamethyltetrasiloxane, 1,5-dichlorohexamethyltrisiloxane, or 1,6-bis(chlorodimethylsilyl)-hexane ($\text{Et}_3\text{N}/\text{THF}$, 4 h, ambient temperature), respectively. All of these compounds led to low viscous oils at 60°C.



Scheme 29: Epoxy resins with three different bismaleimide siloxane crosslinkers developed by Aubert *et al.*[214]

The siloxane moieties led to easily removable encapsulants by rDA, which are promising for the repair of encapsulated electronic components.

More recently, Xia *et al.* described a nontoxic, biocompatible self-healing polysiloxane elastomers based on maleimide propylmethylsiloxane–dimethylsiloxane copolymers, which were converted with 1,3-bis(3-furanopropyl) tetramethyldisiloxane (Figure 26).^[97]

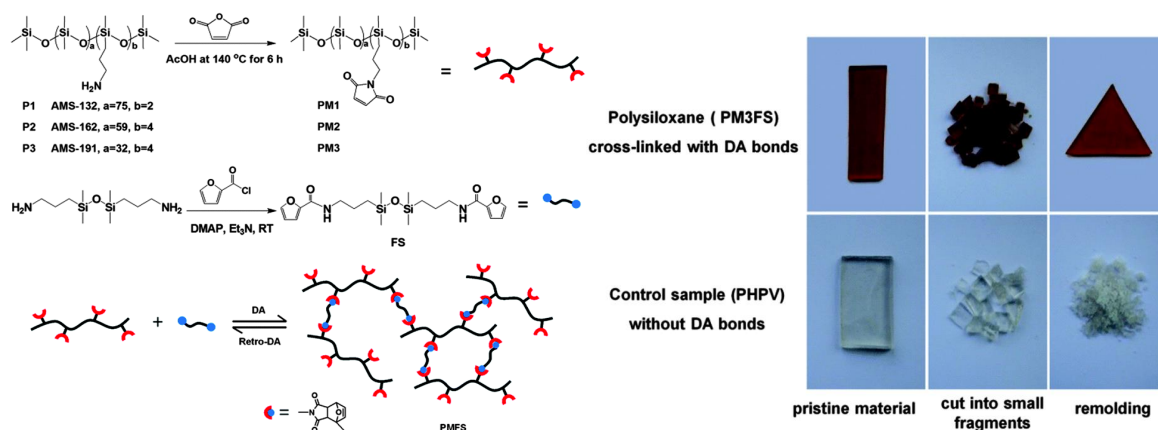


Figure 26: Left: Synthesis of biocompatible self-healing DA crosslinked polysiloxane. Right: Remolding experiment with DA polysiloxane and non-functional siloxane. Reproduced from Ref. [97] with permission from The Royal Society of Chemistry. Copyright The Royal Society of Chemistry 2016.

Crosslinking was realized by mixing both compounds in dichloromethane, evaporating the solvent and leaving the mixture for 4-10 days at 80°C. The healing efficiency was reported to be significantly dependent on the healing time. An increase from 29% to 95% was observed by raising the reaction time from 1 h to 24 h.

Bismaleimidosiloxanes were also already employed in self-healing hybrid materials by Kickelbick *et al.*^[148] and Zelisko *et al.*^[98] as mentioned in chapter 1.6.2.

1.9.2 Thermoplastics and their synthetic access via Controlled Radical Polymerizations

Thermoplastic (polyethylene, polypropylene, polystyrene, polymethacrylate, ...) is probably the most widely used type of plastic. Commonly, they are synthesized by FRPs. But the low level of control of the reaction, due to free radicals, encouraged scientist to develop Controlled Radical Polymerizations (CRPs), which are more useful for the demanding synthesis of smart materials, such as self-healing materials.

Synthetic access to Thermoplastics via Controlled Radical Polymerizations (CRP)

Back in 1982, Otsu and co-workers were the first who described living radical polymerization.^[215]

The "Living Polymerization" was defined by IUPAC in 1996 as follows: "A chain polymerization from which chain transfer and chain termination are absent. Note: In many cases, the rate of chain initiation is fast compared with the rate of chain propagation, so that the number of kinetic-chain carriers is essentially constant throughout the polymerization."^[216]

In 2010, the IUPAC recommended to use the terminology "reversible-deactivation" radical polymerization for the previously called "controlled" radical or "living" radical polymerization, because the word "living" is to unprecise for "radical polymerizations, no matter how minimal the termination might be within such systems." The new definition is: "Chain polymerization, propagated by chain carriers that are deactivated reversibly, bringing them into active-dormant equilibria of which there might be more than one."^[217] Furthermore the authors mention in Note 3, that atom-transfer radical polymerization (ATRP), reversible addition-fragmentation chain-transfer polymerization (RAFT) and polymerization mediated by an aminooxyl (= Nitroxide-mediated Polymerization = NMP) (or a similarly acting substance) belonging to this polymerization category.

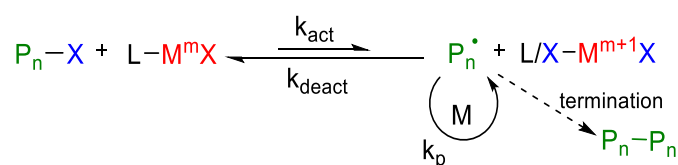
These three main techniques were intensively studied since 1990.^[218] In this work, only the two first mentioned ones were used as a tool to build self-healing materials, so that the NMP will not be described.

This modern techniques enabled scientist to design linear polymer chains, control the molecular weight and its distribution and extend the scope of functional polymers.^[219] A special feature of these reversible deactivation radical polymerizations is, that the dormant species can even be reactivated after isolation of polymer chains. This gave researchers the ability to design novel e.g. mixed polymers, brushes, dendrimers, block copolymers among others to build numerous novel polymeric architectures.

ATRP

IUPAC defined ATRP as "Controlled reversible-deactivation radical polymerization in which the deactivation of the radicals involves reversible atom transfer or reversible group transfer catalyzed usually, though not exclusively, by transition-metal complexes."^[217]

The general mechanism of ATRP is depicted in Scheme 30.^[218] First, a metal, most often copper (along with others, such as Ru, Fe, Mo, Os,...), which is stable in two different oxidation states (M^m and M^{m+1}) form a complex with a chelating N donor ligand. The lower oxidation state complex (activator) react with an alkyl halide initiator (RX) to form the higher oxidation state complex (= deactivator) with coordinating halide and a radical R with a certain rate constant k_{act} . After this activation step, the radical can react either with a monomer, to give a growing polymer chain, with the growing polymer chain itself or termination can occur due to radical recombination. Based on the ability of the coordinating halogen atom on the higher oxidation state complex, to be transferred to an alkyl rest (monomer or growing polymer), a transformation of the the growing polymer into the dormant species P_n-X can occur, while regenerating the lower oxidation state complex (= activator). The ATRP equilibrium is determined by k_{act}/k_{deact} (k_{deact} = deactivation rate constant), which means it is dependent on the activity of the catalyst. Therefore, many catalysts, ligands, solvents and monomers have been tested to control the equilibrium. The deactivation, which means the dormant state should be favored. Thus, a low population of propagating radicals and therefore minimal radical recombination of propagating chains is ensured.



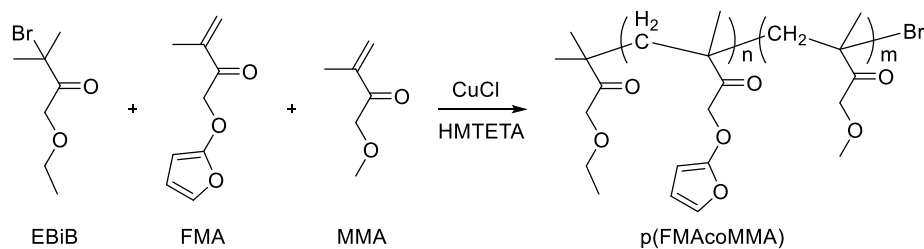
Scheme 30: ATRP mechanism/ equilibrium.

In ATRP, various monomers like acrylates, styrene derivatives, acrylamides and acrylonitrile are tolerated.^[219] Functional groups are tolerated, as long as they do not serve as a competing ligand for the metal complex.^[220] The incorporation of monomers bearing glycidyl, hydroxyethyl, azido, vinyl pyridine, furan and protected maleimide has been reported.^[99, 219, 221, 222, 223]

One of the mayor drawbacks of ATRP is the requirement of high amounts transition metal (up to 5000 ppm)^[224] and the O_2 sensitivity, when e.g. Cu(I) species are employed. Many modifications have been developed, such as AGET (Activators Generated by Electron Transfer), ARGET (Activators ReGenerated by Electron Transfer) and ICAR (Initiators for Continuous Activator Regeneration) amongst others, to overcome these disadvantages.^[219] The aspects of these variated ATRPs have been reviewed.^[218, 219]

Furan/maleimide bearing polymers synthesized by ATRP

ATRP has been used to synthesize thermoreversible methyl- co furfuryl- methacrylates by Singha *et al.*^[99, 225, 226] An exemplary reaction is depicted in Scheme 31.

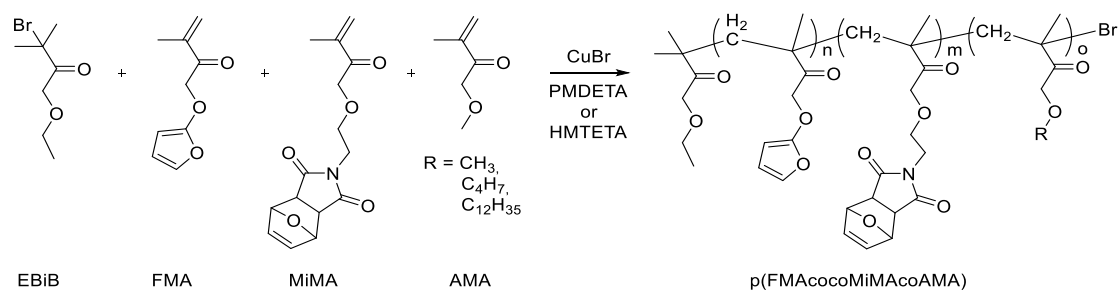


Scheme 31: ATRP of FMA and MMA.

The authors compared FRP with ATRP of methyl(methacrylate) (MMA) and FMA. While FRP led to insoluble, gelled polymers, in ATRP soluble polymers were obtained. In a typical ATRP containing FMA as a monomer, ethyl α -bromoisobutyrate (EBiB) was used as the initiator, CuX (X = Cl or Br) as a catalyst and 1,1,4,7,10,10-hexamethyltriethylenetetramine (HMTETA) as a ligand. Under oxygen-free conditions, the mixtures were heated to 90°C in toluene. The progress of the reaction was monitored with SEC and NMR. A linear increase of the molecular weight and a relatively narrow molecular weight distribution were found. The main advantage of ATRP compared to FRP is, that no undesirable side reactions occur with the double bond of the furan ring. Moreover, ATRP affords linear polymer chains, having a higher mobility than the crosslinked polymers obtained in an FRP. In 2009, Singha reported, that converting FMAcoMMA polymers which were obtained in an ATRP, with BMI, a thermoreversible, self-healing material was observed.^[100]

In 2010, the same group established ABA triblock copolymers (poly(FMA)-*b*-poly(2-ethylhexyl acrylate)-*b*-poly(FMA)) by application of an ATRP. The reaction was carried out at 90°C for 30 min, using CuCl with HMTETA as a catalyst and α,ω -dibromo-poly(2-ethylhexyl acrylate) as a bifunctional macroinitiator. Two T_g 's were found which showed that the polymer consists of a soft and hard phase having a polydispersity index (PDI) of 1.28. The triblock copolymer afforded a self-healing system after conversion with BMI, which showed complete healing of a surface after 4 h in scanning electron microscopy images.

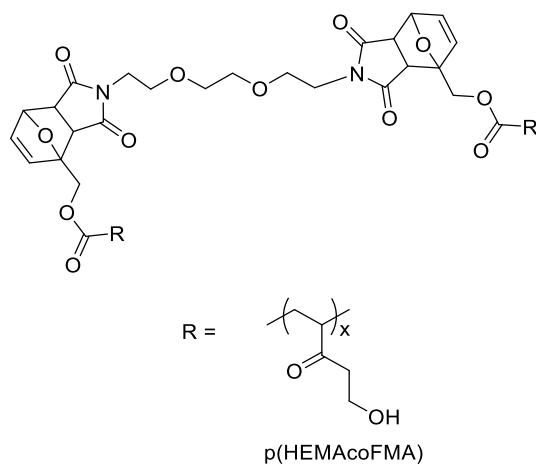
Schubert *et al.* further developed this FMA based system in 2013, by the development of one-component polymers bearing furan and maleimide rings at one polymer backbone (Scheme 32).^[153] To avoid undesired crosslinking during ATRP, the maleimide moiety was protected by furan, as it was established before for FRPs.^[227] The protection is necessary because the maleimide double bond can also undergo polymerizations, which would lead to undesired crosslinking. This system was the first, which had no need of an additional molecular, low molecular weight crosslinker to obtain thermoreversible methacrylates. A ratio of 10 mol% per functional monomer was found to ensure the best healing behavior.



Scheme 32: Schematic representation of the copolymerization of AMA, FMA and MiMA by ATRP.[153]

The same group further developed their system in 2015 by copolymerizing FMA, maleimide (methacrylates) having three different spacers (C_2H_4 , C_6H_{12} , $C_2H_4OC_2H_4$) between both functional groups, and a non-functional comonomer, which is one of the following three: polar 2-hydroxyethyl methacrylate (HEMA) or dimethylaminoethyl methacrylate or non-polar BMA.^[228] EBiB was used as the initiator, CuBr with coordinating HMTETA as a catalyst. Again, each functional was applied in 10 mol%. The polymer consisting of 2-(hydroxyethoxy)ethyl methacrylate and the maleimide unit having $C_2H_4OC_2H_4$ as spacer accomplished the best self-healing behavior and was able to heal millimeter range scratches at $140^\circ C$.

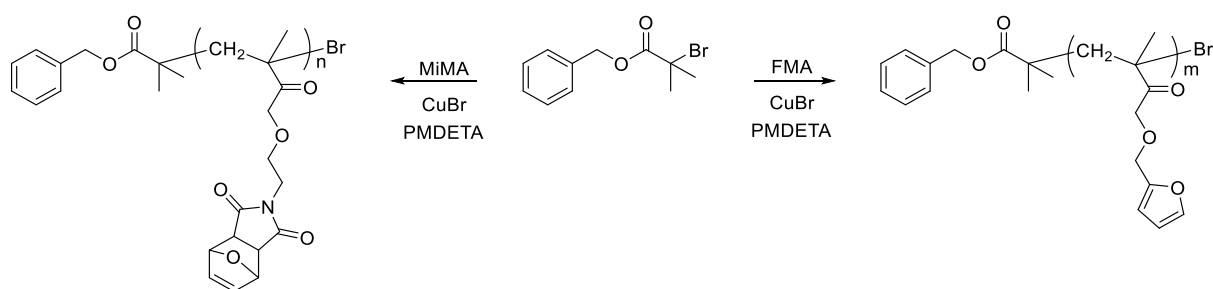
Galbis *et al.* synthesized poly(HEMAcoFMA) (Scheme 33) in various mol% by the employment of EBiB, CuBr/2,2'-bipyridyl ligand in high yields (>95%).^[229] Low PDIs (1.17-1.30) were obtained after reacting the mixtures for 5 h. The polymers were tested concerning their hydrogel-behavior after reacting it with 1,8-dimaleimide-3,6-dioxaoctane.



Scheme 33: Crosslinked poly(HEMA-FMA) copolymer with 1,8-dimaleimide-3,6-dioxaoctane as a crosslinker.[229]

Kickelbick *et al.* described pBMAcoMiMA synthesized using the CuBr/HMTETA system as a catalyst and EBiB as the initiator.^[146] The reaction was carried out in toluene at $70^\circ C$ for 3 h, and again the maleimide monomer had to be protected as mentioned before. A PDI of 1.22 was found and a yield of 36% was obtained. This system was already described in chapter 1.6.2.

In 2016, Oh *et al.* synthesized pMiMA and pFMA using benzylbromide as initiator and CuBr/PMDETA (*N,N,N',N'',N'''*-pentamethyldiethylenetriamine = PMDETA) as catalyst system (Scheme 34).^[230]

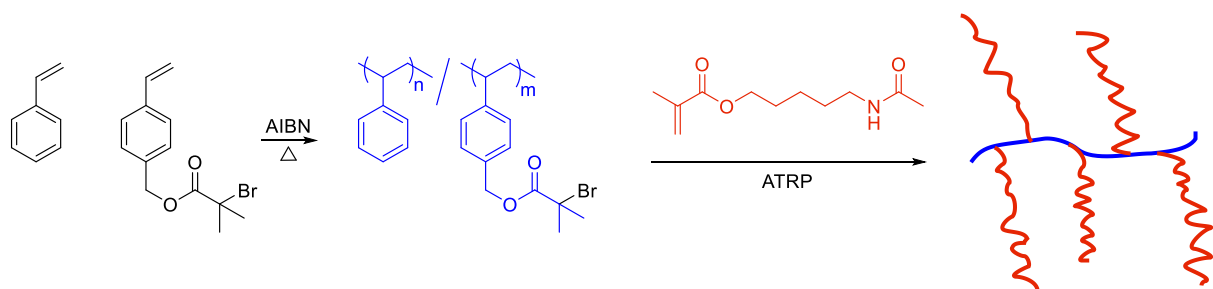


Scheme 34: Synthetic Route to pMiMA and pFMA homopolymers by ATRP.[230]

Rather high PDIs (1.70-1.99) were found, along with conversions between 30 and 60% in 1-7 h reaction time. The crosslinking of both homopolymers afforded healable films.

Hydrogen bond motif bearing polymers synthesized by ATRP

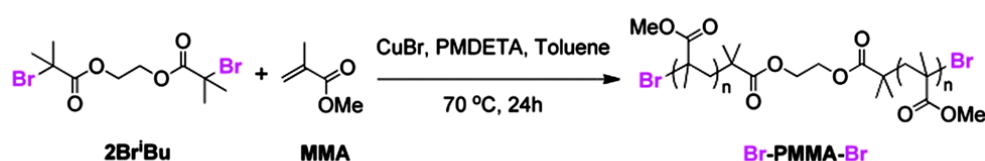
To the best of my knowledge, the group of Guan is the only one who was interested so far in the incorporation of hydrogen bond building motifs in polymers synthesized by ATRP. The first article on this topic was published in 2012, where a system consisting of multiphase polymers polystyrene backbone with polyamide brushes was described (Scheme 35).^[114] The backbone was synthesized by FRP of styrene along with the desired amount ATRP initiator 4-(2-bromoisobutyloylmethyl)-styrene. The amido brushes were attached to this prepolymer in CuBr/PMDETA catalyzed ATRP. These polymers showed autonomic healing behavior, due to its multiphase morphology, which is caused by collapsing of styrene backbone to a hard segment and leaving the dynamic soft amido brushes in the periphery.



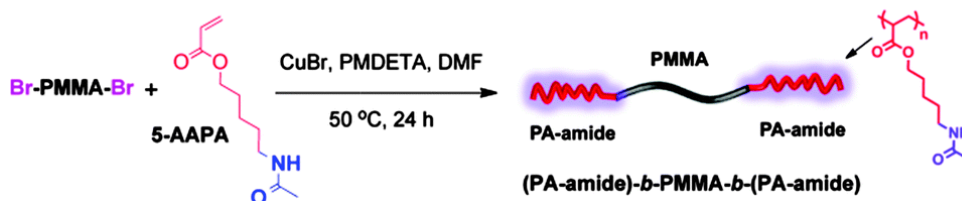
Scheme 35: Polystyrene backbone and PA-amide brushes.[114]

Following this promising concept, the group developed triblock copolymers bearing a pMMA block in the middle and dynamic hydrogen bonding (amide) blocks at both ends using ATRP (Scheme 36).^[231, 232] As the previous system, also this one self-assembles in a microphase-separated morphology consisting of a hard and a soft phase.

a. Synthesis of the glassy PMMA block by ATRP



b. Synthesis of the self-healing ABA triblock copolymer by ATRP



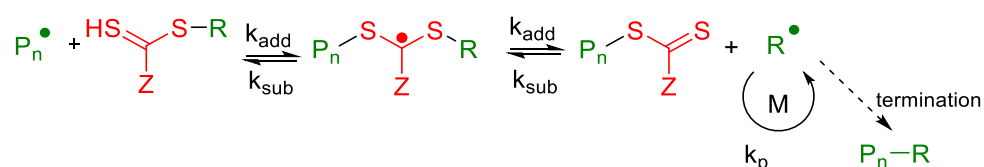
Scheme 36: Triblock copolymer ABA bearing amide blocks on both ends. Reproduced from Ref. [231] with permission from The Royal Society of Chemistry. Copyright The Royal Society of Chemistry 2014.

The same conditions as for the polystyrene system were applied for the ATRP except of using the pMMA macroinitiator in this case. These systems are able to heal at room temperature solely by hydrogen bonds.

RAFT

IUPAC defined RAFT as “Degenerate-transfer radical polymerization in which chain activation and chain deactivation involve a degenerative chain-transfer process, which occurs by a two-step addition-fragmentation mechanism.”^[217]

The mechanism of a RAFT polymerization (Scheme 37)^[220, 233] is based on the so-called RAFT agent (or CTA = Chain Transfer Agent, mostly thiocarbonyl compounds), which can reversibly deactivate propagating chains (radicals) and transfer them into dormant species. Contrary to ATRP, RAFT requires an additional free radical source (initiator), such as azobisisobutyronitrile (AIBN), which has to be initiated first, to form free radicals. These can react with a monomer, to form the propagating chain radical (P_n). The P_n reacts with the CTA on the C=S double bond and forms an intermediate thiocarbonylthio radical, which liberates a radical (R), while the thiocarbonylthio rest remains on the growing polymer chain. The liberated radical can reinitiate polymerization on CTA terminated chains or react with a fresh monomer to form a new propagating chain. When all CTA has reacted, the equilibrium between propagating chains and dormant species of the reaction is reached. Like in FRP, recombination of radicals can occur. Remaining dormant species in the polymeric product give the possibility to further modify the chains or to synthesize block copolymers.



Scheme 37: RAFT mechanism/ equilibrium.

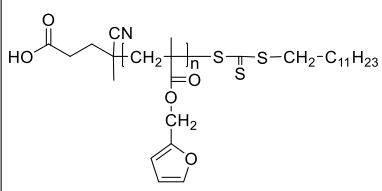
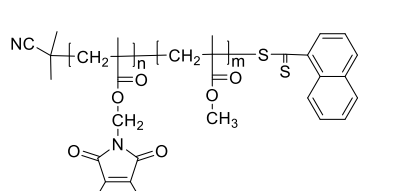
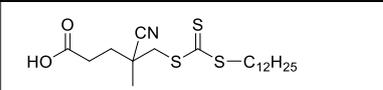
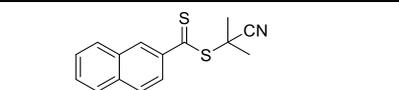
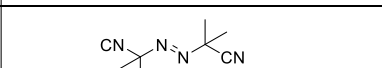
Because the RAFT reaction conditions are almost the same as in conventional polymerizations, nearly the same scope of monomers can be used.^[233] Acrylates, acrylamides, acrylonitrile, styrenes, dienes and vinyl monomers were successfully converted.^[220] In RAFT, also reactive and strong donating functional groups such as isocyanate,^[234, 235] acid chlorides,^[236] and acetylenes^[237] and amines^[235, 238] are tolerated.^[220, 239, 240] This variety of reactive groups opens the way to post-polymerization modifications.^[234, 241, 242]

Although RAFT is a very promising route in CRP techniques, because it proceed without metal catalyst at low temperatures, it suffers from drawbacks like the necessity to carefully adjust the chain transfer agent (CTA) to the monomer, avoid oxygen to control the polymerization and the need of a radical source, which inevitably causes undesired termination reactions.^[233] These aspects have been discussed in a recent review.^[233]

Furan/maleimide bearing polymers synthesized by RAFT

RAFT has already been used for the synthesis of DA based self-healing materials. Singha *et al.* were the first who polymerized FMA using different RAFT reagents and RAFT reagent:initiator mole ratios in toluene at 90°C.^[243] Using the RAFT agent 4-cyano-4-[(dodecylsulfanylthiocarbonyl) sulfanyl] pentanoic acid and 4,4'-azobis(4-cyanovaleric acid) as the initiator, 85% conversion and a PDI of 1.38 were determined after 5 h. These polymers were crosslinked using three different bismaleimides to afford thermally amendable polymer.

Table 2: Two DA polymers synthesized by RAFT polymerization with the corresponding RAFT agent and initiator.^[244, 245]

	pFMA synthesized by Singha <i>et al.</i>	pMMAcoMiMA synthesized by Zhang <i>et al.</i>
Polymer		
RAFT agent	 4-cyano-4-[(dodecylsulfanylthiocarbonyl) sulfanyl] pentanoic acid	 2-cyanoprop-2-yl 1-dithionaphthalate
Initiator		Fe(0)

In an ensuing work, the same procedure was used to obtain pFMAcoBMA in different mol ratios by RAFT polymerization in DMF at 80°C for 16 h.^[240] Treating the polymer having the composition FMA:BMA = 41: 59 with BMI for 24 h at 50°C in chloroform afforded a viscous oil, which solidified upon drying and showed thermoreversible properties due to the DA reaction. In 2016, Singha's group showed a green method of RAFT polymerization of FMA.^[244] The authors used a recyclable ionic liquid (2-butyl-3-methylimidazolium

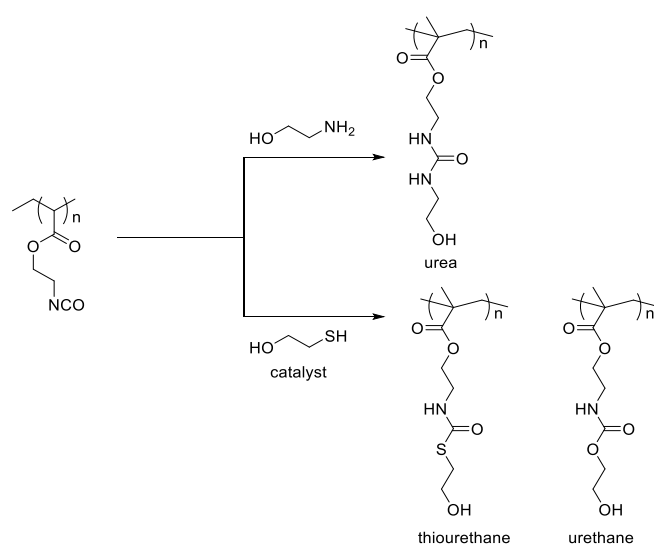
hexafluorophosphate) as a solvent, AIBN as an initiator and again 4-cyano-4-[(dodecylsulfanylthiocarbonyl) sulfanyl] pentanoic acid as a RAFT agent and heated the mixture at 70°C for 1 h. Using chloroform to extract the product, the desired pFMA (Table 2) was obtained with 95% conversion and a PDI of 1.38. An additional advantage is that the reaction is accelerated compared to common organic solvents like toluene or DMF.

In 2018, the first report in which MiMA was used in a RAFT polymerization was published by Zhang *et al.*^[245] The authors copolymerized MMA and ca. 20 mol% MiMA using 2-cyanoprop-2-yl 1-dithionaphthalate as RAFT agent and zero-valent iron powders as an initiator (Table 2). The reaction was carried out at 30°C for 72 h in DMSO. A PDI of 1.21 and a yield of 14.6% was obtained under these conditions. Since the authors were interested in the formation of polymeric nanoparticles, no experiments towards self-healing were conducted.

Hydrogen bond motif bearing polymers synthesized via RAFT polymerization

Since the direct polymerization of hydrogen bond forming monomers is often difficult, a very promising step is to polymerize isocyanate bearing monomers and use the high reactivity towards NH and OH in post-modification methods. The conditions in RAFT polymerization tolerate the isocyanate group and accordingly, several reports of isocyanate group bearing reactive polymers exist in the literature.

Hawker and coworkers synthesized poly(isocyanatoethyl methacrylate coMMA) (pICEMAcMMA; ICEMA = 2-isocyanatoethyl methacrylate) to produce intermolecular collapsed nanoparticles, by post-branching of isocyanate chains by the addition of 2-methoxyethylamine.^[234] The pICEMAcMMA was synthesized by applying S-methoxycarbonylphenylmethyl dithiobenzoate as RAFT agent and AIBN as an initiator in benzene at 75°C for 17 h. The polymer was obtained in 67% yield with a PDI of 1.13. Within 2 h at ambient temperature, the polymer reacted with the diamine to a crosslinked-polymer derived nanoparticles.

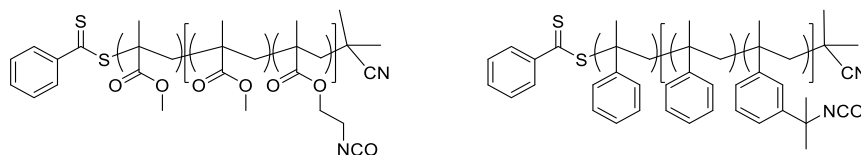


Scheme 38: Post-modification of poly(isocyanatoethyl methacrylate).[235]

McCormick *et al.* described the homopolymerization of 2-(acryloyloxy)ethylisocyanate applying *N,N*-dimethyl-*S*-thiobenzoylthiopropionamide as a RAFT agent and 2,2'-azobis(2,4-dimethylvaleronitrile) as an initiator in dioxane.^[235] At a reaction temperature of 50°C, a conversion of 40% and a PDI of 1.13 was observed within 13 h.

The obtained polymer was reacted with alcohols, amines or thiols (Scheme 38). While the reaction between amine and isocyanate is a click-type reaction, the reaction with thiols affords the presence of a basic catalyst and the conversion with alcohols is very slow but can be completed by the addition of dibutyltin dilaurate.

Perrier *et al.* described a two-step polymerization for block copolymers consisting of either dimethyl meta-isopropenyl benzyl isocyanate (TMI) with styrene or ICEMA and MMA, respectively (Scheme 39).^[239] A pMMA prepolymer was synthesized using cyanoisopropyl dithiobenzoate (CPDB) as RAFT agent and AIBN as initiator at 60°C in dioxane until 75% conversion of monomer and a PDI of 1.23 was observed. Then the isocyanate bearing ICEMA was added to the solution, and the reaction was stopped when 55% conversion of ICEMA was observed. The PDI of the final block copolymer was determined to be 1.60. The authors declare that the rapid increase in PDI is a result of crosslinking between the polymer chains. Previously, Yoon and Lovell suggested a mechanism, involving traces of water, which cause a reaction with the OCN group and results in a carbamic acid.^[246] In the following, CO₂ is split off and leaves an amine group in the polymer. This amine group is able to react with isocyanate groups to form urea bonds. However, most of the isocyanate groups are still present in the block copolymer.



Scheme 39: Block copolymers: left MMA/ICEMA and right TMI/styrene system developed by Perrier *et al.*^[239]

Analogously, the TMI/styrene system (PDI = 1.30) was prepared at 125°C in *p*-xylene, trying (propionic acid)yl butyl trithiocarbonate (PABTC) and CPDB as RAFT agents. The same results regarding the PDI were found for both RAFT agents. PABTC being a trithiocarbonate is known to mediate the polymerization faster than dithiobenzoates, like CPDB, but the dithiobenzoates are better chain transfer agents in RAFT polymerizations. However, Yoon and Lovell reported, that carboxylic acid rest on PABTC is able to catalyze the reaction between TMI and water, to finally form urea bonds as mentioned above.^[246] Therefore, and also because trithiocarbonates are not suited for the RAFT polymerization of methacrylates, the authors decided to do all studies for comparison of the ICEMA/MMA and the TMI/Styrene system using CPDB as RAFT agent. Both systems were coupled with cellulose-OH groups to form urethane bonds. The isocyanate groups of TMI showed a lower reactivity towards post-modification, compared to ICEMA, due to sterical hindrance.

One-component polymers, having DA groups simultaneously with hydrogen-bond motifs, have not been synthesized by CRP techniques so far. The high tolerance towards functional

groups such as isocyanate (RAFT), furan or protected maleimide (ATRP, RAFT) allows to produce polymer chains with reactive moieties, that can be used for post-modification or reversible crosslinking. However, the possibility to tailor molecular weight and mole ratios of functional monomers along with obtaining soluble polymers makes this technique important for the design of self-healing nanocomposites and hybrid materials.

1.10 Knowledge gaps in the known systems

Although a lot of work has been done in the field of DA based healing in polymers, only a few reports on nanocomposites and hybrid materials (1.6) exist. In intrinsic healing systems the mechanical strength is rather low compared to extrinsic systems.^[45] The incorporation of inorganic filler, which lowers the mobility of functional groups, provides a promising way to increase the mechanical strength of intrinsic healing systems. The challenge is, to realize a system, in which healing can still take place as it is known for thermoreversible DA polymers. Additionally, until now, no study dealt explicitly with the understanding of the surface reactivity of DA functionalized spherical nanoparticles. This knowledge would help to not only manufacture self-healing composites phenomenologically and instead to plan the necessary material composition in advance.

Moreover, the usage of inorganic material itself to influence the healing process is barely investigated. Few groups used electrical conductivity (MWCNT's)^[144] or microwaves^[247] to induce a temperature change for DA self-healing. Superparamagnetic iron oxide nanoparticles would be another interesting species because they can be heated in an alternating magnetic field (AMF), which would allow for selective local heating. To the best of my knowledge, only one report has been published in January 2018 by Bose *et al.* comprising magnetite particles in a DA based system. However, these particles were incorporated in reduced graphene oxide, and the authors were not interested in AMF induced healing experiments.^[247] Also, this system does not use the particles as a crosslinking site.

Another promising technique for the design of self-healing materials is the one in which multiple reversible interactions or reactions are assembled. In the rather young field of self-healing materials, this more complex approach is in a very early stage, since researchers have been busy with the understanding of systems, which do not comprise a "cocktail effect". In particular, this concept has not been regarded for nanocomposites or hybrid materials.

In the following chapter, the research goals and studies, which have been made to target these points in the presented work, are introduced and further discussed in chapter 3.

2 Research Goals

2.1 Objective

This work aims to improve the healing capacities of intrinsic self-healing nanocomposites and hybrid materials based on the DA chemistry by studying varying fillers and matrices. Therefore, the careful synthesis of the single components, like coupling agents and monomers have to be done with respect to the tolerance of functional groups in the target molecule (Figure 27). After surface-functionalization of inorganic nanoparticles and polymerization of the monomers, the two ingredients are combined to afford the nanocomposite material.

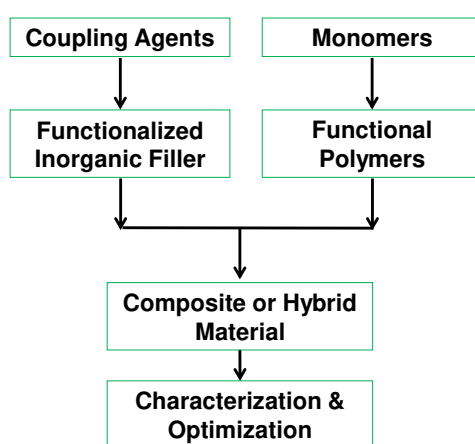


Figure 27: General procedure to synthesize self-healing nanocomposites.

The suitability of DA group modified inorganic nanoparticles as a crosslinking agent, depending on e.g. nanoparticle size, spacer length of coupling agent or crowdedness of the surface shall be investigated. Therefore, DA modified silica nanoparticles have to be embedded within different polymer matrices, such as elastomers or thermoplastics. Monolayer functionalized magnetic iron oxide nanoparticles shall be synthesized by the usage of phosphonic acids. Reacting these particles with either small molecules or sterical demanding derivatives of those, an even deeper understanding of how the particle surface can interact with functional groups bound on polymeric backbones shall be gained.

A further improvement of the self-healing nanocomposites shall be carried out by the incorporation of smaller inorganic fillers, namely spherosilicates and by providing a higher degree of freedom of diene and dienophile at the same time. To realize a greater degree of freedom of diene and dienophile, none of them should be trapped on the inorganic surface. Nevertheless, still an ideal miscibility of filler and polymers has to be provided. Hydrogen bonds can be introduced on the inorganic-organic interface, which would guarantee a perfect matching and integrate a second reversible and intrinsic force in the material.

Therefore, the spherosilicates should be chemically surface modified and conclusively bear hydrogen bond motifs on their surface. The supramolecular interaction rapidly re-equilibrate upon cleavage. This phenomenon realizes close contact of damaged interfaces and consequently guarantees a necessary condition for efficient DA healing.

2.2 Concept

In detail the following studies were carried out:

- DA modified SiO_2 nanoparticles were synthesized and embedded in corresponding matrices. DA group modified siloxanes and poly(butyl methacrylates) are chosen to study the influence of the chemical nature of the polymer matrix. The single components were characterized using FTIR and NMR spectroscopy, and for the particles also dynamic light scattering (DLS), elemental analysis (CHN) and transmission electron microscopy (TEM) measurements were carried out. The crosslinking ability and the healing performance of the materials were tested by optical microscope images, DSC analysis and rheology measurements.
- Iron oxide nanoparticles were synthesized that bear DA group modified phosphonic acids as a monolayer on the surface. The synthesized compounds were characterized using FTIR, CHN, and for the organic molecules also NMR and electrospray ionization – mass spectrometry (ESI-MS) measurements were conducted. This system shall help to understand the chemistry on the particle surface. Small, as well as sterical demanding attacking reagents, were offered to the system, and the difference in conversion, determined by DSC, FTIR and CHN measurements, was analyzed to understand the reactivity towards polymers. One proof-of-principle self-healing experiment was carried out applying BMI as a crosslinker.
- Small molecular SiO_2 units, having no DA groups on the surface, were considered as alternative fillers. Therefore, spherosilicates, having long flexible alkyl substituents and the ability to form hydrogen bonds, shall be synthesized starting from TEOS. The novel cubes were characterized using NMR, ESI-MS, CHN and FTIR analysis. The hydrogen bonds depict a reversible intrinsic force, which equilibrates at ambient conditions. This is a promising feature for the system described in the following point.
- The functional spherosilicates were incorporated into an organic matrix, which contains two intrinsic reversible forces. One of them, the hydrogen bonds are reversible at room temperature and the other, the DA reaction is thermally

triggerable, which allows controlling the healing process. The synthesis were carried out using controlled radical polymerizations (CRPs), namely the ATRP or the RAFT polymerization. The polymers were characterized by NMR, FTIR, DSC and SEC measurements.

In this hybrid material, both diene and dienophile are located in the matrix. Hydrogen bonds on the surface of the inorganic filler and within the matrix shall help to assure homogeneous distribution and reconnection of crack surfaces at ambient temperature. The self-healing behavior was tested using optical microscope images, FTIR, UV/Vis, TEM images of microtome cuts and rheology experiments.

3 Results and Discussion

The results of this work have been published before.

3.1 Self-Healing Polymer Nanocomposites based on Diels-Alder-Reactions with Silica Nanoparticles: The Role of the Polymer Matrix

The self-healing performance of DA modified nanoparticles as crosslinking agents within different polymer matrices, namely the elastomeric siloxanes and the thermoplastic pBMAs, was studied. In a first step, maleimidopropyl- (MPTES) and furanundecyl-trialkoxysilane (FUTES) were synthesized and used as coupling agents for silica nanoparticles with a diameter of 12 - 18 nm. Based on a literature-known reaction for surface functionalization, trialkoxysilanes were attached to silica surfaces using the polar isobutylmethylketone and high temperatures.^[248] The successful surface functionalization with DA alkoxy silanes was shown by FTIR and TGA measurements. The modified particles were further characterized using elemental analysis, nitrogen sorption, DLS and TEM measurements. The surface coverage was found to be 1.23 molecules/ nm² (1.26 mmol/ g) for MPTES@SiO₂ and 0.79 molecules/ nm² (0.86 mmol/ g) in case of FUTES@SiO₂, respectively.

Commercially available side chain or terminal aminopropyl-functionalized dimethylsiloxanes (M_w 3000-5000 g/ mol) were modified to bear maleimide groups. Maleic anhydride was added and the intermediate maleamic acid was catalytically cyclized using ZnCl₂. Analogously, the furan ring was attached to the according hydride dimethylsiloxanes (M_w 400-17000 g/ mol), using a hydrosilylation reaction. Functional pBMA was synthesized in an ATRP according to a literature procedure.^[146] The functional siloxanes were unambiguously characterized using ¹H NMR and FTIR.

The composites are obtained by mixing the functional components in a ratio of 5:1 for diene to dienophile. The excess is always located in the polymer matrix. Ren and Yoshie *et al.* reported, that the non-stoichiometric ratio increases the probability of reconnection after damage.^[249] The synthesized siloxanes from this work contain varying amounts of functional moieties in the backbone. According to this, the materials differ in their appearance because the weight percent of particles range from 18-286 wt%. The ability of crosslinking and therefore healing ability of these materials was investigated using DSC and rheology measurements. While the composites of low T_g elastomeric siloxanes indicated successful reversible crosslinking by an endothermic signal in DSC (0.9 – 0.4 J/g) within the rDA temperature range (100-200°C), the thermoplastic pBMA samples showed no signal. Thus, it was concluded that a high molecular weight and T_g along with small amounts of functional groups per polymeric molecule lowers the conversion with DA group-modified silica nanoparticles. This further supports the literature known dependency from DA polymers of healing efficiency from mobility and flexibility of functional groups within the matrix.^[249] To

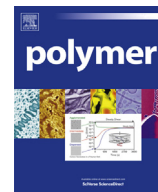
further verify the role of group mobility in conversion of polymers with particles, the reaction was carried out in chloroform and a 10 times higher DSC signal was observed. This result pointed out, that the functional groups can simply not reach each other efficiently within the bulk sample.

A cut healing test was done exemplarily on one siloxanes based composite. Optical microscope images showed that the material is too rigid to heal only by heating. After adding a few drops of chloroform to the surface, the interfaces came back into contact with each other which enabled the healing process.

These results were published in a special issue on self-healing polymers within the journal *Polymer* from Elsevier (Guest editor: Wolfgang Binder). Reproduced by permission of Elsevier. <https://doi.org/10.1016/j.polymer.2015.03.017>

Sandra Schäfer, Guido Kickelbick, Self-healing polymer nanocomposites based on Diels-Alder-reactions with silica nanoparticles: The role of the polymer matrix, *Polymer*, **2015**, 69, 357-368, <https://doi.org/10.1016/j.polymer.2015.03.017>.

Sandra Schäfer has written the publication and carried out all practical work (experiments and characterization). Guido Kickelbick has contributed with discussions about the topic and improvements for the final presentation of data and results within the manuscript.



Self-healing polymer nanocomposites based on Diels–Alder-reactions with silica nanoparticles: The role of the polymer matrix



Sandra Schäfer ^{a, 1}, Guido Kickelbick ^{a, b, *, 1}

^a Inorganic Solid State Chemistry, Saarland University, Am Markt, Zeile 3, 66125 Saarbrücken, Germany

^b INM – Leibniz-Institut für Neue Materialien GmbH, Campus D2₂, 66123 Saarbrücken, Germany

ARTICLE INFO

Article history:

Received 9 January 2015

Received in revised form

4 March 2015

Accepted 5 March 2015

Available online 13 March 2015

Keywords:

Polysiloxane nanocomposites

Self-healing

Thermoreversible crosslinking

ABSTRACT

Self-healing nanocomposites were studied consisting of surface-functionalized silica nanoparticles and polymers with different glass transition temperatures. The silica nanoparticles were synthesized using the Stöber process and afterwards surface-functionalized with the coupling agents 2-furyl-(undecenyl)-11-triethoxysilane or 3-maleimidopropyltriethoxysilane. The obtained nanoparticles were studied as cross-linking agents in thermally triggered self-healing nanocomposites based on Diels–Alder (DA) chemistry. Cross-linking of the nanoparticles with modified poly(butyl methacrylates) containing DA groups revealed that the rigid thermoplasts show only low tendency to undergo the cross-linking reactions. Contrary, similarly modified polysiloxanes display thermally reversible cross-linking in DSC as well as in rheology measurements. The results reveal that a specific extent of mobility and flexibility of the polymer backbones is crucial for a reasonable fast self-healing process if Diels–Alder groups are used as crosslinking agents.

© 2015 Elsevier Ltd. All rights reserved.

1. Introduction

In recent years, self-healing materials became a major research interest due to the public awareness that long lasting materials can save various resources, such as energy and raw materials. Generally, failure, damage, and degradation are natural consequences of material applications. Polymers with self-healing properties could significantly extend the lifetimes of materials [1].

Polysiloxanes are widely used in high-tech applications based on their unique properties such as high flexibility, abrasion and heat resistance, chemical inertness, high transparency, and excellent adhesion to various surfaces [2]. For self-healing applications particularly the extraordinary backbone flexibility is a key property for reversible bond formation. Several self-healing mechanisms applying polysiloxane based structures were previously demonstrated in literature, such as capsule based systems [3], hydrogen bonding mechanisms [4], or ring opening polymerization [5]. Many of these systems are either very sensitive to environmental

conditions because they are based on weak interactions, or self-healing can only be applied once at a localized damage. An alternative route for the production of self-healing polymers is the use of reversible covalent bonds as cross-linking mechanisms in the materials. One of the most studied reaction types with regard to such functional materials is the thermoreversible Diels–Alder (DA) reaction [6] typically based on the combination between furyl and maleimide groups as diene and dienophile. This reaction type showed in the past its efficiency in self-healing materials such as poly(ethylene oxide) [7], polyesters [8], multi-arm polyacrylic systems [9], linear polymerized polyacrylic systems by ATRP [10], poly(ϵ -caprolactone)-urethane chains [11], poly(oxazoline)s [12], and elastomers such as polysiloxanes [13]. Furthermore interpenetrating organic–inorganic hybrid networks were studied applying furan–maleimide systems in conjunction with a silica network generated *in situ* by the sol–gel process [14]. It was shown that the self-healing ability of such systems depends primarily on the mobility of the functional groups and the ratio of maleimide to furan [15].

A further improvement of polysiloxanes in areas like mechanical, thermal, and optical properties can be obtained by the incorporation of inorganic nanoparticles. This approach can also be used to create a new generation of self-healing nanocomposites using inorganic nanoparticles as crosslinkers. In previous studies we

* Corresponding author. Inorganic Solid State Chemistry, Saarland University, Am Markt, Zeile 3, 66125 Saarbrücken, Germany.

E-mail address: guido.kickelbick@uni-saarland.de (G. Kickelbick).

¹ <http://www.uni-saarland.de/lehrstuhl/kickelbick.html>.

showed the importance of the velocity DA/rDA, diffusion, and mobility of the components in the matrix for the self-healing capacity of the material. Smaller inorganic building blocks as well as less viscous polymers generally increase the reaction rates [16]. Core-shell nanoparticles showed slow healing capabilities. Smaller furan-modified spherosilicates could be healed within minutes [17].

The goal of the present study was the systematic investigation of the influence of the polymer matrix viscosity, degree of functionalization, and chain length in reversible cross-linking processes. The nanocomposites analyzed consisted of diene or dienophil modified silica nanoparticles in polysiloxane matrices.

2. Experimental

2.1. Materials

Furan, 10-bromoundec-1-en, triethoxysilane, triphenylphosphine, tetrabromomethane, n-butyllithium (2.5 M in hexanes), butyl methacrylate, isobutyl methyl ketone (IBMK), toluene (abs.), dichloromethane (abs.), and hexamethyldisilazane were purchased from Sigma Aldrich. Silica gel was purchased from Fluka. Alumina oxide 90 active neutral was purchased from Merck Millipore. The polysiloxanes and the Karstedt catalyst (in xylene, Pt 2.1–2.4%) were purchased from ABCR Chemicals. Tetraethyl orthosilicate (TEOS) was provided by Wacker Silicones. Maleic anhydride was purchased from Acros Organics. Zinc chloride was purchased from Grüssing GmbH and purified in boiling dioxane with zinc dust and recrystallized from dioxane. All other chemicals were used without further purification. All synthetic procedures were carried out under inert gas atmosphere applying Schlenk techniques.

2.2. Methods

Fourier transform infrared (FTIR) spectroscopy measurements were performed applying a Bruker Vertex 70 spectrometer under ambient air (40 scans at a resolution of 4 cm^{-1}) in attenuated total reflectance (ATR) mode. Thermogravimetric analysis (TGA) was performed on a Netzsch Iris TG 209C in an alumina crucible heating from room temperature to 700 °C under nitrogen followed by heating to 800 °C under oxygen with a rate of 20 K min^{-1} . Differential scanning calorimetry (DSC) measurements were performed using a Netzsch DSC 204 F1 Phoenix and a TA Instruments Q100 with samples in aluminum crucibles with pierced lids and heated under nitrogen at a rate of 10 K min^{-1} . Solution NMR spectra were recorded with a Bruker Avance 300 spectrometer at 25 °C (^1H at 300.13 MHz, ^{13}C at 75.48 MHz, ^{29}Si at 59.63 MHz). Elemental analysis was performed with a Leco 900 CHN analyzer. Dynamic light scattering (DLS) measurements were performed by noninvasive backscattering with an ALV/CGS-3 compact goniometer system with an ALV/LSE-5003 correlator at a wavelength of 632.8 nm (He–Ne Laser) and at 90 ° goniometer angle. The dispersing media were purified before use applying a syringe filter (200 mesh). The determination of the particle radius was carried out by the analysis of the correlation function by the $g_2(t)$ method followed by a linearized number-weighting (n.w.) of the distribution function. Nitrogen sorption measurements were performed on a Sorptomatic 1900 instrument from Fisons Instruments at 77 K. The samples were degassed under vacuum at 60 °C for at least 2 h prior to measurement. The surface area was calculated according to Brunauer, Emmett, and Teller (BET). Rheological measurements of the polymers and nanocomposites were carried out on an Anton Paar Physica MCR 301 rheometer equipped with a CTD450 convection oven. The silicones were measured in a shear mode and the pressed samples were analyzed in oscillation mode using the CP50

measuring system with 25 mm plate diameter and a plate-to-plate distance of 0.101 mm. Films were compression-molded between baking paper by means of a heatable press (Specac). Transmission electron microscopy (TEM) was carried out using a JEOL JEM-2010 microscope. The samples were attached to Plano S160-3 copper grids by dispersing them in ethanol using an ultrasound cleaning bath, adding 30 μL on the copper grid and evaporating the solvent. Microscope images were recorded under polarized light using an Olympus BX60 microscope equipped with a Sony CCD-Iris color camera.

2.3. Syntheses

2.3.1. 11-Bromo-1-undecene (1) [18]

To an ice-cold solution of 10-undecenol (14 mL, 70.0 mmol) and PPh_3 (20.2 g, 77.0 mmol) in CH_2Cl_2 (abs., 100 mL) was added CBr_4 (23.2 g, 70.0 mmol) portionwise. The solution was stirred at the same temperature for 1 h and concentrated to give a white solid. Hexane was added to the solid, and the mixture was filtered. The solvent was removed in vacuo and the colorless liquid was purified over a pad of silica gel (n-hexane). The filtrate was concentrated, and the residue was distilled to afford 11-bromo-1-undecene. Yield: 16.0 g (70.0 mmol, 100%) colorless oil, bp $90\text{--}91\text{ °C}$ (0.13 mbar). IR 2923, 1640, 994, 910 cm^{-1} . ^1H NMR (300 MHz, CDCl_3) δ 5.80 (ddt, $J = 17, 10, 7\text{ Hz}$, 1H), 5.04–4.88 (m, 2H), 3.40 (t, $J = 6.9\text{ Hz}$, 2H), 2.04 (q, $J = 6.8\text{ Hz}$, 2H), 1.85 (quint, $J = 6.8\text{ Hz}$, 2H), 1.49–1.24 (m, 12H). ^{13}C NMR (75 MHz, CDCl_3) δ 134.3 (C_{allyl}), 109.2 (C_{allyl}), 29.0, 28.7, 27.8, 24.3, 24.0, 23.8, 23.7, 23.1 (C_{alkyl}). CHN ($\text{C}_{11}\text{H}_{21}\text{Br}$) C 55.83% H 8.69% CHN_{theo} C: 56.65% H: 9.01%.

2.3.2. 2-(11-Undecenyl)-furan (2)

THF (abs., 80 mL) was cooled to 0 °C and n-butyllithium (20 mL, 2.5 M solution in hexanes, 48.0 mmol) was added while stirring under argon. Freshly distilled furan (3.4 mL, 50 mmol) was added dropwise, into the n-butyllithium solution. The mixture was stirred for 30 min at 0 °C , then 11-bromo-1-undecene (40.0 mmol, 9.32 g) was added dropwise with vigorous stirring and the mixture was left overnight at room temperature. The reaction was quenched by the addition of saturated NH_4Cl aqueous solution (40 mL) and extracted with ethyl acetate ($3 \times 40\text{ mL}$). The organic phase was separated, dried over MgSO_4 , and the solvent removed in vacuo. The residue purified over silica (n-hexane) resulting in 2-(11-undecenyl)-furan. Yield: 8.80 g, (40.0 mmol, 99%) colorless oil, bp $105\text{--}106\text{ °C}$ (0.13 mbar). IR 2923, 1640, 727 cm^{-1} . ^1H NMR (300 MHz, CDCl_3) δ 7.35 (dd, $J = 1.8, 0.7\text{ Hz}$, 1H), 6.33 (dd, $J = 3.1, 1.9\text{ Hz}$, 1H), 6.06–6.00 (m, 1H), 5.88 (ddt, $J = 16.9, 10.2, 6.7\text{ Hz}$, 1H), 5.12–4.96 (m, 2H), 2.69 (t, $J = 7.6\text{ Hz}$, 2H), 2.11 (dt, $J = 7.0, 3.9\text{ Hz}$, 2H), 1.78–1.65 (m, 2H), 1.54–1.31 (m, 14H). ^{13}C NMR (75 MHz, CDCl_3) δ 156.63 (C_{furan}), 140.68 (C_{furan}), 139.20 (C_{allyl}), 114.25 (C_{furan}), 110.08 (C_{furan}), 104.62 (C_{allyl}), 33.95 (C_{alkyl}), 29.64, 29.61, 29.50, 29.32, 29.27, 29.08, 28.19, 28.11 (C_{alkyl}). CHN ($\text{C}_{15}\text{H}_{24}\text{O}$) C 81.31% H 10.74% CHN_{theo} C: 81.82% H: 10.90%.

2.3.3. 2-Furyl-(undecenyl)-11-triethoxysilane (3)

2-(11-Undecenyl)-furan (2) (9.9 mmol, 2.18 g) and Karstedt catalyst solution (1 μL) were dissolved in toluene (abs., 16 mL). The mixture was heated to 80 °C , then triethoxysilane (10.4 mmol, 1.71 g, 1.92 mL) was added and the temperature was held for 4 h. After cooling to room temperature, the catalyst was removed over neutral Al_2O_3 (1.5 g) and the solvent was removed in vacuo and side products were distilled off at 120 °C at 0.15 mbar, to afford 2-furyl-(undecenyl)-11-triethoxysilan. Yield: 3.80 g (9.90 mmol, 67%). IR 2925, 2973, 1078, 727 cm^{-1} . ^1H NMR (300 MHz, CDCl_3) δ 7.29 (quart, $J = 1.8, 0.8\text{ Hz}$, 1H), 6.27 (dd, $J = 3.1, 1.9\text{ Hz}$, 1H), 5.98–5.94 (m, 1H), 3.82 (dt, $J = 14.0, 4.9\text{ Hz}$, 6H), 2.61 (t, $J = 7.6\text{ Hz}$, 2H), 1.64 (dd,

$J = 14.2, 7.8$ Hz, 2H), 1.34–1.18 (m, 27H), 0.63 (dd, $J = 9.0, 7.1$ Hz, 2H). ^{13}C NMR (75 MHz, CDCl_3) δ 156.80 (C_{furan}), 140.75 (C_{furan}), 110.15 (C_{furan}), 104.64 (C_{furan}), 58.43 (SiOCH_2), 33.34, 32.65, 29.77, 29.68, 29.51, 29.40, 29.34, 28.19, 28.13, 22.91, 18.45 ($\text{SiOCH}_2\text{CH}_3$), 10.54 (CH_2Si). ^{29}Si NMR (60 MHz, CDCl_3) δ -44.75. CHN ($\text{C}_{21}\text{H}_{40}\text{O}_2\text{Si}$) C 65.54% H 10.09% CHN_{theo} C: 65.63% H: 10.12%.

2.3.4. Synthesis of silica nanoparticles

The silica nanoparticles were synthesized according to a modified literature procedure [19]. Methanol (500 mL) was mixed with aqueous ammonia (33%, 5.0 mmol, 255 mg) and water (9.9 g, 550 mmol) and stirred for 10 min. Then TEOS (52.05 g, 250.0 mmol) was added. The solution was stirred for two days, and a small part of the particles was isolated to characterize the unmodified sample. Therefore the particles were precipitated with 10 mL of hexane and 5 mL of diethyl ether. Afterwards they were isolated and washed three times with ethanol by centrifugation at 13,000 rpm and dried overnight in a vacuum oven (≈ 50 mbar) at 60 °C. The remaining particle solution was transferred to *iso*-butyl methyl ketone (IBMK) by adding the high boiling solvent (500 mL) to the methanol solution and removing methanol in vacuo [20]. For a complete exchange, IBMK (250 mL) was added and again 250 mL solvent was removed. This was repeated three times to afford 250 mL particle suspension in IBMK containing 15 g SiO_2 nanoparticles. CHN (SiO_2) C: 6.14%, H: 2.16%, N: -; DLS: diameter in methanol 5.95 ± 0.4 nm, diameter in IBMK 8.8 ± 0.4 nm. BET $755 \text{ m}^2/\text{g}$.

2.3.5. Functionalization of silica nanoparticles [21].

The IBMK-silica nanoparticle suspension (16.67 mL, containing 1.0 g SiO_2 -nanoparticles) was diluted with IBMK (60 mL) and the appropriate coupling agent (FUTES (3) or MPTES (4), 4.31 mmol) was added. The resulting dispersion was stirred at 115 °C for 24 h. After the reaction, the dispersion was concentrated to $\frac{1}{2}$ volume and the particles were isolated and washed three times with ethanol by centrifugation at 13,000 rpm.

MPTES@ SiO_2 : Yield: 0.92 g. IR 1704, 1369, 696 cm^{-1} ; CHN (MPTES@ SiO_2) C: 15.75% H: 2.52% N: 1.12%; DLS: diameter 63.3 ± 0.23 nm. BET $615 \text{ m}^2/\text{g}$. TEM: see Fig. 2.

FUTES@ SiO_2 : Yield: 0.84 g. IR 2978–2852, 1418, 721 cm^{-1} ; CHN (FUTES@ SiO_2) C: 12.60% H: 2.38% N: -; DLS: diameter: 68.1 ± 0.3 nm. BET $654 \text{ m}^2/\text{g}$.

2.3.6. Hydrosilation of polysiloxanes (S1–S4)

The amount of Si–H was determined by ^1H NMR spectroscopy and the vinyl-compound was used in equimolar ratio. 2-(11-Undecenyl)-furan (2) was dissolved in toluene (abs., 10 mL (S1–S3), 20 mL (S4)), the Karstedt catalyst solution (3 μL) was added and the mixture was heated to 100 °C. Then the appropriate polysiloxane was added and the temperature was held for 5–12 h. After that, the solvent was removed in vacuo to afford the furan functionalized polysiloxanes. Completion of the reaction was monitored via IR, ^1H NMR (Supp. Inf.). Rheological measurements were performed.

2.3.7. Synthesis of maleimidopropyl-modified polydimethylsiloxanes (S5–S6)

The amount of Si–(CH_2) $_3$ NH $_2$ was determined by ^1H NMR spectroscopy and the maleic anhydride was used in equimolar ratio. A solution of aminopropyl-modified PDMS (α,ω -diaminopropyl-PDMS or aminopropylmethylsiloxane-dimethylsiloxane copolymer) in CH_2Cl_2 was added dropwise to dissolved maleic anhydride in CH_2Cl_2 . The resulting solution was stirred for 1 h. Afterwards, the solvent was removed in vacuo. The resulting viscous liquid was dissolved in toluene (abs.), and ZnCl_2 was added as the mixture was heated to 80 °C. After the addition of hexamethyldisilazane, the

reaction was continued for 18 h. First, the solid was removed by centrifugation (8000 rpm, 10 min), then the solvent was removed in vacuo. The reaction was monitored via IR, ^1H NMR (Supp. Inf.). Rheological measurements were performed.

2.3.8. Synthesis of siloxane-nanoparticle-composite materials

Polysiloxanes (S1–S6) respectively the cofunctionalized polybutylmethacrylates (CP1–CP2) and modified particles were mixed in a molar ratio of 5:1 of reactive groups in IBMK (Table 1). The solvent was removed in vacuo and the resulting solid was cured at 120 °C, for 12 h. Films were compression-molded between baking paper by means of a heated press at 120 °C for 10 min and 60 °C for 30 min under a pressure of 2 tons. Afterwards the samples were quenched to 20 °C.

2.3.9. Synthesis of polysiloxane-nanoparticle-composite materials in chloroform

The particles and the polysiloxanes were mixed in the same ratios which are given in Table 1. The starting materials were reacted in 6 mL of chloroform at 60 °C for 12 h. Afterwards the solvent was removed to obtain the composite material.

3. Results and discussion

N-((3-Triethoxysilyl)propyl)maleimide (MPTES, 4) [22], furfuryl methacrylate (FMA, 5), the protected maleimide monomer - 3-(3,5-dioxo-10-oxa-4-azatricyclo[5.2.1.0 $_2$,6]dec-8-en-4-yl)-propyl 2-methylprop-2-enoate (pMiMA, 6), poly[(butyl methacrylate)-co-(protected maleimidopropylmethacrylate)] (pMiMAcoBMA, P1) and FMAcoBMA (P2) were synthesized using literature known procedures [16,21].

3.1. Synthesis and characterization of silica nanoparticles

Spherical amorphous silica nanoparticles were synthesized according to a modified Stöber process [19]. Tetraethyl orthosilicate (TEOS) was hydrolyzed and condensed in methanol while using aqueous ammonia solution as a catalyst. Dynamic light scattering (DLS) measurements in methanol showed a diameter of the final particles of 5.95 ± 0.4 nm (Fig. 1).

The surface functionalization was carried out applying a solvent-exchange method, which results in a high surface coverage and a low agglomeration of the modified silica particles [20]. In this procedure, IBMK was added to the freshly prepared silica particles in methanol and the methanol was subsequently removed in vacuo. Using IBMK as the medium during the modification results in ionized OH-groups due to the high dielectric constant of the solvent ($\epsilon = 13.1$). The high boiling point of 115 °C makes the functionalization possible at increased temperatures which favors the elimination of ethoxy groups and condensation of silane coupling agents (FUTES (3) or MPTES (4)).

Table 1
Composition of nanocomposites with S1–S6.!

Composite	Polymer	Particle	wt% particle
C1	S1: 0.5 g	MPTES@ SiO_2 : 0.27 g	54
C2	S2: 0.5 g	MPTES@ SiO_2 : 0.09 g	18
C3	S3: 0.5 g	MPTES@ SiO_2 : 0.57 g	114
C4	S4: 0.5 g	MPTES@ SiO_2 : 1.43 g	286
C5	S5: 0.5 g	FUTES@ SiO_2 : 0.09 g	18
C6	S6: 0.5 g	FUTES@ SiO_2 : 0.14 g	28

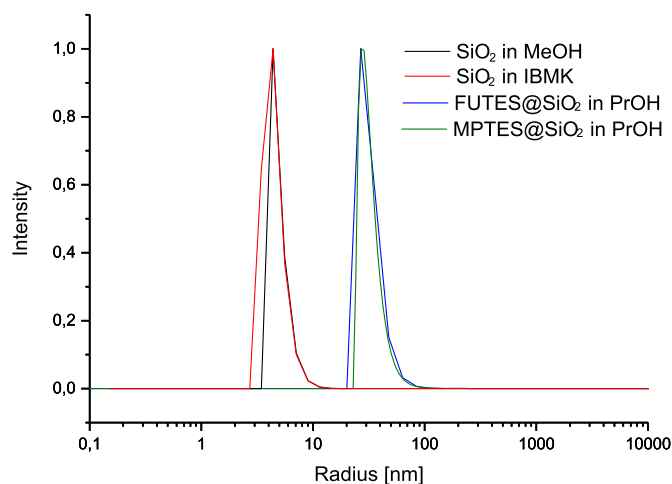


Fig. 1. DLS size distribution of SiO₂ particles before and after solvent exchange and after modification.

3.2. Coupling agents

The two different coupling agents, 2-furyl-(undecenyl)-11-triethoxysilane (FUTES (3)) and *N*-((3-triethoxysilyl)propyl)maleimide (MP TES (4)), were used for surface modification of the nanoparticles. The triethoxysilane group acts as anchoring group on the surface of the nanoparticles and the maleimide or furan, respectively represents the corresponding groups for the reversible DA/rDA reaction with the polymer or siloxane. MP TES (4) was synthesized according to a literature procedure (Scheme 1) with an overall yield of 96% [22].

FUTES (3) was prepared in a three-step synthesis (Scheme 2). The first step is the exchange of the OH-group against a bromo-substituent using PPh₃ and CBr₄ in an Appel-reaction to afford 11-bromo-1-undecene (1) [18,23]. In the second step, furan was deprotonated in 2-position with *n*-butyllithium at 0 °C in THF. Adding 1 dropwise to the 2-lithiumfuranid results in the desired 2-(11-undecenyl)-furan (2) in 99% yield. A selective hydrosilylation at the terminal double with triethoxysilane using the Karstedt catalyst creates the desired product. The furan double bonds show a lower reactivity, because of the aromaticity of the ring, which is the reason for the selectivity of the hydrosilylation reaction for the terminal bond.

3.3. Surface modification and characterization

After modification of the silica particles in IBMK, the particles were isolated and redispersed in 1-propanol for DLS measurements. An increasing hydrodynamic radius of the particles in DLS measurements proves the organic surface modification (Fig. 1). The redispersability is important to make sure that the functional groups are available for the DA-reaction in the nanocomposites. The particles reveal almost the same size after solvent exchange

(Fig. 1) whereas the functionalized particles show a much larger hydrodynamic radius (MP TES@SiO₂ 63.3 ± 0.23 nm; FUTES@SiO₂ 68.1 ± 0.3 nm) but the size distribution remains small after modification.

TEM analysis of MP TES@SiO₂ proves that the particles still have a diameter of about 5 nm, as they had before modification (Fig. 2). Due to low contrast and partial decomposition of the organic functionalization in the electron beam, only the inorganic particle cores are visible in the image. The DLS investigations displayed much higher values due to the organic surface modification, which interacts with the relatively polar solvent 1-propanol.

Nitrogen sorption measurements (BET) reveal a surface area of 755 m²/g before surface modification, and a slightly reduced value of 654 (FUTES@SiO₂) and 615 m²/g (MP TES@SiO₂), respectively afterwards. Potential reasons for the decrease in surface area are the blocking of pores and the lower interaction of the nitrogen molecules with the organically functionalized surface.

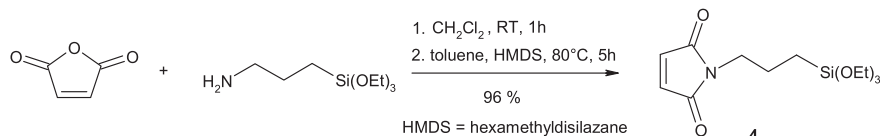
The FTIR analysis of the particles shows the success of the functionalization (Figs. 3 and 4). All samples reveal the typical Si–O-peaks in the area of 1200–600 cm⁻¹. The Si–O–Si vibration at 1100 cm⁻¹ was used to normalize the absorbance.

The FTIR spectra of MP TES@SiO₂ display the characteristic signal for this coupling agent [21]. At 1704 cm⁻¹ is a strong signal for the asymmetric stretch vibration of the C=O-bond. The symmetric C–N–C-bond at 1369 cm⁻¹ and the ring deformation peak at 696 cm⁻¹ proves the successful modification with maleimide.

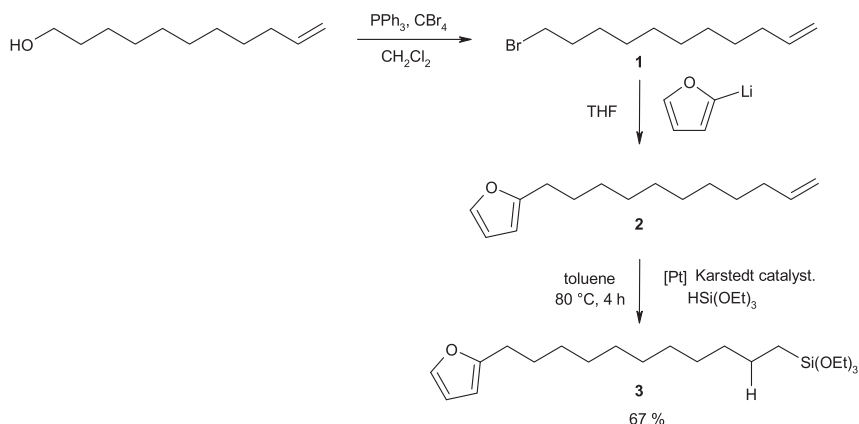
In case of FUTES-modification the strong band at ~3000–2850 cm⁻¹ indicates the successful functionalization as well as the C–H-deformation vibration at 1418 cm⁻¹. The peaks at 3000–2900 cm⁻¹ of pure silica particles before modification belong to the remaining ethoxy groups (CH₂ and CH₃ vibrational modes) on the surface from TEOS. The furan ring deformation is visible at 721 cm⁻¹.

TG and CHN analysis was used to determine the surface coverage of the organic groups on the silica particles.

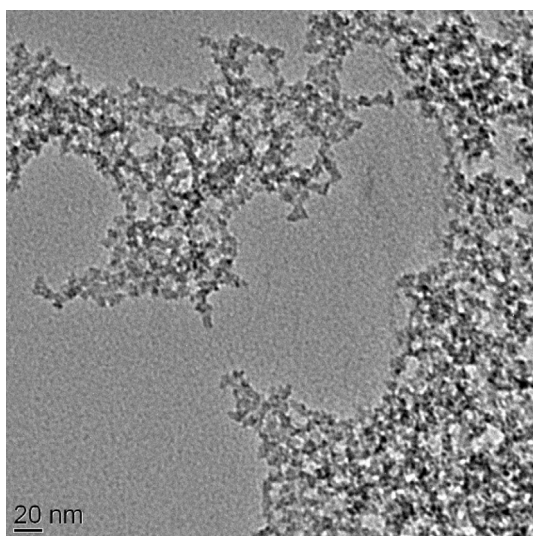
TGA analysis of MP TES@SiO₂ and FUTES@SiO₂ (Fig. 5) was carried out by heating the samples to 700 °C under nitrogen, and from 700 to 800 °C under oxygen. In case of MP TES functionalization an overall mass loss of 28.46% was obtained while in case of FUTES the mass loss was 18.84% [21,24]. Using the CHN analysis of the functionalized nanoparticles (MP TES@SiO₂ C: 15.75 H: 2.52 N: 1.12; FUTES@SiO₂ C: 12.60 H: 2.38; SiO₂: C: 6.14 H: 2.16), the surface coverage can be determined for MP TES@SiO₂ [21]. In case of FUTES@SiO₂ the surface coverage was evaluated using the molar mass of the organic compound on the surface and the residual mass from TGA. For MP TES a surface coverage of 1.23 molecules/nm² (1.26 mmol/g) was obtained and in case of FUTES 0.79 molecules/nm² (0.86 mmol/g). Previous experimental results in our group determined that sterical hindrance in chemisorption of end group functionalized long alkyl chain coupling agents can play a crucial role for the surface coverage compared to the short chain coupling agents. On the other hand we think that there is an advantage when the surface coverage is less crowded because sterical hindrance of densely packed molecules can hinder the six-



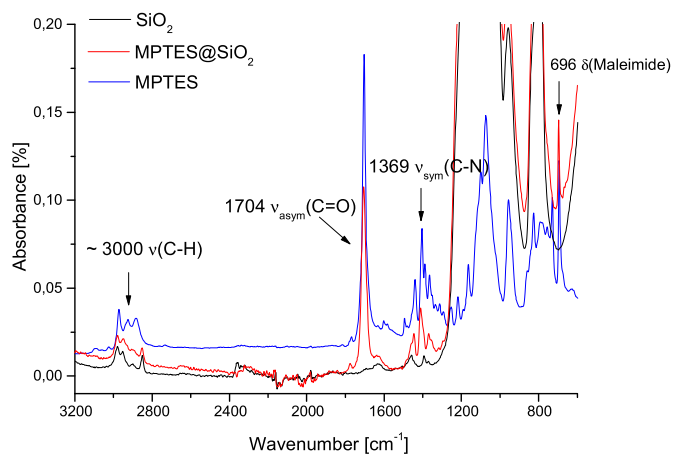
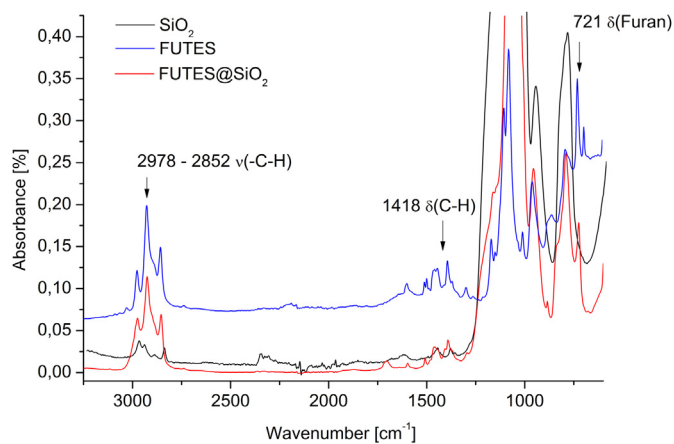
Scheme 1. Preparation of MP TES (4).



Scheme 2. Preparation of FUTES (3).

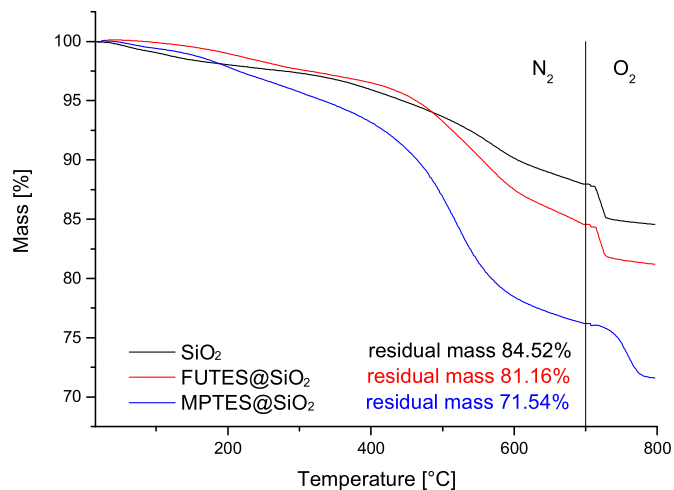
Fig. 2. TEM image of MPTES@SiO₂.

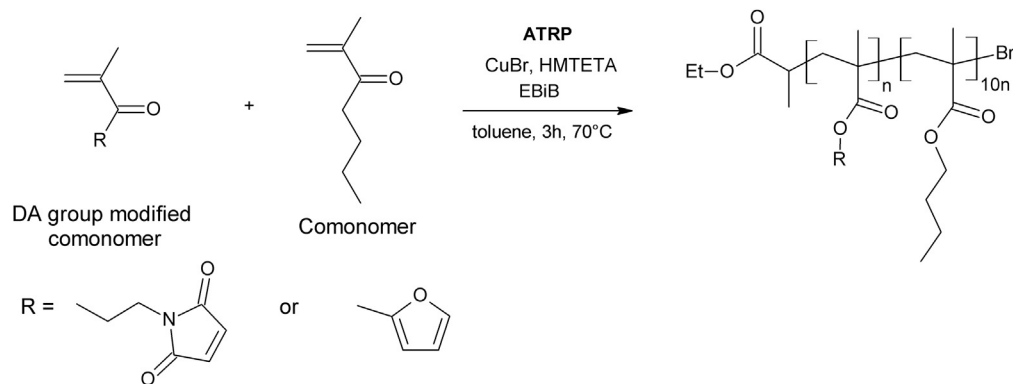
membered transition state required for passing the Diels-Alder reaction as we showed in a previous study [21].

Fig. 3. FTIR of SiO₂ particles and MPTES@SiO₂.Fig. 4. FTIR of SiO₂ particles and FUTES@SiO₂.

3.4. Synthesis of MiMacoBMA and FMAcoBMA (P1&P2)

The modified butylmethacrylat (BMA) polymers (maleimide modified **P1**, furan modified: **P2**) were synthesized referring to a literature procedure applying a copper catalyzed atom transfer radical polymerization (ATRP) using 1,1,4,7,10,10-hexamethyl-triethylenetetramine (HMTETA) as a ligand (Scheme 3) [16].

Fig. 5. TGA curves of MPTES@SiO₂ and FUTES@SiO₂.



Scheme 3. Synthesis of DA-group modified polybutylmethacrylates **P1** and **P2** [16].

Furfurylmethacrylat and protected maleimidopropylmethacrylat were used as comonomers in the polymerization reaction.

By choosing the amount of diene or dienophil-bearing comonomers the degree of substitution was tailored. The BMA to FMA respectively MiMA ratio was 10:1 which was verified by ^1H NMR spectroscopy [16].

3.5. Synthesis of undecenylfuran- and *N*-propylmaleimide modified polydimethylsiloxanes (**S1–S6**)

Commercially available H-terminated polydimethylsiloxanes (**S1–E** & **S2–E**), methylhydrosiloxanedimethylsiloxane copolymers (**S3–E**) (SiMe_3 terminated), and polymethylhydrosiloxanes (**S4–E**) (SiMe_3 terminated) were treated with 2-(11-undecenyl)-furan (**2**) in a hydrosilylation reaction applying Karstedt catalyst in toluene (Scheme 4) at 100 °C to reach quantitative yield. In case of polymethylhydrosiloxanes the reaction time had to be increased to 12 h and a twofold amount of solvent was used, because the system gets highly viscous during the reaction.

The hydrosilylation reaction was monitored using ^1H NMR and IR-spectroscopy (see Supp. Inf.). The disappearance of the Si–H-bond vibration at 2200–2100 cm^{-1} indicates the completion of the reaction (Fig. 6). ^1H NMR spectroscopy shows also the successful modification of PDMS (see Supp. Inf.) due to the disappearance of Si–H and vinyl-H signals. Furthermore, the signals for the furyl group and the alkyl chain can be identified.

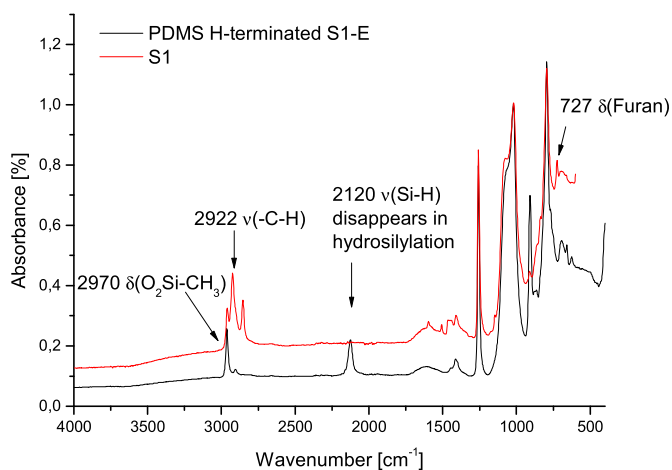
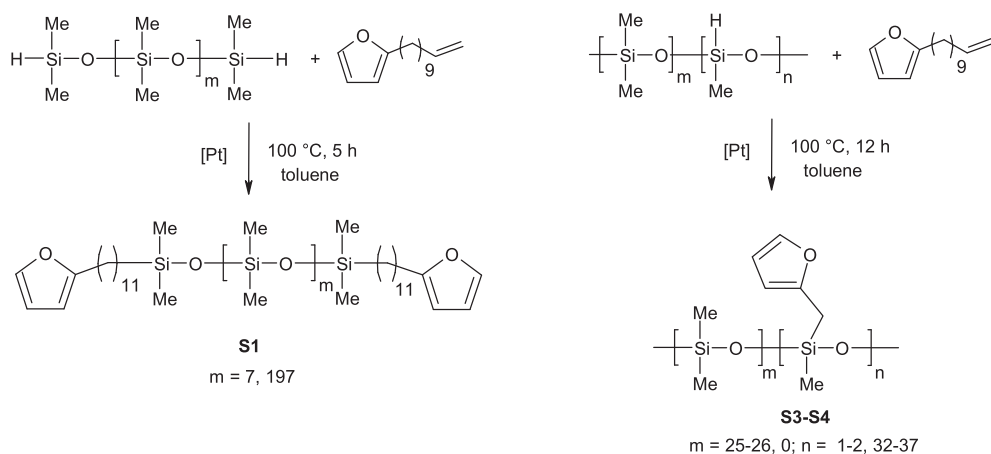
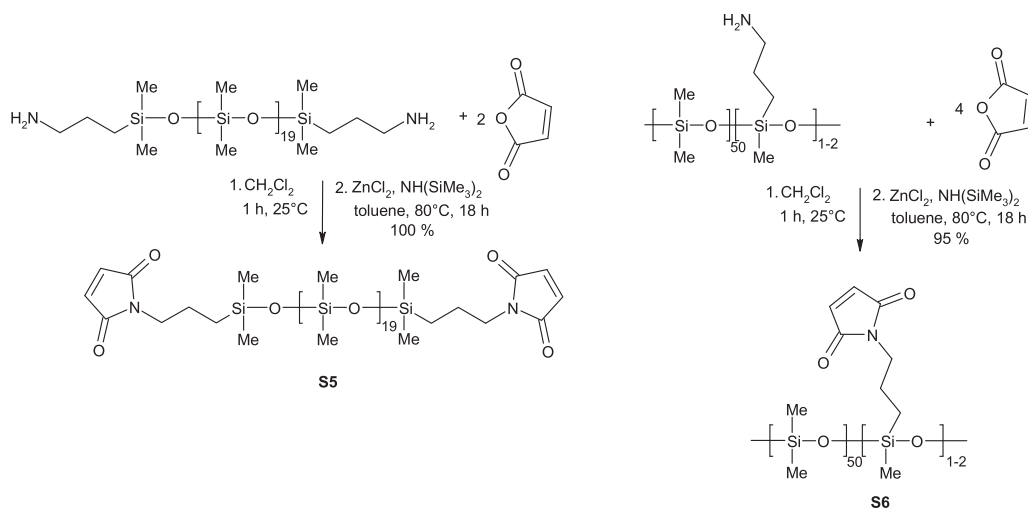


Fig. 6. FTIR spectra of H-terminated PDMS **S1** before and after modification with 2-(11-undecenyl)-furan (**2**).

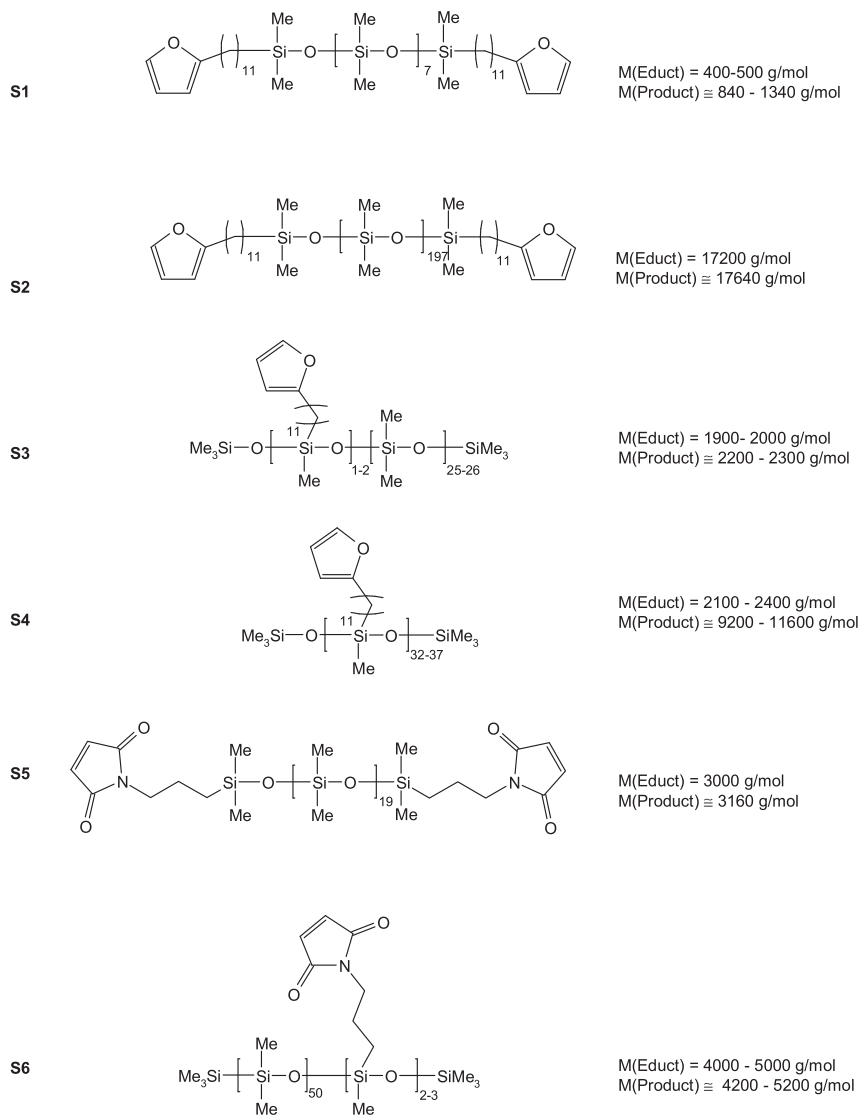
α,ω -Diaminopropyl-PDMS and aminopropylmethylsiloxane-co-dimethylsiloxane copolymer were modified according to a literature procedure to afford the maleimidopropyl-PDMS (Scheme 5) [3c,13,17]. In the first step, the aminopropyl-PDMS was treated with maleic anhydride followed by a ring closure with zinc chloride and hexamethyldisilazane.



Scheme 4. Preparation of furan-modified PDMS (**S1–S4**).



Scheme 5. Preparation of α,ω -bismaleimidopropyl-PDMS (**S5**) and maleimidopropylmethylsiloxane-co-dimethylsiloxane copolymer (**S6**).



Scheme 6. Overview of modified polysiloxanes **S1**–**S6**.

Table 2
Viscosities according to Fig. 7 and the quotients of change in viscosity.!

Polymer	η_{modified} [Pa s]	$\eta_{\text{unmodified}}$ [Pa s]	$\frac{\eta_{\text{modified}}}{\eta_{\text{unmodified}}}$
S1	5.6×10^{-3}	4.8×10^{-4}	11.65
S2	1.05	2.3×10^{-1}	4.57
S3	1.8×10^{-2}	1.4×10^{-2}	1.28
S4	16.78	2.7×10^{-2}	621
S5	5.6×10^{-1}	4.7×10^{-2}	11.91
S6	8.6	8.3×10^{-2}	104

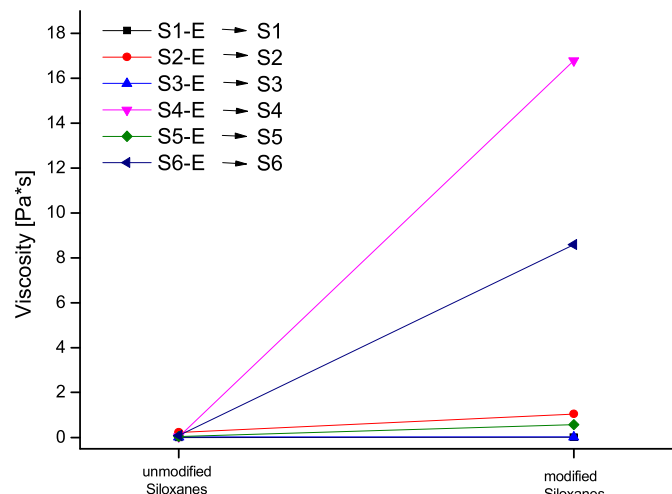


Fig. 7. Viscosity of the PDMS polymers before and after DA group modification (S1–S6).

Because of the macromolecular nature of the compounds, the ring closing time has to be increased from 5 h for molecular systems to 12 h. The ring closure occurred in quantitative yield for α,ω - and in 95% for aminopropylmethylsiloxane-dimethylsiloxane. The yield was determined by ^1H NMR spectroscopy.

Scheme 6 gives an overview of all DA-group modified polysiloxanes (S1–S6) (IR and ^1H NMR see Supp. Inf.).

3.6. Rheological measurements of polysiloxanes

Viscosity is dependent on the molecular mass and the degree of substitution in the functionalized polysiloxanes. As described in literature, unmodified polydimethylsiloxanes show viscosities between 2 and 3 mPa s up to 10,000 mPa s at a molecular weight between 400 and 500 g/mol and 62,000 g/mol, respectively [25]. These values show, that the viscosity depends more on the molecular weight than on the molecular structure. By modifying the polysiloxanes with furan and maleimide moieties, the molecular weight increases (Scheme 5) which is generally correlated with an increase of viscosity. However, one has to distinguish between a terminal substitution and a side chain substitution. In the as

Table 3
Viscosities according to Fig. 8 and the quotients of change in viscosity.!

Composite	$\eta_{\text{comp. before DA}}$ [Pa s]	$\eta_{\text{comp. after DA}}$ [Pa s]	$\frac{\eta_{\text{comp. after DA}}}{\eta_{\text{comp. before DA}}}$
C1	1183	4800	4.06
C2	765	4710	6.16
C3	747	3270	4.38
C4	927	1330	1.43
C5	297	947	3.19
C6	161	3482	21.69

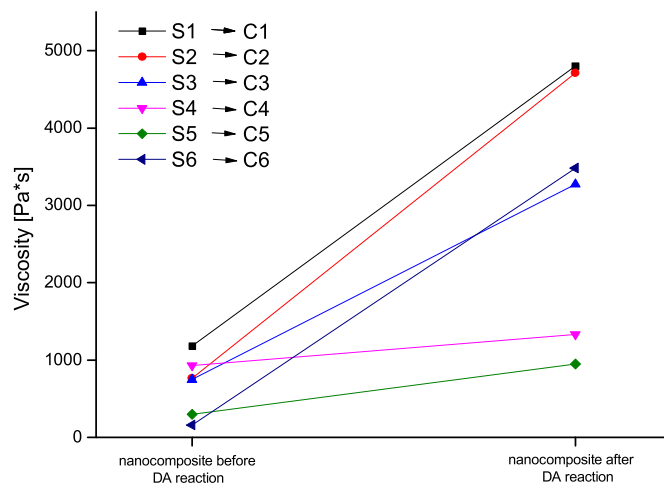


Fig. 8. Viscosity composites (C1–C6) before and after DA reaction.

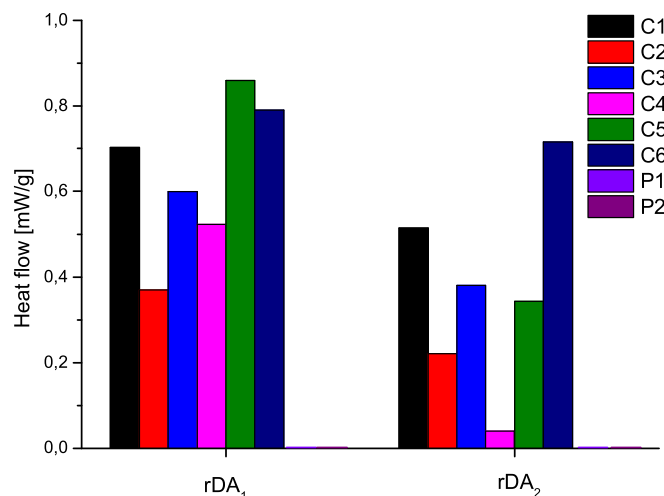


Fig. 9. DSC values of heat flow in nanocomposites. Samples C1–C6: polysiloxane nanocomposites, samples CP1, CP2: poly(butyl methacrylate) nanocomposites.

prepared samples an end group modification shows less change in viscosity than a side chain modified sample (S1 vs. S3 and S5 vs. S6, Table 2). Here the degree of functionalization has a major influence on the rheological properties of the materials.

The results show a small increase of viscosity from unmodified to modified polysiloxanes in case of the terminal substituted polysiloxanes (S1, S2, S5), while side chain modification leads to a substantial increase of viscosity (S4 and S6). In case of S3 the effect was not obvious based on the small degree of substitution and therefore the small change in molecular mass. Compared to α,ω -end-group functionalization the side group functionalization

Table 4
Quotients of DSC values of heat flow in nanocomposites.!

Composite	$\frac{rDA_2}{rDA_1}$
C1	0.73
C2	0.41–0.59
C3	0.30–0.62
C4	0.08–0.61
C5	0.40
C6	0.91

Table 5
Quotients of DSC values of heat flow in nanocomposites.†

Composite synthesized in CHCl_3	rDA_2/rDA_1
C1 _{CHCl₃}	0.40
C2 _{CHCl₃}	0.36
C3 _{CHCl₃}	0.27
C4 _{CHCl₃}	0.44
C5 _{CHCl₃}	0.89
C6 _{CHCl₃}	0.84

increases the molecular weight more drastically and also the interaction between the polymer chains increases.

3.7. Rheological measurements of nanocomposites

The composites **C1–C6** (see [Experimental](#)) were studied in rheological measurements before and after the DA reaction. Non-crosslinked film samples were prepared by pressing the polymers at 2 tons at room temperature between two silicium stamps. The measurements of the crosslinked nanocomposites were conducted on 250 μm films, which were prepared with a heated press by sequential heating to 120 °C for 2 min, cooling to 60 °C, and holding this temperature for 30 min.

In all cases (**C1–C6**) the diene or dienophile in the polymer was in a five-fold excess compared to the functional groups on the particle surface, because a non-stoichiometric ratio increases the probability of new crosslinks after damage [15]. Ren and Yoshie et al. described that the best healing efficiency was achieved by using a six-fold excess of furan to maleimide [15]. They used a furan substituted polymer with different short maleimide crosslinkers. Transferred to our studied systems, in which the silica nanoparticles are the crosslinking agents, it means that the excess of diene/dienophile should be provided by the polymer (see [Table 1](#), [Experimental](#)).

Comparing the rheological measurements of modified polysiloxanes, with the polysiloxanes after adding the nanoparticles, the viscosity increased about 100 times without crosslinking. This is a filler effect due to the interaction of the polymer chains with the surface of the particles. After the DA reaction, there was an additional increase of viscosity, due to crosslinking of the nanoparticles with the polysiloxanes. All samples show an increase of viscosity, which can be explained by the small and flexible linear polymer chains. Samples **C6** and **C3** are both block copolymers, thus the

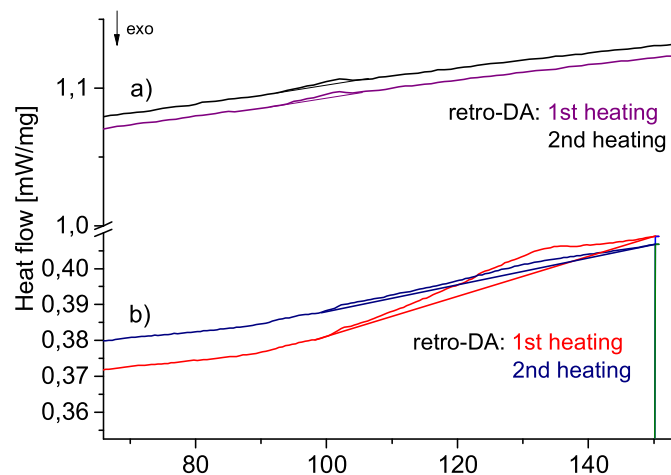


Fig. 10. DSC curves of previously cured a) FUTES@SiO₂ with MiMaCoBMA (**CP1**) nanocomposite and b) FUTES@SiO₂ with α,ω -PDMS nanocomposite (**C5**).

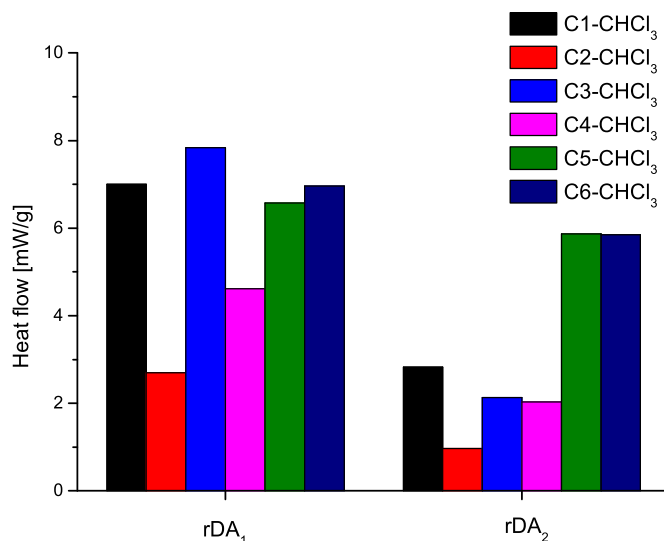


Fig. 11. DSC values of heat flow in nanocomposites samples **C1**_{CHCl₃}–**C6**_{CHCl₃}.

functionalized block crosslinks while the non-functionalized block provides the sample with flexibility during crosslinking. In **C6** the increase of viscosity is more significant, because of the **C11** spacer on the used modified silica nanoparticles, which can result in a higher crosslinking. Sample **C4** provides the lowest increase of viscosity. In this case a high filler concentration was necessary to obtain the best ratio of crosslinking groups. Therefore the effect of crosslinking is not so dominant compared to the other systems.

3.8. DSC Measurements of composites

Cyclic differential scanning calorimetry (DSC) measurements were performed to study the thermally reversible DA crosslinking of the siloxane nanocomposites **C1–C6** (see [Table 3](#)). For reasons of comparison two additional samples of acrylate based composites (**CP1** & **CP2**) were also analyzed. **CP1** consists of FUTES@SiO₂ in maleimide modified poly (butyl methacrylate) **P1** and **CP2** consists of MPTES@SiO₂ in the furan modified derivative **P2**. [Fig. 9](#) shows the comparison of energy consumption in the first and second cycle of rDA reaction of the composites **C1–C6** and **CP1** & **CP2**. All measurements only show small values for the energy consumption and we expect quite high standard deviations (which is shown by repeated measurements). The quotients of the repeated measurements are given in [Table 4](#) as ranges. However, a general trend is that the second healing cycle shows less energy consumption



Fig. 12. Image of nanocomposite **C6** prepared in a teflon mould.

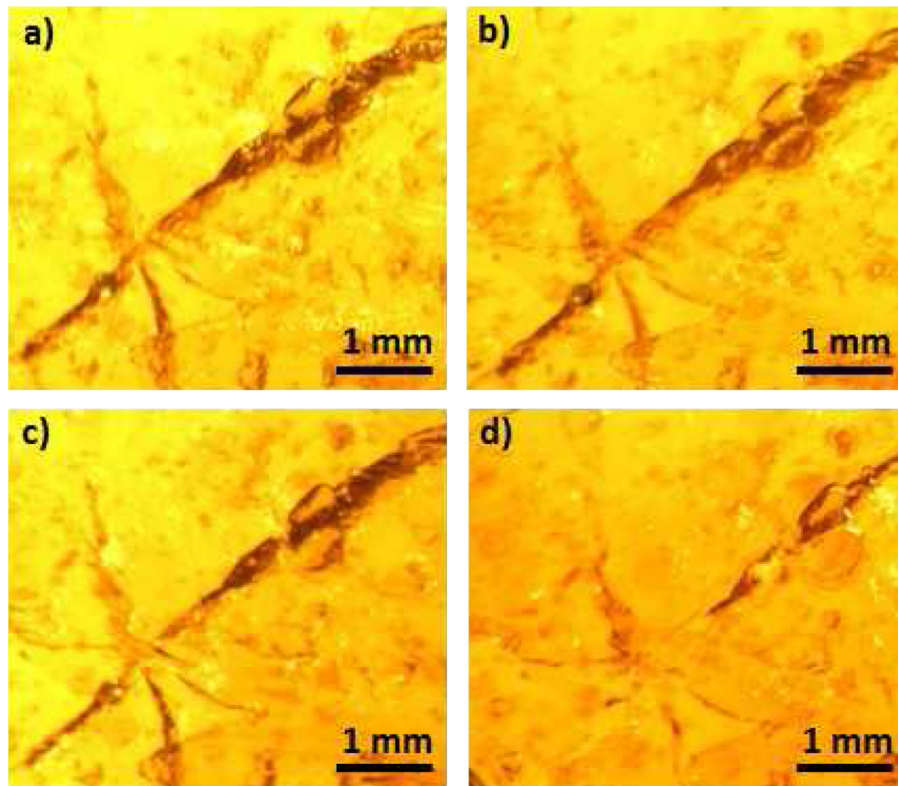


Fig. 13. Microscope images of a cut in nanocomposite **C6** (a) before healing, (b) after heating for 1 h to 60 °C, (c) after heating for 30 min at 120 °C and (d) after heating for 15 min at 120 °C and dropwise adding of CHCl_3 .

(Fig. 9, Table 4) compared to the first. One potential reason is the lack of complete decrosslinking in the first cycle, therefore the composite does not reach the originally condition and a result is less flexibility and mobility of the single components. In conclusion, the DA groups do not have as much corresponding groups in their surrounding as before and the conversion in the second cycle is lower.

The quotient of the heat flow into the nanocomposites for the second to the first rDA reaction can be used to evaluate the self-healing capacity. All samples show a smaller signal in the second cycle. From the values in Table 4 it is obvious that the structure of the polymer and the molecular weight also have a major influence on the self-healing cycles. The best value shows the low molecular weight α,ω -furan functionalized polysiloxane composite (**C1**). The smallest values in the self-healing capacity were detected in case of high filler concentrations (**C4**) and high crosslinking densities.

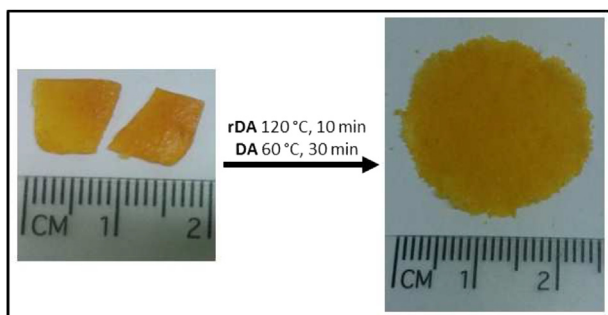


Fig. 14. Reshaping of a broken specimen from teflon mould in the heated press to a 500 μm film.

Fig. 10 shows the heating curve of DSC analysis of **CP1** and **C5**. To crosslink the material the nanocomposites were first heated to 120 °C for 10 min and cured at 60 °C over 12 h in a teflon mould. DSC of the crosslinked nanocomposites show a broad endothermic signal between 90 and 150 °C with an onset temperature of about 100 °C, originating from the rDA reaction (Fig. 10) [16,21]. After cooling the sample with a rate of 10 K/min from 150 °C to –50 °C, the second heating cycle shows a smaller signal which can be explained in the slow formation of DA-bonds during cooling. However, the DSC measurements show the reversibility and provide a measure for the self-healing capacity of the materials.

When using polysiloxanes, the DA/rDA takes place reversibly, whereas using the thermoplastic butyl methacrylate polymers in case of MPTES@SiO₂ with the C3-spacer no DA reaction could be observed. Increasing of the spacer length to C11 with FUTES@SiO₂, a small signal at 100 °C could be detected (Fig. 10a). The reason for the small conversion in case of thermoplastic butyl methacrylates with the modified inorganic nanoparticles, and thus the limited self-healing capacity of this nanocomposites, is most likely the poor mobility of the polymer chains, which causes that the DA groups cannot approach each other in the material. Furthermore, as shown previously there is a sterical hindrance on the particle surface itself, because the DA reaction needs a six-membered transition state to pass the [4 + 2] cycloaddition [21]. The modified particles carry 0.79–1.23 molecules/nm², which is a relatively high surface coverage. The bulky Diels-Alder groups are getting close to each other at the end of the alkyl chain. The used elastomeric polysiloxanes have the advantage that they are lower in viscosity and have smaller molecular masses resulting in a significantly higher conversion in the DA/rDA reaction. However, we expected a more pronounced conversion. To underpin the importance of the group mobility in the self-healing materials we performed the DA

reaction of the composite in solution (CHCl_3 , 60 °C, 12 h). In this case the DSC measurements display at least 10 times higher conversion (Fig. 11, Table 5).

Crosslinking the nanocomposites in chloroform lead to a distinctly higher conversion in general, whereby the quotient of $r_{\text{DA}_2}/r_{\text{DA}_1}$ is similar, except of sample **C4**, due to the high filler concentration as mentioned before. This means, when the DA groups once found each other and are pre-organized, the amount of reacting groups is crucially increased, but the self-healing capacity of the material itself remains or seems to be lower by taking into account the high standard deviation in samples **C1–C6** as mentioned before. One explanation for a lower healing capability is that in the solid state reaction, many of the Diels-Alder groups remain free, so it is easier to find a new reaction partner for the molecules. After the reaction in solvent, the most available dienes and dienophiles reacted probably, and due to the incomplete decrosslinking, the conversion of DA reaction in the second cycle is lower.

Thus these results show that the distance between functional groups (on the particle surface, which can be varied by spacer length and in the polymer, which can be varied by using terminal substituted chains, block copolymers or homopolymers), have an important influence on the DA/rDA reaction in nanocomposites. But the decisive role for the self-healing ability, when working without solvent, seems to be the flexibility and mobility of the polymers. Contrary to the thermoplast systems, in all experiments with the polysiloxane backbone the rDA-reaction could be clearly observed.

3.9. Damage healing of nanocomposites by thermal treatment

To prove the healing ability, the nanocomposite **C6** (Fig. 12) was deliberately cutted, and the damage was thermally treated at 60 °C for 1 h, then 120 °C for 15 min and afterwards treated at 60 °C for 1 h by adding a drop of CHCl_3 every 10 min (Fig. 13). After thermal treatment, the cut were only slightly healed, because the DA groups cannot come into contact. But helping the material to be more flexible by adding chloroform on the cut, the cut disappears nearly completely (Fig. 13d).

This observation is similar to what was found in literature: “a heavily scratched surface of nanocomposite could be healed after thermal treatment, but the scratched surface remained unhealed due to the material loss during scratching. This results suggest that healing takes place only when the damaged parts are closely contacted during heat treatment.” [26] In our case the material cannot close the cut by itself so that the contact is provided by adding solvent.

Another experiment to prove the self-healing ability of the nanocomposite is to reshape a specimen. Therefore, **C6** which was used before for the cutting test, was broken and two parts of it were reshaped in the heated press (Fig. 14). For this experiment, it is necessary to decrosslink the DA groups first at 120 °C in 10 min and crosslink them again at 60 °C in 30 min. In the heated press, a pressure of 2 tons provides the contact of the DA moieties, so that no solvent is necessary for the reshaping.

4. Conclusions

Several new nanocomposites were synthesized by crosslinking of poly (butyl methacrylates) and structurally varied polysiloxanes with surface modified silica nanoparticles via the Diels-Alder reaction. The molecular structure of the coupling agent, especially the spacer length, on the nanoparticle surface plays a key role in determining the healing properties, which was observed by comparing **C3** (MPTES@SiO_2) and **C11** spacer (FUTES@SiO_2) in

poly(butyl methacrylates). Long spacer groups with lower molar amount of coupling agent on the particle seem to be favorable for the six-membered transition state of the Diels-Alder reaction. The more important aspect in self-healing properties and capacity is the nature of polymer as well as its chain length and the type of the polymer. In this study linear and differently branched polysiloxanes were compared. It was shown that terminal modified polymers are more favorable for the use in nanocomposites, because of their high mobility and a lot of space in surrounding of the Diel-Alder moieties. Block copolymers and homopolymers are less suitable, because the mobility of the functional groups is governed by the typical diffusion mechanism of polymeric chains.

Comparing the crosslinking of the elastomeric composites **C1–C6** in solid state with our observations using furan-modified spherosilicates crosslinked with α,ω -bismaleimido-PDMS [17], the heat flow with nanoparticles in this material is just about 10%. But comparing with **C1**_{CHCl3}–**C6**_{CHCl3} which were synthesized in chloroform, nearly the same conversions could be reached, although modified silica particles are less mobile than the molecular spherosilicates. The inorganic core-shell nanoparticles synthesized via ATRP, crosslinked with poly (butyl methacrylates) in previous work [16] showed a higher conversion in the first rDA than **C1–C6**, but the quotient $r_{\text{DA}_2}/r_{\text{DA}_1}$ there is only 0.25. That means, that most of the new polysiloxane nanocomposites have a better self-healing capability than the previously presented system. What has to be taken into account is that nanoparticles provide considerable possibilities, for example when magnetite is used. Then healing can be realized by an alternating external magnetic field, which provides the heat for self-healing. This concept will be shown in a future paper.

Acknowledgments

This work is supported by the German Research Society (DFG) through the priority program “Design and Generic Principles of Self-healing Materials” SPP 1568 (<http://www.spp1568.uni-jena.de/>) grant number KI 1066/2-1. The authors thank Prof. Wulff Possart, Saarland University for the help with DSC measurements.

Appendix A. Supplementary data

Supplementary data related to this article can be found at <http://dx.doi.org/10.1016/j.polymer.2015.03.017>.

Supporting Information

IR and ¹H NMR spectroscopic data of modified polysiloxanes and of the synthesized compounds **1**, **2** and **3**.

References

- [1] Burattini S, Greenland BW, Chappell D, Colquhoun HM, Hayes W. *Chem Soc Rev* 2010;39:1973–85.
- [2] Kamino BA, Bender TP. *Chem Soc Rev* 2013;42:5119–30.
- [3] a) Chen D-H, Hsieh C-H. *J Mater Chem* 2002;12:2412–5;
b) Liu Y-L, Hsieh C-Y. *J Polym Sci Part A: Polym Chem* 2005;44:905–13;
c) Zhang Y, Broekhuis AA, Picchioni F. *Macromolecules* 2009;42:1906–12;
d) Cordier P, Tourmilhac F, Soulie-Ziakovic C, Leibler L. *Nature* 2008;451:977–80;
e) Burattini S, Greenland BW, Merino DH, Weng W, Seppala J, Colquhoun HM, et al. *J Am Chem Soc* 2010;132:12051–8.
- [4] a) Roy N, Buhler E, Lehn J-M. *Chem Eur J* 2013;19:8814–20;
b) Roy N, Buhler E, Lehn J-M. *Polym Int* 2014;63:1400–5.
- [5] Zheng P, McCarthy TJ. *J Am Chem Soc* 2012;134:2024–7.
- [6] a) White SR, Sottos NR, Geubelle PH, Moore JS, Kessler MR, Sriram SR, et al. *Nature* 2001;409:794–7;
b) Toohey KS, Sottos NR, Lewis JA, Moore JS, White SR. *Nat Mater* 2007;6:581–5;

- c) Piermattei A, Karthikeyan S, Sijbesma RP. *Nat Chem* 2009;1:133–7. S133/131-S133/133.
- [7] Sedaghat-Herati R, Chacon A, Hansen ME, Yalaoui S. *Macromol Chem Phys* 2005;206:1981–7.
- [8] a) Watanabe M, Yoshie N. *Polymer* 2006;47:4946–52;
b) Ishida K, Yoshie N. *Macromol Biosci* 2008;8:916–22.
- [9] a) Yamashiro M, Inoue K, Iji M. *Polym J* 2008;40:657–62;
b) Inoue K, Yamashiro M, Iji M. *J Appl Polym Sci* 2009;112:876–85.
- [10] a) Kavitha AA, Singha NK. *J Polym Sci Part A: Polym Chem* 2007;45:4441–9;
b) Kavitha AA, Singha NK. *Macromol Chem Phys* 2007;208:2569–77;
c) Kavitha AA, Singha NK. *ACS Appl Mater Interfaces* 2009;1:1427–36;
d) Kavitha AA, Singha NK. *Macromolecules* 2010;43:3193–205.
- [11] Raquez J-M, Vanderstappen S, Meyer F, Verge P, Alexandre M, Thomassin J-M, et al. *Chem - Eur J* 2011;17:10135–43. S10135/10131-S10135/10134.
- [12] Chujo Y, Sada K, Saegusa T. *Macromolecules* 1990;23:2636–41.
- [13] Gheneim R, Perez-Berumen C, Gandini A. *Macromolecules* 2002;35:7246–53.
- [14] Imai Y, Itoh H, Naka K, Chujo Y. *Macromolecules* 2000;33:4343–6.
- [15] Zeng C, Seino H, Ren J, Hatanaka K, Yoshie N. *Polymer* 2013;54:5351–7.
- [16] Engel T, Kickelbick G. *Polym Int* 2014;63:915–23.
- [17] Engel T, Kickelbick G. *Eur J Inorg Chem* 2015:1226–32.
- [18] Kobayashi Y, Nakano M, Kumar GB, Kishihara K. *J Org Chem* 1998;63:7505–15.
- [19] A F, Stoeber W, Bohn E. *J Colloid Interface Sci* 1968;62–9.
- [20] Huang C, Tassone T, Woodberry K, Sunday D, Green DL. *Langmuir* 2009;25:13351–60.
- [21] Engel T, Kickelbick G. *Chem Mater* 2013;25:149–57.
- [22] Proupin-Perez M, Cosstick R, Liz-Marzan LM, Salgueirino-Maceira V, Brust M. *Nucleosides Nucleotides Nucleic Acids* 2005;24:1075–9.
- [23] Chen SY, Jollie MM. *Synth Commun* 1984;14:591–7.
- [24] Parker SF, Mason SM, Williams KPJ. *Spectrochim Acta Part A* 1990;46A:315–21.
- [25] n. E. ABCR silicon compounds: silanes & silicones. 2008.
- [26] Xu Z, Zhao Y, Wang X, Lin T. *Chem Commun* 2013;49:6755–7.

By comparison of these results with the other previously published in our group,^[146, 148] it becomes obvious that there is a problem with the compatibility of DA surface functionalized inorganic fillers within polymers.

T. Engel a former member of the group of Prof. Kickelbick used octafuran functionalized spherosilicates with a diameter of 3 nm instead of particles.^[148] These spherosilicates were crosslinked either with the molecular crosslinker BMI or with α,ω -maleimidopropyl-PDMS. The systems showed high rDA signals in DSC measurements with 25.5 and 13.9 J/g respectively. The BMI system showed the ability to thermally heal and a specimen of the PDMS sample could be thermally reshaped and reconnected. These results showed, that spherosilicates behave more like a molecule than the surface modified silica nanoparticles does. A disbalance according to the size of polymer and filler decreases the crosslinking density. Also, by incorporating spherosilicates instead of silica nanoparticles, the amount of functional group per area is decreased. Thus, it can be concluded, that this is favorable, because the long polymer chain does not have to organize the whole backbone along one particle.

In another approach, Kickelbick *et al.* situated the functional groups in the periphery of the particle surface by a surface initiated ATRP.^[146] This procedure diluted the functional group density by a factor of ten by adjusting the molar ratio of BMA and FMA to about 10:1. The initial diameter of 43 nm of the silica particles increased by 200% within the surface initiated ATRP. This value makes obvious, that the functional groups are far away from the particle surface. These particles were thermally crosslinked with the corresponding polymer and showed a rDA signal of 5.3 J/g.

In a retrospective, comparing these two works with the approach of the localization of functional groups directly on the surface of silica nanoparticles ($d = 12 - 18$ nm) shown in this work, it is unfavorable to locate all functional groups at one place. The application of elastomers and thermoplastics helped to understand the role of the polymer matrix composition and underlined the necessity of mobility of functional groups and flexibility of the matrix, which is known for pure polymeric systems.

To further investigate the system and understand the limiting factors, a cofunctionalization study was conducted on silica nanoparticles. However, due to the tendency of trialkoxysilanes to form multilayers, the system was further developed to phosphonic acid coupling agents on iron oxide particles. The results are described in the following chapter.

3.2 Diels-Alder Reactions on Surface-Modified Magnetite/Maghemite Nanoparticles: Application in Self-Healing Materials

An elementary study on DA functionalized nanoparticles was performed to gain a deeper understanding of the crucial parameters for the [4+2] cycloaddition conversion on the surface.

Spherical magnetite/maghemite nanoparticles, organically modified with DA phosphonic acids were used to investigate the limiting factor for DA conversions on particles. This could be either the amount of functional groups on the surface or the sterical impact of the emerging DA adducts during the reactions. Using the metal oxide, magnetite/maghemite and the phosphonic acids, which selectively form monolayers, gave us the ability to figure out our initial question concerning the reactivity.

The previously studied trialkoxysilanes on very small silica nanoparticles, which showed a diffuse surface structure, tend to form networks.^[156, 250] Accordingly, it cannot be assured to have only a monolayer of functional groups on the particle surface. However, the monolayer is essential to guarantee the accessibility of functional groups.

Moreover, magnetite/maghemite can be heated when treated in an external magnetic field by Brownian and Néel relaxation,^[251] which incorporates a further tool in self-healing materials. Thus, single parts of a material can be healed, instead of heating the whole specimen.

Novel DA phosphonic acids comprising the chain length C3 and C10 have been synthesized. The most critical step within the synthesis was the cleavage of phosphonic acids esters to the free acids. Applying bromotrimethylsilane, colorless solids were obtained after precipitation and several washing cycles with *n*-hexane. The desired compounds were received in high purity and are storable ambient conditions. However, care has to be taken, because BrTMS partially decomposes to free radicals and HBr, which can cause undesired polymerization of furan and maleimide. Then, insoluble oils are obtained instead of colorless solids.

Using oleic acid coated magnetite/ maghemite from a thermal decomposition reaction,^[190] a suitable exchange protocol against the phosphonic acids was developed. As a model substrate, dodecyl phosphonic acid was applied. An effective exchange took place in a mixture of *n*-hexane and ethanol at room temperature while stirring for 48 h. To ensure the dissolution of phosphonic acids (ethanol) and form a stable dispersion of oleic acid coated magnetite/ maghemite (*n*-hexane), the solvents had to be mixed. Using this protocol, a cofunctionalization of particles with DA and methyl phosphonic acid was done with 0, 25, 50, 75 and 100% functional reagent. Reacting either maleimide/*n*-dodecylmaleimide or methylfuran/ *n*-dodecylfuran with the cofunctionalized magnetite surfaces. We expected that there would be an optimum amount of functional groups on the surface of the particles, which is lower than 100%. The small methyl group should provide space in the surrounding of functional groups, leading to a higher conversion of DA groups.

However, we found out, that the 100% functional reagent particles showed the highest conversion according to FTIR, DSC and CHN analysis. The longer decyl spacer of coupling

reagent led to slightly higher conversions, than the shorter propyl version. In each case, the small attacking derivatives were superior over the dodecyl chain derivatives. This made obvious, that the sterical situation which is created by the formation of the DA adduct has the major impact on the conversion. The dodecyl chains are orientated along the nanoparticle surface and makes further attacks impossible. This explains the three-fold higher conversion with maleimide instead of *N*-dodecyl maleimide. With furan and dodecylfuran, the same impact on the conversion was observed. It should be mentioned, that no numerical statement can be made in this case, because the DSC measurements for the methylfuran samples also include the evaporation of released dienes.

From this study, it can be concluded, that the substituents on the attacking DA reaction partner orients along the surface, instead of orientating away from it. We assumed, that by a dilution of the functional groups on the particle surface, the effect of the substituents on the attacking molecules could be lowered. However, this was not the case. The comparison of the two derivatives, methylfuran/maleimide and dodecylfuran/ dodecylmaleimide allows to estimate the reactivity of the particles towards polymers. Due to the bulky polymer backbones, only a small percentage of functional groups will be able to react with polymers. Nevertheless, the general ability of the particles to react thermoreversible with a crosslinker was proved using 1,1'-(methylenedi-4,1-phenylene)bismaleimide. In a healing experiment on a round, free standing nanocomposite film ($d = 1$ cm), prepared in a heatable press, a scratch of 0.8 mm could be healed. Having these thermoreversible crosslinking nanoparticles it is only a small step to DA self-healing materials, which can be triggered by an external magnetic field. This would enable the heating of a small part of the material without the necessity of warming up the whole sample.

These results were published in ACS Applied Nanomaterials. Reproduced by permission of the American Chemical Society (ACS). <https://pubs.acs.org/doi/abs/10.1021/acsanm.8b00308>

Sandra Schäfer, Guido Kickelbick, Diels–Alder Reactions on Surface-Modified Magnetite/Maghemite Nanoparticles: Application in Self-Healing Nanocomposites: *ACS Applied Nanomaterials*, **2018**, *1*, 2640-2652, <https://doi.org/10.1021/acsanm.8b00308>.

Sandra Schäfer has written the publication and carried out all practical work (experiments and characterization). Guido Kickelbick has contributed with discussions about the topic and improvements for the final presentation of data and results within the manuscript.

Diels–Alder Reactions on Surface-Modified Magnetite/Maghemite Nanoparticles: Application in Self-Healing Nanocomposites

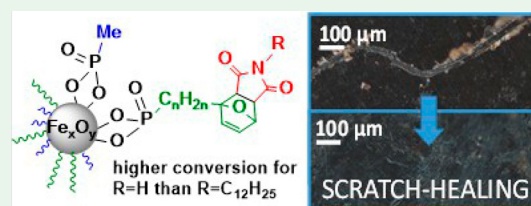
Sandra Schäfer and Guido Kickelbick*¹

Inorganic Solid State Chemistry, Saarland University, Campus C4 1, 66123 Saarbrücken, Germany

Supporting Information

ABSTRACT: Surface-modified inorganic nanoparticles with organic groups allowing thermoreversible cross-linking are versatile building blocks for nanocomposites with improved lifetimes. We studied the synthesis of various organophosphorus coupling agents consisting of phosphonic acid anchor groups, different alkyl spacers (C3, C10), and furan- or maleimide functional groups. The obtained molecules, which are able to undergo Diels–Alder (DA) reactions, were attached to the surface of well-defined preformed magnetite/maghemite nanoparticles by an exchange reaction of the stabilizing oleic acid ligands under mild conditions. A dilution of the reactive functional groups with unreactive methyl phosphonic acid resulted in a cofunctionalization of the surface with nonreactive groups. The reactivity of the modified particle surface toward DA reactions was systematically explored by converting these particles with maleimide/methylfuran or *N*-dodecylmaleimide/dodecylfuran. Fourier transform infrared spectroscopy, differential scanning calorimetry, and CHN elemental analysis measurements revealed a correlation between the quantity of functional reagent on the surface and the conversion in DA reactions. DA conversion of the modified particles is higher if fewer sterical hindered molecules react with the surface, which has implications on the use of these particles as cross-linking agents in polymer matrices. A thin nanocomposite film with thermally triggered healing capacity was successfully prepared by cross-linking the particles with 1,1'-(methylenedi-4,1-phenylene)bismaleimide.

KEYWORDS: magnetite/maghemite, phosphonic acid coupling agents, Diels–Alder reactions, self-healing, cross-linked composites, nanoparticle surface-modification



Nanoparticles containing functional groups on the surface that allow a thermoreversible bond formation are used in applications such as drug delivery systems¹ or as cross-linking agents in self-healing materials.^{2–4} Incorporation of magnetite/maghemite nanoparticles in self-healing materials introduces super-paramagnetic properties, which offer the opportunity for triggered healing based on heating in alternating magnetic fields (AMF). Typically, magnetic iron oxide nanoparticles induce local heat by Néel and/or Brownian relaxation when exposed to an AMF.⁵ Schmidt et al. showed healing of ionomeric elastomers in an AMF. The healing mechanism in these materials is based on dissociation of ionic bonds at higher temperatures, which can reform upon cooling.⁶ N'Guyen et al. reported that a retro-Diels–Alder (rDA) reaction can be induced by an AMF on the surface of modified iron oxide nanoparticles.¹ Wu et al. described maleimide functionalized Fe₃O₄, which was further modified by Diels–Alder (DA) polymerization. The monomers contained benzoxazine groups, which were irreversibly cross-linked afterward.⁷ Bose et al. described the use of magnetic iron oxide particles grafted on graphene oxide (rGO) for self-healing materials.⁸ In their work, furan-modified rGO/Fe₃O₄ sheets of several micrometers were cross-linked with DA-modified polyurethane. This material was healed in a microwave. From these already published studies it becomes clear that iron oxide nanoparticles covered by DA groups are promising for applications within DA-based self-

healing composites. They can extend the application range and allow for selective localized heating within a specific device.

Recently, we developed three different approaches to prepare self-healing nanocomposites using modified silica nanoparticles or spherosilicates as inorganic cross-linking agents. While silica particles functionalized with trialkoxysilanes⁹ showed only low conversion in polysiloxanes,¹⁰ silica particles modified via grafting-from copolymerization³ revealed a higher conversion. Applying modified spherosilicates as inorganic building block, increased conversions were observed using 1,1'-(methylenedi-4,1-phenylene)bismaleimide and a maleimide-modified siloxane.⁴ The study revealed that the amount of DA groups on the surface of the building blocks as well as their degree of freedom are crucial parameters in the self-healing capacity of such materials.⁴ Furthermore, also the size of the building block plays an important role. Until now, self-healing nanocomposite studies based on DA systems were performed with silica-based inorganic building blocks,^{2–4,10} carbon fibers,¹¹ graphene oxide,⁹ and silver nanowires.¹² To extend the work to new functional nanocomposites iron oxides are promising systems. Well-defined, spherical super-paramagnetic iron oxide nanoparticles can be produced by thermal decomposition of

Received: February 26, 2018

Accepted: May 4, 2018

Published: May 4, 2018



Fe(acac)₃.¹³ Although Sun et al. initially described these particles as magnetite, later reports revealed that iron oxide particles below 20 nm consist of a magnetite core and a thin maghemite shell.^{14,15} Therefore, it is better to describe these particles as magnetite/maghemite nanoparticles. In the synthesis of these nanoparticles, oleic acid is commonly employed as stabilizing agent. It can be easily exchanged against phosphonic acid-based molecules due to their higher affinity toward transition-metal oxide surfaces.¹⁶ Stable, irreversible M–O–P bonds are formed under mild conditions even at room temperature resulting in a monolayer formation on the particle surface.^{17,18} Compared to trialkoxysilanes,¹⁹ phosphonic acids have no tendency to form intermolecular networks.¹⁶ Therefore, functional groups will be situated evenly in a monolayer on the surface and will be accessible for reactions with further molecules. Mefford et al. studied the exchange of oleic acid on iron oxide with different anchoring groups, such as amine, carboxylic acid, phosphonic acid, and catechols using ¹⁴C radiolabeled oleic acid.²⁰ They were able to show that catechols and phosphonic acids exchange quantitatively. Cofunctionalization of the particle surfaces is also possible by choosing the desired molar ratio of two or more different coupling agents.²¹ This makes organophosphonic acids an ideal system for the functionalization of metal oxide nanoparticles.

In our study, we investigated the reactivity of the DA functions on the surface of magnetite/maghemite particles depending on parameters such as the density of the functional groups and their distance to the surface. The obtained results reveal important parameters for further studies on self-healing nanocomposites.

RESULTS & DISCUSSION

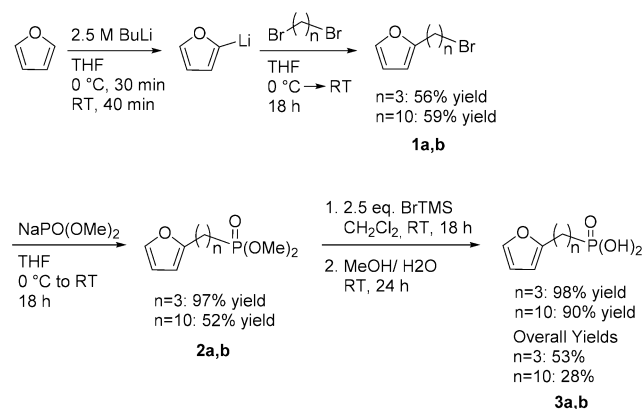
1. Synthesis of DA Phosphonic Acids.

A variety of functionalized organophosphonic acid coupling agents were synthesized, carrying either maleimide or furan groups. In both cases, a short and a long alkyl spacer were incorporated between the phosphonic acid and the DA groups to study the influence of distance between the particle surface and the functional group on the reactivity.

1.1. Furanalkyl Phosphonic Acid (3a,b).

Synthetic access to furanoalkylphosphonic acids (C3, C10 = 3a,b; Scheme 1) is provided by the reaction of dibromoalkanes with 2-lithium furanide. Since the purification of the resulting compounds is difficult, it is advantageous to use lithium furanide in excess;

Scheme 1. Reaction Path to Furan Alkyl Phosphonic Acids



thus, remaining unreacted starting material in the solution can be avoided. The obtained difuran alkanes side products cannot react in the subsequent reaction.

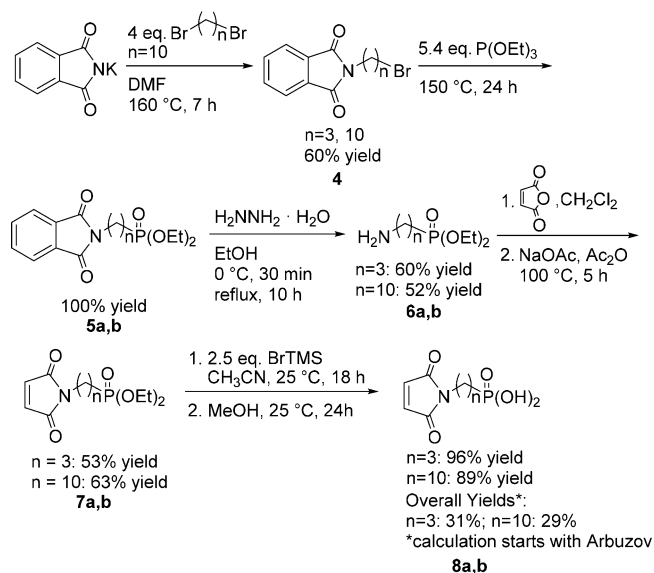
The use of the Michaelis–Becker reaction, which proceeds at room temperature, is the method of choice regarding the thermal instability of furan rings. The bromoalkylfurans (1a,b) were converted, with a slight excess of sodium phosphite resulting in phosphonic acid esters (2a,b), which were cleaved using bromotrimethylsilane (BrTMS) to obtain the silyl ester. The free acids (3a,b = F3P, F10P) formed as colorless solids after hydrolysis in an overall yield of 53% for the C3 chain, and 28% for the C10 chain. After this hydrolysis, it is crucial to purify the free acids from byproducts by precipitation of the solids, because otherwise they decompose upon storage. The purity of the obtained organophosphorus coupling agents was confirmed by ¹H, ³¹P, and ¹³C NMR spectroscopy. ¹H NMR of 3b displays the three typical furan protons at 7.32, 6.26, and 5.98 ppm, respectively (Figure S14). The triplet at 2.60 ppm can be attributed to the CH₂ group next to the furan ring. The remaining protons from the alkyl chain show multiplets between 1.80 and 1.30 ppm. A single signal in ³¹P NMR at 30.24 ppm indicates the high purity of the compound (Figure S15).

Furandecyldimethylphosphonic acid ester (2b, Figure S58) and furandecylphosphonic acid (3b, Figures S59 & S60) were crystallized from methanol after adding a few drops of *n*-hexane. While the protected phosphonic acid esters are not able to form hydrogen bonds, an interaction of several phosphonic acid groups was observed in the case of the crystalline acid (Figure S60). These hydrogen bonds lead to a low solubility of the solid in many common organic solvents. Alcohols, such as methanol and ethanol, are best suited as solvents of the substance.

1.2. Maleimide Alkyl Phosphonic Acid (8a,b).

Because of the reactive nature of the maleimide double bond toward radical additions and polymerizations,²² the functional group must be introduced in one of the last reaction steps. The general reaction path is displayed in Scheme 2. 3-Bromophthalimide is commercially available, and the decyl derivative (4)

Scheme 2. Reaction Path to Maleimide Alkyl Phosphonic Acids



was synthesized by reacting potassium phthalimide with 1,10-dibromodecan.²³ The phosphonate ester group was introduced applying an Arbuzov reaction with triethyl phosphite **5a,b**. A Gabriel synthesis applying hydrazine monohydrate for the C–N bond cleavage provided synthetic access to the necessary primary amines (**6a,b**).²³

Since the amine group tends to react with the phosphonate group at elevated temperature and the byproduct, phthalhydrazide, is difficult to remove, it is advisable to use enough solvent. This procedure leads to a quantitative crystallization of the byproduct upon cooling and simplifies the filtration. Residual phthalhydrazide was precipitated applying dichloromethane, and the desired aminoalkyl phosphonic acid was obtained after filtration (yield = 60% (C = 3) (**6a**), 52% (C = 10) (**6b**)). The reaction of the products with maleic anhydride can be followed by NMR spectroscopy. The complete disappearance of the CH_2NH_2 signals at 2.77 ppm (C3) and 2.69 ppm (C10) indicates the full conversion of the amine (**6a,b**). The maleamic acid phosphonate esters were cyclized in acetic anhydride using sodium acetate as a catalyst to achieve the desired maleimide alkyl phosphonate ester (**7a,b**).

The ester bonds were cleaved using BrTMS in acetonitrile with subsequent addition of methanol. Purification of the free acids is again crucial. The maleimide alkyl phosphonic acids (C3 (**8a** = M3P), C10 (**8b** = M10P)) were obtained as colorless solids (yield = 96/89% (C3/C10); overall yields 31/29%). ¹H, ¹³C, and ³¹P NMR spectroscopy of M3P reveals the high purity of the product (Figures S42–S44). The singlet at 6.77 ppm is attributed to the C=C double bond of the maleimide ring, the triplet at 3.52 ppm to CH_2N , the multiplets at 1.80 ppm to the CH_2 group in the middle, and 1.62 ppm to CH_2P . The ³¹P NMR reveals a single peak at 28.60 ppm.

2. Exchange of Oleic Acid against DA Phosphonic Acid on the Surface of Magnetite/Maghemite Nanoparticles. Oleic acid (OA)-coated magnetite/maghemite ($\text{Fe}_3\text{O}_4/\gamma\text{-Fe}_2\text{O}_3$ hereafter abbreviated with Fe_xO_y) nanoparticles (**11**, $\text{OA}@Fe_x\text{O}_y$) were synthesized using a thermal decomposition reaction of $\text{Fe}(\text{acac})_3$.¹³ X-ray diffraction (XRD) analysis showed the diffraction pattern of a cubic spinel structure, which is typical for magnetite (Fe_3O_4) and maghemite ($\gamma\text{-Fe}_2\text{O}_3$). From the obtained analytical results of the particles (XRD, thermogravimetric analysis (TGA)) no further details of composition can be given. Dynamic light scattering (DLS) and transmission electron microscopy (TEM) measurements revealed a spherical morphology of the particles and an approximate radius of 5 nm. A suitable exchange protocol of oleic acid against dodecylphosphonic acid (DDP), as a model system, was developed. The relevant reaction parameters were studied regarding the solvents, reaction time, and the amount of coupling agents required to establish a complete exchange, within the experimental accuracy,²⁰ to ensure a dense monolayer of phosphonic acids on the surface. Cofunctionalization of the surface was investigated applying different molar ratios of DDP and methyl phosphonic acid (MeP; TGA, IR, & CHN elemental analysis measurements in Supporting Information). Aiming for a precise study regarding the reactivity of DA groups on particle surfaces the described parameters were carefully examined, before proceeding with the cofunctionalization using the DA phosphonic acids.

Solvents used in the exchange reaction should dissolve the coupling agent, but also it is necessary that a stable dispersion of oleic acid-coated magnetite/maghemite particles is formed (**11**). Various solvents and mixtures were studied, aiming for a

complete exchange reaction, for example, chloroform,²⁰ tetrahydrofuran (THF),²⁴ toluene/dioxane/water (12:1:8),²⁵ CHCl_3 /dimethylformamide (DMF) (1:1),²⁶ and *n*-hexane/ethanol (1:1) (further details in Supporting Information). The optimization of the exchange conditions is necessary with regard to the different hydrophobicity of the organic substituents connected to phosphonic acid anchoring groups and the size of the coupling agents.

$\text{OA}@Fe_x\text{O}_y$ nanoparticles form stable dispersions in *n*-hexane (proved by DLS, Figure S62), while the phosphonic acids are soluble in ethanol. Therefore, a 1:1 mixture of *n*-hexane/ethanol was used in the exchange reactions. During the reaction, the particles stayed deep black, which indicates that no changes in the oxidation state occurred. This would alter the magnetic properties and therefore the behavior in an alternating magnetic field. Pourroy et al. described that “phosphatation occurs rapidly, inhibits the dissolution of magnetite and does not modify the structure and the magnetization of magnetite.”²⁷ Chai et al. described oleic-acid-capped and carboxyl–PEG–phosphoric acid-stabilized Fe_3O_4 nanoparticles²⁴ and investigated the effect of the coatings on magnetic properties. They found a marginal reduction in saturation magnetization of 18%. The particles remained super-paramagnetic after modification. On the basis of our observations and measurements (XRD, TGA) and based on the results reported in literature, it is unlikely that a large change in magnetization occurs during the ligand exchange in the *n*-hexane–ethanol mixture. In contrast to that, the dioxane-containing mixture led to a change in color, which indicated redox reactions resulting in variations of the iron oxidation states. Using a DMF/CHCl_3 mixture resulted in an intensively colored supernatant, which indicated dissolved iron ions from the inorganic core.

2.1. Optimization of the Amount of Coupling Agent. IR spectroscopy was used to study the level of exchange of acid molecules and to compare the amount of surface coverage by normalizing the spectra to the Fe–O vibration bands. In literature, the amount of phosphonic acids per gram varies between 0.9 and 2.4 P-groups/ nm^2 .²⁸ Even 2.9–3.0 P-groups per nm^2 ¹⁸ were described to be less than a monolayer. The theoretically possible amount was determined to be 4.16 molecules/ nm^2 taking into account an area of 24 Å^2 /P-groups and a surface area of nanoparticles of 558 m^2/g (detected by nitrogen gas sorption, Brunauer–Emmett–Teller (BET)). Markovich et al. described quasi-bilayers on the surface, which consist of a chemically bound monolayer and a second layer attached to the first one by a mixture of van der Waals forces between alkyl chains and hydrogen bonds between phosphonic acid groups.²⁹ In our systematic exchange reaction studies we used 0.025, 0.05, 0.1, 0.2, 0.3, 0.4, 0.6, and 0.8 mmol per 150 mg nanoparticles in the solution stirring 48 h at 25 °C in *n*-hexane/ethanol (~1:2). This allowed us to analyze the appropriate amount of coupling agent for the formation of a dense monolayer while preventing noncovalently bound acid molecules on the surface (Scheme S1).

Figure S64 compares the IR spectra of $\text{OA}@Fe_x\text{O}_y$ mixed with free dodecylphosphonic acid and dodecylphosphonic acid bound on magnetite/maghemite ($\text{DDP}@Fe_x\text{O}_y$). The first important observation for successful surface modification is the disappearance of the O=P–OH stretching vibrations (3034, 2646, 2287 cm^{-1} , marked with * in Figure S64). The broad shape of these signals is typical for free hydrogen bonds within molecules. Free phosphonic acids reveal sharp peaks in the

range of 1250–900 cm^{-1} resulting from P–C rocking as well as P=O and P–O stretching vibrations.^{27,30–33}

The IR spectra after using 0.2–0.8 mmol DDP in the exchange mixture provided no hint for remaining OA and display the broad P–O–Fe peak as well as the typical signals for bound phosphonates between 1500 and 1250 cm^{-1} (Figure S64). The characteristic broad OH vibrations of free phosphonic acid at 3039, 2656, and 2294 cm^{-1} disappear, but applying more than 0.2 mmol DDP leads to remaining P–OH signals at 933 and 917 cm^{-1} . The P=O vibration at 1217 cm^{-1} disappears almost completely but becomes more pronounced, when more phosphonic acid is used in the exchange reactions. The decreasing P=O signal indicates a dative bond by Lewis acid–base interactions to the magnetite/maghemite surface, which results in delocalization of the π -electrons and therefore a shift to lower frequencies.¹⁶ In all samples, the typical $\text{COO}^-@Fe_xO_y$ stretching vibration in the range of 1500–1250 cm^{-1} vanishes, while the Fe–O–Fe band around 548 cm^{-1} remains. The most significant observation that indicates successful modification is the broad P–O–Fe stretching band from ~ 1150 to 760 cm^{-1} , which is typical for the PO_3^{4-} fragment.^{34,35} This band is also observed in spectra of commercially available FePO_4 (Figure S65). Concentrations of 0.1 mmol organophosphorous agent in the exchange solution seem to be too low for a complete exchange, which is obvious by the persistence of C–O–Fe stretch at 1533 and 1406 cm^{-1} (Figure S66). Various binding modes of phosphonic acids to metal oxide surfaces are described in literature, varying from mono-, bi-, and tridentate to chelating and coordinating, and also hydrogen interactions are known.³⁶ While the interaction with organophosphonates was studied with several other iron oxides,^{37–40} there are almost no investigations on magnetite/maghemite nanoparticles. Magnetite particles seem to consist predominately of (111) surfaces, which means that the top layer consists mainly of iron ions.^{27,41,42} Daou et al. investigated the surface complex starting from hydroxylated magnetite at pH = 3 and found that phosphatation occurs by interaction of Fe^{3+} in octahedral sites with the formation of monoprotonated bimolecular species.²⁷ However, attachment mechanisms can be different, when starting from a carboxylated magnetite/maghemite surface. Gomes et al. described an exchange of 1:1 OA against phosphoric acid (PA) on CdSe, which means that the phosphonate binds as hydrogen phosphonates to the surface.⁴³ In our case, it seems that using only a small excess (0.2–0.3 mmol) of phosphoric acid leads to the formation of a tridentate complex on the surface, which is supported by the total consumption of P=O and P–OH bands in the range of 1115–917 cm^{-1} . Using an under-stoichiometric amount of PA leads to a 2:1 exchange. If a higher excess (≥ 0.4 mmol) of DDP is used residual P–OH bands were observed as well as a small signal for P=O, which indicates that rather a mono- or bidentate complex was formed on the surface.^{33,36}

The supernatants, which were obtained by magnetic decantation of the reaction mixtures, were studied by ^{31}P NMR to determine whether DDP was present in excess. Up to 0.2 mmol, no ^{31}P signal was observed, while an increasing signal was observed in the range from 0.3 to 0.8 mmol (Figure S67).

TGA was performed under nitrogen up to 900 $^\circ\text{C}$ and under oxygen above 900 $^\circ\text{C}$ (Figure S68). The nitrogen segment is important, to evaluate the organic content on the surface. The oxidizing segment was used to prove whether the sample is still composed of magnetite after modification. An increase in mass indicates the oxidation of Fe_3O_4 to Fe_2O_3 . While $\text{OA}@Fe_xO_y$

showed a decomposition between 260 and 370 $^\circ\text{C}$, two decomposition steps for $\text{DDP}@Fe_xO_y$, starting at ~ 400 and 600 $^\circ\text{C}$ were detected within the nitrogen segment, resulting from the decomposition of alkane chains. Within the oxygen segment, an increase of weight was observed resulting from the oxidation of residual phosphonate groups to phosphates and the oxidation of magnetite.

All DDP-modified samples showed the same decomposition steps, and no signal was observed at the degradation temperature of OA. The first derivatives of the TG curves (25–900 $^\circ\text{C}$) were plotted for a better visibility of the described steps in TGA (Figure S69). Elemental analysis was performed to calculate surface coverage in millimoles per gram or molecules per square nanometer (Table S2). Surface coverages between 1.52 and 1.99 molecules/ nm^2 were detected, which is less than half of the theoretical maximum surface coverage previously described. However, the experimental results show that no proportional increase of surface coverage was found by increasing the amount of DDP, which means that the theoretical maximum seems unrealistic. Hence, an amount of 0.3 mmol of phosphonic acid per 150 mg of magnetite/maghemite nanoparticles appears to be an optimum concentration for the reaction. In this case, free phosphonic acid was detected in the ^{31}P NMR within the supernatant, while the IR spectrum did not show a signal for C–O–Fe, and the TGA revealed neither the typical mass loss step for residual carboxylic acid on the surface nor splitting of the Fe–O–P band.

2.2. Optimization of Exchange Reaction Time by FTIR. IR spectroscopy was used to examine the necessary reaction time for the exchange protocol (Figure S70). The exchange starts immediately after adding the phosphonic acid solution to the particle suspension. Already after 1 min, a strong, broad Fe–O–P stretching vibration at 960 cm^{-1} was observed. The completeness of the exchange was evaluated detecting the area between 1475 and 1170 cm^{-1} . While the broad-shaped peak of C–O–Fe decreases, a typical stairlike shape of $\text{DDP}@Fe_xO_y$ became more pronounced. After stirring for 48 h no further change in IR was observed, which indicates the completeness of the reaction. Therefore, this reaction time was chosen for all following experiments.

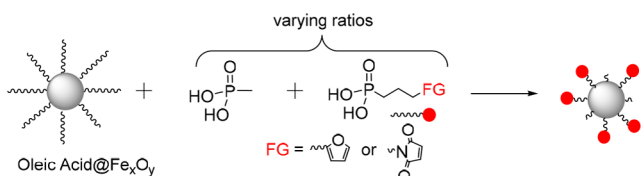
Although phosphonic acid groups can react readily with metal oxides, a relatively long reaction time is required. A possible explanation is that the steric hindrance due to already attached organophosphonate groups and the attractive hydrophobic interactions of the alkyl chains lead to an inhibited desorption of further carboxylic acid. Repulsive interactions between hydrophobic alkyl chains and hydrophilic phosphonic acid groups also lead to a hindered attack of further organophosphonic acid groups (Scheme S1).

This study showed that the desired exchange takes place under mild conditions while stirring for 48 h at room temperature, with a slight excess of phosphonic acid in an *n*-hexane/ethanol mixture. Additionally, TEM measurements proved that the initial shape of the particles is remaining during treatment of $\text{OA}@Fe_xO_y$ with phosphonic acids (Figure S72).

The ability of cofunctionalization of the particles was investigated using a DDP and MeP mixture as a model system. IR, CHN elemental analysis, and TGA showed the successful binding of the coupling agents in the desired ratio (Table S3, Figures S75 & S76). An increased amount of MeP on the particle surface leads to a higher surface polarity.

3. Surface Cofunctionalization of Magnetite/Maghemite Particles with DA Active and Nonactive Phosphonic Acids. With the optimized exchange protocol, Fe_xO_y nanoparticles were cofunctionalized applying the furan- or maleimide alkyl (C3, C10) phosphonic acids (**3a,b** or **8a,b**) and methyl phosphonic acid. This approach allows the dilution of DA functionalities on the surface, and due to the small methyl groups, the DA reaction should be less sterically hindered. To synthesize the cofunctionalized particles, the appropriate mixtures (0.3 mmol in total/150 mg $\text{OA}@Fe_xO_y$, Table S4, Scheme 3) of both acids were dissolved in ethanol/*n*-hexane,

Scheme 3. Schematic Representation of Synthesis of Cofunctionalized Magnetite/Maghemite Nanoparticles



and a suspension of $\text{OA}@Fe_xO_y$ particles (150 mg in 17 mL ethanol) was added. The resulting mixture was stirred 48 h at 25 °C. The particles were magnetically decanted off and washed with ethanol.

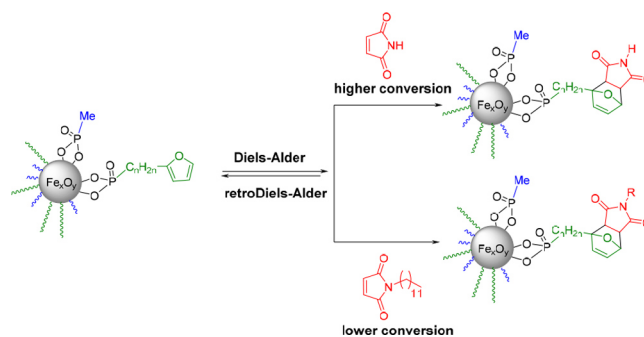
3.1. F10PcoMeP@ Fe_xO_y . CHN, FTIR, and TG measurements were conducted to verify the successful cofunctionalization using F10P (**3b**) and MeP. Elemental analysis reveals decreasing amounts of C and H within the samples with increasing amounts of MeP (Table S6). The surface coverage can only be calculated for the modifications with a single species not for mixtures (TG curves (Figure S82, Table S9)) and was calculated to be between 1.20 and 1.73 mmol/g or 1.30–1.87 molecules/nm² for the samples F10P_100, F3P_100, M10P_100, and M3P_100.

Normalized FTIR spectra (Figure S78) indicate the successful cofunctionalization by increasing peaks from F10P_0 to F10P_100. The small signal at 1506 cm⁻¹ is characteristic for the C=C stretching vibration of furandecyl phosphonic acid (**8b**), and the signal around 2900 cm⁻¹ can be attributed to the CH stretching vibration for the long decyl chain. At the same time the signal at 1304 cm⁻¹ indicates P-CH₃ deformation, and that at 770 cm⁻¹ is for PC-H₃ stretching, which is characteristic for methyl phosphonic acid (MeP) decrease.

3.2. M3PcoMeP@ Fe_xO_y . The cofunctionalization using maleimide phosphonic acids (**8a,b**) can also be followed employing FTIR (Figures S79 & S80). The characteristic signals at 1695 ($\nu(\text{C}=\text{O})$), 1444 ($\nu(\text{R}_2-\text{N}-\text{C})$), 1404 ($\delta(\text{CH})$), 1362 ($\nu(\text{C}-\text{N})$), 824 ($\nu(\text{H}-\text{C}=\text{C})$), and 693 (ring deformation) cm⁻¹ increase with increasing content of M3P (**8a**). The control experiment M3P_0 shows none of these signals. The vibration at 1305 cm⁻¹ originated from MeP increases from M3P_100 to M3P_0.

4. DA Reaction with Molecular Reaction Partners. The activity of the DA surface-functionalized Fe_xO_y particles was investigated by reacting them with a less and a more sterically demanding reactant (Scheme 4). Three parameters were varied: (a) ratio of functional to nonfunctional coupling agent, (b) the spacer length of functional coupling agent, and (c) the chemical nature of dienophile/diene: maleimide (M)/

Scheme 4. DA Reaction on Cofunctionalized Particles



methylfuran (MF) or *N*-dodecylmaleimide (NM)/dodecylfuran (DF).

4.1. DA Reaction of Furan-co-Functionalized Particles with *N*-Dodecylmaleimide or Maleimide. All furan-cofunctionalized particles were reacted with three equivalents (based on mmol furan/mg sample) of dienophile (NM or M) in chloroform at 60 °C for 24 h. The supernatant was magnetically decanted off at the reaction temperature of 60 °C to purify the particles from physisorbed dienophiles. The particles were washed five times with a solvent mixture (ethanol/acetone/ethyl acetate or THF). The dispersibility of 100 and 75% DA functional samples after reaction with dodecyl derivatives was quite high, so methanol was added to the washing mixtures. In the last washing cycle, the suspension was stirred 2 h to equilibrate, and subsequently, the particles were dried in vacuum. This workup procedure was chosen, because washing only with chloroform resulted in nonbonded dienophile or diene on the surface.

IR measurements were used to investigate whether the dienophile reacted with the surface. The typical shift to higher wavenumbers for the C=O bond of maleimide, for example, from 1693 to 1700 cm⁻¹, was observed after forming the DA adduct with furan (Figure S83). The formation of the DA adduct can be correlated with the C=O signal intensity after normalization of the spectra to the Fe–O peak (Figure 1).

The C=O signal increases from F10P_0 to F10P_100 samples, which means the highest conversion in the reaction with maleimide was observed in case of the 100% functional reagent sample.

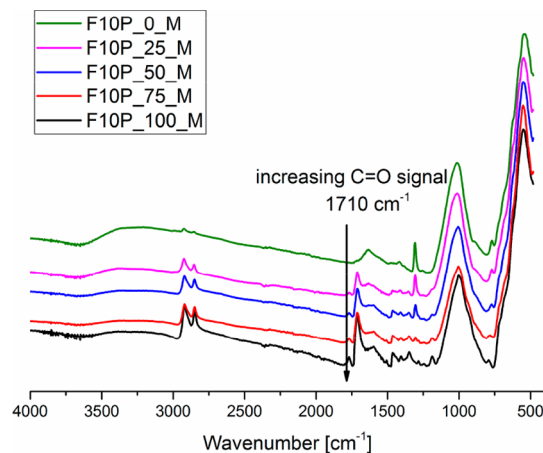


Figure 1. IR spectra of F10PcoMeP@ Fe_xO_y cofunctionalized particles after DA reaction with M.

The same general trend was observed using *N*-dodecylmaleimide (Figure 2) instead of maleimide, but the conversion was

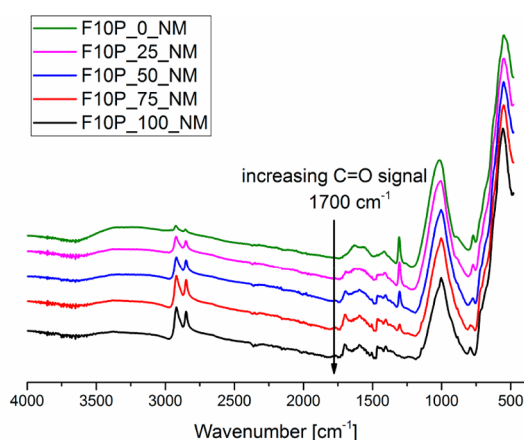


Figure 2. IR spectra of F10PcoMeP@Fe_xO_y cofunctionalized particles after DA reaction with NM.

lower. Evidence is given by the lower C=O intensity of normalized spectra. Again, the control experiment does not show any C=O signal. Another important indication is that no vibration for the maleimide ring was detected at 696 cm⁻¹, which would belong to physisorbed dienophile.

We tried to use CHN measurements to calculate the amount of dienophile per milligram of sample, using the nitrogen value. Unfortunately, the amount of nitrogen is below the detection limit. However, the C and H values follow the expected trends: the more coupling agent used and the more conversion in DA reaction achieved, the higher is the amount of C and H atoms on the surface of the particles (Table 1).

Table 1. DSC & CHN Data of Cofunctionalized F10PcoMeP@Fe_xO_y after DA Reaction with M or NM

	DSC integral J/g	C %	H %
F10P_100_M	15.55	16.67	2.30
F10P_75_M	14.31	15.17	2.17
F10P_50_M	12.80	12.49	1.92
F10P_25_M	2.42	9.24	1.54
F10P_0_M	0	6.42	1.26
F10P_100_NM	4.19	16.21	2.27
F10P_75_NM	3.96	15.06	2.30
F10P_50_NM	2.12	12.73	2.01
F10P_25_NM	0	9.65	1.61
F10P_0_NM	0	7.34	1.32

DSC curves were measured to analyze the rDA reaction via the typical endothermic signal above 100 °C, which appears in the cycloreversion reaction (Figure 3). The measurements were conducted under nitrogen (80 mL/min) at a heating rate of 10 K/min. A 3 min isothermal segment at 50 °C was used to distinguish the background signal from the rDA signal. In a second heating cycle after cooling to 25 °C no signal for rDA reaction was detected. Hence, it can be concluded that the rDA reaction takes place completely in the first cycle. DSC (Table 1, Figure 3) and IR (Figure 1) results agree well. It can be generally stated that an increase in the number of functional groups on the surface results in a higher conversion of the DA reaction independent from the maleimide derivative.

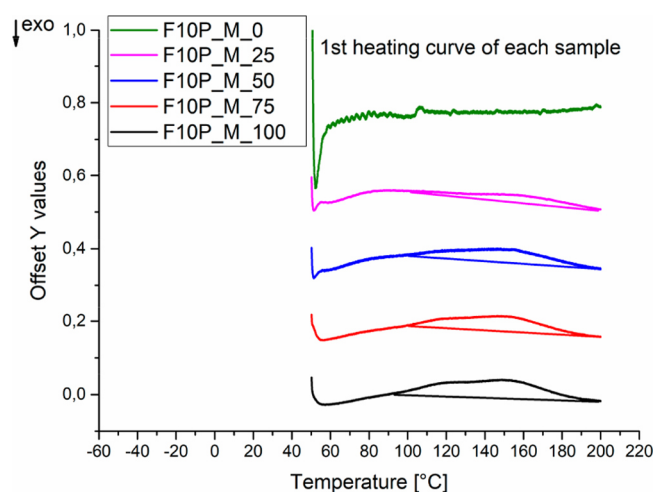


Figure 3. DSC curves of F10PcoMeP@Fe_xO_y cofunctionalized particles after DA reaction with M.

With maleimide as the reaction partner for F10P_100, a signal of 15.55 J/g was detected. With NM, only ~1/3 of this value was detected (4.19 J/g). Within one row of dilution of the functional groups on the particle surface, the signal decreases. This leads to the assumption that the steric demand of the molecules reacting with the surface groups limits the conversion, not the initial steric situation on the surface.

F3P and F10P samples show identical trends regarding the conversions in the DA reactions (see Supporting Information). F3P_100 particles showed a significantly higher conversion with maleimide than with *N*-dodecylmaleimide. Also, a decreasing conversion was observed with a smaller amount functional groups on the surface. Again, the control experiments applying MeP@Fe_xO_y were negative in IR and DSC analysis. The DSC values are evaluated using peak areas in joule per gram, which means they refer to the sample mass. It can be assumed that the areas of rDA reactions of dodecyl samples appear slightly smaller compared to areas of the products after conversion with maleimide. Nevertheless, IR spectra agree well with the lower conversion, as the corresponding signals of the adducts are smaller after using the dodecyl derivatives.

4.2. DA Reaction of Maleimide-co-Functionalized Particles with Dodecylfuran or Methylfuran. All maleimide cofunctionalized particles were reacted with three equivalents (based on mmol of maleimide/mg sample) of dienophile (DF or MF) in chloroform at 60 °C for 24 h. The workup was identical to the corresponding furan-modified particles, except using a solvent mixture of ethanol/acetone/tetrahydrofuran (1:1:1). THF was chosen, because the nonbonded, physisorbed furans can exchange with this solvent. Again, methanol had to be added to the 100 and 75% samples after reaction with dodecyl derivatives because of the better dispersibility compared to more polar samples.

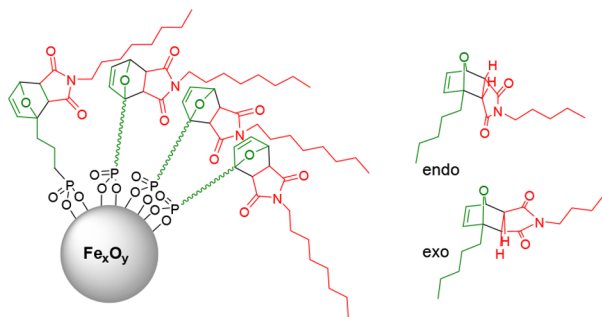
After conversion to the DA adduct, the IR spectra of M3P (Figure S87) indicate the disappearance of the vibrations at 696 (ring deformation) and 826 (H–C=) cm⁻¹ as a result of the full consumption of functional groups while reacting with the smaller MF molecule. When the sterically more demanding DF was applied, significant quantities of these signals are still observed (Figure S88). Further data can be found in the Supporting Information. Again, DSC measurements agree with the IR results. In case of methylfuran, the rDA signal appears to be higher because of the evaporation of the diene after release

(Table S13). Nevertheless, the general trend that the smaller MF shows a higher conversion than DF on the surface of the particles is clear. These observations agree with the ones made for the furan derivatives and are also similar for M10P-modified particles. Results for M10PcoMeP@Fe_xO_y can be found in the Supporting Information.

In summary, it can be concluded that (a) the higher the amount of functional coupling agent the more conversion was detected; (b) an increase in spacer length (C3, C10) results in higher conversion; (c) the DA reactivity is strongly dependent on the added reagent. When dodecyl derivatives were applied, the conversion dropped by a factor of 3 to 4. This comparison gives a hint for the reactivity of the particles toward DA group functionalized polymers. It can be expected that only a small percentage of functional groups will react with polymers, which have bulky polymer backbones.

Initially, we assumed that a less-crowded surface, which can be obtained by the dilution of functional groups using the smaller methyl phosphonic acid, would lead to a higher total conversion. It can be argued that a DA reaction requires a six-membered transition state, which is sterically demanding, and thus more space is needed on the surface. Within the studied range of 100, 75, 50, 25 and 0% functional groups this was not the case. But a significant difference in the DA conversions was observed depending on the steric demand of the reaction partner. Particularly when the dodecyl derivatives were used the conversion in DA reactions decreased. This is most likely due to the long alkyl chain of the DA adduct, which is oriented orthogonal and not perpendicular to the surface (Scheme 5). As a consequence of this orientation further molecules are hindered to undergo a reaction.

Scheme 5. DA Adduct Formation Results in Steric Hindrance Due to the Orthogonal Arrangement of the Groups on the Surface



(simplified scheme of connection of anchoring groups to surface)

5. DA Reaction with Cross-Linking Molecule. The general ability to use the DA group-modified particles as inorganic cross-linking agents was studied applying a free-standing thin film of 250 μm thickness containing F10P_100@Fe_xO_y and 1,1'-(methylenedi-4,1-phenylene)bismaleimide (BMI). The film was produced by mixing F10P_100@Fe_xO_y with BMI in chloroform. After it was shaken for 1 min, the solvent was removed in vacuum. The obtained gray powder was poured between two sheets of aluminum foil within a heatable press. The sample was cross-linked at 60 °C for 24 h at a pressure of 1 t to afford a free-standing round sheet (*d* ≈ 1 cm) of a brittle black film as composite material.

A scratch was produced on the surface by the use of a scalpel (Figure 4). Treatment of the sample at 60 °C for 1 h revealed

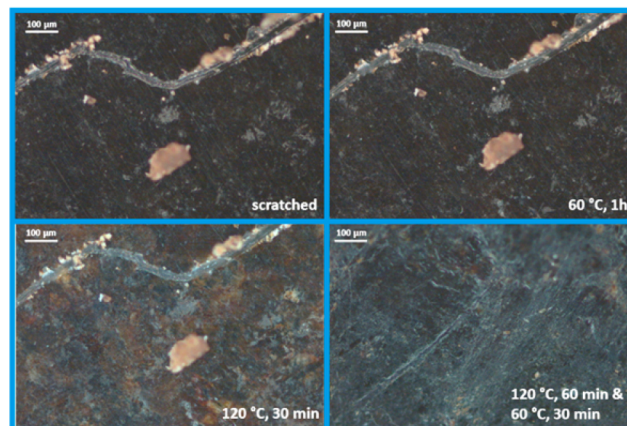


Figure 4. Microscope image of F10P_100@Fe_xO_y cross-linked with BMI.

no change of the defect. Heating to 120 °C for 30 min led to a visible de-cross-linking, which is indicated by the appearance of orange areas due to the liberation and aggregation of bismaleimide in the film. With the second cross-linking at 120 °C for 1 h under gentle pressure, followed by a treatment at 60 °C for 30 min and slowly cooling to room temperature, the bismaleimide again reacts with nearby nanoparticles, which consume free bismaleimide and thus cause the disappearance of visible orange areas. This treatment also resulted in the disappearance of the crack. Thus, the possibility of using these magnetic DA particles for self-healing materials was proved. Only a few cross-linking reactions are expected to occur in this material, due to steric hindrance.⁷ However, there are several evidences that we obtained a cross-linked material. For example, if the material is placed into solvents, which are good dispersion media of the particles as well as for the cross-linking agent (e.g., chloroform), the sample remains stable. In addition, the DSC signals (Figure S101) as well as the resulting IR spectra (Figure S102) of the sample show that at least a part of the DA groups reacted with each other, and thus a cross-linked material was formed. Nevertheless, an optimization must be performed to afford a more stable material.

CONCLUSIONS

Oleic acid-coated magnetite/maghemite particles were cofunctionalized with novel furan- or maleimide alkyl (C3, C10) phosphonic acids and methyl phosphonic acid. Therefore, a suitable exchange protocol was developed on a model system using dodecylphosphonic acid. The amount of DA functions was systematically changed from 100 to 0% in 25% steps to examine the reactivity in DA reactions on the surface. These particles were reacted with maleimide/methylfuran or the corresponding dodecyl derivatives. The dilution of reactive groups on the surface led to a lower conversion. This can be explained by the steric situation created by the formation of the DA adduct, which limits a further conversion. Remaining functional groups on the particle surface cannot be reached by further reaction partners. Changing the spacer length from propyl to decyl resulted in an increase in conversion by a factor of 3 to 4. The principal reactivity of the particles as cross-linkers in self-healing materials was studied by incorporation of the F10P_100 particles in 1,1'-(methylenedi-4,1-phenylene)-bismaleimide. The general curability was shown in microscope images. With these thermoreversible cross-linking nanoparticles

it is only a small step to DA self-healing materials, which can be triggered by an external magnetic field. Thus, heating of small parts of the material would be possible without the necessity of warming the whole device.

EXPERIMENTAL SECTION

Materials & Methods. All syntheses of molecules were performed under an inert atmosphere and using absolute solvents.

Materials. Fe(acac)₃ (97%), benzyl ether (98%), 1,2-dodecandiol (90%), oleyl amine (70%), 1,1'-(methylenedi-4,1-phenylene)-bismaleimide (95%), *n*-butyl lithium (2.5 M solution in hexanes), furan (>99%), sodium hydride (95%), maleimide (98%), dimethyl phosphite (98%), bromotrimethylsilane (97%), and 1-bromododecane (97%) were purchased from Sigma–Aldrich. Dibromoalkanes (C3 (98%), C10 (97%)), triethyl phosphite (98%), hydrazine monohydrate (98+%), dodecylamine (98+%), *N*-(3-bromopropyl)phthalimide (98%), and 1-dodecylphosphonic acid (95%) were purchased from Alfa Aesar. Zinc chloride (98%) was obtained from Grüssing GmbH. Oleic acid (>99%), sodium acetate (>99.999%), maleic anhydride (98%), potassium phthalimide (>99%), acetic anhydride (>99.5%), and silica gel was purchased from Fluka. Methyl phosphonic acid (98%) was purchased from Acros Organics. Hexamethyldisilazane (98.5%) was obtained from ABCR. Methylfuran (>98%) was purchased from TCI chemicals. All chemicals were used as received.

Characterization. FTIR spectroscopy measurements were performed applying a Bruker Vertex 70 spectrometer under ambient air (40 scans at a resolution of 4 cm⁻¹) in attenuated total reflectance (ATR) mode. Selected wavenumbers are listed (s = strong, m = medium, w = weak). Solution NMR spectra were recorded with a Bruker Avance III HD 300 and 400 spectrometers at 25 °C (¹H at 300.13 MHz, ¹³C at 75.48 MHz) with 300 or 400 MHz using CDCl₃ or MeOD-*d*₄ and the residual protons as reference. When numbers are used for signal assignment, compare with the [Supporting Information](#). Elemental analysis was performed with a Leco 900 CHN analyzer. TGA was performed on a Netzsch Iris TG 209C in an alumina crucible heating from room temperature to 900 °C under nitrogen (40 mL/min) followed by heating to 1000 °C under a mixture of nitrogen and oxygen (1:1; 20 mL/20 mL) with a rate of 20 K/min. DSC measurements were performed with a Netzsch DSC 204 F1 Phoenix calorimeter and with a TA Instruments Q100 with samples in aluminum crucibles with pierced lids and heated under nitrogen (80 mL) at a rate of 10 K/min (temperature program: cooling from 20 to -25 °C, heating from -25 to 200 °C, cooling from 200 to -25 °C, heating from -25 to 200 °C, cooling from 200 to 20 °C). DLS measurements were performed by noninvasive backscattering with an ALV/CGS-3 compact goniometer system with an ALV/LSE-S003 correlator at a wavelength of 632.8 nm (HeNe Laser) and at 90° goniometer angle. The particle radius was determined by the analysis of the correlation function by the g₂(t) method followed by a linearized number-weighting (nw) of the distribution function. TEM was performed using a JEOL JEM-2010 microscope. The samples were attached to Plano S160-3 copper grids by dispersing them in ethanol using an ultrasonic cleaning bath, adding 25 μL on the copper grid, and evaporating the solvent. The images were analyzed using image J software. Nitrogen gas-sorption analysis was performed on an Autosorb iQ instrument from Quantachrome. The sample was degassed at 100 mbar at 120 °C for 24 h prior to measurement. The surface area was calculated according to BET. X-ray powder diffraction measurements were conducted on a Bruker D8-A25-Advance with Bragg–Brentano θ - θ -geometry (goniometer radius 280 mm) in a 2 θ range from 7 to 120° (step size 0.013°) and total scan time of 2 h. Cu K α radiation (λ = 154 pm) with a 12 μm Ni K β filter and a LYNXEYE detector were used. Fluorescence-induced back-ground was reduced by discriminating the detector. Single-crystal XRD analysis was performed on a Bruker AXS X8 Apex CCD diffractometer operating with graphite monochromated Mo K α radiation. Microscope images were recorded under polarized light using an Olympus BX60 microscope equipped with a Sony CCD-Iris color camera. High-resolution mass spectrometry (HRMS) was performed with a solarix 7

T FTICR mass spectrometer (Bruker Daltonics). All samples were ionized by electrospray ionization (ESI) and measured in the negative mode.

2-(X-Bromoalkyl)furan, X = 3, 10 (1a,b). THF (absolute, 80 mL) was cooled to 0 °C, *n*-butyl lithium (20 mL, 2.5 M solution in hexanes, 48.0 mmol) was added, and furan (3.4 mL, 50 mmol) was added dropwise. The mixture was stirred for 30 min at 0 °C and another 30 min at room temperature; then, the appropriate dibromo alkane (40.0 mmol) was added rapidly at -20–0 °C with vigorous stirring, and the mixture was left overnight at room temperature. The reaction was quenched by the addition of saturated NH₄Cl aqueous solution (40 mL) and extracted with ethyl acetate (3 × 40 mL). The organic phase was separated and dried over MgSO₄, and the solvent was removed in vacuum. The residue was purified by distillation over 25 cm Vigreux for 2-(3-bromopropyl)furan (very similar boiling points; compare to literature, no pure fraction was obtained) and over silica (*n*-hexane) in case of 2-(10-bromodecyl)furan.

C3 (1a): Colorless oil. Yield: 56% (4.23 g, 22.4 mmol), contains small amounts of propylidifuran. ¹H NMR (300 MHz, CDCl₃) δ 7.35–7.28 (m, 1H, OCH), 6.32–6.24 (m, 1H, OCHCH), 6.11–6.01 (m, 1H, OCCCH), 3.42 (t, *J* = 6.5 Hz, 2H, CH₂Br), 2.81 (t, *J* = 7.1 Hz, 2H, OCCCH₂), 2.19 (p, *J* = 6.8 Hz, 2H, CH₂CH₂Br). ¹³C NMR (75 MHz, CDCl₃) δ 154.33 (OCC), 141.39 (OCH), 110.31 (OCHCH), 105.86 (OCCH), 32.97 (CBr), 31.17 (CCCB), 26.52 (CCBr). IR ν = 2962 (w, CH₂), 2912 (w, CH₂), 2847 (w, CH₂), 1597 (m, C=C), 1506 (w, C=C), 1147 (m, CH), 731 (s, δ (furan ring)), 647 (w, C-Br) cm⁻¹.

C10 (1b): Colorless oil. Yield: 59% (6.78 g, 23.6 mmol) contains small amounts of decylidifuran. ¹H NMR (300 MHz, CDCl₃) δ 7.31–7.28 (m, 1H, OCH), 6.30–6.24 (m, 1H, OCHCH), 5.97 (d, *J* = 3.1 Hz, 1H, OCCCH), 3.41 (t, *J* = 6.9 Hz, 2H, CH₂Br), 2.61 (t, *J* = 7.6 Hz, 2H, OCCCH₂), 1.92–1.80 (m, 2H, CH₂CH₂Br), 1.70–1.57 (m, 2H, OCH₂CH₂), 1.49–1.23 (m, 12H, CH₂CH₂CH₂CH₂CH₂CH₂CH₂CH₂CH₂CH₂Br). ¹³C NMR (75 MHz, CDCl₃) δ 156.76 (OCC), 156.73, 140.75 (OCH), 110.15 (OCHCH), 104.66 (OCCH), 34.15 (CBr), 32.97 (OCCH₂), 29.62 (CCBr), 29.53 (CCCB), 29.44 (OCCH₂), 29.30, 28.88, 28.30, 28.17, 28.11 (CCCCCCCCBr). IR ν = 2922 (s, CH₂), 2852 (s, CH₂), 1597 (m, C=C), 1506 (m, C=C), 1146 (m, CH), 727 (s, δ (furan ring)) cm⁻¹.

X-Furanoalkyl Dimethyl Phosphonate X = 3, 10 (2a,b). To a suspension of sodium hydride (310 mg, 13.8 mmol) in THF_{abs} (40 mL) at 0 °C dimethyl phosphite (1.34 g, 12.2 mmol) was added dropwise. The mixture was stirred at 0 °C for 1.5 h to give sodium dimethyl phosphonate in quantitative yield (release pressure! H₂). The resulting mixture was added dropwise into a solution of X-bromoalkylfuran (1a,b) (X = 3, 10; 11.6 mmol) in THF_{abs} (100 mL) at room temperature and stirred overnight. The conversion was studied using ¹H NMR, and if necessary, a fresh suspension of sodium dimethyl phosphonate (amount calculated from NMR) was added again and stirred at 25 °C for another night. The solid was filtered off, and the solvent was evaporated. The crude product was obtained as a yellowish oil. After purification over silica gel, using a gradient of *n*-hexane/THF from 1:0 (v/v) to 7:3, in case of C3 a colorless oil and in case of C10 a colorless, fast crystallizing solid was obtained.

C3 (2a): Colorless oil. Yield: 97% (2.46 g, 11.3 mmol). ¹H NMR (400 MHz, CDCl₃) δ 7.29 (d, *J* = 1.4 Hz, 1H, OCH), 6.26 (dd, *J* = 2.9, 2.0 Hz, 1H, OCHCH), 6.00 (d, *J* = 2.8 Hz, 1H, OCCCH), 3.72 (d, 6H, (OCH₂)₂), 2.71 (t, *J* = 7.2 Hz, 2H, CH₂CH₂CH₂P), 1.94 (ddt, *J* = 11.3, 9.1, 7.3 Hz, 2H, CH₂CH₂P), 1.82–1.71 (m, 2H, CH₂P). ³¹P NMR (162 MHz, CDCl₃) δ 34.36. ¹³C NMR (101 MHz, CDCl₃) δ 154.73 (OCC), 141.27 (OCH), 110.24 (OCHCH), 105.70 (OCCH), 52.40 (d, *J* = 6.6 Hz, OCH₃), 28.60 (d, *J* = 17.4 Hz CP), 24.79 (CCCP), 21.21 (d, *J* = 4.7 Hz, CCP). IR ν = 2953 (w, CH₂), 2906 (w, CH₂), 2856 (w, CH₂), 1592 (w, C=C), 1508 (w, C=C), 1460 (w, POC-H₃), 1244 (s, P=O), 1030 (s, P-OC), 802 (s, P-OC) cm⁻¹. Elemental analysis: CHN_{theo} (C₉H₁₅O₄P): C: 49.54; H: 6.93; N: 0.00; CHN_{exp}: C: 47.96; H: 7.04; N: 0.00%.

C10 (2b): Colorless solid. Yield: 52% (1.91 g, 6.0 mmol). ¹H NMR (300 MHz, CDCl₃) δ 7.31–7.27 (m, 1H, OCH), 6.30–6.24 (m, 1H,

OCHCH), 6.00–5.93 (m, 1H, OCCCH), 3.73 (d, $J = 10.7$ Hz, 6H, (OCH₂)₂), 2.60 (t, $J = 7.6$ Hz, 2H, OCCH₂), 1.82–1.50 (m, 6H, OCCCH₂CH₂, CH₂CH₂P), 1.41–1.18 (m, 12H, CH₂CH₂CH₂CH₂CH₂CH₂CH₂CH₂P). ³¹P NMR (121 MHz, CDCl₃) δ 35.26. ¹³C NMR (75 MHz, CDCl₃) δ 156.75 (OCC), 140.77 (OCH), 110.17 (OCHCH), 104.66 (OCCH), 52.39 (d, $J = 6.5$ Hz, O(CH₂)₂), 30.84 (OCCH₂), 30.62, 29.58, 29.45, 29.29, 29.21 (CCCCCCP), 28.14 (d, $J = 4.2$ Hz, CP), 25.77, 23.92 (CCCP), 22.45 (d, $J = 5.3$ Hz, CCP). IR $\nu = 2918$ (s, CH₂), 2848 (s, CH₂), 1593 (w, C=C), 1510 (w, C=C), 1470 (w, POC-H₃), 1236 (m, P=O), 1049 (s, P-OC), 1016 (s, P-OC), 825 (s, P-OC) cm⁻¹. Elemental analysis: CHN_{theo} (C₁₆H₂₉O₄P): C: 60.74; H: 9.24; N: 0.00; CHN_{exp} C: 60.61; H: 9.31; N: 0.00%.

X-Furanoalkyl Phosphonic Acid X = 3, 10 (3a,b). X-Furanoalkyl dimethyl phosphonate (2a,b) (X = 3, 11; 1.88 mmol) was dissolved in dichloromethane (20 mL). Bromotrimethylsilane (2.3 equiv, 4.33 mmol, 662 mg, 570 μ L) was added dropwise at 0 °C. After it was stirred for 18 h at 25 °C, degassed methanol (8 mL) was added at 0 °C, and the mixture was stirred for another 16 h at room temperature. The solution was concentrated, and the products were precipitated using *n*-hexane. After it was filtered, the colorless solid was dried in vacuum.

C3 (3a): Colorless solid. Yield: 98% (347 mg, 1.82 mmol). ¹H NMR (400 MHz, MeOD) δ 7.35 (dd, $J = 1.8, 0.7$ Hz, 1H, OCH), 6.29 (dd, $J = 3.1, 1.9$ Hz, 1H, OCHCH), 6.06 (dd, $J = 3.1, 0.7$ Hz, 1H, OCCCH), 2.73 (t, $J = 7.3$ Hz, 2H, CH₂CH₂CH₂P), 2.01–1.85 (m, 2H, CH₂CH₂P), 1.79–1.63 (m, 2H, CH₂P). ³¹P NMR (162 MHz, MeOD) δ 29.52. ¹³C NMR (101 MHz, MeOD) δ 156.35 (OCC), 142.31 (OCH), 111.08 (OCHCH), 106.41 (OCCH), 29.48 (d, $J = 17.6$ Hz, CP), 27.47 (d, $J = 138.6$ Hz, CCCP), 22.84 (d, $J = 4.4$ Hz, CCP). IR $\nu = 2997$ (w, OH), 2949 (w, CH₂), 2906 (w, CH₂), 2611 (w, OH), 2254 (w, OH), 1595 (w, C=C), 1510 (m, C=C), 1099 (m, P=O), 987 (s, P-OH), 937 (s, P-OH) cm⁻¹. Elemental analysis: CHN_{theo} (C₇H₁₁O₄P): C: 44.22; H: 5.83; N: 0.00; CHN_{exp} C: 43.93; H: 5.52; N: 0.00%. ESI-MS: ⁻MS: [M-H⁺]: 189.0326 *m/z*.

C10 (3b): Colorless solid. Yield: 90% (488 mg, 1.69 mmol). ¹H NMR (400 MHz, MeOD) δ 7.32 (dd, $J = 1.8, 0.7$ Hz, 1H, OCH), 6.26 (dd, $J = 3.1, 1.9$ Hz, 1H, OCHCH), 5.98 (dd, $J = 3.1, 0.8$ Hz, 1H, OCCCH), 2.60 (t, $J = 7.5$ Hz, 2H, OCCH₂), 1.68–1.54 (m, 4H, CH₂P & OCCH₂CH₂), 1.46–1.27 (m, 14H, rest of alkyl chain). ³¹P NMR (162 MHz, MeOD) δ 30.24. ¹³C NMR (101 MHz, MeOD) δ 157.54 (OCC), 141.84 (OCH), 110.99 (OCHCH), 105.64 (OCCH), 31.77 (d, $J = 16.7$ Hz), 30.61, 30.47, 30.42, 30.27, 30.17, 29.25, 28.78 (rest of alkyl chain), 27.42 (OCCH₂), 23.92 (d, $J = 5.0$ Hz). IR $\nu = 3007$ (w, OH), 2922 (m, CH₂), 2852 (m, CH₂), 2663 (w, OH), 2303 (w, OH), 1597 (w, C=C), 1508 (w, C=C), 1032 (m, P=O), 995 (s, P-OH), 953 (s, P-OH) cm⁻¹. Elemental analysis: CHN_{theo} (C₁₄H₂₅O₄P): C: 58.32; H: 8.74; N: 0.00; CHN_{exp} C: 57.60; H: 8.07; N: 0.00%. ESI-MS: ⁻MS: [M-H⁺]: 287.1414 *m/z*.

N-(10-Bromodecyl)phthalimide (4). The synthesis of 4 was similar to that of a literature procedure.²³ Potassium phthalimide (3.55 g, 19.2 mmol) was added in a suspension of 1,10-dibromodecane (25.00 g, 76.2 mmol) in absolute DMF (35 mL) and stirred for 7 h at 160 °C. After it cooled, a mixture of petrolether/diethyl ether (140 mL; (v/v) 1:1) was added, and phase separation was observed after adding brine (70 mL). The organic layer was dried over magnesium sulfate, and the solvent was removed under reduced pressure. The crude product was purified by column chromatography using silica gel, first with hexane, then with a solvent gradient of *n*-hexane/ethyl acetate from 7:3 to 1:1 (v/v). Compound 2 was obtained as a colorless solid that crystallizes in long colorless needles.

Yield: 60% (4.21 g, 11.5 mmol). ¹H NMR (300 MHz, CDCl₃) δ 7.83 (d, $J = 4.0$ Hz, 2H, C3&C6), 7.71 (d, $J = 3.1$ Hz, 2H, C1&C2), 3.67 (t, $J = 7.1$ Hz, 2H, CH₂N), 3.40 (t, $J = 6.9$ Hz, 2H, CH₂Br), 1.91–1.77 (m, 2H, CH₂CH₂Br), 1.75–1.60 (m, 2H, CH₂CH₂N), 1.48–1.19 (m, 12H, C14–19). ¹³C NMR (75 MHz, CDCl₃) δ 168.62 (C=O), 133.98 (C1&2), 132.35 (C4&5), 123.30 (C3&6), 38.20 (CN), 34.16 (CBr), 32.97, 29.47, 29.46, 29.25, 28.84, 28.71, 28.29, 26.96 (C19–20). IR $\nu = 2931$ (s, CH₂), 2854 (s, CH₂), 1714 (s, C=O), 1364 (m,

C–N) cm⁻¹. Elemental analysis: CHN_{theo} (C₁₈H₂₄BrNO₂): C: 59.02; H: 6.60; N: 3.82; CHN_{exp} C: 59.52; H: 6.75; N: 3.27%.

N-(X-Phthalimidoalkyl)diethyl Phosphonate X = 3, 10 (5a,b). The synthesis of 5a,b was similar to that of a literature procedure.⁴⁴ N-(3-Bromoalkyl)phthalimide (C3,C10; 10.0 mmol) was added to triethyl phosphite (4 equiv, 66.5 g, 69 mL, 40 mmol) slowly at room temperature. The reaction mixture was refluxed (150 °C) for 24 h; then, excess triethyl phosphite was removed under reduced pressure (3 mmHg) at 60 °C, and diethyl ethylphosphonate was distilled out in high vacuum (5 \times 10⁻³ mbar, 80 °C).

C3 (5a): Colorless solid (solidifies upon storage at –25 °C). Yield: 100% (3.25 g, 10.0 mmol). ¹H NMR (300 MHz, CDCl₃) δ 7.84 (dd, $J = 8.2, 4.0$ Hz, 2H, H3&6), 7.78–7.67 (m, 2H, H1&H2), 4.20–3.97 (m, 4H, OCH₂CH₃), 3.75 (t, $J = 6.9$ Hz, 2H, NCH₂), 2.10–1.89 (m, 2H, CH₂CH₂P), 1.87–1.69 (m, 2H, CH₂P), 1.30 (t, $J = 7.0$ Hz, 6H, (CH₃)₂). ³¹P NMR (121 MHz, CDCl₃) δ 30.70. ¹³C NMR (75 MHz, CDCl₃) δ 168.40 (C=O), 134.17 (C1&C2), 132.17 (C4&C5), 123.43 (C3&C6), 61.80 (d, $J = 6.5$ Hz, OCH₂), 38.40 (d, $J = 20.0$ Hz, CN), 23.58 (d, $J = 143.2$ Hz, CH₂P), 22.14 (d, $J = 4.6$ Hz, CH₂CH₂P), 16.59 (d, $J = 5.9$ Hz, OCH₂CH₃). IR $\nu = 2978$ (w, CH₂), 2906 (w, CH₂), 1705 (s, C=O), 1369 (m, C–N), 1244 (s, P=O), 1030 (s, P-OC), 958 (s, P-OC) cm⁻¹. Elemental analysis: CHN_{theo} (C₁₅H₂₀NO₃P): C: 55.38; H: 6.20; N: 4.31; CHN_{exp} C: 55.32; H: 6.24; N: 4.15%.

C10 (5b): Colorless oil. Yield: 100% (4.23 g, 10.0 mmol). ¹H NMR (400 MHz, CDCl₃) δ 7.87–7.79 (m, 2H, H3&H6), 7.75–7.65 (m, 2H, H1&H2), 4.17–3.99 (m, 4H, OCH₂), 3.72–3.62 (m, 2H, CH₂N), 1.78–1.50 (m, 6H, C13 & C20), 1.41–1.21 (m, 18H, C14–19 & (CH₃)₂). ³¹P NMR (121 MHz, CDCl₃) δ 32.61. ¹³C NMR (75 MHz, CDCl₃) δ 168.56 (C=O), 133.94 (C1&2), 132.30 (C4&5), 123.25 (C3&6), 61.46 (d, $J = 6.5$ Hz, OCH₂), 38.15 (CN), 30.68 (d, $J = 16.9$ Hz, CH₂CH₂P), 29.43 (d, $J = 8.1$ Hz, CH₂CH₂CH₂P), 29.23, 29.14, 28.68, 26.94, 26.73, 24.87 (C13–18), 22.51 (d, $J = 5.2$ Hz, CH₂P), 16.59 (d, $J = 6.0$ Hz, OCH₂CH₃). IR: $\nu = 2982$ (w, CH₂), 2928 (m, CH₂), 2954 (m, CH₂), 1709 (s, C=O), 1394 (m, C–N), 1234 (m, P=O), 1055 (s, P-OC), 1024 (s, P-OC), 957 (s, P-OC) cm⁻¹. Elemental analysis: CHN_{theo} (C₂₂H₃₄NO₃P): C: 62.40; H: 8.09; N: 3.31; CHN_{exp} C: 62.37; H: 8.31; N: 3.05.

N-(X-Aminoalkyl)diethylphosphonate X = 3, 10 (6a,b). The synthesis of N-(3-aminopropyl)diethylphosphonate was similar to that of a literature procedure.²³ Hydrazine monohydrate (650 mg, 630 μ L, 13.0 mmol) was added to a solution of the appropriate phthalimide (5a,b; 4.61 mmol) in absolute ethanol (200 mL) at 0 °C. After 30 min, the reaction mixture was heated to reflux for 10 h. After it slowly cooled to room temperature, the crystallized precipitate, phthalhydrazide, was filtered off, and the solvent was removed under reduced pressure. To the crude mixture, 10 mL of absolute dichloromethane was added, and again, the mixture was filtered. Evaporation of the solvent gave the desired amino phosphonates (6a,b) as colorless oils. No residual ethanol should be left, as it would react in the following reaction. The crude products with high purity (compare NMR) were used without further purification.

C3 (6a): Colorless oil. Yield: 60% (540 mg, 2.77 mmol). ¹H NMR (400 MHz, CDCl₃) δ 4.35–3.80 (m, 4H, OCH₂CH₃), 2.83–2.70 (m, 2H, CH₂N), 1.86–1.66 (m, 4H, CH₂CH₂P), 1.65–1.45 (m, 2H, NH₂), 1.32 (t, $J = 7.0$ Hz, 6H, (CH₃)₂). ³¹P NMR (162 MHz, CDCl₃) δ 32.32. ¹³C NMR (101 MHz, CDCl₃) δ 61.64 (d, $J = 6.5$ Hz, OC), 42.71 (d, $J = 17.1$ Hz, CN), 26.65 (d, $J = 5.0$ Hz, CH₂P), 23.24 (d, $J = 142.3$ Hz, CH₂P), 16.62 (d, $J = 6.0$ Hz, CH₃). IR $\nu = 2985$ (w, CH₂), 2935 (w, CH₂), 2904 (w, CH₂), 1444 (w, NCH₂), 1390 (w, C–N), 1228 (s, P=O), 1022 (s, P-OC), 955 (m, P-OC) cm⁻¹.

C10 (6b): Colorless oil. Yield: 52% (709 mg, 2.40 mmol). ¹H NMR (400 MHz, CDCl₃) δ 4.16–3.97 (m, 4H), 2.69 (t, $J = 7.1$ Hz, 2H), 2.21 (s, 2H), 1.77–1.65 (m, 2H), 1.64–1.51 (m, 2H), 1.44 (dd, $J = 13.6, 6.7$ Hz, 2H), 1.40–1.21 (m, 18H). ³¹P NMR (162 MHz, CDCl₃) δ 32.68. ¹³C NMR (101 MHz, CDCl₃) δ 61.52 (d, $J = 6.5$ Hz, OC), 42.17 (CN), 33.50 (CCN), 30.74 (d, $J = 16.9$ Hz, CH₂P), 29.61 (d, $J = 10.2$ Hz, CH₂CH₂CH₂P), 29.45, 29.21, 26.99, 26.53, 25.13 (C4–C8), 22.53 (d, $J = 5.2$ Hz, CH₂CH₂P), 16.62 (d, $J = 6.0$ Hz, CH₃). IR $\nu = 3419$ (w, NH), 2983 (w, CH₂), 2928 (w, CH₂), 2954 (w, CH₂), 1572

(m, CH₂), 1443 (m, NCH₂), 1389 (m, C–N), 1215 (m, P=O), 1049 (s, P–OC), 1024 (s, P–OC), 958 (s, P–OC) cm⁻¹.

N-(*X*-Maleimidealkyl)diethylphosphonate *X* = 3, 10 (**7a,b**). Maleic anhydride (235 mg, 2.40 mmol) was suspended in dry dichloromethane (10 mL). A mixture of *N*-(3-aminoalkyl) diethylphosphonic acid (C3, C10, 2.40 mmol) in dry dichloromethane (10 mL) was added dropwise while stirring. After the mixture was allowed to stir for 1 h at room temperature, the solvent was removed under vacuum. The intermediate products were collected as a colorless oils.

C3 Maleamic Acid. ¹H NMR (400 MHz, CDCl₃) δ 9.00 (br s, 1H, OH), 6.34 (m, 2H, C=C), 4.20–4.01 (m, 4H, (OCH₂CH₂)₂), 3.46 (dd, *J* = 11.8, 5.8 Hz, 2H, NCH₂), 2.01–1.80 (m, 4H, NCH₂CH₂CH₂), 1.34 (t, *J* = 7.1 Hz, 6H, (OCH₂CH₂)₂). ³¹P NMR (162 MHz, CDCl₃) δ 32.64. ¹³C NMR (101 MHz, CDCl₃) δ 166.34 (HNC=O), 165.43 (HOC=O), 136.14 (HO(C=O)C=), 131.57 (HN(C=O)C=), 62.50 (d, *J* = 6.8 Hz, OC), 40.71 (d, *J* = 9.2 Hz, CN), 23.64 (d, *J* = 141.4 Hz, CCN), 21.32 (d, *J* = 4.7 Hz, CP), 16.56 (d, *J* = 6.1 Hz, OCH₂CH₂). IR ν = 3232 and 3063 (w, OH & NH) 2983 (w, CH₂), 2935 (w, CH₂), 2906 (w, CH₂), 1716 (s, C=O), 1211 (s, P=O), 1020 (s, P–OC), 962 (m, P–OC) cm⁻¹.

C10 Maleamic Acid. ¹H NMR (400 MHz, CDCl₃) δ 8.21 (s, 1H, OH), 6.54–6.22 (m, 2H, C=C), 4.17–3.98 (m, 4H, (OCH₂CH₂)₂), 3.44–3.25 (m, 2H, NCH₂), 1.80–1.65 (m, 2H, CH₂P), 1.65–1.49 (m, 4H, CH₂CH₂P & CH₂CH₂N), 1.49–1.22 (m, 18H, C11–17 & (OCH₂CH₂)₂). ³¹P NMR (162 MHz, CDCl₃) δ 32.67. ¹³C NMR (101 MHz, CDCl₃) δ 166.23 (HOC=O), 165.80 (HNC=O), 135.51 (HO(C=O)C=), 132.19 (HN(C=O)C=), 61.86 (d, *J* = 6.6 Hz, OC), 40.49 (CN), 30.06 (d, *J* = 16.1 Hz, CCCP), 28.82, 28.76, 28.62, 28.59, 28.53, 26.59 (C12–17), 25.33 (d, *J* = 140.1 Hz, CP), 22.06 (d, *J* = 5.0 Hz, CCP), 16.58 (d, *J* = 6.0 Hz, OCH₂CH₂). IR ν = 3441 and 3240 (m, NH & OH), 2985 (m, CH₂), 2926 (s, CH₂), 2854 (s, CH₂), 1716 (m, C=O), 1215 (s, P=O), 1053 (s, P–O–C), 1026 (s, P–OC), 964 (m, P–OC) cm⁻¹.

In the next step, the appropriate intermediate product (2.40 mmol) was dissolved in acetic anhydride (8.0 mL, 8.65 g, 84.8 mmol), and sodium acetate (98 mg, 1.20 mmol) was added. The mixture was heated to 100 °C for 5 h. After the mixture cooled, ethyl acetate (8 mL) was added to the mixture and extracted with distilled water (3 × 8 mL) and with brine (1 × 8 mL). The organic layer was dried over Na₂SO₄. The solvent was evaporated, and residual acetic anhydride and part of HOAc was distilled off in high vacuum (5 × 10⁻³ mbar, 100 °C). The crude products were used without further purification due to high yield losses trying purification over silica column.

C3 (7a): Colorless oil. Yield: 53% (350 mg, 1.27 mmol). ¹H NMR (400 MHz, CDCl₃) δ 6.69 (s, 2H, 2H, HC=CH), 4.17–3.97 (m, 2H, (OCH₂CH₂)₂), 3.56 (t, *J* = 7.0 Hz, 2H, CH₂N), 1.94–1.80 (m, 2H, CH₂CH₂N), 1.78–1.62 (m, 2H, CH₂P), 1.30 (t, *J* = 5.1 Hz, 6H, (OCH₂CH₂)₂). ³¹P NMR (162 MHz, CDCl₃) δ 30.64. ¹³C NMR (101 MHz, CDCl₃) δ 170.77 (C=O), 134.27 (C=C), 61.84 (d, *J* = 6.5 Hz, OC), 38.26 (d, *J* = 19.9 Hz, CN), 23.44 (d, *J* = 143.3 Hz, CP), 22.08 (d, *J* = 4.5 Hz, CCP), 16.57 (d, *J* = 6.0 Hz, OCH₂CH₂). IR ν = 2982 (w, CH₂), 2945 (w, CH₂), 2912 (w, CH₂), 1703 (s, C=O), 1444 (m, NCH₂), 1408 (m, C–H), 1371 (m, C–N), 1248 (m, P=O), 1022 (s, P–OC), 964 (s, P–OC), 827 (m, =C–H), 694 (s, maleimide ring deformation) cm⁻¹.

C10 (7b): Colorless oil. Yield: 63% (565 mg, 1.51 mmol). ¹H NMR (400 MHz, CDCl₃) δ 6.68 (s, 2H, HC=CH), 4.16–3.98 (m, 4H, (OCH₂CH₂)₂), 3.50 (dd, *J* = 13.4, 6.1 Hz, 2H, CH₂N), 1.79–1.64 (m, 2H, CH₂P), 1.64–1.49 (m, 4H, CH₂CH₂P & CH₂CH₂N), 1.40–1.19 (m, 18H, C10–C15 & (OCH₂CH₂)₂). ³¹P NMR (162 MHz, CDCl₃) δ 32.66. ¹³C NMR (101 MHz, CDCl₃) δ 171.04 (C=O), 134.18 (C=C), 61.53 (d, *J* = 6.5 Hz, OC), 38.05 (CN), 30.72 (d, *J* = 17.2 Hz, CCCP), 29.52, 29.39, 29.17, 29.19 (two C), 28.65, 26.84 (C9–15), 25.82 (d, *J* = 140.2 Hz, CP), 22.53 (d, *J* = 5.2 Hz, CCP), 16.62 (d, *J* = 5.9 Hz, OCH₂CH₂). IR ν = 2983 (m, CH₂), 2926 (s, CH₂), 2854 (s, CH₂), 1705 (s, C=O), 1441 (m, NCH₂), 1406 (m, C–H), 1367 (m, C–N), 1234 (m, P=O), 1053 (s, P–OC), 1028 (s, P–OC), 958 (s, P–OC), 829 (m, =C–H), 696 (s, maleimide ring deformation) cm⁻¹.

N-(*X*-Maleimide alkyl)phosphonic Acid *X* = 3, 10 (**8a,b**). *N*-(3-Maleimidepropyl) diethylphosphonate (**8a,b**) (*X* = 3, 11; 1.27 mmol)

was dissolved in absolute acetonitrile (10 mL). BrTMS (2.3 equiv, 447 mg, 385 μL, 2.92 mmol) was added dropwise at 0 °C. The mixture was stirred for 18 h at 25 °C. The solvent, byproducts, and excess BrTMS were removed in vacuum (5 × 10⁻³ mbar, 25 °C). Degassed methanol (8 mL) was added at 0 °C, and the mixture was stirred for another 16 h at room temperature. The solution was reduced to the half volume, and the products were precipitated using *n*-hexane. After the solution was filtered, the colorless solid was dried in vacuum.

C3 (8a): Colorless solid. Yield: 96% (267 mg, 1.22 mmol). ¹H NMR (400 MHz, MeOD) δ 6.77 (s, 2H, HC=CH), 3.52 (t, NCH₂, *J* = 6.9 Hz, 2H), 1.90–1.71 (m, 2H, CH₂CH₂P), 1.70–1.54 (m, 2H, CH₂P). ³¹P NMR (162 MHz, MeOD) δ 28.60. ¹³C NMR (101 MHz, MeOD) δ 172.51 (C=O), 135.38 (C=C), 39.11 (d, *J* = 20.5 Hz, CN), 25.65 (d, *J* = 139.9 Hz, CP), 23.45 (d, *J* = 4.1 Hz, CCP). IR ν = 3442 (w, OH), 3111 (w, CH₂), 2951 (w, CH₂), 2754 (w, OH), 2318 (w, OH), 1697 (s, C=O), 1446 (m, NCH₂), 1408 (m, C–H), 1363 (m, C–N), 1200 (m, P=O), 1113 (m, =P–O), 991 (s, P–OH), 954 (s, P–OH), 827 (s, =C–H), 694 (s, δ(maleimide ring)) cm⁻¹. Elemental analysis: CHN_{theo} (C₇H₁₀NO₃P): C: 38.37; H: 4.60; N: 6.39; CHN_{exp}: C: 37.34; H: 5.28; N: 6.25%. ESI-MS: ⁻MS: [M–H⁺]: 218.0220 *m/z*.

C10 (8b): Colorless solid. Yield: 89% (359 mg, 1.13 mmol). ¹H NMR (400 MHz, MeOD) δ 6.80 (s, 2H, HC=CH), 3.48 (t, *J* = 7.1 Hz, 2H, CH₂N), 1.75–1.50 (m, 6H, CH₂CH₂N, CH₂P, CH₂CH₂P), 1.49–1.22 (m, 12H, C14–19). ³¹P NMR (162 MHz, MeOD) δ 30.28. ¹³C NMR (101 MHz, MeOD) δ 172.60 (C=O), 135.33 (C=C), 38.52 (CN), 31.75 (d, *J* = 16.8 Hz, CCCP), 30.52, 30.41, 30.25, 30.14, 29.47, 27.74 (C15–C20), 28.09 (d, *J* = 134.0 Hz, CP), 23.92 (d, *J* = 4.9 Hz, CCP). IR: ν = 3034 (w, P–OH), 2912 (m, CH₂), 2848 (m, CH₂), 2652 (w, PO–H), 2299 (w, P–OH), 1693 (s, C=O), 1470 (m, NCH₂), 1421 (m, C–H), 1375 (m, C–N), 1099 (m, P=O), 1014 (m, P–OH), 952 (s, P–OH), 833 (s, =C–H), 696 (δ(maleimide ring)) cm⁻¹. Elemental analysis: CHN_{theo} (C₁₄H₂₄NO₃P): C: 52.99; H: 7.62; N: 4.41; CHN_{exp}: C: 52.79; H: 7.59; N: 4.64%. ESI-MS: ⁻MS: [M–H⁺]: 316.1317 *m/z*.

Synthesis of *N*-Dodecylmaleimid (9). A mixture of dodecylamine (3.26 g, 17.6 mmol) in dry dichloromethane (20 mL) was added to maleic anhydride (1.73 g, 17.6 mmol) dry dichloromethane (60 mL). After the mixture was allowed to stir for 1 h at room temperature, the solvent was removed under vacuum. The intermediate product was collected as a colorless solid. In the next step, the intermediate product was dissolved in dry toluene (60 mL), and zinc chloride (2.40 g, 17.6 mmol) was added at once. After the mixture was heated to 80 °C, a solution of hexamethyldisilazane (2.84 g, 17.6 mmol) and toluene (20 mL) was added dropwise. The temperature was held for 5 h at 80 °C. After it cooled, the solution was filtered, and the solvent was removed in vacuum to afford the desired product as a colorless solid. Yield: 91% (4.25 g, 16.0 mmol). ¹H NMR (400 MHz, CDCl₃) δ 6.68 (s, 2H, CH=CH), 3.50 (t, *J* = 8.0 Hz, 2H, CH₂N), 1.62–1.50 (m, 2H, CH₂CH₂N), 1.35–1.17 (m, 18H, C10–18), 0.87 (t, *J* = 6.8 Hz, 3H, CH₃). ¹³C NMR (101 MHz, CDCl₃) δ 171.06 (C=O), 134.18 (C=C), 38.10 (CN), 32.05, 29.76, 29.69, 29.63, 29.49, 29.28, 28.69, 26.90, 22.83 (C9–18), 14.27 (CH₃). IR ν = 2918 (m, CH₂), 2850 (m, CH₂), 1697 (s, C=O), 1446 (m, NCH₂), 1402 (m, C–H), 1369 (m, C–N), 692 (s, δ(maleimide ring)) cm⁻¹. Elemental analysis: CHN_{theo} (C₁₄H₂₄NO₃P): C: 72.41; H: 10.25; N: 5.28; CHN_{exp}: C: 71.35; H: 9.95; N: 5.59%.

Synthesis of Dodecylfuran (10). THF (absolute, 80 mL) was cooled to 0 °C, *n*-butyllithium (20 mL, 2.5 M solution in hexanes, 48.0 mmol) was added, and furan (3.4 mL, 50.0 mmol) was added dropwise. The mixture was stirred for 30 min at 0 °C and for another 30 min at room temperature; then, 1-bromo dodecane (9.97 g, 40.0 mmol) was added at –20–0 °C with vigorous stirring, and the mixture was left overnight at room temperature. The reaction was quenched by the addition of saturated NH₄Cl aqueous solution (40 mL) and extracted with ethyl acetate (3 × 40 mL). The organic phase was separated and dried over MgSO₄, and the solvent was removed in vacuo. The residue was purified by column chromatography (silica; eluent: *n*-hexane) to afford the product as colorless oil. Yield: 87% (8.23 g, 34.8 mmol). ¹H NMR (400 MHz, CDCl₃) δ 7.29 (d, *J* = 1.0 Hz, 1H, H3), 6.30–6.25 (m, 1H, H4), 5.97 (d, *J* = 2.6 Hz, 1H, H5),

2.61 (t, $J = 7.6$ Hz, 2H, H1), 1.68–1.58 (m, 2H, H2), 1.37–1.21 (m, 18H, H8–16), 0.88 (t, $J = 6.8$ Hz, 3H, CH₃). ¹³C NMR (101 MHz, CDCl₃) δ 156.81 (C6), 140.75 (C3), 110.16 (C4), 104.63 (C5), 32.07, 29.82, 29.79 (two C), 29.71, 29.52, 29.51, 29.35, 28.19, 28.13, 22.84 (C1–16), 14.27 (CH₃). IR $\nu = 2922$ (s, CH₂), 2852 (s, CH₂), 1597 (m, C=C). Elemental analysis: CHN_{theo} (C₁₆H₂₈O): C: 81.29; H: 11.94; N: 0%. CHN_{exp}: C: 80.51; H: 11.41; N: 0%.

Magnetite/Maghemite Nanoparticles (11).¹³ The magnetite/maghemite particles were produced using a modified literature procedure via thermal decomposition of Fe(acac)₃. Fe(acac)₃ (3.53 g, 10 mmol), dodecandiol (10.10 g, 10.0 mmol), oleic acid (10 mL), and oleyl amine (10 mL) dissolved in benzyl ether (100 mL) were heated to 200 °C. The temperature was held for 30 min, and the mixture was heated to 300 °C. This temperature again was held for 30 min. Then the heating source was removed, and the mixture was cooled to room temperature. The particles were magnetically decanted off and washed with ethanol (3 × 100 mL). The particles were stored in dispersion in ethanol (96 mL). An aliquot of 2 mL of the sample was taken out, and the particles were magnetically decanted off and dried in vacuum to estimate the concentration and yield (17.7 mg/2 mL; ca. 850 mg; TGA: 78.65% residual mass after N₂ segment; this residual mass can be attributed to the inorganic core, calculating with the molar mass of Fe_xO_y; the yield can be estimated to ~663 mg of Fe_xO_y = 2.86 mmol = 81%). The exact yield varies from batch to batch, but it is always in the same range.

Ligand Exchange Protocol. The appropriate phosphonic acid (0.3 mmol) was dissolved in *n*-hexane/ethanol (8 mL/2 mL). Ethanol particle dispersion (16.9 mL, 150 mg of OA@Fe_xO_y) was added, and the mixture was stirred at 25 °C for 48 h. Afterward, the particles were magnetically decanted off, washed with ethanol (3 × 15 mL), and stored in ethanol (20 mL). The concentration and the yield were determined as described in the synthesis of OA@Fe_xO_y.

Cofunctionalization. The cofunctionalization was performed identically as the ligand exchange, except for choosing the millimolar ratios of the appropriate functional coupling agent and methyl phosphonic acid. The ratios used are displayed in Table S4 within the Supporting Information. The functionalized particles were stored in ethanol (20 mL).

DA Reaction on Particle Surface. Conversion with three equivalents of dienophile: 47.76 mg of NM or 13.1 mg of M = 0.06 mmol.

An aliquot of 4 mL (ca. 30 mg particles) of each sample of cofunctionalized particles was magnetically decanted off; chloroform (5 mL) was added with the appropriate DA reagent (3 equiv, 0.06 mmol). The mixtures were stirred at 60 °C for 24 h. At this temperature, the supernatant was removed by magnetic decantation, and the “furan” particles were washed with a mixture of ethanol/acetone/ethyl acetate (= 1:1:1; 5 × 5 mL). The “maleimide” particles were washed using THF (5 × 5 mL).

Synthesis of Composite. F10P₁₀₀@Fe_xO_y particles (30 mg) dispersed in chloroform (5 mL) were mixed with 1,1'-(methylene-di-4,1-phenylene)bismaleimide (150 mg, 0.465 mmol) dissolved in chloroform (5 mL). After it was shaken for 1 min, the solvent was removed in vacuum. The gray powder was poured between two sheets of aluminum foil within a heatable press. The aluminum foils were used to separate the composite film from the heatable press after cross-linking. The sample was cross-linked at 60 °C for 24 h at a pressure of 1 t, which led to a black brittle free-standing film of 250 μ m.

■ ASSOCIATED CONTENT

● Supporting Information

The Supporting Information is available free of charge on the ACS Publications website at DOI: 10.1021/acsnm.8b00308.

Further data to particles: DLS, XRD, TEM, TG curves, FTIR, CHN values, DLS; NMR and IR spectra of organic molecules (PDF)
Structural data (CIF)

■ AUTHOR INFORMATION

Corresponding Author

*E-mail: guido.kickelbick@uni-saarland.de.

ORCID

Guido Kickelbick: 0000-0001-6813-9269

Author Contributions

Experiments were conducted by S.S. The manuscript was written through contributions of S.S. and G.K.

Funding

Both authors received funding from Saarland Univ.

Notes

The authors declare no competing financial interest.

■ ACKNOWLEDGMENTS

We thank V. Huch for the single X-ray diffraction measurements.

■ ABBREVIATIONS

OA, oleic acid
PA, phosphonic acid
DDP, dodecylphosphonic acid
MeP, methyl phosphonic acid
F10P, furan decyl phosphonic acid
F3P, furan propyl phosphonic acid
M10P, maleimide decyl phosphonic acid
M3P, maleimide propyl phosphonic acid
M, maleimide
NM, *N*-dodecylmaleimide
MF, methyl furan
DF, dodecylfuran
HMDS, hexamethyl disilazane

■ REFERENCES

- (1) N'Guyen, T. T. T.; Duong, H. T. T.; Basuki, J.; Montebault, V.; Pascual, S.; Guibert, C.; Fresnais, J.; Boyer, C.; Whittaker, M. R.; Davis, T. P.; Fontaine, L. Functional Iron Oxide Magnetic Nanoparticles with Hyperthermia-Induced Drug Release Ability by Using a Combination of Orthogonal Click Reactions. *Angew. Chem., Int. Ed.* **2013**, *52*, 14152–14156.
- (2) Xu, Z.; Zhao, Y.; Wang, X.; Lin, T. A Thermally Healable Polyhedral Oligomeric Silsesquioxane (POSS) Nanocomposite based on Diels-Alder chemistry. *Chem. Commun.* **2013**, *49*, 6755–6757.
- (3) Engel, T.; Kickelbick, G. Self-Healing Nanocomposites from Silica – Polymer Core – Shell Nanoparticles. *Polym. Int.* **2014**, *63*, 915–923.
- (4) Engel, T.; Kickelbick, G. Furan-Modified Spherosilicates as Building Blocks for Self-Healing Materials. *Eur. J. Inorg. Chem.* **2015**, *2015*, 1226–1232.
- (5) Torres-Lugo, M.; Rinaldi, C. Thermal Potentiation of Chemotherapy by Magnetic Nanoparticles. *Nanomedicine* **2013**, *8*, 1689–1707.
- (6) Hohlbein, N.; Shaaban, A.; Bras, A. R.; Pyckhout-Hintzen, W.; Schmidt, A. M. Self-healing Dynamic Bond-based Rubbers: Understanding the Mechanisms in Ionomeric Elastomer Model Systems. *Phys. Chem. Chem. Phys.* **2015**, *17*, 21005–21017.
- (7) Wu, C.-S.; Kao, T.-H.; Li, H.-Y.; Liu, Y.-L. Preparation of Polybenzoxazine-functionalized Fe₃O₄ Nanoparticles through in situ Diels-Alder Polymerization for High Performance Magnetic Polybenzoxazine/Fe₃O₄ Nanocomposites. *Compos. Sci. Technol.* **2012**, *72*, 1562–1567.
- (8) Menon, A. V.; Madras, G.; Bose, S. Ultrafast Self-Healable Interfaces in Polyurethane Nanocomposites Designed Using Diels-Alder “Click” as an Efficient Microwave Absorber. *ACS Omega* **2018**, *3*, 1137–1146.

- (9) Engel, T.; Kickelbick, G. Thermoreversible Reactions on Inorganic Nanoparticle Surfaces: Diels–Alder Reactions on Sterically Crowded Surfaces. *Chem. Mater.* **2013**, *25*, 149–157.
- (10) Schäfer, S.; Kickelbick, G. Self-Healing Polymer Nanocomposites based on Diels–Alder-reactions with Silica Nanoparticles: The Role of the Polymer Matrix. *Polymer* **2015**, *69*, 357–368.
- (11) Park, J. S.; Darlington, T.; Starr, A. F.; Takahashi, K.; Riendeau, J.; Thomas Hahn, H. Multiple Healing Effect of Thermally Activated Self-Healing Composites based on Diels–Alder reaction. *Compos. Sci. Technol.* **2010**, *70*, 2154–2159.
- (12) Li, J.; Liang, J.; Li, L.; Ren, F.; Hu, W.; Li, J.; Qi, S.; Pei, Q. Healable Capacitive Touch Screen Sensors Based on Transparent Composite Electrodes Comprising Silver Nanowires and a Furan/Maleimide Diels–Alder Cycloaddition Polymer. *ACS Nano* **2014**, *8*, 12874–12882.
- (13) Sun, S.; Zeng, H.; Robinson, D. B.; Raoux, S.; Rice, P. M.; Wang, S. X.; Li, G. Monodisperse MFe_2O_4 ($M = Fe, Co, Mn$) Nanoparticles. *J. Am. Chem. Soc.* **2004**, *126*, 273–279.
- (14) Frison, R.; Cernuto, G.; Cervellino, A.; Zaharko, O.; Colonna, G. M.; Guagliardi, A.; Masciocchi, N. Magnetite–Maghemite Nanoparticles in the 5–15 nm Range: Correlating the Core–Shell Composition and the Surface Structure to the Magnetic Properties. A Total Scattering Study. *Chem. Mater.* **2013**, *25*, 4820–4827.
- (15) Santoyo Salazar, J.; Perez, L.; de Abril, O.; Truong Phuoc, L.; Ihiawakrim, D.; Vazquez, M.; Greneche, J.-M.; Begin-Colin, S.; Pourroy, G. Magnetic Iron Oxide Nanoparticles in 10–40 nm Range: Composition in Terms of Magnetite/Maghemite Ratio and Effect on the Magnetic Properties. *Chem. Mater.* **2011**, *23*, 1379–1386.
- (16) Guerrero, G.; Mutin, P. H.; Vioux, A. Anchoring of Phosphonate and Phosphinate Coupling Molecules on Titania Particles. *Chem. Mater.* **2001**, *13*, 4367–4373.
- (17) Babu, K.; Dhamodharan, R. Grafting of Poly(methyl methacrylate) Brushes from Magnetite Nanoparticles Using a Phosphonic Acid Based Initiator by Ambient Temperature Atom Transfer Radical Polymerization (ATATRP). *Nanoscale Res. Lett.* **2008**, *3*, 109–117.
- (18) Mohapatra, S.; Pramanik, P. Synthesis and Stability of Functionalized Iron Oxide Nanoparticles using Organophosphorus Coupling Agents. *Colloids Surf., A* **2009**, *339*, 35–42.
- (19) Larsen, B. A.; Hurst, K. M.; Ashurst, W. R.; Serkova, N. J.; Stoldt, C. R. Mono- and Dialkoxysilane Surface Modification of Superparamagnetic Iron Oxide Nanoparticles for Application as Magnetic Resonance Imaging Contrast Agents. *J. Mater. Res.* **2012**, *27*, 1846–1852.
- (20) Davis, K.; Qi, B.; Witmer, M.; Kitchens, C. L.; Powell, B. A.; Mefford, O. T. Quantitative Measurement of Ligand Exchange on Iron Oxides via Radiolabeled Oleic Acid. *Langmuir* **2014**, *30*, 10918–10925.
- (21) Feichtenschlager, B.; Pabisch, S.; Peterlik, H.; Kickelbick, G. Nanoparticle Assemblies as Probes for Self-Assembled Monolayer Characterization: Correlation between Surface Functionalization and Agglomeration Behavior. *Langmuir* **2012**, *28*, 741–750.
- (22) Musa, O. M. *Handbook of Maleic Anhydride Based Materials: Syntheses, Properties and Applications*; Springer International Publishing: Switzerland, 2016; p 175ff.
- (23) Sauer, R.; Froimowicz, P.; Scholler, K.; Cramer, J. M.; Ritz, S.; Mailander, V.; Landfester, K. Design, Synthesis, and Miniemulsion Polymerization of New Phosphonate Surfmers and Application Studies of the Resulting Nanoparticles as Model Systems for Biomimetic Mineralization and Cellular Uptake. *Chem. - Eur. J.* **2012**, *18*, 5201–5212.
- (24) Lu, C.; Bhatt, L. R.; Jun, H. Y.; Park, S. H.; Chai, K. Y. Carboxyl–Polyethylene Glycol–Phosphoric Acid: A Ligand for highly stabilized Iron Oxide Nanoparticles. *J. Mater. Chem.* **2012**, *22*, 19806–19811.
- (25) Patsula, V.; Kosinova, L.; Lovric, M.; Ferhatovic Hamzic, L.; Rabyk, M.; Konefal, R.; Paruzel, A.; Slouf, M.; Herynek, V.; Gajovic, S.; Horak, D. Superparamagnetic Fe_3O_4 Nanoparticles: Synthesis by Thermal Decomposition of Iron(III) Glucuronate and Application in Magnetic Resonance Imaging. *ACS Appl. Mater. Interfaces* **2016**, *8*, 7238–7247.
- (26) Pothayee, N.; Balasubramaniam, S.; Davis, R. M.; Riffle, J. S.; Carroll, M. R. J.; Woodward, R. C.; St Pierre, T. G. Synthesis of ‘ready-to-adsorb’ Polymeric Nanoshells for Magnetic Iron Oxide Nanoparticles via Atom Transfer Radical Polymerization. *Polymer* **2011**, *52*, 1356–1366.
- (27) Daou, J.; Begin-Colin, S.; Grenèche, J. M.; Thomas, F.; Derory, A.; Bernhardt, P.; Legaré, P.; Pourroy, G. Phosphate Adsorption Properties of Magnetite-Based Nanoparticles. *Chem. Mater.* **2007**, *19*, 4494–4505.
- (28) Breucker, L.; Landfester, K.; Taden, A. Phosphonic Acid-Functionalized Polyurethane Dispersions with Improved Adhesion Properties. *ACS Appl. Mater. Interfaces* **2015**, *7*, 24641–24648.
- (29) Sahoo, Y.; Pizem, H.; Fried, T.; Golodnitsky, D.; Burstein, L.; Sukenik, C. N.; Markovich, G. Alkyl Phosphonate/Phosphate Coating on Magnetite Nanoparticles: A Comparison with Fatty Acids. *Langmuir* **2001**, *17*, 7907–7911.
- (30) Longo, R. C.; Cho, K.; Schmidt, W. G.; Chabal, Y. J.; Thissen, P. Monolayer Doping via Phosphonic Acid Grafting on Silicon: Microscopic Insight from Infrared Spectroscopy and Density Functional Theory Calculations. *Adv. Funct. Mater.* **2013**, *23*, 3471–3477.
- (31) Lushtinetz, R.; Seifert, G.; Jaehne, E.; Adler, H.-J. P. Infrared Spectra of Alkylphosphonic Acid Bound to Aluminium Surfaces. *Macromol. Symp.* **2007**, *254*, 248–253.
- (32) Thomas, L. C.; Chittenden, R. A. Characteristic Infrared Absorption Frequencies of Organophosphorus Compounds-II. P-O(X) Bonds. *Spectrochim. Acta* **1964**, *20*, 489–502.
- (33) Quinones, R.; Shoup, D.; Behnke, G.; Peck, C.; Agarwal, S.; Gupta, R. K.; Fagan, J. W.; Mueller, K. T.; Iulucci, R. J.; Wang, Q. Study of Perfluorophosphonic Acid Surface Modifications on Zinc Oxide Nanoparticles. *Materials* **2017**, *10*, 1–16.
- (34) Lalatonne, Y.; Paris, C.; Serfaty, J. M.; Weinmann, P.; Lecouvey, M.; Motte, L. Bis-Phosphonates-Ultra Small Superparamagnetic Iron Oxide Nanoparticles: A Platform towards Diagnosis and Therapy. *Chem. Commun.* **2008**, 2553–2555.
- (35) Jastrzebski, W.; Sitarz, M.; Rokita, M.; Bulat, K. Infrared Spectroscopy of different Phosphates Structures. *Spectrochim. Acta, Part A* **2011**, *79*, 722–727.
- (36) Brodard-Severac, F.; Guerrero, G.; Maquet, J.; Florian, P.; Gervais, C.; Mutin, P. H. High-Field ^{17}O MAS NMR Investigation of Phosphonic Acid Monolayers on Titania. *Chem. Mater.* **2008**, *20*, 5191–5196.
- (37) Brice-Profeta, S.; Arrio, M. A.; Tronc, E.; Menguy, N.; Letard, I.; CartierditMoulin, C.; Noguès, M.; Chanéac, C.; Jolivet, J. P.; Sainctavit, P. Magnetic Order in $g-Fe_2O_3$ Nanoparticles: A XMCD Study. *J. Magn. Magn. Mater.* **2005**, *288*, 354–365.
- (38) Tronc, E.; Ezzir, A.; Cherkaoui, R.; Chanéac, C.; Noguès, M.; Kachkachi, H.; Fiorani, D.; Testa, A. M.; Grenèche, J. M.; Jolivet, J. P. Surface-Related Properties of $g-Fe_2O_3$ Nanoparticles. *J. Magn. Magn. Mater.* **2000**, *221*, 63–79.
- (39) Yee, C.; Kataby, G.; Ulman, A.; Prozorov, T.; White, H.; King, A.; Rafailovich, M.; Sokolov, J.; Gedanken, A. Self-Assembled Monolayers of Alkanesulfonic and -phosphonic Acids on Amorphous Iron Oxide Nanoparticles. *Langmuir* **1999**, *15*, 7111–7115.
- (40) Jolivet, J. P.; Chaneac, C.; Tronc, E. Iron Oxide Chemistry. From Molecular Clusters to Extended Solid Networks. *Chem. Commun.* **2004**, 481–487.
- (41) Campbell, V. E.; Tonelli, M.; Cimatti, I.; Moussy, J. B.; Tortech, L.; Dappe, Y. J.; Riviere, E.; Guillot, R.; Delprat, S.; Mattana, R.; Seneor, P.; Ohresser, P.; Choueikani, F.; Otero, E.; Koprowiak, F.; Chilkuri, V. G.; Suaud, N.; Guihery, N.; Galtayries, A.; Miserque, F.; Arrio, M. A.; Sainctavit, P.; Mallah, T. Engineering the Magnetic Coupling and Anisotropy at the Molecule-Magnetic Surface Interface in Molecular Spintronic Devices. *Nat. Commun.* **2016**, *7*, 13646–10.
- (42) Pabisiak, T.; Winiarski, M. J.; Ossowski, T.; Kiejna, A. Adsorption of Gold Subnano-Structures on a Magnetite (111) Surface and their Interaction with CO. *Phys. Chem. Chem. Phys.* **2016**, *18*, 18169–18179.

(43) Gomes, R.; Hassinen, A.; Szczygiel, A.; Zhao, Q.; Vantomme, A.; Martins, J. C.; Hens, Z. Binding of Phosphonic Acids to CdSe Quantum Dots: A Solution NMR Study. *J. Phys. Chem. Lett.* **2011**, *2*, 145–152.

(44) Chun, Y.-J.; Park, J.-N.; Oh, G.-M.; Hong, S.-I.; Kim, Y.-J. Synthesis of ω -Phthalimidoalkylphosphonates. *Synthesis* **1994**, *1994*, 909–910.

It can be concluded, that localizing the DA functionalities on nanoparticle surfaces is not the most promising strategy for self-healing nanocomposites. Based on this knowledge, the structure of the system was adjusted. To provide the same mobility of diene and dienophile, both functions shall be located in the matrix. Additional hydrogen bonds shall provide a second reversible intrinsically interaction and ensure the ideal miscibility of inorganic filler within the matrix. The realization of this plan is explained in the next two chapters.

3.3 Simple and High Yield Access to Octafunctional Azido, Amine and Urea Group bearing Cubic Spherosilicates

To further develop the inorganic – organic nanocomposites or hybrid materials, hydrogen bond forming spherosilicates were synthesized. The small spherosilicate molecules were applied in this study, because previously we were able to show that it is advantageous to apply molecular scale inorganic components in hybrid self-healing materials due to mobility reasons.^[79, 148] Starting from commercial available TEOS, octa(dimethylsilylhydrido)spherosilicate was synthesized applying a literature known procedure.^[174, 175] In a subsequent hydrosilylation reaction with ω -bromo alkenes (C_nH_{2n} ; $n = 4, 5, 6, 11$), various organic substituents were attached to the silica cubes. The bromofunction allows further derivatization applying substitution reactions. The reaction with NaN_3 yields in azides which were catalytically reduced to primary amines. Although, this reaction proceeded fast and quantitatively, problems with the isolation of the product occurred. Previously, several authors in literature claimed that they successfully synthesized and isolated octa(aminopropyl)silsesquioxane starting from APTES.^[252, 253, 254] However, rather the protonated ammonium salts or probably ladder like polysilsesquioxanes were produced. Mass spectrometry (MS) data, which would definitely prove the closed cage structure is missing in these studies. In our study, we observed the degradation of the cubic structure, when the alkyl amine groups are attached to the corners. The free electron pair of the primary amine can cleave Si-O-Si bonds^[253, 255] and irreversibly degrade the cubic structure. Such a degradation also occurs in aminopropyldimethylsiloxanes^[255] and APTES@SiO₂.^[256] By the conduction of an *in situ* following reaction step, the cubic structure was maintained. Therefore, an isocyanato propyl was added to the reaction mixture. The OCN group reacts readily and quantitatively with the eight primary amine groups per cube. The desired octakis(X-(3-propylurea)alkyl-1-dimethylsiloxy)octasilsesquioxanes (alkyl = butyl, pentyl, hexyl, undecyl) were obtained in high yields (83-88%) and purity. These cubes were the first having solely long flexible alkyl arms with a primary amine group, which allows for numerous modifications. In literature, predominantly the propylspacer is described or phenyl groups were used, to prevent the attack on Si-O-Si by the primary amine, due to the rigidity of the spacer (Chapter 1.8.2). The as synthesized cubes were used as inorganic filler within a double reversible polymer. The matrix consisting of linear pBMA was cofunctionalized with DA functions and hydrogen bonds. More details about this are presented in the next chapter.

These results were published in Dalton Transactions. Reproduced with permission of The Royal Society of Chemistry. <http://pubs.rsc.org/en/content/articlehtml/2017/dt/c6dt03872g>

Sandra Schäfer, Guido Kickelbick, Simple and high yield access to octafunctional azido, amine and urea group bearing cubic sphaerosilicates: *Dalton Trans.* **2017**, *46*, 1, 221-226. <http://pubs.rsc.org/en/content/articlehtml/2017/dt/c6dt03872g>.

Sandra Schäfer conceived of the presented idea, has written the publication and carried out all practical work (experiments and characterization). Guido Kickelbick has contributed with discussions about the topic and improvements for the final presentation of data and results within the manuscript.

CrossMark
click for updatesCite this: *Dalton Trans.*, 2017, **46**, 221

Simple and high yield access to octafunctional azido, amine and urea group bearing cubic spherosilicates†

Sandra Schäfer^a and Guido Kickelbick^{*a,b}

Spherosilicates and polyhedral oligomeric silsesquioxanes represent unique well-defined rigid building blocks for molecular and hybrid materials. Drawbacks in their synthesis are often low yields and the restricted presence of functional groups either based on incomplete transformation of all corners or the reactivity of the functional groups. Particularly amine-functionalization reveals some synthetic challenges. In this study we report the synthesis of a new class of octafunctionalized hydrogen bond forming spherosilicates *via* a facile route based on octabromo alkyl functionalized cubic spherosilicates. Four different alkyl chain lengths, namely C₄, C₅, C₆ and C₁₁, were realized starting from ω-alkenylbromides *via* hydrosilylation of Q₈M₈^H. Using sodium azide in a mixture of acetonitrile : DMF = 10 : 1, the octaazide was obtained quantitatively and could be rapidly transformed in an octaamine cube *via* catalytic hydrogenation over Pd/C in absolute ethanol. The following reaction to hydrogen bond forming spherosilicates was performed *in situ* by adding propyl isocyanate. All transformations proceed quantitatively at the eight corners of the cube, which was evidenced by NMR spectroscopy and ESI-MS measurements. The Q₈-target compound can be separated after each reaction step over simple chemical workup while no cage rearrangement was observed. The structures were confirmed using ¹H, ¹³C, ²⁹Si-NMR, FT-IR, elemental analysis and ESI-MS. The method opens a high yield route (overall isolated yield 83–88%) for structural building blocks in hybrid materials.

Received 6th October 2016,
Accepted 28th November 2016

DOI: 10.1039/c6dt03872g

www.rsc.org/dalton

Introduction

Functionalized cage siloxanes, consisting of polyhedral oligomeric silsesquioxanes or spherosilicates, being well-defined relatively rigid nanobuilding blocks, have emerged as an additive that allows the improvement of thermal and mechanical properties if incorporated into polymers and thus results in novel nanocomposite materials.^{1–6} Polyhedral oligomeric silsesquioxane (POSS) as well as spherosilicate based nanofillers offer the advantages of molecular defined structure, monodispersity and complete solubility in many different monomers and polymers. Studies carried out with these molecular precursors not only allow for the preparation of novel nanocomposites but also make them ideal model compounds for nanoparticle based systems.⁷

Novel cubes generate new applications, as their chemical properties can be selected by choosing the functional groups. For example, octa-furan-modified spherosilicates were

synthesized as building blocks for self-healing materials.^{8,9} In continuation of our previous studies the herein developed spherosilicate bearing groups capable of hydrogen bonding shall act as restoring force within shape memory and self-healing polymers. Spherosilicates incorporated into thermoplastics are known to provide excellent properties including resistance to atomic oxygen and mechanical robustness.^{10–12}

The synthesis of octaamino functional silsesquioxanes usually starts from trialkoxysilanes leading to ammonium salt derivatives.^{13,14} The deprotonation of these systems to free amine was described as ‘surprisingly difficult without destroying the Si/O framework’¹³ and poor yields (<40%) were reported. Previous reports further show that the opening of the cage structure is caused by the attack of primary aliphatic amine groups at silicon atoms of the cage. With traces of water a further reaction to open-cage-like silanols takes place.^{14,15} The possible storage of the aminopropyl-POSS is described very differently in the literature: it ranges from storage which is only possible in dry alcohols at –35 °C¹⁴ while others describe that storage is possible for one day at 25 °C.¹⁶ The observations indicate that an intra- or intermolecular attack at the Si–O cage takes place in the presence of primary aliphatic amines. It was shown that if the primary amine group was blocked with one propyl group, such an opening did not occur.^{17,18}

^a*Inorganic Solid State Chemistry, Saarland University, Am Markt, Zeile 3, 66125 Saarbrücken, Germany. E-mail: guido.kickelbick@uni-saarland.de*

^b*INM – Leibniz-Institut für Neue Materialien GmbH, Campus D2 2, 66123 Saarbrücken, Germany*

† Electronic supplementary information (ESI) available: Experimental procedures, NMR, IR, ESI-MS spectra and TG curves. See DOI: 10.1039/c6dt03872g

We introduce a simple access to octa-bromo-, -azido and -amino functionalized cages with promising high potential for further chemical conversions such as the derivatization of the amine, catalytic conversions or click chemistry. The formed amine functions could be modified with propyl isocyanate, yielding the hydrogen bond forming urea group. By varying the alkyl chain length, the organic content in the rigid inorganic-organic hybrid molecules was tailored and thus leads to promising new building blocks for hybrid materials forming hydrogen interactions.

Results and discussion

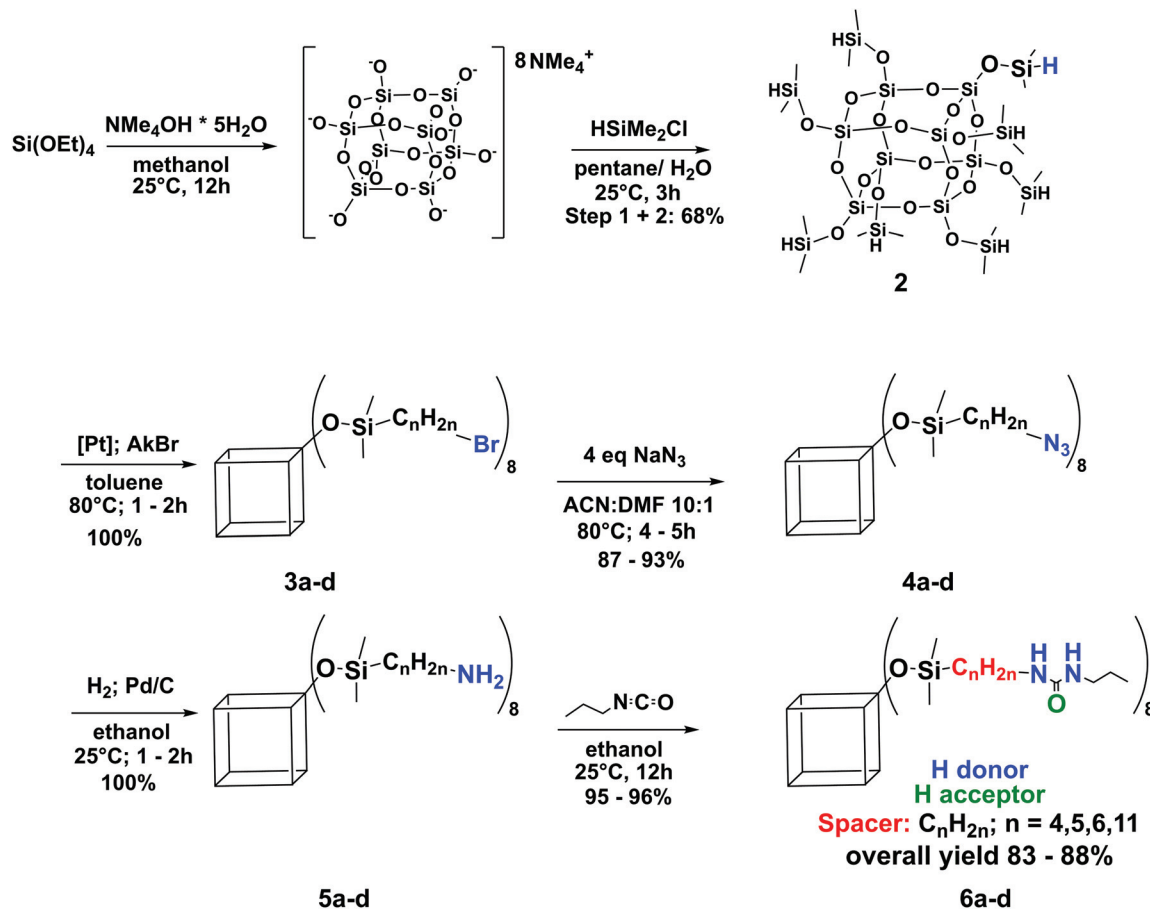
Octakis[1-(5-(1,1-dimethyldisiloxanyl)-alkyl-3-propylurea)] silsesquioxane (**6a-d**) can easily be prepared *via* a four step procedure affording only two workups. The intermediate products are interesting from a synthetic point of view and offer access to a wide range of aliphatic substituted derivatives.

For the synthesis of the inorganic building block initially a controlled condensation of 3-aminopropyltriethoxysilane (APTES) was planned as the synthetic route to form a polyhedral oligomeric silsesquioxane bearing the required functional groups. But the various reactions starting from APTES

do not result in high yields and mixtures of various products are common.^{13,14} Often also ladder like polysilsesquioxane are described.¹⁹ Therefore, we developed a facile synthetic route to an octafunctional amino spherosilicate (Scheme 1).

Starting from tetraethylorthosilicate, an octaanion cube was synthesized under basic conditions, which was directly transformed with chlorodimethylsilane to octakis(hydridodimethylsiloxy)octasilsesquioxane according to a literature procedure.^{20,21} This inorganic building block should be hydrosilylated with allyl bromide, but the allyl bromide reacts partly under formation of HBr; the phenomenon is known for isomerizable double bonds.^{22,23} Eventually, the isomerization can be suppressed by using iridium as a catalyst and making the C3 derivative accessible.^{23,24} In this work, ω -alkenylbromides (**1a-d**) with longer, non-isomerizable carbon chains were chosen for the hydrosilylation reaction. Long alkyl chains provide additional advantages, for instance that no undesired side products appear, as they are described in the case of allyl halogenides.^{24,25}

Hydrosilylation of the Si-H modified cube with alkenyl bromides results in end-standing bromide groups which can be transformed into an azide using NaN_3 . A subsequent catalytic hydrogenation over Pd/C in ethanol results in the quantitative formation of amine functions. The latter was



Scheme 1 Quantitative route to octakis(X-(3-propylurea)alkyl-1-dimethylsiloxy)octasilsesquioxane (X = 4, 5, 6, 11) (**6a-d**).

transformed into an urea group bearing spherosilicate with an overall isolated yield of 83–88%.

Hydrosilylation was carried out using Karstedt's catalyst, different ω -alkenylbromides (C4–C6, C11; **1a–d**) and octakis (hydridodimethylsiloxy)octasilsesquioxane (**2**) which leads to the desired products within hours. It should be mentioned that ω -alkenylbromides were initially synthesized using an Appel reaction,²⁵ but the resulting products, except for ω -undecylbromide (**1d**), could not be purified from bromoform by distillation. Applying bromoform-containing alkenylbromides leads to free radicals when thermally treated and consequently to a decomposition of the cube structure. Hence, the alkenylbromides were synthesized starting from dibromoalkanes. Formally HBr was eliminated by adding KO^tBu, while the reaction was catalyzed by 18-crown-6.²⁶ This reaction also leads to a byproduct, namely di-*tert*-butylether, which could not be separated by distillation, but it could be removed by passing the reaction mixture through a silica column (eluent: *n*-hexane).

In the next step, the octabromo cubes (**3a–d**) were azidated with sodium azide. In the literature, a cage-rearrangement phenomenon of the T₈ cage to the thermodynamically more stable T₁₀ and T₁₂ cube is described by nucleophilic substitutions with strong nucleophiles including nitrogen (azide)²⁷ anions in polar aprotic solvents (*e.g.* DMF) at high temperatures. The described rearrangement of the “propyl-cubes”, when strong nucleophiles were applied,²⁸ was not observed using chain length >C4. The conversion with the relatively strong nucleophile N₃[−] in a S_N2 reaction was studied in the polar aprotic solvents acetonitrile and DMF. They solvate the cation Na⁺ and therefore increase the nucleophilic character of the anion N₃[−]. While the reaction achieved completion in DMF within four hours, in acetonitrile under the same reaction conditions, the conversion was still incomplete after three days. An explanation for this behavior is the good solubility of the bromo cubes (**3a–d**) in DMF and their insolubility in acetonitrile. However, DMF produces methylamine, when heated for a long time, which attacks the Q₈ cage and leads to degradation. A mixture of acetonitrile : DMF (10 : 1 v/v) results in a full conversion after 4–5 h and seems to be the best compromise to synthesize the octaazide cubes (**4a–d**) without side reactions. **4a–d** were isolated by extraction with *n*-hexane/water and are storable and stable in air. A preliminary experiment to click the octaazide cube with 1-pentyne or 1-octyne by applying CuBr(PPh₃)₃ as a catalyst in absolute and degassed acetone revealed a decomposition of the cube structure according to ²⁹Si and IR spectroscopy, while the conversion seems to be complete after the reaction at room temperature over 24 h according to ¹H and IR. The first step of copper catalyzed azide alkyne cycloaddition (CuAAC) involves the dissociation of the catalyst in [Cu(PPh₃)₃]⁺ and Br[−] and the coordination of copper to the alkyne. Within this step, formally HBr is generated, which could probably attack the cage structure.

Octakisaminospherosilicates (**5a–d**) were synthesized *in situ*, applying hydrogen on a mixture of the appropriate azide substituted cube (**4a–d**) and 10 wt% palladium on

carbon in absolute ethanol. The completion of the reaction was confirmed by IR and ¹H NMR spectroscopy. A slight excess of propyl isocyanate was added to this mixture and stirring was performed overnight at room temperature. Scheme 1 shows the complete reaction path to the octakisurea cubes (**6a–d**).

The IR spectra of siloxysilsesquioxanes (**2**, **3–6d**) were used to prove the presence of the basic cubic structure (Fig. 1). We applied the typical strong Si–O–Si stretching peak at 1070 cm^{−1} for normalization. The silsesquioxane skeletal deformation vibration (557 cm^{−1})²⁹ would disappear if the cube structure was degraded. The persistent presence of this peak demonstrates that the initial structure of the cube is maintained during all conversions. All transformations were carried out in quantitative yields including the reaction with propyl isocyanate in ethanol.

On hydrosilylating ω -alkenylbromides (**1a–d**) with **2**, the Si–H-stretching mode (~2200 cm^{−1}) disappears, which indicates a quantitative conversion. The typical azide signal at 2090 cm^{−1} becomes visible exchanging bromide for azide. After accomplishing hydrogenation to the amine, no azide signal was detected. However, the IR measurements (Fig. 2) show that the amine-spherosilicate (**5a–d**) should be synthesized *in situ* for further reaction with propyl isocyanate. While freshly prepared samples reveal high purity (IR, NMR, ESI-MS), the samples which were stored in ethanolic solution in a fridge or at 25 °C show decomposition products in ESI-MS and IR measurements. As Fig. 2 reveals, the silsesquioxane deformation band disappears at room temperature within 24 h and at 8 °C at least within one week.

²⁹Si NMR of the degraded samples reveal that the M-peak shifts from 13 ppm to 20 ppm, while the Q₄ signal entirely disappears. A small, broad signal at 12 ppm was detected, which could not be assigned so far. The chemical shift indicates some kind of M species. The moderate ring-strained cyclic azasilanes with Si–N bonds along with high oxophilic silicon enables high reactivity towards hydroxyl groups. When the cube degrades, and all corner modifications were “removed” as M-units, formally an octaanion should be left, which most

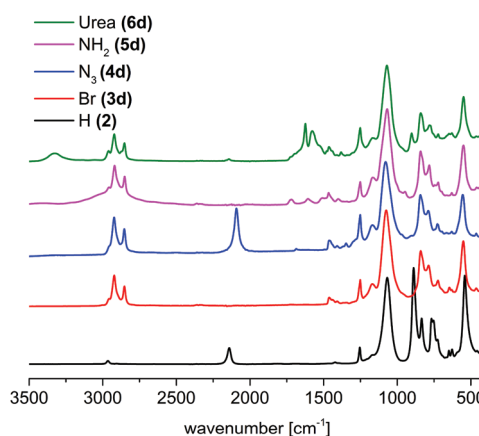


Fig. 1 IR-spectra of the synthesized C₁₁-spherosilicates (**3–6d**).

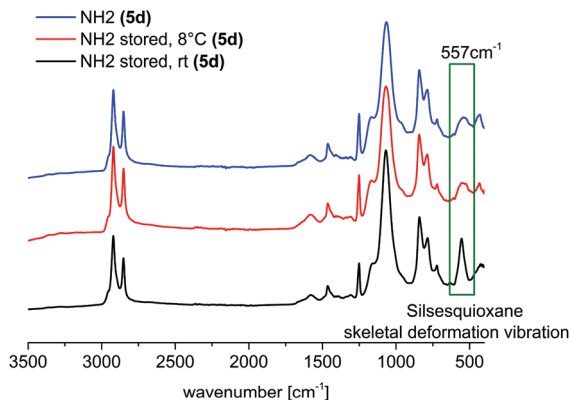
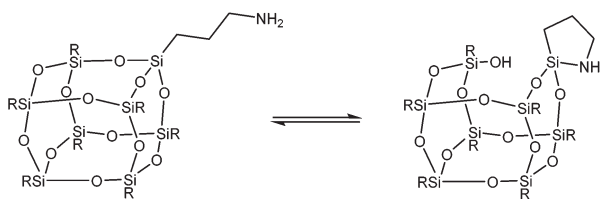


Fig. 2 The IR spectra of $C_{11}NH_2$ -spherosilicate (**5d**) before and after storage are displayed. The disappearance of the cage deformation band at 557 cm^{-1} indicates the degradation of the Si–O framework.

likely further decomposes in the reaction with the cyclic azasilanes under cleavage of the Si–N bond. This reaction explains the consistency of the CH_2NH_2 signal in 1H NMR and the maintained reactivity of the NH_2 group.

As the ESI-MS measurements of degraded samples never showed significantly higher molecular masses compared to the molecule itself, while the reaction mixture is completely dissolved, an intermolecular reaction is unlikely to occur and has not been described so far. The fragmentation pattern in positive MS showed mass losses that indicate intramolecular attacks similar to Scheme 2 even when the alkyl chains increase (C4–C6). These fully condensed frameworks containing primary amino groups seem to be unstable.

According to the literature, the same reactivity was found in commercially available systems, such as aminopropyl functionalized PDMS (polydimethyl siloxanes)³⁰ and APTES@ SiO_2 .³¹ Primary amines are known to attack Si–O–Si bonds which occurs as a backbiting from the lone pair of the nitrogen atom at a Si center.³² Commonly rings are formed as degradation products, which can afterwards build chainlike structures. According to the literature, the degradation process depends (among other reaction parameters) on the alkyl chain length and the nature of the amine.³³ Herein lies a possible explanation for the deviation of amino propyl silsesquioxane from the reported spherosilicates: it forms a five membered ring by intramolecular attack¹⁴ (Scheme 2), which is energetically more attractive than 6, 7, 8 or 15-atom membered rings, as it



Scheme 2 Intramolecular degradation of the Si–O cage in amino-propylsilsesquioxane.¹⁴

would be the case in the synthesized compounds (**6a–d**). Contrary to octakis(aminopropyl)octasilsesquioxane,¹⁴ the $C_{11}NH_2$ -derivative (**6d**) could be isolated as a slightly yellow solid directly after synthesis. This solid is stable under ambient conditions for at least several months. Eventually, the long, folded alkyl chains provide better shielding of the inorganic cage compared to short alkyl chains and therefore hinder the degradation.

Anyhow, if freshly prepared amine cubes were converted *in situ* with propyl isocyanate, the hydrogen bond moieties bearing octaurea-spherosilicate (**6a–d**) could be obtained in quantitative yield. It should be emphasized that the octazide cube precursors are stable under ambient conditions and storable, which prevents the necessity to store the octamines and makes them easily accessible. The presented procedure quantitatively supplies free amine cubes without impurities. The formation of all the desired products and the complete conversion were further confirmed by 1H NMR. After hydrosilylation, there are no residual peaks for $-CH=CH_2$ (5.74 and 4.89 ppm) or $-Si-H$ (4.75 ppm) protons. Particularly the shift of the CH_2 group next to the transformed functional group, from bromide to azide, to amine and to amide indicates the complete conversion in each synthetic step: CH_2Br 3.41 ppm ($CDCl_3$), CH_2N_3 3.26 ppm ($CDCl_3$), CH_2NH_2 group 2.66 ppm (CD_3OD) and $CH_2NHCONH$ 3.08 ppm (CD_3OD) (Fig. 3).

The 1H NMR spectra in Fig. 4 display the product spectra of bromide substituted spherosilicates (**3a–d**). While C4–C6 display only the β configuration, a small amount α configuration was found when using 11-bromoundecene.

Quantitative conversion in each step is necessary to yield an octafunctional spherosilicate. Besides NMR, IR and ESI-MS measurements further proved that the Q_8 cage is preserved: the amines showed mainly $[M + H]^+$ ions; while the urea derivatives showed mainly $[M + 2Na]^{2+}$, $[M + Na + K]^{2+}$ and $[M + 2K]^{2+}$ ions. The mass spectrum of C6-urea spherosilicate (**6c**) is shown in Fig. 5 (further spectra: ESI⁺).

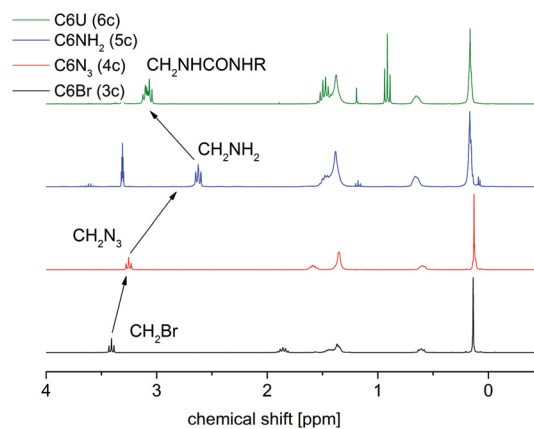


Fig. 3 1H NMR spectra display the complete conversion in each synthesis step of compounds **3–6c**. In particular, the CH_2 group next to the functional group is indicative for that (arrows).

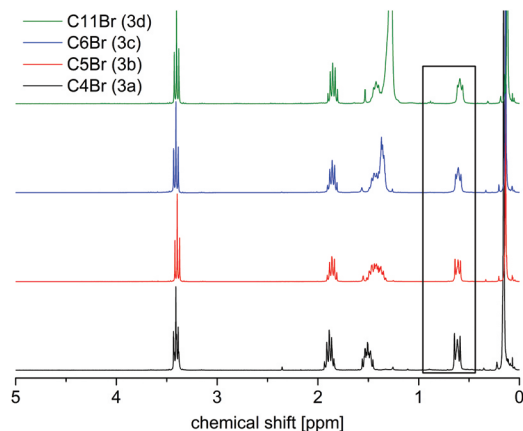


Fig. 4 ^1H NMR spectra of bromo substituted spherosilicates (3a–d), showing the high selectivity of hydrosilylation.

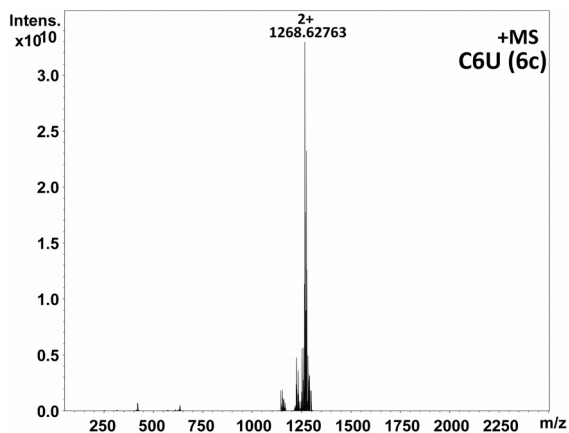


Fig. 5 ESI-MS spectra of octa-C6-urea POSS (6c).

As thermal stability is an important point for organic-inorganic nanofillers the behavior upon thermal treatment of the final products was studied *via* TG and DSC measurements.

The comparison of the TGA measurements of **2** and **5a–d** was conducted from 20–800 °C with a heating rate of 20 K min⁻¹. Up to 700 °C nitrogen was used as carrier gas, from 700–800 °C a 50 : 50% mixture of nitrogen and oxygen was used (Fig. 6). The results are in good agreement with the literature.³⁴ Octakis(hydridodimethylsiloxy)octasilsesquioxane (**2**) sublimes under an inert atmosphere nearly completely 98.76% starting at 230 °C, without recognizable decomposition processes. [(H₂N(CH₂)₁₁Me₂SiO)SiO_{1.5}]₈ (**5d**) shows two mass loss steps: the first one is probably due to partial degradation of amino alkyl chains, while the second mass loss presumably involves the cleavage of Si–C-bonds. Because of the higher molecular weight, the modified octakis(aminoundecyl)-silsesquioxane (**5d**) does not sublime, but decomposing starts at about 257 °C and a residue of SiO₂ is obtained after thermal treatment.

Since, for self-healing nanocomposites, the thermal degradation behavior under air is interesting, the measurement of

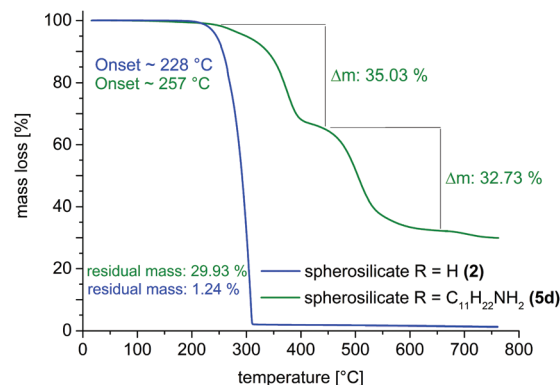


Fig. 6 Thermogravimetric measurement of **2** and **5d** under N₂.

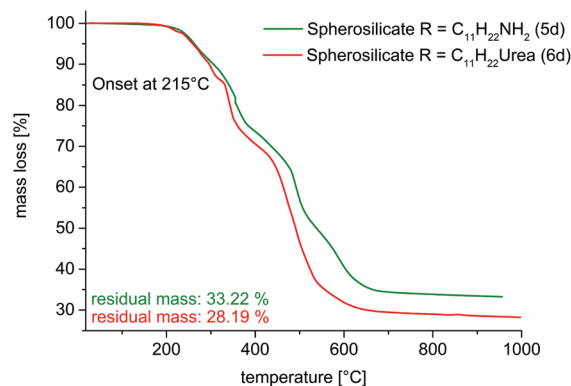


Fig. 7 Thermogravimetric measurement of **5d** and **6d** under O₂ : N₂.

octakis(aminoundecyldimethyl-siloxy)octasilsesquioxane (**5d**) and the final product octakis[1-(5-(1,1-dimethyldisiloxanyl)-undecyl-3-propylurea)]silsesquioxane (**6d**) was conducted under synthetic air, additionally (Fig. 7).

Indeed, the decomposition temperature under synthetic air is a bit lower at 215 °C. As technical and engineering plastics show a thermal stability up to 150 °C, the filler should at least be stable up to this point. Some of the high performance plastics with continuous service temperatures above 150 °C could also be improved with the presented spherosilicates. With a decomposition temperature of 215 °C the filler is appropriate for composite materials.

Conclusions

We have developed a straightforward and high yield synthesis to aliphatic octafunctional bromo-, azido-, amino- and urea group (83–88% overall isolated yield) bearing spherosilicates. Particularly amine-functionalization reveals some synthetic challenges, which we overcome by using a catalytic hydrogenation over Pd/C, starting from an air and moisture stable precursor. All the results based on NMR, FTIR and ESI-MS analysis were indicative of the successful synthesis of

octafunctional spherosilicates, consisting only of the not degraded Q₈ cube after each reaction step. Octakis[1-(5-(1,1-dimethyldisiloxanyl)-pentyl-3-propylurea)]silsesquioxane was synthesized to prepare hydrogen bond-bearing and building spherosilicates. In further work, they can interact with appropriate polymers and consequently act as homogeneously distributed nanoconstruction sites. In particular, they are interesting building blocks for shape memory and self-healing materials.

References

- 1 P. G. Harrison, *J. Organomet. Chem.*, 1997, **542**, 141.
- 2 E. Ayandele, B. Sarkar and P. Alexandridis, *Nanomaterials*, 2012, **2**, 445.
- 3 T. A. Tereshchenko, *Polym. Sci., Ser. B*, 2008, **50**, 249.
- 4 J. Pyun and K. Matyjaszewski, *Chem. Mater.*, 2001, **13**, 3436.
- 5 B. J. Scott, G. Wirnsberger and G. D. Stucky, *Chem. Mater.*, 2001, **13**, 3140.
- 6 D. B. Cordes, P. D. Lickiss and F. Rataboul, *Chem. Rev.*, 2010, **110**, 2081.
- 7 G. Kickelbick, in *Functional Molecular Silicon Compounds I: Regular Oxidation States*, ed. D. Scheschkewitz, Springer International Publishing, Cham, 2014, p. 1.
- 8 T. Engel and G. Kickelbick, *Eur. J. Inorg. Chem.*, 2015, **7**, 1226.
- 9 Z. Xu, Y. Zhao, X. Wang and T. Lin, *Chem. Commun.*, 2013, **49**, 6755.
- 10 F. J. Feher and T. A. Budzichowski, *J. Organomet. Chem.*, 1989, **379**, 33.
- 11 J. W. Gilman, D. S. Schlitzer and J. D. Lichtenhan, *J. Appl. Polym. Sci.*, 1996, **60**, 591.
- 12 H. G. Jeon, P. T. Mather and T. S. Haddad, *Polym. Int.*, 2000, **49**, 453.
- 13 F. J. Feher and K. D. Wyndham, *Chem. Commun.*, 1998, 323.
- 14 F. J. Feher, K. D. Wyndham, D. Soulivong and F. Nguyen, *J. Chem. Soc., Dalton Trans.*, 1999, 1491.
- 15 S. Neyertz, D. Brown, M. Pilz, N. Rival, B. Arstad, F. Männle and C. Simon, *J. Phys. Chem. B*, 2015, **119**, 6433.
- 16 Z. Zhang, G. Liang and T. Lu, *J. Appl. Polym. Sci.*, 2007, **103**, 2608.
- 17 M. Janeta, Ł. John, J. Ejfler and S. Szafert, *Chem. – Eur. J.*, 2014, **20**, 15966.
- 18 M. Janeta, Ł. John, J. Ejfler, T. Lis and S. Szafert, *Dalton Trans.*, 2016, **45**, 12312.
- 19 R. H. Baney, M. Itoh, A. Sakakibara and T. Suzuki, *Chem. Rev.*, 1995, **95**, 1409.
- 20 M. Dutkiewicz, H. Maciejewski, B. Marciniak and J. Karasiewicz, *Organometallics*, 2011, **30**, 2149.
- 21 I. Hasegawa and S. Motojima, *J. Organomet. Chem.*, 1992, **441**, 373.
- 22 M. Igarashi, T. Matsumoto, T. Kobayashi, K. Sato, W. Ando, S. Shimada, M. Hara and H. Uchida, *J. Organomet. Chem.*, 2014, **749**, 421.
- 23 P. Gigler, M. Drees, K. Riener, B. Bechlars, W. A. Herrmann and F. E. Kühn, *J. Catal.*, 2012, **295**, 1.
- 24 K. Riener, T. K. Meister, P. Gigler, W. A. Herrmann and F. E. Kühn, *J. Catal.*, 2015, **331**, 203.
- 25 Y. Kobayashi, M. Nakano, G. B. Kumar and K. Kishihara, *J. Org. Chem.*, 1998, **63**, 7505.
- 26 T. W. Baughman, J. C. Sworen and K. B. Wagener, *Tetrahedron*, 2004, **60**, 10943.
- 27 V. Ervithayasuporn, X. Wang and Y. Kawakami, *Chem. Commun.*, 2009, 5130.
- 28 S. Chimjarn, R. Kunthom, P. Chancharone, R. Sodkhomkhum, P. Sangtrirutnugul and V. Ervithayasuporn, *Dalton Trans.*, 2015, **44**, 916.
- 29 D. R. Carmo, N. L. D. Filho and N. R. Stradiotto, *Mater. Res.*, 2004, **7**, 499.
- 30 M. Vincenti, E. Pelizzetti, A. Guarini and S. Costanzi, *Anal. Chem.*, 1992, **64**, 1879.
- 31 H.-S. Jung, D.-S. Moon and J.-K. Lee, *J. Nanomater.*, 2012, **2012**, 1.
- 32 H. Chen, *J. Am. Soc. Mass Spectrom.*, 2003, **14**, 1039.
- 33 E. Asenath Smith and W. Chen, *Langmuir*, 2008, **24**, 12405.
- 34 N. Auner, B. Ziemer, B. Herrschaft, W. Ziche, P. John and J. Weis, *Eur. J. Inorg. Chem.*, 1999, **7**, 1087.

3.4 Double Reversible Network – Improvement of Self-Healing in Hybrid Materials via the combination of Diels-Alder-Crosslinking and Hydrogen Bonds

The healing ability of inorganic-organic nanocomposites or hybrid materials was optimized. In the initial systems, in which the DA groups were located on the particle surface, low conversions in DA reaction with siloxanes and no reaction with pBMAs were observed (Chapter 3.1). In the new approach, diene and dienophile are solely localized in the matrix and thus both functions have the same mobility and distribution. Hydrogen bond forming moieties were introduced as a second reversible intrinsic force and to incorporate the inorganic filler, octakis(6-(3-propylurea)hexyl-1-dimethylsiloxy)octasilsesquioxane (C6U), homogeneously within the matrix. In addition, the hydrogen bond forming groups in self-healing materials provide close contact within the nanometer scale of damaged surfaces. When hydrogen bonds are mechanically separated, these supramolecular interactions immediately equilibrate again. Using this phenomenon, freshly formed interfaces can be brought back into contact again and form a connection within less than a minute. This reconnection provides the necessary closeness of damaged interfaces, so that the desired covalent crosslinking by DA moieties can occur.

Novel polymers were synthesized applying CRP techniques. ATRP and RAFT were tested to react furan, maleimide, amide and imide group containing monomers. Polymers, bearing both DA moieties as well as one hydrogen bond building moiety, are called "one-component polymers" in this work. The Cu(I) catalyzed ATRP was found to be unsuitable, because of the N-H donating monomers, which can coordinate to copper and degrade the complex. By the addition of fresh ligand HMTETA and hydrazine hydrate as reducing agent, the polymerization took place. The obtained PDIs were rather large (2.07-3.25) but still the polymers were mostly linear and soluble. The degree of functionalization was determined to be between 4.3 and 9.9% using ^1H NMR spectroscopy. RAFT polymerization, using AIBN as radical source (initiator) and 2-cyano-2-propyl benzodithioate as RAFT agent, tolerated all functional groups. In these reactions, the polymerizations proceeded moderately controlled (PDI: 2.76 – 5.51) and the degree of substitution with functional monomers was found to be between 5.6 and 9.8%. Also these polymers were found to be still soluble and therefore they are suited for the desired application.

Octakis(6-(3-propylurea)hexyl-1-dimethylsiloxy)octasilsesquioxane (C6U, 20 wt%) was incorporated in various matrices. Either one-component polymers or a polymer mixture, consisting of three monofunctional polymers was applied to afford the composites (C1-C5). It was shown, that having no corresponding amide or imide groups within the matrix led to an inhomogeneous distribution of the filler (C1, C2). These materials showed also "healing" – pBMA+C6U (C1) because of heating above T_g , and the pBMA+pFMA+pMiMA+ C6U (C2) because of the DA reaction within the matrix. The C2 system behaves like the pure matrix (mixture of pBMA+pFMA+pMiMA) would behave. As long as the surfaces are reconnected by pressure within the Teflon mold, DA-caused healing occurs. If there was no contact provided

by pressure, no significant healing took place, because of the missing hydrogen bonds to reconnect the surfaces. The other composites (C3-C5) including all functions, which means diene, dienophile and amide or imide, showed a good to excellent healing behavior. Cut surfaces become reconnected by hydrogen bonds under ambient conditions, which is advantageous because the contact is necessary for the subsequent DA healing. The healing was evidenced by optical microscope images and the reversibility of the system by DSC measurements. According to microscope images, the amide groups seem to be slightly better in crack healing performance, possibly due to the hard segment character of imide moieties, when too many imides are assembled. STEM measurements of microtome slices were performed to visualize the nanostructure of the materials. The images show a completely homogeneous material, which means the inorganic moieties do not form any agglomerates within the hydrogen bond motive functionalized polymer matrix. Rheological measurements were conducted to show mechanically the ability of the system to crosslink. UV/Vis measurements over 24 h revealed that 80% conversion is reached within the first 4 h – in the pure polymer as well as in the hybrid material.

These results were published in ACS Macromolecules. Reproduced by permission of the American Chemical Society (ACS). <https://pubs.acs.org/doi/10.1021/acs.macromol.8b00601>

Sandra Schäfer, Guido Kickelbick, Double Reversible Networks – Improvement of Self-Healing in Hybrid Materials via Combination of Diels-Alder-Crosslinking and Hydrogen Bonds, *Macromolecules*, **2018**, xx, xx-xx. <https://pubs.acs.org/doi/10.1021/acs.macromol.8b00601>.

Sandra Schäfer conceived of the presented idea, has written the publication and carried out all practical work (experiments and characterization). Guido Kickelbick has contributed with discussions about the topic and improvements for the final presentation of data and results within the manuscript.

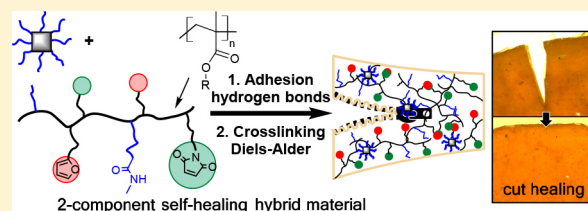
Double Reversible Networks: Improvement of Self-Healing in Hybrid Materials via Combination of Diels–Alder Cross-Linking and Hydrogen Bonds

Sandra Schäfer and Guido Kickelbick*[✉]

Inorganic Solid State Chemistry, Saarland University, Campus C4, 66123 Saarbrücken, Germany

Supporting Information

ABSTRACT: Intrinsic self-healing materials rely on a reversible bond formation after failure. In this study we report hybrid materials that contain two intrinsic self-healing forces: The reversible covalent bond formation of Diels–Alder groups is supported by intrinsic hydrogen bonds, which form supramolecular interactions and contribute to the mobility and proximity of the DA groups. This concept was realized by a combination of urea group containing spherosilicates with butyl methacrylate based polymers bearing both DA moieties and self-assembling hydrogen bonds. Multifunctional one-component polymers were synthesized and studied regarding their application in self-healing hybrid materials. The self-healing behavior was investigated following the signals for bond release and formation of DA groups in the material using IR, UV-vis, and CP-MAS NMR spectroscopy. Furthermore, DSC and rheological measurements were performed and revealed that the materials are superior compared to previously studied systems concerning their healing capacity. The self-healing behavior of the formed hybrid materials was proven by a cut healing test of several millimeters using microscope images. We can conclude that it is advantageous to combine several reversible functions in one material to promote the self-healing capacity particularly in nanocomposites where the flexibility of the network is restricted.



1. INTRODUCTION

Intrinsic self-healing materials are based on reversible bond formation on the molecular scale, which requires quite flexible polymer structures to foster the connectivity of damaged surfaces. This is necessary for the re-formation of the bonds, which only takes place at the nanometer scale or below, when the proximity of reactants is reached.¹ During the past two decades the Diels–Alder (DA) reaction was identified as one of the most promising reaction types in polymer self-healing materials.² The thermoreversible [4 + 2] cycloaddition between electron-rich dienes and electron-deficient dienophiles, like furan and maleimide, works at temperatures between 100 and 150 °C and thus in a region that allows its use in daily applications.

Generally chain diffusion, in particular the mobility of functional groups, is one of the most important parameters with respect to the ability to heal intrinsic systems. Regarding self-healing nanocomposites compared to polymers, additional challenges have to be considered. Inorganic fillers increase, for example, hardness and T_g , but both are disadvantageous for the previously described requirements concerning healing mechanisms. Furthermore, there is a huge difference between the usage of fibers or particles as the inorganic moiety in such composites. While fibers can break or change their alignment,³ which cannot be reorganized applying polymer healing mechanisms, spherical particles or large isotropic molecules have no translational preferred direction, are not aligned, and do not tend to break because of brittleness within the softer

matrix. Because of these multiple challenges only a few studies have been conducted in self-healing nanocomposites based on DA cross-linking. Generally the organic polymers and the inorganic moieties have to be optimized for the best performing nanocomposites or hybrid materials. Several research groups already studied polymer nanocomposites based on click chemistry reactions^{4–6} and revealed that MWCNT's (multiwalled carbon nanotubes), GO (graphene oxide), or inorganic NPs (SiO₂) have a potential in self-healing nanocomposites. Careful control of the chemical surface modification is necessary for a homogeneous distribution of inorganic nanoparticles in organic polymers.

A few studies have been conducted using SiO₂ nanoparticles in DA based healing composites. Chujo et al. synthesized a 20% furan modified polystyrol, which was reacted *in situ* with tetraethyl orthosilicate and a maleimido alkoxy silanes.⁷ This procedure resulted under appropriate conditions a colorless, transparent hybrid material that revealed retro-Diels–Alder (rDA) reactions in DSC. In our group a system was developed in which a grafting-from polymerization applying SI-ATRP was used to modify 40 nm SiO₂ with a copolymer of butyl methacrylate and 10 mol % protected maleimidoethyl methacrylate. These particles were incorporated in the corresponding furan and butyl methacrylate group containing

Received: March 20, 2018

Revised: June 25, 2018

polymers to form a self-healing composite, which is able to heal scratches on a micrometer scale.⁸ For a deeper understanding of the limiting parameters when reacting molecular surface functionalized particles with the corresponding molecules⁹ or different matrices,¹⁰ in particular siloxanes and poly(butyl methacrylate)s (pBMA), a study using different spacer lengths was conducted. While the pBMA samples showed no conversion in DSC, the elastomers indicated a conversion. This leads to the assumption that again the mobility of functional groups and also the flexibility of the matrix are the key for effective healing. In a recent study we developed a system based on spherical magnetite/maghemite nanoparticles, which was modified using a monolayer of phosphonic acids on the surface.¹¹ Reacting these particles with different types of molecules, we found that the sterical demand of the attacking reagent is the limiting factor in this type of materials rather than the crowdedness of the surface. This result is further supported by the observation that smaller molecular inorganic building blocks lead to a faster healing in the nanocomposites. Thus, spherosilicate or silsesquioxane based DA systems heal more efficiently than the ones with SiO₂ nanoparticles. Liu et al. described an octamethyl methacrylate modified POSS (polymeric octahedral silsesquioxane) which was reacted with furfurylamine.¹² A partially thermoreversible network was formed via the reaction of the methacrylate double bond with either the amine in a Michael addition or the furan in a DA reaction. Lin et al. described an octafurfurylamine POSS, which was cross-linked using the commercial 1,1'-(methylene-di-4,1-phenylene)bismaleimide (BMI) and formed a curable solid.¹³ We described furan modified spherosilicates prepared via hydrosilylation, which were incorporated in BMI or linear maleimide siloxanes and resulted in hybrid materials that showed a high conversion in DA reactions.¹⁴ Zelisko et al. also synthesized furan modified spherosilicates cross-linked with maleimide siloxanes starting from different precursors and found an intrinsically healing system.¹⁵

Besides DA cross-linking reactions also other interaction types were used for intrinsic healing systems. For example, spontaneous supramolecular assembly by a hydrogen bond donor–acceptor interaction results in a fast reconnection of surfaces. Although individual hydrogen bonds are weak, collectively they form a strong network that is dynamic at room temperature¹⁶ and allow autonomic healing. Liu et al. studied solvent induced healing of PMMA at 40–60 °C and found that, in addition to mechanical lock of the broken chains, hydrogen bonds promoted the mechanical strength of the healed sample because of the interaction between methanol and broken polymeric chains.¹⁷

According to the literature, chemical networks show a kind of molecular memory when covalent and supramolecular groups are combined.¹⁸ Weaker hydrogen bonds can break and build again spontaneously, while covalent bonds provide the basic stability and robustness.

Probably the first who studied the combination of DA and hydrogen bonds was the group of Picchioni.^{19,20} The first attempt was the chemical modification of aliphatic polyketones with furan and primary amines. The polymers were cross-linked with commercial bismaleimides. The incorporation of hydrogen bonds between amine and carbonyl groups leads to a significant increase in T_g and thus extends the possible application of the material. One drawback in this polymeric material is the side reaction between amine and carbonyl groups, which leads to irreversible links.¹⁹ In a subsequent

study, this drawback was overcome by OH-group containing derivatives instead of amines.²⁰ In 2017, Raquez et al. reported one-component DA based polyurethanes and achieved a free-standing healable film, when an appropriate ratio of hydrogen bonds to DA functions was adjusted.²¹

In this work, intrinsic healing hybrid materials that contain two types of independent reversible interactions are investigated. Physical hydrogen bonds, which can form spontaneously and are located in the matrix and on the surface of the inorganic moiety, provide the ideal miscibility and homogeneous distribution of the filler. Covalent bonds, which can be thermally triggered by the DA reaction, are located only in the polymer chains to ensure good mobility and accessibility of these groups. One-component polymers, bearing diene, dienophile, and amide or urea groups, were synthesized using controlled radical polymerizations (CRPs). ATRP (atom transfer radical polymerization), ARGET ATRP (activator regenerated by electron transfer), and RAFT (reversible addition–fragmentation chain transfer) were performed with a mixture of previously synthesized monomers. The resulting linear poly(butyl methacrylates) contain maleimide, furan, and hydrogen bond moieties at the same backbone. Octafunctional spherosilicates²² were chosen as inorganic moiety, as they are molecular, soluble, three-dimensional nanobuilding blocks. The received materials showed a superior self-healing potential according to DSC measurements and microscope images.

2. EXPERIMENTAL SECTION

Materials. CuBr₂ (99%), hydrazine hydrate solution in H₂O (78–82%), 2-cyano-2-propyl benzodithioate (>97%), triethylamine_{abs} (>99.5%), furan (≥97%), furfuryl alcohol (98%), 3-aminopropanol (99%), 2-aminoethanol (≥99%), isopropenyl acetate (99%), methacryloyl chloride (97%), butyl methacrylate (BMA, 99%), ethyl 2-bromoisobutyrate (EBiB, 98%), 1,1,4,7,10,10-hexamethyltriethylenetetramine (HMTETA, 97%), maleic anhydride (98%), *n*-butylamine (99.5%), and anhydrous toluene were purchased from Sigma-Aldrich. 2-Isocyanatoethyl methacrylate (≥99%) was purchased from TCI Chemicals. Aluminum oxide 90 active neutral (70–230 mesh ASTM) was purchased from Merck Millipore. Na₂SO₃ (>98%) and 2,2'-azobis(2-methylpropionitrile) (AIBN, ≥98%) were purchased from Merck. The stabilizer of BMA was removed by passing it through active neutral alumina. AIBN was recrystallized from methanol. A stock solution containing 100 mg in 5 mL anhydrous toluene was prepared directly prior to use. CuBr was synthesized by reducing CuBr₂ with Na₂SO₃ in distilled water. The precipitating colorless solid was filtered, washed three times with ethanol, dried under vacuum, and stored under argon. All other chemicals were used as received. Synthetic procedures were performed under inert gas atmosphere applying Schlenk techniques.

Characterization. Fourier transform infrared (FTIR) spectroscopy measurements were performed applying a Bruker Vertex 70 spectrometer under ambient air (40 scans at a resolution of 4 cm⁻¹) in attenuated total reflectance (ATR) mode. Differential scanning calorimetry (DSC) measurements were carried out using a Netzsch DSC 204 F1 Phoenix with samples in aluminum crucibles with pierced lids and heated under nitrogen at a rate of 10 K/min. Solution NMR spectra were recorded with a Bruker Avance III HD 300/400 spectrometer at 25 °C (¹H at 300.13/400.13 MHz, ¹³C at 75.48/100.61 MHz) using CDCl₃ as reference. The degree of substitution (dS) in polymers was determined using ¹H NMR integrals, where dS = (integral functional group) × 100/(integral OCH₂) [%]. Peak assignments of polymers can be found in the [Supporting Information](#). Solid-state CP-MAS NMR spectra were recorded on a Bruker Avance 400WB spectrometer at 25 °C (¹³C at 100.62 MHz, ²⁹Si at 79.50 MHz) and a contact time of 2.0 ms with a variable power contact time

(ramp 10050). The rotor spin rate was 13 kHz, with delay time of 3–6 s. Adamantane was used as an external standard for ^{13}C NMR and octakis(trimethylsiloxy)silsesquioxane for ^{29}Si NMR. Elemental analysis was performed with a Leco 900 CHN analyzer. Films were compression-molded at 70 °C 24 h in a Teflon form (3 cm × 1 cm × 0.1 cm) which was held with a vice. Microscope images were recorded under polarized light using an Olympus BX60 microscope equipped with a Sony CCD-Iris color camera. Size exclusion chromatography (SEC) measurements in tetrahydrofuran (THF) were performed with a PSS (Polymers Standards Service) system, which included a Viscotek VE1121 pump, a Shodex refractive index detector, a PSS SLD 7000 multiangle light scattering detector, and styrene-divinylbenzene copolymer columns (PSS SDV) at a rate of 1 mL min^{-1} . A linear polystyrene standard was used for calibration, which causes deviations from expected molecular masses. UV–vis transmission spectra were recorded on a Lambda 750 instrument (PerkinElmer Inc., USA) equipped with a 100 mm integrating sphere from 500 to 248 nm with a 4 nm increment on 1 mm cuvettes with a drop-cast film of the sample. Rheological measurements were carried out on an Anton Paar Physica MCR 301 rheometer equipped with a CTD450 convection oven. Thin films (500 μm thick, 25 mm diameter) of the samples were compression-molded in a heatable press (Specac, 60 °C, 2 t, 1 min, baking paper for separation) and measured in oscillation mode using the PP25 measuring system with 25 mm plate diameter and a plate-to-plate distance of 0.5 mm. The measurements were conducted in the temperature range where the materials are present as a melt. The measurement starts at 70 °C; the temperature was increased to 120 °C, held for 1 h, and subsequently decreased to 70 °C. This temperature was held constant until the sample solidifies. STEM measurements were performed on a cold field emission gun TEM/STEM (JEOL JEM-ARM 200F) instrument, operated at an accelerating voltage of 200 kV and equipped with a STEM Cs corrector (CESCOR; CEOS GmbH Heidelberg). Images were obtained using a high angle annular bright-field (ABF) detector with a camera length of 8 cm. The sample was prepared by the ultramicrotomy technique with a thickness of about 20 nm and put on a copper grid coated with thin pure carbon holey film.

Synthesis. 3-Acetylaminopropanol (1).²³ A mixture of isopropyl acetate (25.97 g, 28.57 mL, 259.36 mmol) and 3-aminopropanol (5.0 g, 5.1 mL, 64.84 mmol) was heated at 60 °C for 3 h in a sealed vial. After the reaction was finished the residual isopropyl acetate and acetone were distilled off under vacuum. The product was obtained as a yellow oil and used without further purification to synthesize 2. Yield: 7.60 g (64.84 mmol, 100%). ^1H NMR (300 MHz, CDCl_3): δ 6.80 (s, 1H, H8 or H4), 4.12 (1H, H8 or H4), 3.58 (t, J = 5.7 Hz, 2H, H1), 3.32 (td, J = 6.0 Hz, 2H, H3), 1.93 (s, 3H, H7), 1.63 (quint, 2H, H2). ^{13}C NMR (75 MHz, CDCl_3): δ 171.64 (C5), 59.40 (C1), 36.56 (C3), 32.05 (C2), 23.03 (C7).

3-Acetamidopropyl Methacrylate (2). To a stirred solution of 3-acetylaminopropanol (1) (7.60 g, 64.84 mmol, 1.0 equiv) and triethylamine (7.87 g, 10.94 mL, 77.81 mmol, 1.2 equiv) in anhydrous CH_2Cl_2 (170 mL) a solution of methacryloyl chloride (8.13 g, 77.81 mmol, 1.2 equiv) in anhydrous CH_2Cl_2 (20 mL) was added dropwise at 0 °C. After complete addition, the mixture was allowed to warm to room temperature and stirred overnight. The orange slurry was concentrated to half of the volume, cooled to 0 °C, and filtered; the filtrate was extracted with water (2 × 25 mL). Afterward, the organic phase was separated, dried over MgSO_4 , and concentrated *in vacuo*. The crude product was obtained as an orange oil. After purification via distillation *in vacuo* (132 °C, 7×10^{-3} mbar) pure 2 could be obtained as a colorless oil. Yield: 10.77 g (58.13 mmol, 90%). ^1H NMR (300 MHz, CDCl_3): δ 6.14–6.02 (m, J = 1.5, 1.0 Hz, 2H, H12, and H4), 5.58–5.50 (m, 1H, H12), 4.18 (t, J = 6.0 Hz, 2H, H1), 3.28 (td, J = 6.0 Hz, 2H, H3), 1.95 (s, 3H, H7), 1.92–1.90 (m, 3H, H13), 1.85 (quint, J = 6.0 Hz, 2H, H2). ^{13}C NMR (75 MHz, CDCl_3): δ 170.34 (C5), 167.65 (C9), 136.24 (C11), 125.83 (C12), 62.26 (C1), 36.47 (C3), 28.79 (C2), 23.31 (C7), 18.35 (C13). CHN_{theo} ($\text{C}_9\text{H}_{15}\text{NO}_3$): C, 58.36; H, 8.16; N, 7.56. CHN_{exp} : C, 57.68; H, 8.10; N, 7.22. IR: ν = 3290 $\nu(\text{N-H})$, w; 3088 $\nu(\text{N-H})$ w; 2960, 2931, 2871 (m, $\nu(\text{C-H})$); 1716 (s, $\nu(\text{C=O})$); 1639 (s, amide I

$\nu(\text{C=O})$); 1551 (s, amide II $\nu(\text{C-N})$ with contributions of $\delta(\text{N-H})$); 1443 (m, $\delta(\text{C-H})$); 1294 (s, $\nu(\text{C-O-C})$) cm^{-1} .

2-(4-Butylureido)ethyl Methacrylate (3). 2-Isocyanatoethyl methacrylate (1 g, 6.44 mmol) was dissolved in absolute dichloromethane (30 mL), and *n*-butylamine (0.47 g, 0.64 mL, 6.44 mmol) was added dropwise. The colorless precipitate was filtered off and dried *in vacuo*. Yield: 1.47 g (6.44 mmol, 100%). ^1H NMR (400 MHz, CDCl_3): δ 6.19–6.07 (m, 1H, H1), 5.64–5.53 (m, 1H, H1), 4.68 (s, 1H, H9 or H11), 4.44 (s, 1H, H1, H9 or H11), 4.24 (t, J = 5.4 Hz, 2H, H6), 3.50 (q, J = 5.4 Hz, 2H, H8), 3.18–3.11 (m, 2H, H12), 1.94 (s, 3H, H4), 1.52–1.42 (m, 2H, H13), 1.41–1.27 (m, 2H, H15), 0.91 (t, J = 7.3 Hz, 3H, H16). ^{13}C NMR (75 MHz, CDCl_3): δ 167.73 (C5), 158.12 (C10), 136.22 (C2), 126.11 (C1), 64.37 (C6), 40.54 (C8), 39.88 (C12), 32.38 (C13), 20.15 (C4), 18.44 (C15), 13.89 (C16). CHN_{theo} ($\text{C}_{10}\text{H}_{11}\text{NO}_4$): C, 57.87; H, 8.83; N, 12.27. CHN_{exp} : C, 57.78; H, 8.57; N, 12.23. IR: ν = 3336 (w, $\nu(\text{N-H})$); 2964, 2931, 2858 (m, $\nu(\text{C-H})$); 1708 (s, $\nu(\text{C=O})$); 1618 (s, amide I $\nu(\text{C=O})$); 1574 (s, amide II $\nu(\text{C-N})$ with contributions of $\delta(\text{N-H})$); 1446 (m, $\delta(\text{C-H})$); 1292 (s, $\nu(\text{C-O-C})$) cm^{-1} .

2-(2-Hydroxyethyl)-3a,4,7,7a-Tetrahydro-1H-4,7-epoxyisindole-1,3(2H)-dione (4). A solution of 4,7,7a-tetrahydro-4,7-epoxyisobenzofuran-1,3-dione (10 g, 60.3 mmol) in methanol (250 mL) was purged with nitrogen for 10 min in an ice bath. Subsequently, ethanolamine (4 mL, 60.3 mmol) and triethylamine (6.10 g, 8.4 mL, 60.3 mmol) were added. The reaction mixture was allowed to warm up, and the temperature was increased to 70 °C for 20 h. Subsequently, ethanolamine (0.4 mL, 6.0 mmol) was added, and stirring was continued for 2 h at 70 °C. The solution turned pale yellow. After cooling to room temperature, the solution volume was reduced and stored at –18 °C. The precipitate was collected by vacuum filtration washed with isopropanol and used without further purification. Dissolving the solid in isopropanol and storing it at –18 °C leads to crystalline 4. Yield: 10.72 g (51.25 mmol, 85%). ^1H NMR (300 MHz, CDCl_3): δ 6.53–6.48 (m, 2H, H1&2), 5.27 (t, J = 0.9 Hz, 2H, H3&6), 3.79–3.72 (m, 2H, H14), 3.71–3.63 (m, 2H, H13), 2.88 (s, 2H, H4&5), 2.37 (s, 1H, H15). ^{13}C NMR (75 MHz, CDCl_3): δ 176.92 (C7/9), 136.67 (C1/2), 81.15(C3/6), 60.57 (C14), 47.65 (C4/5), 41.97 (C13). CHN_{theo} ($\text{C}_{10}\text{H}_{11}\text{NO}_4$): C, 57.41; H, 5.30; N, 6.70. CHN_{exp} : C, 57.85; H, 5.56; N, 6.72.

Furfuryl methacrylate (FMA) (5)²⁴ and 2-(1,3-dioxo-3a,4,7,7a-tetrahydro-1H-4,7-epoxyisindol-2(3H)-yl)ethyl methacrylate (MIMA, 6)²⁵ were synthesized according to literature procedures. NMR and IR spectra can be found in SI2.

General Procedure for the Synthesis of Copolymers P1–P3 via ATRP. BMA (100 equiv, 13.86 mL, 86.0 mmol), FMA (1.34 g) or MIMA (2.49 g) each 10 equiv (8.6 mmol), according to the polymer, and anhydrous toluene (54 mL) were mixed under an argon atmosphere. The mixture was degassed using four freeze–pump–thaw cycles. To the frozen mixture CuBr (1 equiv, 124 mg, 0.86 mmol) and HMTETA (1 equiv, 224 μL , 0.86 mmol) were added, and another two vacuum–argon cycles were performed. The reaction was carried out after addition of degassed EBiB (1 equiv, 126 μL , 0.86 mmol) by heating the mixture at 70 °C for 16 h. The polymers (listed in Table 1) were purified by passing the solution through an alumina

Table 1. Polymers Prepared via ATRP

	polymer	yield [%]	dS_{F} [%]	dS_{M} [%]	dS_{H} [%]	PDI
P1	pBMA	84	–	–	–	1.52
P2	FMAcoBMA	85	8.33	–	–	1.66
P3	MIMAcoBMA	60	–	–	6.0	2.40

column (active, neutral) to remove the catalyst. The polymers were precipitated from concentrated THF solution two times in ice-cold *n*-hexane and dried at room temperature under reduced pressure. Parts of the polymer samples were analyzed by SEC and ^1H NMR to determine the molar mass and molar mass distribution.

P1. ^1H NMR (300 MHz, CDCl_3): δ 4.10–3.82 (m, 1H, OCH_2), 2.14–0.59 (m, 6H, pBMA backbone). IR: ν = 2958, 2931, 2874 (m,

$\nu(\text{C-H})$); 1720 (s, $\nu(\text{C=O})$); 1460 (m, $\delta(\text{C-H})$); 1386 (m, $\delta(\text{CH}_3)$); 1242–1142 (s, $\nu(\text{C-O-C})$); 746 (m, $\rho((\text{CH}_2)_n)$) cm^{-1} .

P2. $^1\text{H NMR}$ (300 MHz, CDCl_3): δ 7.42 (s, 1H), 6.44–6.29 (m, 2H), 5.02–4.88 (m, 2H), 4.08–3.81 (m, 21H), 2.12–0.64 (m, 140H). IR: ν = 2958, 2931, 2874 (m, $\nu(\text{C-H})$); 1720 (s, $\nu(\text{C=O})$); 1460 (m, $\delta(\text{C-H})$); 1386 (m, $\delta(\text{CH}_3)$); 1242–1142 (s, $\nu(\text{C-O-C})$); 746 (m, $\rho((\text{CH}_2)_n)$) cm^{-1} .

P3. $^1\text{H NMR}$ (300 MHz, CDCl_3): δ 6.58–6.45 (m, 1H), 5.32–5.15 (m, 1H), 4.13–3.81 (m, 24H), 3.68–3.48 (m, 1H), 2.91–2.79 (m, 1H), 2.14–0.62 (m, 149H). **P3** deprotected: $^1\text{H NMR}$ (400 MHz, CDCl_3): δ 6.80–6.68 (m, 1H), 4.05–3.83 (m, 20H), 3.67–3.54 (m, 1H), 2.18–0.51 (m, 132H). IR: ν = 2958, 2931, 2874 (m, $\nu(\text{C-H})$); 1720 (s, $\nu(\text{C=O})$); 1460 (m, $\delta(\text{C-H})$); 1403 (m, $\delta(\text{C-N})$); 1386 (m, $\delta(\text{CH}_3)$); 1242–1142 (s, $\nu(\text{C-O-C})$); 746 (m, $\rho((\text{CH}_2)_n)$) cm^{-1} . **P3** deprotected: same signals +696 $\delta(\text{maleimide})$ cm^{-1} .

General Procedure for the Synthesis of Copolymers P4–P6 via ARGET ATRP. BMA (100 equiv, 13.86 mL, 86.0 mmol), a hydrogen bond forming monomer (H1 = 3-acetamidopropyl methacrylate (1.59 g) (2), H2 = 2-(3-butylureido)ethyl methacrylate (1.96 g) (3)), FMA (5) (1.34 g), MIMA (6) (2.49 g) (each 10 equiv, 8.6 mmol), and anhydrous toluene (54 mL) were mixed under an argon atmosphere. The mixture was degassed using four freeze–pump–thaw cycles. In the case of H2 (3) absolute methanol (3 mL) were added to ensure complete dissolution. To the frozen mixture CuBr (1 equiv, 124 mg, 0.86 mmol) and HMTETA (1 equiv, 224 μL , 0.86 mmol) were added, and another two vacuum–argon cycles were carried out. The reaction was carried out after addition of degassed EBIB (1 equiv, 126 μL , 0.86 mmol) by heating the mixture at 70 °C for 12 h. Because of the low conversion, fresh HMTETA (1 equiv, 224 μL) and $\text{H}_2\text{NNH}_2 \cdot \text{H}_2\text{O}$ (200 μL = 0.206 mg \rightarrow 80% 0.165 mg = 3.29 μmol) were added to the reaction mixture, and stirring was continued for another 12 h at 70 °C. The polymers (listed in Table 2) were purified by passing the

Table 2. Polymers Prepared via ARGET ATRP

polymer	yield [%]	dS_F [%]	dS_M [%]	dS_H [%]	PDI
P4 BMAcoH1	69	–	–	–	1.60
P5 FMAcoMIMAcOBMAcOH1 = EKHI _A	75	7.5	6.6	7.0	3.25
P6 FMAcoMIMAcOBMAcOH2 = EKHI _{2A}	62	7.0	4.3	9.9	2.07

solution through an alumina column (active, neutral) to remove the catalyst. The polymers were precipitated from concentrated THF solution two times in ice-cold *n*-hexane and dried at room temperature under reduced pressure. Parts of the polymer samples were analyzed by SEC and $^1\text{H NMR}$ to determine the molar mass, molar mass distribution, and dS .

P4. $^1\text{H NMR}$ (300 MHz, CDCl_3): δ 4.08–3.85 (m, 15H), 3.44–3.25 (m, 1H), 2.11–0.63 (m, 100H). IR: ν = 3396 (w, $\nu(\text{N-H})$); 2958, 2931, 2874 (m, $\nu(\text{C-H})$); 1720 (s, $\nu(\text{C=O})$); 1460 (m, $\delta(\text{C-H})$); 1533 (m, $\nu(\text{C-N})$ and $\delta(\text{N-H})$); 1388 (m, $\nu(\text{C-N})$), 1386 (m, $\delta(\text{CH}_3)$); 1242–1142 (s, $\nu(\text{C-O-C})$); 746 (s, $\rho((\text{CH}_2)_n)$) cm^{-1} .

P5. $^1\text{H NMR}$ (400 MHz, CDCl_3): δ 7.51–7.34 (m, 1H), 6.64–6.48 (m, 2H), 6.48–6.29 (m, J = 19.8 Hz, 2H), 5.34–5.18 (m, 1H), 5.06–4.88 (m, 1H), 4.19–3.83 (m, 22H), 3.83–3.68 (m, 2H), 3.48–3.24 (m, 2H), 3.10–2.86 (m, 1H), 2.33–0.48 (m, 163H). IR: ν =

3396 (w, $\nu(\text{N-H})$), 2958, 2931, 2874 (m, $\nu(\text{C-H})$); 1720 (s, $\nu(\text{C=O})$); 1460 (m, $\delta(\text{C-H})$), 1525 (m, $\nu(\text{C-N})$ and $\delta(\text{N-H})$); 1392 (m, $\nu(\text{C-N})$), 1386 (m, $\delta(\text{CH}_3)$); 1242–1142 (s, $\nu(\text{C-O-C})$); 746 (m, $\rho((\text{CH}_2)_n)$) cm^{-1} .

P6. $^1\text{H NMR}$ (400 MHz, CDCl_3): δ 7.40 (s, 1H), 6.51 (d, J = 16.7 Hz, 1H), 6.34 (d, J = 20.6 Hz, 2H), 5.26 (s, 2H), 4.94 (s, 2H), 3.91 (s, 22H), 3.78 (dd, J = 14.9, 9.6 Hz, 2H), 3.50 (s, 2H), 3.17 (s, 2H), 2.96 (s, 1H), 2.03–1.69 (m, 21H), 1.69–1.50 (m, 23H), 1.51–1.28 (m, 27H), 1.27–0.57 (m, 73H). IR: ν = 3400 (w, $\nu(\text{N-H})$); 2958, 2931, 2874 (m, $\nu(\text{C-H})$); 1720 (s, $\nu(\text{C=O})$); 1637 (m, amide I $\nu(\text{C=O})$); 1558 (m, amide II $\nu(\text{C-N})$ with contributions of $\delta(\text{N-H})$); 1460 (m, $\delta(\text{C-H})$); 1392 (m, ($\nu(\text{C-N-C})$, $\delta(\text{N-H})$ and $\delta(\text{CH}_3)$)); 1242–1142 (s, $\nu(\text{C-O-C})$); 746 (m, $\rho((\text{CH}_2)_n)$) cm^{-1} .

General Procedure for the Synthesis of Copolymers P7–P10 via RAFT. BMA (10 equiv, 1.39 mL, 8.6 mmol), a hydrogen bond forming monomer (H1 = 3-acetamidopropyl methacrylate (159 mg) (2), H2 = 2-(3-butylureido)ethyl methacrylate (196 mg) (3)), 2-isocyanatoethyl methacrylate (133 mg), FMA (5) (134 mg), MIMA (6) (249 mg) (each 1 equiv, 0.86 mmol), and anhydrous toluene (5.4 mL) were mixed under an argon atmosphere. In the case of H2 (3) absolute methanol (0.3 mL) was added to ensure complete dissolution. The mixture was degassed using four freeze–pump–thaw cycles. To the frozen mixture 2-cyanopropan-2-yl benzodithioate (19 mg, 0.086 mmol) and AIBN (10 mg, 0.061 mmol in 0.5 mL of toluene (abs) from stock solution, previously degassed) were added, and two more freeze–pump–thaw cycles were carried out. The reaction mixture was stirred at 70 °C for 20 h. In the case of the 2-isocyanatoethyl methacrylate modified polymer (**P10**), *n*-butylamine (55 mg, 0.086 mmol) was added to the reaction mixture after cooling to room temperature, and stirring was continued for another 12 h. The polymers (listed in Table 3) were purified by precipitation in ice-cold *n*-hexane and dried at room temperature under reduced pressure. Parts of the polymer samples were analyzed by SEC and $^1\text{H NMR}$ to determine the molar mass and molar mass distribution.

P7. $^1\text{H NMR}$ (400 MHz, CDCl_3): δ 7.49–7.33 (m, 1H), 6.62–6.46 (m, 2H), 6.46–6.28 (m, J = 21.6 Hz, 2H), 5.35–5.24 (m, J = 10.8 Hz, 2H), 5.09–4.87 (m, 2H), 4.09–3.83 (m, 21H), 3.83–3.66 (m, J = 6.7 Hz, 3H), 3.04–2.90 (m, 1H), 2.78–2.60 (m, 2H), 2.13–0.55 (m, 153H). IR: ν = 3403 (w, $\nu(\text{N-H})$); 2958, 2931, 2874 (m, $\nu(\text{C-H})$); 1720 (s, $\nu(\text{C=O})$); 1460 (m, $\delta(\text{C-H})$); 1535 (m, $\nu(\text{C-N})$ and $\delta(\text{N-H})$); 1388 (m, $\nu(\text{C-N})$); 1386 (m, $\delta(\text{CH}_3)$); 1242–1142 (s, $\nu(\text{C-O-C})$); 746 (m, $\rho((\text{CH}_2)_n)$) cm^{-1} . **P7** deprotected: same signals +696 $\delta(\text{maleimide})$ cm^{-1} .

P8. $^1\text{H NMR}$ (400 MHz, CDCl_3): δ 7.49–7.33 (m, 1H), 6.62–6.46 (m, 2H), 6.46–6.28 (m, J = 21.6 Hz, 2H), 5.35–5.24 (m, J = 10.8 Hz, 2H), 5.09–4.87 (m, 2H), 4.09–3.83 (m, 21H), 3.83–3.66 (m, J = 6.7 Hz, 3H), 3.04–2.90 (m, 1H), 2.78–2.60 (m, 2H), 2.13–0.55 (m, 153H). IR: ν = 3400 (w, $\nu(\text{N-H})$); 2958, 2931, 2874 (m, $\nu(\text{C-H})$); 1720 (s, $\nu(\text{C=O})$); 1637 (m, amide I $\nu(\text{C=O})$); 1558 (m, amide II $\nu(\text{C-N})$ with contributions of $\delta(\text{N-H})$); 1460 (m, $\delta(\text{C-H})$); 1392 (m, $\nu(\text{C-N-C})$, $\delta(\text{N-H})$ and $\delta(\text{CH}_3)$); 1242–1142 (s, $\nu(\text{C-O-C})$); 746 (m, $\rho((\text{CH}_2)_n)$) cm^{-1} .

P9. $^1\text{H NMR}$ (400 MHz, CDCl_3): δ 7.47–7.32 (m, 1H), 6.59–6.47 (m, 1H), 6.44–6.28 (m, 2H), 5.31–5.22 (m, 1H), 5.05–4.86 (m, 2H), 4.11–3.83 (m, J = 58.4 Hz, 19H), 3.81–3.68 (m, 2H), 3.55 (dd, J = 10.5, 5.4 Hz, 2H), 3.04–2.89 (m, 1H), 2.09–1.70 (m, 20H), 1.70–1.49 (m, 22H), 1.51–1.29 (m, 21H), 1.29–0.67 (m, 61H). IR: ν = 2958, 2931, 2874 (m, $\nu(\text{C-H})$); 2270 (m, $\nu(\text{OCN})$); 1720 (s, $\nu(\text{C=O})$); 1460 (m, $\delta(\text{C-H})$); 1386 (m, $\delta(\text{CH}_3)$); 1242–1142 (s, $\nu(\text{C-O-C})$); 746 (m, $\rho((\text{CH}_2)_n)$) cm^{-1} .

Table 3. Polymers Prepared via RAFT

polymer	yield [%]	dS_F [%]	dS_M [%]	dS_H [%]	PDI
P7 FMAcoMIMAcOBMAcOH1 = EKHI _R	68	8.6	6.4	5.6	5.51
P8 FMAcoMIMAcOBMAcOH2 = EKHI _{2R}	79	8.7	6.5	9.8	2.76
P9 FMAcoMIMAcOBMAcOCN = EKOCN _R	–	9.1	5.9	9.6	–
P10 EK(OCN+amine) _R = EKHI _{2R}	84	7.8	5.9	9.4	3.48

Table 4. Composition of Polymers P1–P10

		W	X	Y	Z	M_n theor [g/mol]	M_n ^1H NMR [g/mol]	M_n SEC [g/mol]	PDI SEC	T_g ($^{1/2}\Delta c_p$) [°C]
P1	pBMA	–	–	–	n	14200	13100	17200	1.52	29
P2	pBMAcoFMA	–	1n	–	10n	15900	14800	21800	1.66	26
P3	pBMAcoMiMA	1n	–	–	10n	17000	15800	11800	2.40	30
P4	pBMAcoH1	–	–	1n	10n	16100	15600	19200	1.60	34
P5	EKH1 _A	1n	1n	1n	10n	20900	17800	16500	3.25	63
P6	EKH2 _A	1n	1n	1n	10n	21300	16800	20300	2.07	63
P7	EKH1 _R	1n	1n	1n	10n	20900	16500	9070	5.51	53
P8	EKH2 _R	1n	1n	1n	10n	21300	19400	17000	2.76	53
P9	EK(OCN) _R	1n	1n	1n	10n	20600	18500	–	–	63
P10	EK(OCN+amine) _R	1n	1n	1n	10n	21300	postmod	18000	3.48	61

P10. ^1H NMR (400 MHz, CDCl_3): δ 7.42 (s, 1H), 6.59–6.50 (m, 1H), 6.45–6.31 (m, 2H), 5.32–5.22 (m, 2H), 5.04–4.89 (m, 2H), 4.12–3.84 (m, 22H), 3.86–3.70 (m, 3H), 3.63–3.41 (m, 2H), 3.27–3.12 (m, 2H), 3.06–2.90 (m, 1H), 2.10–1.71 (m, 22H), 1.71–1.53 (m, 29H), 1.53–1.30 (m, 28H), 1.30–0.55 (m, 74H). IR: ν = 3400 (w, $\nu(\text{N-H})$); 2958, 2931, 2874 (m, $\nu(\text{C-H})$); 1720 (s, $\nu(\text{C=O})$); 1637 (m, amide I $\nu(\text{C=O})$); 1558 (m, amide II $\nu(\text{C-N})$ with contributions of $\delta(\text{N-H})$); 1460 (m, $\delta(\text{C-H})$); 1392 (m, $\nu(\text{C-N-C})$, $\delta(\text{N-H})$ and $\delta(\text{CH}_3)$); 1242–1142 (s, $\nu(\text{C-O-C})$); 746 (m, $\rho((\text{CH}_2)_n)$) cm^{-1} .

Synthesis of Octafunctional Hydrogen Bond Bearing Spherosilicate.²² Tetraethyl orthosilicate was condensed with tetramethylammonium pentahydrate to an SiO_2 octaanion, which was transferred to the Si-H terminated cube by conversion with dimethylchlorosilane.^{26,27} Hydrosilylation with ω -bromoalkenes resulted in cubes, which could be further converted with NaN_3 to the corresponding azides. After catalytic reduction to the amine, the highly reactive cube could be converted with propyl isocyanate to the desired hydrogen bond bearing spherosilicate.²²

Synthesis of Composites (C1–C5). The hybrid materials C1–C5 (Scheme 2 and Table 4) were synthesized by mixing (a) P1 with C6U = C1 (control) with OctaUreaPOSS (C6U), (b) P1, P2, and P3 with C6U = C2, (c) P2, P3, and P4 with C6U = C3, (d) one-component polymer EKH1_A = (P5) with C6U = C4, and (e) one-component polymer EKH2_R = (P6) with C6U = C5. The polymers or polymer mixtures (500 mg in total, 167 mg each) were dissolved in THF (5 mL) and C6U (125 mg, M_w = 2478.20 g/mol, 0.05 mmol) in methanol (10 mL). After mixing, the solvents were evaporated at room temperature in a vacuum, and the respective precipitated solid was pressed into a Teflon mold. The deprotection of maleimide in MIMA (6) containing hybrid materials (C2–C5) was performed in the bulk material for 30 min at 120 °C. Cross-linking was realized by heating the samples at 70 °C for 20 h.

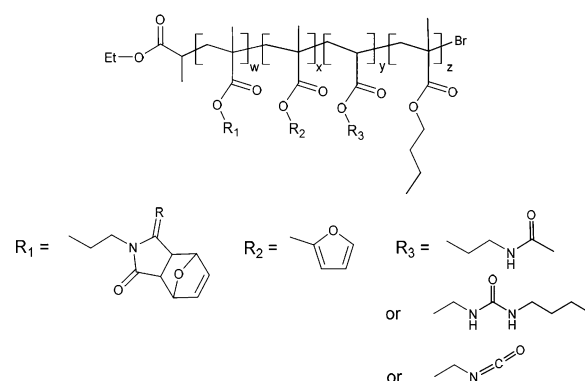
3. RESULTS AND DISCUSSION

Synthesis and Characterization of Polymers P1–P10.

Polymers containing DA as well as hydrogen donor and acceptor functions were synthesized via controlled radical polymerization (CRP), in particular ATRP, ARGET ATRP, or RAFT. In the present work, we decided to locate the diene as well as the dienophile in the polymer matrix to ascertain a high degree of freedom of these chemical reaction partners. Applying this approach, it can be guaranteed that the maleimide and furan functional groups are statistical distributed and therefore equal in their availability to undergo DA reaction.¹⁰ As a second reversible network, we introduced amide and urea motifs as supramolecular units because of their ability to form hydrogen bonds. The precursors are commercially available and the monomers can be produced in one or two reaction steps. Hydrogen bonds equilibrate at room temperature after damage and according to that a reconnection of cut interfaces at or below nanometer scale is

immediately possible to ensure the proximity of DA moieties. Scheme 1 and Table 4 summarize the synthesized polymers.

Scheme 1. Statistical Copolymers P1–P10



All macromolecules were statistical copolymers from butyl methacrylate, furfuryl methacrylate ($5 = R_2$), protected maleimidoethyl methacrylate ($6 = R_1$), and a hydrogen bond building moiety, namely 3-acetamidopropyl methacrylate ($2 = R_3$), 2-(4-butylureido)ethyl methacrylate ($3 = R_3$), or 2-isocyanatoethyl methacrylate (R_3) as functional monomers (Scheme 1 and Table 4). The protection of maleimide is necessary because otherwise cross-linking with the reactive maleimide double bond would occur.⁸ The main component within the polymer is butyl methacrylate (70–90 equiv), and each functional monomer was applied in 10 equiv.

P1–P3 containing only BMA, FMA, and protected MIMA could be polymerized similar to literature known procedures applying a Cu(I)-catalyzed ATRP using HMTEA as a ligand.^{8,28} When hydrogen bond donors, particularly nitrogen donors, were added to the mixture, only very little conversion was observed. Literature procedures describe the polymerization of 3-acetamidopropyl methacrylate ($2 = R_3 = H1$) applying an ATRP with CuBr PMDETA catalyst in DMF.²⁹ In our systems, the polymerization remained quite incomplete. Trying to polymerize hydrogen bond bearing 2-(4-butylureido)ethyl methacrylate ($3 = R_3 = H2$) under the same conditions, almost no conversion was obtained after 16 h. Adjusting the reaction conditions to an ARGET ATRP like polymerization instead, even the strong donating monomers could be polymerized in high quantity (up to 90%). $[\text{CuBr}(\text{HMTETA})]\text{Br}$ seems to be not stable long enough under the given reaction conditions. Therefore, hydrazine hydrate was applied as reducing agent. In addition, fresh ligand was added after 12 h, and the desired products (P4–P6) could be synthesized in up to 95% conversion (as determined by ^1H

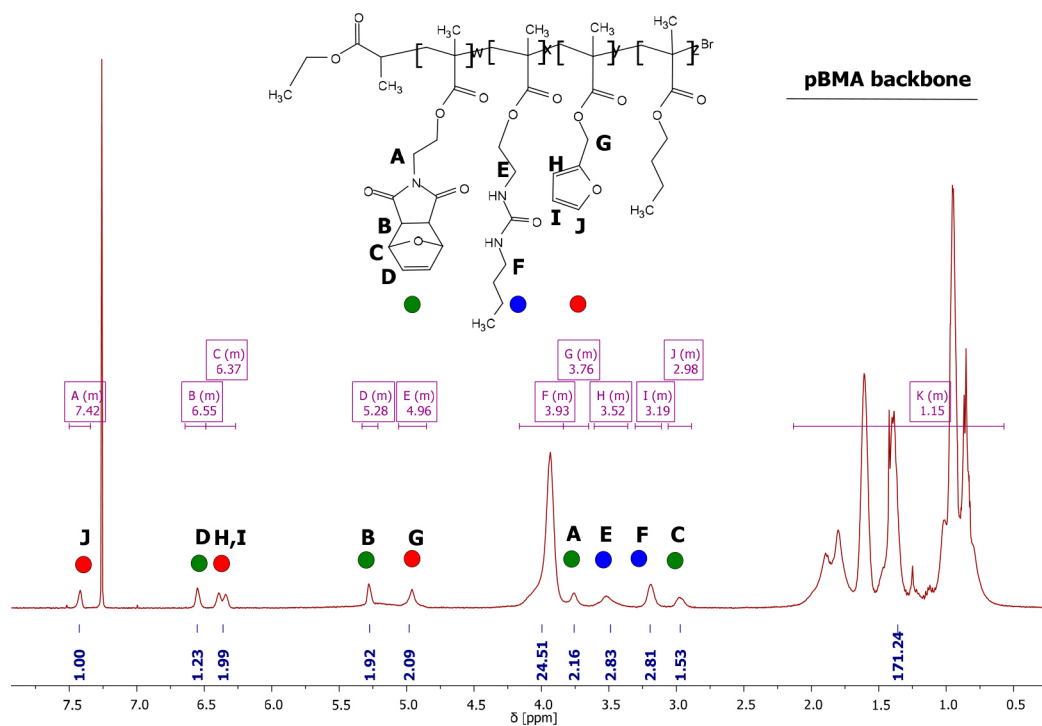


Figure 1. ^1H NMR of one-component polymer $\text{EKH2}_A = \text{P6}$.

NMR). SEC measurements revealed a rather broad mass distribution ($\text{PDI} = 1.52\text{--}2.40$). The highest value was obtained for maleimide containing **P3**, presumably because of impurities of small amounts of deprotected maleimide, which can undergo irreversible cross-linking.⁸ The obtained one-component polymers are soluble in common organic solvents such as acetone, CHCl_3 , or THF.

As an alternative route a reversible addition–fragmentation chain transfer (RAFT) polymerization was applied because it tolerates more functional groups than ATRP and requires no metal catalyst. Using 2-cyanopropan-2-yl benzodithioate as RAFT agent and AIBN as initiator, the hydrogen bond bearing monomers could be incorporated without difficulties within the polymer. As the urea bearing monomer (**3**) is insoluble in toluene, a small amount of methanol had to be added to the mixture. To keep the reaction parameters more similar to the polymerization of EKH1_A (**P5**) and EKH1_R (**P7**), the polymerization of the 2-isocyanatoethyl methacrylate was also investigated. The successful polymerizations of isocyanates in RAFT have been described before.^{30,31} In a post-modification, the crude polymer could be directly converted with *n*-butylamine to the desired EKH2_R (**P10**). Conversions of 79–91% were obtained, and molar mass distributions from $\text{PDI} = 2.76\text{--}5.51$ were determined.

^1H NMR spectra were used to verify that there are no unreacted monomers left after work-up. The degree of substitution was determined by setting the integral of all OCH_2 signals (at 3.93 and 4.96 ppm), which represents the complete polymer backbone, in relation to one proton of each functional comonomer. SEC measurements revealed that the PDIs are between 1.5 and 5.5. The reason for these relatively broad molar mass distributions, in particular, when maleimide participates within the reaction, is mentioned above. However, the obtained polymer chains are still soluble and linear and have low molecular weights (below 22000 g/mol). The desired

functional monomers were incorporated in a good substitution degree ($\text{dS} = 4.3\text{--}9.9\%$).

Figure 1 displays the ^1H NMR of one-component polymer $\text{EKH2}_A = \text{P6}$. The red dots at 7.42, 6.37, and 4.96 ppm indicate protons belonging to the furan moiety, the green dots at 6.55, 5.28, 3.76, and 2.98 ppm show the signals of protected maleimide group, and the blue dots at 3.52 and 3.19 ppm show the CH_2N groups of copolymerized urea derivative. After ARGET ATRP, furan was found in 7.0%, protected maleimide in 4.3%, and 2-(4-butylureido)ethyl methacrylate (**3** = **H2**) in 9.9% for $\text{EKH2}_A = \text{P6}$. By use of RAFT polymerization for $\text{EKH2}_R = \text{P8}$, a substitution degree of 8.7% for furan, 6.5% protected maleimide, and 9.8% for **3** (**H2**) was observed. ^1H NMR spectra and degree of substitution of all other polymers can be found in the [Supporting Information](#).

By comparison of the IR spectra of functional polymers with the pure pBMA polymer **P1**, the incorporation of functional groups could be further verified (**Figure 2**). Pure pBMA shows similar bands like PMMA: 2958–2874 cm^{-1} C–H stretching, 1720 cm^{-1} C=O stretching, 1460 cm^{-1} C–H bending, 1386 and 746 cm^{-1} $\alpha\text{-CH}_3$ -vibration, 1242–1142 cm^{-1} C–O–C stretching. The functional polymer shows additional peaks, which are typical for the urea structure motive. At 3400 cm^{-1} the N–H stretching vibration, at 1637 cm^{-1} amide I (C=O stretching), 1558 cm^{-1} amide II bands (C–N stretching with contributions of N–H bending), and 1392 cm^{-1} (C–N–C stretching, N–H deformation and CH_3 deformation).^{32,33} The **H2** monomer (**3**) shows the corresponding peaks at 3336, 1620, 1574, and 1382 cm^{-1} . Further IR spectra can be found in the [Supporting Information](#).

Analysis of Polymers via DSC. All polymers were analyzed using DSC by cooling the samples to $-25\text{ }^\circ\text{C}$ and heating to $200\text{ }^\circ\text{C}$ twice. The presence of only one T_g in all polymers evidences an ideal miscibility and a homogeneous, statistical distribution of each comonomer (**Table 4** and **Figure 3**).³⁴

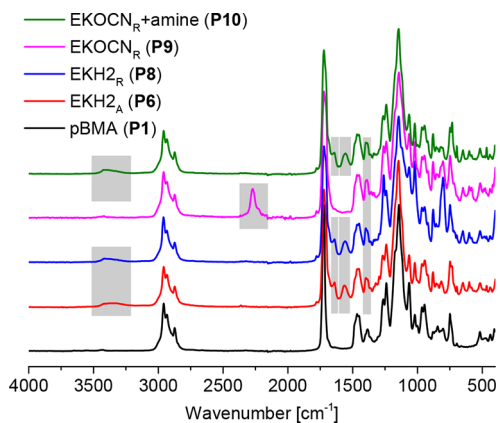


Figure 2. Comparison of IR spectra of pure pBMA with functional one-component polymers EKH₂.

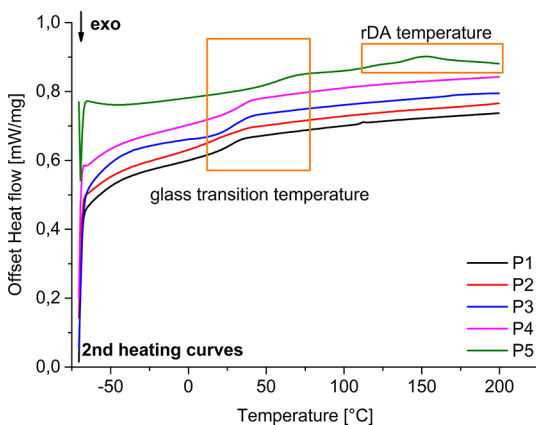


Figure 3. DSC measurements of second heating curve to determine the glass transition temperature from P1–P5.

The T_g is a function of molecular weight, amount, chemical nature of side chains, the thermal history of a polymer, and the cross-linking between the single chains. In polymers containing the maximum number of two comonomers (P1–P4) the glass transition is significantly lower with 26–34 °C, while in one-component polymers consisting of four comonomers (P5–P12) the T_g 's are between 53 and 63 °C. The T_g 's were analyzed using the second heating curve, in which cross-linking of single polymer chains already took place to a certain amount. Consequently, the T_g 's of P5–P12 are about 20–30 °C higher than those of P1–P4 (Table 4). A second effect should be the hydrogen bond forming side chains on a hydrogen bond forming spine, which makes an interlock more probable and thus leads also to an increased T_g . All protected maleimide-containing polymers (P3, P5–P10) show a broad endothermic signal between 100 and 200 °C belonging to the rDA reaction in the first heating cycle, which corresponds to the deprotection of maleimide and evaporation of furan (compare Figure 5). DSC curves of other polymers (P6–P10) are displayed in the Supporting Information (Figure S28).

FTIR spectra (Figure 4) show the appearance of maleimide deformation band after deprotection of the polymer P5 in bulk. This observation further confirms that after synthesis all maleimide moieties are still protected. After heating to 120 °C for 30 min, a small and sharp signal at 696 cm⁻¹ for ring deformation can be detected, which indicates free, unprotected, and intact maleimide.

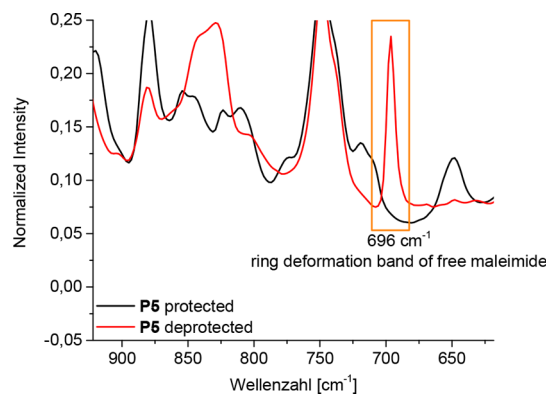


Figure 4. Observation of maleimide deformation band as indicator for successful deprotection of polymer P5.

The DSC curve in Figure 5 shows the deprotection of EKH₂ (P8) in the first heating cycle, which causes the high

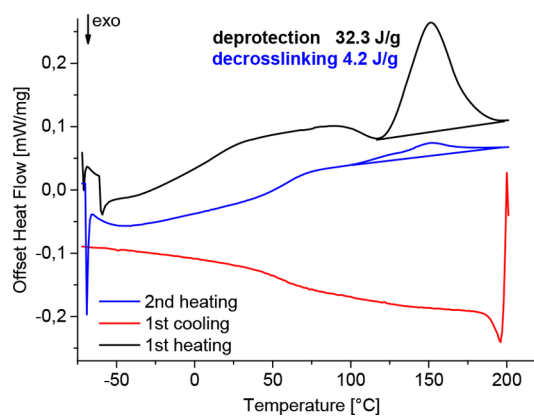


Figure 5. DA/rDA cycles of P8 = EKH₂.

endothermic signal (32.3 J/g) between 120 and 200 °C. Because of the evaporation energy of furan, the signal is much higher than the one in the second heating cycle. During the measurement, the sample passes the DA temperature and thus parts of the one-component polymer cross-link. Upon the second heating to rDA temperature, the de-cross-linking causes an endothermic signal (4.2 J/g).

The FTIR and DSC measurements show the efficient reversibility of synthesized one-component polymer P9.

Synthesis of Composites. Hybrid materials (Scheme 2 and Table 5) were synthesized by mixing (a) P1 with OctaUreaPOSS (C6U) = C1 (control), (b) P1, P2, and P3 with C6U = C2, (c) P2, P3, and P4 with C6U = C3, (d) one-component polymer EKH1_A = P5 with C6U = C4, and (e) one-component polymer EKH2_R = P8 with C6U = C5 in an appropriate solvent mixture. C1 is the pure nonfunctional pBMA mixed with the filler as a control experiment. C2 also misses hydrogen bonds within the matrix but has the DA moieties for covalent cross-linking. C3 is a mixture of all desired functions, but each is located in its own polymer. C4 is the one-component matrix bearing amide and C5 the one that is bearing urea groups in the backbone. By investigation of these different compositions, the contributions of the single forces should be judged.

For a good solubility the polymers were dissolved in THF and C6U in methanol. After mixing, the solvents were

Scheme 2. General Procedure for Synthesis of Hybrid Materials: (1) Dissolve and Mix Components in THF/Methanol (20 wt % C6U); (2) Evaporate Solvent; (3) Placing Solid Mixture in Teflon Mold, Heating Sample at 120 °C, 30 min (Deprotection) and 70 °C, 20 h (Cross-Linking)

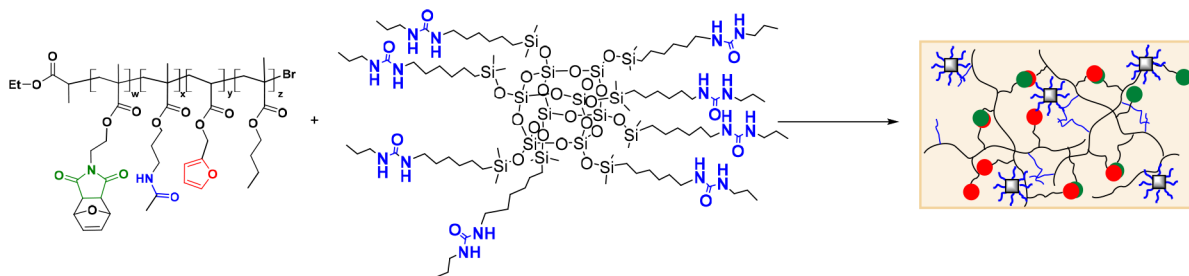


Table 5. Synthesized Composites and Their Abbreviations

	organic matrix	inorganic filler
C1	pBMA	each hybrid material contains 20 wt % C6U cube
C2	pBMA + pBMAcoFMA + pBMAcoMIMA	
C3	pBMAcoFMA + pBMAcoMIMA + pBMAcoH1	
C4	EKH1 _A	
C5	EKH2 _R	

evaporated at room temperature in a vacuum and the respective precipitated solid was pressed into a Teflon mold.

In Figure 6, the resulting hybrid material specimens with 1 mm thickness and edge length of 1 cm × 1 cm of C1, C2, C3, C4,

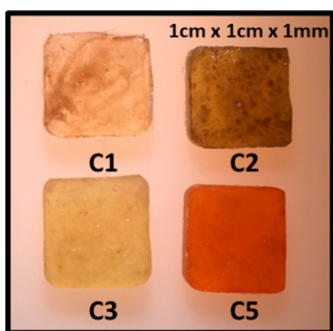


Figure 6. Images of hybrid materials C1, C2, C3, and C5.

and C5 are shown. In C1 and C2 a macroscopically visible inhomogeneous distribution was found, although the solvent was evaporated during stirring, while C3, C4, and C5 show a uniform material (Figure 6).

The deprotection of maleimide in MIMA (6) containing hybrid materials (C2–C5) was performed by heating the bulk material to 120 °C for 30 min. Subsequently, the materials were cross-linked by heating the specimens at 70 °C for 20 h.

Reversibility of DA Reaction in Hybrid Materials. FTIR measurements (Figure 7) confirm the incorporation of C6U by the appearance of typical Si–O–Si bonds and the cage deformation vibration at 557 cm⁻¹. The position of the N–H vibration can be seen as an indicator that hydrogen bonds are formed. In dilute solutions, the signals for the urea N–H bond is typically observed around 3400 cm⁻¹, which means no hydrogen bonds are formed. In bulk, the lower wavenumber of 3300 cm⁻¹ indicates hydrogen bonds within the hybrid material.^{32,33} The presence of only one N–H vibration at 3336 cm⁻¹ indicates the formation of a dynamic

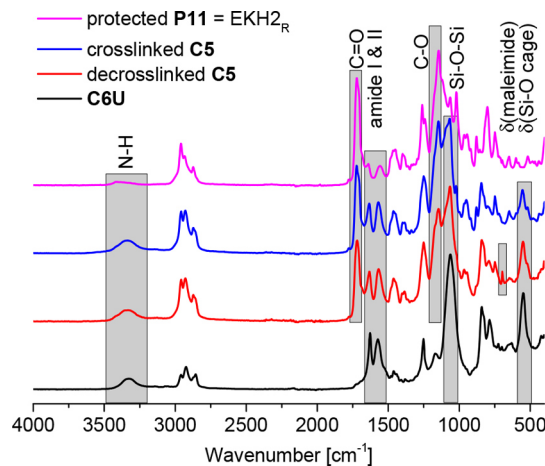


Figure 7. IR spectra of P11 and C6U = C5.

hydrogen bond network, formed between filler and matrix. Further IR spectra of composites are shown in Figure S29.

Although the absorbance of urea groups (0.4 mmol in 125 mg of C6U) cause strong vibrations, the typical maleimide (maximum 0.24 mmol in 500 mg of PS) deformation vibration at 696 cm⁻¹ becomes visible after deprotection of the hybrid material in bulk. After cross-linking at 70 °C for 20 h, this vibration disappears again, which indicates cross-linking within the material.

DSC measurements from –25 to 200 °C with a heating rate of 10 K/min were used to visualize DA cycles by thermal treatment of the composites. Although temperatures up to 200 °C could lead to polymerization and decomposition of maleimides in the sample, this temperature program was chosen to display the whole energy consumption of rDA reaction. For the one-component cross-linked composite C5, the first heating cycle show a broad endothermic signal from 100 to 200 °C of 18.5 J/g (Figure 8).

The T_g signal is located around 53 °C, like in the initial polymer, but it should be considered that the signal may have contributions from the DA reaction. After the first deprotection within DSC measurement, the sample is maximum 22 min in the DA temperature range, which is quite a short time to reconnect for the DA groups compared to the normally applied 20 h in bulk. However, the appearance of the rDA signal with 3.1 J/g in the second heating cycle shows that cross-linking took place. Directly after that, the sample was heated isothermal at 70 °C for 20 h in DSC (Figure 8, third heating). This heating represents the experimental conditions, like they are applied for the bulk material. A signal of 4.4 J/g

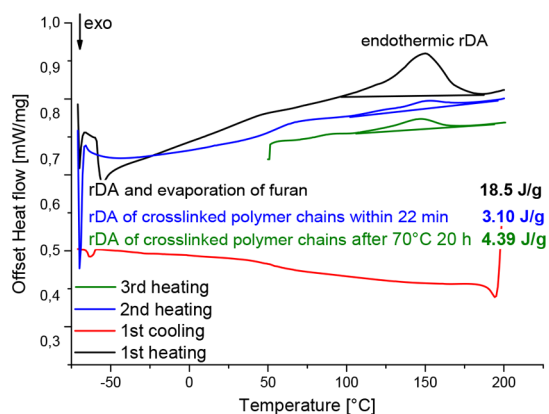


Figure 8. DA/rDA cycles of C5.

which is 15% higher was observed compared to the short cross-linking time of 22 min in DSC.

The DSC measurements display a good reversibility of DA reactions in this hybrid material. Situating the DA functional groups only within the matrix polymers seems to be advantageous compared to systems where the groups are located on inorganic surfaces.¹⁰ Even with a high filler content of 20 wt % the spherosilicate does not limit the DA reaction, as can be concluded from the rDA signal after cross-linking of C5. The hybrid material shows a signal of 3.1, and the pure polymer EKH_{2R} (P8, Figure 5) shows a signal of 4.2 J/g after short cross-linking time of 22 min.

Self-Healing Studies. ¹³C CP MAS NMR measurements were conducted to follow the cross-linking ability of the produced materials. The measurements were performed on protected P5 and cross-linked C4 (Figure 9).

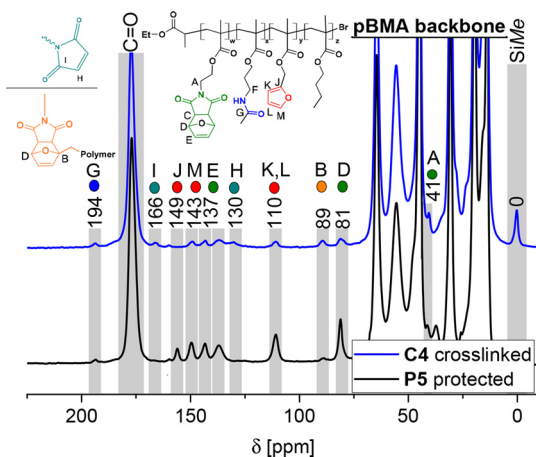


Figure 9. ¹³C CP-MAS NMR spectra of protected P5 and cross-linked composite C4.

In ¹³C CP-MAS NMR, the ratio of signals that belong to DA/rDA can be visualized. The colored dots in Figure 9 indicate the relevant peaks, which are the signals of the CH₂ group next to maleimide nitrogen at 41 ppm, the bridgehead carbons of the C–O–C motive in the DA product at 81 and 89 ppm, and the double bond of the DA adduct at 137 ppm. After deprotection the signals at 130 and 166 ppm of free maleimide became visible. The signals at 110, 143, and 149 ppm belong to the four carbon atom signals of the furan ring and at 194 ppm the characteristic signals for the C=O group

of the imide can be observed. The successful incorporation of spherosilicates is indicated by the signal of Si–CH₃ groups at 0 ppm. ²⁹Si CP-MAS NMR spectra of composite C4 evidence that the silica framework remains intact and in its original high symmetry, as indicated by only two sharp signals: –11.99 ppm (OSi(CH₃)₂R) and –109.21 ppm (SiOSi) (Figure 10). This spectrum is in good agreement with solution ²⁹Si NMR of the pure compound C6U.

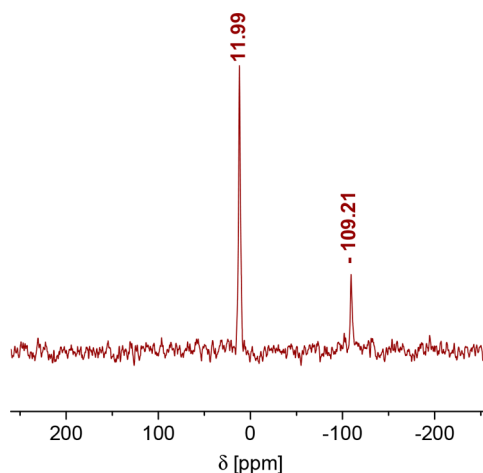


Figure 10. ²⁹Si CP-MAS of cross-linked composite C4.

UV-vis measurements were performed to follow the DA reaction as a function of temperature within 24 h (Figure 11).

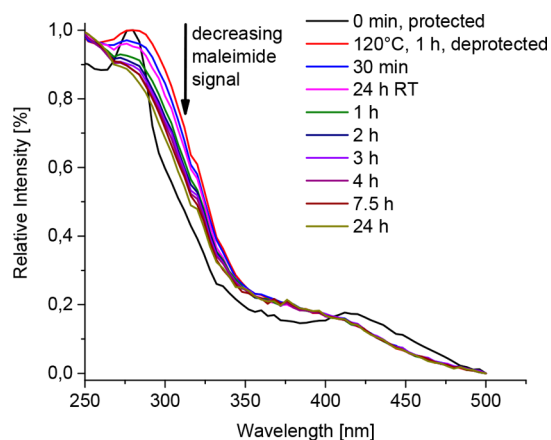


Figure 11. UV-vis spectra followed over time during the cross-linking reaction of C4 at 70 °C.

A comparison of the free maleimide UV-vis absorption around 284 nm was used to plot the conversion over time (Figure 12). Cross-linking proceeds mostly within the first 4 h. A conversion of 80% was reached already within this short period in the pure polymer P8 (Figures S37–39) as well as in the hybrid material (C4). These results show that the reactivity of the one-component polymer is not decreased by the addition of C6U.

Rheological measurements of pure polymer P8 and hybrid material C4 were conducted. The storage modulus was observed over time while the temperature was varied from 70 °C (protected maleimide) to 120 °C for 1 h (deprotection) and back to 70 °C (cross-linking). In the pure polymer (Figure S41), an increasing storage modulus was observed after

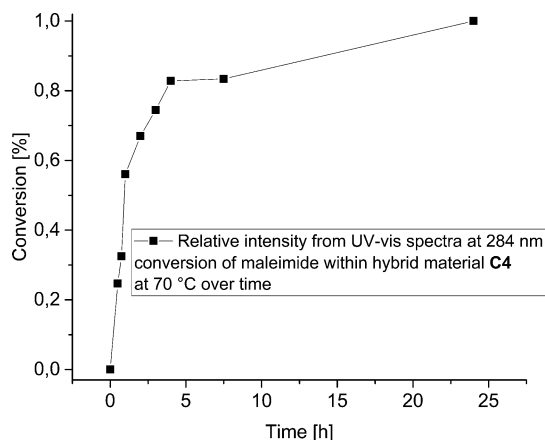


Figure 12. DA conversion over time of C4 determined from UV-vis spectra.

deprotection, upon cooling to the cross-linking temperature of 70 °C. After approximately 1 h at 70 °C, the polymer melt solidifies, and the observation of storage modulus was no longer possible. The increasing modulus as well as turning from polymer melt to a solid already at 70 °C indicates a successful DA cross-linking reaction within the one-component polymer.

The same temperature program was applied to the hybrid material C4, and the same general trend was observed (Figure 13). The ability to measure a storage modulus in the protected

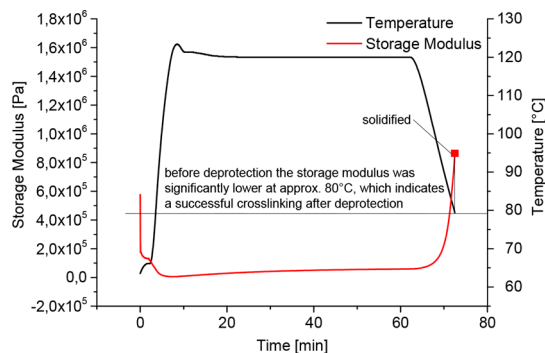


Figure 13. Temperature dependent rheology measurement of C4.

state of the sample below 80 °C compared to the solidification of the hybrid material, upon cooling within 10 min, indicates a successful and rapid DA cross-linking.

STEM images of microtome cutting slices (~20 nm depth) of C3 were prepared to investigate the nanostructure of the hybrid material (Figure 14 and Figure S42). The images show a homogeneous distribution of C6U within the hydrogen bond motive functionalized polymer matrix. No agglomerates could be found, in neither a low nor a high magnification. Notice that the black lines in Figure 14 (left) belong to the TEM grid. An EDX spectrum of this sample was recorded to prove that the silica nanocages (C6U) are part of the microtome cutting slice (Figure S43).

Optical Microscope Images: Proof of Principle. Self-healing studies were performed applying a 1 cm × 1 cm × 1 mm sample by creating a cut of 5 mm through the entire specimen (Figure 15).

As mentioned above, C1 and C2 showed an inhomogeneous distribution of the urea group bearing spherosilicate C6U.

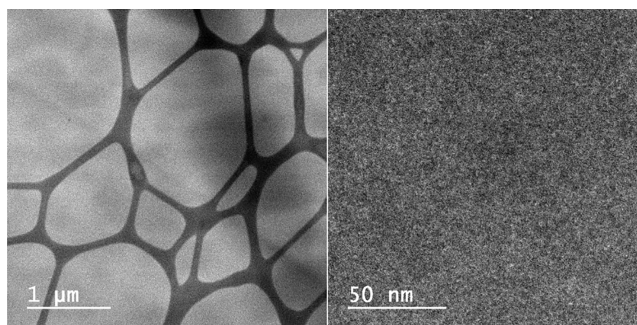


Figure 14. STEM images of microtome cutting slice (~20 nm depth) of C3.

Healing experiments were performed identically to the other samples: a cut was prepared, the interfaces were gently pressed together at room temperature, the samples were placed in an oven at 120 °C for 30 min, and treated at 70 °C for 20 h afterward. Figure S34 shows the control experiment with composite C1, which only consists of pBMA with the filler C6U. When the interfaces were pressed together at 30 °C, the hydrogen bonds of C6U provide close contact. By heating the sample to 120 °C, the material “healed” almost completely by simple flowing together of the polymer matrix. However, the material is significantly softer than the DA-containing hybrid materials. While C1 “healed” because the material was heated above T_g , C2 first seemed to heal quite efficiently, when heated to 120 °C because it seemed to behave like the pure polymer matrix (Figure S35). After heating to 70 °C for 20 h, the crack was still visible, which should be reasoned by a mismatch of the cut surfaces due to the lack of supramolecular forces.

C3 (Figure S36) healed equally to C4, which is discussed in the following section. As shown in Figure 15, composites C4 and C5 reveal a relatively high self-healing potential. After a macroscopic damage of several millimeters, the interfaces could be recombined at 30 °C. Because of a glue-like effect of hydrogen bonds, the specimens could recombine by gently pressing the two interfaces together at 30 °C (Figure 15, left d, right d)).

Healing the sample by thermal treatment led to the disappearance of the cut in sample C4 (Figure 15, left f) and to reduction of the crack in sample C5 (Figure 15, right, f). Therefore, the DA groups were de-cross-linked by heating the sample 30 min at 120 °C. Thus, linear polymer chains can move again, and a complete closure (C4) and partial closure (C5) of the cut occurs by the help of newly organized hydrogen bonds and re-formed DA product after cross-linking again at 70 °C within 20 h. The difference between C4 and C5 should be attributed to the urea groups within the polymer matrix, which lowers the mobility of the chains due to stronger interlock between filler and polymer compared to the amide.

4. CONCLUSIONS

Novel functional pBMA-based hybrid materials containing the DA moieties FMA and MiMA as well as hydrogen bond forming monomer H1 or H2 were synthesized. The linear polymers were prepared via living radical polymerizations ATRP or RAFT at 70 °C and characterized by ¹H NMR, IR, DSC, and SEC measurements. A homogeneous distribution of inorganic filler is ensured using spherosilicates modified with urea groups, which affords two H donors and one H acceptor. Self-healing was demonstrated using a FTIR, DSC, CP-MAS

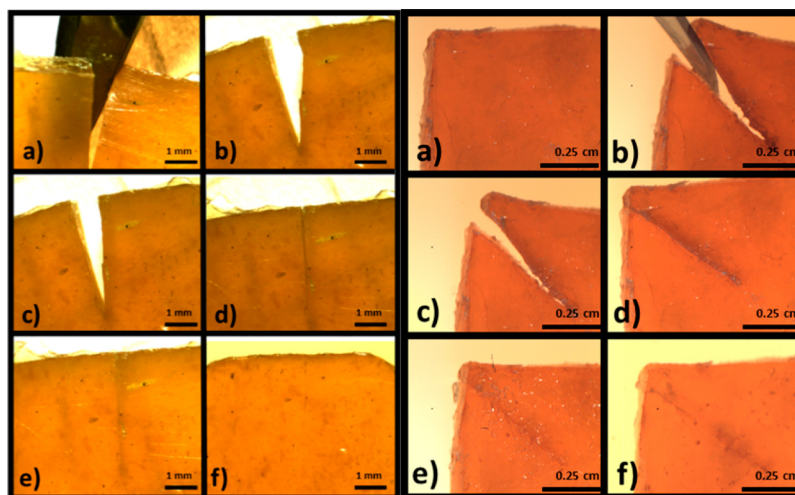


Figure 15. Microscope images of self-healing experiments on samples C4 (left) and C5 (right). C4: (a) cut through whole sample; (b, c) recombination of surfaces; (d) gently pressed together interfaces at 30 °C; (e) de-cross-linked at 120 °C and (f) cross-linked at 70 °C; C5: (a) initial sample; (b) cut through whole sample; (c) recombination of surfaces; (d) gently pressed together interfaces at 30 °C; (e) de-cross-linked at 120 °C and (f) cross-linked at 70 °C.

NMR, and an optical microscope. DSC measurements showed high endothermic peak areas between 120 and 200 °C for de-cross-linking of the DA bonds. Optical microscope images revealed a promising self-healing ability of the obtained materials. Cuts of 1 mm depth and at least 5 mm length could be healed completely. Localizing both Diels–Alder moieties within the matrix of the hybrid materials is superior compared to the Diels–Alder cross-linking between inorganic filler surface and organic matrix. Furthermore, placing hydrogen bonds within the polymers leads to a glue-like effect, which provides immediately close contact of the cut interfaces. This contact is a necessary condition for effective healing.

■ ASSOCIATED CONTENT

Supporting Information

The Supporting Information is available free of charge on the ACS Publications website at DOI: 10.1021/acs.macromol.8b00601.

¹H and ¹³C NMR spectra of synthesized molecules (1–10) and polymers (P1–P10), DSC curves (second heating) of polymers P6–P10, IR spectra of composites C1–C4, DSC curves of C1–C4, microscope images of composites C1–C3, UV-vis spectra and time over conversion plot for P8, rheological measurement for P8, STEM images and EDX for C3 (PDF)

■ AUTHOR INFORMATION

Corresponding Author

*E-mail: guido.kickelbick@uni-saarland.de (G.K.).

ORCID

Guido Kickelbick: 0000-0001-6813-9269

Notes

The authors declare no competing financial interest.

■ ACKNOWLEDGMENTS

We thank J. Schmauch for the STEM images of microtome cutting slices and the INM for providing access to the JEOL JEM-ARM 200F instrument.

■ REFERENCES

- (1) Diesendruck, C. E.; Sottos, N. R.; Moore, J. S.; White, S. R. Biomimetic Self-Healing. *Angew. Chem., Int. Ed.* **2015**, *54*, 10428–10447.
- (2) Tasdelen, M. A. Diels–Alder “click” reactions: recent applications in polymer and material science. *Polym. Chem.* **2011**, *2* (10), 2133–2145.
- (3) Ruiz de Luzuriaga, A.; Martin, R.; Markaide, N.; Rekondo, A.; Cabanero, G.; Rodríguez, J.; Odriozola, I. Epoxy resin with exchangeable disulfide crosslinks to obtain reprocessible, repairable and recyclable fiber-reinforced thermoset composites. *Mater. Horiz.* **2016**, *3*, 241–247.
- (4) Thakur, V. K.; Kessler, M. R. Self-healing polymer nanocomposite materials: A review. *Polymer* **2015**, *69*, 369–383.
- (5) Zhong, N.; Post, W. Self-repair of structural and functional composites with intrinsically self-healing polymer matrices: A review. *Composites, Part A* **2015**, *69*, 226–239.
- (6) Arslan, M.; Tasdelen, M. Polymer Nanocomposites via Click Chemistry Reactions. *Polymers* **2017**, *9*, 499.
- (7) Adachi, K.; Achimuthu, A. K.; Chujo, Y. Synthesis of Organic-Inorganic Polymer Hybrids Controlled by Diels–Alder Reaction. *Macromolecules* **2004**, *37*, 9793–9797.
- (8) Engel, T.; Kickelbick, G. Self-healing nanocomposites from silica – polymer core – shell nanoparticles. *Polym. Int.* **2014**, *63* (5), 915–923.
- (9) Engel, T.; Kickelbick, G. Thermoreversible Reactions on Inorganic Nanoparticle Surfaces: Diels–Alder Reactions on Sterically Crowded Surfaces. *Chem. Mater.* **2013**, *25* (2), 149–157.
- (10) Schäfer, S.; Kickelbick, G. Self-healing polymer nanocomposites based on Diels–Alder-reactions with silica nanoparticles: The role of the polymer matrix. *Polymer* **2015**, *69*, 357–368.
- (11) Schäfer, S.; Kickelbick, G. Diels–Alder Reactions on Surface-Modified Magnetite/Maghemite Nanoparticles: Application in Self-Healing Nanocomposites. *ACS Appl. Nano Mater.* **2018**, *1*, 2640.
- (12) Chuo, T.-W.; Liu, Y.-L. Preparation of self-healing organic–inorganic nanocomposites with the reactions between methacrylated polyhedral oligomeric silsesquioxanes and furfurylamine. *Compos. Sci. Technol.* **2015**, *118*, 236–243.
- (13) Xu, Z.; Zhao, Y.; Wang, X.; Lin, T. A thermally healable polyhedral oligomeric silsesquioxane (POSS) nanocomposite based on Diels–Alder chemistry. *Chem. Commun.* **2013**, *49* (60), 6755–6757.

(14) Engel, T.; Kickelbick, G. Furan-Modified Spherosilicates as Building Blocks for Self-Healing Materials. *Eur. J. Inorg. Chem.* **2015**, *2015* (7), 1226–1232.

(15) Nasresfahani, A.; Zelisko, P. M. Synthesis of a self-healing siloxane-based elastomer cross-linked via a furan-modified polyhedral oligomeric silsesquioxane: investigation of a thermally reversible silicon-based cross-link. *Polym. Chem.* **2017**, *8* (19), 2942–2952.

(16) Ciferri, A. Bond Scrambling and Network Elasticity. *Chem. - Eur. J.* **2009**, *15* (28), 6920–6925.

(17) Liu, C. K.; Yang, T. J.; Shen, J. S.; Lee, S. Some recent results on crack healing of poly(methyl methacrylate). *Eng. Fract. Mech.* **2008**, *75* (17), 4876–4885.

(18) Fang, X.; Zhang, H.; Chen, Y.; Lin, Y.; Xu, Y.; Weng, W. Biomimetic Modular Polymer with Tough and Stress Sensing Properties. *Macromolecules* **2013**, *46* (16), 6566–6574.

(19) Araya-Hermosilla, R.; Broekhuis, A. A.; Picchioni, F. Reversible polymer networks containing covalent and hydrogen bonding interactions. *Eur. Polym. J.* **2014**, *50*, 127–134.

(20) Araya-Hermosilla, R.; Lima, G. M. R.; Raffa, P.; Fortunato, G.; Pucci, A.; Flores, M. E.; Moreno-Villoslada, I.; Broekhuis, A. A.; Picchioni, F. Intrinsic self-healing thermoset through covalent and hydrogen bonding interactions. *Eur. Polym. J.* **2016**, *81*, 186–197.

(21) Willocq, B.; Khelifa, F.; Brancart, J.; Van Assche, G.; Dubois, Ph.; Raquez, J.-M. One-component Diels–Alder based polyurethanes: a unique way to self-heal. *RSC Adv.* **2017**, *7*, 48047–48053.

(22) Schäfer, S.; Kickelbick, G. Simple and high yield access to octafunctional azido, amine and urea group bearing cubic spherosilicates. *Dalton Trans* **2017**, *46* (1), 221–226.

(23) Pelagalli, R.; Chiarotto, L.; Feroci, M.; Vecchio, S. Isopropenyl acetate, a remarkable, cheap and acylating agent of amines under solvent- and catalyst-free conditions: a systematic investigation. *Green Chem.* **2012**, *14* (8), 2251.

(24) Kavitha, A. A.; Singha, N. K. Atom-Transfer Radical Copolymerization of Furfuryl Methacrylate (FMA) and Methyl Methacrylate (MMA): A Thermally-Amendable Copolymer. *Macromol. Chem. Phys.* **2007**, *208* (23), 2569–2577.

(25) Dispinar, T.; Sanyal, R.; Sanyal, A. A Diels-Alder/retro Diels-Alder strategy to synthesize polymers bearing maleimide side chains. *J. Polym. Sci., Part A: Polym. Chem.* **2007**, *45* (20), 4545–4551.

(26) Hasegawa, I.; Motojima, S. Dimethylvinylsilylation of $\text{Si}_8\text{O}_{20}^{8-}$ silicate anion in methanol solutions of tetramethylammonium silicate. *J. Organomet. Chem.* **1992**, *441* (3), 373–380.

(27) Dutkiewicz, M.; Maciejewski, H.; Marciniak, B.; Karasiewicz, J. New Fluorocarboxyfunctional Spherosilicates: Synthesis and Characterization. *Organometallics* **2011**, *30* (8), 2149–2153.

(28) Kötteritzsch, J.; Stumpf, S.; Hoepfener, S.; Vitz, J.; Hager, M. D.; Schubert, U. S. One-Component Intrinsic Self-Healing Coatings Based on Reversible Crosslinking by Diels-Alder Cycloadditions. *Macromol. Chem. Phys.* **2013**, *214* (14), 1636–1649.

(29) Chen, Y.; Kushner, A. M.; Williams, G. A.; Guan, Z. <34 Yulin Chen†, Aaron M. Kushner†, Gregory A. Williams and Zhibin Guan nchem.1314.pdf>. *Nat. Chem.* **2012**, *4*, 467–472.

(30) Beck, J. B.; Killops, K. L.; Kang, T.; Sivanandan, K.; Bayles, A.; Mackay, M. E.; Wooley, K. L.; Hawker, C. J. Facile Preparation of Nanoparticles by Intramolecular Crosslinking of Isocyanate Functionalized Copolymers. *Macromolecules* **2009**, *42* (15), 5629–5635.

(31) Flores, J. D.; Shin, J.; Hoyle, C. E.; McCormick, C. L. Direct RAFT polymerization of an unprotected isocyanate-containing monomer and subsequent structopendant functionalization using “click”-type reactions. *Polym. Chem.* **2010**, *1* (2), 213–220.

(32) Mido, Y. An infrared study of various dialkylureas in solution. *Spectrochim. Acta* **1973**, *29* (3), 431–438.

(33) Rao, C. N. R.; Chaturvedi, G. C.; Gosavi, R. K. Infrared spectra and configurations of alkylurea derivatives: Normal vibrations on N, N'-dimethyl- and tetramethylurea. *J. Mol. Spectrosc.* **1968**, *28* (4), 526–535.

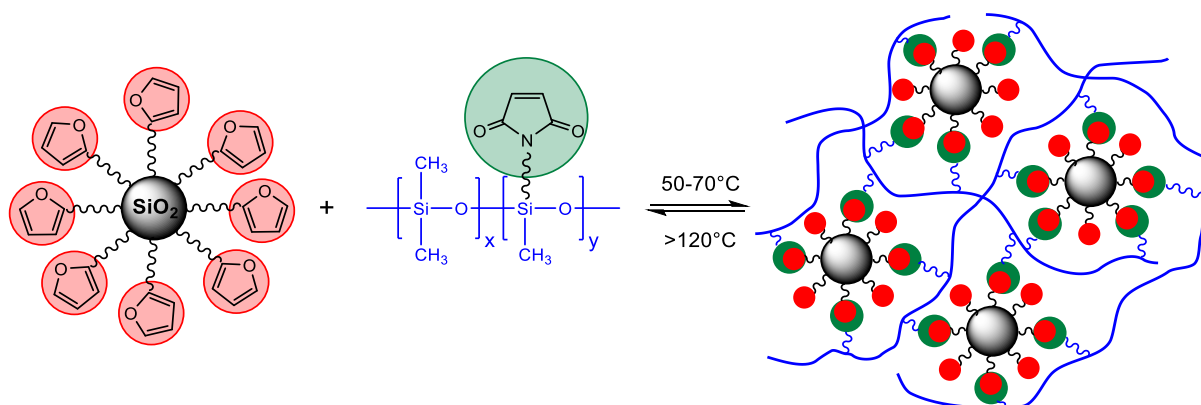
(34) Mettler_Toledo, Interpreting DSC curves: Part 1: Dynamic measurements. *User Com* **2000**, *11*, 1–26.

4 Summary and Outlook

The presented work deals with the question how DA based self-healing nanocomposites and hybrid materials can be developed with a homogeneous distribution of the filler and high crosslink density. The thermoreversible healing without the need of an additional healing agent or mechanical force was realized in a composite material.

Various parameters, such as the role of the polymer matrix, the design of the interface, the localization of DA functional groups and the effect of a second supporting physically reversible interaction, namely the hydrogen bonds as supramolecular forces, were investigated with regard to the healing capacity of the final material.

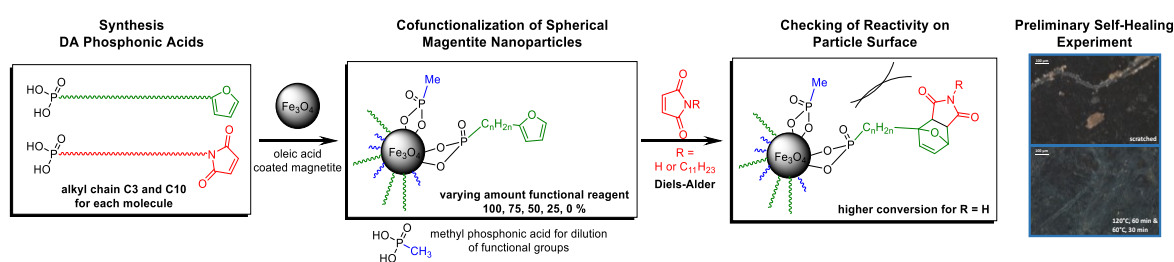
The first studied system investigated DA surface functionalized silica nanoparticles by trialkoxysilanes, which were incorporated either in DA modified siloxanes or pBMA to afford thermoreversible composites (Scheme 40).



Scheme 40: Illustration of DA modified silica particles reacting with corresponding siloxanes to crosslinked nanocomposite.

This procedure enabled the filler-matrix interface to act as the thermoreversible zone. The low degree of substitution with functional groups on the linear polymer backbone of pBMA was identified to be not suitable for the crosslinking with DA coupling agent modified silica nanoparticles. The reason is a mismatch of the densely localized functional groups on the particles and the widely distributed ones in the polymer. A better matching was achieved applying elastomeric siloxanes with side chain or α,ω -functionalizations. The lower molecular weight along with a higher amount of functional groups per chain, compared to pBMA, led to the desired thermoreversible crosslinking. The ability to heal by the thermoreversible DA reaction on particle interfaces was shown in a cut-healing experiment on the surface of a siloxane-particle composite. Due to the rigidity of the composite material, a small amount of chloroform had to support the interface-rematch. Thus, the necessary mobility of damaged interfaces for the chemical reaction in the bulk material was realized and the healing took place.

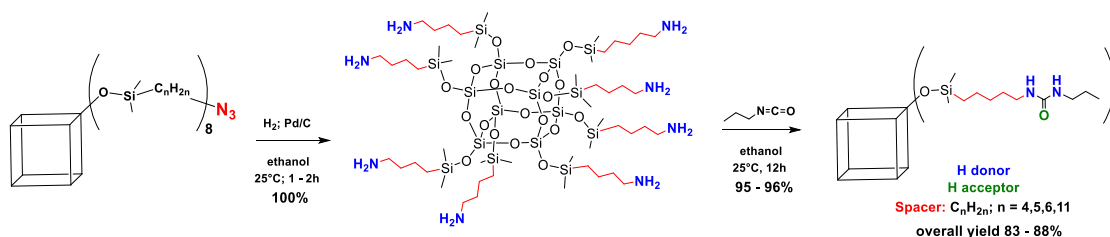
To further understand the reasons of mismatch between surface functionalized nanoparticles and polymers, we carried out a cofunctionalization study on the particle surface. As the sol-gel chemistry led to difficulties, concerning the tendency to form networks, and also the required relatively high temperature to bind alkoxysilanes onto silica, which are non-favorable working with temperature sensitive compounds like furan and maleimide, a further optimization was indicated. Magnetite/maghemite particles provide several advantages, and can be heated by an external magnetic field. Small spherical nanoparticles can be easily synthesized through a thermal decomposition reaction. Using metal oxide surfaces, the application of phosphonic acids as anchoring groups is possible. Contrary to alkoxysilanes, they do not form networks and consequently they selectively build a monolayer on metal oxides. Phosphonic acids react readily under mild reaction conditions with the substrate.



Scheme 41: Synthesis of monolayer DA phosphonic acid@ Fe_xO_y to examine the limiting factors of DA reaction on nanoparticle surfaces.

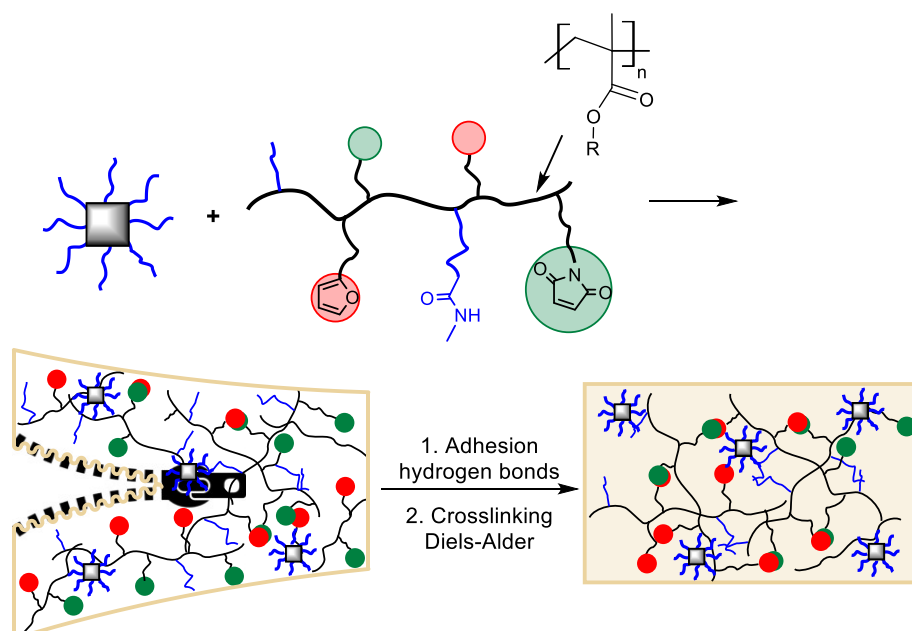
Therefore, four novel different DA phosphonic acids were synthesized (Scheme 41). A suitable exchange protocol was developed for phosphonic acid against oleic acid, which is bound to the magnetite/maghemite surface after synthesis. The propyl-/decyl DA and non-functional methyl phosphonic acid cofunctionalized particles were reacted with methylfuran/maleimide or the corresponding dodecyl derivatives. The particles with solely DA functional coupling agent on the surface showed the highest conversion in all cases. But a significant drop in conversion was observed from small methylfuran/maleimide compared to the corresponding dodecyl derivatives. This result demonstrated, that rather the sterical situation which is generated by the DA reaction is the limiting parameter, than the sterical situation on the surface itself. This has drastic consequences regarding the reaction with polymers. When one polymer chain, for example is laying along the particle surface, it prevents further reactions to occur. Consequently, we decided to distribute the DA groups more homogeneously and not to use them as a reversible force to reconnect the matrix and the filler. Nevertheless, the homogeneous embedding of the filler should be assured while providing an attractive, reversible and efficient interaction. Like in nature, hydrogen bonds, which always tend to be in an equilibrium and re-organize very fast should be the proper complement in the system. A synthesis of urea group bearing spherosilicates was developed (Scheme 42), involving a high yield access to octakis(aminoalkyl)octasilsesquioxanes. Although the primary amine group has a strong tendency to cleave Si-O-Si bonds, the desired hydrogen bond building cubes were quantitatively synthesized by reacting the amine cubes *in situ* with propylisocyanate. The cube structure was evidenced by ESI-MS amongst other methods. Their surface is reasonable for the

interaction with the matrix. Having eight hydrogen building urea groups on the surface, a strong interaction with the matrix was realized.



Scheme 42: Synthesis of octakis(6-(3-propylurea)hexyl-1-dimethylsiloxy)octasilsesquioxane (C6U) and high yield access to octakis(amino alkyl)octasilsesquioxane.

Therefore, one-component polymers were designed using controlled-radical polymerization techniques. Furan, maleimide and hydrogen bond building groups (amide and imide) were copolymerized with BMA. ATRP turns out to be disadvantageous because the catalyst system does not tolerate strongly electron donating monomers. By providing hydrazine hydrate as reducing agent and the addition of fresh ligand, the polymerization was promoted in an ARGET ATRP like process. The RAFT polymerization technique was tested for the same monomer mixtures and showed up to better tolerate the mixture of functional groups. Although high PDIs were observed, the polymers were still soluble. ^1H NMR revealed the degrees of substitution, which is between 4 and 10%. The crosslinking density indicates the quality of polymerization of the various monomers and gives valuable information for the possible crosslinking density in the final material.



Scheme 43: Illustration of intrinsic double reversible network nanocomposites.

Several hybrid materials with high self-healing potential were synthesized. Octakis(6-(3-propylurea)hexyl-1-dimethylsiloxy)octasilsesquioxane (C6U) and functional poly(butylmethacrylate) were dissolved separately and mixed afterwards to achieve a

homogeneous blend. After the solvent was evaporated in vacuum under stirring, the blend was crosslinked in a certain temperature program (Scheme 43). The high self-healing potential stems from the incorporated supramolecular forces, which enables a quick reconnection of the interfaces at 30°C. Thus, the necessary proximity of DA groups at the damaged interfaces is guaranteed and healing by DA crosslinking proceeds efficiently.

In future work, it will be interesting to combine the advantages of the above described systems. Magnetite particles could be easily surface modified with hydrogen bond motifs. Starting from *N*-(*X*-Aminoalkyl) diethyl phosphonate, e.g. imide bearing phosphonic acids could be synthesized and attached to the surface. Embedding those particles in the described one-component polymers would lead to nanocomposites, which could be healed in an external magnetic field.

The synthesized thermoreversible hybrid material composed of a blend of one-component polymer and spherosilicate could be optimized to a potential application, such as functional coatings, e.g. scratch resistant, corrosion protection, repairable running surfaces for skis and snowboards or protective shells for electronic devices. Mechanical tests, like dynamic mechanical analysis or tensile tests would be interesting, when a certain application and therefore specific demand according to the material properties are given.

The influence of other polymer backbones, in particular non-polar ones such as siloxanes contrary to polar ones like polyurethanes on the self-healing ability of one-component-polymer-C6U hybrid materials should be tested. But the variation of the polarity of the matrix, the interaction of the hydrogen bonds can be directed.

To achieve higher amounts of hybrid materials, FRP could be tested for the one-component polymers. The presented hybrid materials were synthesized in the laboratory scale (polymer around 15 g). In the case of an FRP, the filler should be already stirred with the reaction mixture. This would enable a homogeneous distribution, although the resulting polymers would be insoluble.

Also, spherosilicates or particles could be attached covalently to the polymer backbone. Both, polymer and inorganic filler, namely spherosilicates or particles can be easily synthesized bearing isocyanate or amine group, respectively. These functional groups offer versatile possibilities for post-modifications. The material, the inorganic filler is made of, can be varied according to the desired properties of the resulting material. Various metal oxides or metals could be applied for specific applications, to provide electrical conductivity, transparency or hardness for example.

Further intrinsically reversible interactions, such as ionic forces could be tested on the inorganic- organic interface. Depending on the substrates, the effort to synthesize the specific fillers, coupling agents and polymers should be concerned. When aiming for a bulk material application, the components should be affordable and accessible in large amounts.

5 References

- [1] T. Seilnacht http://www.seilnacht.com/Lexikon/k_gesch.html (Accessed on 03 March 2018).
- [2] R. Geyer; J. R. Jambeck; K. L. Law, Production, use, and fate of all plastics ever made. *Sci. Adv.* **2017**, *Band 3*, 1-5.
- [3] FRED ECONOMIC DATA <https://fred.stlouisfed.org/series/PCU325211325211> (Accessed on 05 March 2018).
- [4] OPEC IEA Statista 2018, <https://www.statista.com/statistics/262858/change-in-opec-crude-oil-prices-since-1960/> (Accessed on 19 March 2018).
- [5] R. Braun, Der Menschenplanet - Aufbruch ins Anthropozän. *Nachr. Chem. - Inlay* **2014**, 1-22.
- [6] I. K. Cohen, From: The Diabetic Foot, Second Edition Chapter 3: The Evolution of Wound Healing - From Art to Science. In Humana Press Inc. Edt. A. Veves, J. M. G., and F. W. LoGerfo, Ed. Totowa, NJ, **2006**.
- [7] B. J. Blaiszik; S. L. B. Kramer; S. C. Olugebefola; J. S. Moore; N. R. Sottos; S. R. White, Self-Healing Polymers and Composites. *Annu. Rev. Mater. Sci.* **2010**, *40*, 179-211.
- [8] M. D. Hager; P. Greil; C. Leyens; S. van der Zwaag; U. S. Schubert, Self-Healing Materials. *Adv. Mater.* **2010**, *22*, 5424-5430.
- [9] Marie D. Jackson; Eric N. Landis; Philip F. Brune; Massimo Vitti; Heng Chen; Qinfei Li; Martin Kunz; Hans-Rudolf Wenk; Paulo J. M. Monteiro; A. R. Ingraffea, Mechanical Resilience and Cementitious Processes in Imperial Roman Architectural Mortar. *PNAS* **2014**, *111*, 18484-18489.
- [10] B. Lubelli; T.G. Nijland; R. P. J. v. Hees, Self-healing of Lime based Mortars: Microscopy Observations on Case Studies. *Heron* **2011**, *56*, 1-18.
- [11] search phrase "self healing polymer" SciFinder, Version 42.032117; Chemical Abstracts Service: Columbus, OH, 2014 (accessed March 21, 2018).
- [12] "Heal." Merriam-Webster.com, www.merriam-webster.com/dictionary/healing. Accessed 19 June 2018.
- [13] C. E. Diesendruck; N. R. Sottos; J. S. Moore; S. R. White, Biomimetic Self-Healing. *Angew. Chem. Int. Ed.* **2015**, *54*, 10428-10447.
- [14] B. Aïssa; D. Therriault; E. Haddad; W. Jamroz, Self-Healing Materials Systems: Overview of Major Approaches and Recent Developed Technologies. *Adv. Mater. Sci. Eng.* **2012**, *2012*, 1-17.
- [15] R. P. Wool, Self-Healing Materials: A Review. *Soft Matter* **2008**, *4*, 400-418.
- [16] V. K. Thakur; M. R. Kessler, Self-Healing Polymer Nanocomposite Materials: A Review. *Polymer* **2015**, *69*, 369-383.
- [17] P. G. de Gennes, Reptation of a Polymer Chain in the Presence of Fixed Obstacles. *J. Chem. Phys.* **1971**, *55*, 572-579.
- [18] S. Prager; M. Tirrell, The Healing Process at Polymer-Polymer Interfaces. *J. Chem. Phys.* **1981**, *75*, 5194-5198.
- [19] R. P. Wool; K. M. O'Connor, A Theory of Crack Healing in Polymers. *J. Appl. Phys.* **1981**, *52*, 5953-5963.
- [20] K. Jud; H. H. Kausch, Load Transfer Through Chain Molecules After Interpenetration at Interfaces. *Polym. Bull.* **1979**, *1*, 697-707.
- [21] M. M. Caruso; D. A. Davis; Q. Shen; S. A. Odom; N. R. Sottos; S. R. White; J. S. Moore, Mechanically-Induced Chemical Changes in Polymeric Materials. *Chem. Rev.* **2009**, *109*, 5755-5798.

- [22] S. Burattini; H. M. Colquhoun; J. D. Fox; D. Friedmann; B. W. Greenland; P. J. Harris; W. Hayes; M. E. Mackay; S. J. Rowan, A Self-Repairing, Supramolecular Polymer System: Healability as a Consequence of Donor-Acceptor π - π Stacking Interactions *Chem. Commun.* **2009**, 6717-6719.
- [23] S. Burattini; B. W. Greenland; D. Hermida Merino; W. Weng; J. Seppala; H. M. Colquhoun; W. Hayes; M. E. Mackay; I. W. Hamley; S. J. Rowan, A Healable Supramolecular Polymer Blend Based on Aromatic π - π Stacking and Hydrogen-Bonding Interactions. *J. Am. Chem. Soc.* **2010**, *132*, 12051-12058.
- [24] H. M. Colquhoun; Z. Zhu; C. J. Cardin; Y. Gan, Principles of Sequence-Recognition in Aromatic Polyimides. *Chem. Commun.* **2004**, *0*, 2650-2652.
- [25] Howard M. Colquhoun; Zhixue Zhu; Christine J. Cardin; Yu Gan; M. G. B. Drew, Sterically Controlled Recognition of Macromolecular Sequence Information by Molecular Tweezers. *J. Am. Chem. Soc.* **2007**, *129*, 16163-16174.
- [26] R. P. Sijbesma; F. H. Beijer; L. Brunsveld; B. J. B. Folmer; J. H. K. Ky Hirschberg; R. F. M. Lange; J. K. L. Lowe; E. W. Meijer, Reversible Polymers Formed from Self-Complementary Monomers Using Quadruple Hydrogen Bonding. *Science* **1997**, *278*, 1601-1604.
- [27] A. W. Bosman; R. P. Sijbesma; E. W. Meijer, Supramolecular Polymers at Work. *Mater. Today* **2004**, *7*, 34-39.
- [28] P. Cordier; F. Tournilhac; C. Soulie-Ziakovic; L. Leibler, Self-Healing and Thermoreversible Rubber from Supramolecular Assembly. *Nature* **2008**, *451*, 977-980.
- [29] J. Fox; J. J. Wie; B. W. Greenland; S. Burattini; W. Hayes; H. M. Colquhoun; M. E. Mackay; S. J. Rowan, High-Strength, Healable, Supramolecular Polymer Nanocomposites. *J. Am. Chem. Soc.* **2012**, *134*, 5362-5368.
- [30] A. Reisch; E. Roger; T. Phoeung; C. Antheaume; C. Orthlieb; F. Boulmedais; P. Lavallo; J. B. Schlenoff; B. Frisch; P. Schaaf, On the Benefits of Rubbing Salt in the Cut: Self-Healing of Saloplastic PAA/PAH Compact Polyelectrolyte Complexes. *Adv. Mater.* **2014**, *26*, 2547-2551.
- [31] T. J. Cuthbert; J. J. Jadischke; J. R. de Bruyn; P. J. Ragona; E. R. Gillies, Self-Healing Polyphosphonium Ionic Networks. *Macromol.* **2017**, *50*, 5253-5260.
- [32] S. Huang; L. Yang; M. Liu; S. L. Phua; W. A. Yee; W. Liu; R. Zhou; X. Lu, Complexes of Polydopamine-modified Clay and Ferric Ions as the Framework for Pollutant-Absorbing Supramolecular Hydrogels. *Langmuir* **2013**, *29*, 1238-1244.
- [33] M. Burnworth; L. Tang; J. R. Kumpfer; A. J. Duncan; F. L. Beyer; G. L. Fiore; S. J. Rowan; C. Weder, Optically Healable Supramolecular Polymers. *Nature* **2011**, *472*, 334-337.
- [34] S. Coulibaly; A. Roulin; S. Balog; M. V. Biyani; E. J. Foster; S. J. Rowan; G. L. Fiore; C. Weder, Reinforcement of Optically Healable Supramolecular Polymers with Cellulose Nanocrystals. *Macromol.* **2013**, *47*, 152-160.
- [35] F. Herbst; D. Döhler; P. Michael; W. H. Binder, Self-Healing Polymers via Supramolecular Forces. *Macromol. Rapid Commun.* **2013**, *34*, 203-220.
- [36] D. L. Taylor; M. In Het Panhuis, Self-Healing Hydrogels. *Adv. Mater.* **2016**, *28*, 9060-9093.
- [37] X. Chen; M. A. Dam; K. Ono; A. Mal; H. Shen; S. R. Nutt; K. Sheran; F. Wudl, A Thermally Remendable Cross-Linked Polymeric Material. *Science* **2002**, *295*, 1698-1702.
- [38] S. D. Bergman; F. Wudl, Mendable Polymers. *J. Mater. Chem.* **2008**, *18*, 41-62.
- [39] C. Yuan; M. Z. Rong; M. Q. Zhang; Z. P. Zhang; Y. C. Yuan, Self-Healing of Polymers via Synchronous Covalent Bond Fission/ Radical Recombination. *Chem. Mater.* **2011**, *23*, 5076-5081.
- [40] S. Nevejans; N. Ballard; J. I. Miranda; B. Reck; J. M. Asua, The Underlying Mechanisms for Self-Healing of Poly(disulfide)s. *Phys. Chem. Chem. Phys.* **2016**, *18*, 27577-27583.

- [41] H. Ying; Y. Zhang; J. Cheng, Dynamic Urea Bond for the Design of Reversible and Self-Healing Polymers. *Nature Commun.* **2014**, *5*, 3218.
- [42] O. R. Cromwell; J. Chung; Z. Guan, Malleable and Self-Healing Covalent Polymer Networks through Tunable Dynamic Boronic Ester Bonds. *J. Am. Chem. Soc.* **2015**, *137*, 6492-6495.
- [43] F. Altuna; C. Hoppe; R. Williams, Epoxy Vitrimers: The Effect of Transesterification Reactions on the Network Structure. *Polymers* **2018**, *10*, 43.
- [44] M. Capelot; D. Montarnal; F. Tournilhac; L. Leibler, Metal-Catalyzed Transesterification for Healing and Assembling of Thermosets. *J. Am. Chem. Soc.* **2012**, *134*, 7664-7667.
- [45] J. Dahlke; S. Zechel; M. D. Hager; U. S. Schubert, How to Design a Self-Healing Polymer: General Concepts of Dynamic Covalent Bonds and Their Application for Intrinsic Healable Materials. *Adv. Mater. Interf.* **2018**, 1800051.
- [46] W. G. Skene; J. M. Lehn, Dynamers: Polyacylhydrazone Reversible Covalent Polymers, Component Exchange, and Constitutional Diversity. *Proc Natl Acad Sci U S A* **2004**, *101*, 8270-8275.
- [47] G. Deng; C. Tang; F. Li; H. Jiang; Y. Chen, Covalent Cross-Linked Polymer Gels with Reversible Sol-Gel Transition and Self-Healing Properties. *Macromol.* **2010**, *43*, 1191-1194.
- [48] L. He; D. E. Fullenkamp; J. G. Rivera; P. B. Messersmith, pH Responsive Self-Healing Hydrogels formed by Boronate-Catechol Complexation. *Chem Commun (Camb)* **2011**, *47*, 7497-7499.
- [49] A. Chao; I. Negulescu; D. Zhang, Dynamic Covalent Polymer Networks Based on Degenerative Imine Bond Exchange: Tuning the Malleability and Self-Healing Properties by Solvent. *Macromol.* **2016**, *49*, 6277-6284.
- [50] S. Mukherjee; M. R. Hill; B. S. Sumerlin, Self-Healing Hydrogels Containing Reversible Oxime Crosslinks. *Soft Matter.* **2015**, *11*, 6152-6161.
- [51] W. Schmolke; N. Perner; S. Seiffert, Dynamically Cross-Linked Polydimethylsiloxane Networks with Ambient-Temperature Self-Healing. *Macromol.* **2015**, *48*, 8781-8788.
- [52] P. Zheng; T. J. McCarthy, A Surprise from 1954: Siloxane Equilibration is a Simple, Robust, and Obvious Polymer Self-Healing Mechanism. *J Am Chem Soc* **2012**, *134*, 2024-2027.
- [53] Z. P. Zhang; M. Z. Rong; M. Q. Zhang; C. e. Yuan, Alkoxyamine with Reduced Homolysis Temperature and its Application in Repeated Autonomous Self-Healing of Stiff Polymers. *Polym. Chem.* **2013**, *4*, 4648-4654.
- [54] S. Telitel; Y. Amamoto; J. Poly; F. Morlet-Savary; O. Soppera; J. Lalevée; K. Matyjaszewski, Introduction of Self-Healing Properties into Covalent Polymer Networks via the Photodissociation of Alkoxyamine Junctions. *Polym. Chem.* **2014**, *5*, 921-930.
- [55] J. L. Hodgson; L. B. Roskop; M. S. Gordon; C. Y. Lin; M. L. Coote, Side Reactions of Nitroxide-Mediated Polymerization: N-O versus O-C Cleavage of Alkoxyamines. *J. Phys. Chem. A* **2010**, *114*, 10458-10466.
- [56] A. Fürstner, Olefin Metathesis and Beyond. *Angew. Chem. Int. Ed.* **2000**, *39*, 3012-3043.
- [57] Y. X. Lu; Z. Guan, Olefin Metathesis for Effective Polymer Healing via Dynamic Exchange of Strong Carbon-Carbon Double Bonds. *J Am Chem Soc* **2012**, *134*, 14226-14231.
- [58] X. Chen; M. A. Dam; K. Ono; A. Mal; H. Shen; S. R. Nutt; K. Sheran; F. Wudl, A Thermally Remendable Cross-Linked Polymeric Material. *Science* **2002**, *295*, 1698-1702.
- [59] N. Kuhl; R. Geitner; R. K. Bose; S. Bode; B. Dietzek; M. Schmitt; J. Popp; S. J. Garcia; S. van der Zwaag; U. S. Schubert; M. D. Hager, Self-Healing Polymer Networks Based on Reversible Michael Addition Reactions. *Macromol. Chem. Phys.* **2016**, *217*, 2541-2550.

- [60] N. Kuhl; R. Geitner; J. Vitz; S. Bode; M. Schmitt; J. Popp; U. S. Schubert; M. D. Hager, Increased Stability in Self-Healing Polymer Networks based on Reversible Michael Addition Reactions. *J. Appl. Polym. Sci.* **2017**, *134*, 44805, 1-8.
- [61] P. Chakma; L. H. Rodrigues Possarle; Z. A. Digby; B. Zhang; J. L. Sparks; D. Konkolewicz, Dual Stimuli Responsive Self-Healing and Malleable Materials based on Dynamic Thiol-Michael Chemistry. *Polym. Chem.* **2017**, *8*, 6534-6543.
- [62] C. E. Mortimer; U. Müller, *Chemie: das Basiswissen der Chemie*. Georg Thieme Verlag: Stuttgart, **2007**; Vol. 9. Auflage.
- [63] T. Engel; G. Kickelbick, Thermally Remendable Polymers. In *Self-Healing Polymers: From Principles to Applications*, Binder, W. H., Ed. Wiley-VCH; 1. Auflage: **2013**.
- [64] H. Staudinger; A. Brunson, Hochpolymere Verbindungen. 7. Mitteilung. Über das Dicyclopentadien und Weitere Polymere Cyclopentadiene. *Liebigs Ann.* **1926**, *447*, 97-110.
- [65] A. J. Inglis; S. Sinnwell; M. H. Stenzel; C. Barner-Kowollik, Ultrafast click conjugation of macromolecular building blocks at ambient temperature. *Angew Chem Int Ed Engl* **2009**, *48*, 2411-2414.
- [66] R. S. Dickson; B. J. Dobney; F. W. Eastwood, Preparation of Cyclopentadiene from its Dimer. *J. Chem. Educ.* **1987**, *64*, 898-898.
- [67] J. K. Stille; L. Plummer, Polymerization by the Diels-Alder Reaction. *J. Org. Chem.* **1961**, *26*, 4026-4029.
- [68] J. P. Kennedy; K. F. Castner, Thermally Reversible Polymer Systems by Cyclopentadienylation. I. A Model for Termination by Cyclopentadienylation of Olefin Polymerization. *J. Polym. Sci. Polym. Chem. Ed.* **1979**, *17*, 2039-2054.
- [69] J. P. Kennedy; K. F. Castner, Thermally Reversible Polymer Systems by Cyclopentadienylation. II. The Synthesis of Cyclopentadiene-Containing Polymers. *J. Polym. Sci. Polym. Chem. Ed.* **1979**, *17*, 2055-2070.
- [70] E. B. Murphy; E. Bolanos; C. Schaffner-Hamann; F. Wudl; S. R. Nutt; M. L. Auad, Synthesis and Characterization of a Single-Component Thermally Remendable Polymer Network: Staudinger and Stille Revisited. *Macromol.* **2008**, *41*, 5203-5209.
- [71] M. A. Tasdelen, Diels-Alder "Click" Reactions: Recent Applications in Polymer and Material Science. *Polym. Chem.* **2011**, *2*, 2133-2145.
- [72] Y.-L. Liu; T.-W. Chuo, Self-Healing Polymers based on Thermally Reversible Diels-Alder Chemistry. *Polym. Chem.* **2013**, *4*, 2194-2205.
- [73] A. Gandini, The Furan/Maleimide Diels-Alder Reaction: A versatile Click-Unclick Tool in Macromolecular Synthesis. *Prog. Polym. Sci.* **2013**, *38*, 1-29.
- [74] L. Rulisek; P. Sebek; Z. Havlas; R. Hrabal; P. Capek; A. Svatos, An Experimental and Theoretical Study of Stereoselectivity of Furan-Maleic Anhydride and Furan-Maleimide Diels-Alder Reactions. *J. Org. Chem.* **2005**, *70*, 6295-6302.
- [75] O. N. Hans R. Kricheldorf, Graham Swift, Handbook of Polymer Synthesis: Second Edition. In CRC Press: New York, **2004**.
- [76] A. B. Koldobskii; N. P. Tsvetkov; V. N. Kalinin, Universal Method for the Functionalization of β -Bromovinyl Trifluoromethyl Ketones of Cyclobutene Series. *Dokl. Chem.* **2010**, *432*, 133-135.
- [77] K. C. Nicolaou; C. Nilewski; C. R. Hale; C. F. Ahles; C. A. Chiu; C. Ebner; A. ElMarrouni; L. Yang; K. Stiles; D. Nagrath, Synthesis and Biological Evaluation of Dimeric Furanoid Macroheterocycles: Discovery of new Anticancer Agents. *J. Am. Chem. Soc.* **2015**, *137*, 4766-4770.

- [78] M. Wouters; E. Craenmehr; K. Tempelaars; H. Fischer; N. Stroeks; J. van Zanten, Preparation and Properties of a Novel Remendable Coating Concept. *Prog. Org. Coat.* **2009**, *64*, 156-162.
- [79] Z. Xu; Y. Zhao; X. Wang; T. Lin, A Thermally Healable Polyhedral Oligomeric Silsesquioxane (POSS) Nanocomposite based on Diels-Alder Chemistry. *Chem. Commun.* **2013**, *49*, 6755-6757.
- [80] O. Diels; K. Alder, Syntheses in the Hydroaromatic Series. I. Addition of "Diene" Hydrocarbons. *Liebigs Ann. Chem.* **1928**, *460*, 98-122.
- [81] J. M. Craven; C. Wilmington, Cross-linked Thermally Reversible Polymers Produced from Condensation Polymers with Pendant Furan Groups Cross-linked with Maleimides. US3435003, June 1, 1966, **1969**.
- [82] M. J. Arco, One-Part Solvent-Free Thermosettable Blocked Prepolymer Composition Containing a Diene, together with Chain Extender, Chain Terminator and a Dienophile. US Re.31670, September 11, 1984, **1983**.
- [83] M. P. Stevens; A. D. Jenkins, Crosslinking of Polystyrene via Pendant Maleimide Groups. *J. Polym. Sci. Pol. Chem.* **1979** *17*, 3675-3685.
- [84] Y. Chujo; K. Sada; T. Saegusa, Reversible Gelation of Polyoxazoline by Means of Diels-Alder Reaction. *Macromolecules* **1990**, *23*, 2636-2641.
- [85] A. Gandini; M. N. Belgacem, Furans in Polymer Chemistry. *Prog. Polym. Sci.* **1997** *22*, 1203-1379.
- [86] J. R. McElhanon; D. R. Wheeler, Thermally Responsive Dendrons and Dendrimers Based on Reversible Furan-Maleimide Diels-Alder Adducts. *Org. Lett.* **2001**, *3*, 2681-2683.
- [87] Y.-L. Liu; C.-Y. Hsieh, Crosslinked Epoxy Materials Exhibiting Thermal Remendability and Removability from Multifunctional Maleimide and Furan Compounds. *J. Polym. Sci. Pol. Chem.* **2006**, *44*, 905-913.
- [88] Xiangxu Chen; Fred Wudl; Ajit K. Mal; Hongbin Shen; S. R. Nutt, New Thermally Remendable Highly Cross-Linked Polymeric Materials. *Macromol.* **2003**, *36*, 1802-1807.
- [89] R. Gheneim; C. Perez-Berumen; A. Gandini, Diels-Alder Reactions with Novel Polymeric Dienes and Dienophiles: Synthesis of Reversibly Cross-Linked Elastomers. *Macromol.* **2002**, *35*, 7246-7253.
- [90] N. Kuramoto; K. Hayashi; K. Nagai, Thermoreversible Reaction of Diels-Alder Polymer Composed of Difurufuryladipate with Bismaleimidodiphenylmethane. *J. Polym. Sci., Polym. Chem.* **1994**, *32*, 2501-2504.
- [91] M. Watanabe; N. Yoshie, Synthesis and Properties of Readily Recyclable Polymers from Bisfuranic terminated Poly(ethylene adipate) and Multi-Maleimide Linkers. *Polymer* **2006**, *47*, 4946-4952.
- [92] S. A. Canary; M. P. Stevens, Thermally Reversible Crosslinking of Polystyrene via the Furan-Maleimide Diels-Alder Reaction. *J. Polym. Sci., Polym. Chem.* **1992**, *30*, 1755-1760.
- [93] S. Y. Kim; T. H. Lee; Y. I. Park; J. H. Nam; S. M. Noh; I. W. Cheong; J. C. Kim, Influence of Material Properties on Scratch-Healing Performance of Polyacrylate- Graft -Polyurethane Network that undergo Thermally Reversible Crosslinking. *Polymer* **2017**, *128*, 135-146.
- [94] P. Du; M. Wu; X. Liu; Z. Zheng; X. Wang; T. Joncheray; Y. Zhang, Diels-Alder-Based Crosslinked Self-Healing Polyurethane/Urea from Polymeric Methylene Diphenyl Diisocyanate. *J. Appl. Polym. Sci.* **2014**, *131*, 40234.
- [95] P. Du; X. Liu; Z. Zheng; X. Wang; T. Joncheray; Y. Zhang, Synthesis and Characterization of Linear Self-Healing Polyurethane based on Thermally Reversible Diels-Alder Reaction. *RSC Adv.* **2013**, *3*, 15475-15482.

- [96] S. Dello Iacono; A. Martone; A. Pastore; G. Filippone; D. Acierno; M. Zarrelli; M. Giordano; E. Amendola, Thermally Activated Multiple Self-Healing Diels-Alder Epoxy System. *Polym. Eng. Sci.* **2017**, *57*, 674-679.
- [97] J. Zhao; R. Xu; G. Luo; J. Wub; H. Xia, A Self-Healing, Re-Moldable and Biocompatible Crosslinked Polysiloxane Elastomer. *J. Mater. Chem. B* **2016**, *4*, 982-989.
- [98] A. Nasresfahani; P. M. Zelisko, Synthesis of a Self-Healing Siloxane-based Elastomer Cross-linked via a Furan-modified Polyhedral Oligomeric Silsesquioxane: Investigation of a Thermally Reversible Silicon-based Cross-link. *Polym. Chem.* **2017**, *8*, 2942-2952.
- [99] A. A. Kavitha; N. K. Singha, Atom-Transfer Radical Copolymerization of Furfuryl Methacrylate (FMA) and Methyl Methacrylate (MMA): A Thermally-Amendable Copolymer. *Macromol. Chem. Phys.* **2007**, *208*, 2569-2577.
- [100] A. A. Kavitha; N. K. Singha, "Click Chemistry" in Tailor-Made Polymethacrylates bearing Reactive Furfuryl Functionality: A New Class of Self-Healing Polymeric Material. *ACS Appl. Mater. Interfaces* **2009**, *1*, 1427-1436.
- [101] H.-L. Wei; Z. Yang; L.-M. Zheng; Y.-M. Shen, Thermosensitive Hydrogels Synthesized by fast Diels-Alder Reaction in Water. *Polymer* **2009**, *50*, 2836-2840.
- [102] E. Vedejs; T. H. Eberlein; D. J. Mazur; C. K. McClure; D. A. Perry; R. Ruggeri; E. Schwartz; J. S. Stults; D. L. Varié; R. G. Wilde; S. Wittenberger, Thioaldehyde Diels-Alder Reactions. *J. Org. Chem.* **1986**, *51*, 1556-1562.
- [103] W. M. McGregor; D. C. Sherrington, Some Recent Synthetic Routes to Thioketones and Thioaldehydes. *Chem. Soc. Rev.* **1993**, *22*, 199-204
- [104] J. Rapp; R. Huisgen, Diels-Alder Reactions of Diaryl Thioketones with Dienophiles. *Tetrahedron* **1997**, *53*, 961-970.
- [105] A. J. Inglis; L. Nebhani; O. Altintas; F. G. Schmidt; C. Barner-Kowollik, Rapid Bonding/Debonding on Demand: Reversibly Cross-Linked Functional Polymers via Diels-Alder Chemistry. *Macromol.* **2010**, *43*, 5515-5520.
- [106] M. Glassner; G. Delaittre; M. Kaupp; J. P. Blinco; C. Barner-Kowollik, (Ultra)fast Catalyst-free Macromolecular Conjugation in Aqueous Environment at Ambient Temperature. *J Am Chem Soc* **2012**, *134*, 7274-7277.
- [107] K. K. Oehlenschlaeger; N. K. Guimard; J. Brandt; J. O. Mueller; C. Y. Lin; S. Hilf; A. Lederer; M. L. Coote; F. G. Schmidt; C. Barner-Kowollik, Fast and Catalyst-free Hetero-Diels-Alder Chemistry for on Demand Cyclable Bonding/Debonding Materials. *Polym. Chem.* **2013**, *4*, 4348-4355.
- [108] K. K. Oehlenschlaeger; J. O. Mueller; J. Brandt; S. Hilf; A. Lederer; M. Wilhelm; R. Graf; M. L. Coote; F. G. Schmidt; C. Barner-Kowollik, Adaptable Hetero Diels-Alder Networks for Fast Self-Healing under Mild Conditions. *Adv Mater* **2014**, *26*, 3561-3566.
- [109] L. Brunsveld; B. J. B. Folmer; E. W. Meijer; R. P. Sijbesma, Supramolecular Polymers. *Chem. Rev.* **2001**, *101*, 4071-4097.
- [110] T. Steiner, The Hydrogen Bond in the Solid State. *Angew. Chem. Int. Ed.* **2002**, *41*, 48-76.
- [111] S. Strandman; X. X. Zhu, Self-Healing Supramolecular Hydrogels Based on Reversible Physical Interactions. *Gels* **2016**, *2*, 16.
- [112] J.-L. Wietor; A. Dimopoulos; L. E. Govaert; R. A. T. M. van Benthem; G. de With; R. P. Sijbesma, Preemptive Healing through Supramolecular Cross-Links. *Macromol.* **2009**, *42*, 6640-6646.
- [113] Aaron M. Kushner; John D. Vossler; Gregory A. Williams; Z. Guan, A Biomimetic Modular Polymer with Tough and Adaptive Properties. *J. Am. Chem. Soc.* **2009**, *131*, 8766-8768.
- [114] Y. Chen; A. M. Kushner; G. A. Williams; Z. Guan, Multiphase Design of Autonomic Self-Healing Thermoplastic Elastomers. *Nat. Chem.* **2012**, *4*, 467-472.

- [115] J. Hentschel; A. M. Kushner; J. Ziller; Z. Guan, Self-Healing Supramolecular Block Copolymers. *Angew. Chem. Int. Ed.* **2012**, *51*, 10561-10565.
- [116] R. Araya-Hermosilla; A. A. Broekhuis; F. Picchioni, Reversible Polymer Networks Containing Covalent and Hydrogen Bonding Interactions. *Eur. Polym. J.* **2014**, *50*, 127-134.
- [117] H. Lodish; A. Berk; S. L. Zipursky; P. Matsudaira; D. Baltimore; J. Darnell, Hierarchical Structure of Proteins. In *Molecular Cell Biology. 4th edition.*, S. Tenney, K. A., R. Steyn, K. Ueno, Ed. W. H. Freeman & Co Ltd: New York, **2000**; 1296.
- [118] M. V. Trivedi; J. S. Laurence; T. J. Siahaan, The Role of Thiols and Disulfides in Protein Chemical and Physical Stability. *Curr. Protein Pept. Sci.* **2009**, *10*, 614-625.
- [119] Lumen-Learning, Biology I: Biological Macromolecules <https://courses.lumenlearning.com/suny-biology1/chapter/biological-molecules/> (Accessed on 18 July 2018).
- [120] X. Fang; H. Zhang; Y. Chen; Y. Lin; Y. Xu; W. Weng, Biomimetic Modular Polymer with Tough and Stress Sensing Properties. *Macromol.* **2013**, *46*, 6566-6574.
- [121] J. Collins; M. Nadgorny; Z. Xiao; L. A. Connal, Doubly Dynamic Self-Healing Materials Based on Oxime Click Chemistry and Boronic Acids. *Macromol Rapid Commun* **2017**, *38*, 1600760.
- [122] J. Chen; Q. Su; R. Guo; J. Zhang; A. Dong; C. Lin; J. Zhang, A Multitasking Hydrogel Based on Double Dynamic Network with Quadruple-Stimuli Sensitiveness, Autonomic Self-Healing Property, and Biomimetic Adhesion Ability. *Macromol. Chem. Phys.* **2017**, *218*, 1700166.
- [123] X. Jian; Y. Hu; W. Zhou; L. Xiao, Self-Healing Polyurethane based on Disulfide Bond and Hydrogen Bond. *Polym. Adv. Technol.* **2018**, *29*, 463-469.
- [124] G. Deng; F. Li; H. Yu; F. Liu; C. Liu; W. Sun; H. Jiang; Y. Chen, Dynamic Hydrogels with an Environmental Adaptive Self-Healing Ability and Dual Responsive Sol–Gel Transitions. *ACS Macro Letters* **2012**, *1*, 275-279.
- [125] G. Schaeffer; E. Buhler; S. J. Candau; J.-M. Lehn, Double Dynamic Supramolecular Polymers of Covalent Oligo-Dynamers. *Macromol.* **2013**, *46*, 5664-5671.
- [126] E. Kolomiets; J. M. Lehn, Double Dynamers: Molecular and Supramolecular Double Dynamic Polymers. *Chem Commun (Camb)* **2005**, 1519-1521.
- [127] N. Roy; E. Buhler; J.-M. Lehn, Double Dynamic Self-Healing Polymers: Supramolecular and Covalent Dynamic Polymers based on the Bis-Iminocarbohydrazide Motif. *Polymer International* **2014**, *63*, 1400-1405.
- [128] R. Araya-Hermosilla; G. M. R. Lima; P. Raffa; G. Fortunato; A. Pucci; M. E. Flores; I. Moreno-Villoslada; A. A. Broekhuis; F. Picchioni, Intrinsic Self-Healing Thermoset through Covalent and Hydrogen Bonding Interactions. *Eur. Polym. J.* **2016**, *81*, 186-197.
- [129] B. Willocq; F. Khelifa; J. Brancart; G. Van Assche; P. Dubois; J.-M. Raquez, One-Component Diels–Alder based Polyurethanes: A Unique Way to Self-Heal. *RSC Adv.* **2017**, *7*, 48047-48053.
- [130] G. Kickelbick, Introduction to Hybrid Materials. In *Hybrid Materials*, Wiley-VCH: **2007**.
- [131] J. V. Alemán; A. V. Chadwick; J. He; M. Hess; K. Horie; R. G. Jones; P. Kratochvíl; I. Meisel; I. Mita; G. Moad; S. Penczek; R. F. T. Stepto, Definitions of Terms Relating to the Structure and Processing of Sols, Gels, Networks, and Inorganic–Organic Hybrid Materials (IUPAC Recommendations 2007). *Pure and Appl. Chem.* **2007**, *79*, 1801-1829.
- [132] E. D'Elia; S. Eslava; M. Miranda; T. K. Georgiou; E. Saiz, Autonomous Self-Healing Structural Composites with Bio-Inspired Design. *Sci. Rep.* **2016**, *6*, 25059.

- [133] M. Arslan; M. Tasdelen, Polymer Nanocomposites via Click Chemistry Reactions. *Polymers* **2017**, *9*, 499.
- [134] E. H. Anderson; T. A. Plaisted; A. Vakil Amirkhizi; D. Arbelaez; S. C. Nemat-Nasser; S. Nemat-Nasser, Self-Healing Structural Composites with Electromagnetic Functionality. *Smart Struct. Mater.* **2003**, *5054*, 372-381.
- [135] S. Nemat-Nasser; A. Vakilamirkhizi; T. A. Plaisted; C. Santos; A. Starr; S. C. Nemat-Nasser, Thermal, Self-Healing and Self-Sensing Functionality. In *Composites with Negative Refractive Index*, **2004**; 138-143.
- [136] J. S. Park; T. Darlington; A. F. Starr; K. Takahashi; J. Riendeau; H. T. Hahn, Multiple Healing Effect of Thermally Activated Self-Healing Composites based on Diels–Alder Reaction. *Compos. Sci. Technol.* **2010**, *70*, 2154-2159.
- [137] F. Ghezzi; D. R. Smith; T. N. Starr; T. Perram; A. F. Starr; T. K. Darlington; R. K. Baldwin; S. J. Oldenburg, Development and Characterization of Healable Carbon Fiber Composites with a Reversibly Cross Linked Polymer. *J. Compos. Mater.* **2010**, *44*, 1587-1603.
- [138] A. M. Peterson; R. E. Jensen; G. R. Palmese, Room-temperature Healing of a Thermosetting Polymer using the Diels-Alder Reaction. *ACS Appl Mater Interfaces* **2010**, *2*, 1141-1149.
- [139] A. M. Peterson; R. E. Jensen; G. R. Palmese, Thermoreversible and Remendable Glass–Polymer Interface for Fiber-Reinforced Composites. *Compos. Sci. Technol.* **2011**, *71*, 586-592.
- [140] J. Li; G. Zhang; L. Deng; S. Zhao; Y. Gao; K. Jiang; R. Sun; C. Wong, *In situ* Polymerization of Mechanically Reinforced, Thermally Healable Graphene Oxide/Polyurethane Composites based on Diels–Alder Chemistry. *J. Mater. Chem. A* **2014**, *2*, 20642-20649.
- [141] Y. Yang; B. Zhu; D. Yin; J. Wei; Z. Wang; R. Xiong; J. Shi; Z. Liu; Q. Lei, Flexible Self-Healing Nanocomposites for Recoverable Motion Sensor. *Nano Energy* **2015**, *17*, 1-9.
- [142] H. Hayden; Y. K. Gun'ko; T. S. Perova, Chemical Modification of Multi-Walled Carbon Nanotubes using a Tetrazine Derivative. *Chem. Phys. Lett.* **2007**, *435*, 84-89.
- [143] Y.-H. Wang; C.-M. Chang; Y.-L. Liu, Benzoxazine-functionalized Multi-Walled Carbon Nanotubes for Preparation of Electrically-Conductive Polybenzoxazines. *Polymer* **2012**, *53*, 106-112.
- [144] B. Willocq; R. K. Bose; F. Khelifa; S. J. Garcia; Ph. Dubois; J.-M. Raquez, Healing by the Joule Effect of Electrically Conductive Poly(ester-urethane)/Carbon Nanotube nanocomposites. *J. Mater. Chem. A* **2016**, *4*, 4089-4097.
- [145] K. Adachi; A. K. Achimuthu; Y. Chujo, Synthesis of Organic-Inorganic Polymer Hybrids Controlled by Diels-Alder Reaction. *Macromol.* **2004**, *37*, 9793-9797.
- [146] T. Engel; G. Kickelbick, Self-Healing Nanocomposites from Silica – Polymer Core – Shell Nanoparticles. *Polym. Int.* **2014**, *63*, 915-923.
- [147] T.-W. Chuo; Y.-L. Liu, Preparation of Self-Healing Organic–Inorganic Nanocomposites with the Reactions between Methacrylated Polyhedral Oligomeric Silsesquioxanes and Furfurylamine. *Compos. Sci. Technol.* **2015**, *118*, 236-243.
- [148] T. Engel; G. Kickelbick, Furan-Modified Spherosilicates as Building Blocks for Self-Healing Materials. *Eur. J. Inorg. Chem.* **2015**, *2015*, 1226-1232.
- [149] S. Gupta; Q. Zhang; T. Emrick; A. C. Balazs; T. P. Russell, Entropy-Driven Segregation of Nanoparticles to Cracks in Multilayered Composite Polymer Structures. *Nat. Mater.* **2006**, *5*, 229-233.
- [150] A. C. Balazs, Modeling Self-Healing Materials. *Mater. Today* **2007**, *10*, 18-23.
- [151] A. C. Balazs; T. Emrick; T. P. Russell, Nanoparticle Polymer Composites: Where Two Small Worlds Meet. *Science* **2006**, *314*, 1107-1110.

- [152] J. Y. Lee; G. A. Buxton; A. C. Balazs, Using Nanoparticles to Create Self-Healing Composites. *J. Chem. Phys.* **2004**, *121*, 5531-5540.
- [153] J. Kötteritzsch; S. Stumpf; S. Hoepfner; J. Vitz; M. D. Hager; U. S. Schubert, One-Component Intrinsic Self-Healing Coatings Based on Reversible Crosslinking by Diels-Alder Cycloadditions. *Macromol. Chem. Phys.* **2013**, *214*, 1636-1649.
- [154] D. V. Talapin; E. V. Shevchenko, Introduction: Nanoparticle Chemistry. *Chem. Rev.* **2016**, *116*, 10343-10345.
- [155] K. Zarschler; L. Rocks; N. Licciardello; L. Boselli; E. Polo; K. P. Garcia; L. De Cola; H. Stephan; K. A. Dawson, Ultrasmall Inorganic Nanoparticles: State-of-the-Art and Perspectives for Biomedical Applications. *Nanomedicine* **2016**, *12*, 1663-1701.
- [156] S. P. Pujari; L. Scheres; A. T. Marcelis; H. Zuilhof, Covalent Surface Modification of Oxide Surfaces. *Angew. Chem. Int. Ed.* **2014**, *53*, 6322-6356.
- [157] W. Stöber; A. Fink; E. Bohn, Controlled Growth of Monodisperse Silica Spheres in the Micron Size Range. *J. Colloid Interface Sci.* **1968**, *26*, 62-69.
- [158] L. L. Hench; J. K. West, The Sol-Gel Process. *Chem. Rev.* **1990**, *90*, 33-72.
- [159] E. P. Plueddemann, Silane Coupling Agents. In Springer, US: **1991**.
- [160] R. M. Shaltout; D. A. Loy; D.R. Wheeler, In *Materials Research Society Symposium - Proceedings*, Maleimide Functionalized Siloxane Resins, Proceedings of the 1999 MRS Spring Meeting - Symposium DD, 'Organic/Inorganic Hybrid Materials' - San Francisco, CA, USA, Materials Research Society: **1999**, 15-20.
- [161] P. Y. Reddy; S. Kondo; T. Toru; Y. Ueno, Lewis Acid and Hexamethyldisilazane-Promoted Efficient Synthesis of N-Alkyl- and N-Arylimide Derivatives. *J. Org. Chem.* **1997**, *62*, 2652-2654.
- [162] M. Proupin-Perez; R. Cosstick; L. M. Liz-Marzan; V. Salgueiriño-Maceira; M. Brust, Studies on the Attachment of DNA to Silica-Coated Nanoparticles through a Diels-Alder Reaction. *Nucleosides, Nucleotides and Nucleic Acids* **2005**, *24*, 1075-1079.
- [163] H. I. Lim; P. M. Oliver; J. Marzillier; D. V. Vezenov, Heterobifunctional Modification of DNA for Conjugation to Solid Surfaces. *Anal Bioanal Chem* **2010**, *397*, 1861-1872.
- [164] L. Mancuso; T. Knobloch; J. Buchholz; J. Hartwig; L. Moller; K. Seidel; W. Collisi; F. Sasse; A. Kirschning, Preparation of Thermocleavable Conjugates based on Ansamitocin and Superparamagnetic Nanostructured Particles by a Chemobiosynthetic Approach. *Chemistry* **2014**, *20*, 17541-17551.
- [165] N. Moszner; I. Lamparth; T. Bock; K. Fischer; U. Salz; V. Rheinberger; R. Liska, Dental Materials based on Monomers having Debonding-on-Demand Properties. US9668946B2, September 10, 2012, **2017**.
- [166] B. Patel, Process for Preparing unsaturated Imidoalkoxysilanes. US20070123728A1, May 31, 2007, **2007**.
- [167] B. Oktay; E. Çakmakçı, DOPO Tethered Diels Alder Clickable Reactive Silica Nanoparticles for Bismaleimide Containing Flame Retardant Thiol-ene Nanocomposite Coatings. *Polymer* **2017**, *131*, 132-142.
- [168] H. Mori, Design and Synthesis of Functional Silsesquioxane-Based Hybrids by Hydrolytic Condensation of Bulky Triethoxysilanes. *Int. J. Polym. Sci.* **2012**, *2012*, 1-17.
- [169] P. Eisenberg; R. Erra-Balsells; Y. Ishikawa; J. C. Lucas; A. N. Mauri; H. Nonami; C. C. Riccardi; R. J. J. Williams, Cage-like Precursors of High-Molar-Mass Silsesquioxanes Formed by the Hydrolytic Condensation of Trialkoxysilanes. *Macromol.* **2000**, *33*, 1940-1947.
- [170] T. A. Tereshchenko, Synthesis and Application of Polyhedral Oligosilsesquioxanes and Spherosilicates. *Polym. Sci. Ser. B* **2008**, *50*, 249-262.

- [171] M. G. Voronkov; T. N. Martynova; R. G. Mirskov; V. I. Belyi, Octavinylsilsesquioxane. *Zh. Obshch. Khim.* **1979**, *49*, 1522-1525.
- [172] K. Larsson, Crystal structure of $(\text{HSiO}_{1.5})_8$. *Ark. Kemi* **1960**, *16*, 215-219.
- [173] C. Zhang; R. M. Laine, Hydrosilylation of Allyl Alcohol with $[\text{HSiMe}_2\text{OSiO}_{1.5}]_8$: Octa(3-hydroxypropyldimethylsiloxy)octasilsesquioxane and Its Octamethacrylate Derivative as Potential Precursors to Hybrid Nanocomposites. *J. Am. Chem. Soc.* **2000**, *122*, 6979-6988.
- [174] I. Hasegawa; S. Motojima, Dimethylvinsilylation of $\text{Si}_8\text{O}_{20}^{8-}$ Silicate Anion in Methanol Solutions of Tetramethylammonium Silicate. *J. Org. Chem.* **1992**, *441*, 373-380.
- [175] M. Dutkiewicz; H. Maciejewski; B. Marciniak; J. Karasiewicz, New Fluorocarbofunctional Spherosilicates: Synthesis and Characterization. *Organomet.* **2011**, *30*, 2149-2153.
- [176] R. Tamaki; Y. Tanaka; M. Z. Asuncion; J. Choi; R. M. Laine, Octa(aminophenyl)silsesquioxane as a Nanoconstruction Site. *J. Am. Chem. Soc.* **2001**, *123*, 12416-12417.
- [177] P. K. Behera; P. Mondal; N. K. Singha, Self-Healable and Ultrahydrophobic Polyurethane-POSS Hybrids by Diels-Alder "Click" Reaction: A New Class of Coating Material. *Macromol.* **2018**, *51*, 4770-4781.
- [178] S.-W. Kuo; H.-C. Lin; W.-J. Huang; C.-F. Huang; F.-C. Chang, Hydrogen Bonding Interactions and Miscibility between Phenolic Resin and Octa(acetoxystyryl) Polyhedral Oligomeric Silsesquioxane (AS-POSS) Nanocomposites. *J. Polym. Sci. B Polym. Phys.* **2006**, *44*, 673-686.
- [179] H. Liu; S.-i. Kondo; N. Takeda; M. Unno, Synthesis of Octacarboxy Spherosilicate. *J. Am. Chem. Soc.* **2008**, *130*, 10074-10075.
- [180] K. Madhavan; B. S. R. Reddy, Synthesis and Characterization of Polyurethane Hybrids: Influence of the Polydimethylsiloxane Linear Chain and Silsesquioxane Cubic Structure on the Thermal and Mechanical Properties of Polyurethane Hybrids. *J. Appl. Polym. Sci.* **2009**, *113*, 4052-4065.
- [181] V. K. Daga; E. R. Anderson; S. P. Gido; J. J. Watkins, Hydrogen Bond Assisted Assembly of Well-Ordered Polyhedral Oligomeric Silsesquioxane-Block Copolymer Composites. *Macromol.* **2011**, *44*, 6793-6799.
- [182] V. Ervithayasuporn; T. Tomeechai; N. Takeda; M. Unno; A. Chaiyanurakkul; R. Hamkool; T. Osotchan, Synthesis and Characterization of Octakis(3-propyl ethanethioate)octasilsesquioxane. *Organomet.* **2011**, *30*, 4475-4478.
- [183] B. Marciniak; M. Dutkiewicz; H. Maciejewski; M. Kubicki, New, Effective Method of Synthesis and Structural Characterization of Octakis(3-chloropropyl)octasilsesquioxane. *Organomet.* **2008**, *27*, 793-794.
- [184] Z. Shen; J. Kim; J. Shen; C. M. Downing; S. Lee; H. H. Kung; M. C. Kung, Spherosilicates with Peripheral Malonic Acid and Vinyl End Groups. *Chem. Commun.* **2013**, *49*, 3357-3359.
- [185] M. Janeta; L. John; J. Ejfler; S. Szafert, High-Yield Synthesis of Amido-Functionalized Polyoctahedral Oligomeric Silsesquioxanes by using Acyl Chlorides. *Chemistry* **2014**, *20*, 15966-15974.
- [186] N. Kanfar; A. Mehdi; P. Dumy; S. Ulrich; J.-Y. Winum, Polyhedral Oligomeric Silsesquioxane (POSS) Bearing Glyoxylic Aldehyde as Clickable Platform Towards Multivalent Conjugates. *Chem. Eur. J.* **2017**, *23*, 17867-17869.
- [187] M. Fernández-García; J. A. Rodríguez, Metal Oxide Nanoparticles. In *Encyclopedia of Inorganic Chemistry*, R. B. King, R. H. C., C. M. Lukehart, D. A. Atwood, R. A. Scott, Ed. John Wiley & Sons, Ltd: **2009**.
- [188] J. Pal; T. Pal, Faceted Metal and Metal Oxide Nanoparticles: Design, Fabrication and Catalysis. *Nanoscale* **2015**, *7*, 14159-14190.

- [189] S. Stankic; S. Suman; F. Haque; J. Vidic, Pure and Multi Metal Oxide Nanoparticles: Synthesis, Antibacterial and Cytotoxic Properties. *J. Nanobiotechnology* **2016**, *14*, 73.
- [190] S. Sun; H. Zeng; D. B. Robinson; S. Raoux; P. M. Rice; S. X. Wang; G. Li, Monodisperse MFe_2O_4 ($M = Fe, Co, Mn$) Nanoparticles. *J. Am. Chem. Soc.* **2004**, *126*, 273-279.
- [191] J. A. Rodríguez; M. Fernández-García, The World of Oxide Nanomaterials. In *Synthesis, Properties and Applications of Oxide Nanomaterials*, John Wiley & Sons, Inc.: **2006**; 1-5.
- [192] Y. S. Kang; S. Risbud; J. F. Rabolt; P. Stroeve, Synthesis and Characterization of Nanometer-Size Fe_3O_4 and γ - Fe_2O_3 Particles. *Chem. Mater.* **1996**, *8*, 2209-2211.
- [193] M. Klokkenburg; J. Hilhorst; B. H. Erne, Surface Analysis of Magnetite Nanoparticles in Cyclohexane Solutions of Oleic Acid and Oleylamine. *Vib. Spectrosc.* **2007**, *43*, 243-248.
- [194] A. K. Yuen; G. A. Hutton; A. F. Masters; T. Maschmeyer, The Interplay of Catechol Ligands with Nanoparticulate Iron Oxides. *Dalton Trans.* **2012**, *41*, 2545-2559.
- [195] R. Frison; G. Cernuto; A. Cervellino; O. Zaharko; G. M. Colonna; A. Guagliardi; N. Masciocchi, Magnetite–Maghemite Nanoparticles in the 5–15 nm Range: Correlating the Core–Shell Composition and the Surface Structure to the Magnetic Properties. A Total Scattering Study. *Chem. Mater.* **2013**, *25*, 4820-4827.
- [196] J. Santoyo Salazar; L. Perez; O. de Abril; L. Truong Phuoc; D. Ihiwakrim; M. Vazquez; J.-M. Greneche; S. Begin-Colin; G. Pourroy, Magnetic Iron Oxide Nanoparticles in 10–40 nm Range: Composition in Terms of Magnetite/Maghemite Ratio and Effect on the Magnetic Properties. *Chem. Mater.* **2011**, *23*, 1379-1386.
- [197] M. Szekeres; O. Kamalin; R. A. Schoonheydt; K. Wostyn; K. Clays; A. Persoons; I. Dékány, Ordering and Optical Properties of Monolayers and Multilayers of Silica Spheres Deposited by the Langmuir–Blodgett Method. *J. Mater. Chem.* **2002**, *12*, 3268-3274.
- [198] M. Raza; A. Bachinger; N. Zahn; G. Kickelbick, Interaction and UV-Stability of Various Organic Capping Agents on the Surface of Anatase Nanoparticles. *Materials (Basel)* **2014**, *7*, 2890-2912.
- [199] P. H. Mutin; G. Guerrero; A. Vioux, Hybrid Materials from Organophosphorus Coupling Molecules. *J. Mater. Chem.* **2005**, *15*, 3761-3768.
- [200] C. Queffelec; M. Petit; P. Janvier; D. A. Knight; B. Bujoli, Surface Modification using Phosphonic Acids and Esters. *Chem. Rev.* **2012**, *112*, 3777-3807.
- [201] F. Brodard-Severac; G. Guerrero; J. Maquet; P. Florian; C. Gervais; P. H. Mutin, High-Field ^{17}O MAS NMR Investigation of Phosphonic Acid Monolayers on Titania. *Chem. Mater.* **2008**, *20*, 5191-5196.
- [202] K. Davis; B. Qi; M. Witmer; C. L. Kitchens; B. A. Powell; O. T. Mefford, Quantitative Measurement of Ligand Exchange on Iron Oxides via Radiolabeled Oleic Acid. *Langmuir* **2014**, *30*, 10918-10925.
- [203] B. Iorga; F. Eymery; D. Carmichael; P. Savignac, Dialkyl 1-Alkynylphosphonates: A Range of Promising Reagents. *Eur. J. Org. Chem.* **2000**, 3103-3115.
- [204] B. A. Arbuzov; B. P. Lugovkin, Synthesis of Esters of Phosphonic Acids Containing Heterocyclic Radicals. II. Ethyl Esters of Phosphonic Acids with Oxygen-Bearing Heterocyclic Radicals. *Zh. Obshch. Khim.* **1952**, *22*, 1193-1198.
- [205] C.-W. Lee; W. S. Shin; D. Y. Oh, A Facile Preparation of 2-Arylethenephosphonates. *Synth. Commun.* **1995**, *25*, 2013-2017.
- [206] D.-Q. Shi; Y.-M. Wang; R.-Y. Chen, Synthesis and Stereoselectivity of a New Type of Unsaturated Phosphonates. *Heteroat. Chem.* **2000**, *11*, 261-266.
- [207] P. Golborn; J. J. Duffy, Imidomethyl Phosphonates. US3890275A, August 2, 1974, **1975**.
- [208] M. Imai; T. Sorori, Presensitized Plate for Use in Making Lithographic Printing Plates. EP5061592A1, April 25, 1990, **1991**.

- [209] P. Kurzweil; P. Scheipers, *Chemie: Grundlagen, Aufbauwissen, Anwendungen und Experimente*. Vieweg+Teubner Verlag, Springer: Wiesbaden, **2010**.
- [210] J. E. Mark, Overview of Siloxane Polymers. In *Silicones and Silicone-Modified Materials*, Stephen J. Clarson, J. J. F., Michael J. Owen, Steven D. Smith, Ed. ACS Symposium Series: **2000**; Vol. 729, 1-10.
- [211] A. Purkayastha; J. B. Baruah, Synthetic Methodologies in Siloxanes. *Appl. Organomet. Chem.* **2004**, *18*, 166-175.
- [212] K. Mojsiewicz-Pienkowska; D. Krenczkowska, Evolution of Consciousness of Exposure to Siloxanes-Review of Publications. *Chemosphere* **2018**, *191*, 204-217.
- [213] G. C. Tesoro; V. R. Sastri, Synthesis of Siloxane-Containing Bis(furans) and Polymerization with Bis(maleimides). *Ind. Eng. Chem. Prod. Res. Dev.* **1986**, *25*, 444-448.
- [214] J. R. McElhanon; E. M. Russick; D. R. Wheeler; D. A. Loy; J. H. Aubert, Removable Foams based on an Epoxy Resin Incorporating Reversible Diels-Alder Adducts. *J. Appl. Polym. Sci.* **2002**, *85*, 1496-1502.
- [215] T. Otsu; M. Yoshida; T. Tazaki, A Model for Living Radical Polymerization. *Makromol. Chem. Rapid Commun.* **1982**, *3*, 133-140.
- [216] A. D. Jenkins; P. Kratochvíl; R. F. T. Stepto; W. Suter, Glossary of Basic Terms in Polymer Science. *Pure Appl. Chem.* **1996**, *68*, 2287-2311.
- [217] A. D. Jenkins; R. G. Jones; G. Moad, Terminology for Reversible-Deactivation Radical Polymerization Previously called "Controlled" Radical or "Living" Radical Polymerization (IUPAC Recommendations 2010). *Pure Appl. Chem.* **2010**, *82*, 483-491.
- [218] K. Matyjaszewski, Atom Transfer Radical Polymerization (ATRP): Current Status and Future Perspectives. *Macromol.* **2012**, *45*, 4015-4039.
- [219] C. Boyer; N. A. Corrigan; K. Jung; D. Nguyen; T. K. Nguyen; N. N. Adnan; S. Oliver; S. Shanmugam; J. Yeow, Copper-Mediated Living Radical Polymerization (Atom Transfer Radical Polymerization and Copper(0) Mediated Polymerization): From Fundamentals to Bioapplications. *Chem. Rev.* **2016**, *116*, 1803-1949.
- [220] Sigma-Aldrich, Controlled Radical Polymerization Guide. *Aldrichs Materials Science* **2012**, 1-52.
- [221] S. Coca; C. B. Jasieczek; K. L. Beers; K. Matyjaszewski, Polymerization of Acrylates by Atom Transfer Radical Polymerization. Homopolymerization of 2-Hydroxyethyl Acrylate. *J. Polym. Sci. A Pol. Chem.* **1998**, *36*, 1417-1424.
- [222] K. Matyjaszewski; S. Coca; C. B. Jasieczek, Polymerization of Acrylates by Atom Transfer Radical Polymerization. Homopolymerization of Glycidyl Acrylate. *Macromol. Chem. Phys.* **1997**, *198*, 4011-4017.
- [223] K. Matyjaszewski; Y. Nakagawa; S. G. Gaynor, Synthesis of Well-Defined Azido and Amino Endfunctionalized Polystyrene by Atom Transfer Radical Polymerization. *Macromol. Rapid Commun.* **1997**, *18*, 1057-1064.
- [224] Jin-Shan Wang; K. Matyjaszewski, Controlled/ "Living" Radical Polymerization. Atom Transfer Radical Polymerization in the Presence of Transition-Metal Complexes. *J. Am. Chem. Soc.* **1995**, *117*, 5614-5615.
- [225] A. A. Kavitha; A. Choudhury; N. K. Singha, Controlled Radical Polymerization of Furfuryl Methacrylate. *Macromol. Symp.* **2006**, *240*, 232-237.
- [226] A. A. Kavitha; N. K. Singha, A Tailor-Made Polymethacrylate Bearing a Reactive Diene in Reversible Diels-Alder Reaction. *J. Polym. Sci. A Pol. Chem.* **2007**, *45*, 4441-4449.
- [227] T. Dispinar; R. Sanyal; A. Sanyal, A Diels-Alder/retro Diels-Alder Strategy to Synthesize Polymers Bearing Maleimide Side Chains. *J. Polym. Sci. A Polym. Chem.* **2007**, *45*, 4545-4551.

- [228] J. Kötteritzsch; M. D. Hager; U. S. Schubert, Tuning the Self-Healing Behavior of One-Component Intrinsic Polymers. *Polymer* **2015**, *69*, 321-329.
- [229] E. Galbis; M. V. de Paz; K. L. McGuinness; M. Angulo; C. Valencia; J. A. Galbis, Tandem ATRP/Diels–Alder Synthesis of polyHEMA-based Hydrogels. *Polym. Chem.* **2014**, *5*, 5391-5402.
- [230] D. Arunbabu; S. M. Noh; J. H. Nam; J. K. Oh, Thermoreversible Self-Healing Networks Based on a Tunable Polymethacrylate Crosslinker Having Pendant Maleimide Groups. *Macromol. Chem. Phys.* **2016**, *217*, 2191-2198.
- [231] Y. Chen; Z. Guan, Multivalent Hydrogen Bonding Block Copolymers Self-Assemble into Strong and Tough Self-Healing Materials. *Chem. Commun.* **2014**, *50*, 10868-10870.
- [232] Y. Chen; Z. Guan, Self-Healing Thermoplastic Elastomer Brush Copolymers Having a Glassy Polymethylmethacrylate Backbone and Rubbery Polyacrylate-Amide Brushes. *Polymer* **2015**, *69*, 249-254.
- [233] M. R. Hill; R. N. Carmean; B. S. Sumerlin, Expanding the Scope of RAFT Polymerization: Recent Advances and New Horizons. *Macromol.* **2015**, *48*, 5459-5469.
- [234] J. B. Beck; K. L. Killops; T. Kang; K. Sivanandan; A. Bayles; M. E. Mackay; K. L. Wooley; C. J. Hawker, Facile Preparation of Nanoparticles by Intramolecular Crosslinking of Isocyanate Functionalized Copolymers. *Macromol.* **2009**, *42*, 5629-5635.
- [235] J. D. Flores; J. Shin; C. E. Hoyle; C. L. McCormick, Direct RAFT Polymerization of an unprotected Isocyanate-Containing Monomer and Subsequent Structopendant Functionalization using "Click"-Type Reactions. *Polym. Chem.* **2010**, *1*, 213-220.
- [236] M. Seo; M. A. Hillmyer, RAFT Copolymerization of Acid Chloride-Containing Monomers. *Polym. Chem.* **2014**, *5*, 213-219.
- [237] A. Sanchez-Sanchez; I. Asenjo-Sanz; L. Buruaga; J. A. Pomposo, Naked and Self-Clickable Propargylic-Decorated Single-Chain Nanoparticle Precursors via Redox-Initiated RAFT Polymerization. *Macromol. Rapid. Commun.* **2012**, *33*, 1262-1267.
- [238] G. Moad; E. Rizzardo; S. H. Thang, Toward Living Radical Polymerization. *Acc. Chem. Res.* **2008**, *41*, 1133-1142.
- [239] J. Moraes; T. Maschmeyer; S. Perrier, "Clickable" Polymers via a Combination of RAFT Polymerization and Isocyanate Chemistry. *J. Polym. Sci. A Pol. Chem.* **2011**, *49*, 2771-2782.
- [240] N. B. Pramanik; G. B. Nando; N. K. Singha, Self-Healing Polymeric Gel via RAFT Polymerization and Diels–Alder Click Chemistry. *Polymer* **2015**, *69*, 349-356.
- [241] R. K. Iha; K. L. Wooley; A. M. Nystrom; D. J. Burke; M. J. Kade; C. J. Hawker, Applications of Orthogonal "Click" Chemistries in the Synthesis of Functional Soft Materials. *Chem. Rev.* **2009**, *109*, 5620-5686.
- [242] C. S. Boyer, M. H.; Davis, T. P., Building Nanostructures Using RAFT Polymerization. *J. Polym. Sci. A Polym. Chem.* **2011**, *49*, 551-595.
- [243] N. B. Pramanik; D. S. Bag; S. Alam; G. B. Nando; N. K. Singha, Thermally Amendable Tailor-Made Functional Polymer by RAFT Polymerization and "Click Reaction". *J. Polym. Sci. A Polym. Chem.* **2013**, *51*, 3365-3374.
- [244] N. K. Singha; N. B. Pramanik; P. K. Behera; A. Chakrabarty; J. W. Mays, Tailor-Made Thermoreversible Functional Polymer via RAFT Polymerization in an Ionic Liquid: A Remarkably Fast Polymerization Process. *Green Chem.* **2016**, *18*, 6115-6122.
- [245] Y. Zhou; Y. Qu; Q. Yu; H. Chen; Z. Zhang; X. Zhu, Controlled Synthesis of Diverse Single-Chain Polymeric Nanoparticles Using Polymer Bearing Furan-Protected Maleimide Moieties. *Polym. Chem.* **2018**, *9*, 3238-3247.

- [246] J. Yoon; P. A. Lovell, Model Reaction Studies and Crosslinking of Dimethyl-meta-isopropenylbenzyl Isocyanate Containing Ambient Crosslinkable Latex. *Macromol. Chem. and Phys.* **2008**, *209*, 279-289.
- [247] A. V. Menon; G. Madras; S. Bose, Ultrafast Self-Healable Interfaces in Polyurethane Nanocomposites Designed Using Diels–Alder “Click” as an Efficient Microwave Absorber. *ACS Omega* **2018**, *3*, 1137-1146.
- [248] C. Huang; T. Tassone; K. Woodberry; D. Sunday; D. L. Green, Impact of ATRP Initiator Spacer Length on Grafting Poly(methyl methacrylate) from Silica Nanoparticles. *Langmuir* **2009**, *25*, 13351-13360.
- [249] C. Zeng; H. Seino; J. Ren; K. Hatanaka; N. Yoshie, Self-Healing bio-based Furan Polymers Cross-Linked with various Bis-Maleimides. *Polymer* **2013**, *54*, 5351-5357.
- [250] B. A. Larsen; K. M. Hurst; W. R. Ashurst; N. J. Serkova; C. R. Stoldt, Mono and Dialkoxysilane Surface Modification of Superparamagnetic Iron Oxide Nanoparticles for Application as Magnetic Resonance Imaging Contrast Agents. *J. Mater. Sci.* **2012**, *27*, 1846-1852.
- [251] M. Torres-Lugo; C. Rinaldi, Thermal Potentiation of Chemotherapy by Magnetic Nanoparticles. *Nanomedicine* **2013**, *8*, 1689-1707.
- [252] F. J. Feher; K. D. Wyndham, Amine and Ester-Substituted Silsesquioxanes: Synthesis, Characterization and Use as a Core for Starburst Dendrimers. *Chem. Commun.* **1998**, *0*, 323-324.
- [253] F. J. Feher; K. D. Wyndham; D. Soulivong; F. Nguyen, Syntheses of Highly Functionalized Cube-Octameric Polyhedral Oligosilsesquioxanes ($R_8Si_8O_{12}$). *J. Chem. Soc. Dalton Trans.* **1999**, *0*, 1491-1497.
- [254] Z. Zhang; G. Liang; T. Lu, Synthesis and Characterization of Cage Octa(aminopropylsilsesquioxane). *J. Appl. Polym. Sci.* **2007**, *103*, 2608-2614.
- [255] H. Chen, Endgroup-Assisted Siloxane Bond Cleavage in the Gas Phase. *J. Am. Soc. Mass Spectrom.* **2003**, *14*, 1039-1048.
- [256] E. A. Smith; W. Chen, How to Prevent the Loss of Surface Functionality Derived from Aminosilanes. *Langmuir* **2008**, *24*, 12405-12409.

6 Supporting Information

Supporting Information

Self-Healing Polymer Nanocomposites based on Diels-Alder-Reactions with Silica Nanoparticles: The Role of the Polymer Matrix

Sandra Schäfer , Guido Kickelbick*^[a,b]

[a] Inorganic Solid State Chemistry, Saarland University, Am Markt, Zeile 3, 66125 Saarbrücken, Germany

[b] INM – Leibniz-Institut für Neue Materialien GmbH, Campus D2₂, 66123 Saarbrücken, Germany

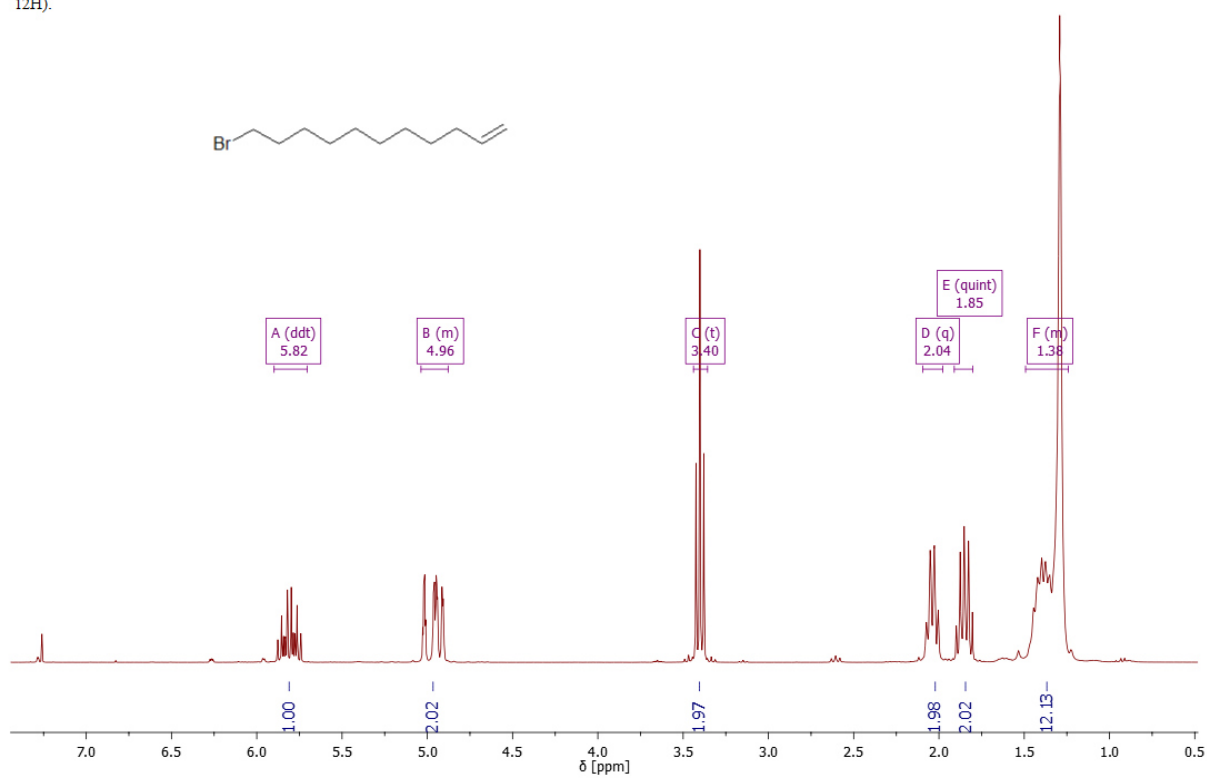
E-mail: guido.kickelbick@uni-saarland.de

<http://www.uni-saarland.de/lehrstuhl/kickelbick.html>

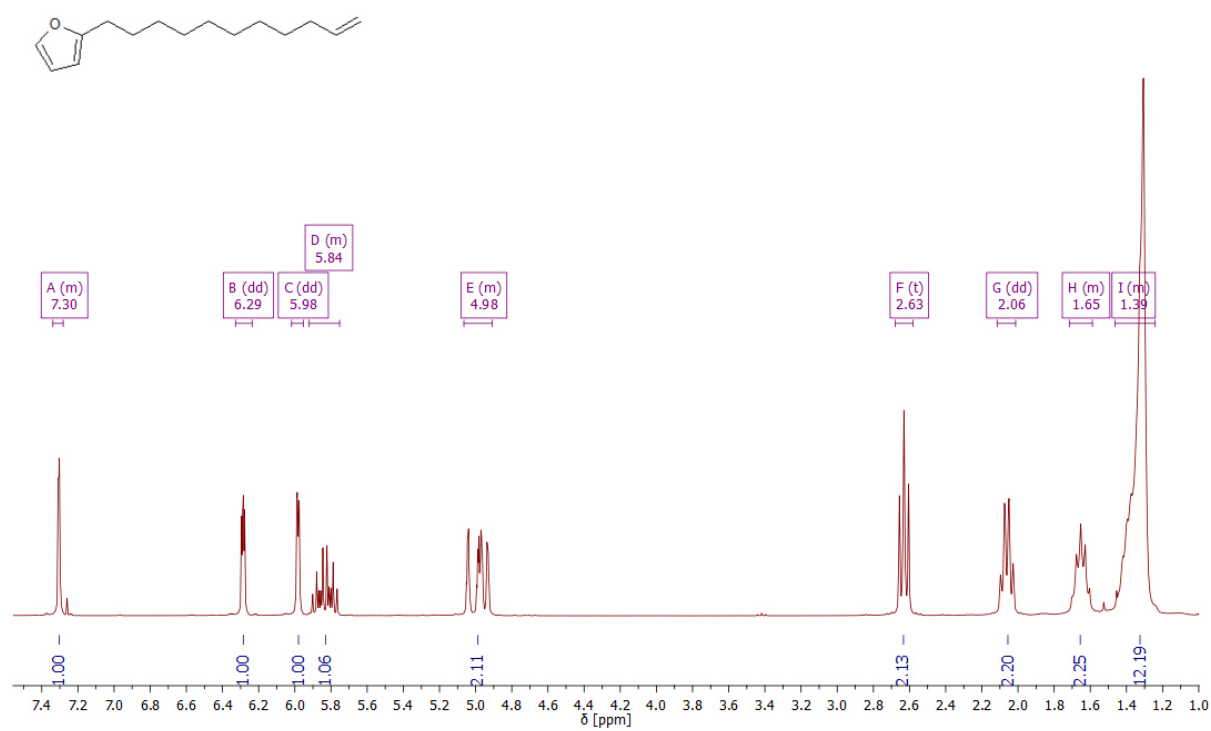
IR and ¹H-NMR spectra

All ¹H NMR Spectras were recorded in CDCl₃ at 300 MHz.

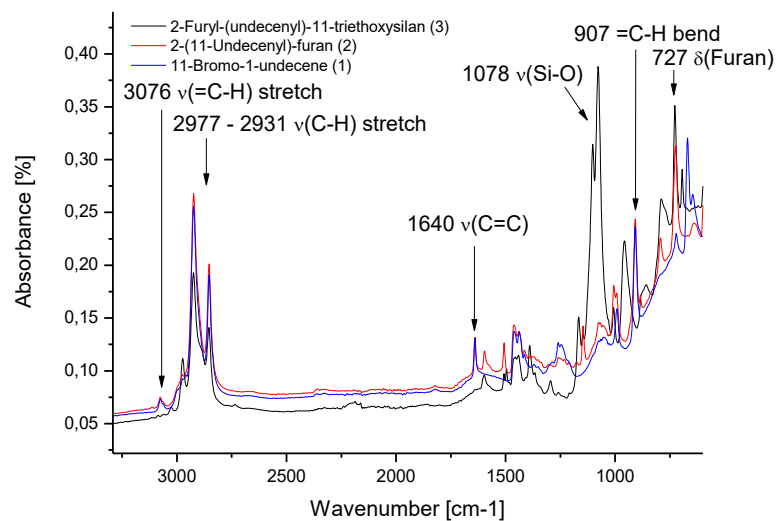
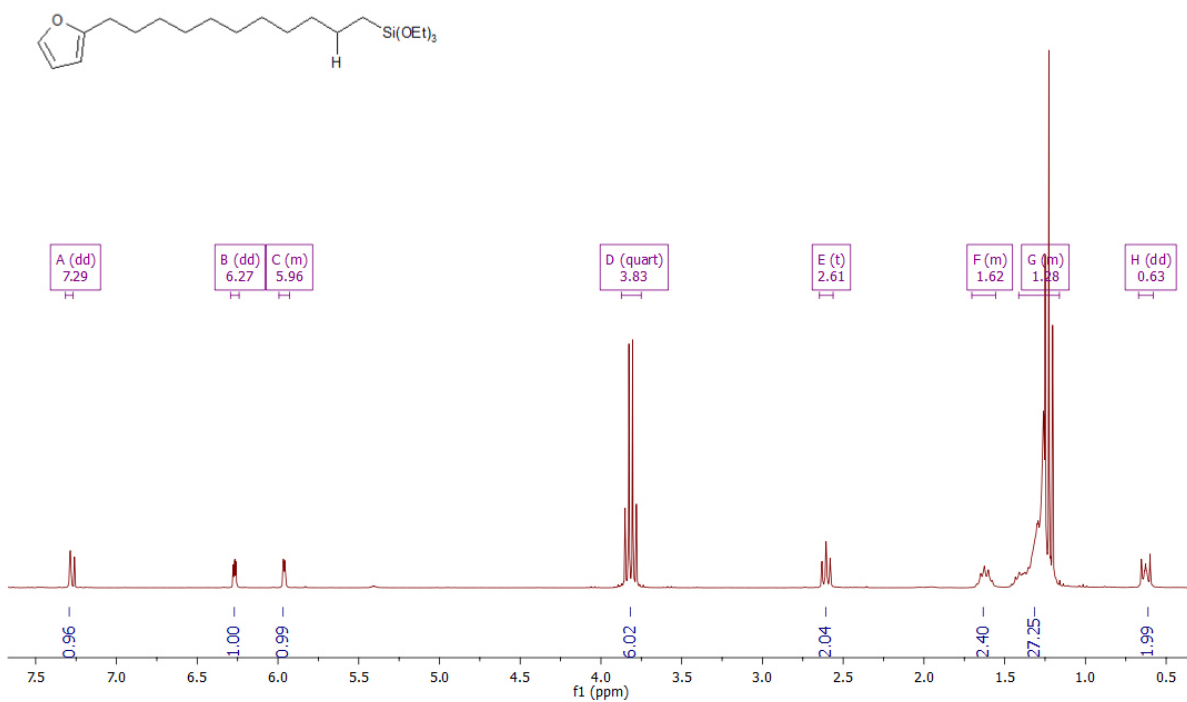
^1H NMR (300 MHz, CDCl_3) δ 5.80 (ddt, $J = 17, 10, 7$ Hz, 1H), 5.04 – 4.88 (m, 2H), 3.40 (t, $J = 6.9$ Hz, 2H), 2.04 (q, $J = 6.8$ Hz, 2H), 1.85 (quint, $J = 6.8$ Hz, 2H), 1.49 – 1.24 (m, 12H).



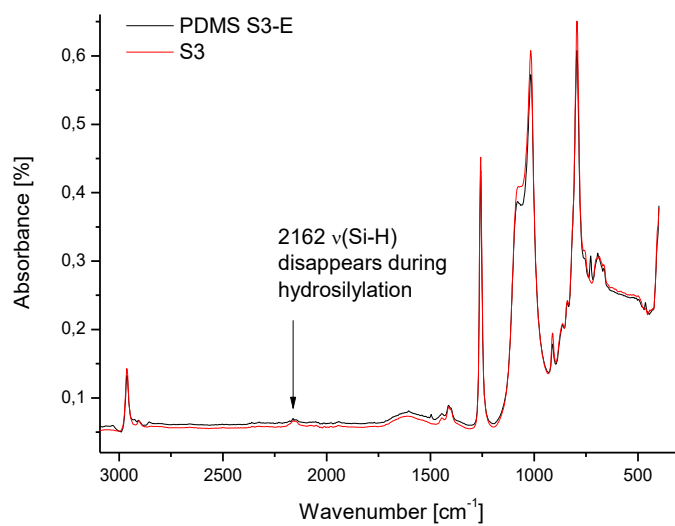
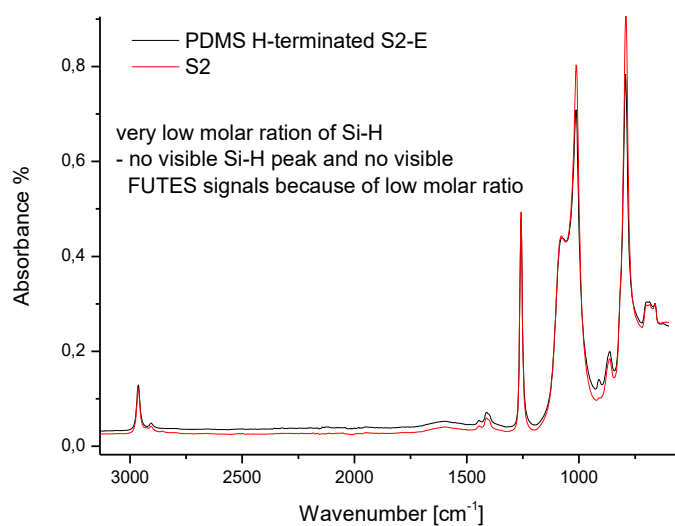
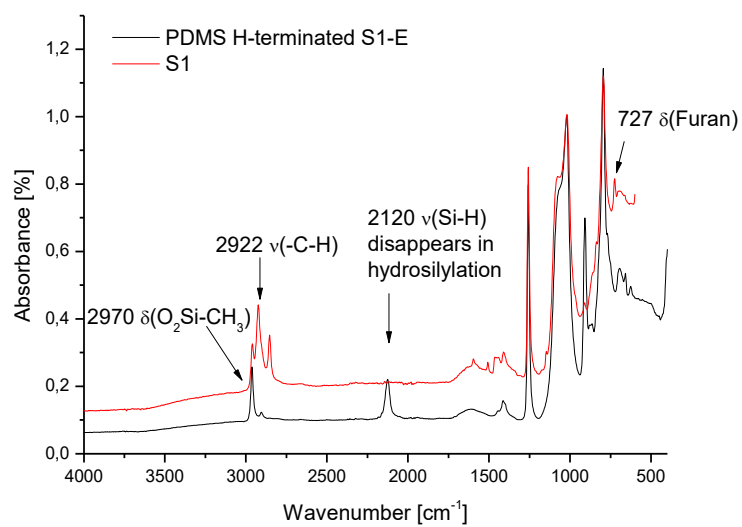
^1H NMR (300 MHz, CDCl_3) δ 7.34 – 7.28 (m, 1H), 6.29 (dd, $J = 3.0, 1.9$ Hz, 1H), 5.98 (dd, $J = 3.1, 0.7$ Hz, 1H), 5.92 – 5.75 (m, 1H), 5.06 – 4.91 (m, 2H), 2.63 (t, $J = 7.6$ Hz, 2H), 2.06 (dd, $J = 14.2, 6.8$ Hz, 2H), 1.72 – 1.59 (m, 2H), 1.46 – 1.24 (m, 13H).

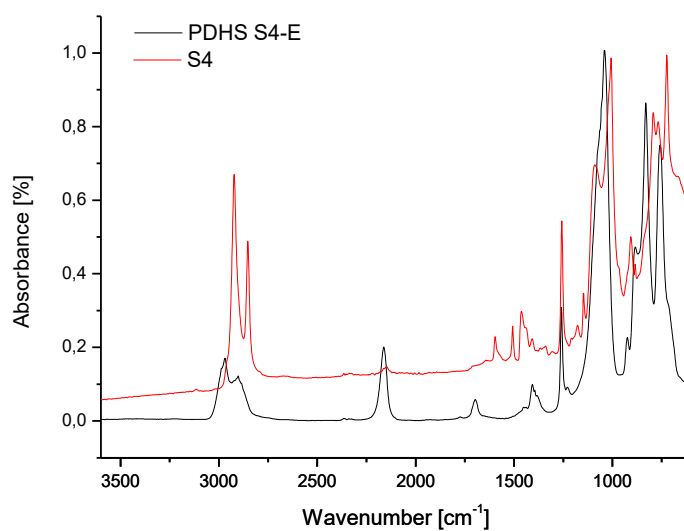
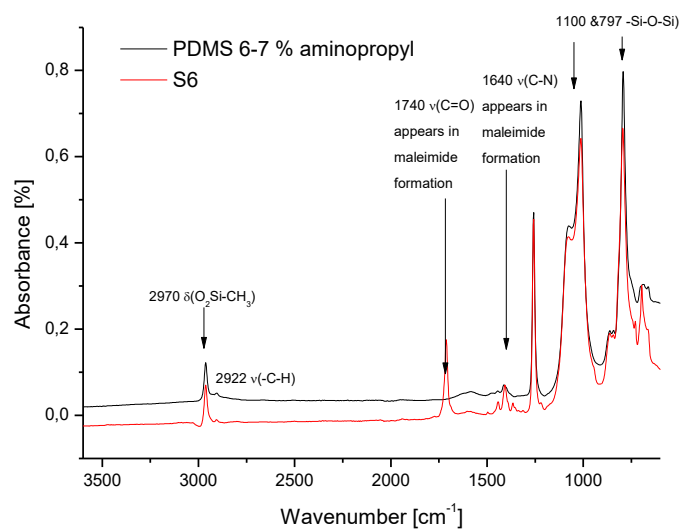
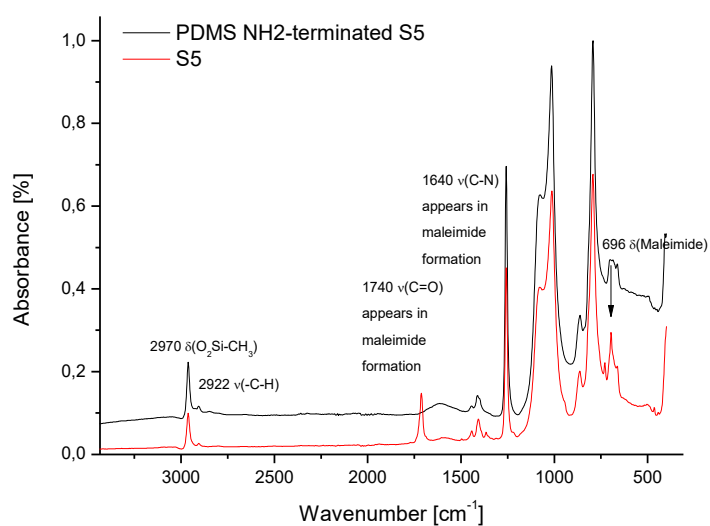


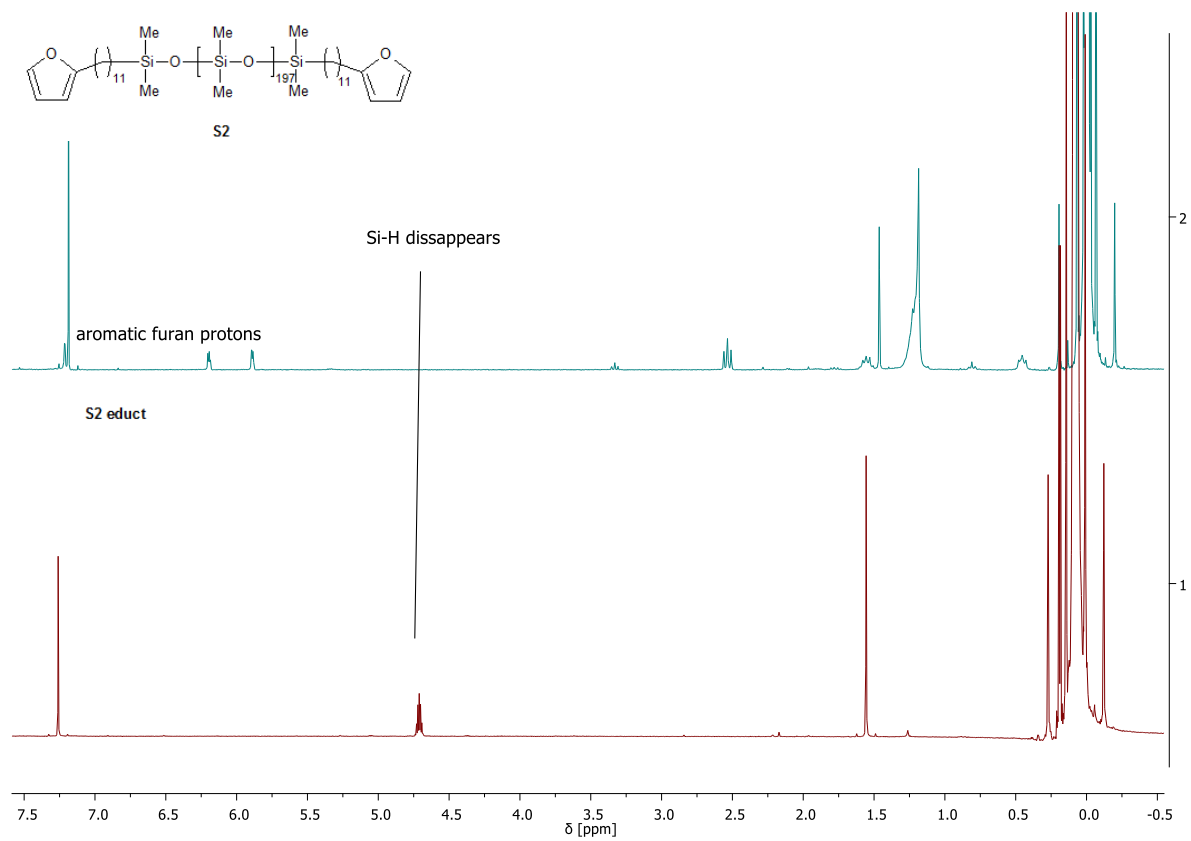
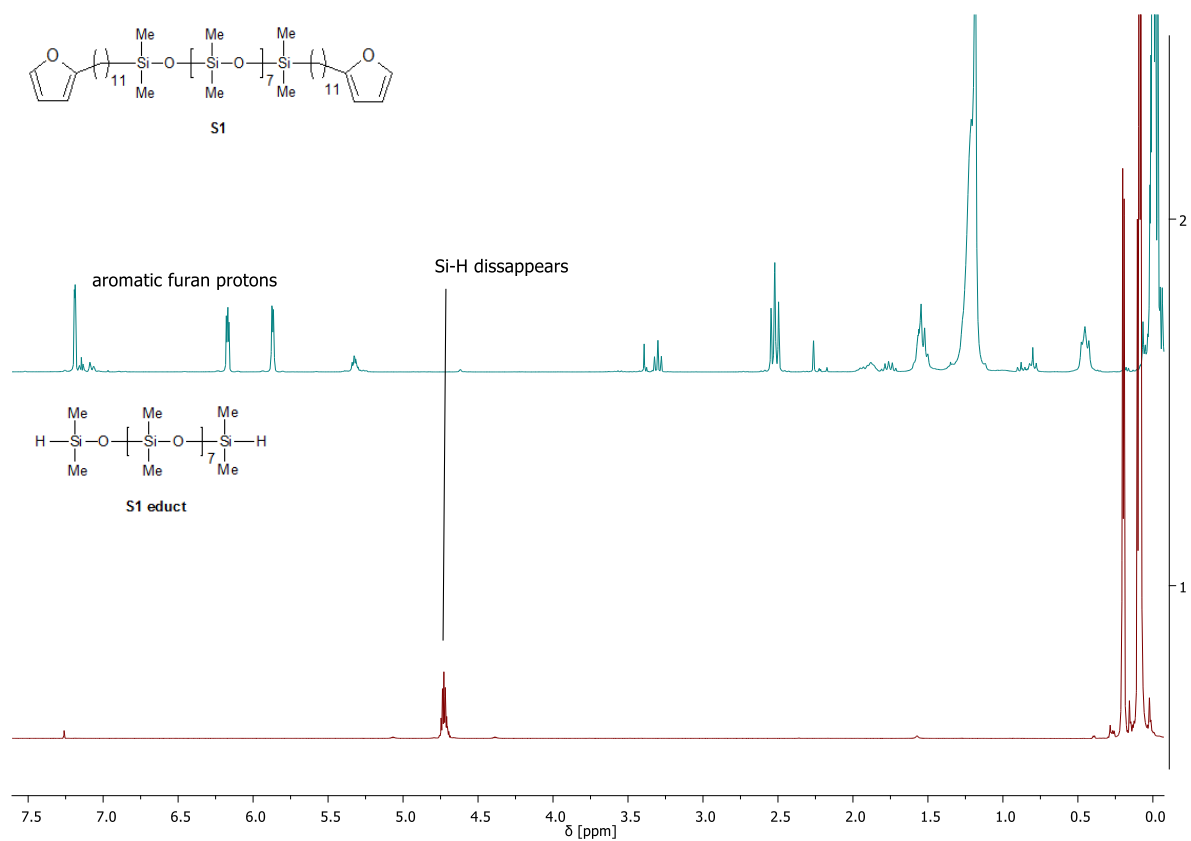
¹H NMR (300 MHz, CDCl₃) δ 7.29 (dd, *J* = 1.8, 0.8 Hz, 1H), 6.27 (dd, *J* = 3.1, 1.9 Hz, 1H), 5.99 – 5.93 (m, 1H), 3.83 (quart, 7.0 Hz, 6H), 2.61 (t, *J* = 7.6 Hz, 2H), 1.70 – 1.56 (m, 3H), 1.41 – 1.16 (m, 28H), 0.63 (dd, *J* = 9.0, 7.1 Hz, 2H).

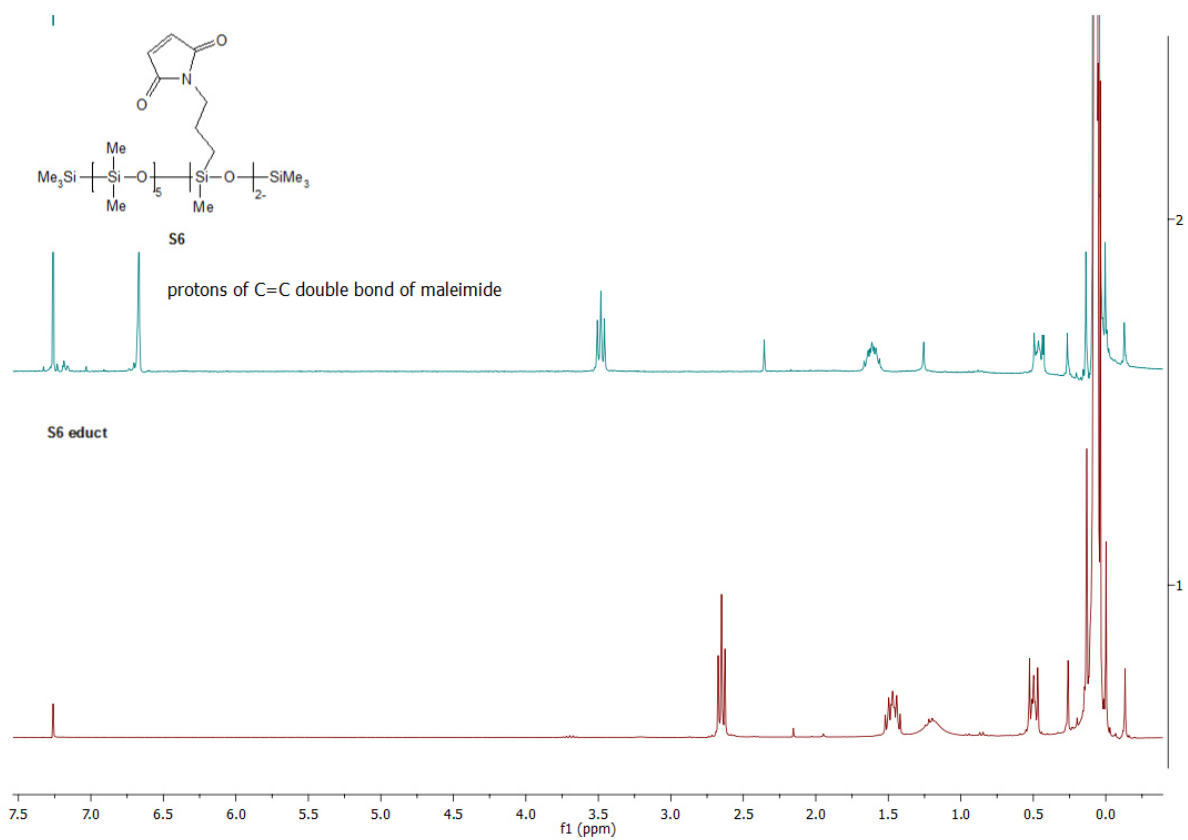
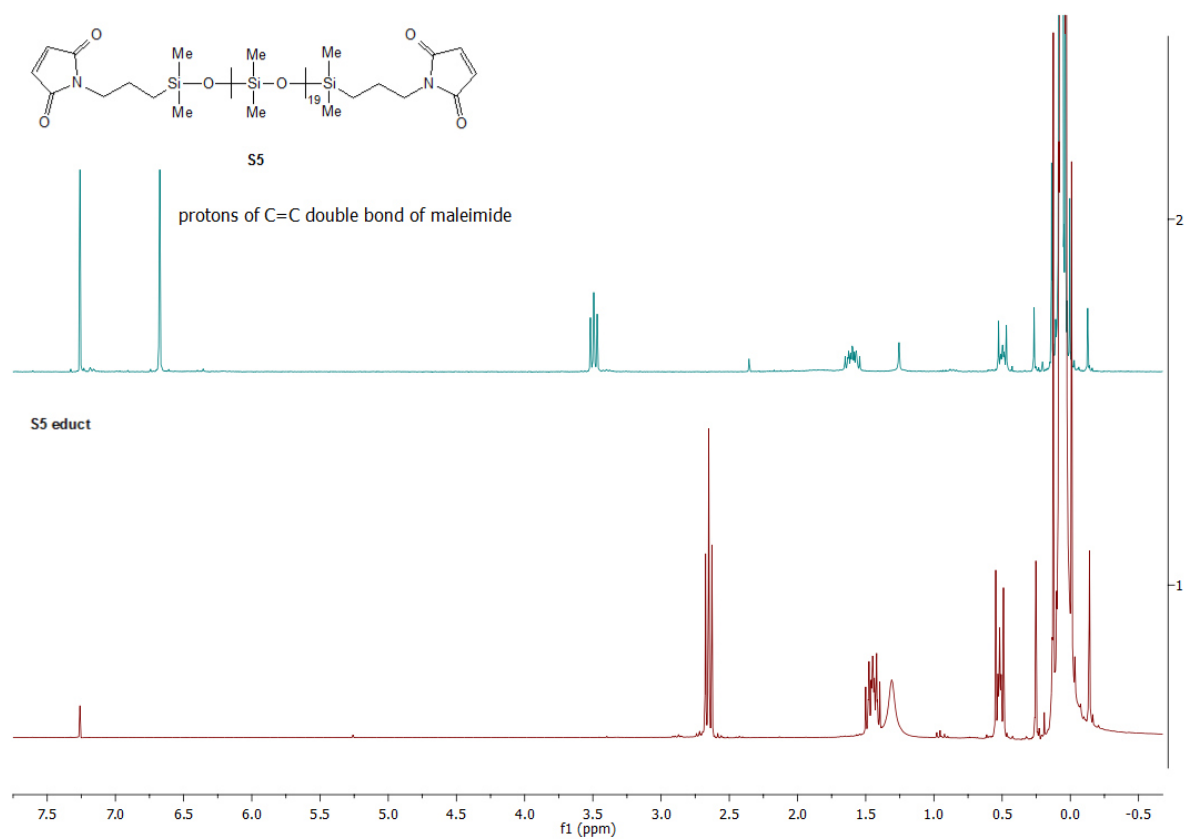


IR spectra of Furan-modified Siloxanes



**IR spectra of Maleimide-modified Siloxanes**

^1H NMR of modified Siloxanes



Supporting Information

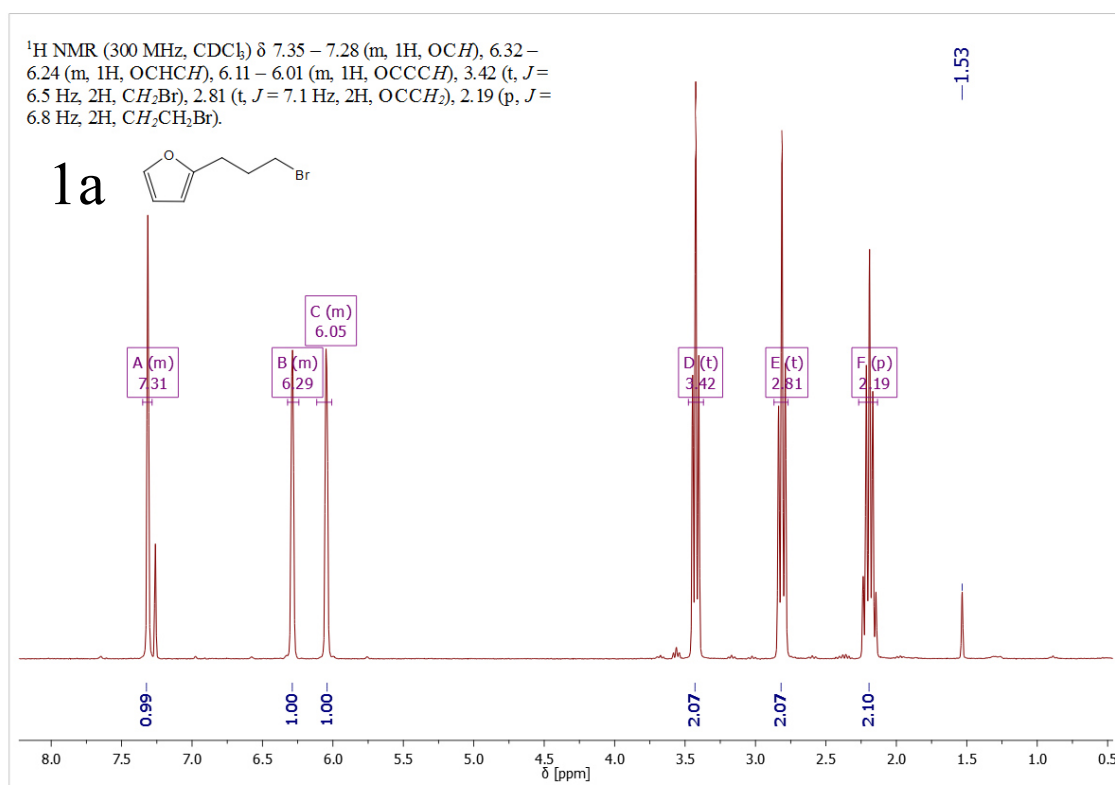
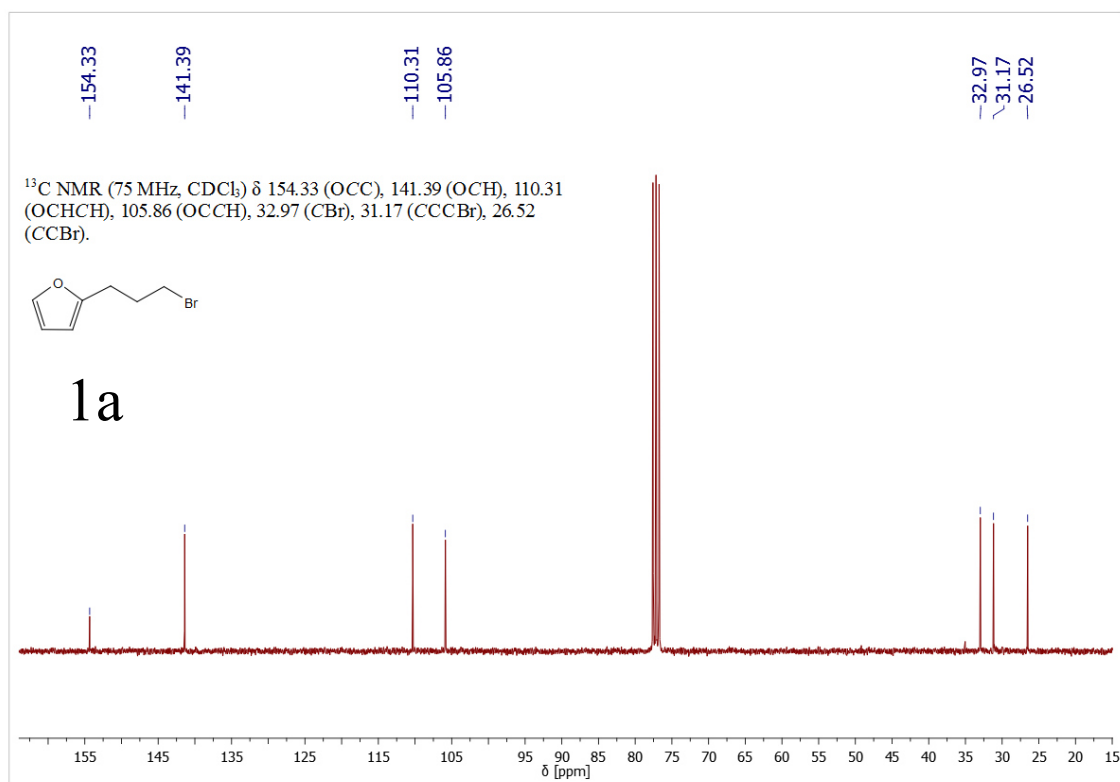
Diels-Alder Reactions on Surface-Modified Magnetite/Maghemite Nanoparticles: Application in Self-Healing Nanocomposites

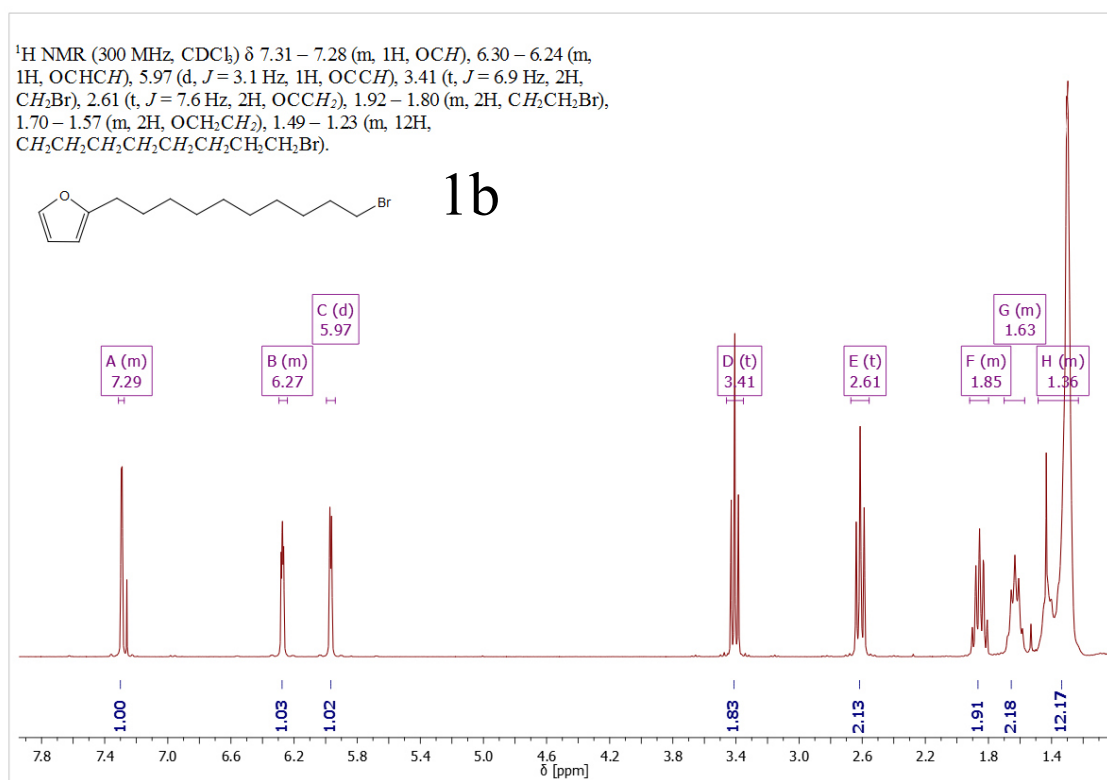
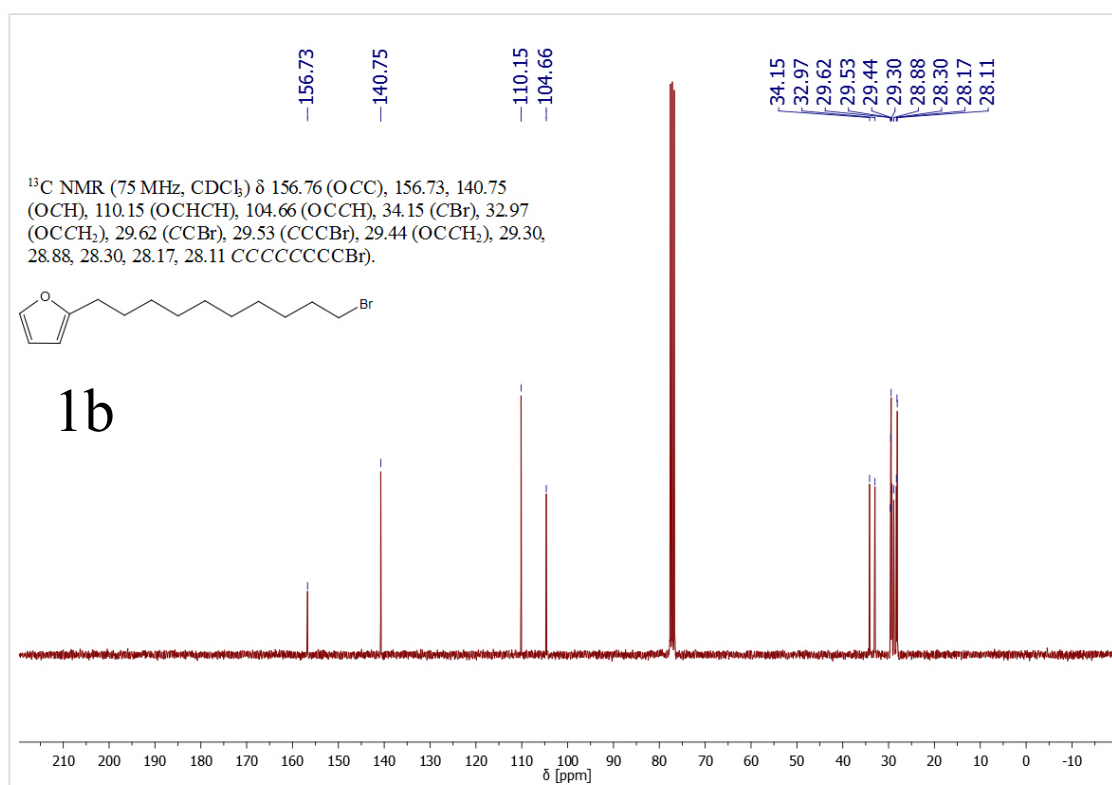
Sandra Schäfer and Guido Kickelbick*

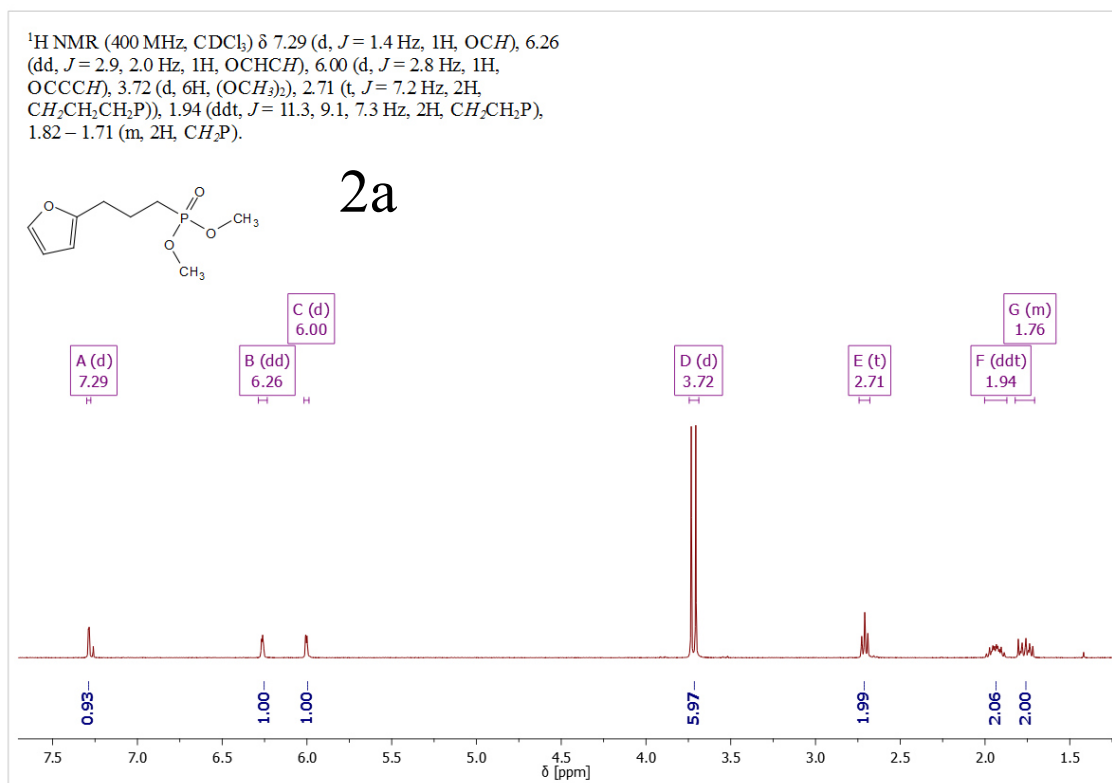
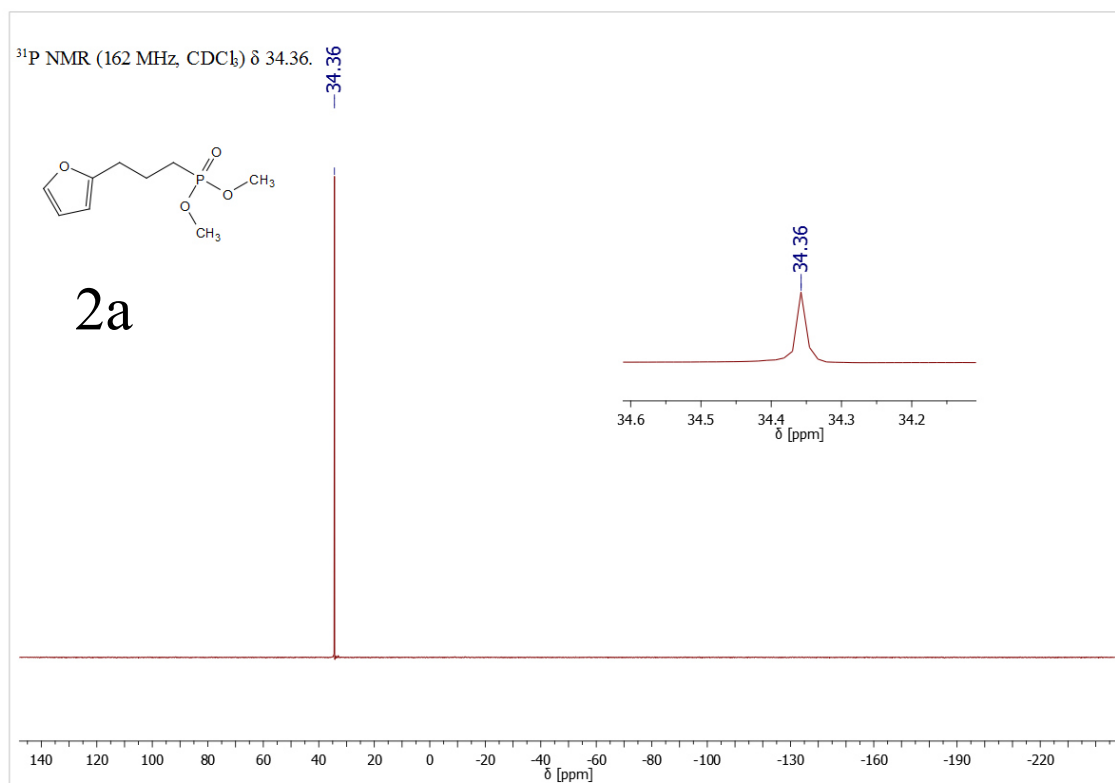
Inorganic Solid State Chemistry, Saarland University, Campus C4 1, 66123 Saarbrücken, Germany

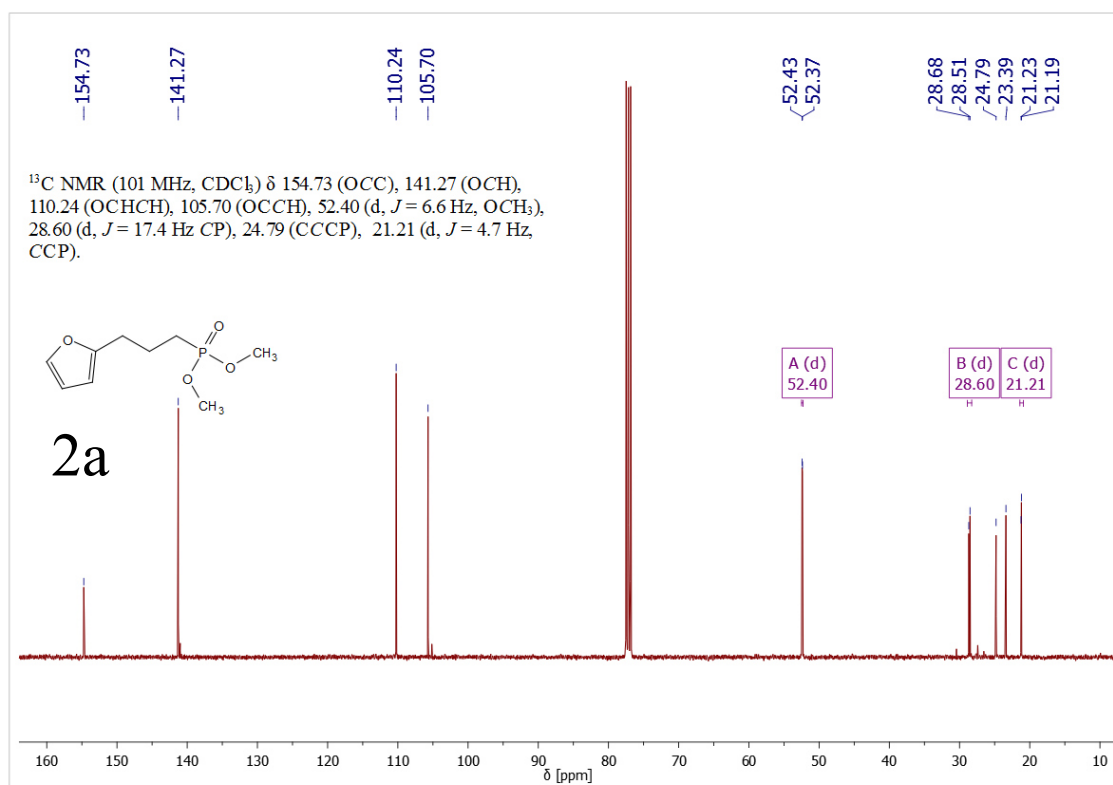
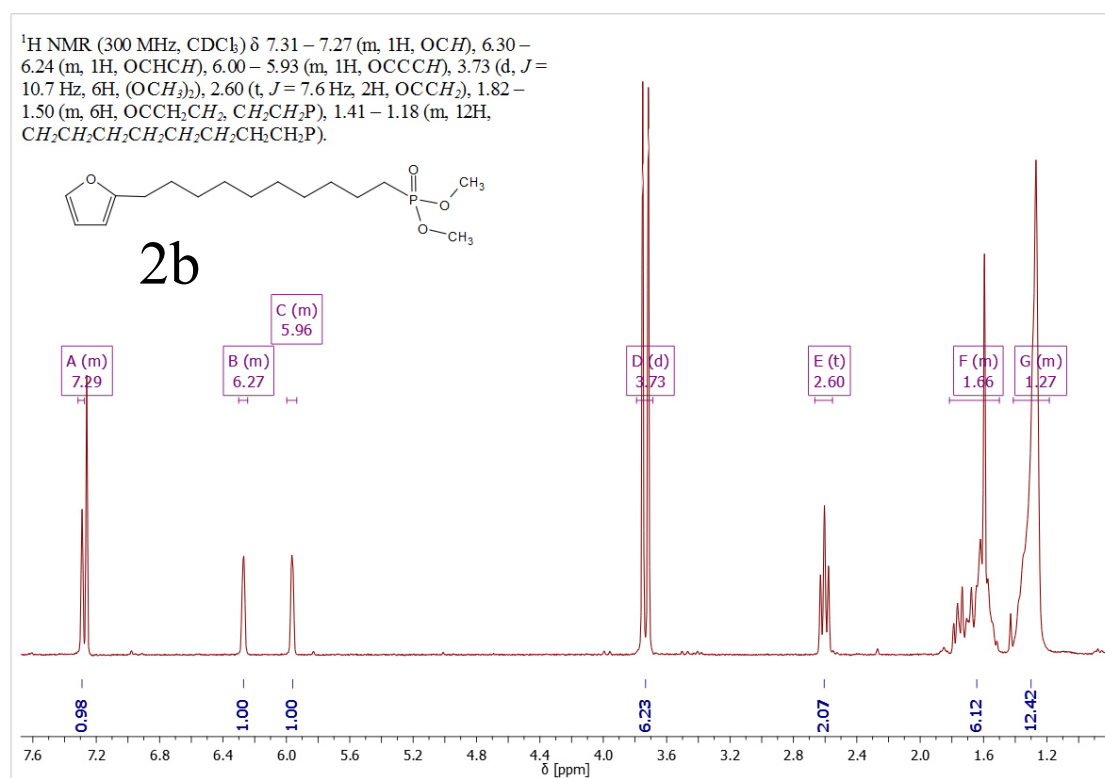
E-mail: guido.kickelbick@uni-saarland.de

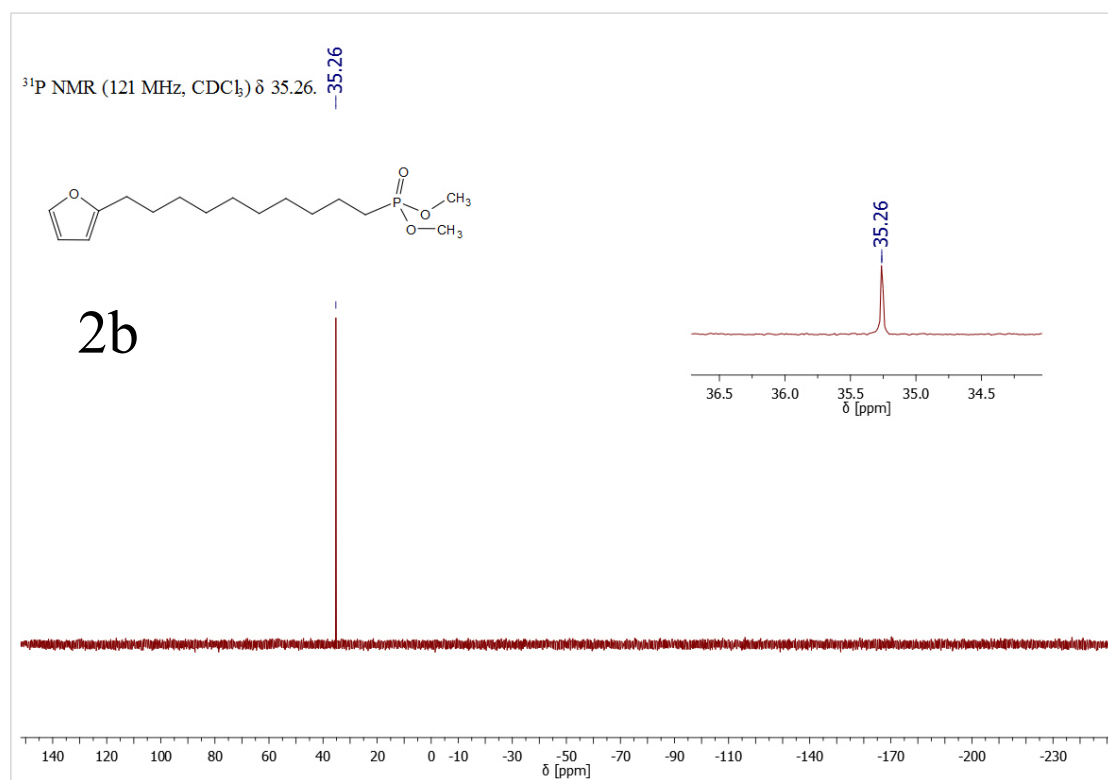
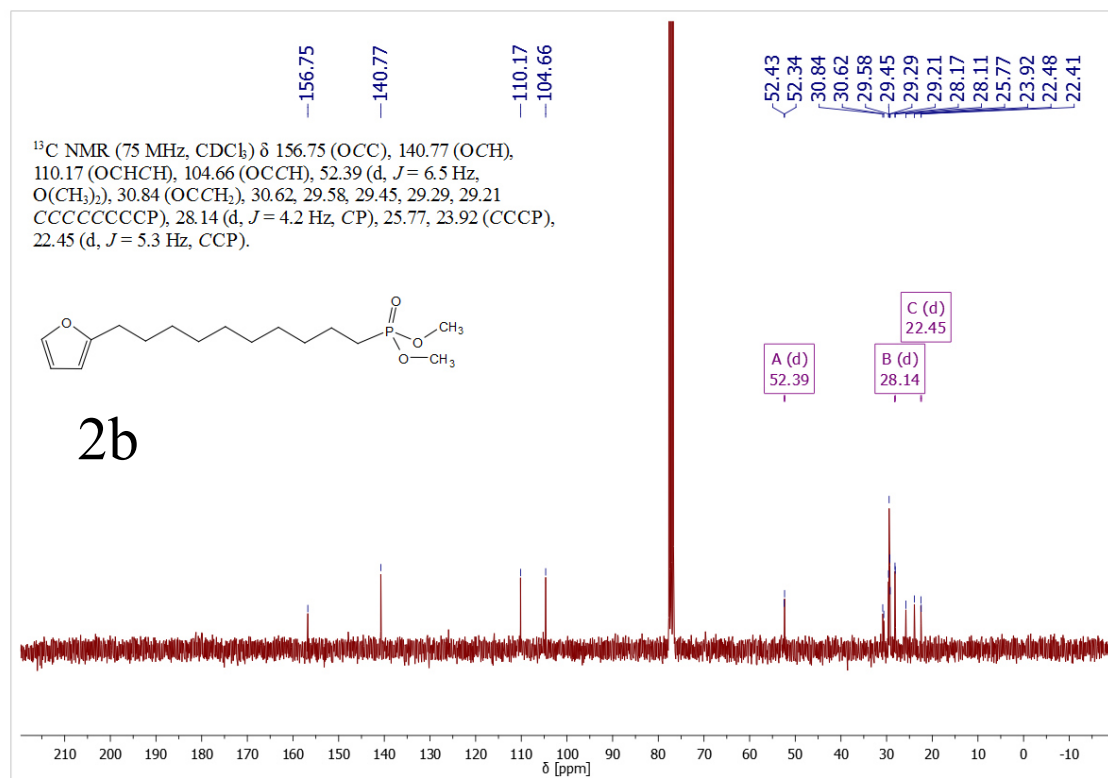
1. ^1H , ^{31}P & ^{13}C NMR spectra of synthesized molecules (1-10)
2. FTIR spectra of synthesized molecules (1-10)
3. Molecular structure of F10PE (**2b**) and F10P (**3b**) as obtained by single crystal X-ray diffraction analysis
4. OA@Fe_xO_y: further analytical data: TG, DLS
5. DDP@Fe_xO_y: further analytical data: TG, XRD
6. Control experiment, OA@Fe_xO_y & DDP mixed as solids to a physical blend.
7. Cofunctionalization with DDP&MeP@Fe_xO_y: TG, FTIR
8. Cofunctionalization with DA- and Methylphosphonic acids: CHN, FTIR
9. IR spectra of molecular Dien & Dienophile and the corresponding DA adduct
10. DA reaction on cofunctionalized DA-particles: FTIR, DSC, CHN
 - 10.1 F3PcoMeP@Fe_xO_y: DA-reaction of Furan-cofunctionalized particles with N-Dodecyl maleimide or Maleimide
 - 10.2 M3PcoMeP@Fe_xO_y.
 - 10.3 M10PcoMeP@Fe_xO_y.
11. DSC Graphs and listed values for all cofunctionalized particles
12. DSC and IR data to composite

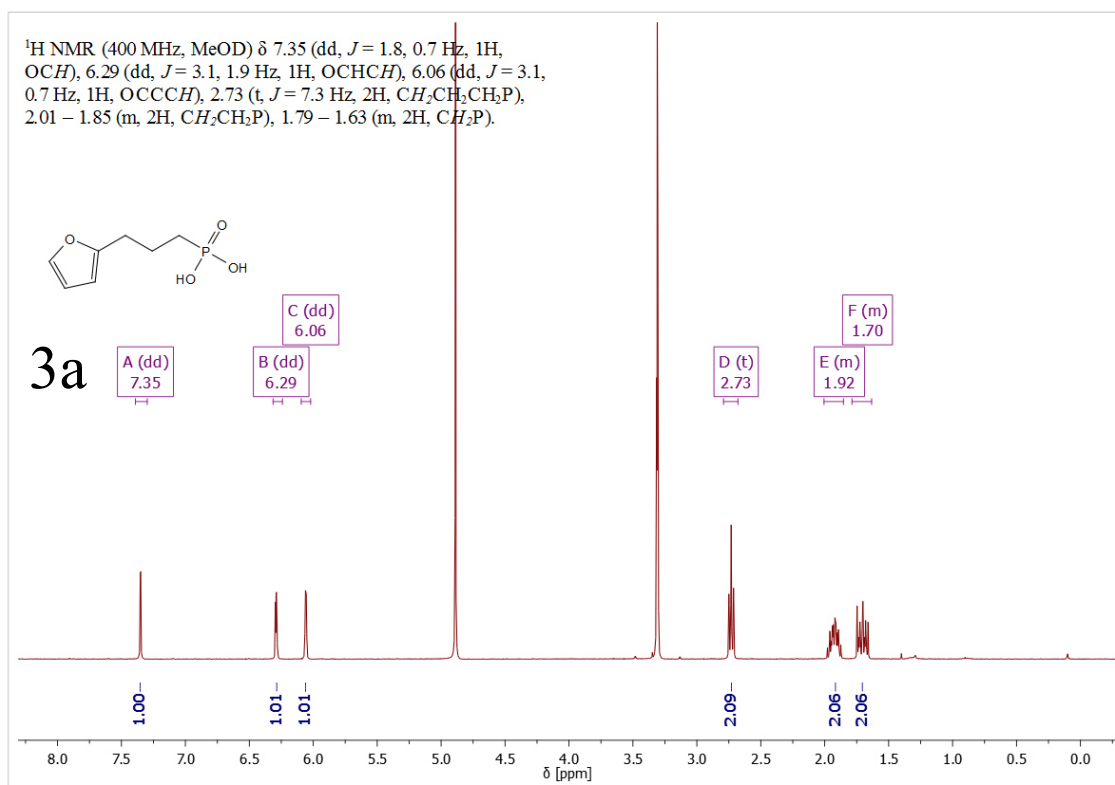
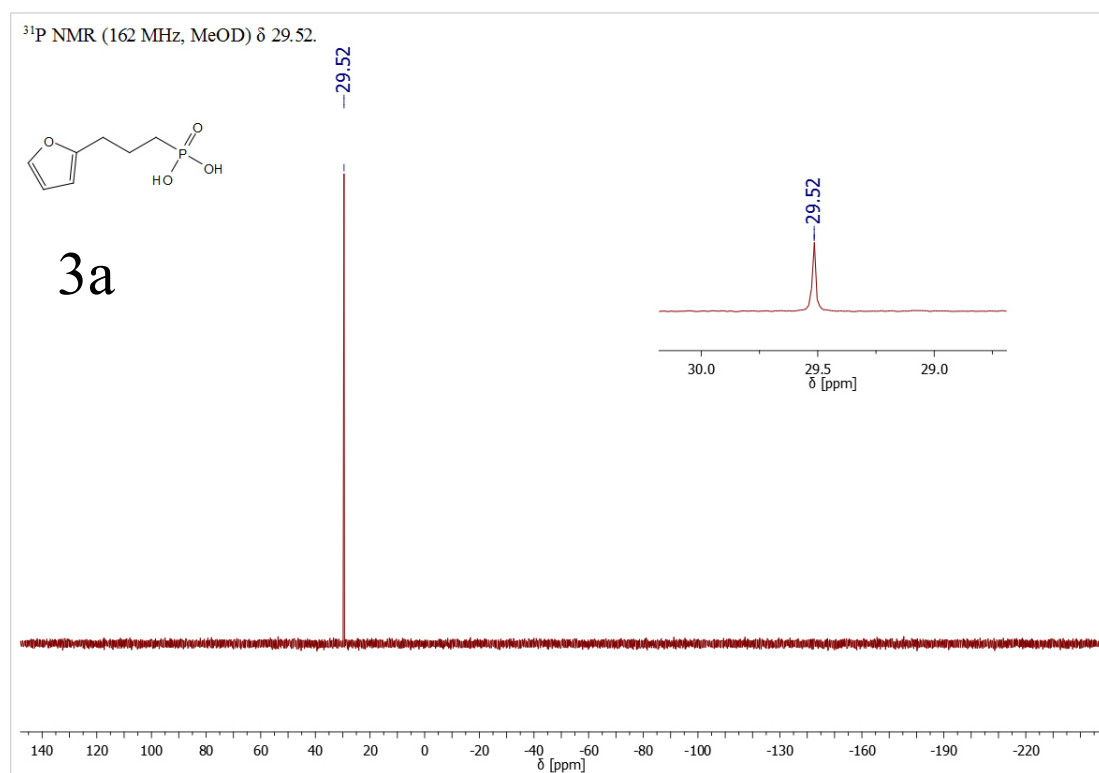
1. ^1H , ^{31}P & ^{13}C NMR spectra of synthesized molecules (1-10)Figure S1: ^1H NMR of 1a.Figure S2: ^{13}C NMR of 1a.

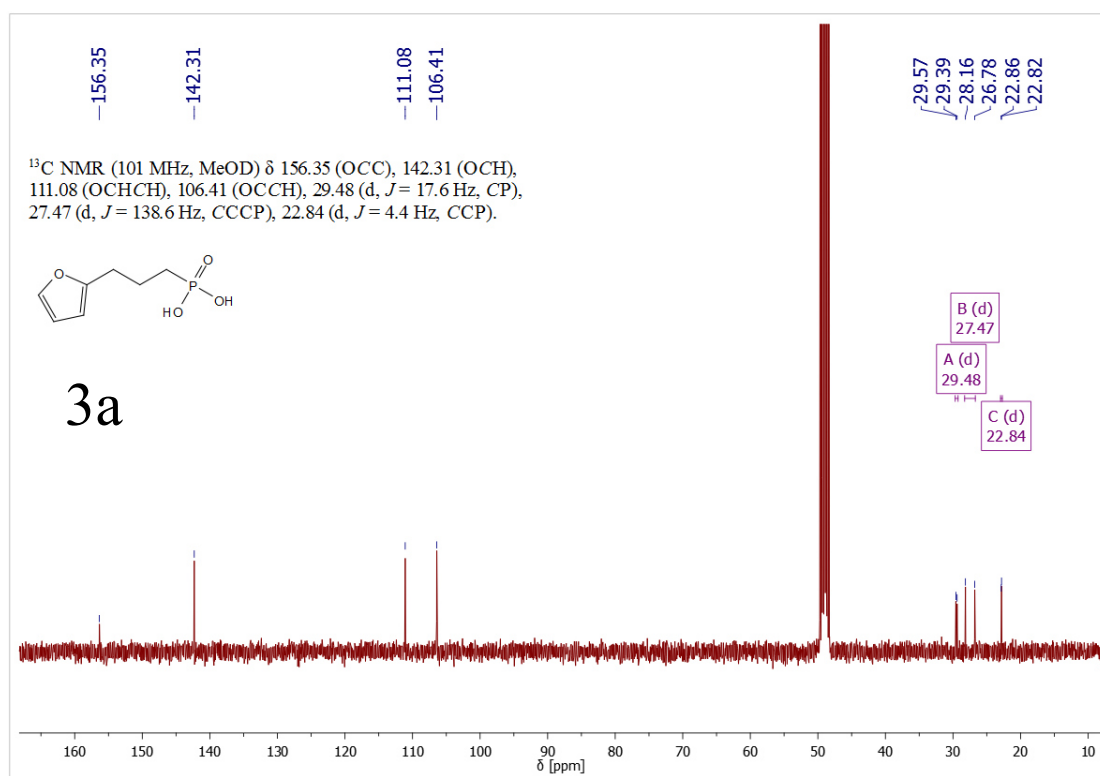
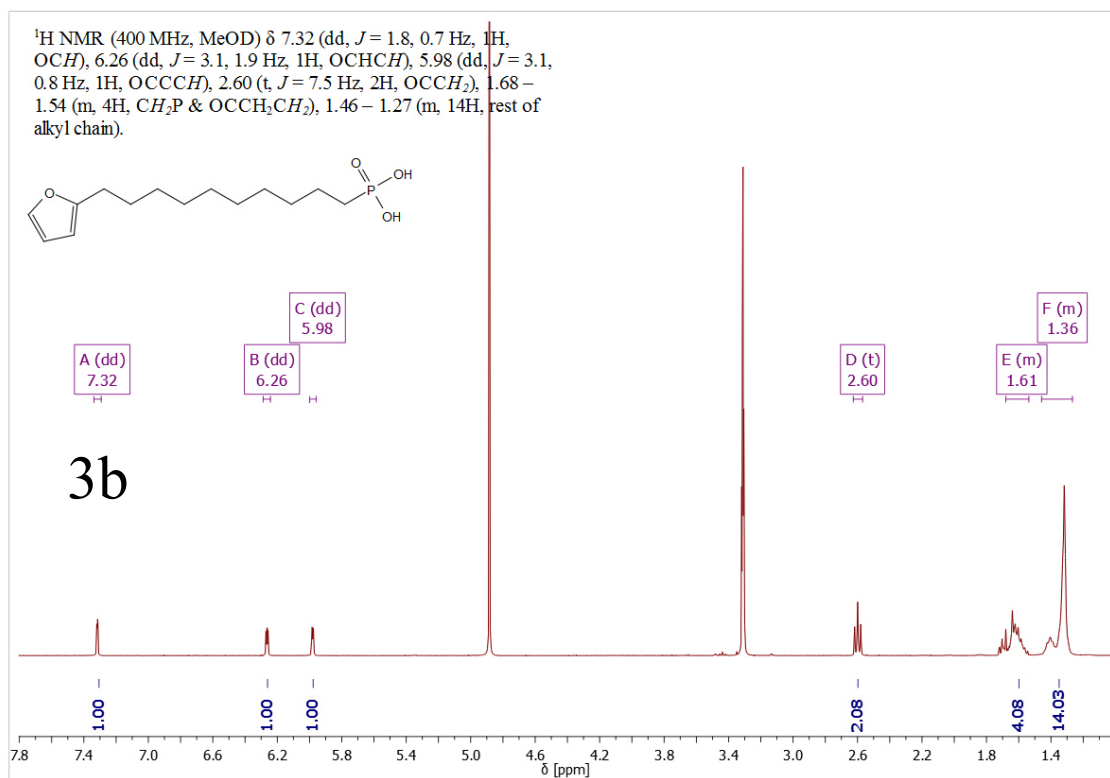
Figure S3: ¹H NMR of 1b.Figure S4: ¹³C NMR of 1b.

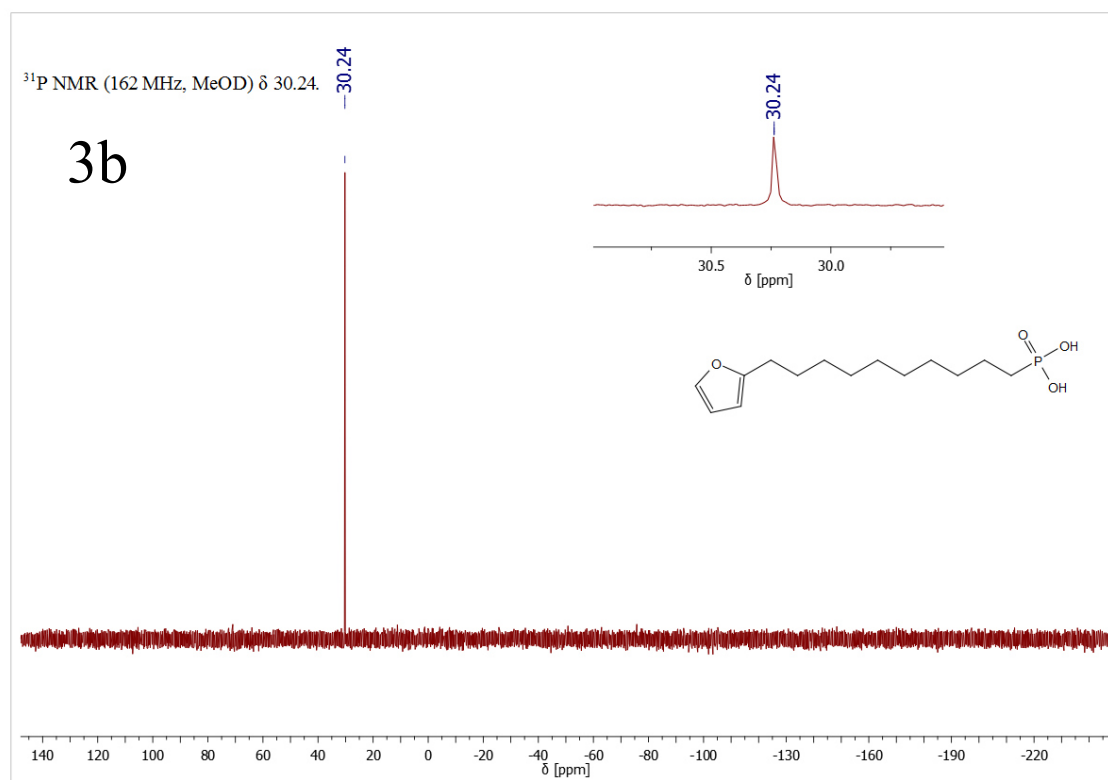
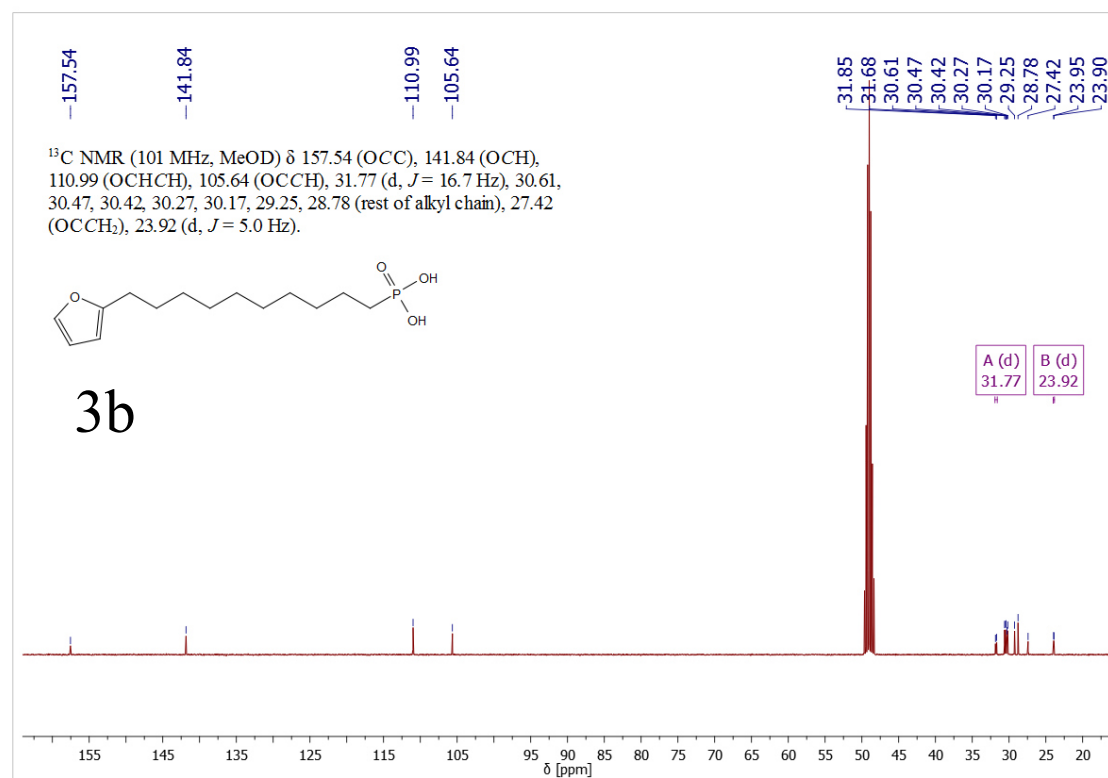
Figure S5: ¹H NMR of 2a.Figure S6: ³¹P NMR of 2a.

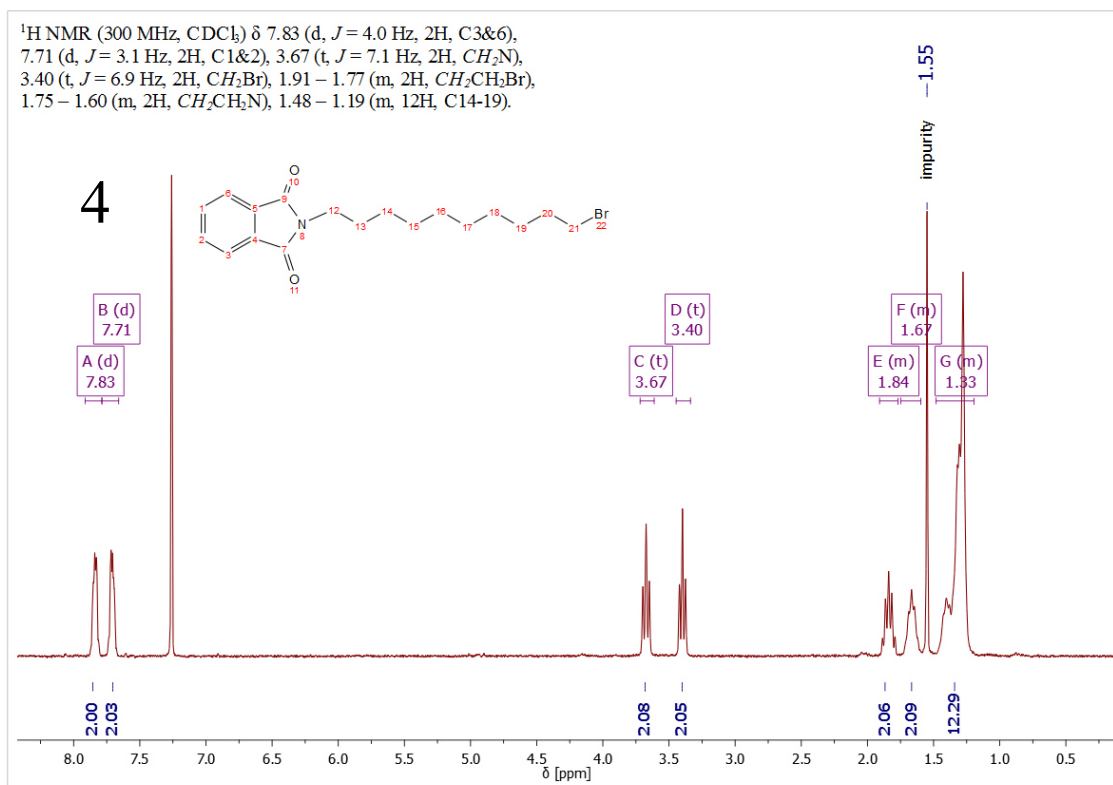
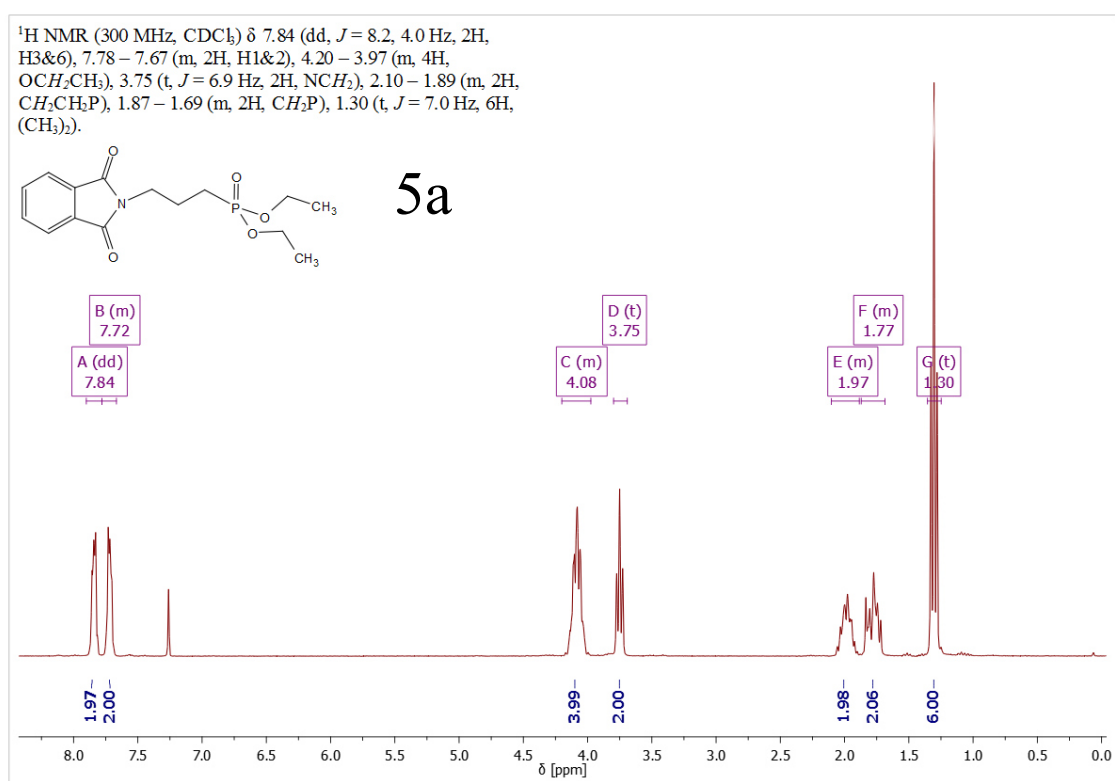
Figure S7: ^{13}C NMR of 2a.Figure S8: ^1H NMR of 2b.

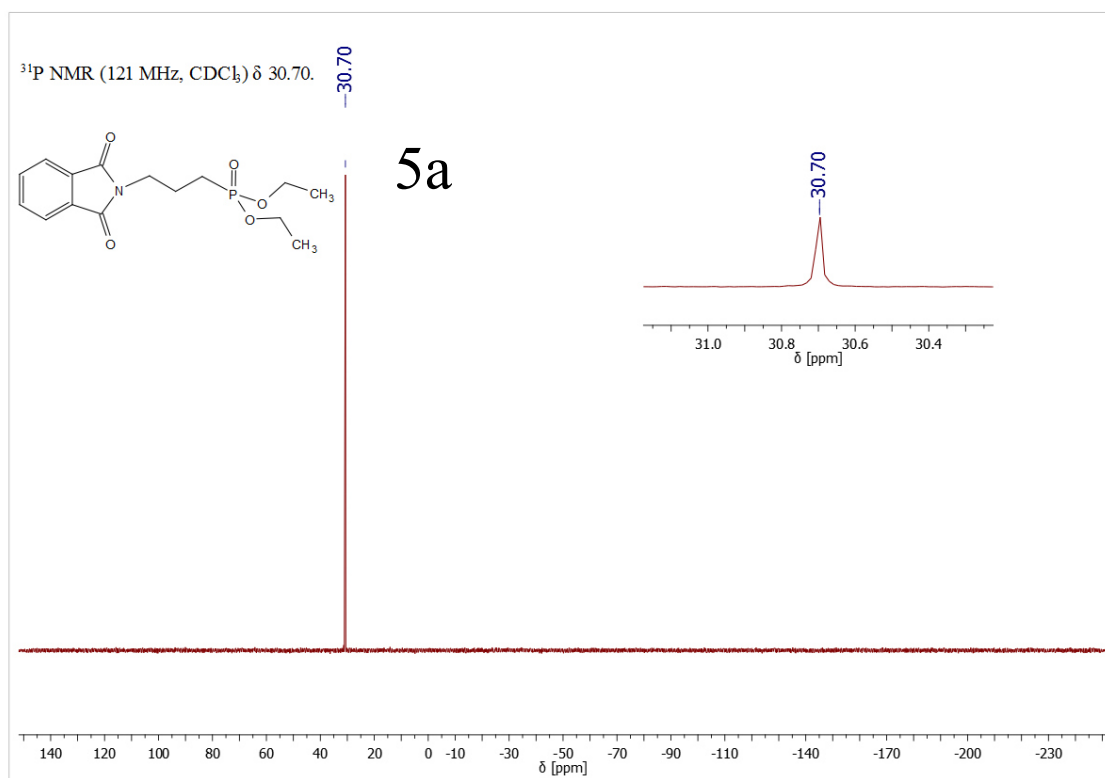
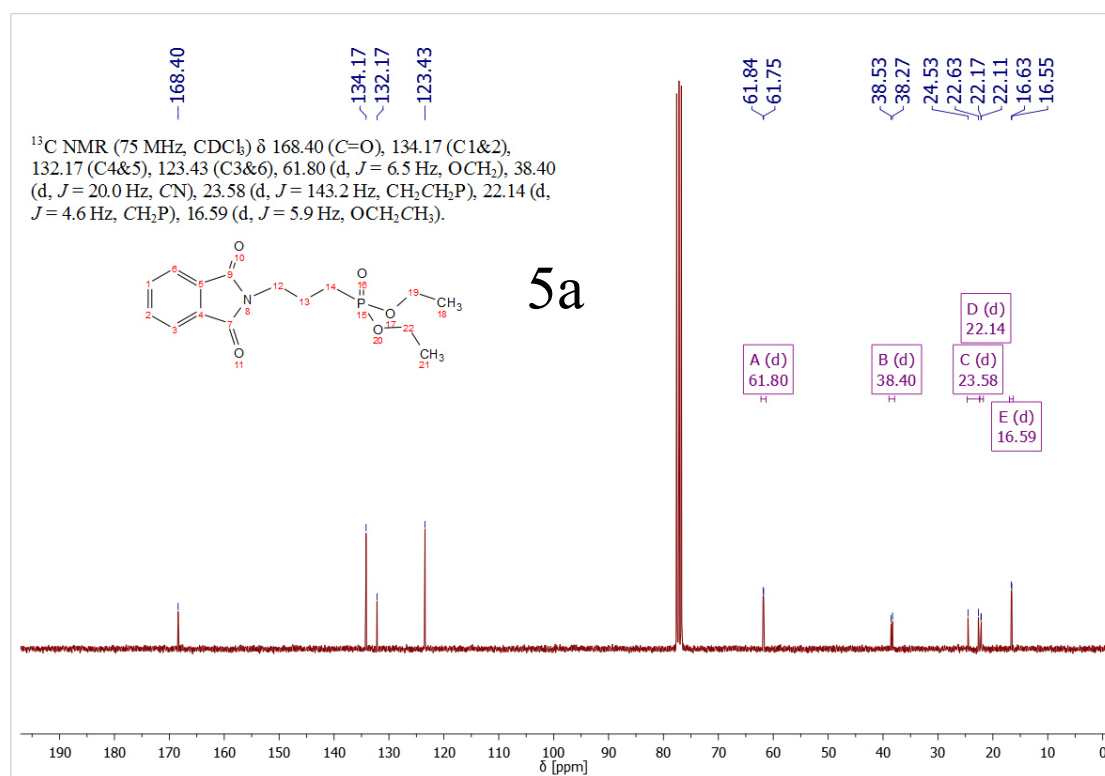
Figure S9: ³¹P NMR of 2b.Figure S10: ¹³C NMR of 2b.

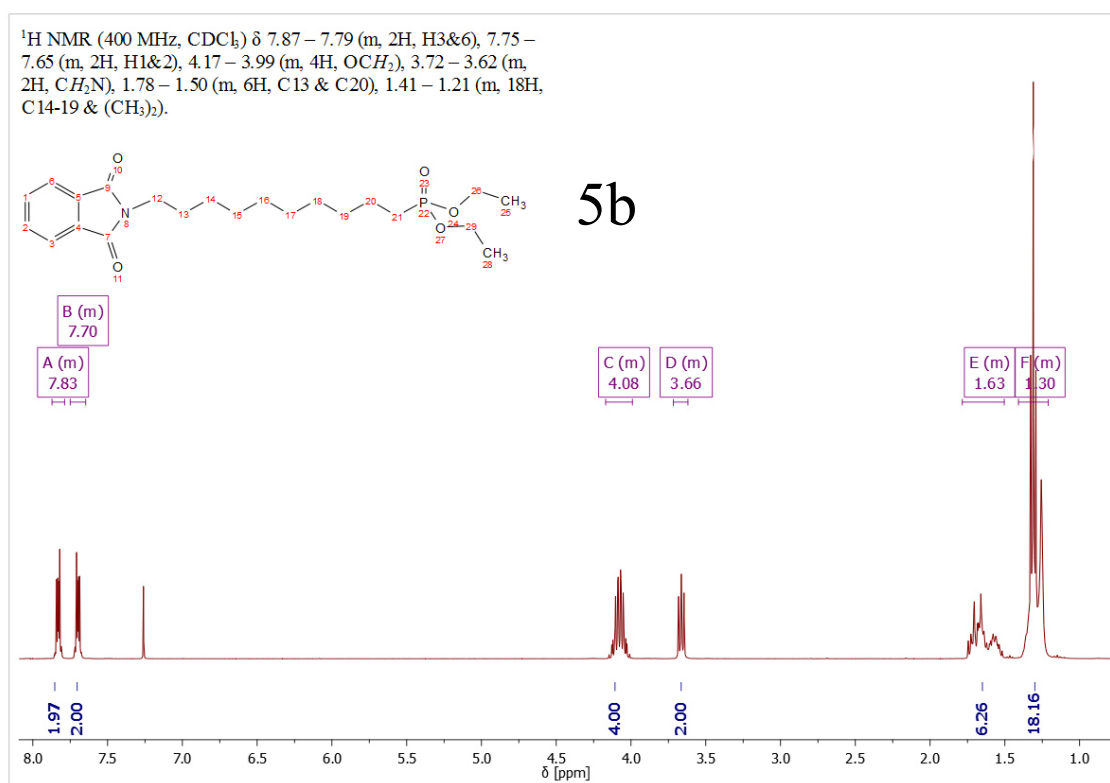
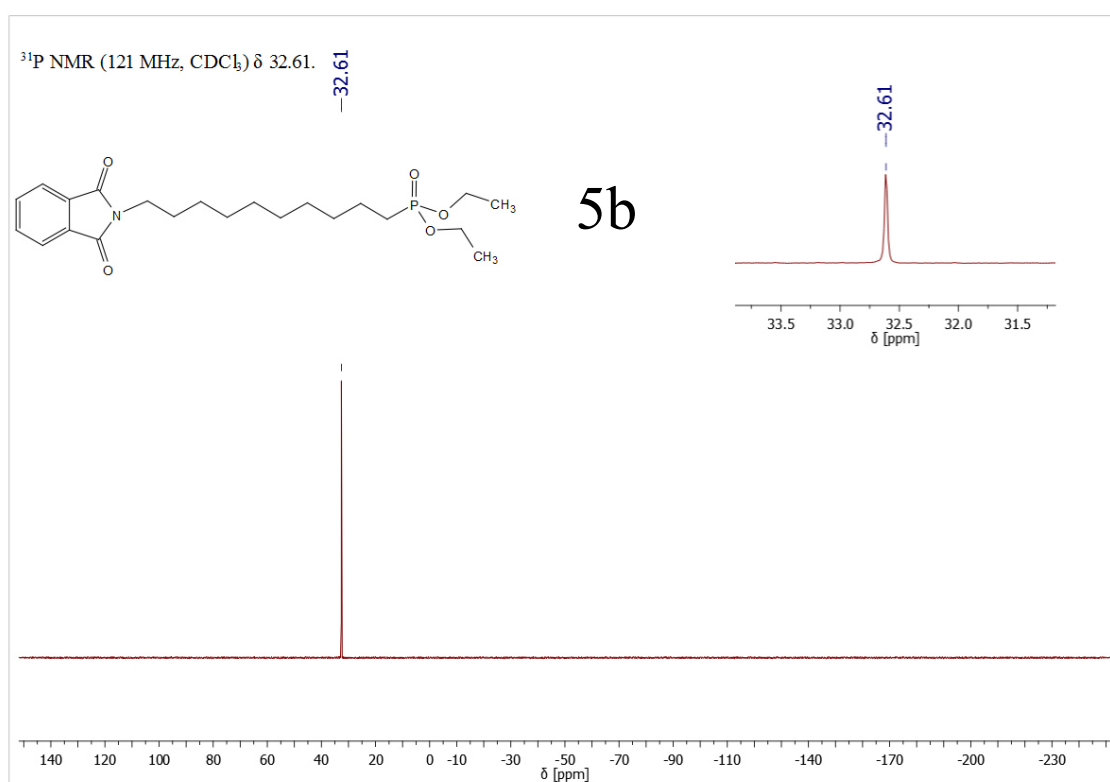
Figure S11: ¹H NMR of 3a.Figure S12: ³¹P NMR of 3a.

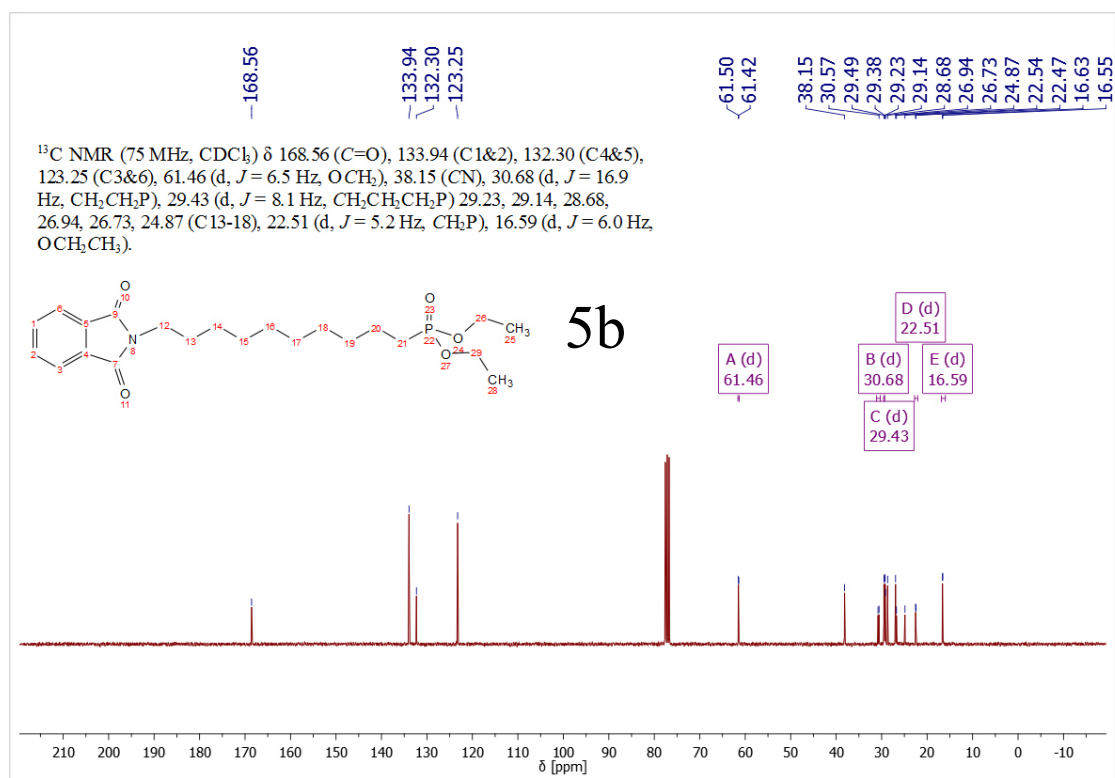
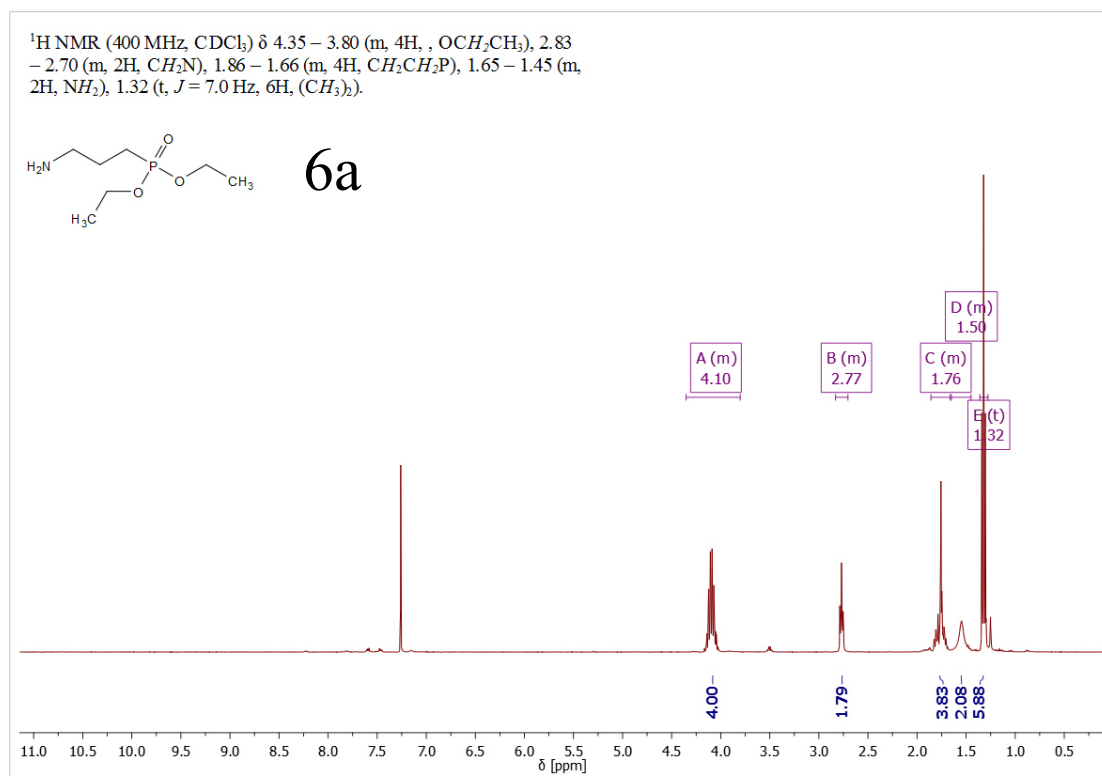
Figure S13: ¹³C NMR of 3a.Figure S14: ¹H NMR of 3b.

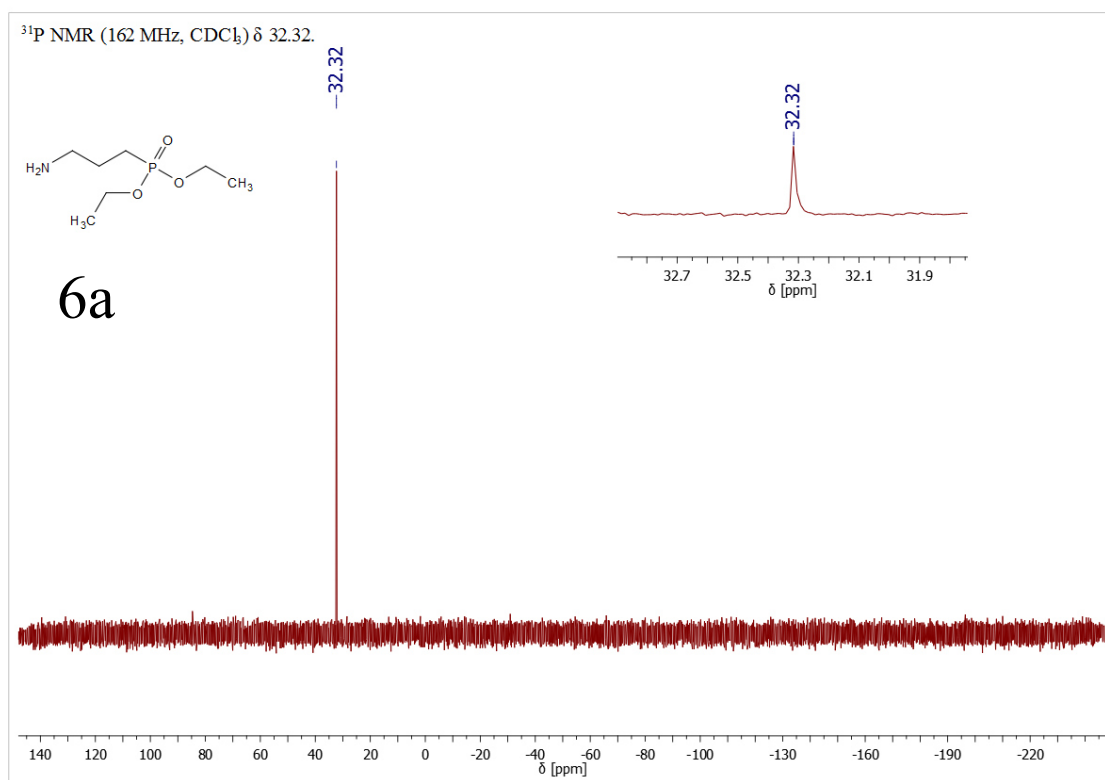
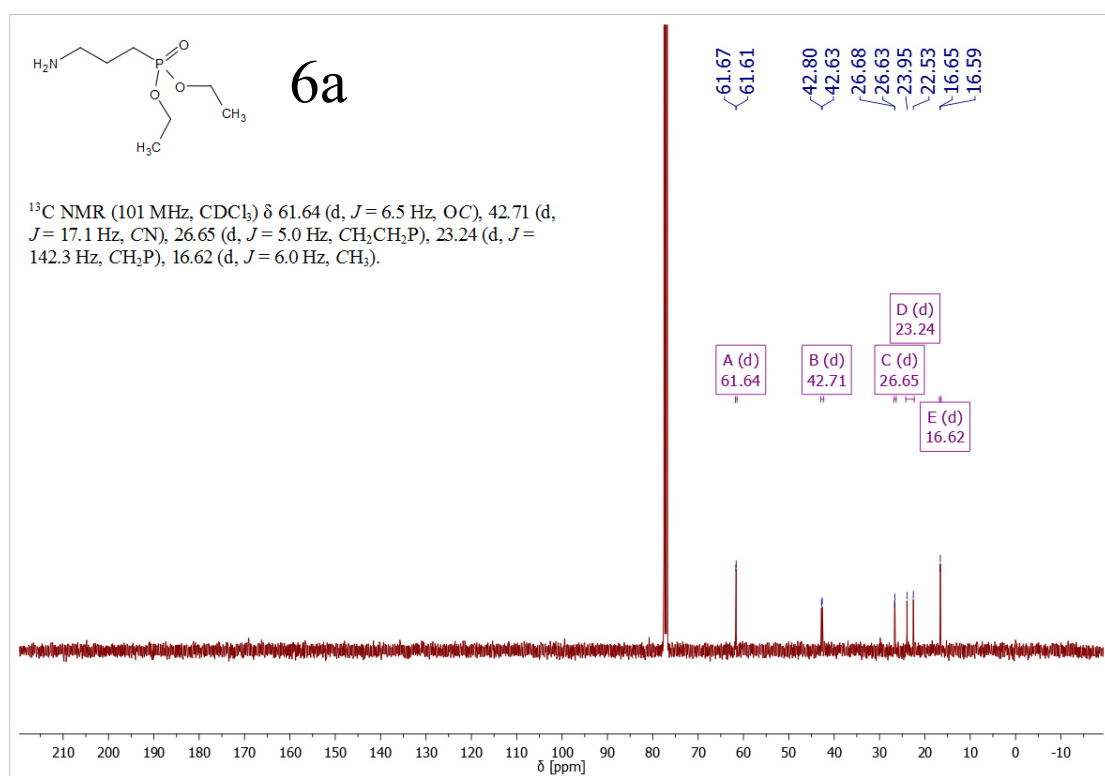
Figure S15: ³¹P NMR of 3b.Figure S16: ¹³C NMR of 3b.

Figure S17: ¹H NMR of **4**.Figure S18: ¹H NMR of **5a**.

Figure S19: ^{31}P NMR of 5a.Figure S20: ^{13}C NMR of 5a.

Figure S21: ¹H NMR of 5b.Figure S22: ³¹P NMR of 5b.

Figure S23: ¹³C NMR of 5b.Figure S24: ¹H NMR of 6a.

Figure S25: ³¹P NMR of 6a.Figure S26: ¹³C NMR of 6a.

^1H NMR (400 MHz, CDCl_3) δ 4.16 – 3.97 (m, 4H), 2.69 (t, $J = 7.1$ Hz, 2H), 2.21 (s, 2H), 1.77 – 1.65 (m, 2H), 1.64 – 1.51 (m, 2H), 1.44 (dd, $J = 13.6, 6.7$ Hz, 2H), 1.40 – 1.21 (m, 18H).

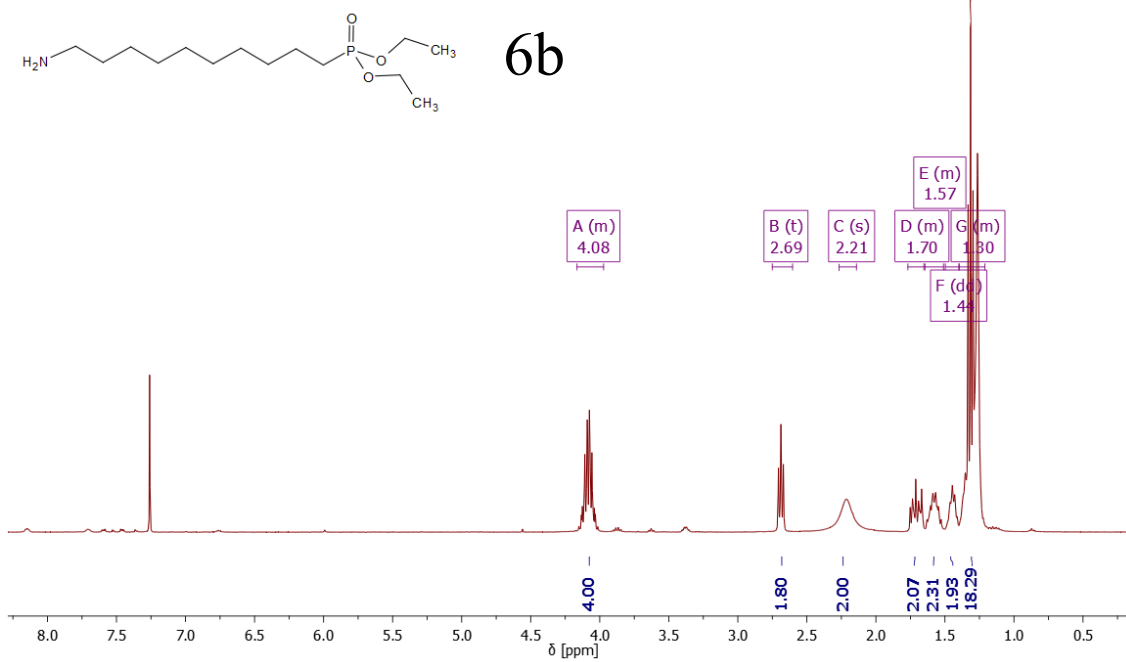


Figure S27: ^1H NMR of **6b**.

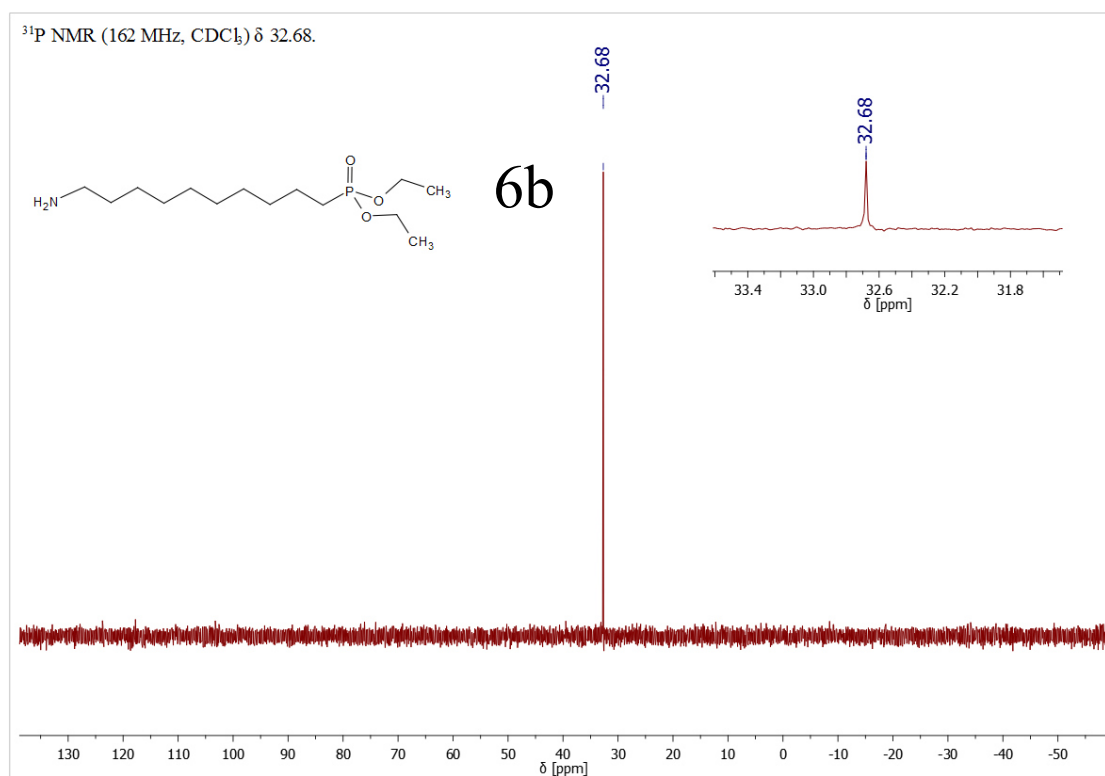
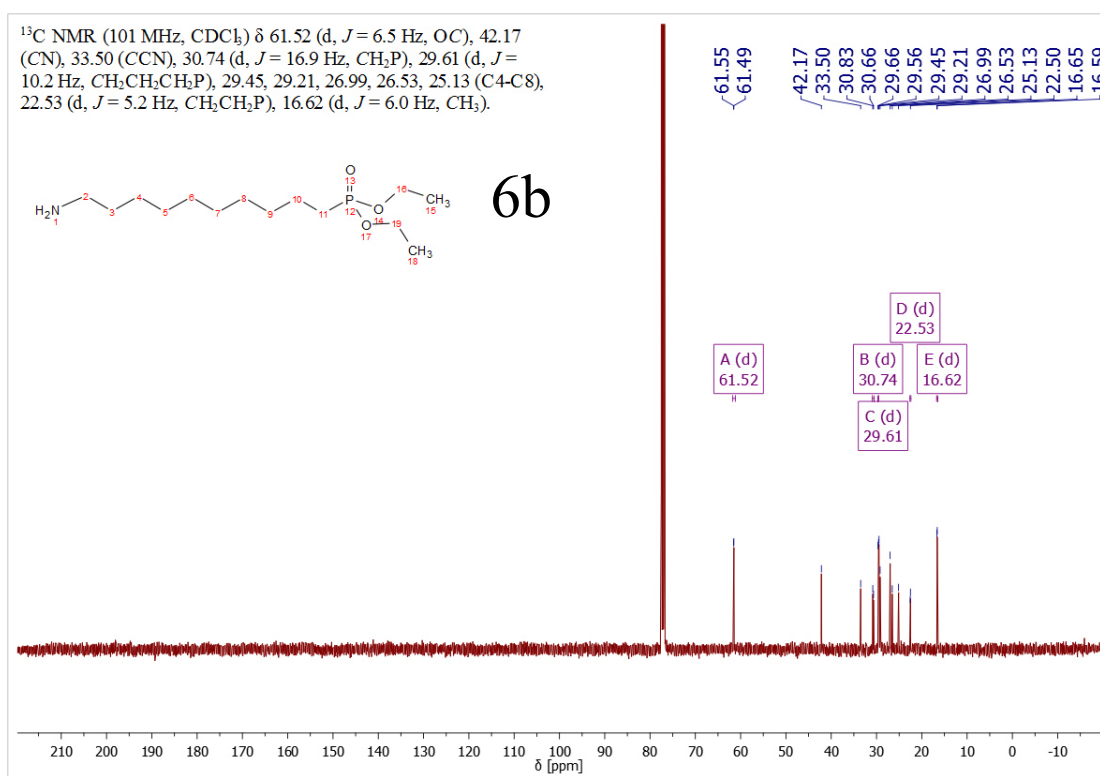
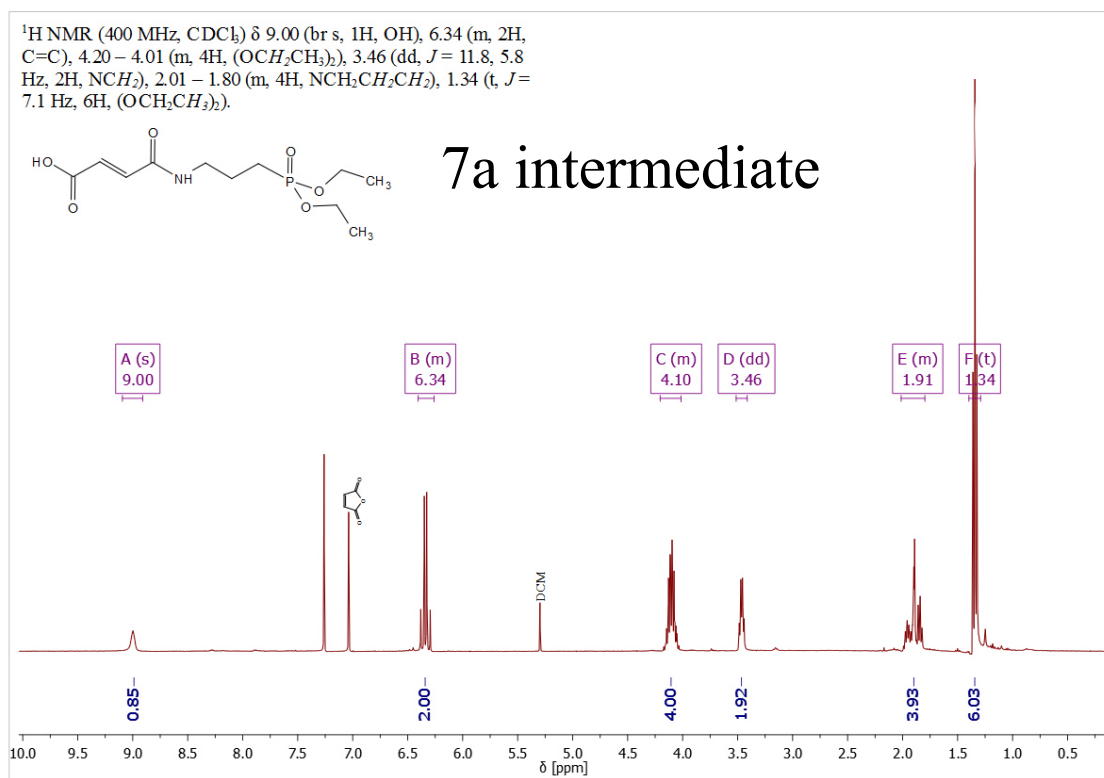
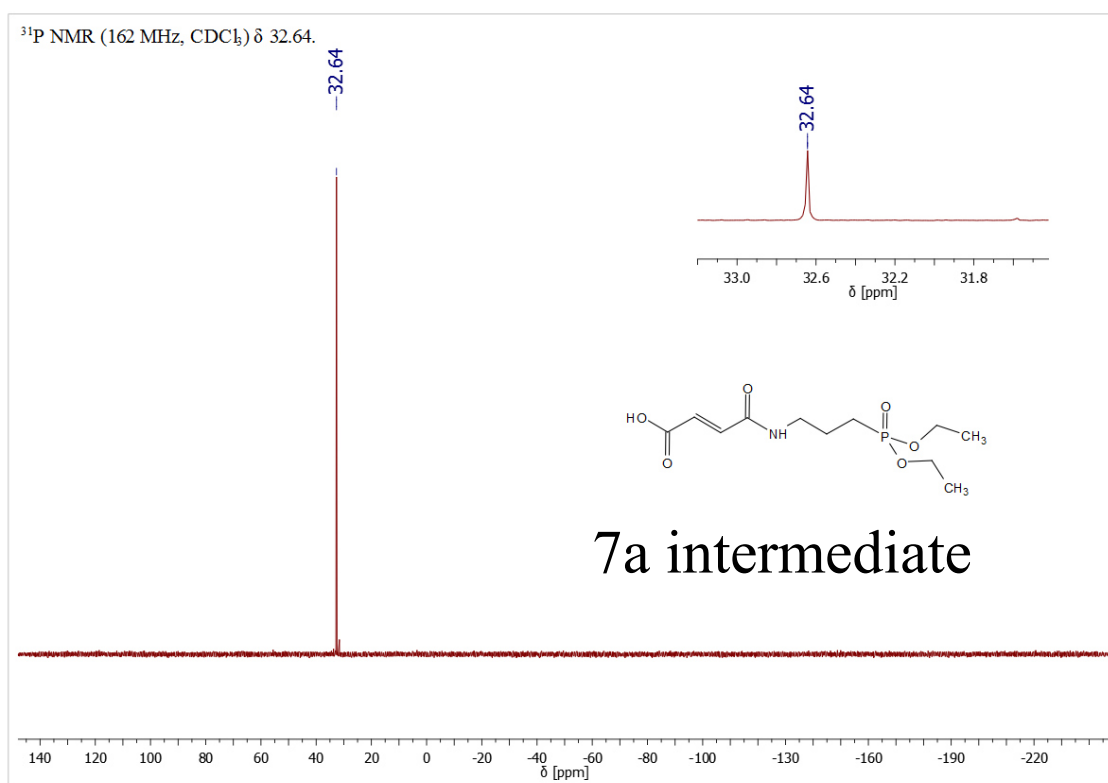
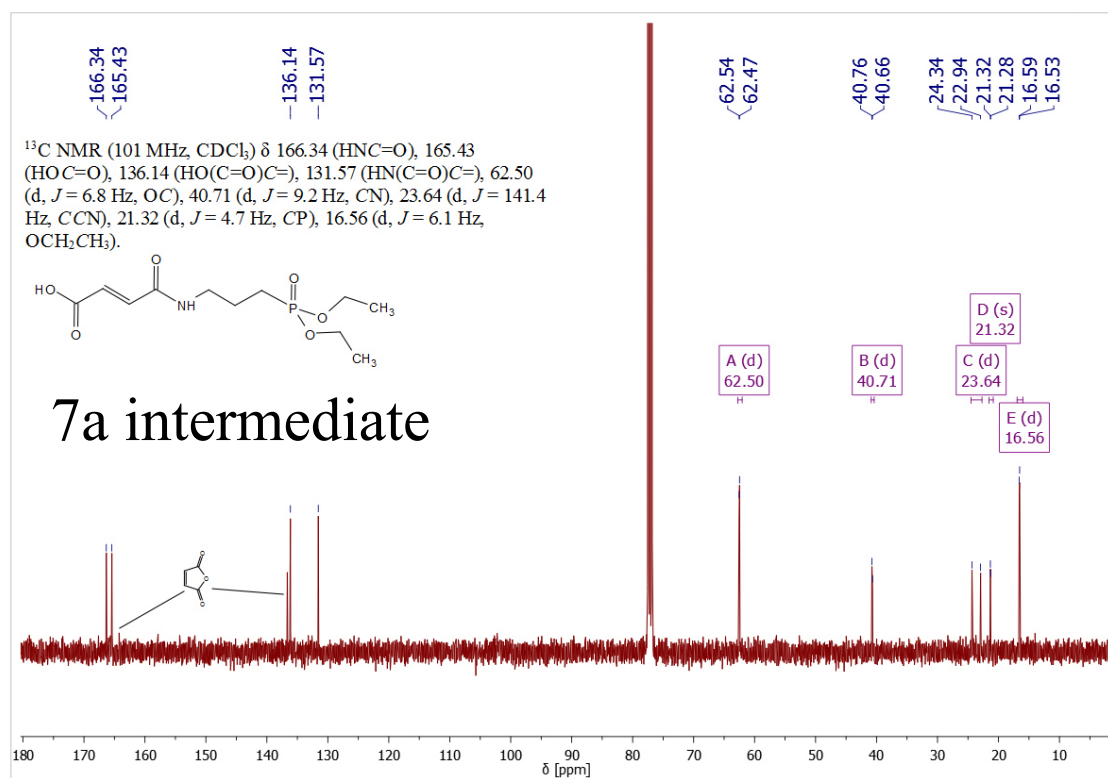
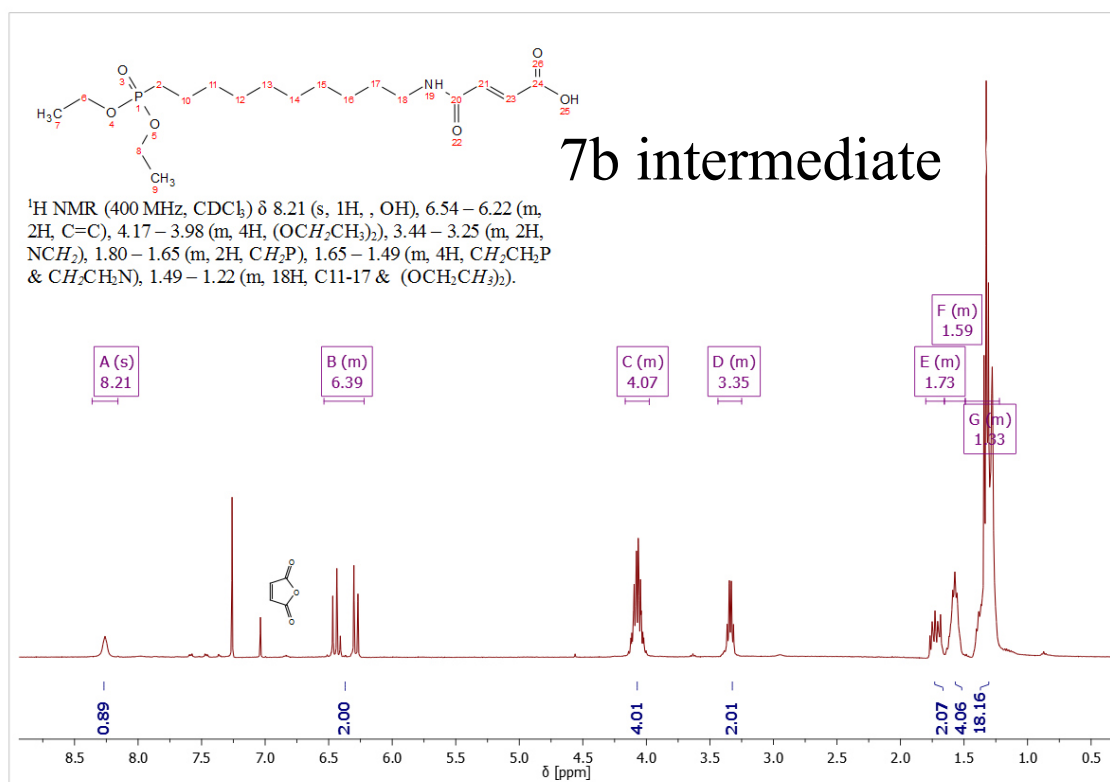
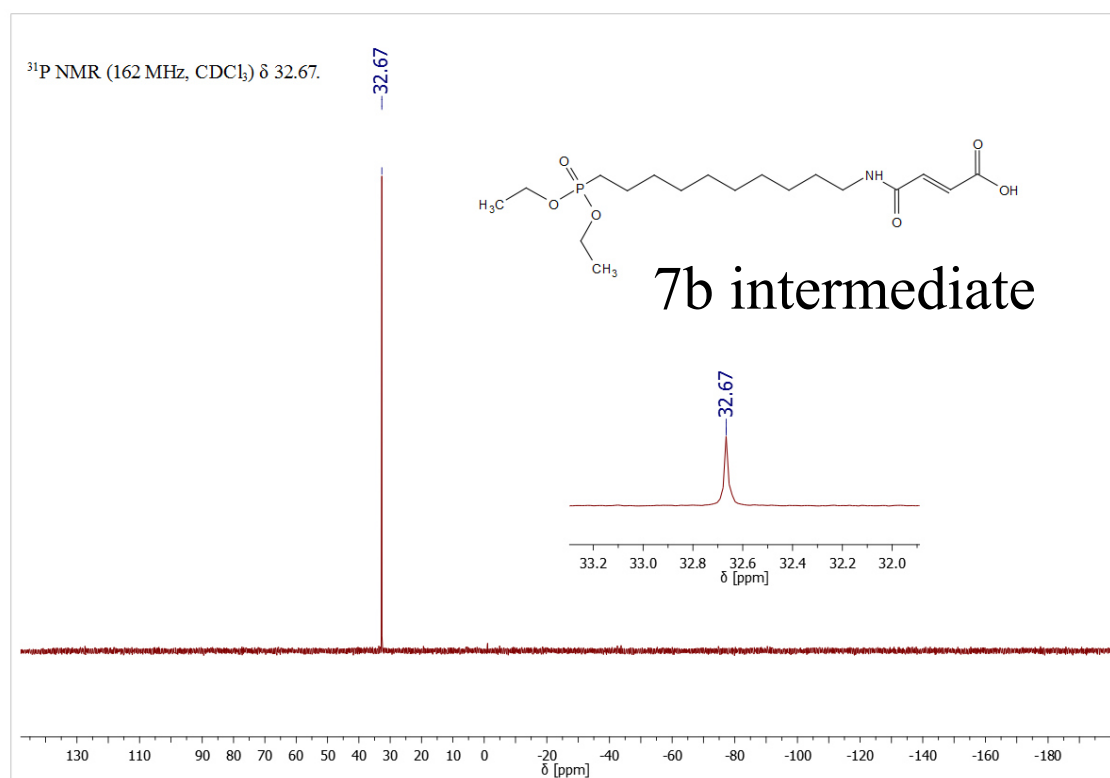
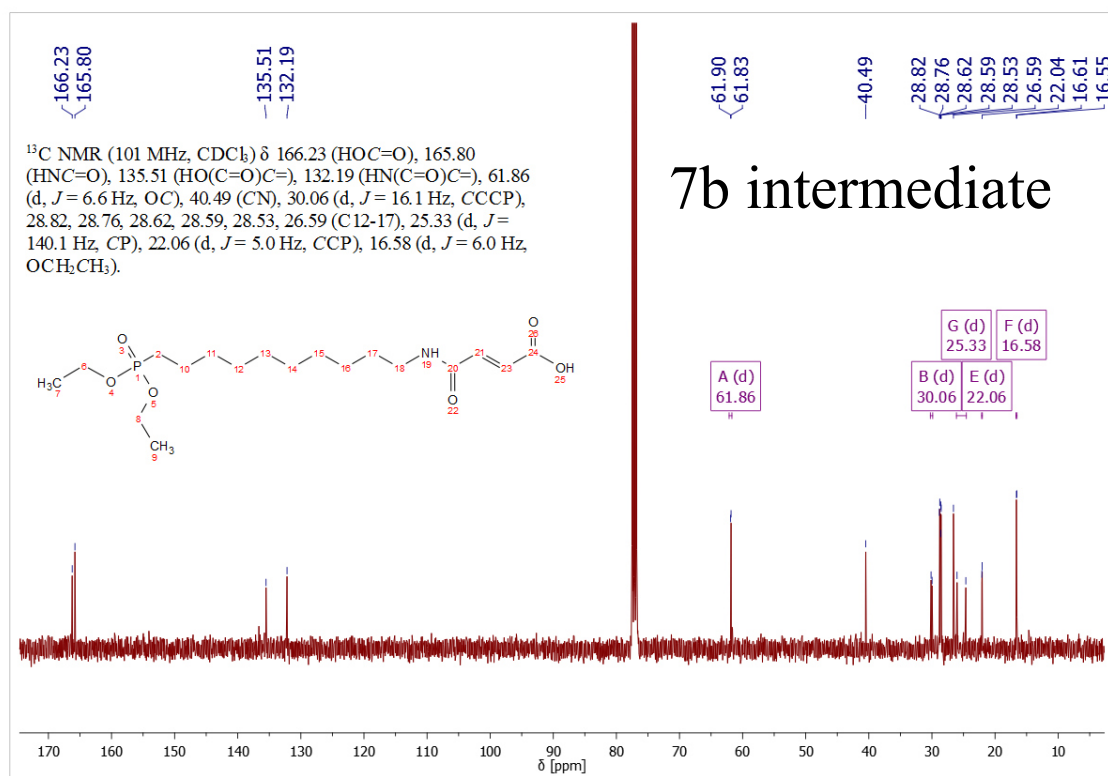
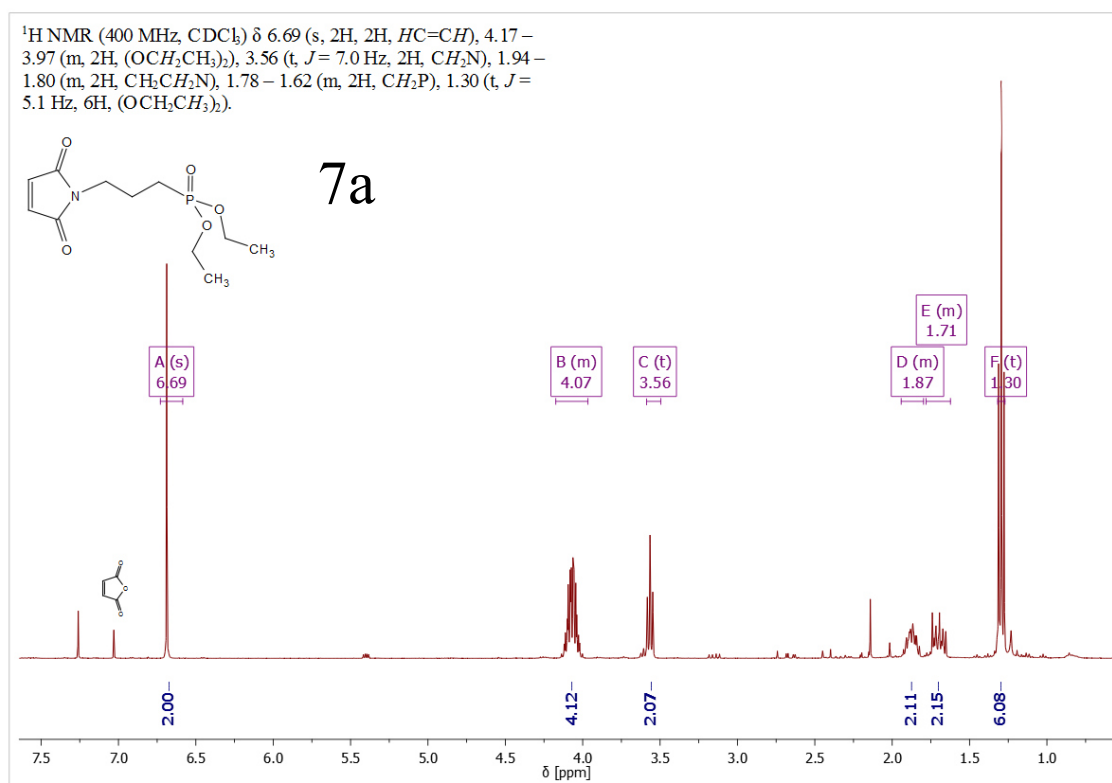


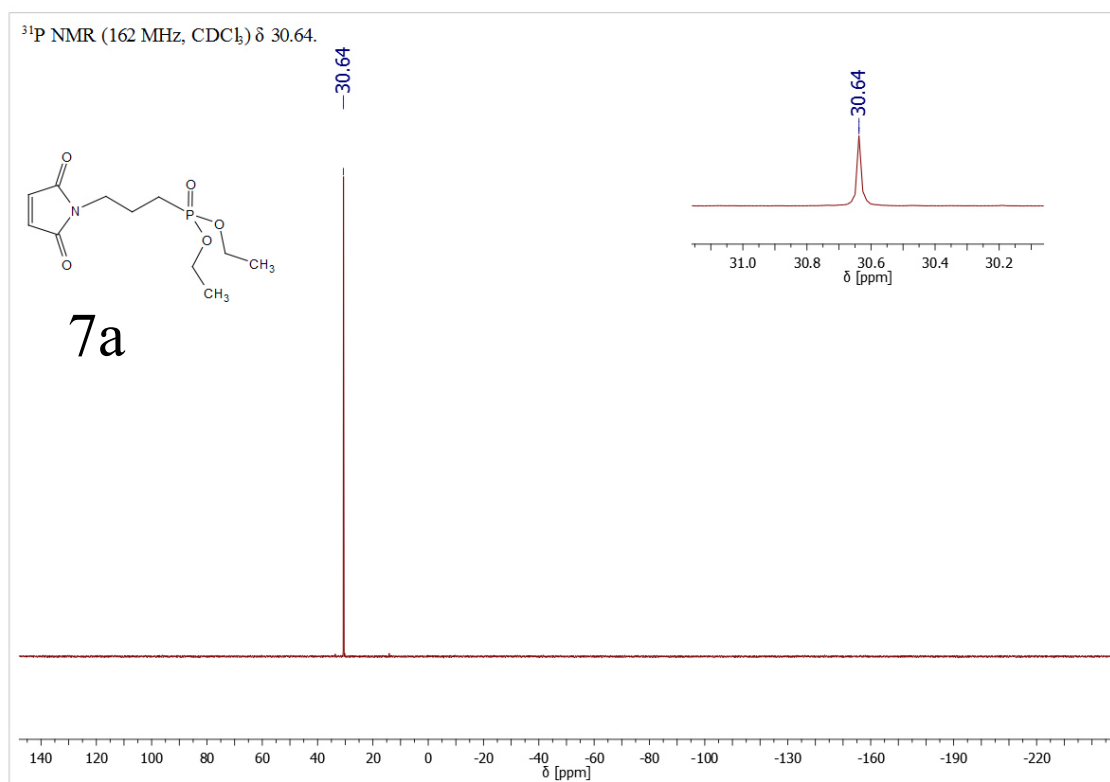
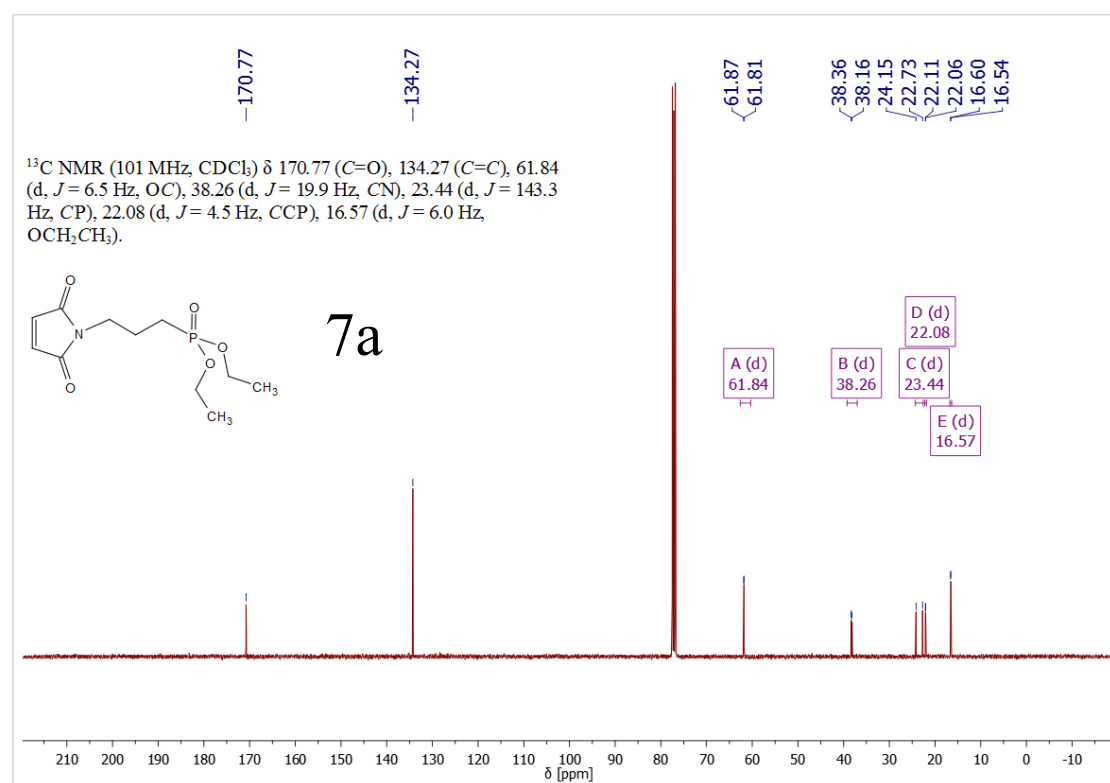
Figure S28: ^{31}P NMR of **6b**.

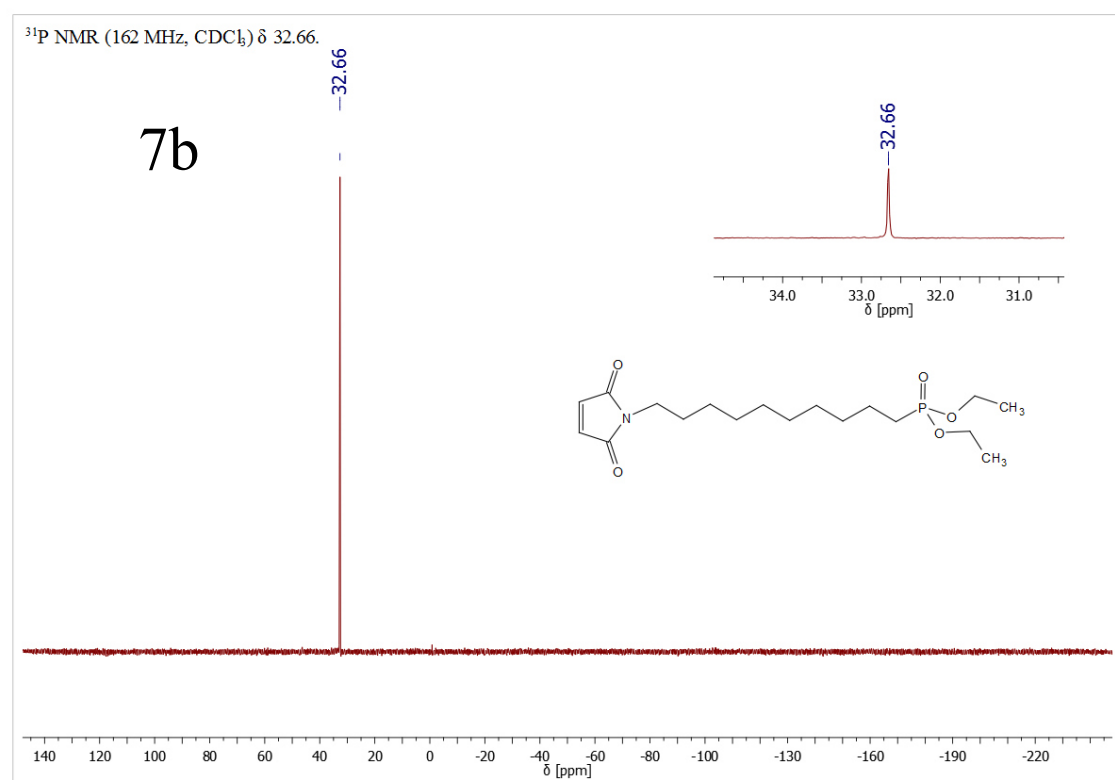
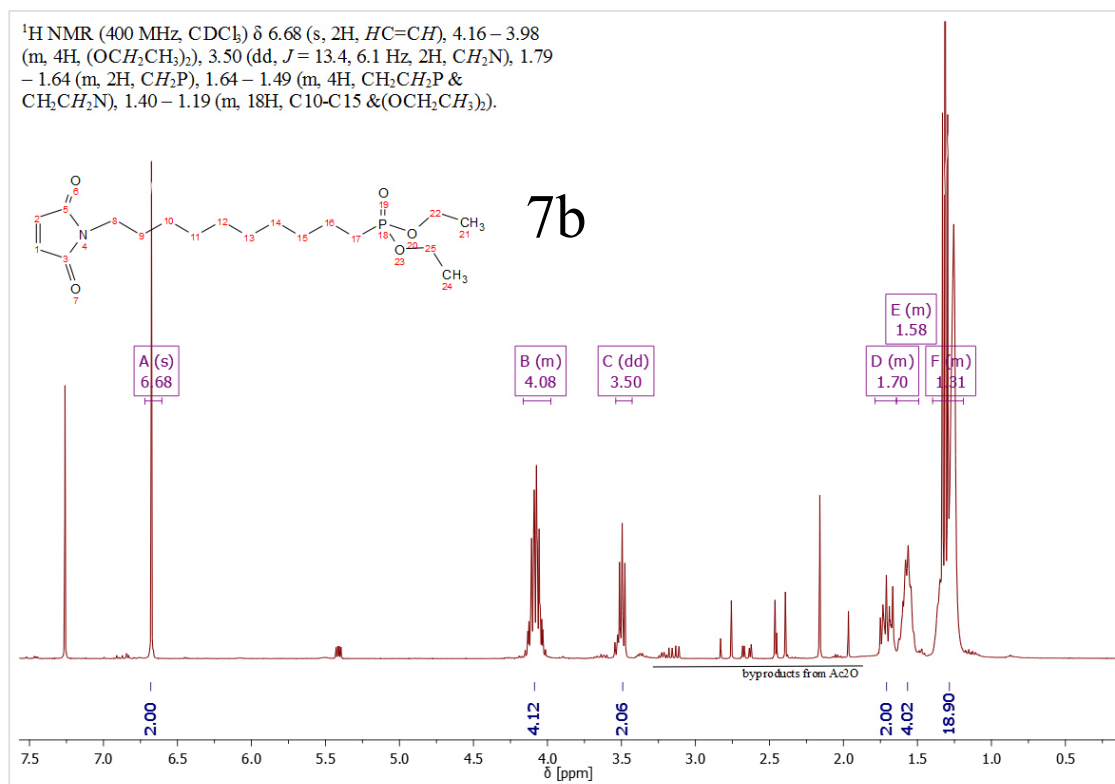
Figure S29: ¹³C NMR of 6b.Figure S30: ¹H NMR of 7a intermediate.

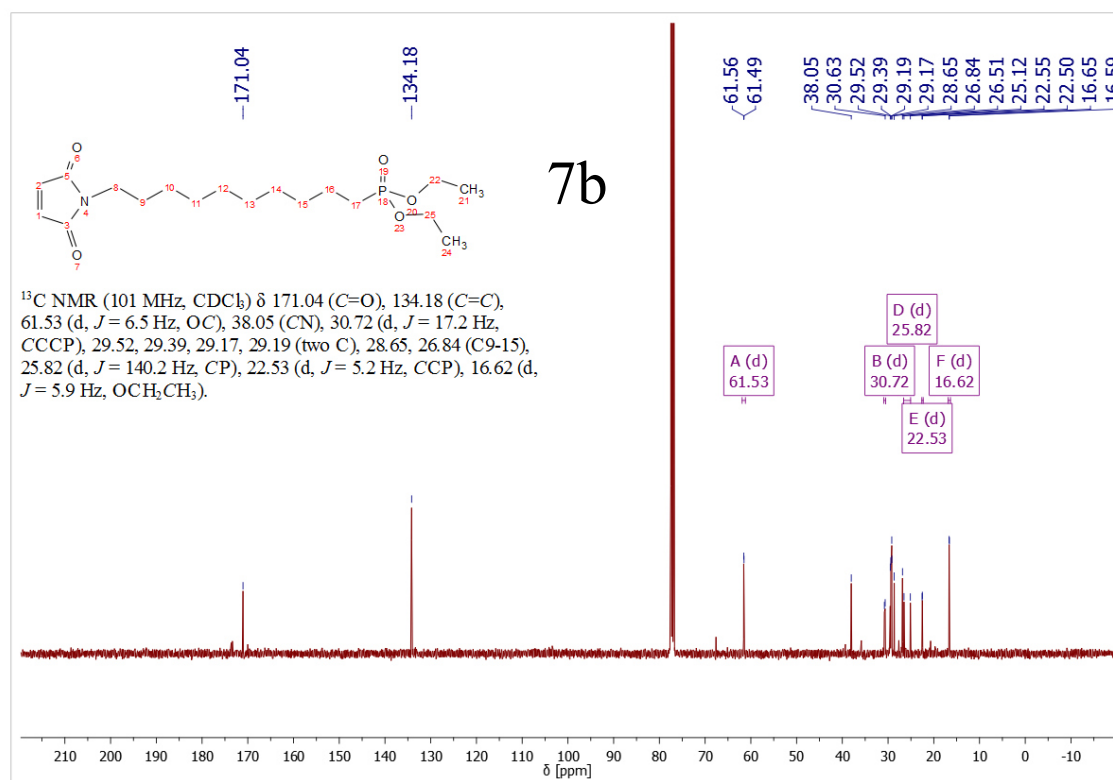
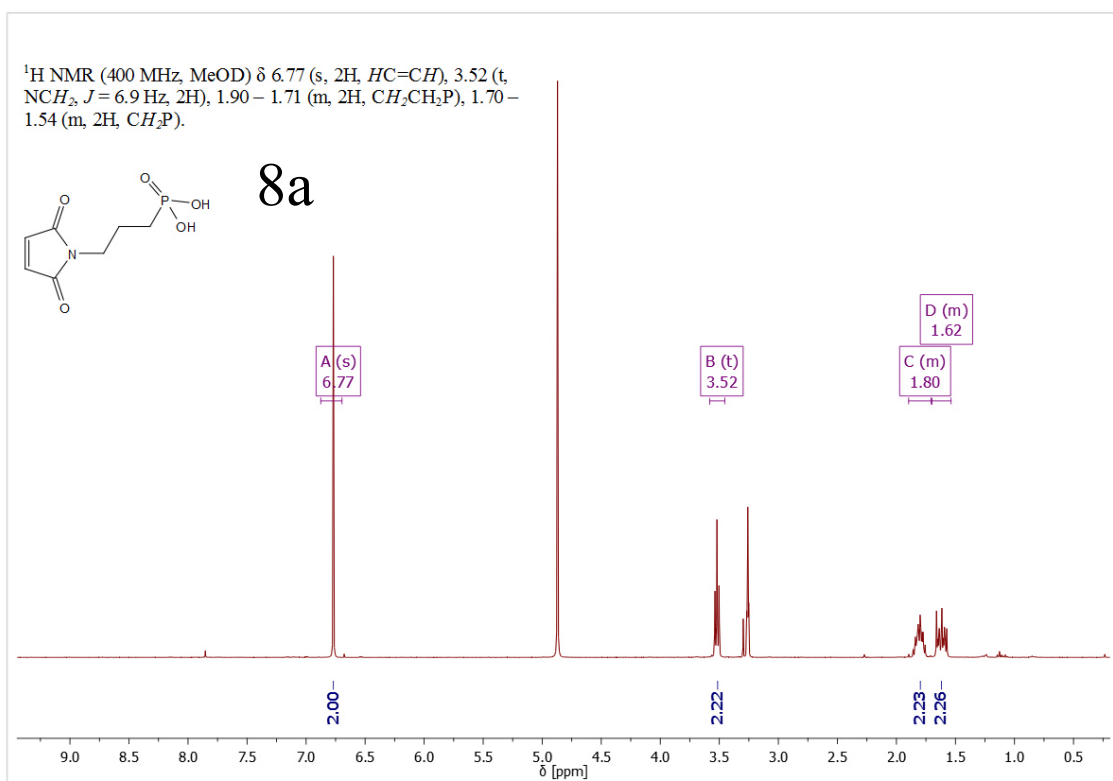
Figure S31: ^{31}P NMR of 7a intermediate.Figure S32: ^{13}C NMR of 7a intermediate.

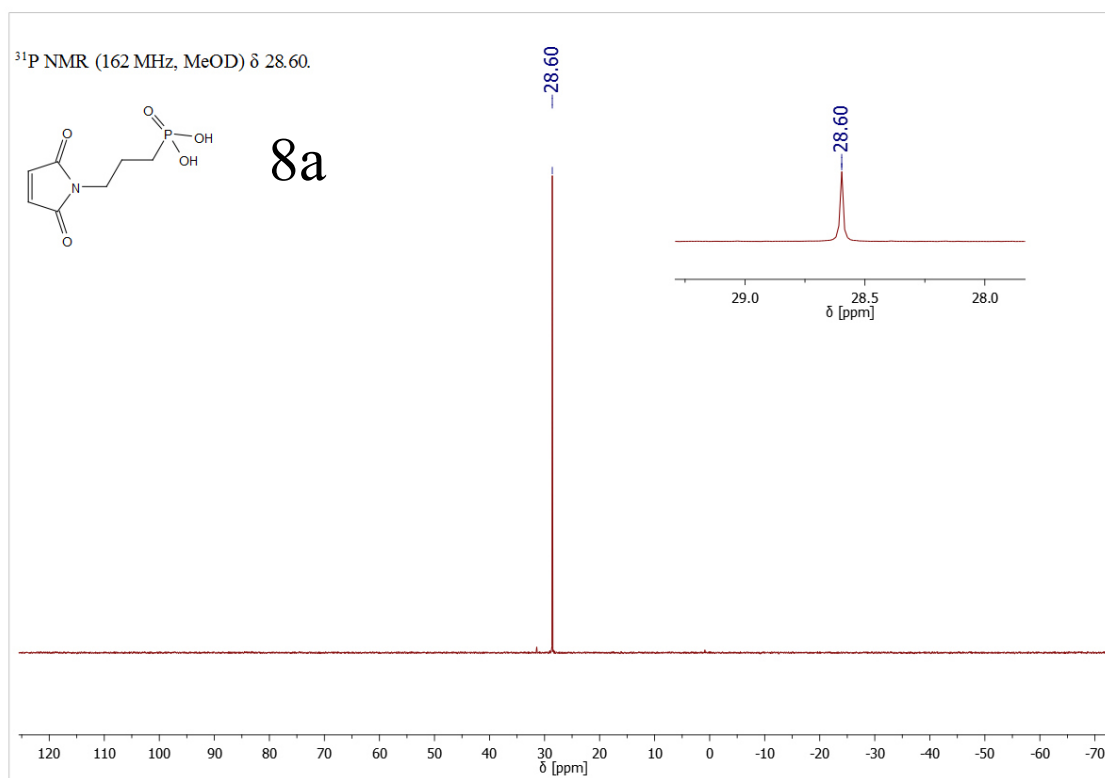
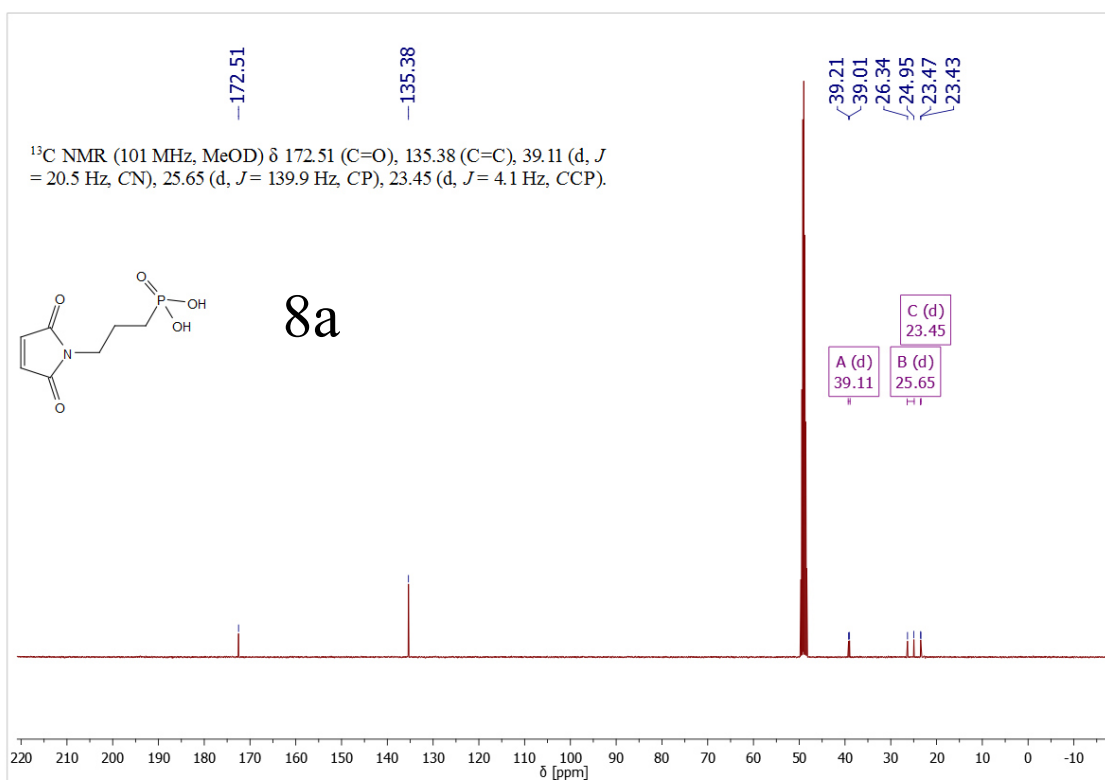
Figure S33: $^1\text{H NMR}$ of 7b intermediate.Figure S34: $^{31}\text{P NMR}$ of 7b intermediate.

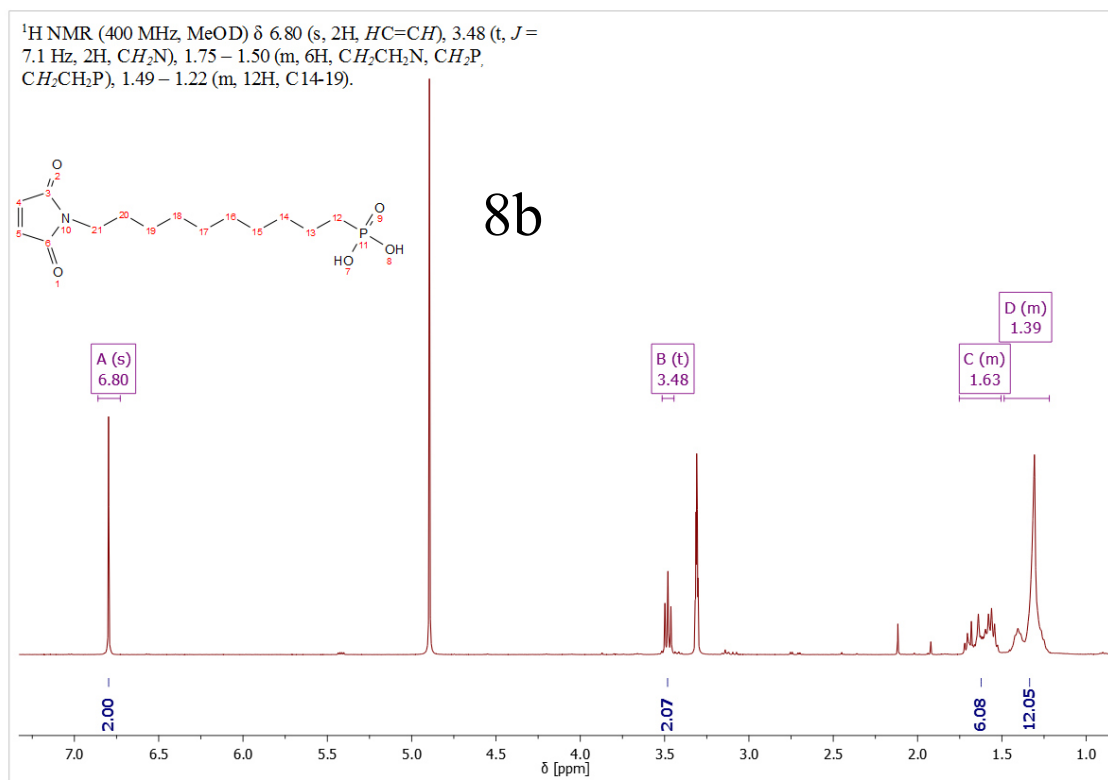
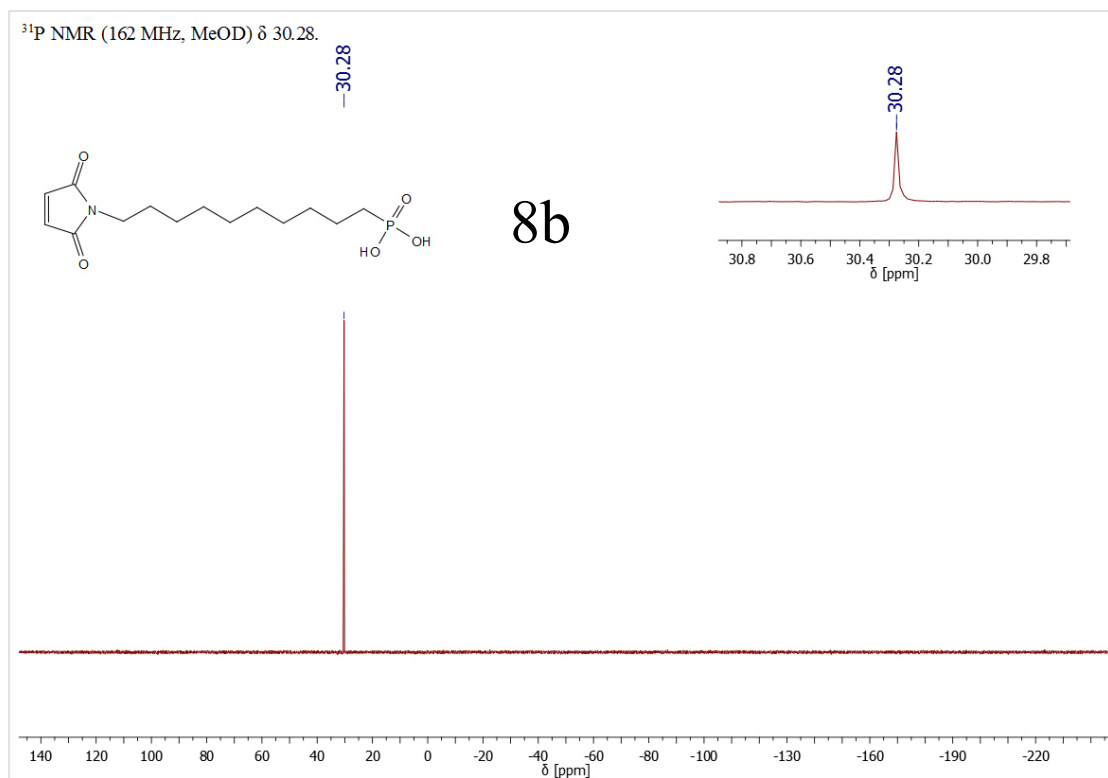
Figure S35: ¹³C NMR of 7b intermediate.Figure S36: ¹H NMR of 7a.

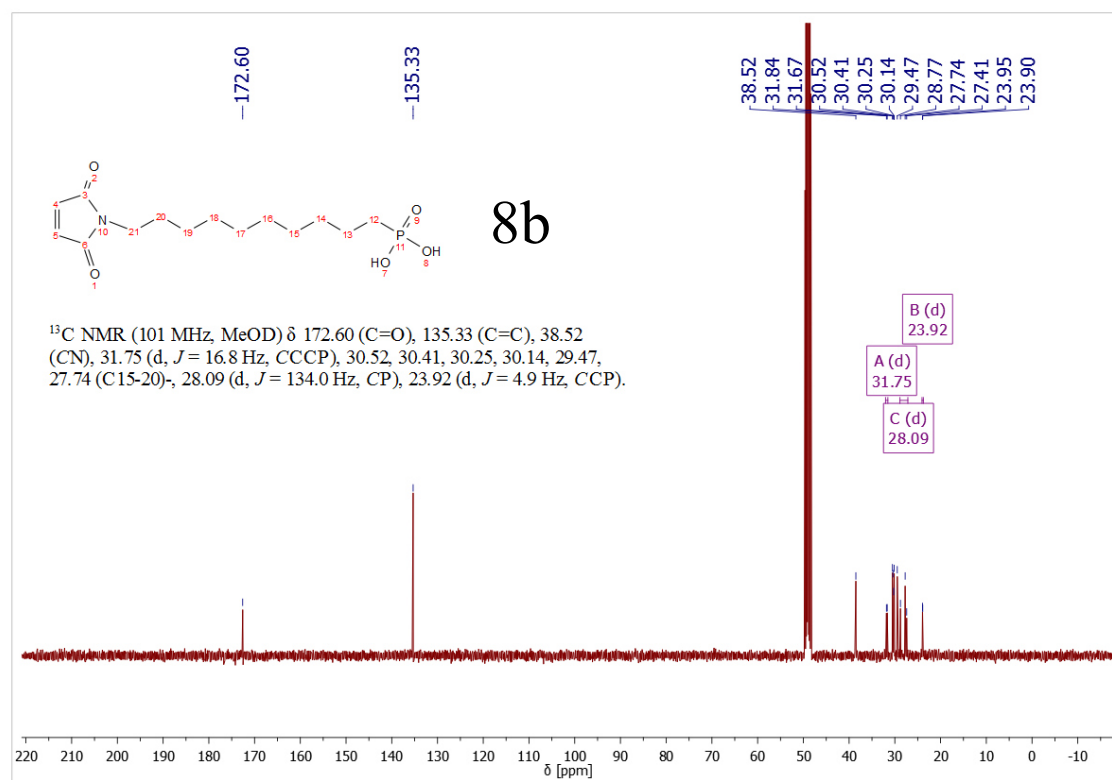
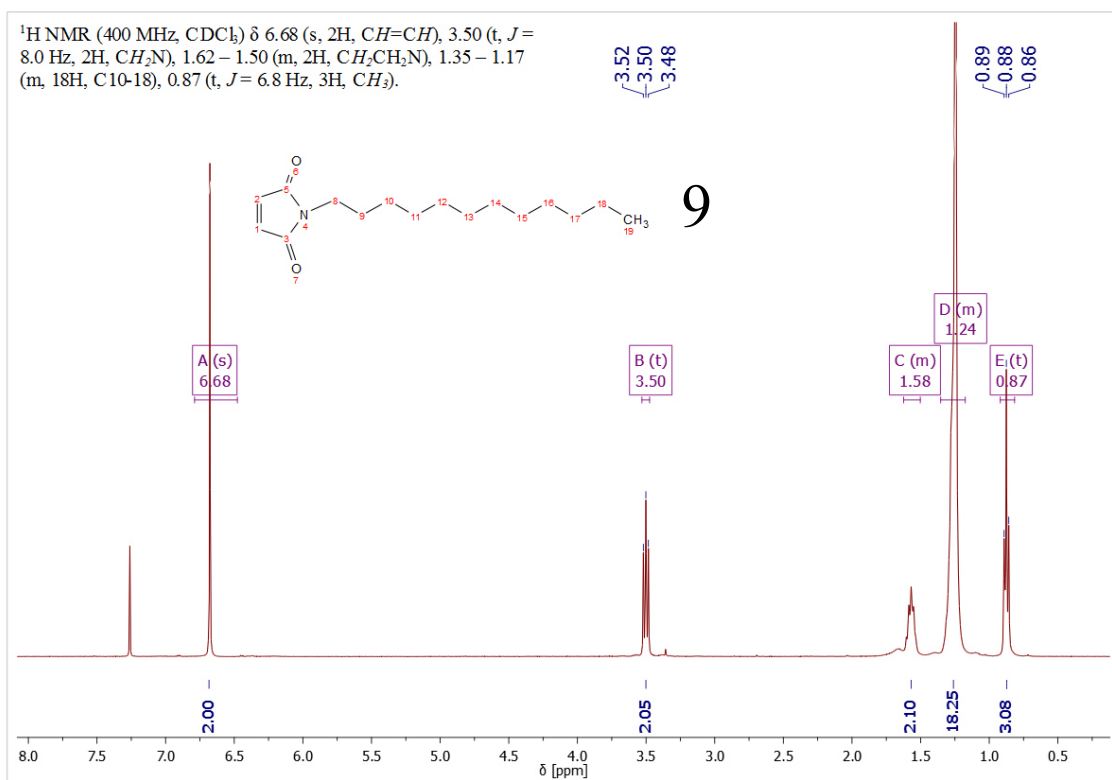
Figure S37: ³¹P NMR of **7a**.Figure S38: ¹³C NMR of **7a**.

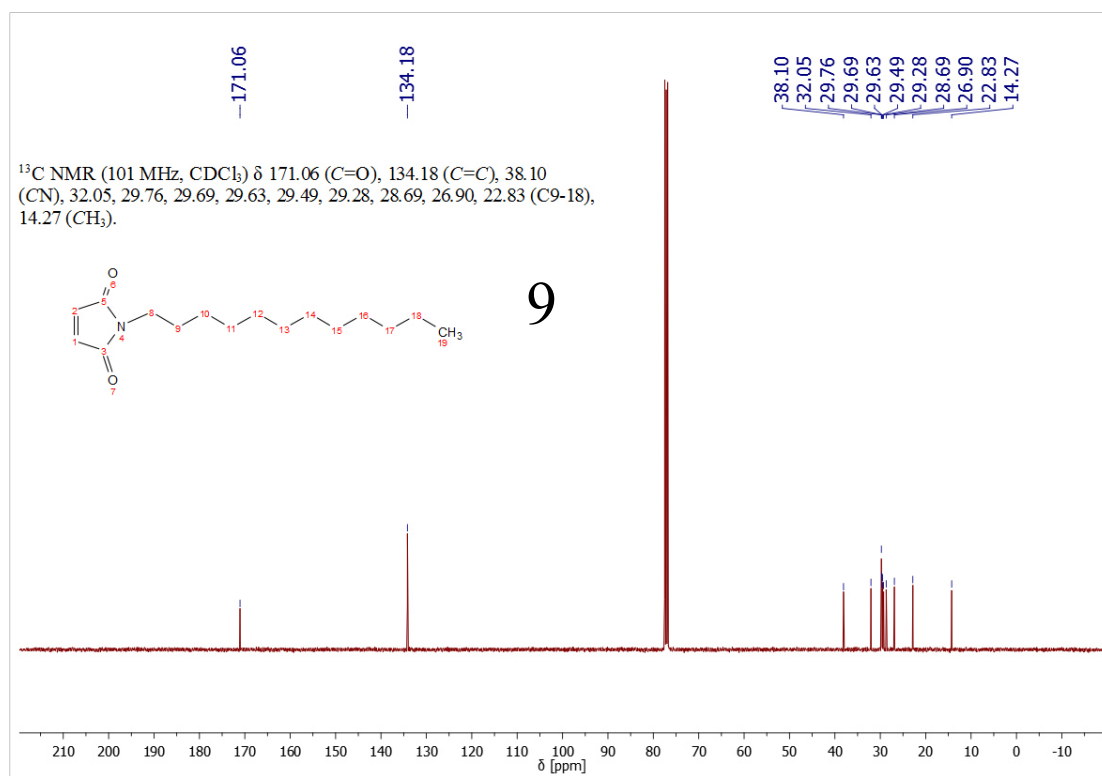
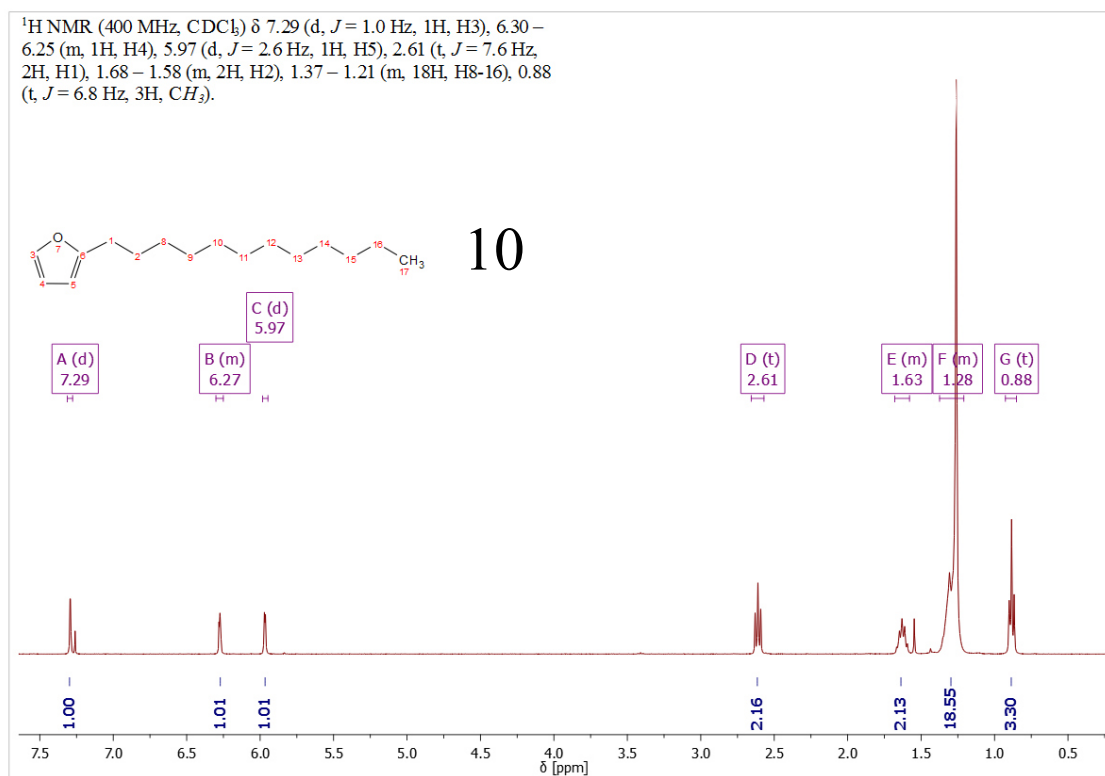


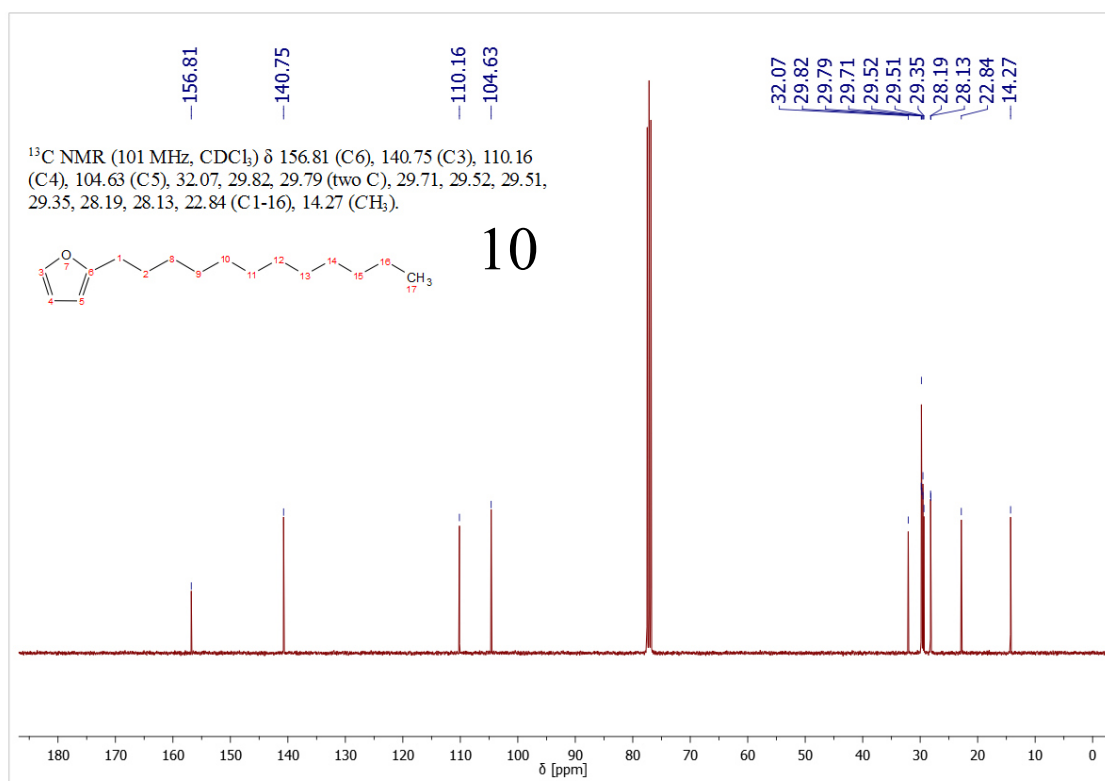
Figure S41: ^{13}C NMR of 7b.Figure S42: ^1H NMR of 8a.

Figure S43: ³¹P NMR of **8a**.Figure S44: ¹³C NMR of **8a**.

Figure S45: ¹H NMR of 8b.Figure S46: ³¹P NMR of 8b.

Figure S47: ^{13}C NMR of 8b.Figure S48: ^1H NMR of 9.

Figure S49: ^{13}C NMR of 9.Figure S50: ^1H NMR of 10.

Figure S51: ¹³C NMR of 10.

2. FTIR spectra of synthesized molecules (1-10)

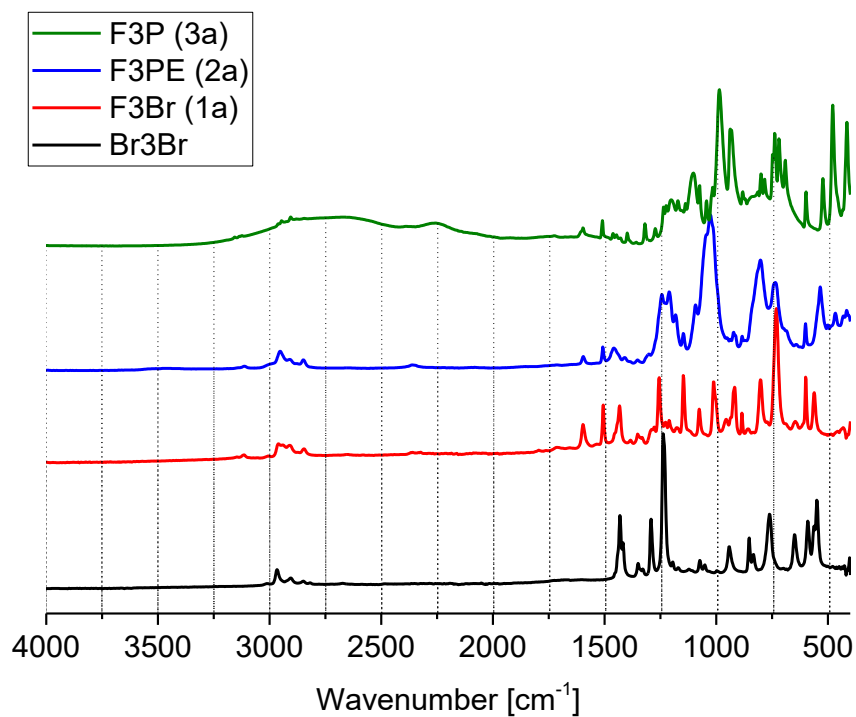


Figure S52: IR spectra of 1a-3a.

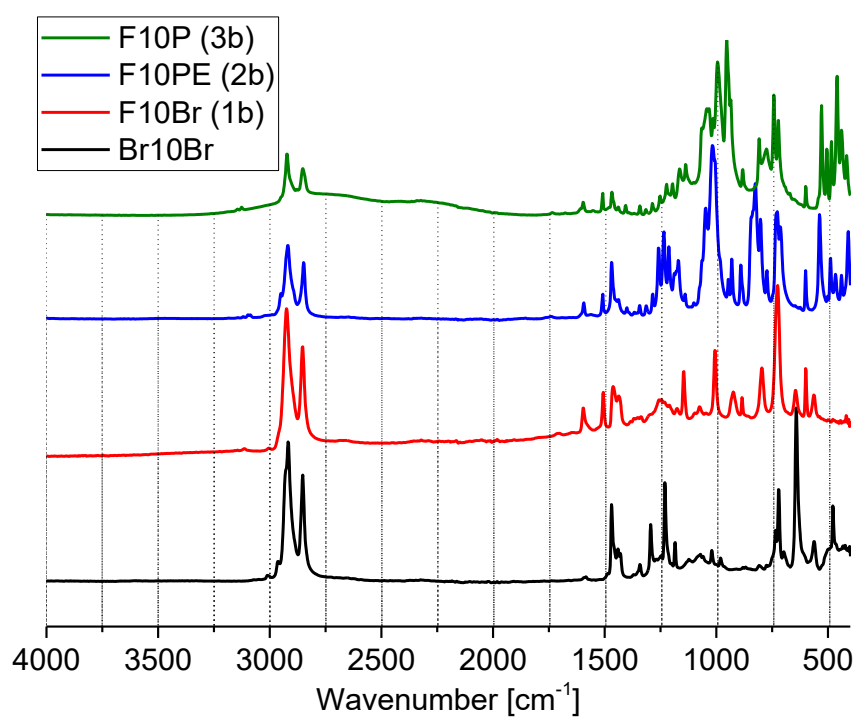
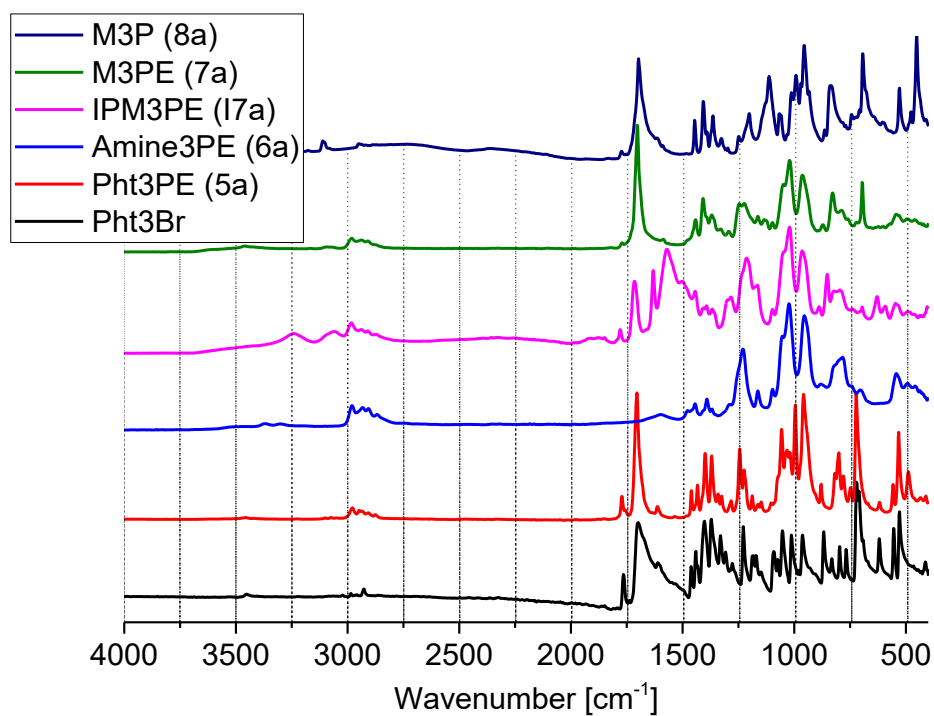
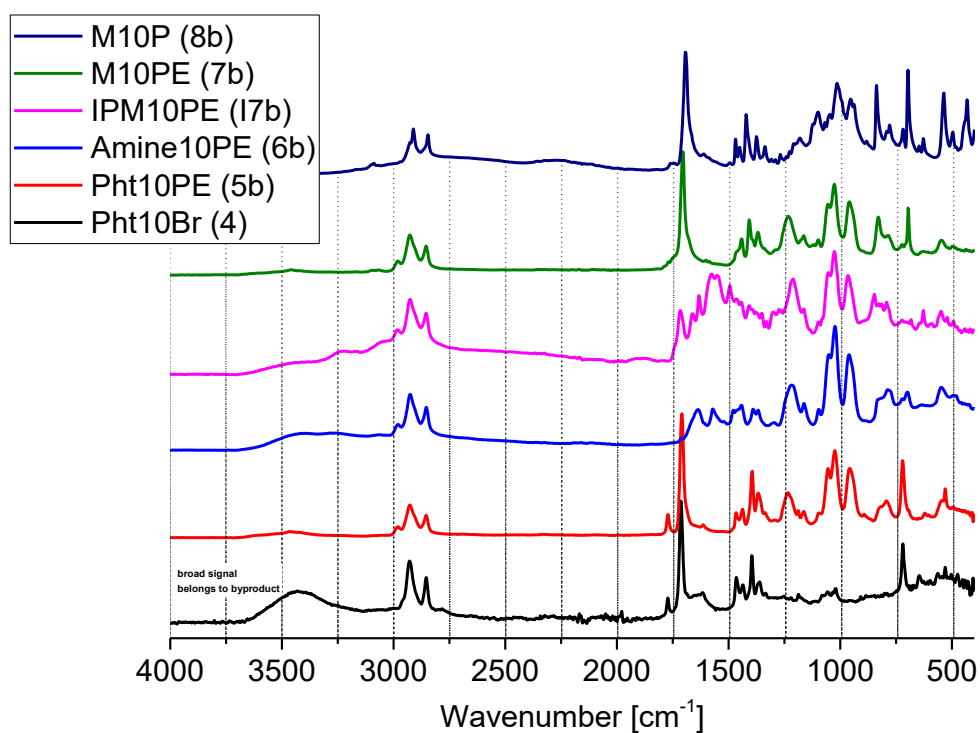


Figure S53: IR spectra of 1b-3b.

**Figure S54:** IR spectra of 5a-8a.**Figure S55:** IR spectra of 4, 5b-8b.

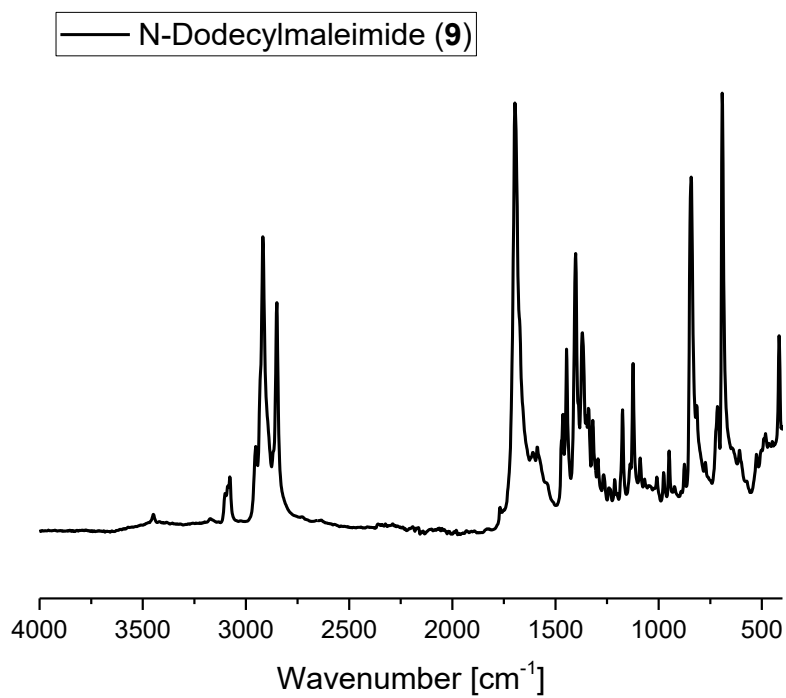


Figure S56: IR spectrum of **9**.

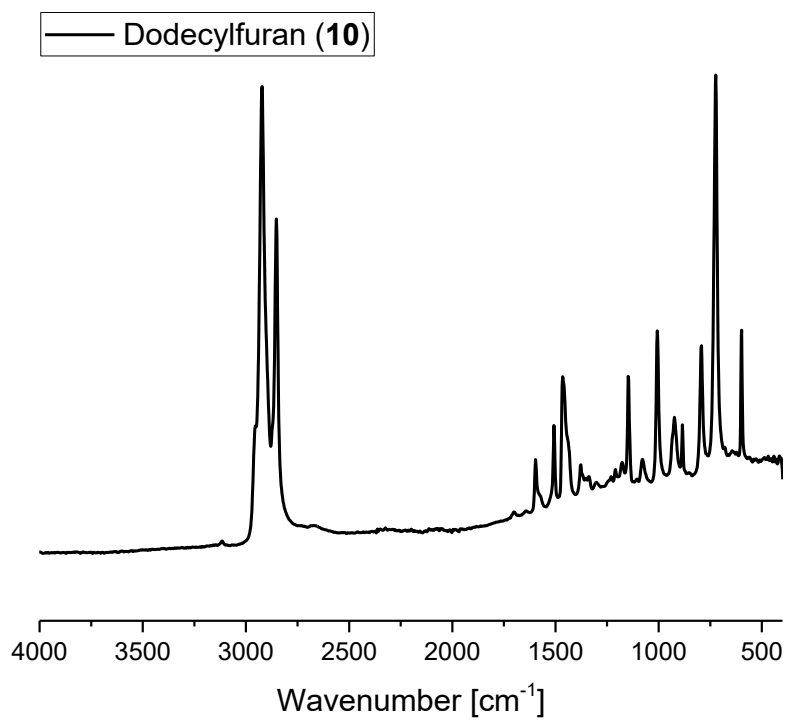


Figure S57: IR spectrum of **10**.

3. Molecular structure of F10PE (2b) and F10P (3b) as obtained by single crystal X-ray diffraction analysis

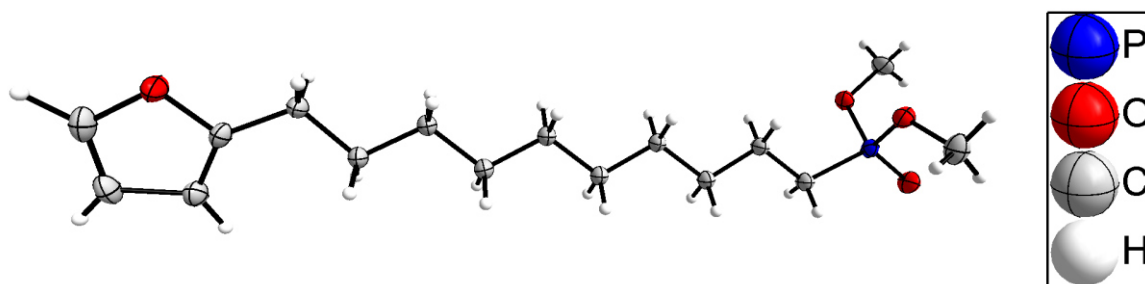


Figure S58: Crystal Structure of furandecyl phosphonic acid ester (**2b**)

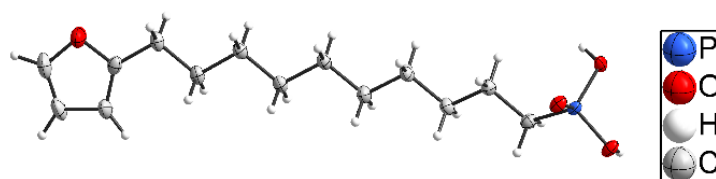


Figure S59: Crystal Structure of furandecyl phosphonic acid (**3b**)

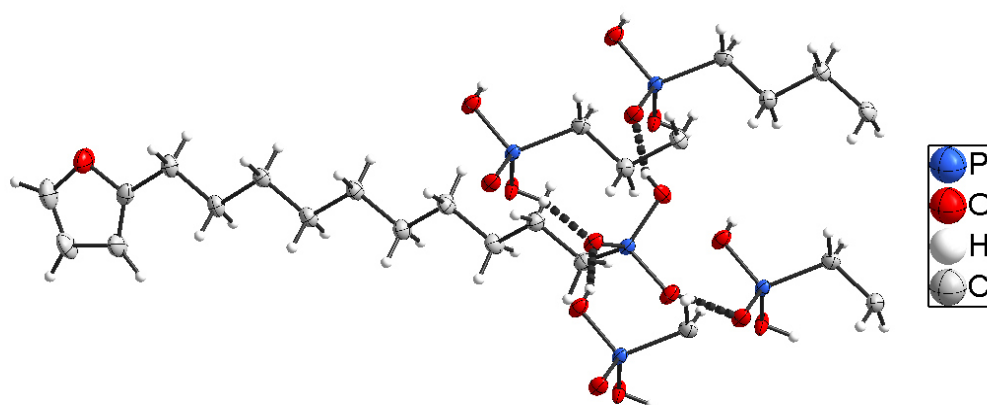


Figure S60: Crystal Structure of furandecyl phosphonic acid (**3b**)

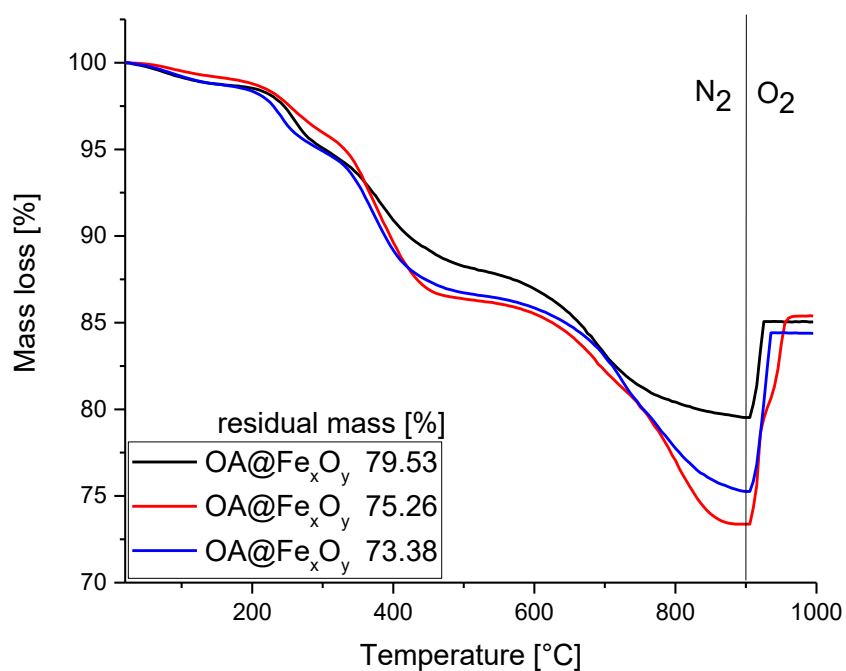
4. OA@Fe_xO_y: further analytical data: TG, DLS

Figure S61: TG curves of OA@Fe_xO_y from three different batches.

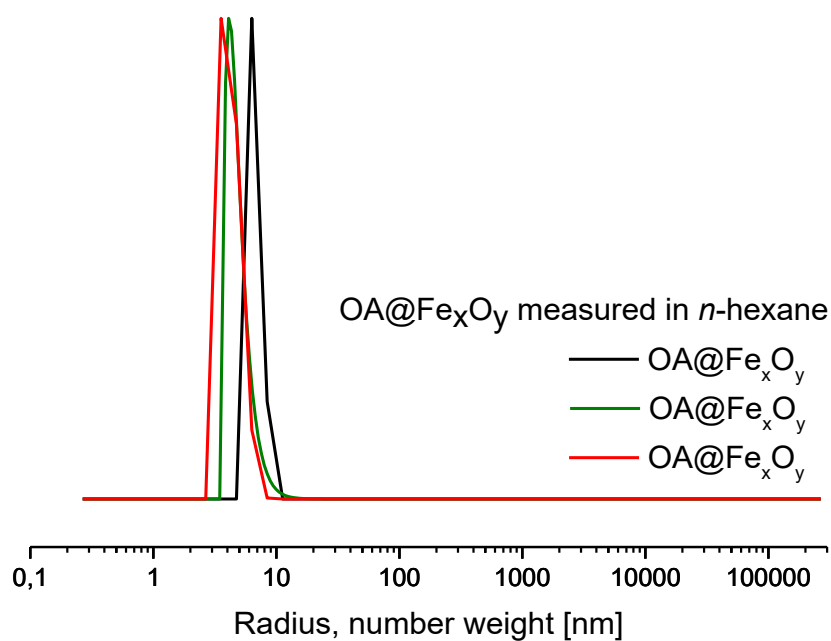


Figure S62: DLS curves of OA@Fe_xO_y from three different batches in *n*-hexane.

5. DDP@Fe_xO_y: further analytical data: TG, XRD

Table S1: Various solvent or solvent mixtures tested for exchange of OA against DDP on Fe _x O _y surface	
solvent	reaction parameters
chloroform	shaking, 12 h, 25°C
toluene/dioxane/water (12:1:8)	stirring, 72 h, 70 °C, Ar
<i>n</i> -hexane/EtOH (1:2)	stirring, 24 h, 25°C
THF	reflux, 12 h, 25°C
CHCl ₃ /DMF (1:1)	stirring, 24 h, 25°C
total volume of solvent: 10 mL; 80 mg OA@Fe _x O _y ; 0.18 mmol DDP.	

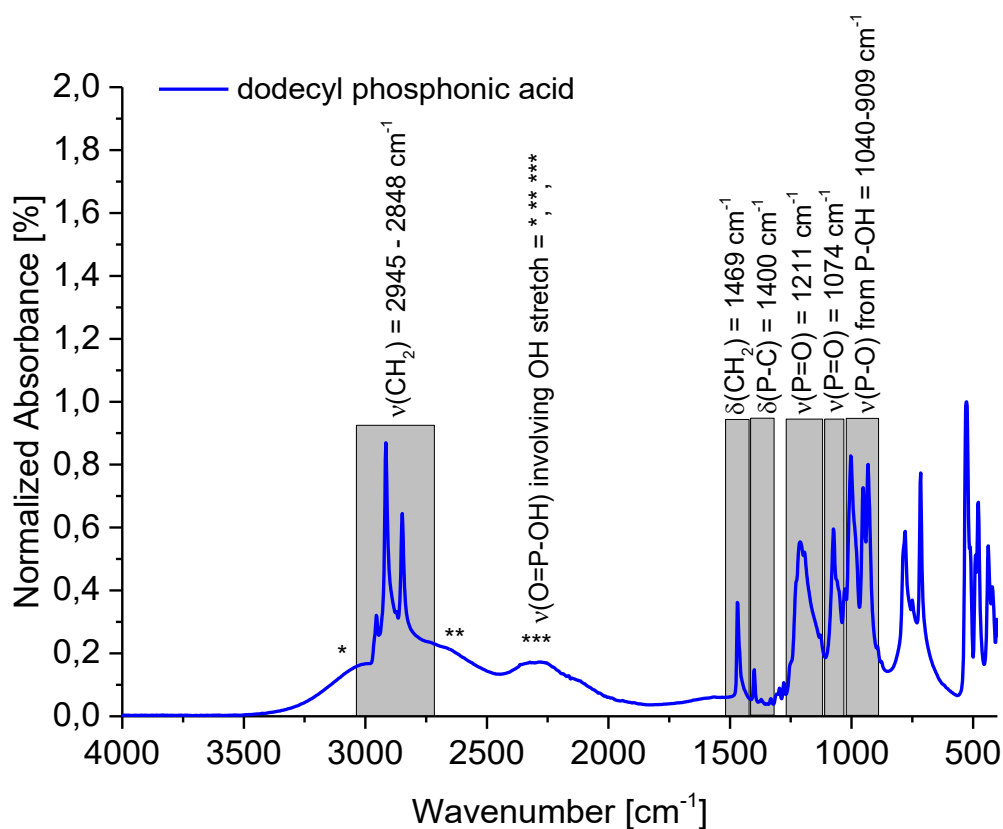


Figure S63: IR spectrum of dodecyl phosphonic acid.

Peaks assigned using following literature the literature given at the end of the document.¹⁻⁵

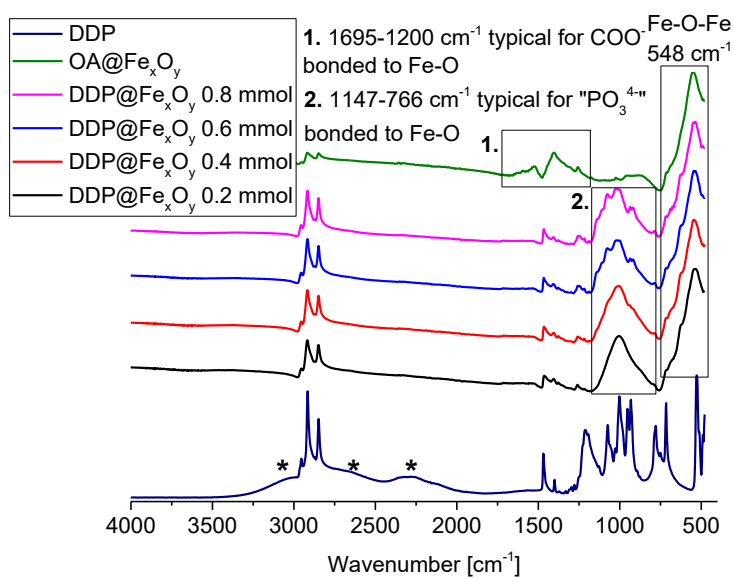


Figure S64: IR spectra of OA@Fe_xO_y vs. DDP@Fe_xO_y (various amounts DDP) and DDP.

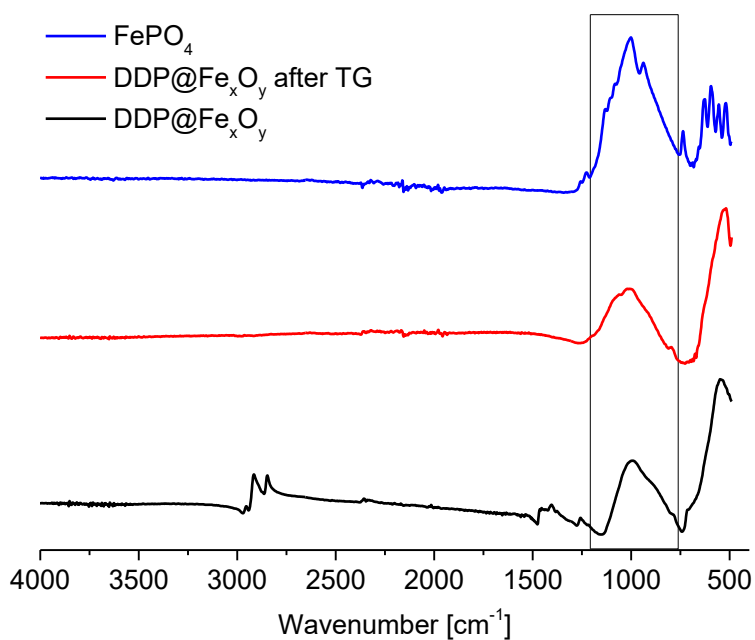


Figure S65: IR spectra of DDP@Fe_xO_y, DDP@Fe_xO_y after TG and commercial FePO₄.

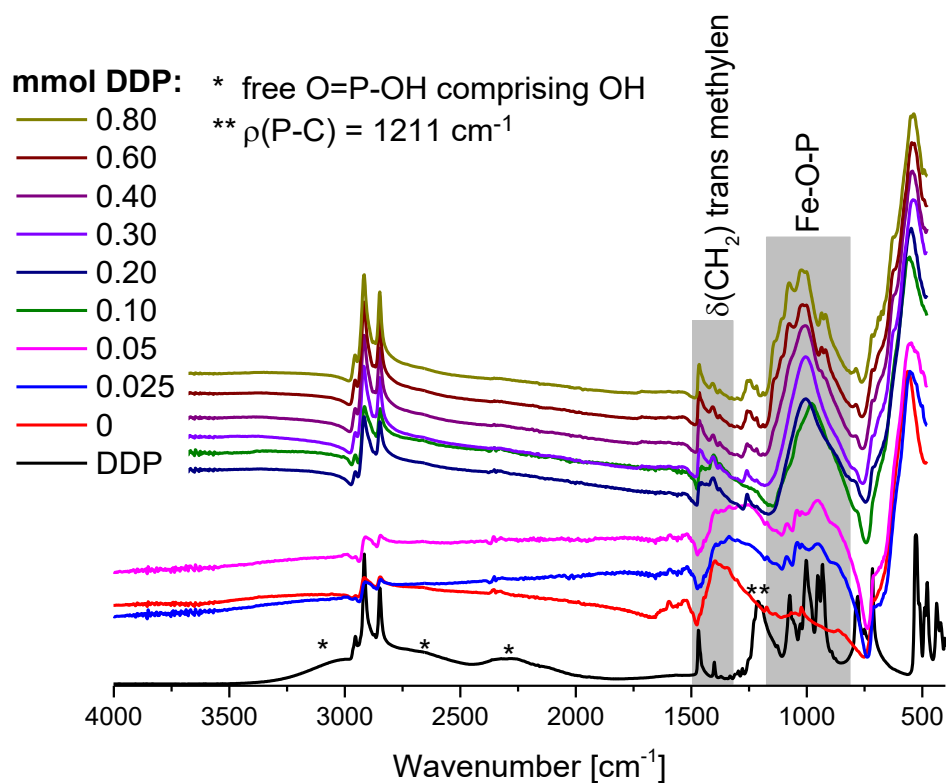


Figure S66: IR spectra of DDP@Fe_xO_y after (various amounts DDP).

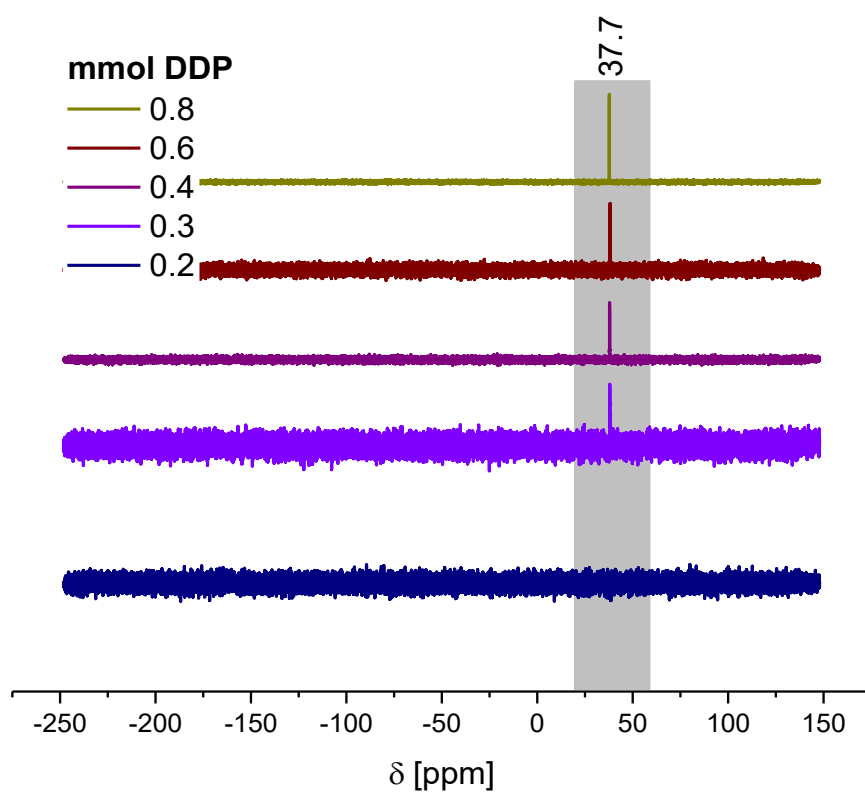


Figure S67: ^{31}P NMR spectra of supernatant of DDP@Fe_xO_y (various amounts DDP).

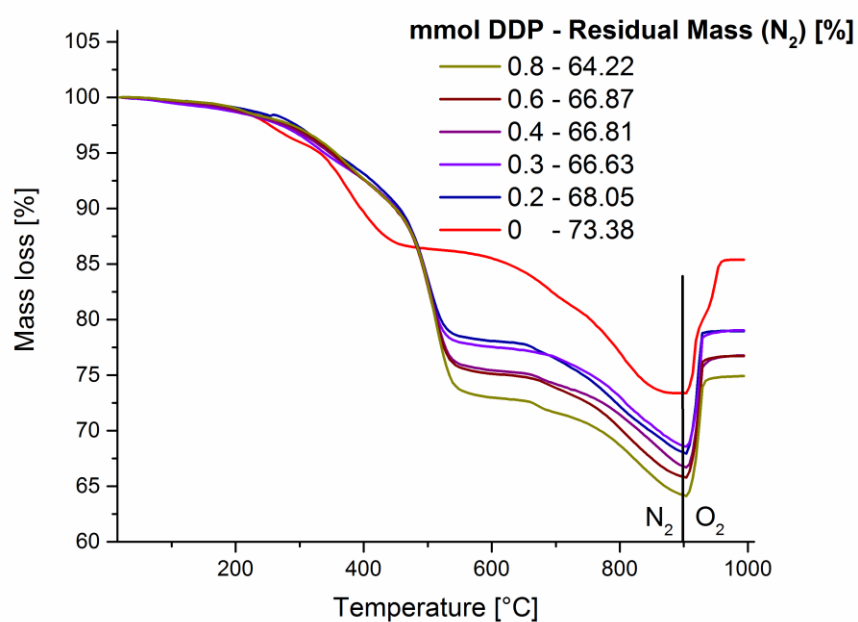


Figure S68: TG curves of OA@Fe_xO_y vs. DDP@Fe_xO_y (various amounts DDP).

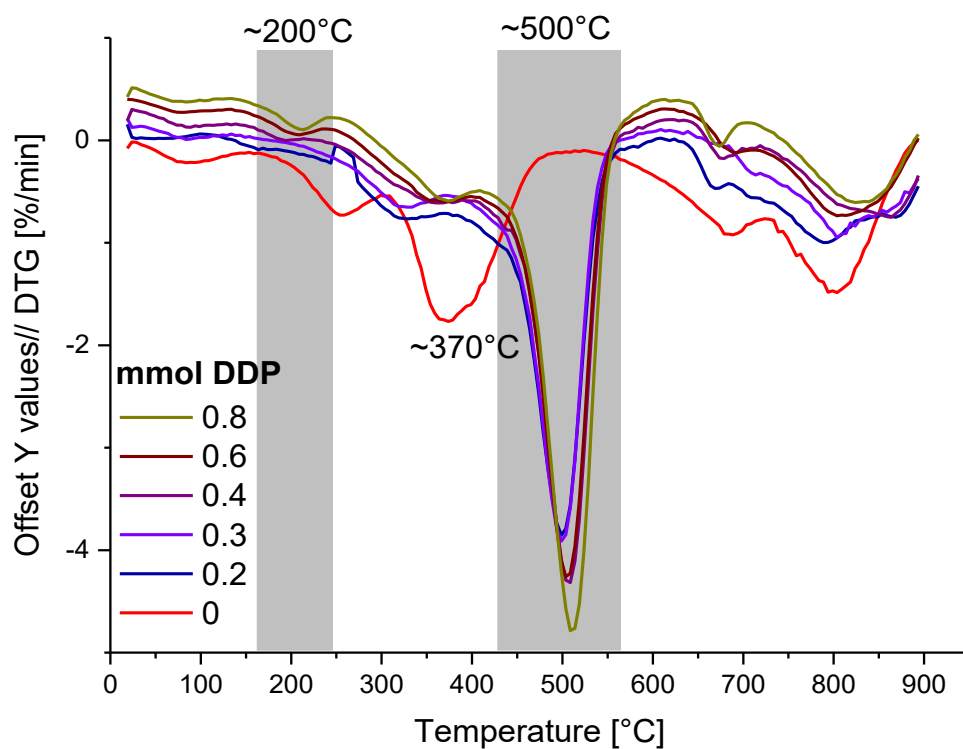


Figure S69: DTG curves of OA@Fe_xO_y vs. DDP@Fe_xO_y (various amounts DDP).

Table S2: TG and CHN values of DDP@Fe_xO_y (various amounts DDP)

Sample	TG _{residual mass} [%]		CHN [%]			Surface coverage (TG 900°C value)				mmol DDP/150mg
	25-900°C	900- 1000°C	C	H	N	[mmol/g]		[molecules/ nm ²]		
						C	H	C	H	
OA@Fe _x O _y	78.65	86.43	13.73	2.27	-	0.69	0.80	0.745	0.863	0
^{0.2} DDP@Fe _x O _y	68.08	79.04	17.47	3.14	-	1.52	1.92	1.640	2.072	0.2
^{0.3} DDP@Fe _x O _y	68.65	78.89	17.40	3.18	-	1.51	1.93	1.630	2.083	0.3
^{0.4} DDP@Fe _x O _y	66.84	76.66	19.67	3.63	-	1.75	2.26	1.889	2.439	0.4
^{0.6} DDP@Fe _x O _y	65.88	76.59	19.83	3.67	-	1.79	2.32	1.932	2.503	0.6
^{0.8} DDP@Fe _x O _y	64.24	74.88	21.50	3.99	-	1.99	2.59	2.148	2.795	0.8

The following equations were used to determine the amount of coupling agent in the phosphonic acid functionalized samples. TG-and CHN-analysis were used for that. Because of the oxidation of the sample when O₂ was used in the measurement, the residual mass from the nitrogen segment was used (although residual carbon maybe was left on the sample). However, these calculation could have a small error because of the different desorption behavior of the coupling agents. OA completely desorbs, while the anchoring group of dodecylphosphonic acid, formally PO₃H₂ does not desorb from the inorganic core, even in the oxidizing segment.

$$n_{ca} = \frac{X}{Y} * \frac{1000}{M * N} * \frac{1}{1g}$$

n_{ca} : amount coupling agent per particle mol/g (CA = coupling agent)

X : CHN value in % of relevant element

Y : residual mass of particles from TGA in % after N₂ segment

M : molar mass of element in g/mol

N : number of atoms per molecule

Surface coverages in molecules/ nm² were calculated using the following formula:

$$\sigma = n_{ca} * N_A * \frac{1}{A} * 10^{-18}$$

σ : surface coverage of coupling agents in molecules/nm²

A : surface area of particles in m²/g (determined by BET; 558 m²/g for OA@Fe_xO_y; under assumption that no relevant changes were caused by functionalization, all values were calculated using this area).

N_A : Avogadro constant

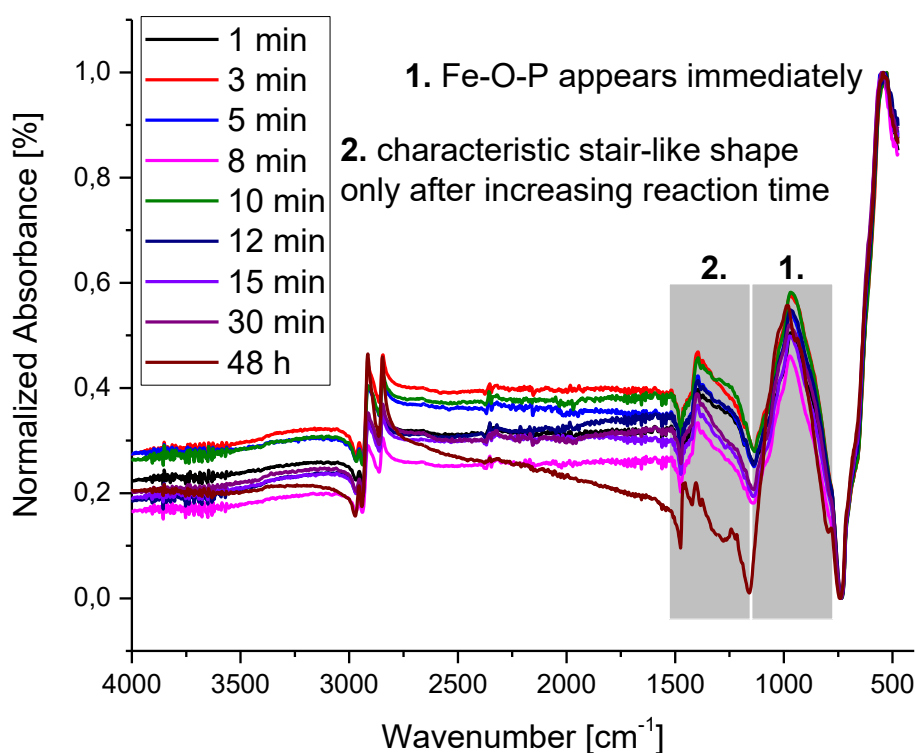
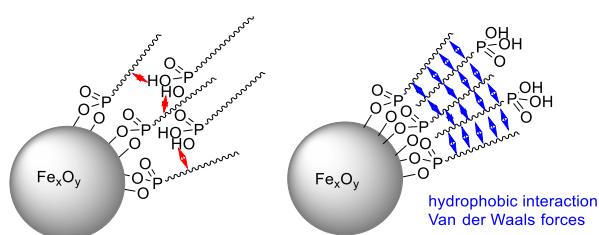


Figure S70: IR spectra of DDP@Fe_xO_y after various reaction times.

Scheme S1: Hindering of further attack during functionalization; possible interactions while exchange; right: possible second layer.



XRD

XRD measurements were conducted to check if the crystal structure is maintained during functionalization. The typical reflexes for cubic structure (*Fd3m*) was found before and after functionalization. The drift of the blue curve is caused because of the usage of a silicium single crystal and only small sample amounts, while OA@Fe_xO_y was measured in a flat plate sample holder and therefore no underground is visible.

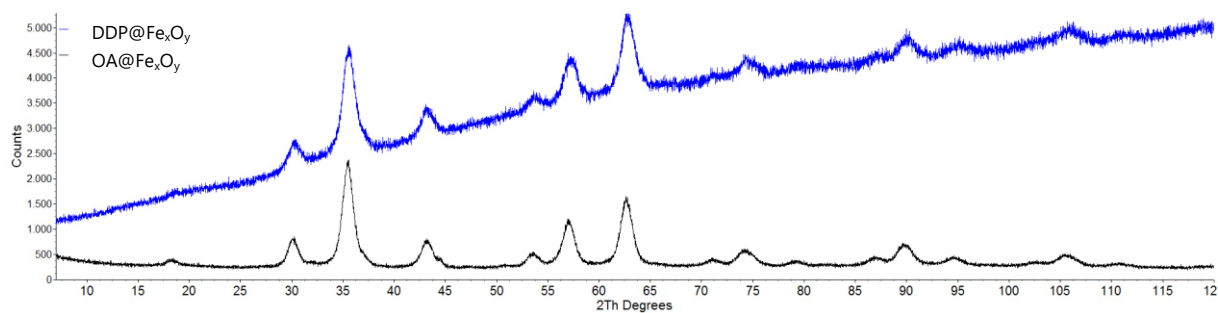


Figure S71: XRD patterns: black: OA@Fe_xO_y; blue: DDP@Fe_xO_y.

TEM images

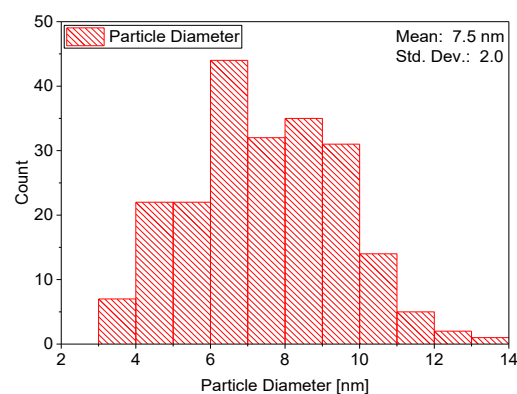
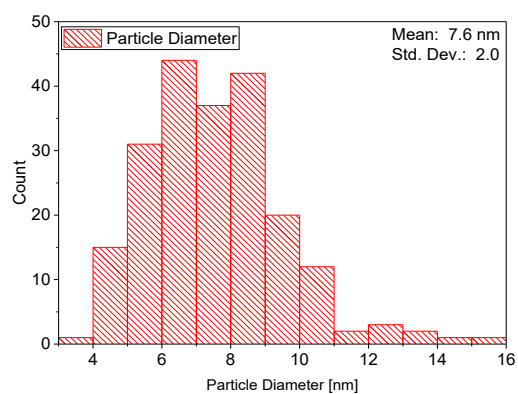
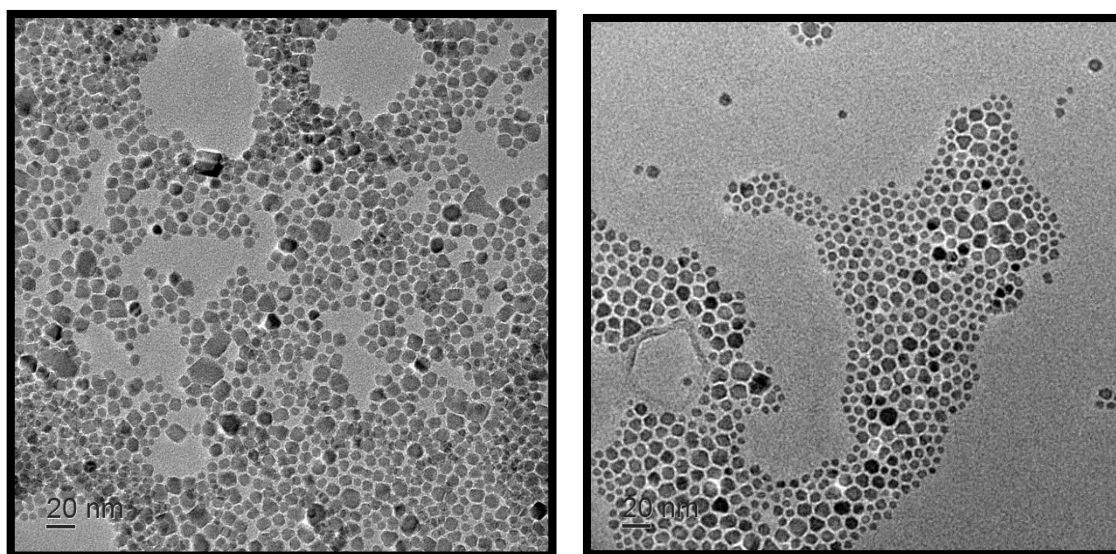


Figure S72: TEM images: left: OA@Fe_xO_y; right: DDP@Fe_xO_y. Histograms: Statistical Size Distribution of Particles. 200 particles counted with Image J.

6. Control experiment, OA@Fe_xO_y & DDP mixed as solids to a physical blend.

As a control experiment, OA@Fe_xO_y & DDP were mixed as solids to a physical blend. IR spectra and TG curves were compared with the system after applying the exchange protocol using a mixture of *n*-hexane and ethanol as solvents. While in the physical blend, the broad OH signals are clearly visible (compare IR spectrum of DDP), and the signal for bonded oleic acid is present, this is not the case after reaction in the solvent mixture.

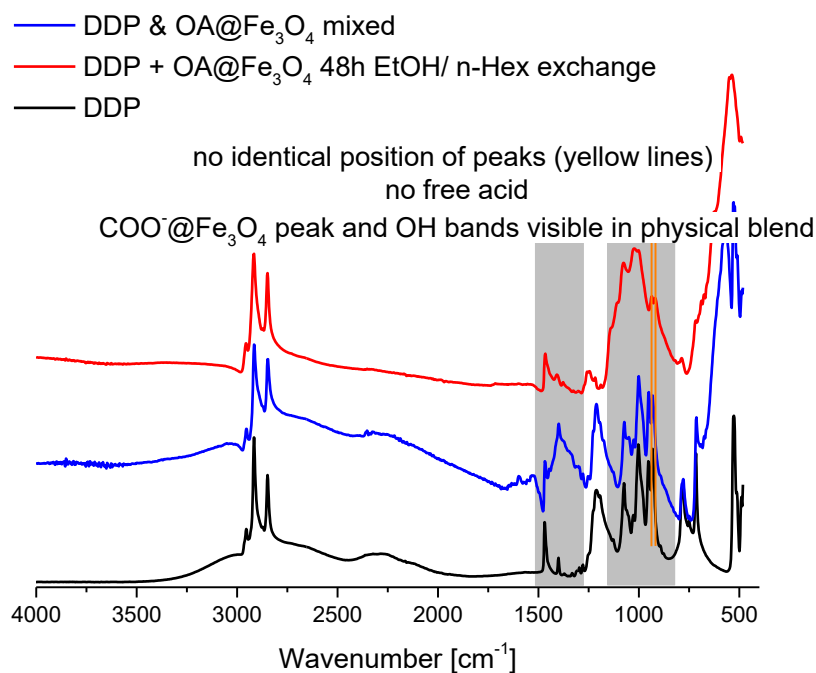


Figure S73: IR spectra of mixed OA@Fe_xO_y & DDP, DDP@Fe_xO_y and free DDP.

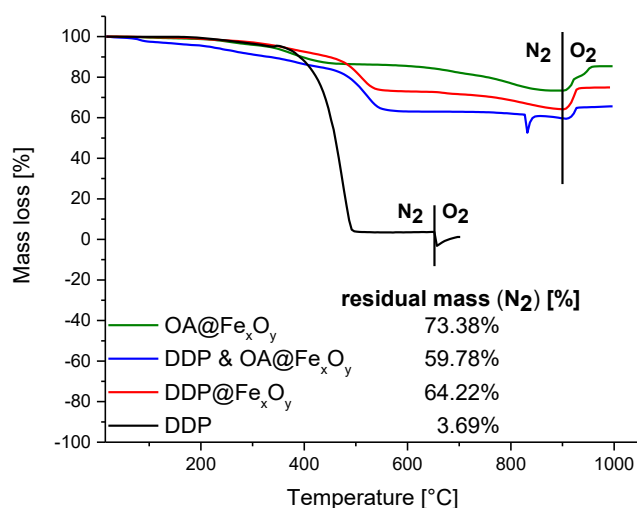


Figure S74: Thermogravimetric curves of mixed OA@Fe_xO_y & DDP, DDP@Fe_xO_y and free DDP.

7. Cofunctionalization with DDP&MeP@Fe_xO_y: TG, FTIR

A mixture of DDP and MeP (total: 0.16 mmol) were dissolved in ethanol: *n*-hexane (4.25 mL: 1 mL) and mixed with OA@Fe_xO_y (80 mg) in *n*-hexane (9 mL).

Table S3: Used ratios for cofunctionalization with DDP & MeP.

	ratio [%]	DDP [mmol]	MeP [mmol]	C-gehalt [%]	H-Gehalt [%]	N-Gehalt [%]
DDP_100	100:0	0.16	0	14,25	2,89	0
DDP_75	75:25	0.12	0.04	10,84	2,27	0
DDP_25	25:75	0.04	0.12	6,60	1,62	0
DDP_0	0:100	0	0.16	3,01	1,00	0

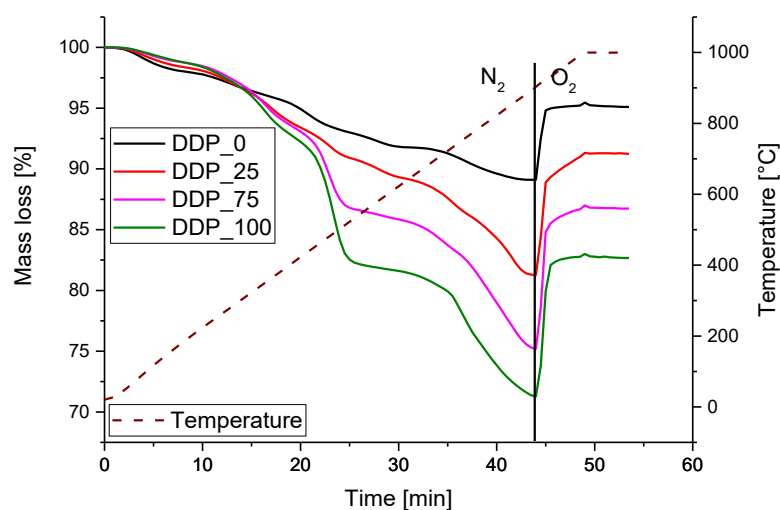


Figure S75: Thermogravimetric curves of DDPcoMeP@Fe_xO_y in different ratios.

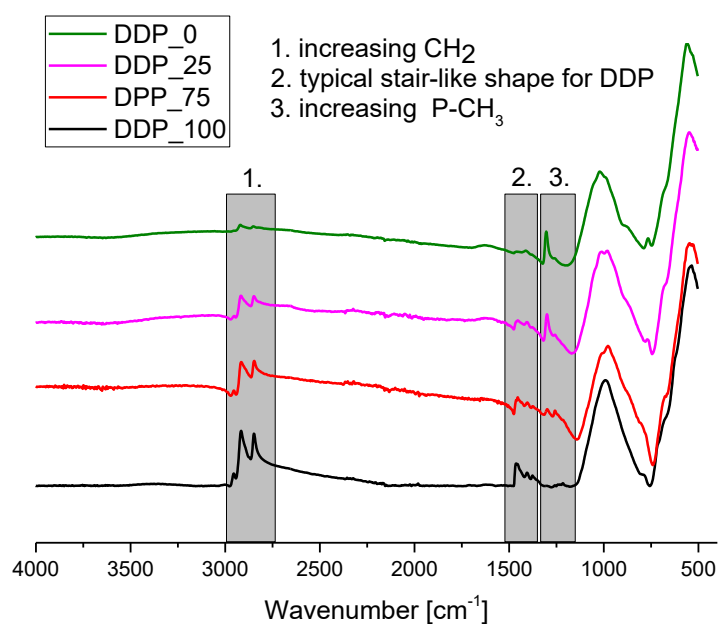


Figure S76: IR spectra of DDPcoMeP@Fe_xO_y in different ratios.

8. Cofunctionalization with DA- and Methylphosphonic acids: CHN, FTIR

Table S4: Experimental series of cofunctionalization with exemplary the weights of F10P (3a) and MeP

	F10P (3a)			MeP		
	%	mmol	mg	%	mmol	mg
F10P_100	100	0.30	84.50	0	0	0
F10P_75	75	0.225	64.87	25	0.075	7.20
F10P_50	50	0.15	43.25	50	0.15	14.40
F10P_25	25	0.075	21.64	75	0.225	21.60
F10P_0	0	0	0	100	0.30	28.81

Table S5: CHN values of F3PcoMeP@Fe_xO_y.

Sample	CHN [%]		
	C	H	N
F3P_100	10.41	1.69	-
F3P_75	10.06	1.75	-
F3P_50	7.62	1.75	-
F3P_25	6.35	1.70	-
F3P_0	4.23	1.65	-

Table S6. CHN values of F10P-co-funtionalized Fe_xO_y.

	C [%]	H [%]
F10P_100	16.13	2.51
F10P_75	14.92	2.32
F10P_50	12.17	2.04
F10P_25	8.85	1.63
F10P_0	5.59	1.32

F10P_xx means xx = percentage of functional group on surface

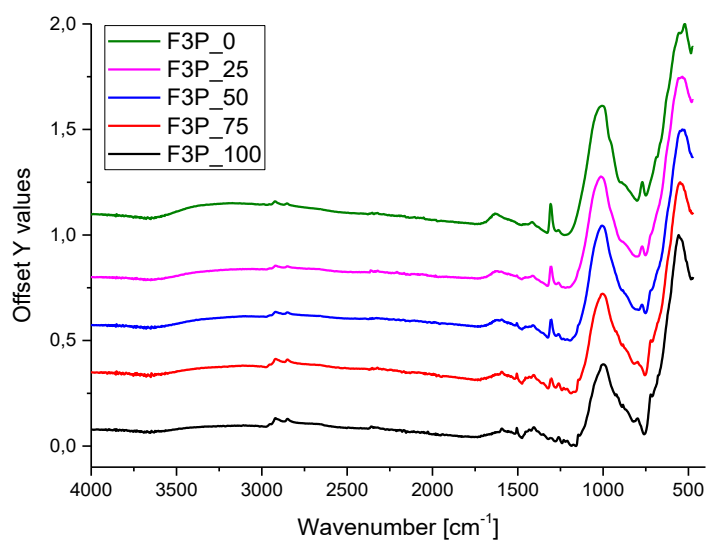


Figure S77: IR spectra of F3PcoMeP@Fe_xO_y.

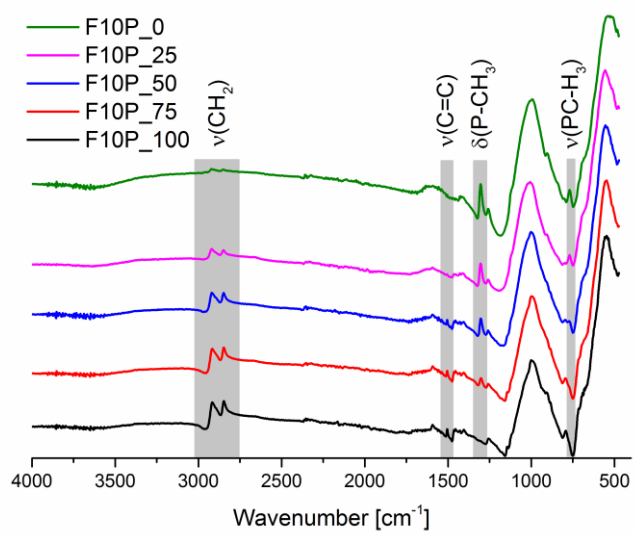
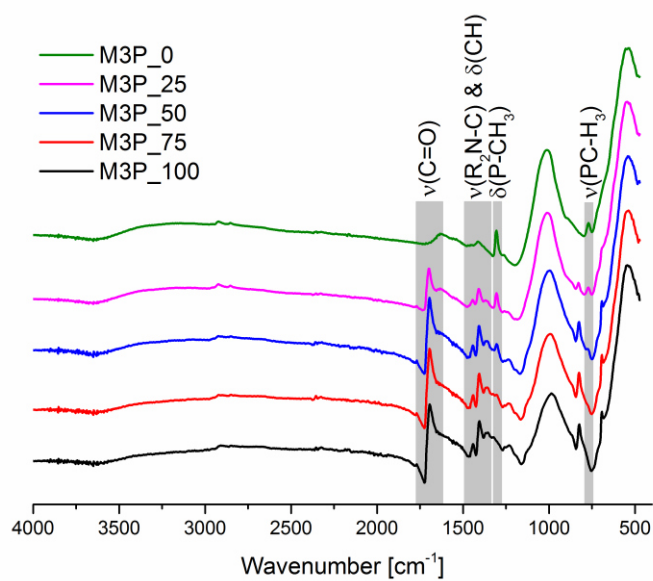


Figure S78: IR spectra of F10PcoMeP@Fe_xO_y.

Table S7: CHN values of M3PcoMeP@Fe_xO_y.

Sample	CHN [%]		
	C	H	N
M3P_100	8.22	1.50	1.80
M3P_75	8.12	1.55	1.65
M3P_50	7.41	1.54	1.45
M3P_25	5.59	1.48	0.98
M3P_0	2.69	1.23	0

**Figure S79:** IR spectra of M3PcoMeP@Fe_xO_y.

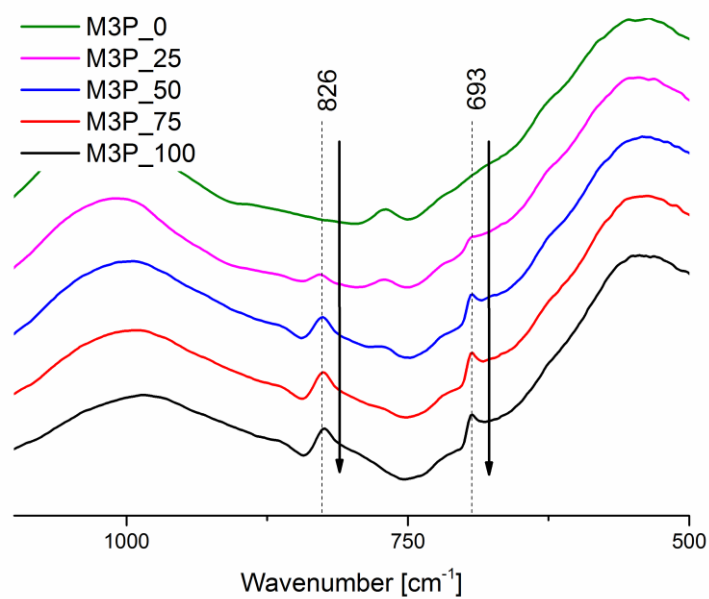


Figure S80: Zoomed IR spectra of M3PcoMeP@Fe_xO_y.

Table S8: CHN values of M10PcoMeP@Fe_xO_y.

Sample	CHN [%]		
	C	H	N
M10P_100	16.99	2.71	1.50
M10P_75	16.07	2.76	1.58
M10P_50	12.82	2.27	1.08
M10P_25	9.24	2.09	1.16
M10P_0	4.93	1.61	0

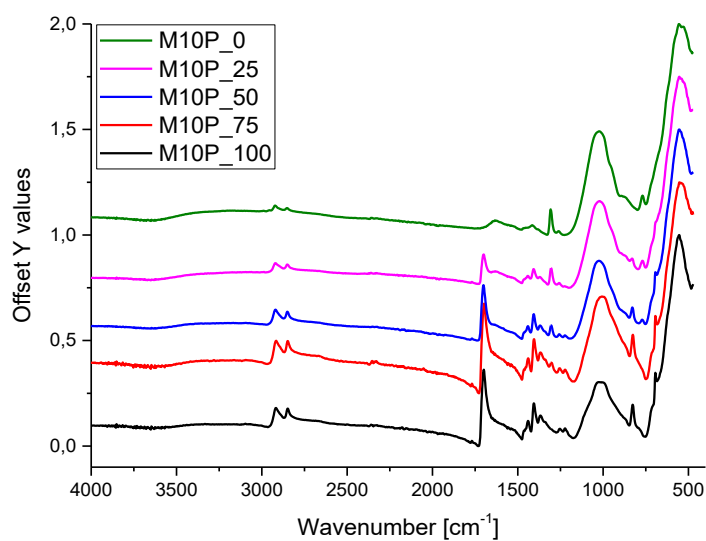


Figure S81: IR spectra of M10PcoMeP@Fe_xO_y.

Surface coverage with 100% functional reagent

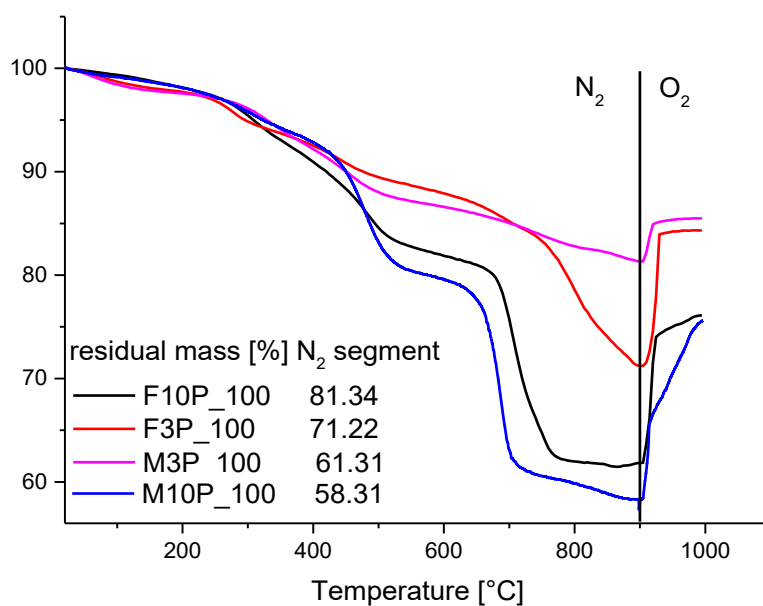


Figure S82: Thermogravimetric curves of F10P-, F3P-, M3P- and M10P_100@Fe_xO_y.

Table S9: CHN values and surface coverage of F10P-, F3P-, M3P- and M10P_100@Fe_xO_y.

Sample	CHN [%]			surface coverage					
	C	H	N	[mmol/g]			[molecules/ nm ²]		
				C	H	N	C	H	N
F10P_100	16.13	2.51	-	1.55	1.75	-	1.67	1.88	-
F3P_100	10.41	1.69	-	1.73	2.62	-	1.87	2.83	-
M10P_100	16.91	2.69	1.39	1.73	2.08	1.70	1.86	2.25	1.84
M3P_100	8.22	1.50	1.80	1.20	2.28	1.57	1.30	2.46	1.69

Formulas used are described under Table S2. TG residual masses are in the FigureS82 above.

9. IR spectra of molecular Diene & Dienophile and the corresponding DA adduct

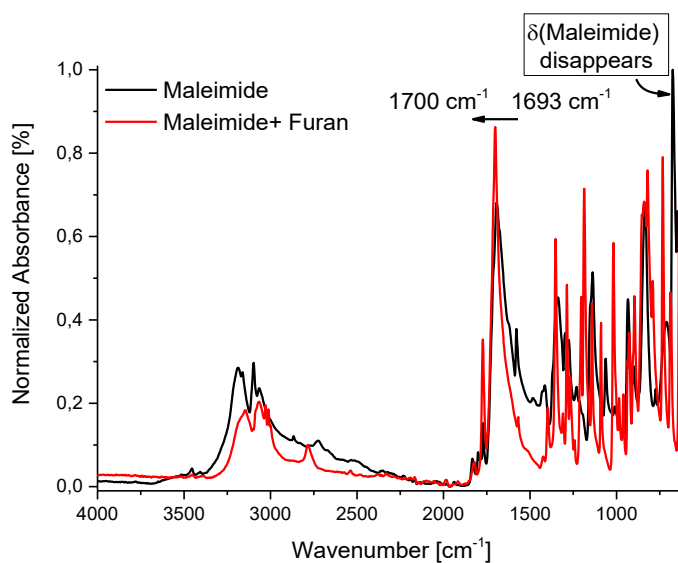


Figure S83: Typical shift of C=O band and consumption of $\delta(\text{ring})$ at 696cm⁻¹ in DA reaction shown on maleimide vs. maleimide+furan-DA-adduct.

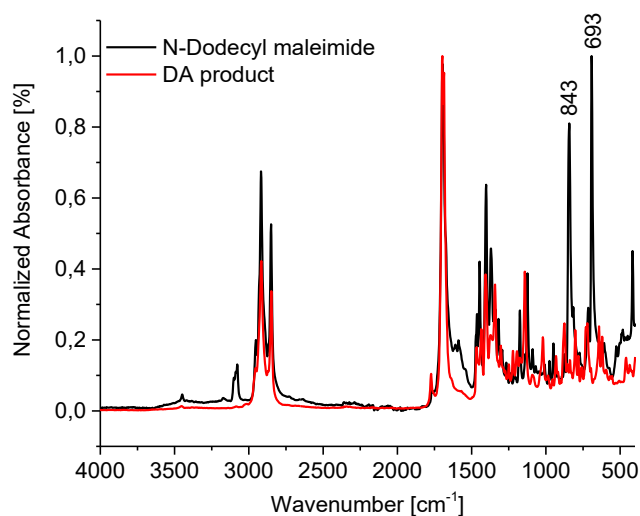


Figure S84: Typical consumption of =C-H band at 843 and $\delta(\text{ring})$ at 693cm⁻¹ in DA reaction shown on *N*-dodecylmaleimide vs. maleimide+furan-DA-adduct.

10. DA reaction on cofunctionalized DA-particles: FTIR, DSC, CHN

10.1 F3PcoMeP@Fe_xO_y: DA-reaction of Furan-cofunctionalized particles with *N*-Dodecyl maleimide or Maleimide

Table S10: CHN data to cofunctionalized F3PcoMeP@Fe_xO_y.

Sample	C [%]	H [%]
F3P_100_NM	13.90	2.26
F3P_75_NM	12.81	2.15
F3P_50_NM	9.25	1.97
F3P_25_NM	8.21	1.99
F3P_0_NM	5.70	1.67
F3P_100_M	12.26	1.86
F3P_75_M	11.12	1.83
F3P_50_M	8.69	1.77
F3P_25_M	6.94	1.73
F3P_0_M	4.76	1.61

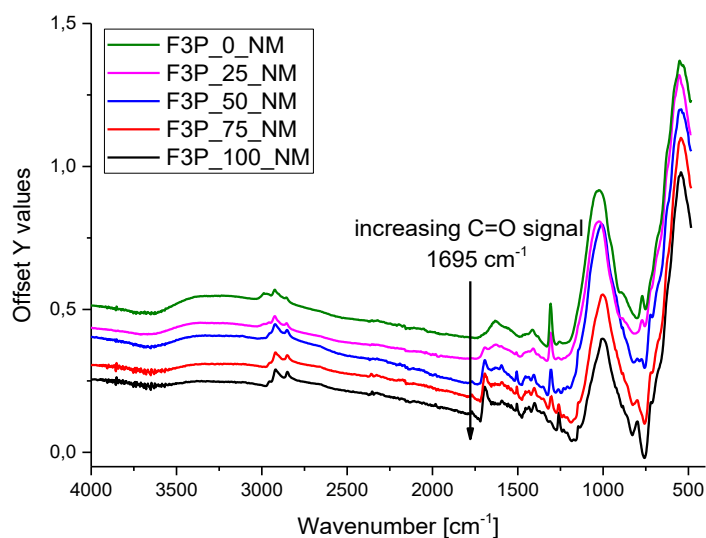


Figure S85: IR spectra of F3PcoMeP cofunctionalized particles after DA-reaction with NM.

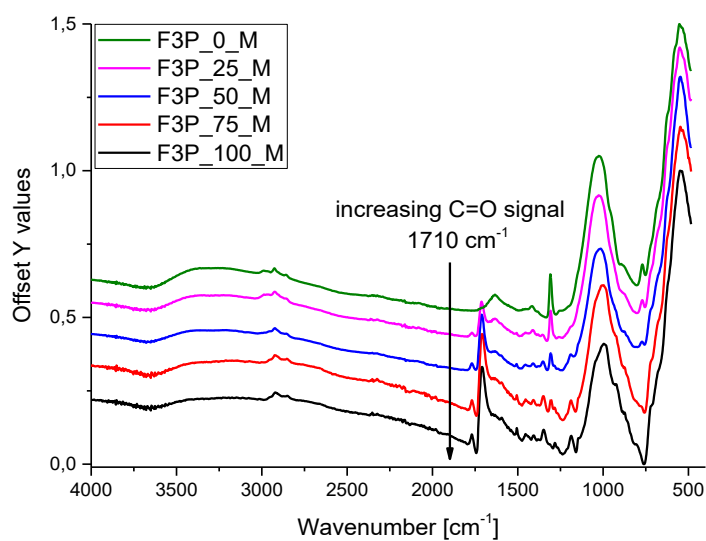


Figure S86: IR spectra of F3PcoMeP cofunctionalized particles after DA-reaction with M.

10.2 M3PcoMeP@Fe_xO_y.

Table S11: CHN data to cofunctionalized M3PcoMeP@Fe_xO_y.

	C [%]	H [%]	H [%]
M3P_100_MF	8.70	1.50	1.63
M3P_75_MF	8.99	1.56	1.50
M3P_50_MF	8.32	1.58	1.43
M3P_25_MF	5.96	1.48	1.25
M3P_0_MF	3.09	1.12	0
M3P_100_DF	8.62	1.79	1.34
M3P_75_DF	8.59	1.80	1.90
M3P_50_DF	8.00	1.63	1.45
M3P_25_DF	5.86	1.49	1.06
M3P_0_DF	2.65	1.16	0

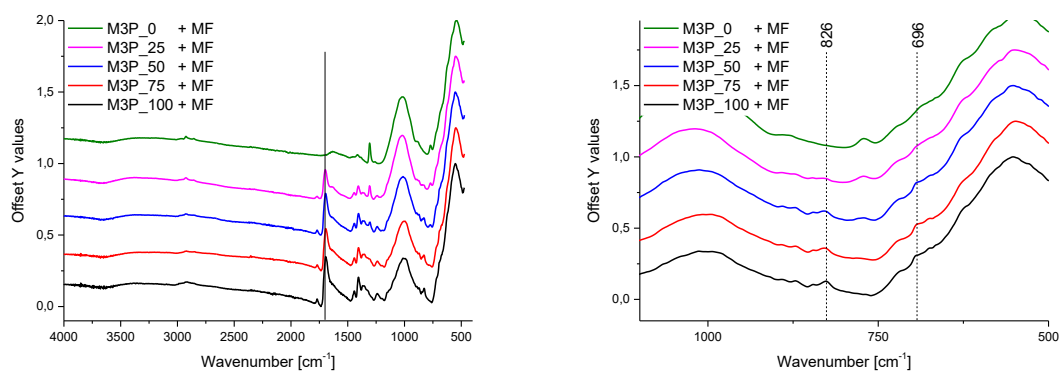


Figure S87: IR spectra of M3PcoMeP@Fe_xO_y cofunctionalized particles after DA-reaction with MF.

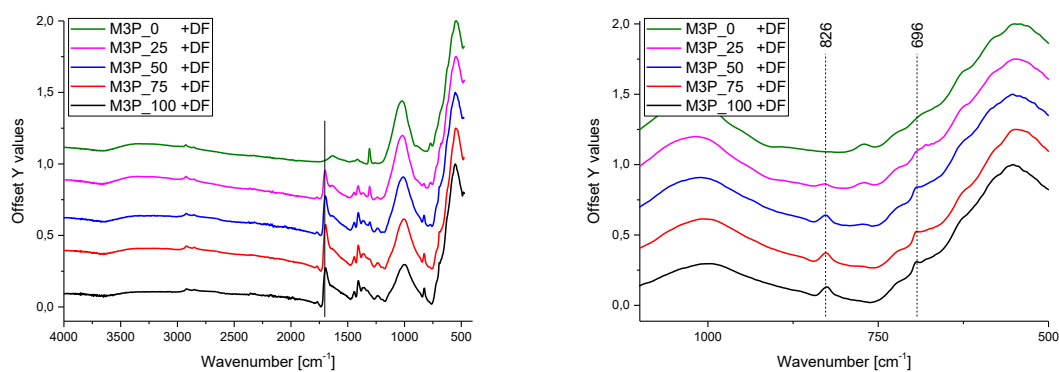


Figure S88: IR spectra of M3PcoMeP@Fe_xO_y cofunctionalized particles after DA-reaction with DF.

10.3 M10PcoMeP@Fe_xO_y.

Table S12: CHN data to cofunctionalized M10PcoMeP@Fe_xO_y_DF and M10PcoMeP@Fe_xO_y_MF.

Sample	C [%]	H [%]	N [%]
M10P_100_DF	16.19	2.60	1.61
M10P_75_DF	15.96	2.65	1.59
M10P_50_DF	12.82	2.33	1.31
M10P_24_DF	8.87	1.96	1.19
M10P_0_DF	4.59	1.47	0
M10P_100_MF	15.23	2.52	1.30
M10P_75_MF	15.70	2.53	1.25
M10P_50_MF	12.27	2.21	1.22
M10P_24_MF	9.00	1.93	1.08
M10P_0_MF	3.98	1.35	0

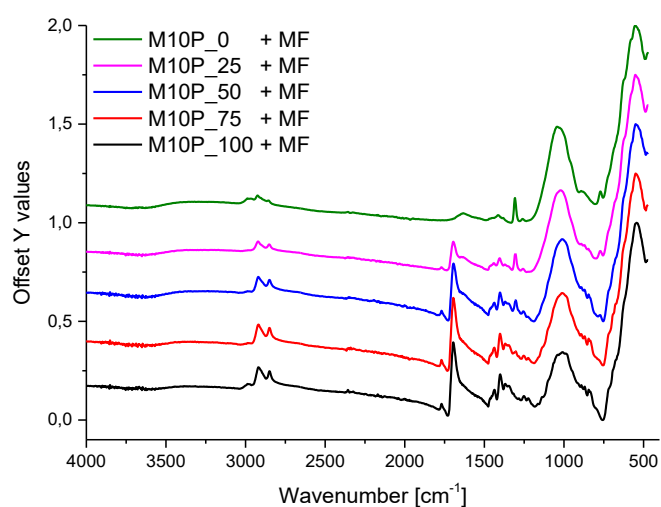


Figure S89: IR spectra of M10PcoMeP@Fe_xO_y cofunctionalized particles after DA-reaction with MF.

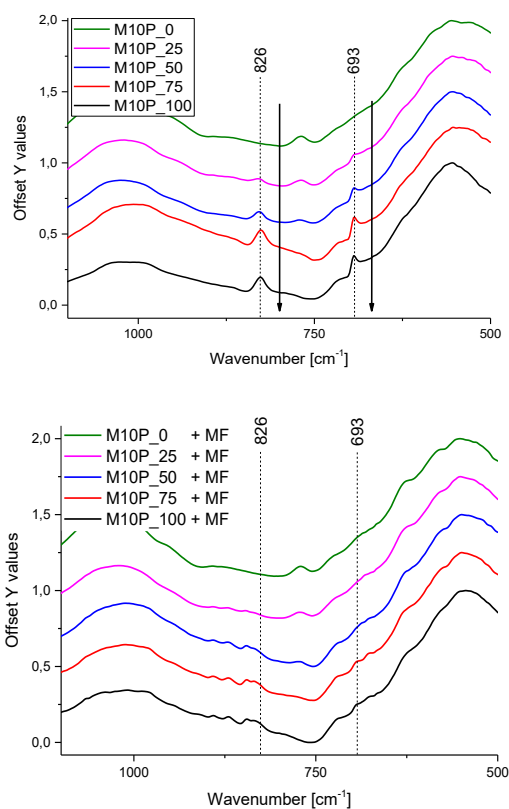


Figure S90: IR spectra of M10PcoMeP@Fe_xO_y cofunctionalized particles before (left) and after (right) DA-reaction with MF.

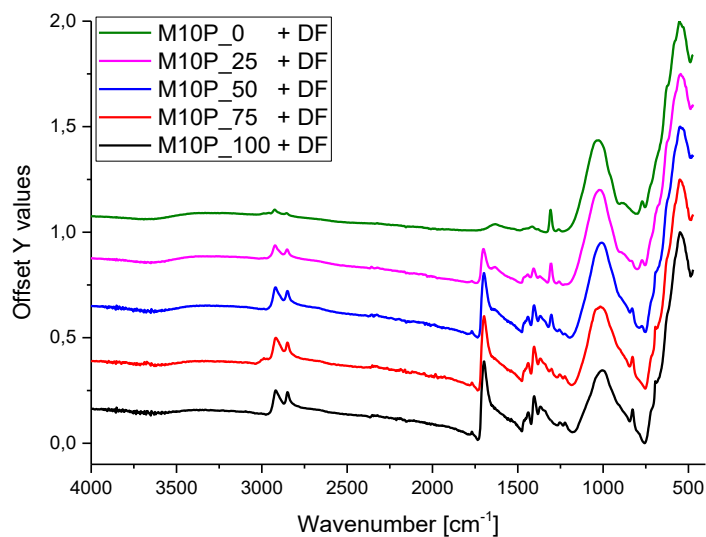


Figure S91: IR spectra of M10PcoMeP@Fe_xO_y cofunctionalized particles after DA-reaction with DF.

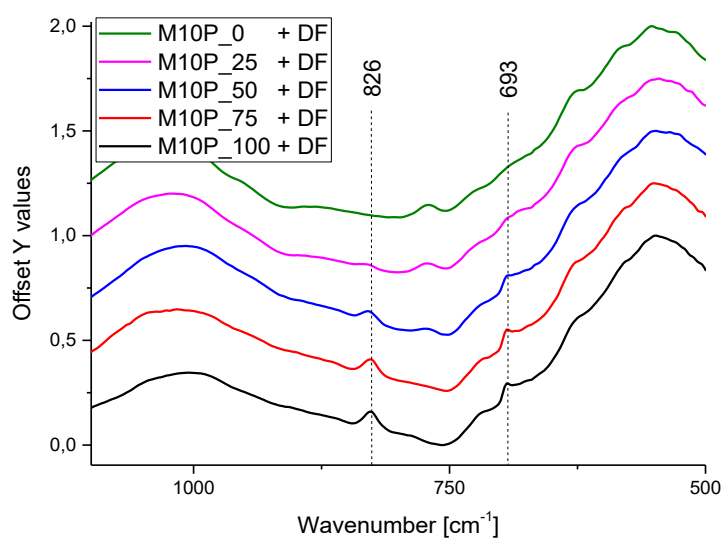


Figure S92: IR spectra of M10PcoMeP@Fe_xO_y cofunctionalized particles after DA-reaction with DF.

11. DSC Graphs and listed values for all cofunctionalized particles

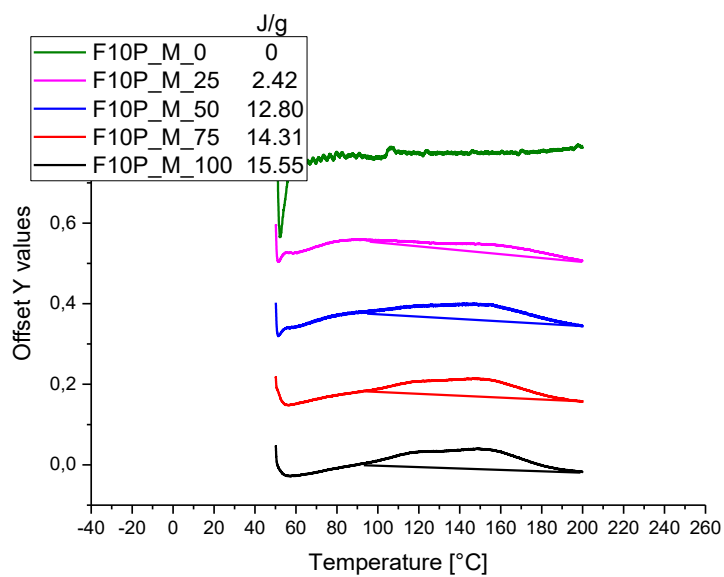
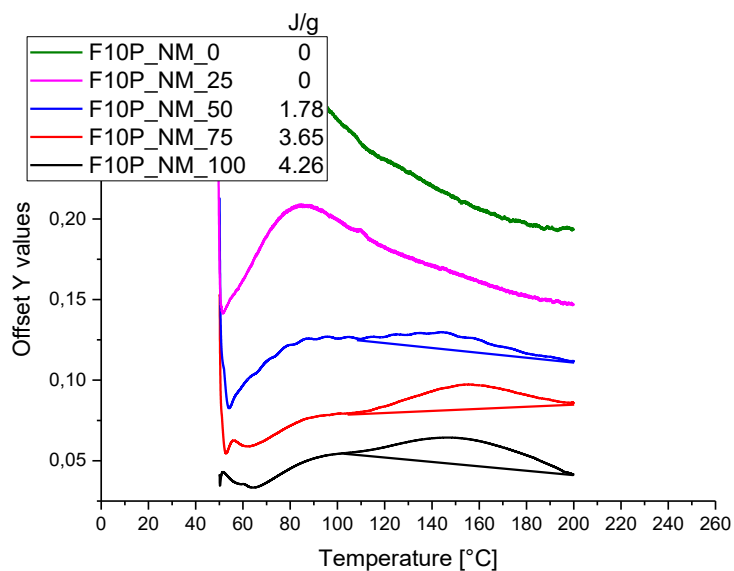
Table S13: Listed values of endothermic rDA signal from DSC measurement for all cofunctionalized particles

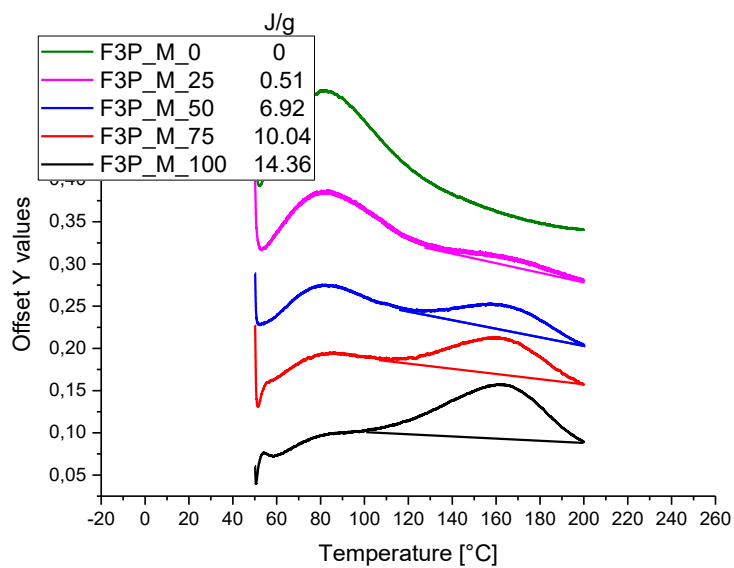
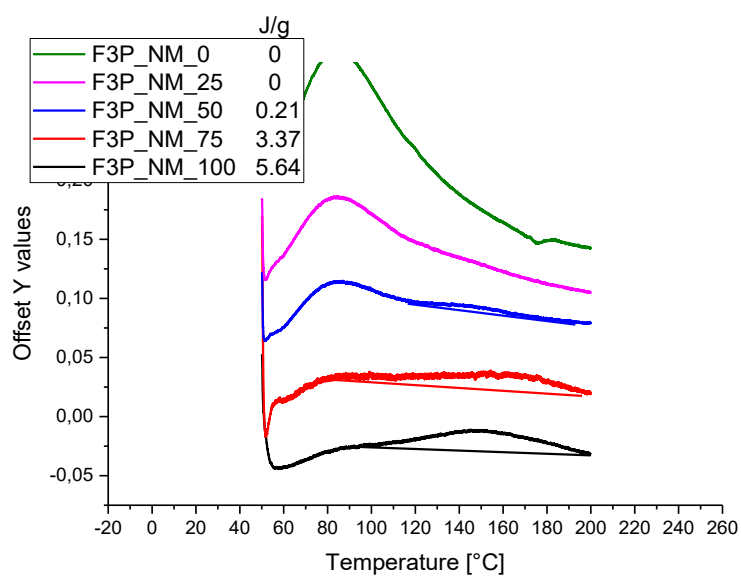
	Maleimide conversion in J/g	N-Dodecylmaleimide conversion in J/g
F10P_100	15.55	4.26
F10P_75	14.31	3.65
F10P_50	12.80	1.78
F10P_25	2.42	0
F10P_0	0	0

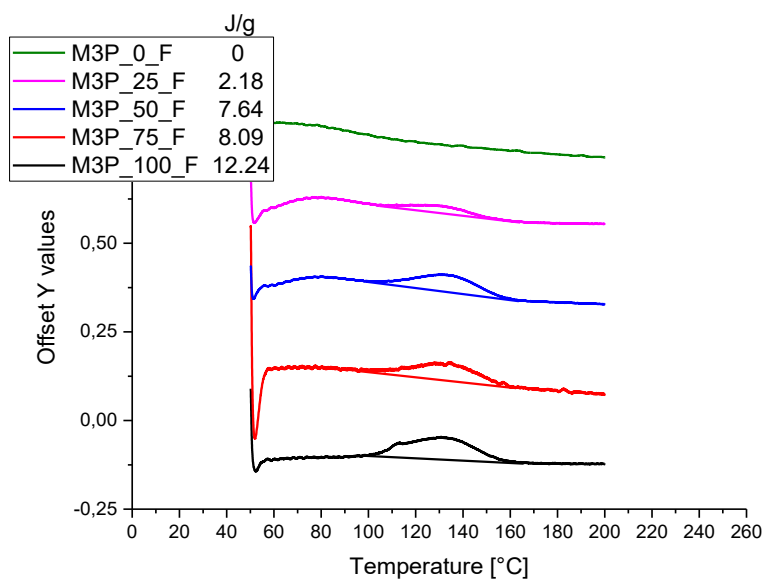
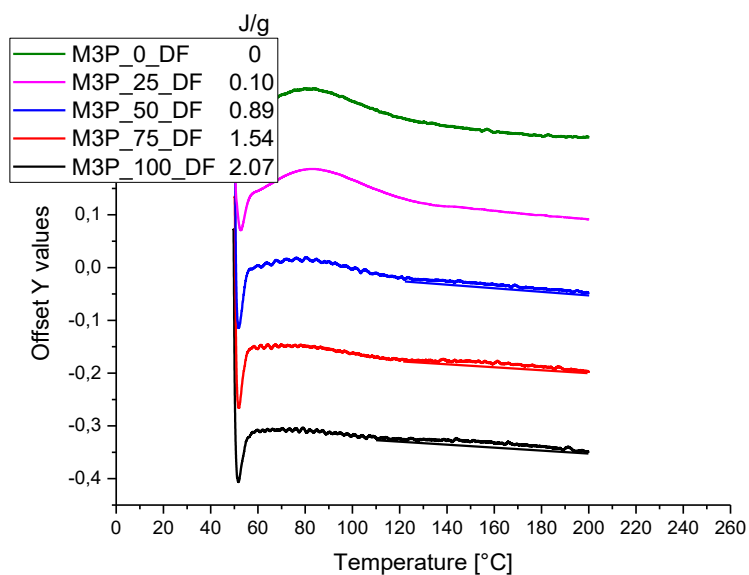
	Maleimide conversion in J/g	N-Dodecylmaleimide conversion in J/g
F3P_100	14.36	5.64
F3P_75	10.04	3.37
F3P_50	6.92	0.21
F3P_25	0.51	0
F3P_0	0	0

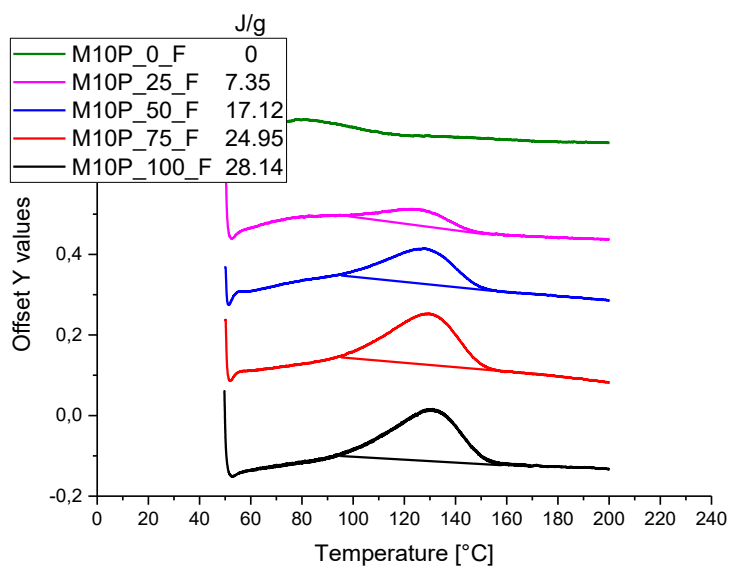
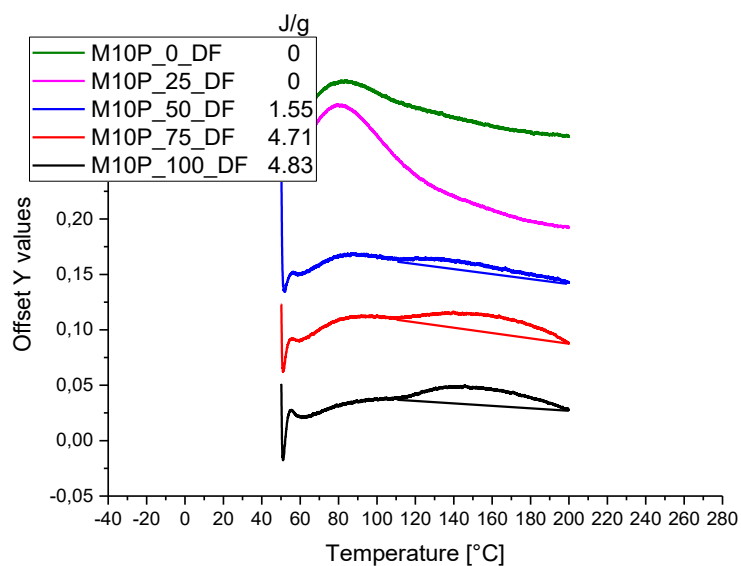
	Furan conversion in J/g	Dodecylfuran conversion in J/g
M3P_100	12.24	2.07
M3P_75	8.09	1.54
M3P_50	7.64	0.89
M3P_25	2.18	0.10
M3P_0	0	0

	Maleimide conversion in J/g	N-Dodecylmaleimide conversion in J/g
M10P_100	28.14	4.83
M10P_75	24.95	4.71
M10P_50	17.12	1.55
M10P_25	7.35	0
M10P_0	0	0

**Figure S93:** DSC curves of F10P_M.**Figure S94:** DSC curves of F10P_NM.

**Figure S95:** DSC curves of F3P_M.**Figure S96:** DSC curves of F3P_NM.

**Figure S97:** DSC curves of M3P_F.**Figure S 98:** DSC curves of M3P_DF.

**Figure S99:** DSC curves of M10P_F.**Figure S100:** DSC curves of M10P_DF.

12. DSC and IR data to composite

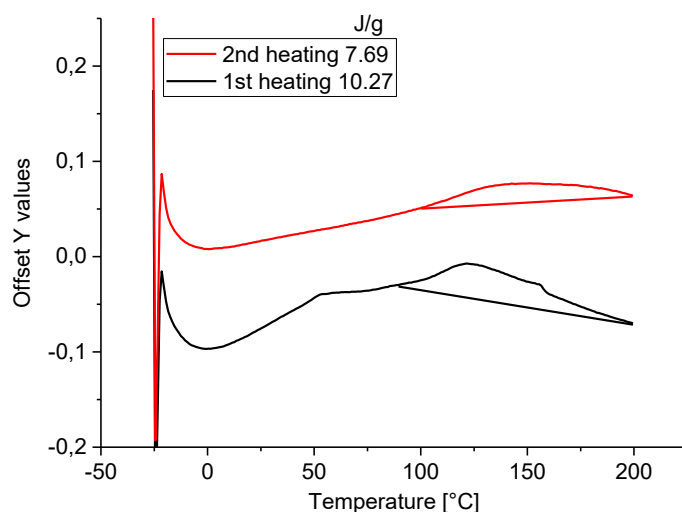


Figure S101: DSC curve of nanocomposite.

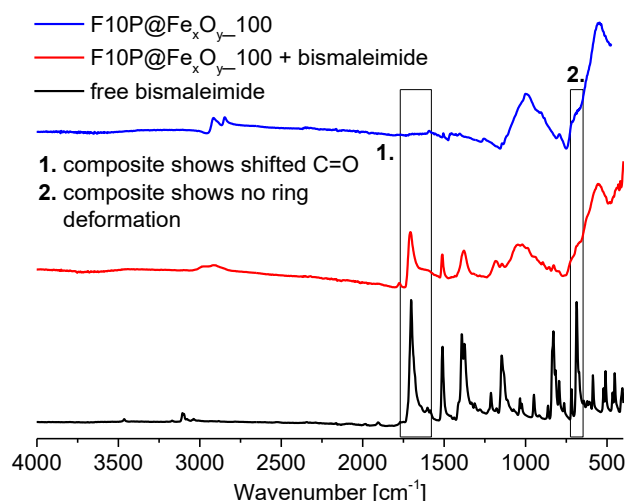


Figure S102: IR spectra of single components and nanocomposite.

References

- (1) Longo, R. C.; Cho, K.; Schmidt, W. G.; Chabal, Y. J.; Thissen, P., Monolayer Doping via Phosphonic Acid Grafting on Silicon: Microscopic Insight from Infrared Spectroscopy and Density Functional Theory Calculations. *Adv. Funct. Mater.* **2013**, *23*, 3471-3477.
- (2) Thomas, L. C.; Chittenden, R. A., Characteristic Infrared Absorption Frequencies of Organophosphorus Compounds-II. P-O-(X) Bonds. *Spectrochim. Acta* **1964**, *20*, 489-502.
- (3) Daou, J.; Begin-Colin, S.; Grenèche, J. M.; Thomas, F.; Derory, A.; Bernhardt, P.; Legaré, P.; Pourroy, G., Phosphate Adsorption Properties of Magnetite-Based Nanoparticles. *Chem. Mater.* **2007**, *19*, 4494-4505.
- (4) Quinones, R.; Shoup, D.; Behnke, G.; Peck, C.; Agarwal, S.; Gupta, R. K.; Fagan, J. W.; Mueller, K. T.; Iulicci, R. J.; Wang, Q., Study of Perfluorophosphonic Acid Surface Modifications on Zinc Oxide Nanoparticles. *Materials (Basel)* **2017**, *10*, 1-16.
- (5) Lushtinetz, R.; Seifert, R.; Jaehne, G.; Adler, E.; Adler, H.-J. P., Infrared Spectra of Alkylphosphonic Acid Bound to Aluminium Surfaces. *Macromol. Symp.* **2007**, *254*, 248-253.

Supporting Information

Simple and High Yield Access to Octafunctional Azido, Amine and Urea Group bearing Cubic SpherosilicatesSandra Schäfer, Guido Kickelbick*^[a,b]

[a] Inorganic Solid State Chemistry, Saarland University, Am Markt, Zeile 3, 66125 Saarbrücken, Germany

[b] INM – Leibniz-Institut für Neue Materialien GmbH, Campus D2₂, 66123 Saarbrücken, Germany

E-mail: guido.kickelbick@uni-saarland.de

<http://www.uni-saarland.de/lehrstuhl/kickelbick.html>

Materials. Tetraethoxysilane was provided by Wacker Silicones. Chlorodimethylsilane, and Karstedt catalyst (in xylene, Pt 2.1-2.4%) were purchased from ABCR. Tetramethylammonium hydroxide pentahydrate, 10-undecen-1-ol, triphenylphosphine, tetrabromomethane, NaN₃, Pd/C on carbon (10 wt%), propyl isocyanate, 18-crown-6, toluene (abs.), ACN (abs.), DMF (abs.) and ethanol (abs.) were purchased from Sigma–Aldrich. 1,4- dibromobutane, 1,5- dibromopentane, 1,6-dibromohexane and potassium *tert*-butoxide were purchased from Alfa Aesar. Alumina 90 active neutral was purchased from Merck Millipore. All chemicals were used as received. All synthetic procedures were carried out under inert gas atmosphere applying Schlenk techniques.

Characterization. Fourier transform infrared (FTIR) spectroscopy measurements were performed applying a Bruker Vertex 70 spectrometer under ambient air (40 scans at a resolution of 4 cm⁻¹) in attenuated total reflectance (ATR) mode. Solution NMR spectra were recorded with a Bruker Avance 300 spectrometer at 25 °C (¹H at 300.13 MHz, ¹³C at 75.48 MHz, ²⁹Si at 59.63 MHz) with 400 MHz using CDCl₃, or MeOD-*d*4 and the residual protons as reference. Elemental analysis was performed with a Leco 900 CHN analyzer. High-resolution mass spectrometry (HRMS) was performed with a solarix 7 Tesla FTICR mass spectrometer (Bruker Daltonics, Bremen, Germany). All samples were ionized by electrospray ionization (ESI). In MS/MS mode, precursor ions were isolated first in the quadrupole and externally accumulated in the hexapole for 0.1 s. For collision- induced dissociation (CID), a collision voltage of 2–10 V was applied. Thermogravimetric analysis (TGA) was performed on a Netzsch Iris TG 209C in an alumina crucible heating from room temperature to 700 °C under nitrogen followed by heating to 800 °C under a mixture of nitrogen and oxygen (1:1) with a rate of 20 K/min or completely under mixture of nitrogen and oxygen (1:1) with the same rate. Differential scanning calorimetry (DSC) measurements were performed with a Netzsch DSC 204 F1 Phoenix calorimeter and with a TA instruments Q100 with samples in aluminum crucibles with pierced lids and heated under nitrogen at a rate of 10 K/min.

Synthesis

ω -alkenylbromides (C4-C6, C11; **1a-d**). 4-Bromo-1-butene, 5-Bromo-1-Pentene, 6-Bromo-1-hexene were synthesized according to literature^[i], using an elimination reaction with potassium *tert*-butoxide in diethyl ether. The reaction was catalyzed via 18-crown-6 ether. Synthesis of 11-bromo undecene (**1d**)^[ii] was described elsewhere.

Octakis(hydridodimethylsiloxy)octasilsesquioxane (**2**) was synthesized according to a literature procedure.^[iii]

Octakis(bromoalkyldimethylsiloxy)octasilsesquioxane (3a-d).

Octakis(hydridodimethylsiloxy)octasilsesquioxane (**2**) (3.00 g, 2.95 mmol) and ω -bromo alkene (**1a-d**) (23.6 mmol) were dissolved in anhydrous toluene (30 mL). Karstedt-catalyst (2 % in xylene, 350 μ L) was added and the mixture was heated to 80 °C for 1-2 h. The mixture was filtered through Al₂O₃ (active neutral) and the solvent was removed under reduced pressure. The product was obtained as colorless oil and used without further purification for the following reactions.

3a (C4): Colorless Oil. **Yield:** 6.12 g (100 %, 2.95 mmol). **¹H NMR** (300 MHz, CDCl₃) δ 3.41 (t, *J* = 6.8 Hz, 16H, CH₂Br), 1.97 – 1.80 (m, 16H, CH₂CH₂Br), 1.56 – 1.45 (m, 16H, CH₂CH₂Si), 0.67 – 0.54 (m, 16H, CH₂Si), 0.16 (s, 48H, Si(CH₃)₂). **¹³C NMR** (75 MHz, CDCl₃) δ 36.14 (CH₂Br), 33.44 (CH₂CH₂Br), 21.72 (CH₂Si), 16.81 (CH₂CH₂Si), -0.16 (Si(CH₃)₂). **²⁹Si NMR** (60 MHz, CDCl₃) δ 12.68 (OSi(CH₃)₂R), -108.96 (SiO₄). **IR** ν = 2960 (v C-H), 2935 (v C-H), 1254 (v Si-C), 1072 (v Si-O), 840 (δ C-H), 694 (v C-Br), 548 (δ Si-O cage deformation) cm⁻¹. **CHN**_{theo} (C₄₈H₁₁₂Br₈O₂₀Si₁₆): C: 27.48; H: 5.38; N – **CHN**_{exp}. C: 27.36; H: 5.37; N –.

3b (C5): Colorless Oil. **Yield:** 6.52 g (100 %, 2.95 mmol). **¹H NMR** (300 MHz, CDCl₃) δ 3.40 (t, *J* = 6.9 Hz, 16H, CH₂Br), 1.86 (m, 16H, CH₂CH₂Br), 1.54 – 1.31 (m, 32H, CH₂CH₂CH₂Si), 0.66 – 0.56 (m, 16H, CH₂Si), 0.13 (s, 48H, Si(CH₃)₂). **¹³C NMR** (75 MHz, CDCl₃) δ 33.93 (CH₂Br), 32.72 (CH₂CH₂Br), 31.91 (CH₂CH₂CH₂Br), 22.36 (CH₂Si), 17.65 (CH₂CH₂Si), -0.14 (Si(CH₃)₂). **²⁹Si NMR** (60 MHz, CDCl₃) δ 12.66 (OSi(CH₃)₂R), -108.93 (SiO₄). **IR** ν = 2958 (v C-H), 2926 (v C-H), 1253 (v Si-C), 1070 (v Si-O), 835 (δ C-H), 694 (v C-Br), 546 (δ Si-O cage deformation) cm⁻¹. **CHN**_{theo} (C₅₆H₁₂₈Br₈O₂₀Si₁₆): C: 30.43; H: 5.84; N – **CHN**_{exp}. C: 30.43; H: 5.84; N –.

3c (C6): Colorless Oil. **Yield:** 6.85 g (100 %, 2.95 mmol). **¹H NMR** (300 MHz, CDCl₃) δ 3.40 (t, *J* = 6.9 Hz, 2H, CH₂Br), 1.85 (m, 2H, CH₂CH₂Br), 1.52 – 1.27 (m, 48H, CH₂CH₂CH₂CH₂Si), 0.65 – 0.54 (m, 16H, CH₂Si), 0.13 (s, 48H, Si(CH₃)₂). **¹³C NMR** (75 MHz, CDCl₃) δ 34.08 (CH₂Br), 32.93 (CH₂CH₂Br), 32.58 (CH₂CH₂CH₂Br), 28.03 (CH₂CH₂CH₂Si), 22.94 (CH₂Si), 17.73 (CH₂CH₂Si), -0.14 (Si(CH₃)₂). **²⁹Si NMR** (60 MHz, CDCl₃) δ 12.68 (OSi(CH₃)₂R), -108.91 (SiO₄). **IR** ν = 2958 (v C-H), 2924 (v C-H), 1252 (v Si-C), 1071 (v Si-O), 839 (δ C-H), 694 (v C-Br), 548 (δ Si-O cage deformation) cm⁻¹. **CHN**_{theo} (C₆₄H₁₄₄Br₈O₂₀Si₁₆): C: 33.10; H: 6.25; N – **CHN**_{exp}. C: 33.54; H: 6.34; N –.

3d (C11): Colorless Oil. **Yield:** 8.51 g (100 %, 2.95 mmol). **¹H NMR** (300 MHz, CDCl₃) δ 3.40 (t, *J* = 6.9 Hz, 16H, CH₂Br), 1.91 – 1.80 (m, 16H, CH₂CH₂Br), 1.48 – 1.18 (m, 128H, CH₂ alkyl), 0.88 (t, *J* = 6.7 Hz, 1H, CH₂Si small amount α product), 0.67 – 0.51 (m, 15H, CH₂Si), 0.13 (s, 48H, Si(CH₃)₂). **¹³C NMR** (75 MHz, CDCl₃) δ 34.13 (CH₂Br), 33.64 (CH₂CH₂Br), 33.03 (C_{alkyl}), 29.82 (C_{alkyl}), 29.81 (C_{alkyl}), 29.66 (C_{alkyl}), 29.58 (C_{alkyl}), 28.99 (C_{alkyl}), 28.37 (C_{alkyl}), 23.14 (CH₂Si), 17.87 (CH₂CH₂Si), -0.17 ((CH₃)₂Si). **²⁹Si NMR** (60 MHz, CDCl₃) δ 12.58 (OSi(CH₃)₂R), -108.88 (SiO₄). **IR** ν = 2921 (v C-H), 2856 (v C-H), 1252 (v Si-C), 1074 (v Si-O), 838 (δ C-H), 548 (δ Si-O cage deformation) cm⁻¹. **CHN**_{theo} (C₁₀₄H₂₄₄Br₈O₂₀Si₁₆): C: 43.51; H: 7.89; N – **CHN**_{exp}. C: 43.23; H: 7.75; N –.

Octakis(azidoalkyldimethylsiloxy)octasilsesquioxane (4a-d): Sodium azide (4.60 g, 70.8 mmol, 4 eq per C-Br group) was suspended in a mixture of anhydrous ACN:DMF (10:1 v/v; 40 mL) and the appropriate octakis(bromoalkyldimethylsiloxy)octasilsesquioxane (2.95 mmol) was added. The reaction mixture was heated to 80 °C for 4-5 h. After cooling to room temperature, the mixture was extracted with *n*-hexane (3 x 20 mL). Afterwards, the hexane layer was extracted with water to remove the residual DMF. The organic layer was dried over MgSO₄ and the solvent was removed in vacuo. The product was obtained as colorless oil.

4a: Colorless Oil. **Isolated Yield:** 4.58 g (87 %, 2.57 mmol). **Conversion:** 100 %. **¹H NMR** (300 MHz, CDCl₃) δ 3.27 (t, *J* = 6.9 Hz, 16H, CH₂N₃), 1.69 – 1.57 (m, 16H, CH₂CH₂N₃), 1.51 – 1.37 (m, 16H, CH₂CH₂Si), 0.68 – 0.56 (m, 16H, CH₂Si), 0.15 (s, 48H, Si(CH₃)₂). **¹³C NMR** (75 MHz, CDCl₃) δ 51.19 (CH₂N₃), 32.36 (CH₂CH₂CH₂Si), 20.33 (CH₂Si), 17.30 (CH₂CH₂Si), -0.23 ((CH₃)₂Si). **²⁹Si NMR** (60 MHz, CDCl₃) δ 12.66 (OSi(CH₃)₂R), -108.95 (SiO₄). **IR** ν = 2956 (ν C-H), 2928 (ν C-H), 2092 (ν N₃), 1254 (ν Si-C), 1072 (ν Si-O), 827 (δ C-H), 552 (δ Si-O cage deformation) cm⁻¹. **CHN**_{theo} (C₄₈H₁₁₂N₂₄O₂₀Si₁₆): C: 32.12; H: 6.29; N: 18.73 **CHN**_{exp}: C: 31.78, H: 6.10; N: 18.22.

4b: Colorless Oil. **Isolated Yield:** 5.23 g (93 %, 2.74 mmol). **Conversion:** 100 %. **¹H NMR** (300 MHz, CDCl₃) δ 3.25 (t, *J* = 6.9 Hz, 16H, CH₂N₃), 1.69 – 1.49 (m, 16H, CH₂CH₂N₃), 1.47 – 1.26 (m, 32H, CH₂CH₂CH₂Si), 0.69 – 0.49 (m, 16H, CH₂Si), 0.13 (s, 48H, Si(CH₃)₂). **¹³C NMR** (75 MHz, CDCl₃) δ 51.57 (CH₂N₃), 30.49 (CH₂CH₂CH₂Si), 28.72 (CH₂CH₂CH₂CH₂Si), 22.72 (CH₂Si), 17.70 (CH₂CH₂Si), -0.20 ((CH₃)₂Si). **²⁹Si NMR** (60 MHz, CDCl₃) δ 12.67 (OSi(CH₃)₂R), -108.90 (SiO₄). **IR** ν = 2956 (ν C-H), 2928 (ν C-H), 2091 (ν N₃), 1252 (ν Si-C), 1070 (ν Si-O), 837 (δ C-H), 550 (δ Si-O cage deformation) cm⁻¹. **CHN**_{theo} (C₅₆H₁₂₈N₂₄O₂₀Si₁₆): C: 35.27; H: 6.77; N: 17.63 **CHN**_{exp}: C: 35.26; H: 6.69; N: 16.89.

4c: Colorless Oil. **Isolated Yield:** 5.41 g (91 %, 2.68 mmol). **Conversion:** 100 %. **¹H NMR** (300 MHz, CDCl₃) δ 3.25 (t, *J* = 6.9 Hz, 16H, CH₂N₃), 1.66 – 1.52 (m, 16H, CH₂CH₂N₃), 1.44 – 1.28 (m, 48H), 0.68 – 0.53 (m, 16H, CH₂Si), 0.13 (s, 48H, Si(CH₃)₂). **¹³C NMR** (75 MHz, CDCl₃) δ 51.63 (CH₂N₃), 32.98 (CH₂CH₂CH₂Si), 28.96 (CH₂CH₂N₃), 26.57 (CH₂CH₂CH₂N₃), 22.97 (CH₂Si), 17.72 (CH₂CH₂Si), -0.19 ((CH₃)₂Si). **²⁹Si NMR** (60 MHz, CDCl₃) δ 12.67 (OSi(CH₃)₂R), -108.90 (SiO₄). **IR** ν = 2958 (ν C-H), 2926 (ν C-H), 2092 (ν N₃), 1252 (ν Si-C), 1062 (ν Si-O), 839 (δ C-H), 548 (δ Si-O cage deformation) cm⁻¹. **CHN**_{theo} (C₆₄H₁₄₄N₂₄O₂₀Si₁₆): C: 38.07; H: 7.19; N: 16.65 **CHN**_{exp}: C: 37.95; H: 7.13; N: 16.25.

4d: Colorless Oil. **Isolated Yield:** 6.79 g (89 %, 2.63 mmol). **Conversion:** 100 %. **¹H NMR** (300 MHz, CDCl₃) δ 3.26 (t, *J* = 6.9 Hz, 16H, CH₂N₃), 1.66 – 1.54 (m, 16H, CH₂CH₂N₃), 1.46 – 1.22 (m, 128H, CH₂ alkyl), 0.91 – 0.85 (m, 1H, CH₂Si small amount α product), 0.66 – 0.52 (m, 15H, CH₂Si), 0.09 (s, 48H, Si(CH₃)₂). **¹³C NMR** (75 MHz, CDCl₃) δ 51.64 (CH₂N₃), 33.64 (CH₂CH₂N₃), 29.80, 29.70, 29.58, 29.37, 29.01, 26.91, 23.14 (CH₂Si), 17.86 (CH₂CH₂Si), -0.18 ((CH₃)₂Si). **²⁹Si NMR** (60 MHz, CDCl₃) δ 12.58 (OSi(CH₃)₂R), -108.88 (SiO₄). **IR** ν = 2921 (ν C-H), 2856 (ν C-H), 2091 (ν N₃), 1252 (ν Si-C), 1074 (ν Si-O), 838 (δ C-H), 548 (δ Si-O cage deformation) cm⁻¹. **CHN**_{theo} (C₁₀₄H₂₄₄N₈O₂₀Si₁₆): C 48.41; H: 8.75; N 13.03 **CHN**_{exp}: C: 48.54; H: 8.10; N 12.15.

Octakis(aminoalkyldimethylsiloxy)octasilsesquioxane (5a-d).

Octakis(azidoalkyldimethylsiloxy)octasilsesquioxane (Yield from **4a-d**) and palladium catalyst on activated carbon (10 wt%, ca. 200 mg) was suspended in anhydrous ethanol (200 mL). Hydrogen was bubbled slowly through the suspension for 1-2 h at 20-25 °C. The quantitative conversion was determined by ¹H NMR spectroscopy. Therefore, the catalyst was removed by filtering through a glas

filter under inert atmosphere and the solvent was evaporated at room temperature in vacuo. ^{29}Si was not possible to acquire due to long measurement time in which the cube structure decomposes.

5a: Not isolated. **Conversion:** 100 %, 2.57 mmol. $^1\text{H NMR}$ (300 MHz, MeOD) δ 2.64 (t, 16H, CH_2NH_2), 1.55 – 1.37 (m, 32H, $\text{CH}_2\text{CH}_2\text{CH}_2\text{Si}$), 0.68 – 0.59 (m, 16H, CH_2Si), 0.11 (s, 42H (should be 48, $(\text{CH}_3)_2\text{Si}$)). $^{13}\text{C NMR}$ (75 MHz, CDCl_3) δ 42.20 (CH_2NH_2), 37.37 ($\text{CH}_2\text{CH}_2\text{NH}_2$), 21.58 (CH_2Si), 16.59 ($\text{CH}_2\text{CH}_2\text{Si}$), -2.69 ($(\text{CH}_3)_2\text{Si}$). **IR** ν = 3300 (ν N-H), 2958 (ν C-H), 2924 (ν C-H), 1579 (δ N-H), 1251 (ν Si-C), 1045 (ν Si-O), 836 (δ C-H), 545 (δ Si-O cage deformation) cm^{-1} . **ESI-MS:** +MS: $[\text{M}+\text{H}^+]$: 1586.59, $[\text{M}+2\text{H}^+]$: 793.33 m/z.

5b: Not isolated. **Conversion:** 100 %, 2.74 mmol. $^1\text{H NMR}$ (300 MHz, MeOD) δ 2.63 (t, J = 6.9 Hz, 16H, CH_2NH_2), 1.55 – 1.37 (m, 48H, $\text{CH}_2\text{CH}_2\text{CH}_2\text{CH}_2\text{Si}$), 0.72 – 0.61 (m, 16H, CH_2Si), 0.17 (s, 48H, $(\text{CH}_3)_2\text{Si}$). $^{13}\text{C NMR}$ (75 MHz, MeOD) δ 42.50 (CH_2NH_2), 33.53 ($\text{CH}_2\text{CH}_2\text{NH}_2$), 31.74 ($\text{CH}_2\text{CH}_2\text{CH}_2\text{NH}_2$), 24.10 (CH_2Si), 16.70 ($\text{CH}_2\text{CH}_2\text{Si}$), -2.69 ($(\text{CH}_3)_2\text{Si}$). **IR** ν = 3300 (ν N-H), 2958 (ν C-H), 2924 (ν C-H), 1579 (δ N-H), 1251 (ν Si-C), 1045 (ν Si-O), 836 (δ C-H), 545 (δ Si-O cage deformation) cm^{-1} . **ESI-MS:** +MS: $[\text{M}+\text{H}^+]$: 1699.70 $[\text{M}+2\text{H}^+]$: 849.89 m/z.

5c: Not isolated. **Conversion:** 100 %, 2.68 mmol. $^1\text{H NMR}$ (300 MHz, MeOD) δ 2.70 – 2.57 (m, 16H, CH_2NH_2), 1.45 (dd, J = 21.1, 14.2 Hz, 64H, $\text{CH}_2\text{CH}_2\text{CH}_2\text{CH}_2\text{CH}_2\text{Si}$), 0.66 (s, 16H, CH_2Si), 0.16 (d, J = 3.3 Hz, 48H, $(\text{CH}_3)_2\text{Si}$). $^{13}\text{C NMR}$ (75 MHz, MeOD) δ 42.60 (CH_2NH_2), 34.35 ($\text{CH}_2\text{CH}_2\text{CH}_2\text{CH}_2\text{NH}_2$), 33.78 ($\text{CH}_2\text{CH}_2\text{NH}_2$), 27.72 ($\text{CH}_2\text{CH}_2\text{CH}_2\text{NH}_2$), 24.16 (CH_2Si), 16.68 ($\text{CH}_2\text{CH}_2\text{Si}$), -2.69 ($(\text{CH}_3)_2\text{Si}$). **IR** ν = 3300 (ν N-H), 2958 (ν C-H), 2924 (ν C-H), 1579 (δ N-H), 1251 (ν Si-C), 1045 (ν Si-O), 836 (δ C-H), 545 (δ Si-O cage deformation) cm^{-1} . **ESI-MS:** +MS: $[\text{M}+\text{H}^+]$: 1811.90, $[\text{M}+2\text{H}^+]$: 906.42 m/z.

5d: Slightly yellow solid. **Conversion:** 100 %, 2.63 mmol. **Isolated Yield:** 4.49 g (1.89 mmol, 72 %). $^1\text{H NMR}$ (300 MHz, MeOD) δ 2.92 (d, J = 7.1 Hz, 16H, CH_2NH_2), 1.74 – 1.58 (m, 16H, $\text{CH}_2\text{CH}_2\text{NH}_2$), 1.48 – 1.24 (m, 128H, , CH_2 alkyl), 0.69 – 0.62 (m, 16H, CH_2Si), 0.16 (s, 48H, $\text{Si}(\text{CH}_3)_2$). $^{13}\text{C NMR}$ (75 MHz, MeOD) δ 40.82 (CH_2NH_2), 34.70 ($\text{CH}_2\text{CH}_2\text{N}$), 30.92 (C_{alkyl}), 30.89 (C_{alkyl}), 30.72 (C_{alkyl}), 30.68 (C_{alkyl}), 30.41 (C_{alkyl}), 28.66 (C_{alkyl}), 27.62 (C_{alkyl}), 24.26 (CH_2Si), 18.75 ($\text{CH}_2\text{CH}_2\text{Si}$), 0.09 ($\text{Si}(\text{CH}_3)_2$). $^{29}\text{Si NMR}$ (60 MHz, MeOD) δ 13.00 ($\text{OSi}(\text{CH}_3)_2\text{R}$), -108.63 (SiO_4). **CHN**_{theo} ($\text{C}_{104}\text{H}_{240}\text{N}_8\text{O}_{20}\text{Si}_{16}$): C, 52.65; H, 10.20; N, 4.72 **CHN**_{exp}. C, 47.44; H, 9.25; N, 4.78. **IR** ν = 3300 (ν N-H), 2921 (ν C-H), 2856 (ν C-H), 1579 (δ N-H), 1252 (δ C-H), 1074 (ν Si-O), 838 (δ C-H), 548 (δ Si-O cage deformation) cm^{-1} . **TG residual mass:** N_2 : 29.93 %, O_2 : 33.22 % (theoretical residual mass: 32.43%). **ESI-MS:** $[\text{M}+2\text{H}^+]$: 1186.73, $[\text{M}+3\text{H}^+]$: 791.49 m/z.

Octakis(X-(3-propylurea)alkyl-1-dimethylsiloxy)octasilsesquioxane (X = 4, 5, 6, 11).

The amine cube solutions in ethanol were filtered off from reaction solution under inert atmosphere. Propyl isocyanate (1 eq) was added at room temperature to the reaction mixture. Afterwards, the solvent was removed in vacuo and in case of residual free propyl isocyanate, the product was extracted with chloroform.

6a: Colorless Solid. **Yield:** 5.53 g (95 %, 2.44 mmol). $^1\text{H NMR}$ (300 MHz, MeOD) δ 3.20 – 3.01 (m, 32H, $\text{CH}_2\text{NHCONHCH}_2$), 1.49 (td, J = 14.6, 7.3 Hz, 48H, $\text{CH}_2\text{CH}_2\text{CH}_2\text{NHCONHCH}_2\text{CH}_2$), 0.91 (t, J = 7.4 Hz, 24H, CH_3), 0.75 – 0.61 (m, 16H, CH_2Si), 0.18 (s, 48H, $\text{Si}(\text{CH}_3)_2$). $^{13}\text{C NMR}$ (75 MHz, MeOD) δ 161.33 (CO), 42.83 (CONHCH₂), 40.74 (CONHCH₂—Si), 35.01 (C_{alkyl}), 24.57 (CH_2Si), 21.46 (C_{alkyl}), 18.39 ($\text{CH}_2\text{CH}_2\text{Si}$), 11.69 (CH_3), 0.01 ($\text{Si}(\text{CH}_3)_2$). $^{29}\text{Si NMR}$ (60 MHz, MeOD) δ 13.31 ($\text{OSi}(\text{CH}_3)_2\text{R}$), -108.57 (SiO_4). **IR** ν = 3332 (ν N-H), 2960 (ν C-H), 2928 (ν C-H), 1632 (amide I ν C=O), 1568 (amide II, δ N-H, C=O, ν C-N), 1252 (δ C-H), 1070 (ν Si-O), 842 (δ C-H), 554 (δ Si-O cage deformation) cm^{-1} . **ESI-MS:** $[\text{M}+\text{H}^++\text{Na}^+]$: 1156.50 m/z.

6b: Colorless Solid. **Yield:** 6.19 g (95 %, 2.60 mmol). **¹H NMR** (300 MHz, MeOD) δ 3.09 (dt, J = 13.9, 6.9 Hz, 32H, $\text{CH}_2\text{NHCONHCH}_2$), 1.57 – 1.33 (m, 64H, $\text{CH}_2\text{CH}_2\text{CH}_2\text{CH}_2\text{NHCONHCH}_2\text{CH}_2\text{CH}_3$), 0.91 (t, J = 7.4 Hz, 24H, CH_3), 0.73 – 0.59 (m, 16H, CH_2Si), 0.17 (s, 48H, $\text{Si}(\text{CH}_3)_2$). **¹³C NMR** (75 MHz, MeOD) δ 161.33 (CO), 42.84 (CONHCH_2), 41.07 ($\text{CONHCH}_2\text{—Si}$), 31.81 (C_{alkyl}), 31.21 (C_{alkyl}), 24.56 (C_{alkyl}), 23.99 (C_{alkyl}), 23.56 (CH_2Si), 18.70 ($\text{CH}_2\text{CH}_2\text{Si}$), 11.68 (CH_3), 0.04 ($\text{Si}(\text{CH}_3)_2$). **²⁹Si NMR** (60 MHz, MeOD) δ 13.24 ($\text{OSi}(\text{CH}_3)_2\text{R}$), -108.55 (SiO_4). **IR** ν = 3333 (ν N-H), 2960 (ν C-H), 2926 (ν C-H), 1628 (amide I ν C=O), 1570 (amide II, δ N-H, C=O, ν C-N), 1252 (ν Si-C), 1070 (ν Si-O), 839 (δ C-H), 548 (δ Si-O cage deformation) cm^{-1} . **ESI-MS:** $[\text{M}+\text{H}^++\text{Na}^+]$: 1212.56 m/z .

6c: Colorless Solid. **Yield:** 6.41 g (96 %, 2.57 mmol). **¹H NMR** (300 MHz, MeOD) δ 3.16 – 2.99 (m, 32H, $\text{CH}_2\text{NHCONHCH}_2$), 1.57 – 1.27 (m, 80H, $\text{CH}_2\text{CH}_2\text{CH}_2\text{CH}_2\text{CH}_2\text{NHCONHCH}_2\text{CH}_2$), 0.91 (t, J = 7.4 Hz, 24H, CH_3), 0.72 – 0.55 (m, J = 14.7 Hz, 16H, CH_2Si), 0.16 (s, 48H, $\text{Si}(\text{CH}_3)_2$). **¹³C NMR** (75 MHz, MeOD) δ 161.34 (CO), 42.84 (CONHCH_2), 41.15 ($\text{CONHCH}_2\text{—Si}$), 34.51 (C_{alkyl}), 31.51 (C_{alkyl}), 27.78 (C_{alkyl}), 24.56 (C_{alkyl}), 24.16 (CH_2Si), 18.84 ($\text{CH}_2\text{CH}_2\text{Si}$), 11.68 (CH_3), 0.07 ($\text{Si}(\text{CH}_3)_2$). **²⁹Si NMR** (60 MHz, MeOD) δ 13.23 ($\text{OSi}(\text{CH}_3)_2\text{R}$), -108.56 (SiO_4). **IR** ν = 3329 (ν N-H), 2960 (ν C-H), 2924 (ν C-H), 2858 (ν C-H), 1628 (amide I ν C=O), 1572 (amide II, δ N-H, C=O, ν C-N), 1252 (δ Si-C), 1062 (ν Si-O), 839 (δ C-H), 548 (δ Si-O cage deformation) cm^{-1} . **ESI-MS:** $[\text{M}+2\text{Na}^+]$: 1268.63 m/z .

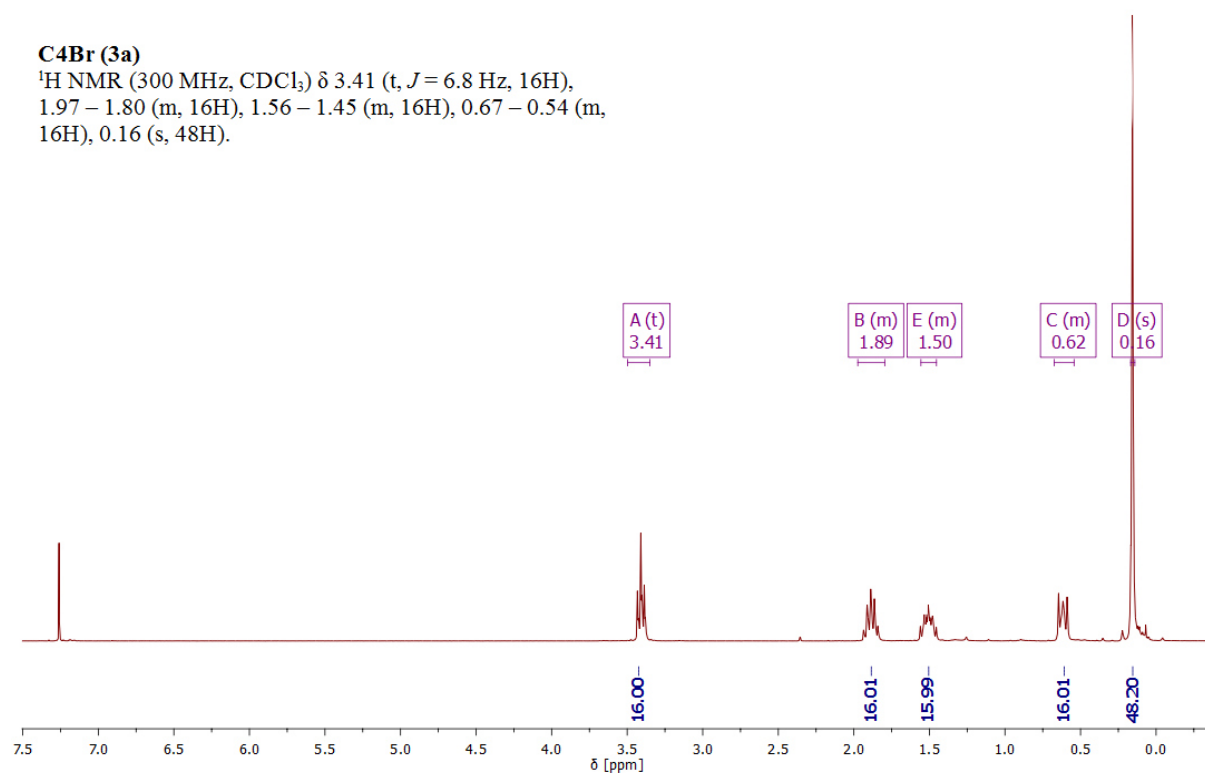
6d: Colorless Solid. **Yield:** 7.63 g (2.50 mmol, 95 %). **¹H NMR** (300 MHz, MeOD) δ 3.16 – 3.03 (m, J = 9.7, 7.0 Hz, 32H, $\text{CH}_2\text{NHCONHCH}_2$), 1.56 – 1.23 (m, 160H, $\text{CH}_{2\text{alkyl}}$), 0.91 (t, J = 7.4 Hz, 24H, CH_3), 0.70 – 0.61 (m, 16H, CH_2Si), 0.14 (s, 48H, $\text{Si}(\text{CH}_3)_2$). **¹³C NMR** (75 MHz, MeOD) δ 161.36 (CO), 42.84 (CONHCH_2), 41.10 ($\text{CONHCH}_2\text{—Si}$), 34.69 (C_{alkyl}), 31.49 (C_{alkyl}), 30.94 (C_{alkyl}), 30.69 (C_{alkyl}), 28.10 (C_{alkyl}), 24.55 (C_{alkyl}), 24.27 (CH_2Si), 18.77 ($\text{CH}_2\text{CH}_2\text{Si}$), 11.67 (CH_3), 0.15 ($\text{Si}(\text{CH}_3)_2$). **²⁹Si NMR** (60 MHz, MeOD) δ 12.98 ($\text{OSi}(\text{CH}_3)_2\text{R}$), -108.63 (SiO_4). **IR** ν = 3325 (ν N-H), 2960 (ν C-H), 2922 (ν C-H), 1624 (amide I, ν C=O), 1579 (amide II, δ N-H, C=O, ν C-N), 1252 (ν Si-C), 1072 (ν Si-O), 840 (δ C-H), 550 (δ Si-O cage deformation) cm^{-1} . **TG residual mass:** N_2 : 28.19 %, (theoretical residual mass: 29.39 %). **ESI-MS:** $[\text{M}+2\text{Na}^+]$: 1549.40, $[\text{M}+\text{Na}^++\text{K}^+]$: 1557.39, $[\text{M}+2\text{K}^+]$: 1564.89 m/z .

NMR

C4Br (3a)

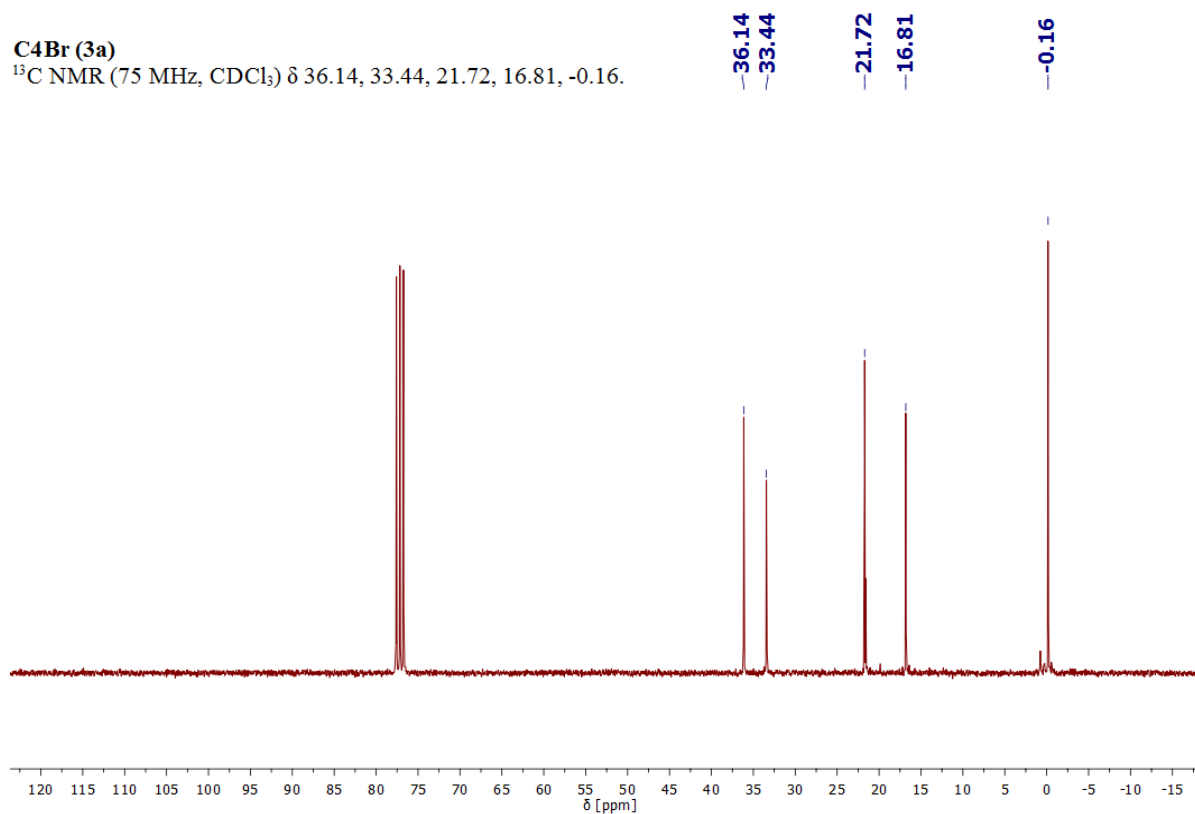
C4Br (3a)

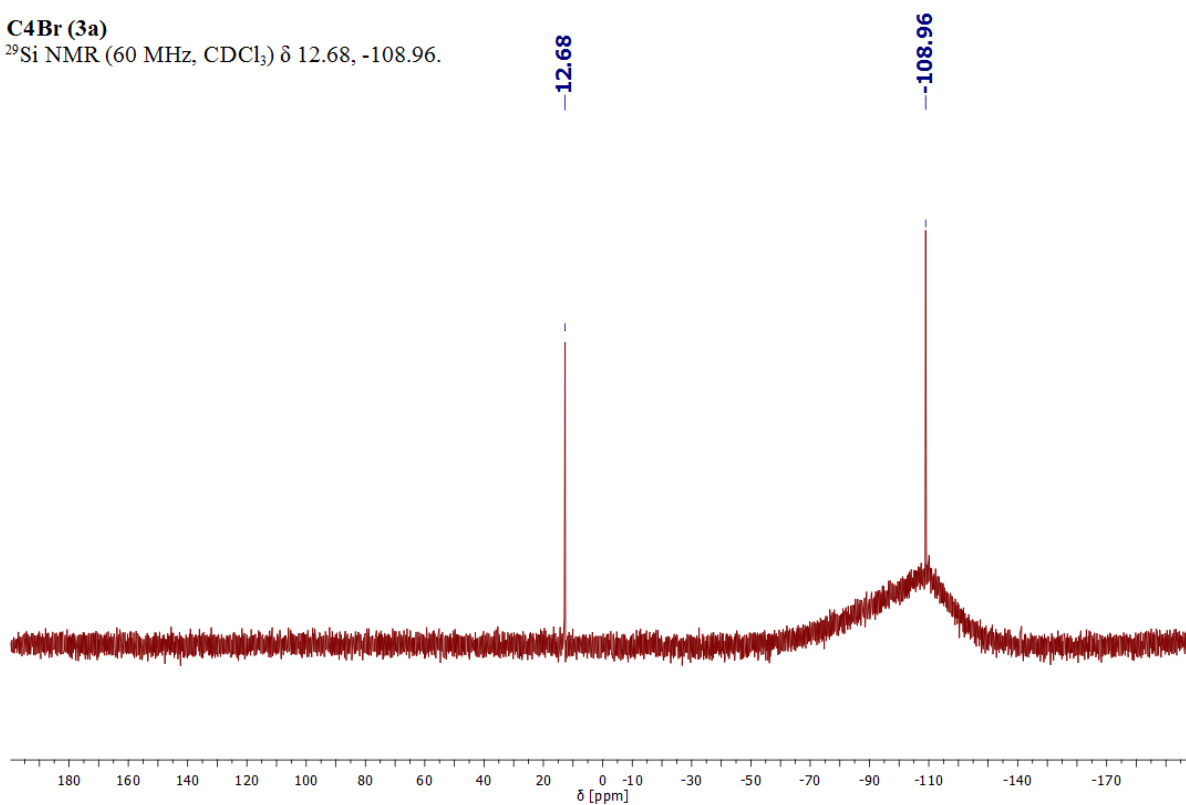
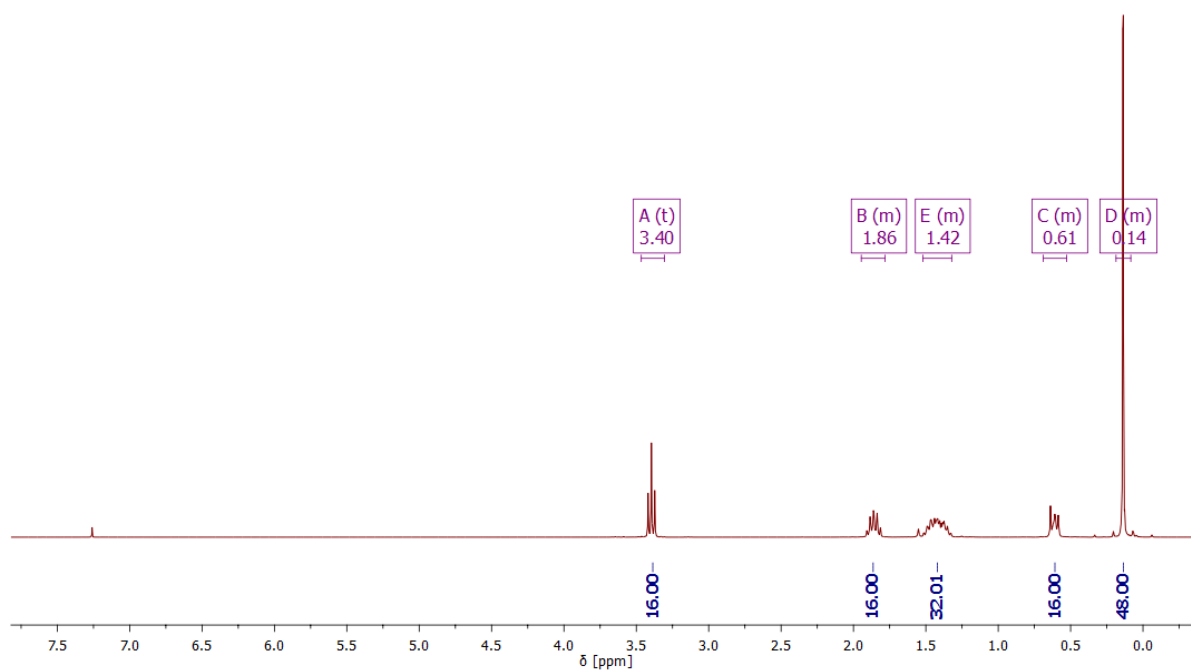
^1H NMR (300 MHz, CDCl_3) δ 3.41 (t, $J = 6.8$ Hz, 16H),
1.97 – 1.80 (m, 16H), 1.56 – 1.45 (m, 16H), 0.67 – 0.54 (m,
16H), 0.16 (s, 48H).

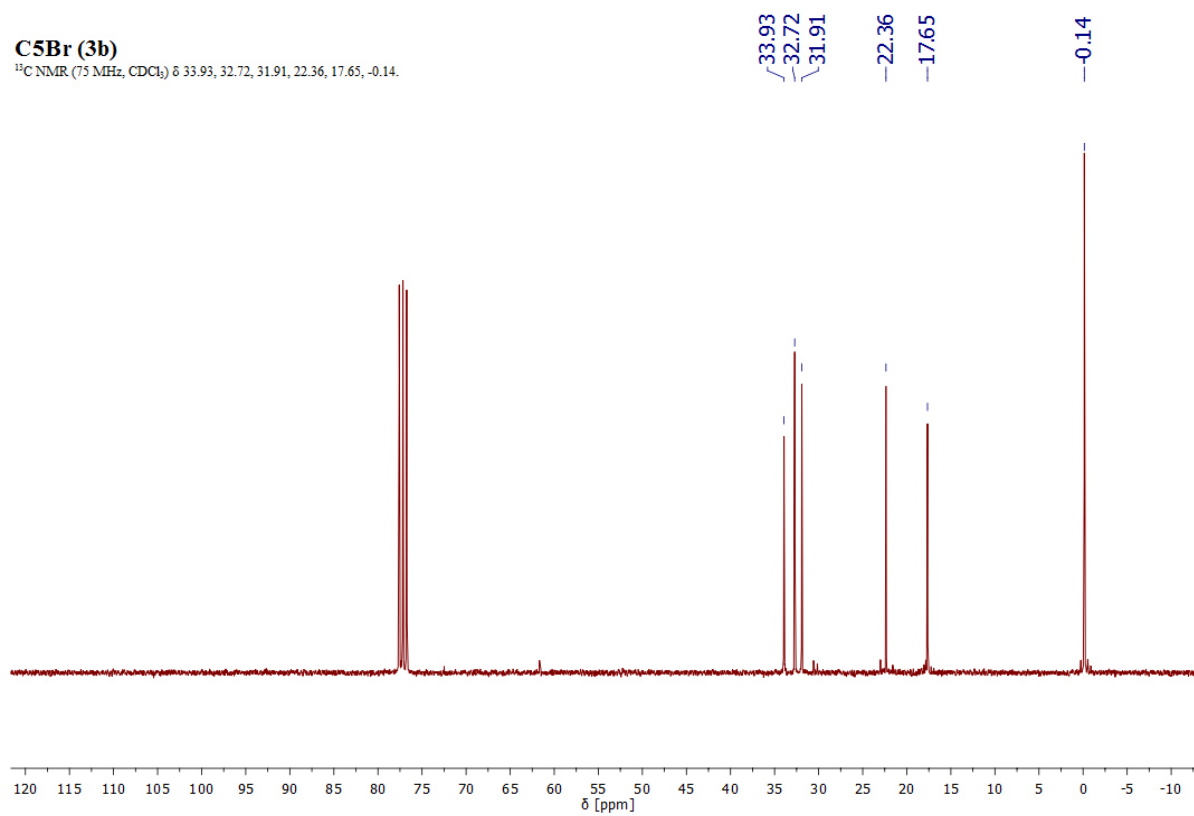
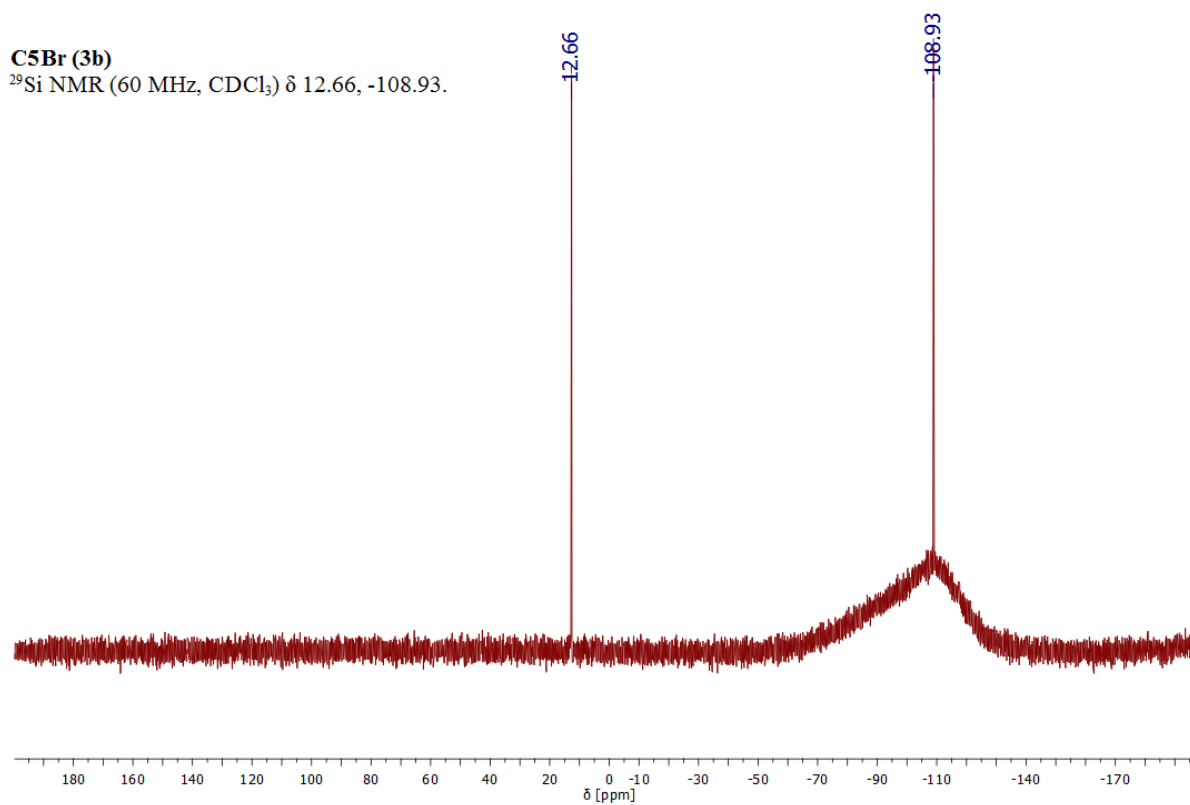


C4Br (3a)

^{13}C NMR (75 MHz, CDCl_3) δ 36.14, 33.44, 21.72, 16.81, -0.16.

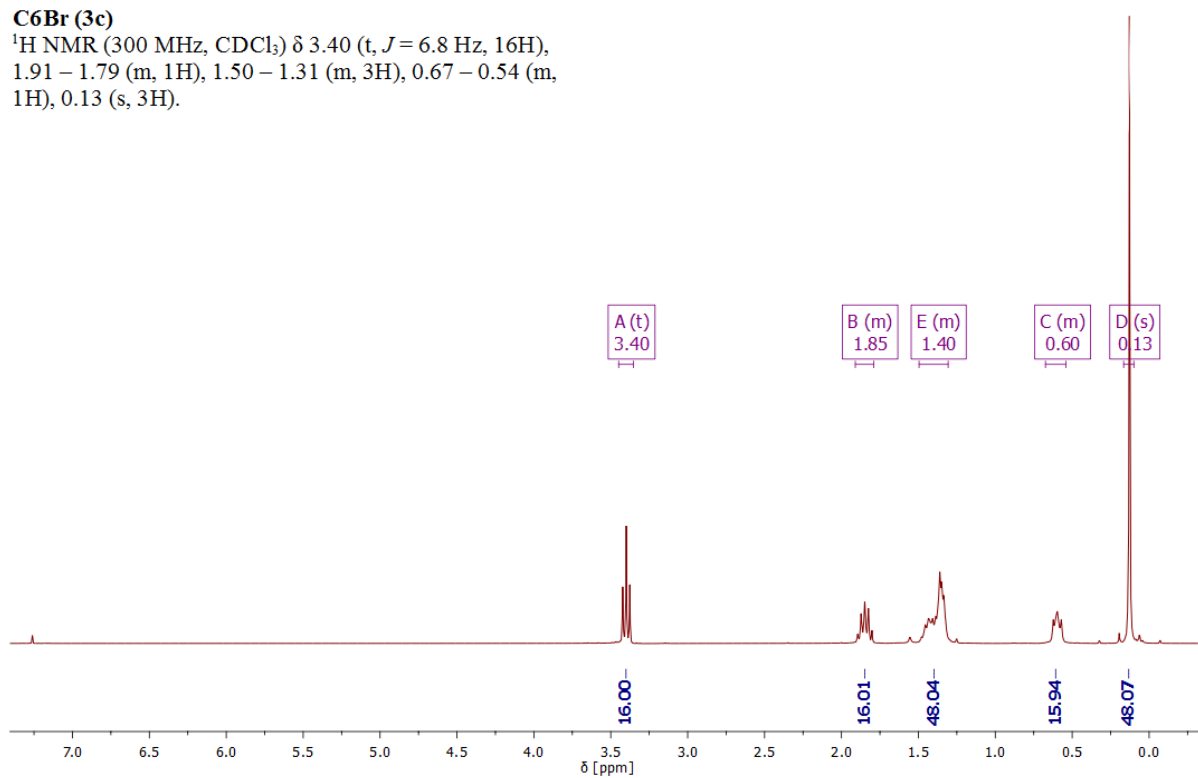


C4Br (3a)²⁹Si NMR (60 MHz, CDCl₃) δ 12.68, -108.96.**C5Br (3b)****C5Br (3b)**¹H NMR (300 MHz, CDCl₃) δ 3.40 (t, *J* = 6.9 Hz, 1H), 1.95 – 1.78 (m, 16H), 1.52 – 1.32 (m, 2H), 0.69 – 0.53 (m, 1H), 0.19 – 0.08 (m, 3H).

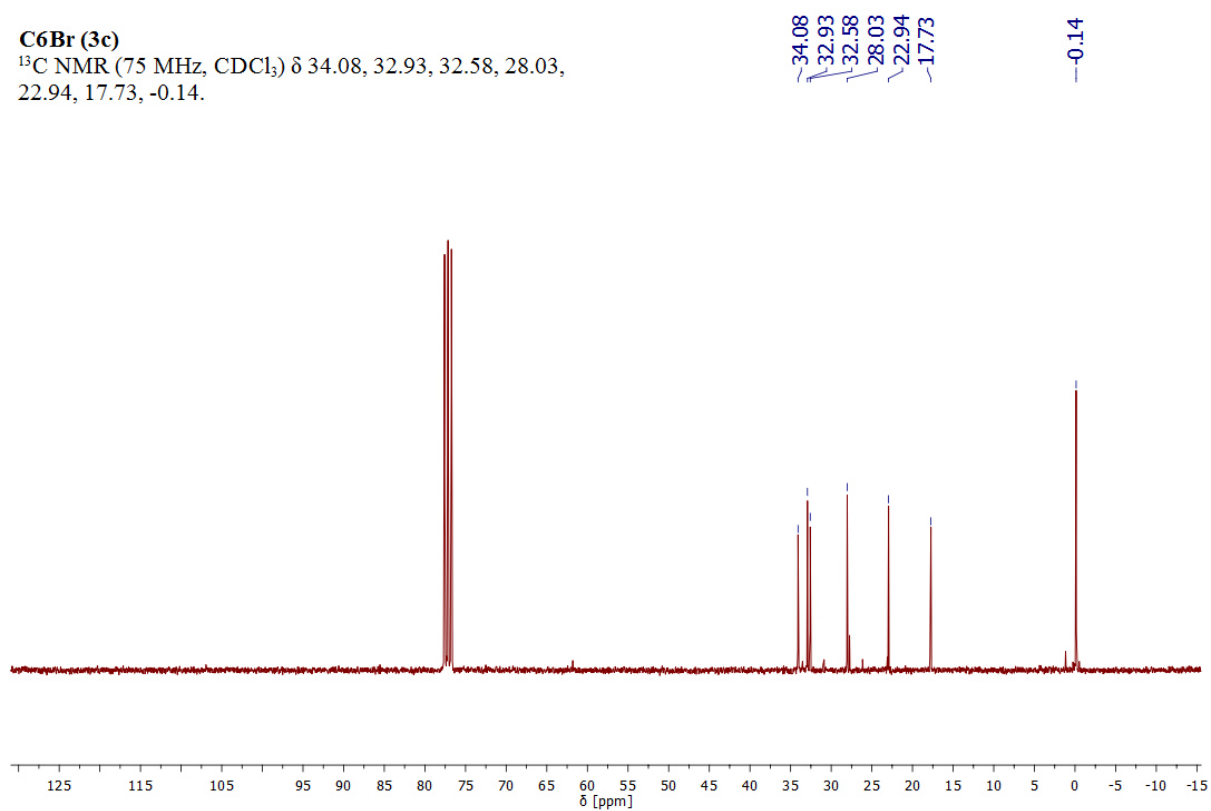
C5Br (3b) ^{13}C NMR (75 MHz, CDCl_3) δ 33.93, 32.72, 31.91, 22.36, 17.65, -0.14.**C5Br (3b)** ^{29}Si NMR (60 MHz, CDCl_3) δ 12.66, -108.93.

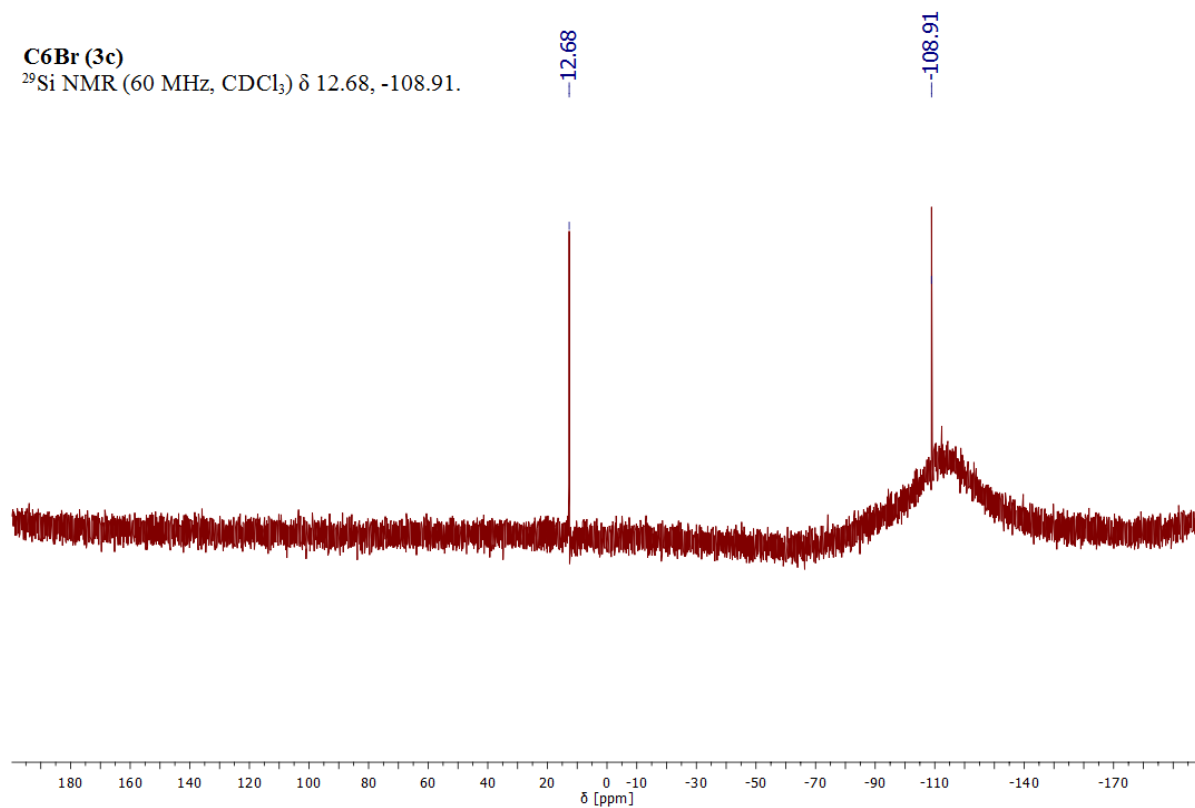
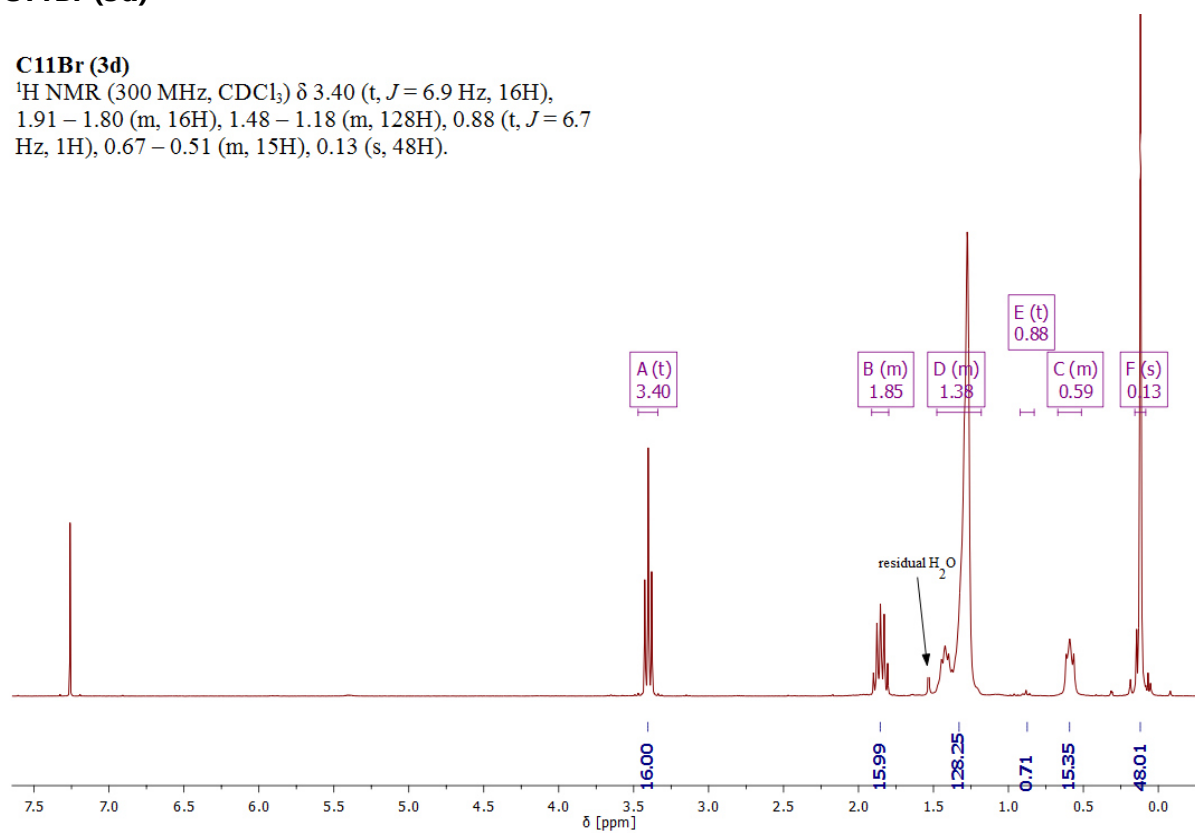
C6Br (3c)**C6Br (3c)**

^1H NMR (300 MHz, CDCl_3) δ 3.40 (t, $J = 6.8$ Hz, 16H), 1.91 – 1.79 (m, 1H), 1.50 – 1.31 (m, 3H), 0.67 – 0.54 (m, 1H), 0.13 (s, 3H).

**C6Br (3c)**

^{13}C NMR (75 MHz, CDCl_3) δ 34.08, 32.93, 32.58, 28.03, 22.94, 17.73, -0.14.

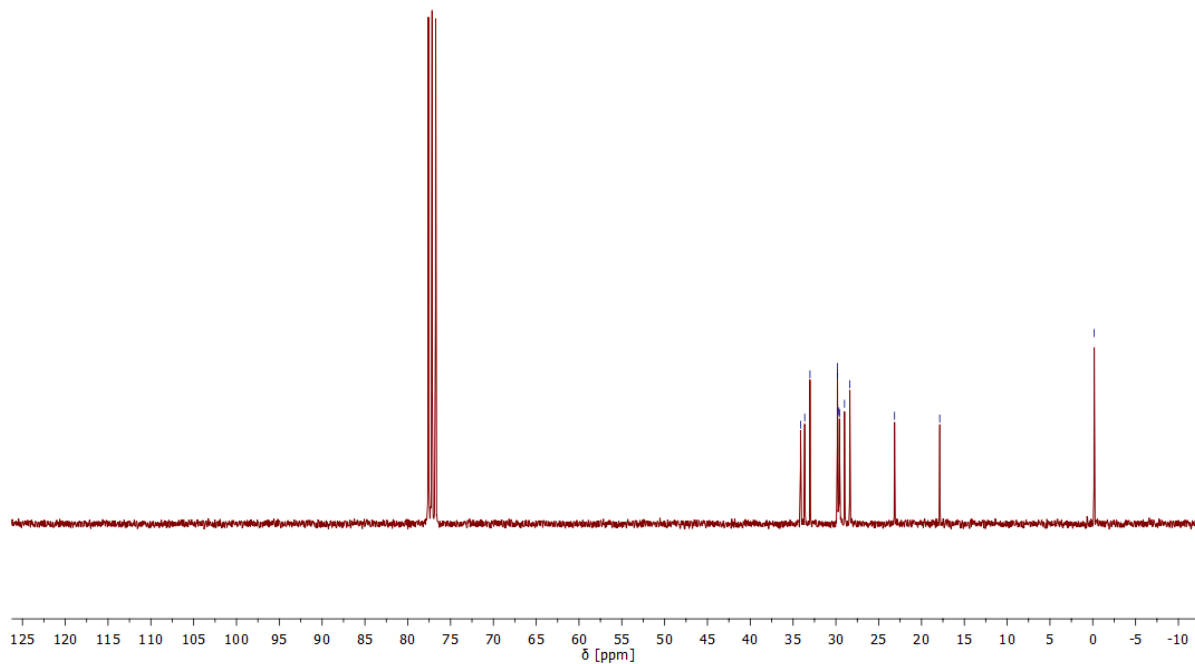


C6Br (3c) ^{29}Si NMR (60 MHz, CDCl_3) δ 12.68, -108.91.**C11Br (3d)****C11Br (3d)** ^1H NMR (300 MHz, CDCl_3) δ 3.40 (t, $J = 6.9$ Hz, 16H), 1.91 – 1.80 (m, 16H), 1.48 – 1.18 (m, 128H), 0.88 (t, $J = 6.7$ Hz, 1H), 0.67 – 0.51 (m, 15H), 0.13 (s, 48H).

C11Br (3d)

^{13}C NMR (75 MHz, CDCl_3) δ 34.13, 33.64, 33.03, 29.82, 29.81, 29.66, 29.58, 28.99, 28.37, 23.14, 17.87, -0.17.

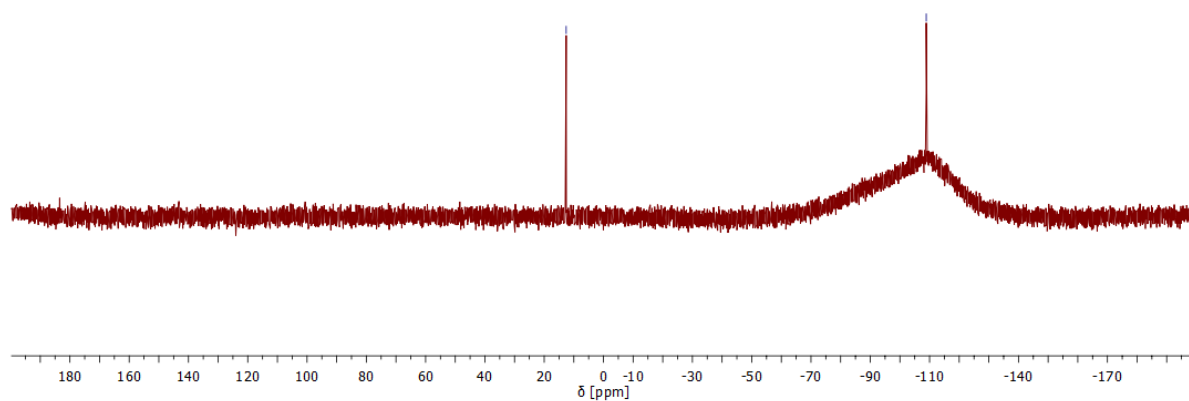
34.13
33.64
33.03
29.82
29.81
29.66
29.58
28.99
28.37
23.14
17.87
-0.17

**C11Br (3d)**

^{29}Si NMR (60 MHz, CDCl_3) δ 12.58, -108.88.

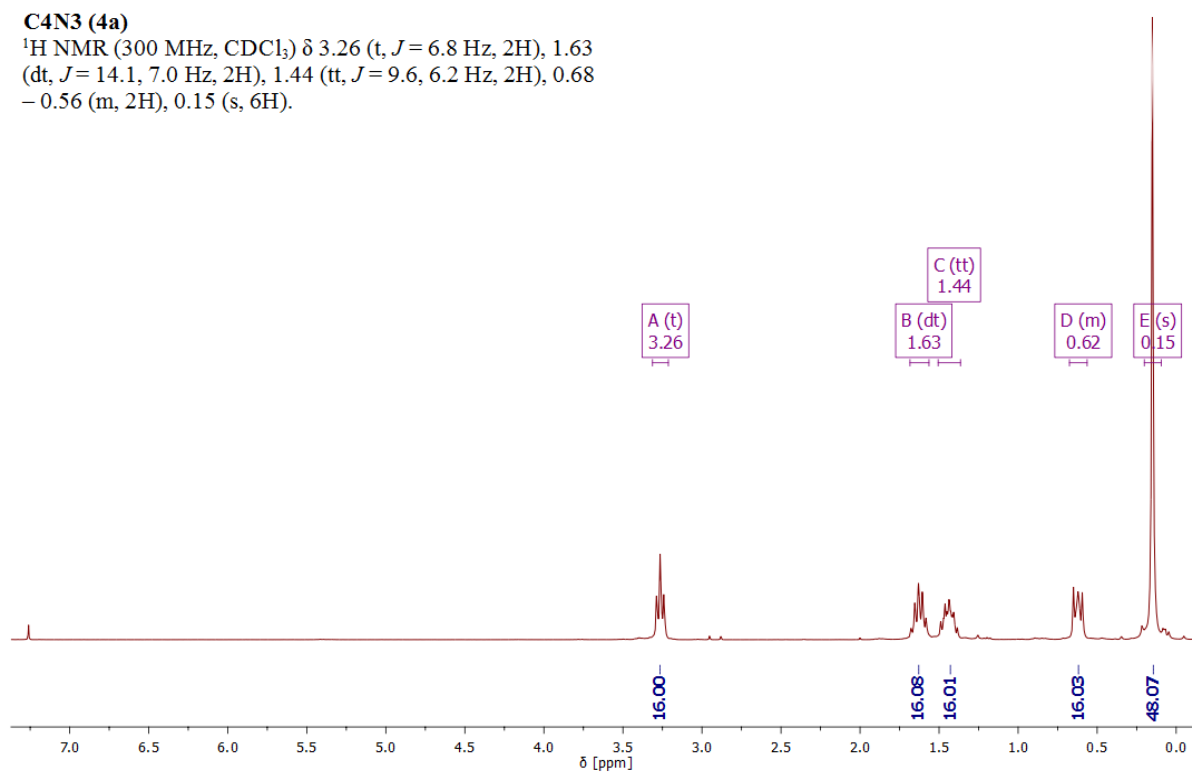
12.58

-108.88

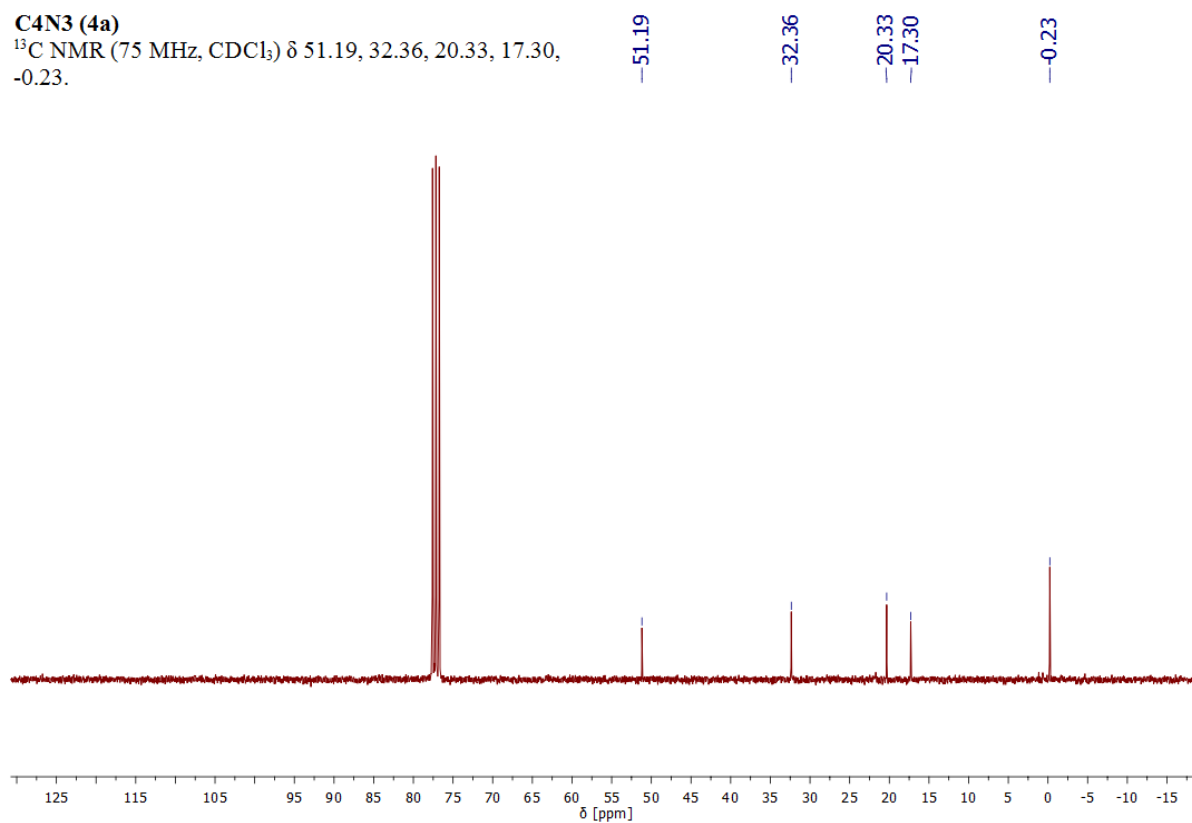


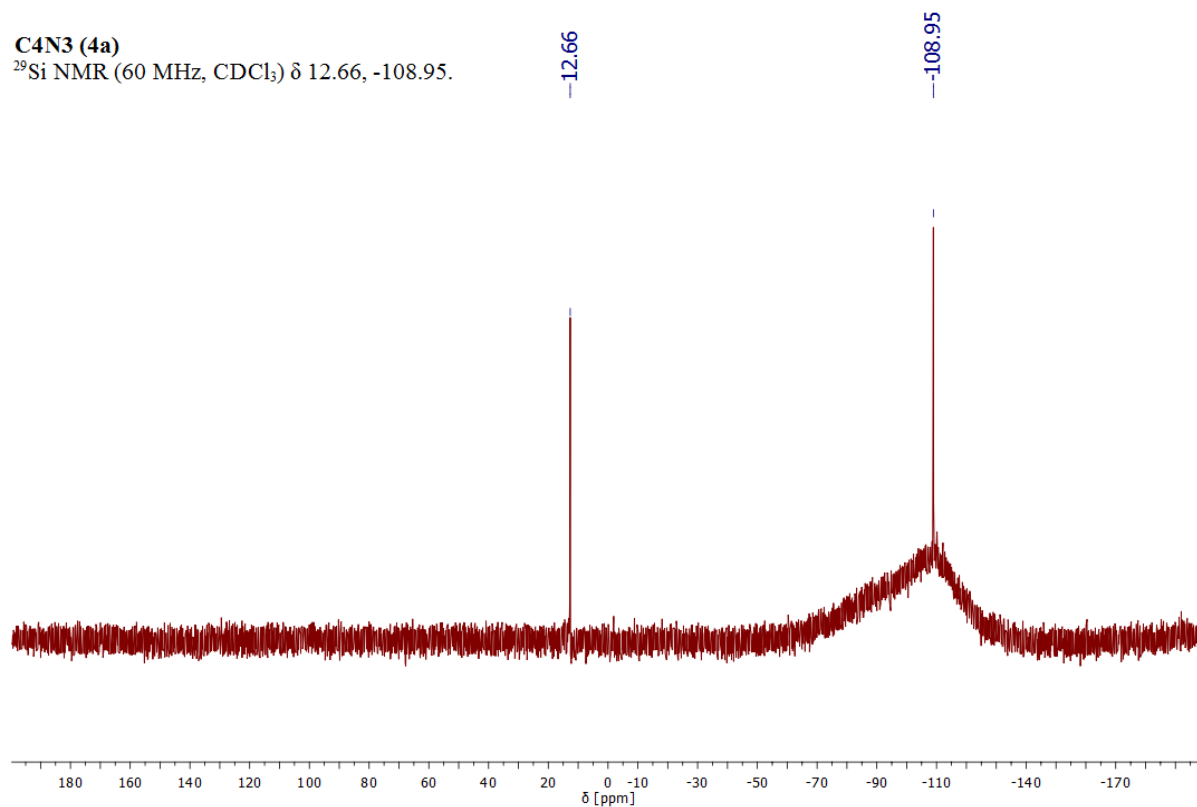
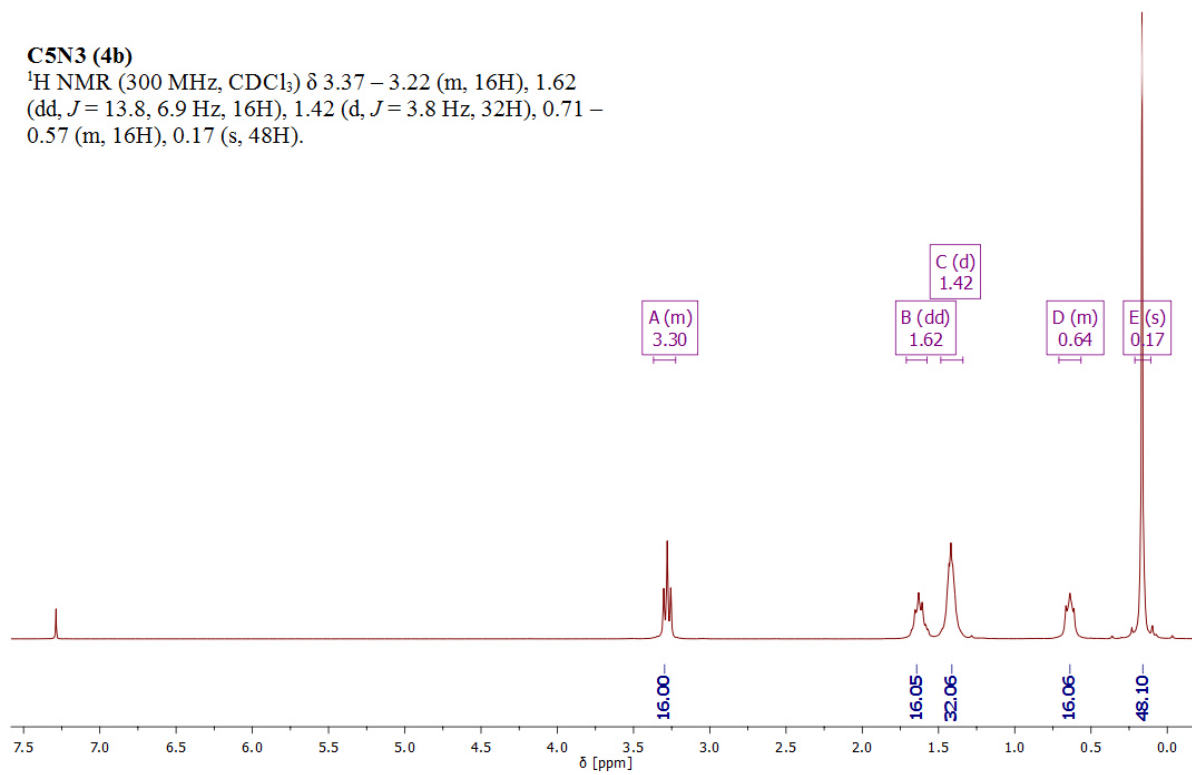
C4N3 (4a)**C4N3 (4a)**

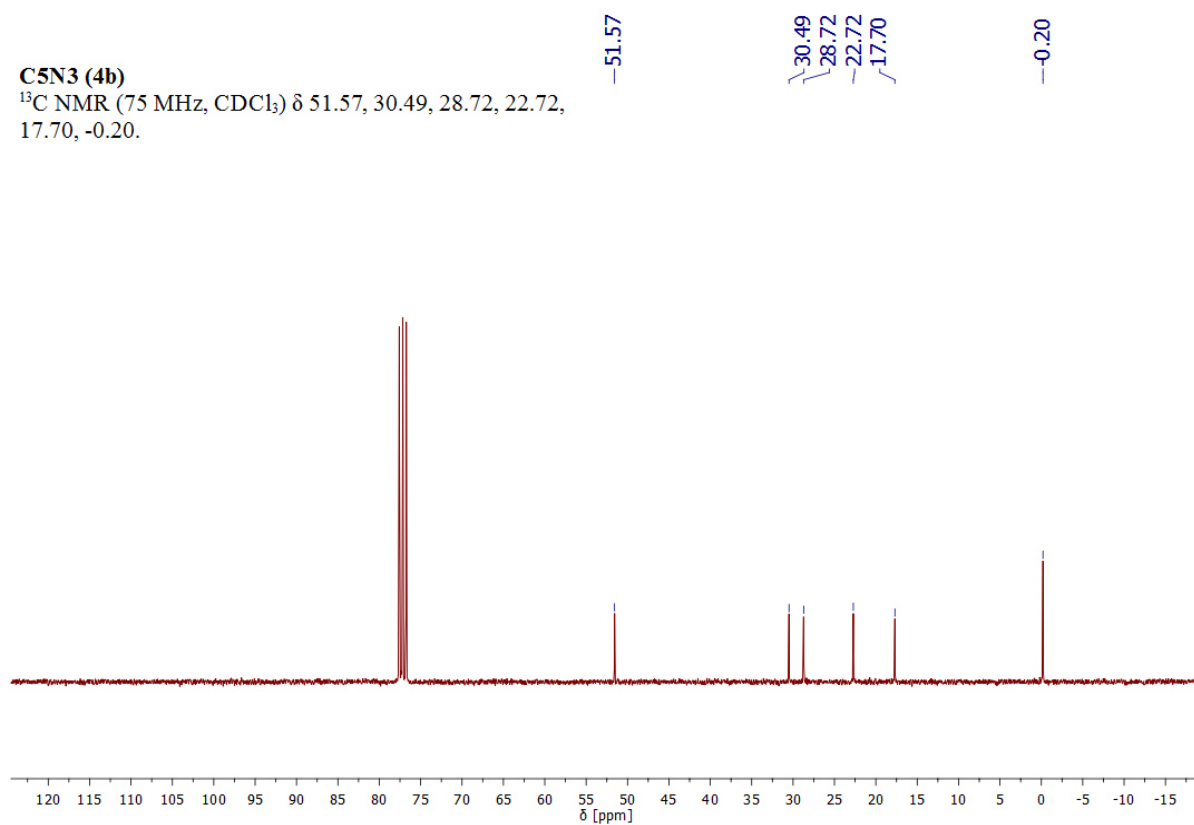
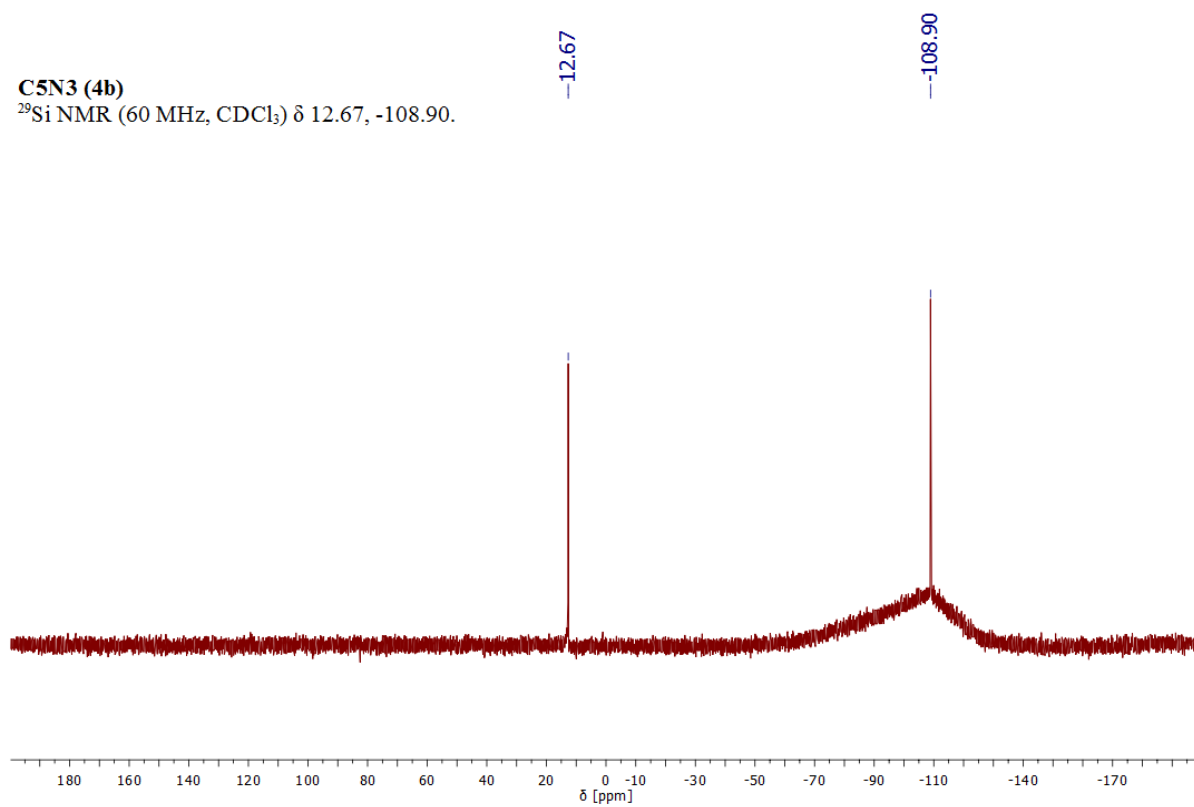
^1H NMR (300 MHz, CDCl_3) δ 3.26 (t, $J = 6.8$ Hz, 2H), 1.63 (dt, $J = 14.1, 7.0$ Hz, 2H), 1.44 (tt, $J = 9.6, 6.2$ Hz, 2H), 0.68 – 0.56 (m, 2H), 0.15 (s, 6H).

**C4N3 (4a)**

^{13}C NMR (75 MHz, CDCl_3) δ 51.19, 32.36, 20.33, 17.30, -0.23.

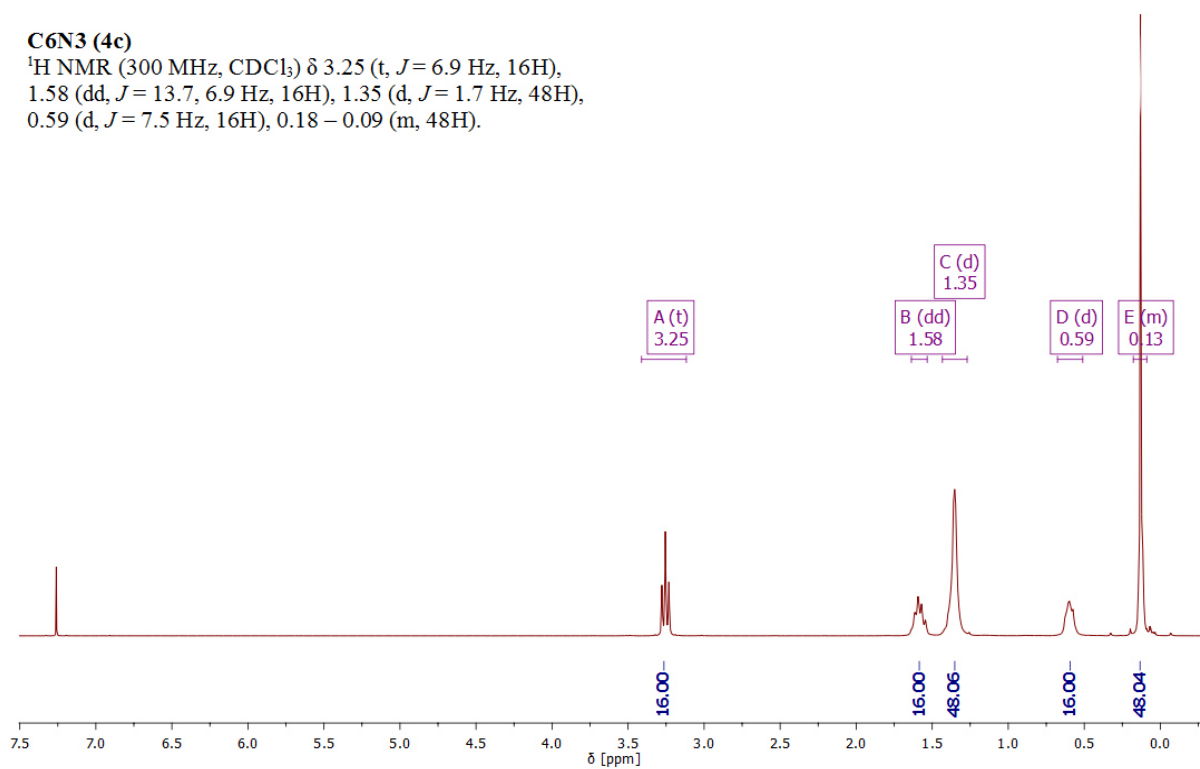


C4N3 (4a)²⁹Si NMR (60 MHz, CDCl₃) δ 12.66, -108.95.**C5N3 (4b)****C5N3 (4b)**¹H NMR (300 MHz, CDCl₃) δ 3.37 – 3.22 (m, 16H), 1.62 (dd, *J* = 13.8, 6.9 Hz, 16H), 1.42 (d, *J* = 3.8 Hz, 32H), 0.71 – 0.57 (m, 16H), 0.17 (s, 48H).

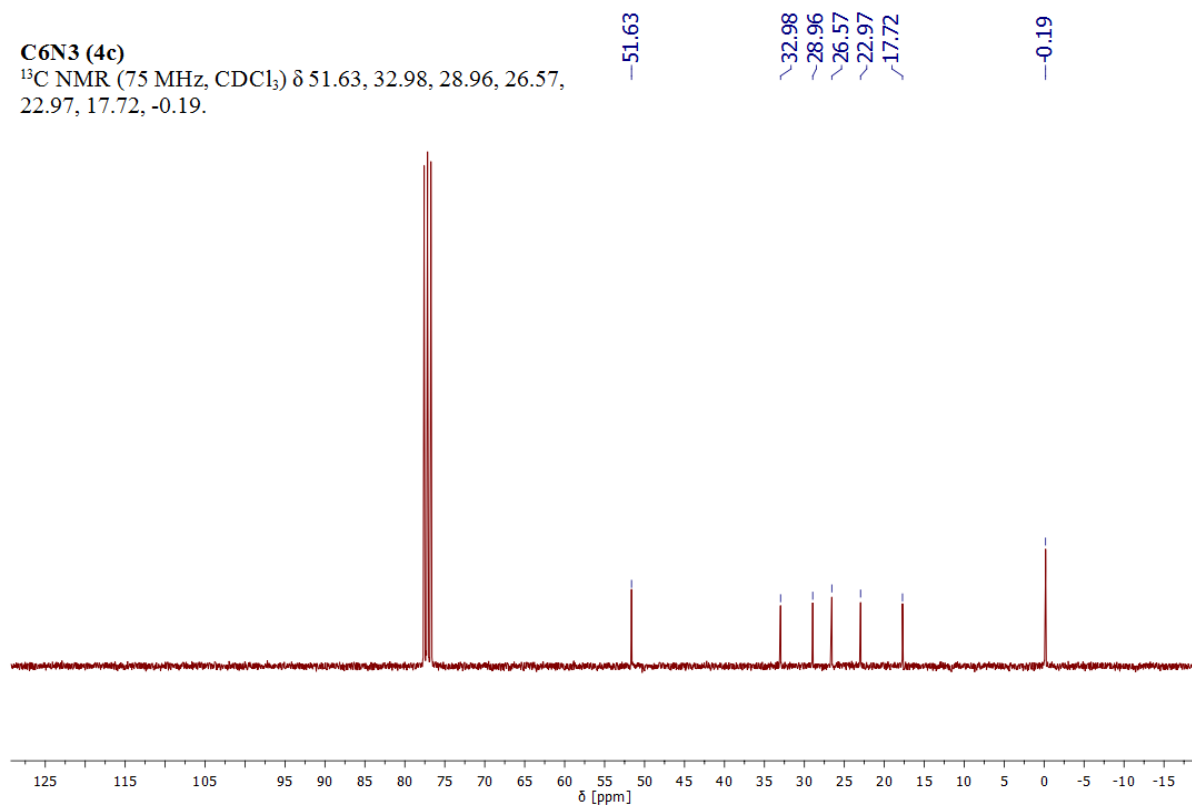
C5N3 (4b) ^{13}C NMR (75 MHz, CDCl_3) δ 51.57, 30.49, 28.72, 22.72, 17.70, -0.20.**C5N3 (4b)** ^{29}Si NMR (60 MHz, CDCl_3) δ 12.67, -108.90.

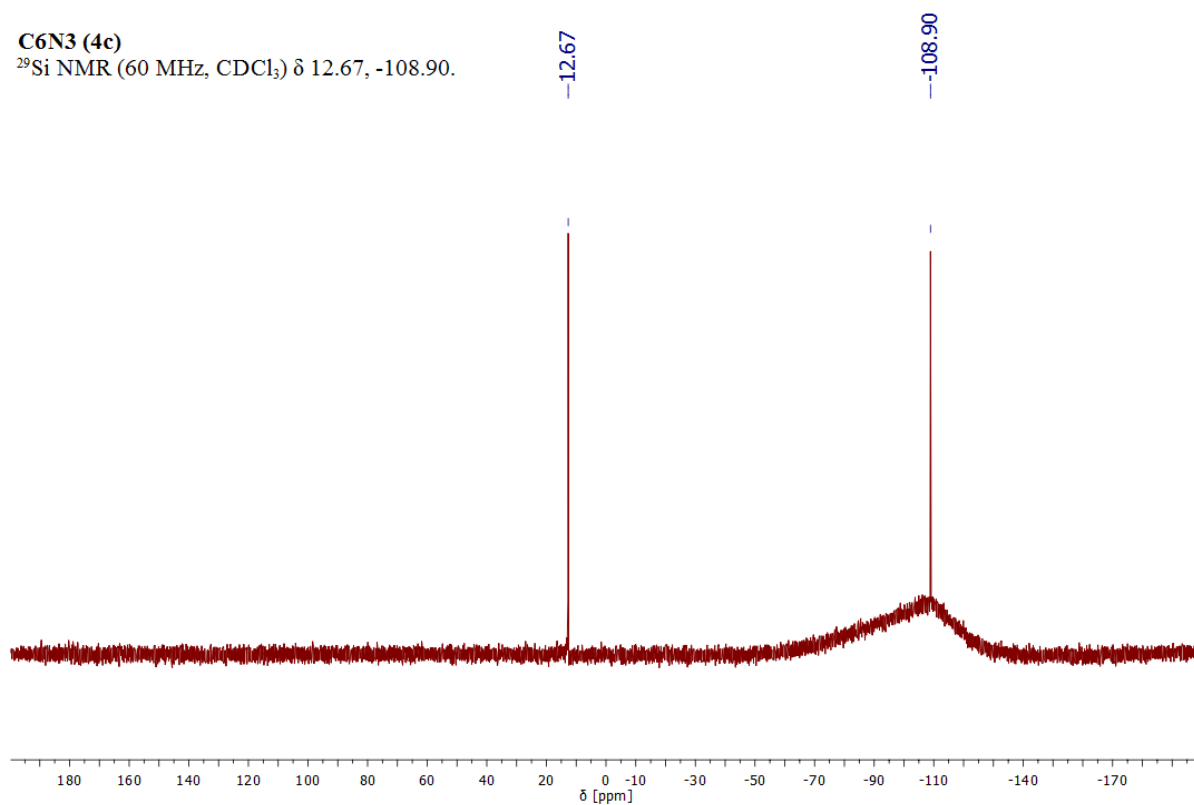
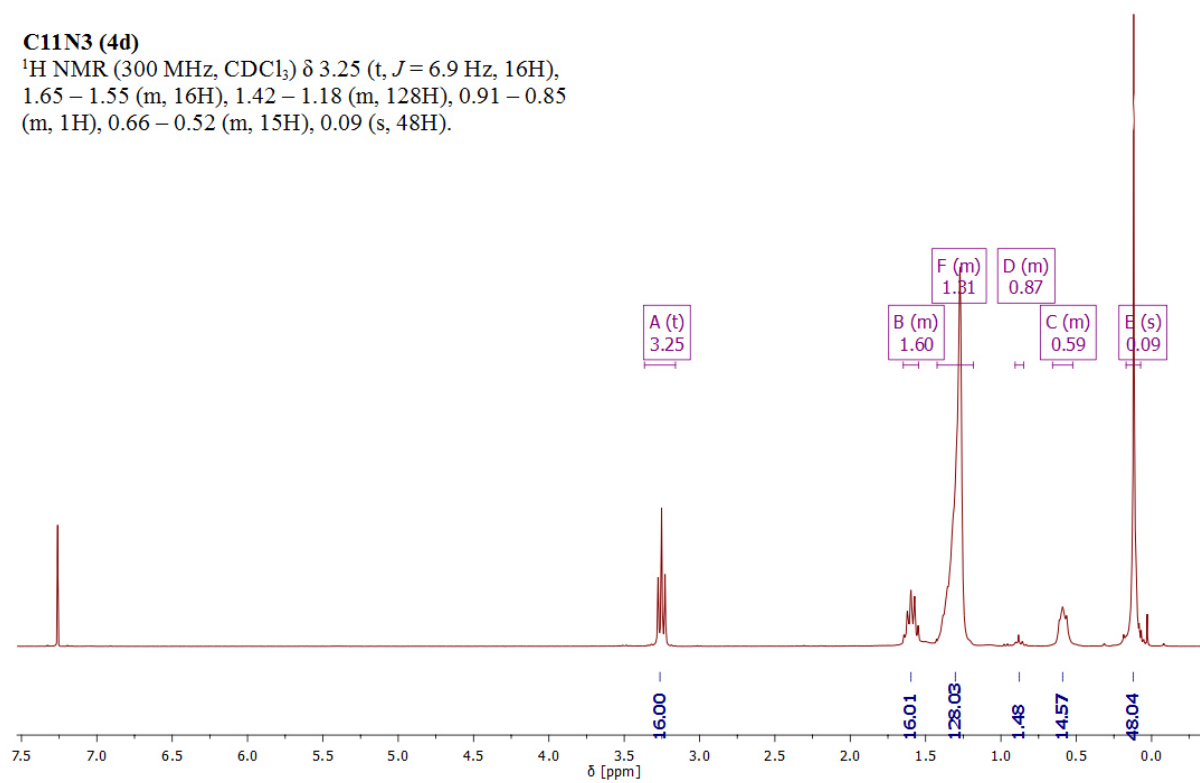
C6N3 (4c)**C6N3 (4c)**

^1H NMR (300 MHz, CDCl_3) δ 3.25 (t, $J = 6.9$ Hz, 16H), 1.58 (dd, $J = 13.7, 6.9$ Hz, 16H), 1.35 (d, $J = 1.7$ Hz, 48H), 0.59 (d, $J = 7.5$ Hz, 16H), 0.18 – 0.09 (m, 48H).

**C6N3 (4c)**

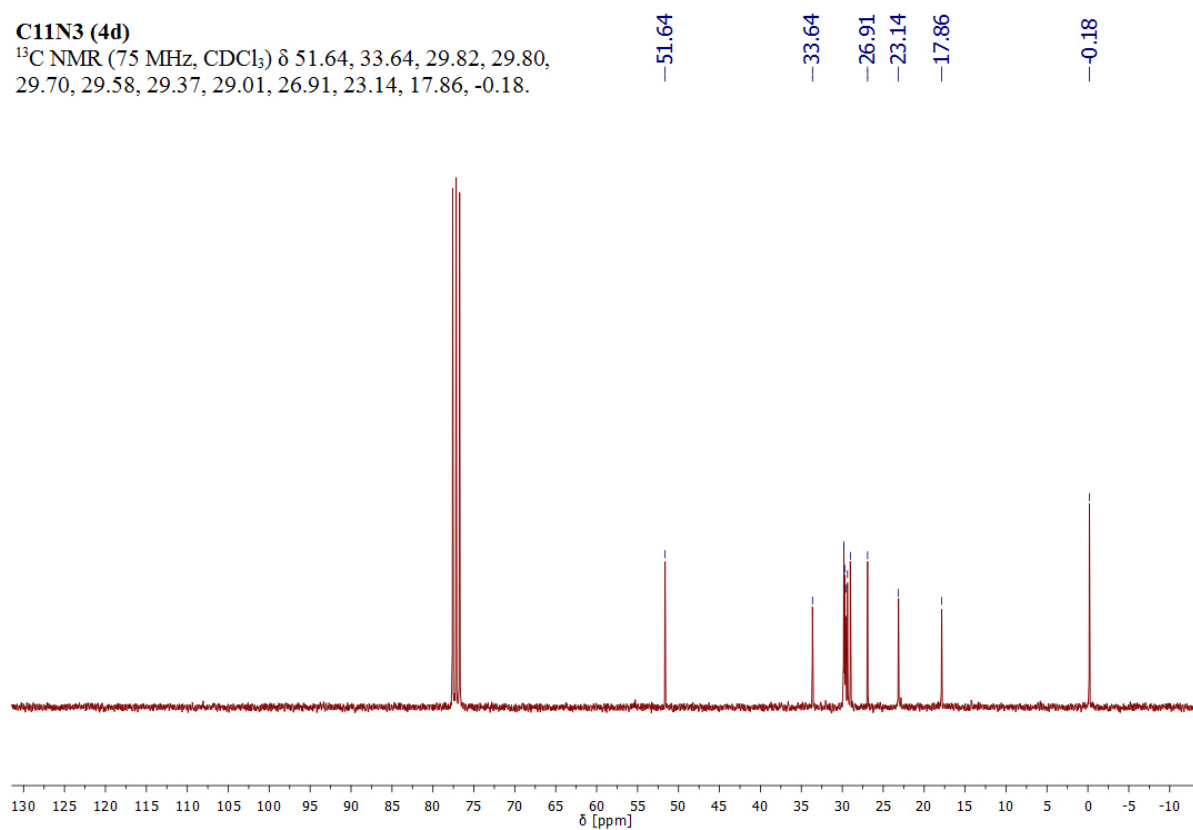
^{13}C NMR (75 MHz, CDCl_3) δ 51.63, 32.98, 28.96, 26.57, 22.97, 17.72, -0.19.



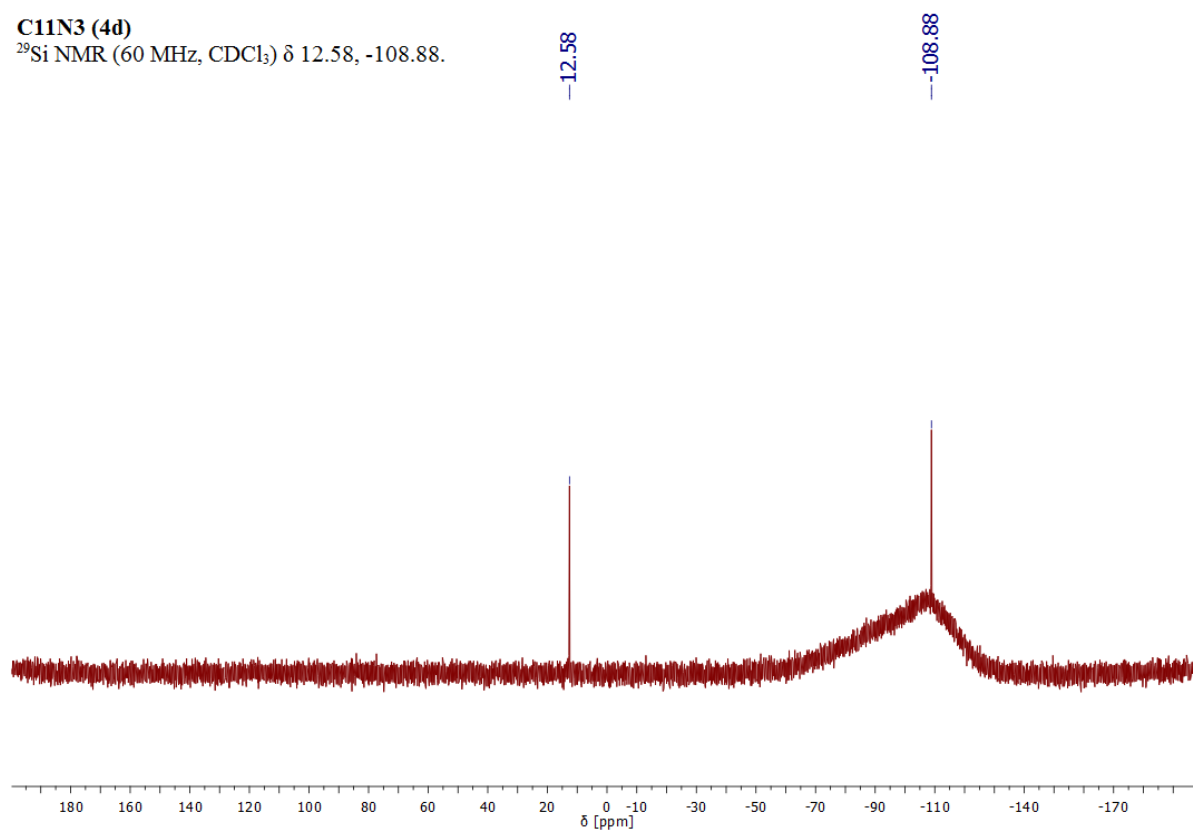
C6N3 (4c)²⁹Si NMR (60 MHz, CDCl₃) δ 12.67, -108.90.**C11N3 (4d)****C11N3 (4d)**¹H NMR (300 MHz, CDCl₃) δ 3.25 (t, *J* = 6.9 Hz, 16H), 1.65 – 1.55 (m, 16H), 1.42 – 1.18 (m, 128H), 0.91 – 0.85 (m, 1H), 0.66 – 0.52 (m, 15H), 0.09 (s, 48H).

C11N3 (4d)

^{13}C NMR (75 MHz, CDCl_3) δ 51.64, 33.64, 29.82, 29.80, 29.70, 29.58, 29.37, 29.01, 26.91, 23.14, 17.86, -0.18.

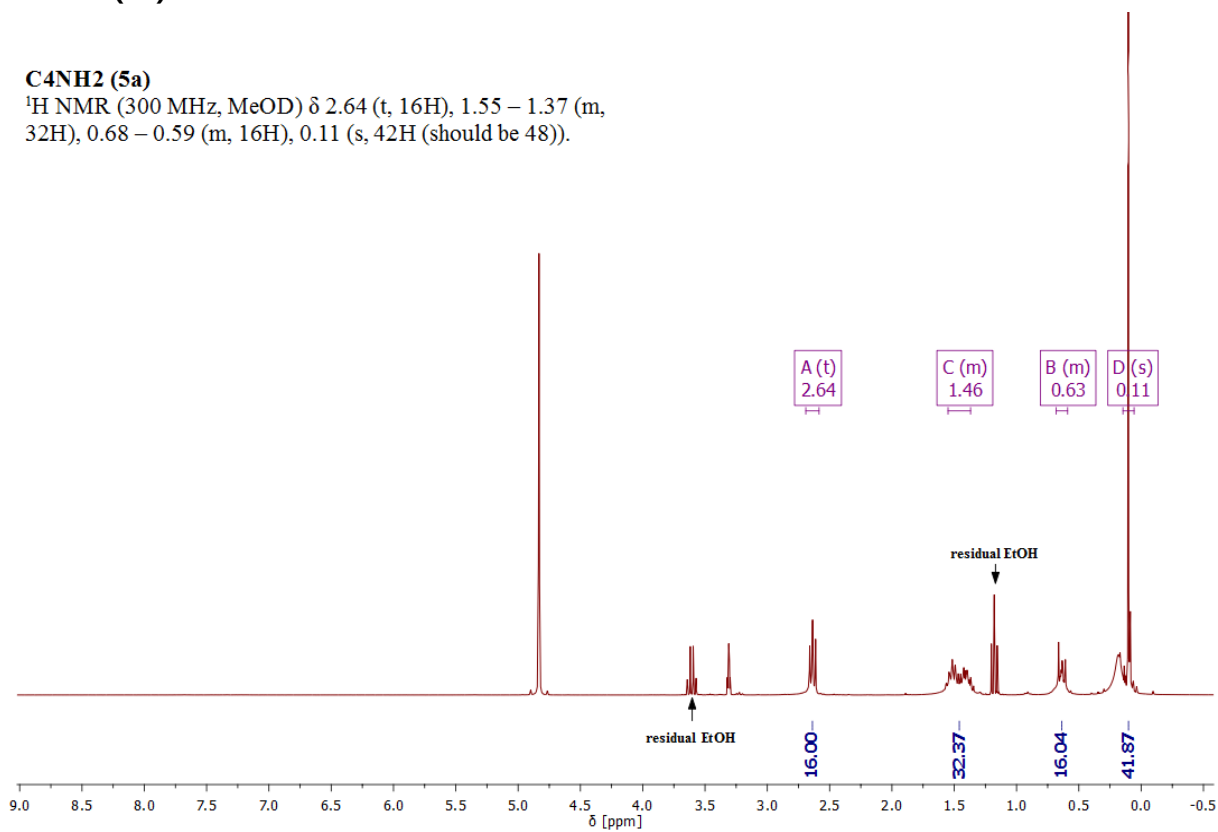
**C11N3 (4d)**

^{29}Si NMR (60 MHz, CDCl_3) δ 12.58, -108.88.

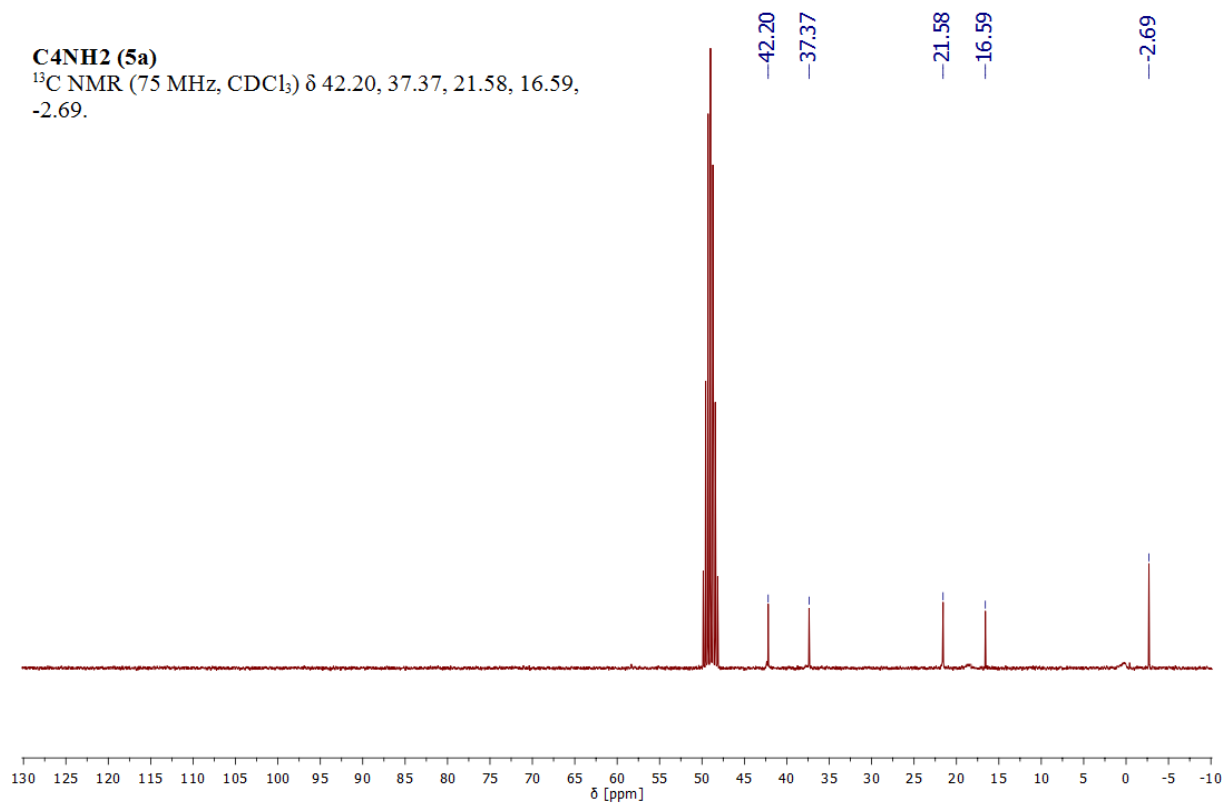


C4NH2 (5a)**C4NH2 (5a)**

^1H NMR (300 MHz, MeOD) δ 2.64 (t, 16H), 1.55 – 1.37 (m, 32H), 0.68 – 0.59 (m, 16H), 0.11 (s, 42H (should be 48)).

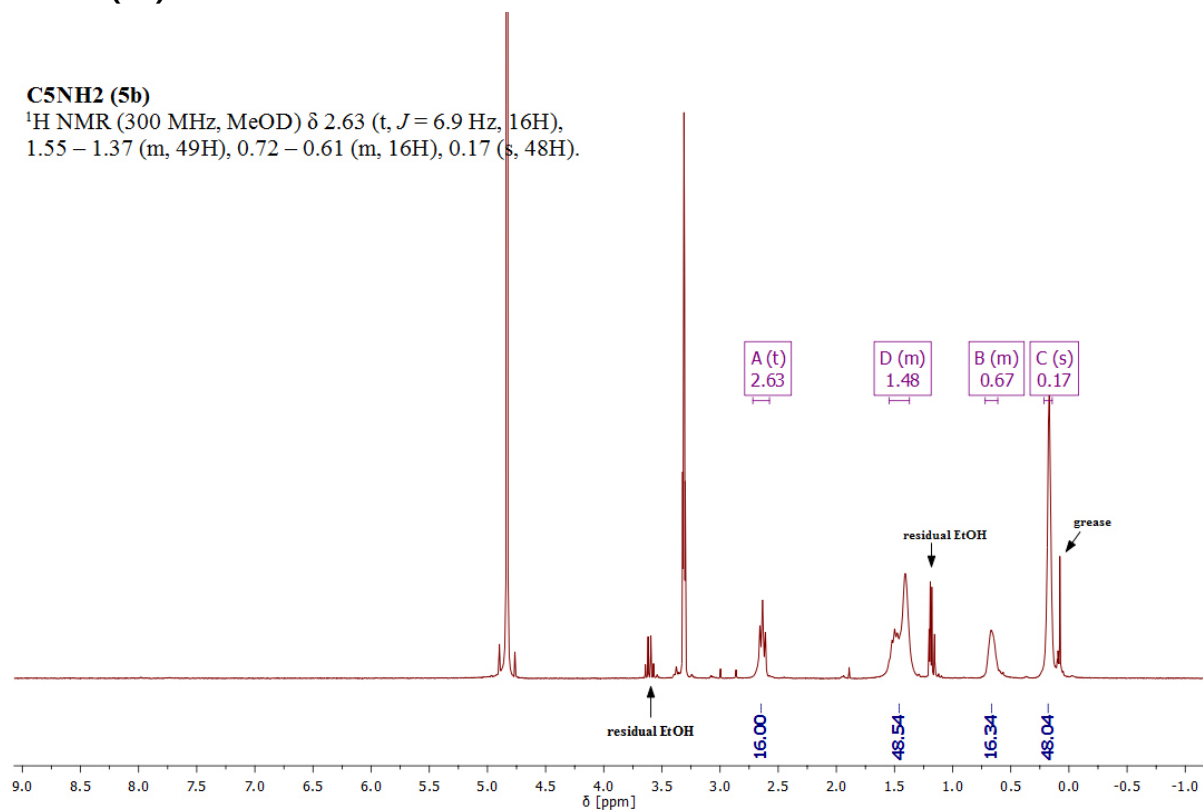
**C4NH2 (5a)**

^{13}C NMR (75 MHz, CDCl_3) δ 42.20, 37.37, 21.58, 16.59, -2.69.

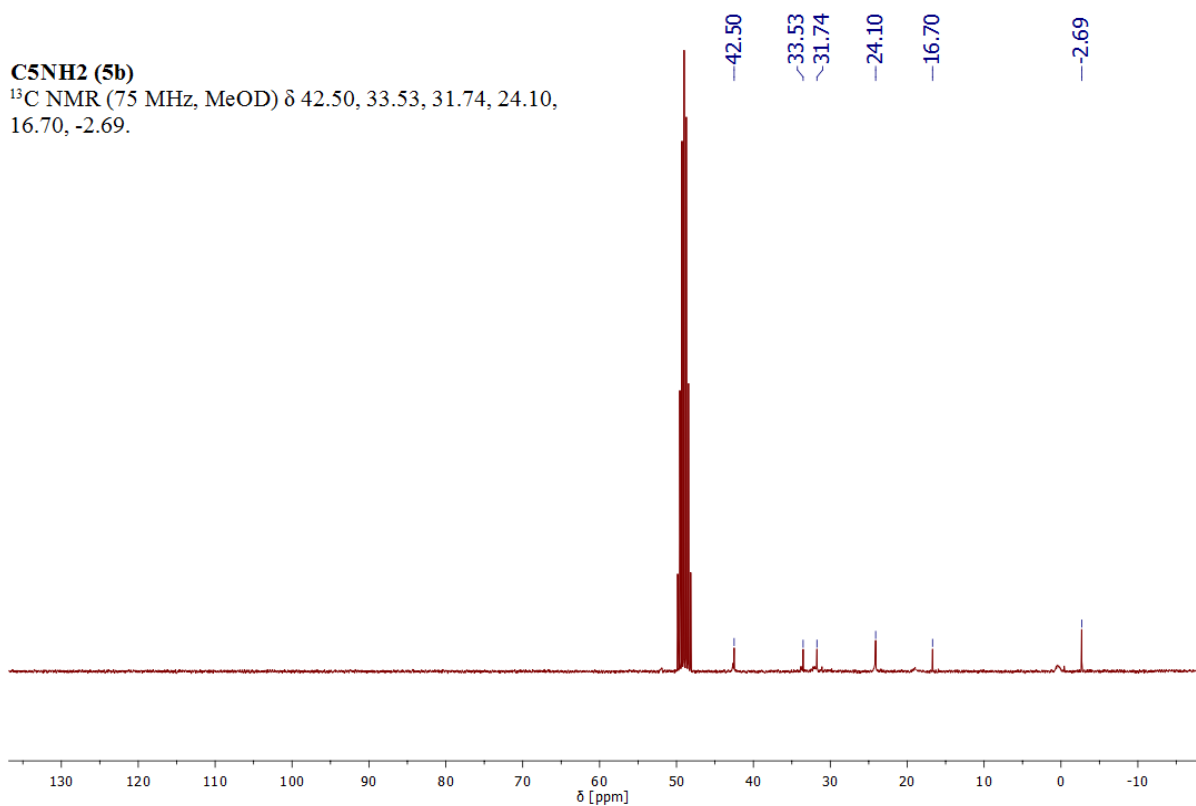


C5NH2 (5b)**C5NH2 (5b)**

^1H NMR (300 MHz, MeOD) δ 2.63 (t, $J = 6.9$ Hz, 16H),
1.55 – 1.37 (m, 49H), 0.72 – 0.61 (m, 16H), 0.17 (s, 48H).

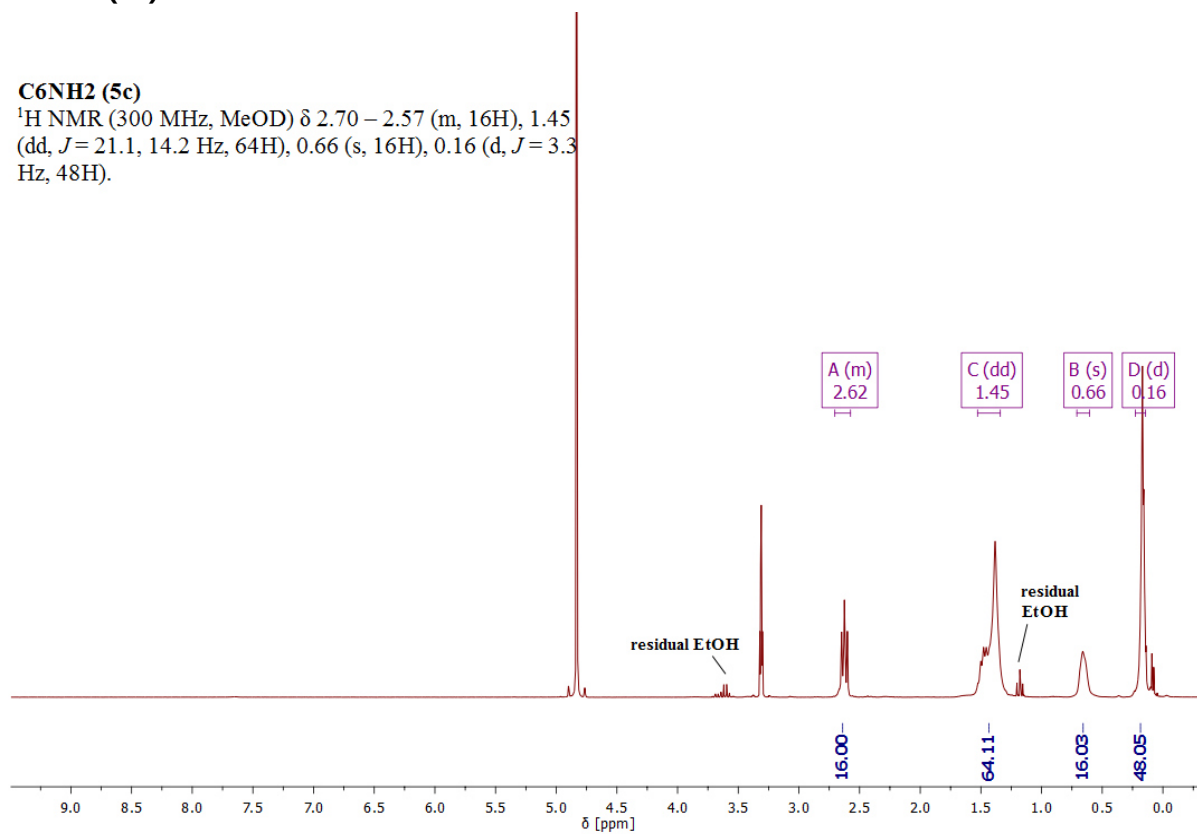
**C5NH2 (5b)**

^{13}C NMR (75 MHz, MeOD) δ 42.50, 33.53, 31.74, 24.10,
16.70, -2.69.

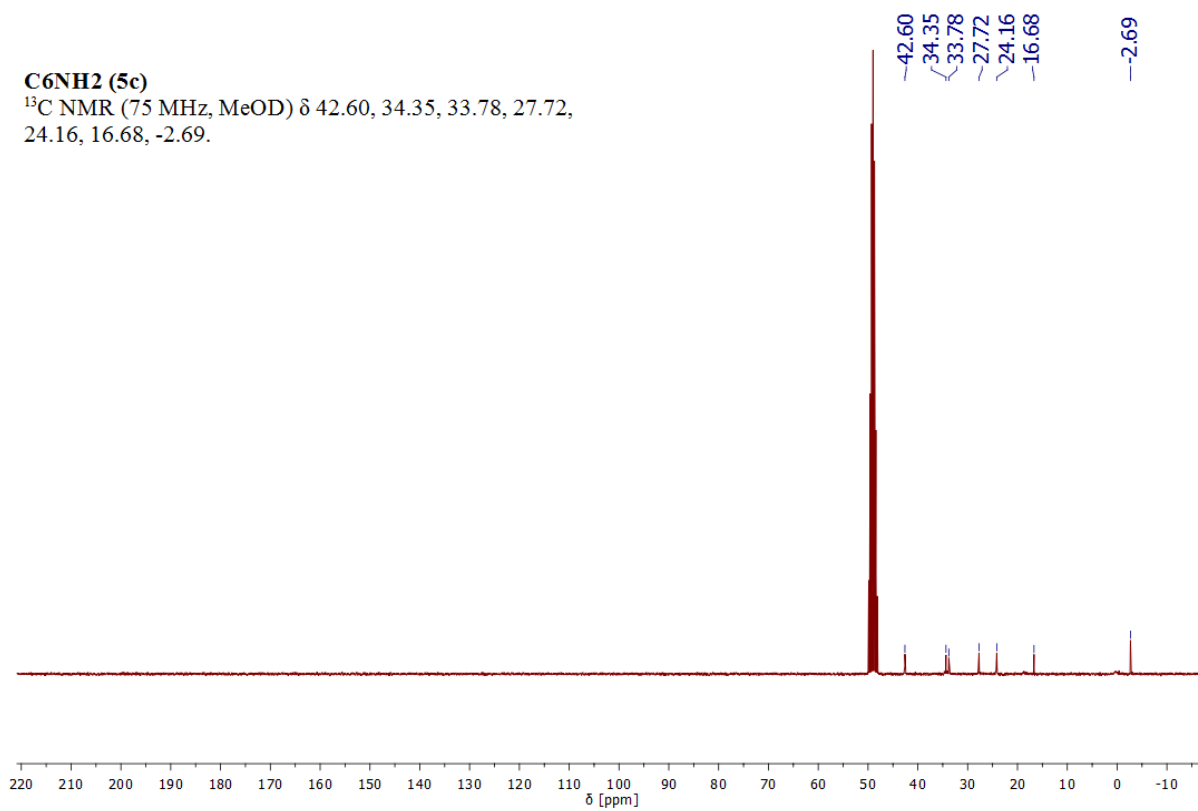


C6NH2 (5c)**C6NH2 (5c)**

^1H NMR (300 MHz, MeOD) δ 2.70 – 2.57 (m, 16H), 1.45 (dd, $J = 21.1, 14.2$ Hz, 64H), 0.66 (s, 16H), 0.16 (d, $J = 3.3$ Hz, 48H).

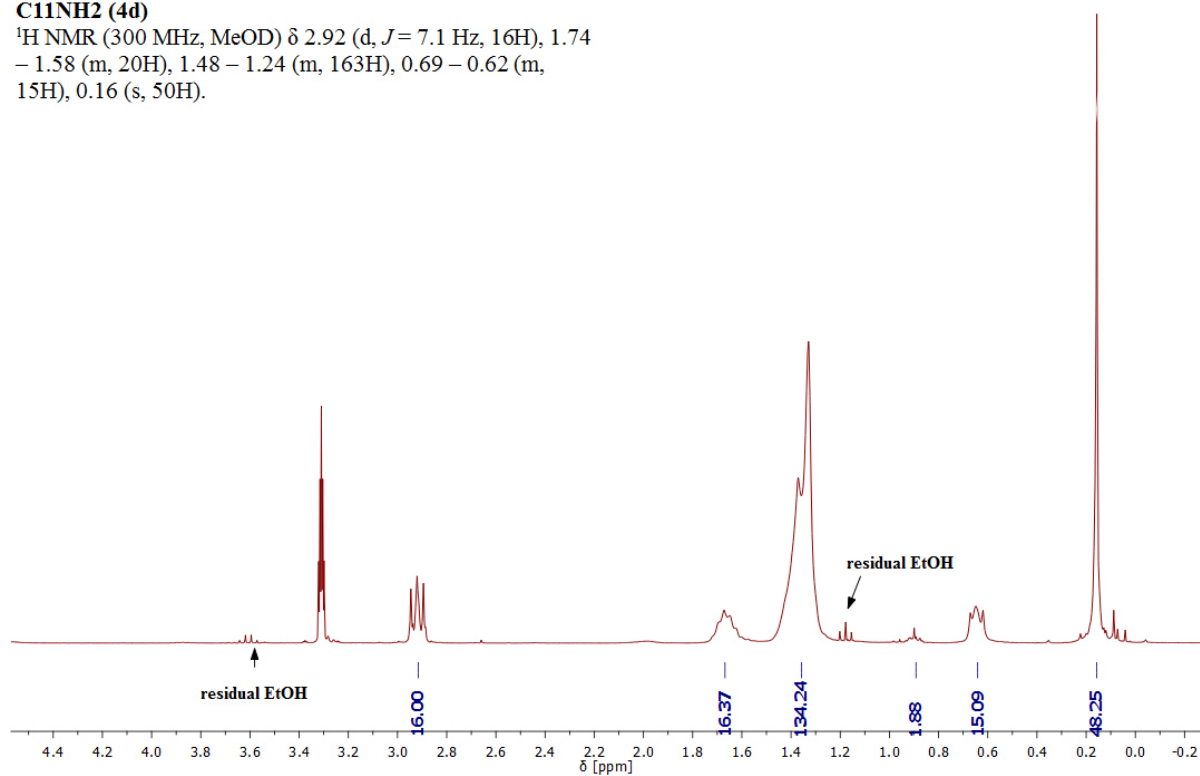
**C6NH2 (5c)**

^{13}C NMR (75 MHz, MeOD) δ 42.60, 34.35, 33.78, 27.72, 24.16, 16.68, -2.69.

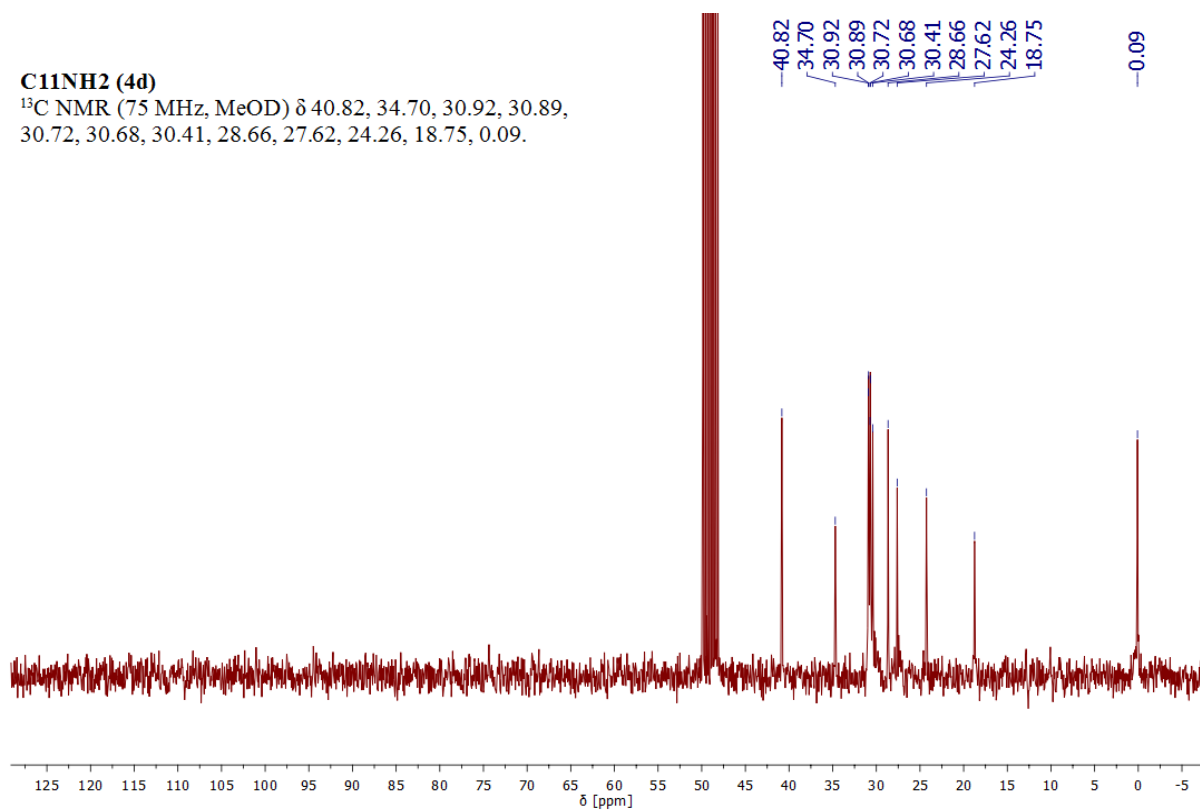


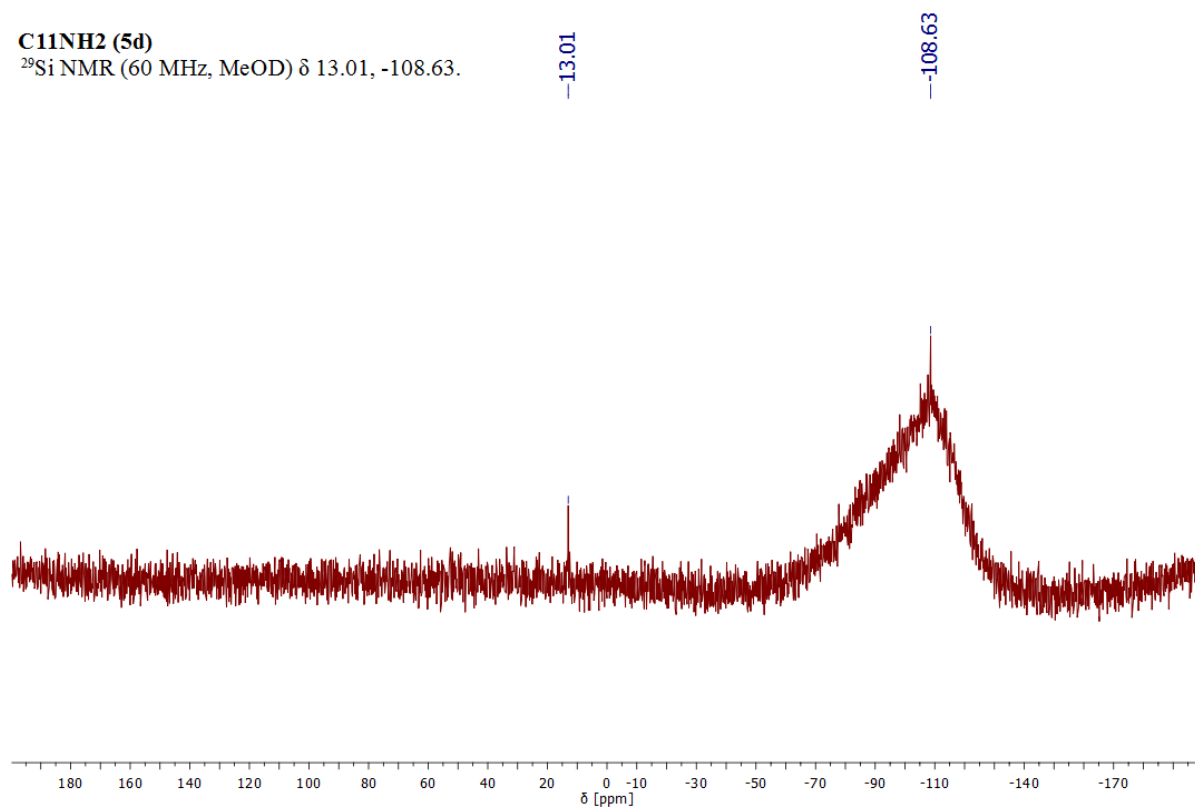
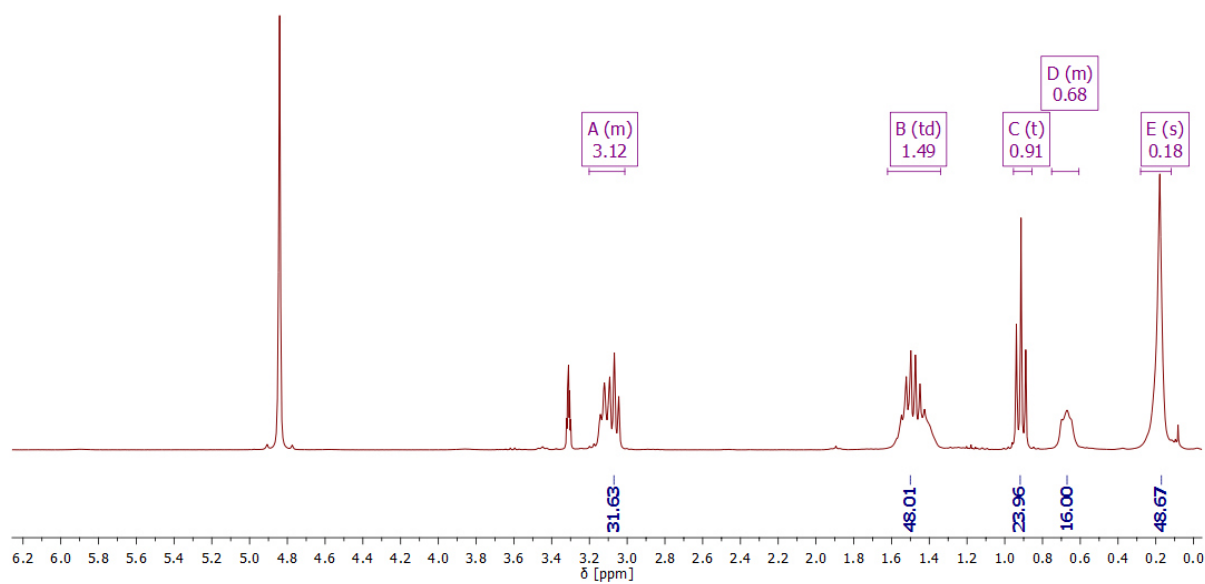
C11NH2 (5d)**C11NH2 (4d)**

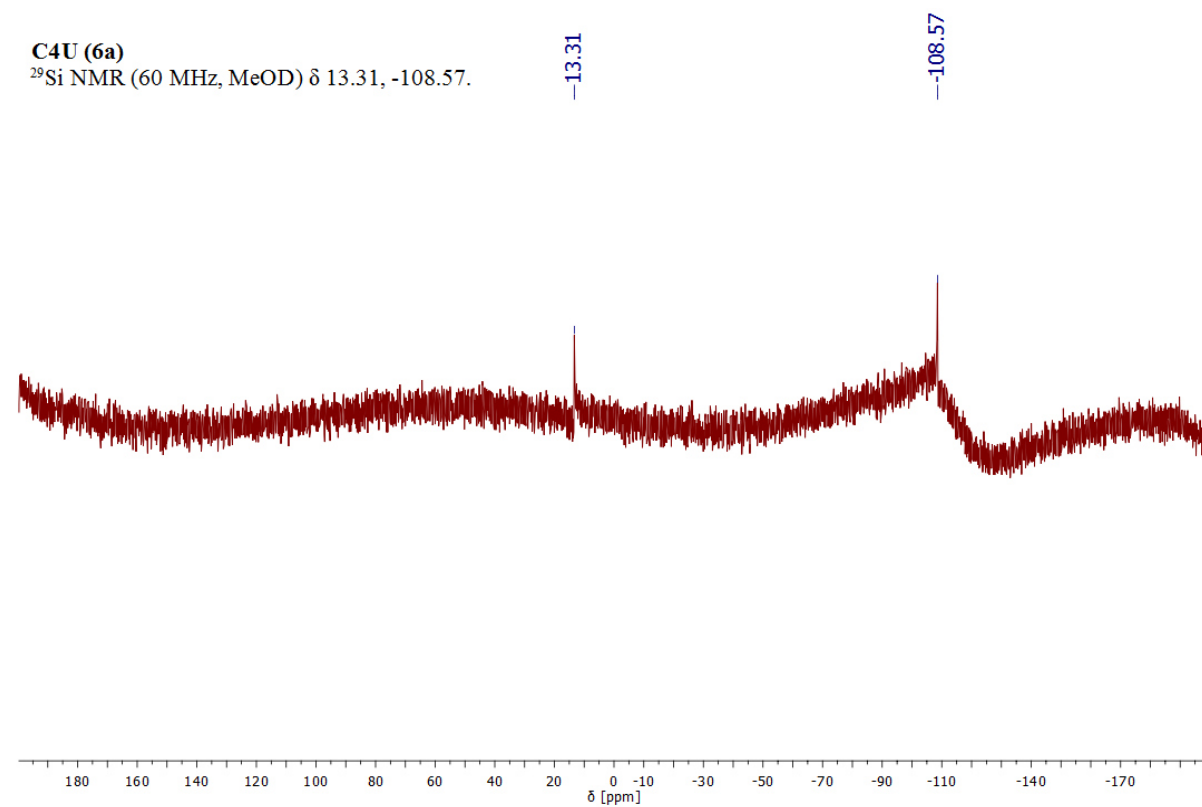
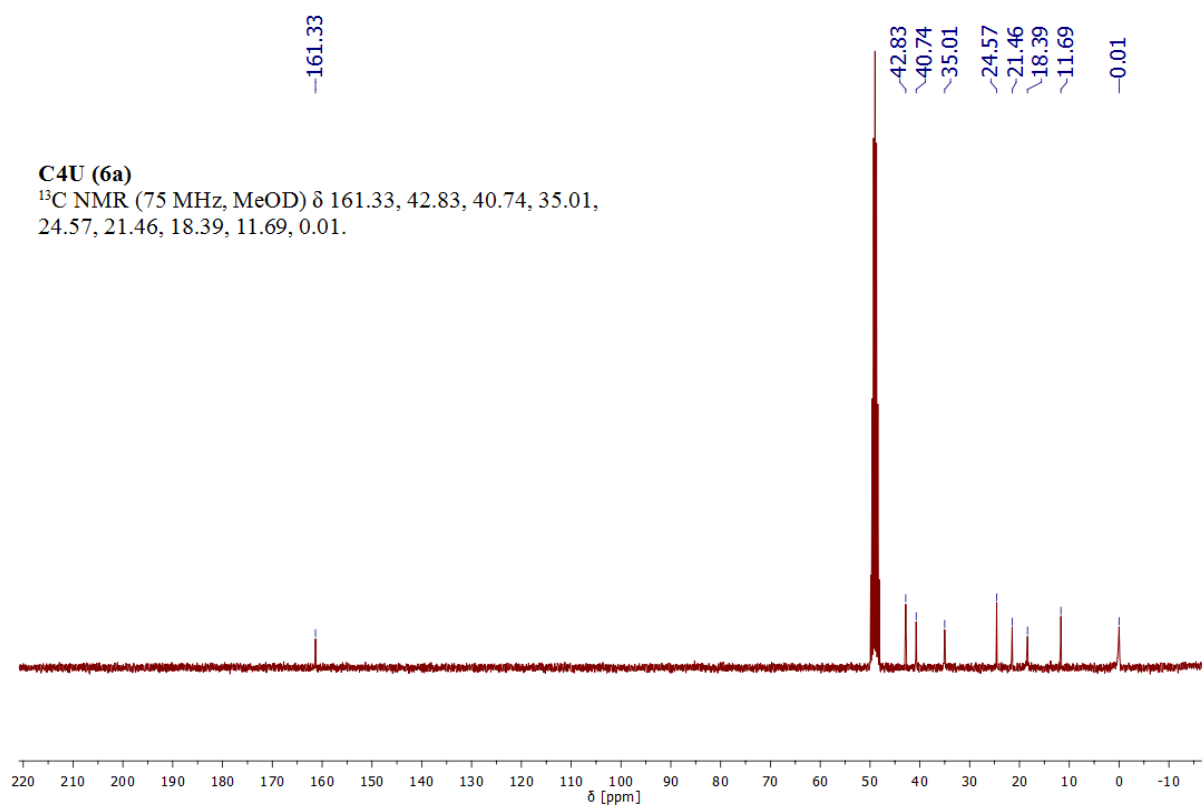
^1H NMR (300 MHz, MeOD) δ 2.92 (d, $J = 7.1$ Hz, 16H), 1.74 – 1.58 (m, 20H), 1.48 – 1.24 (m, 163H), 0.69 – 0.62 (m, 15H), 0.16 (s, 50H).

**C11NH2 (4d)**

^{13}C NMR (75 MHz, MeOD) δ 40.82, 34.70, 30.92, 30.89, 30.72, 30.68, 30.41, 28.66, 27.62, 24.26, 18.75, 0.09.

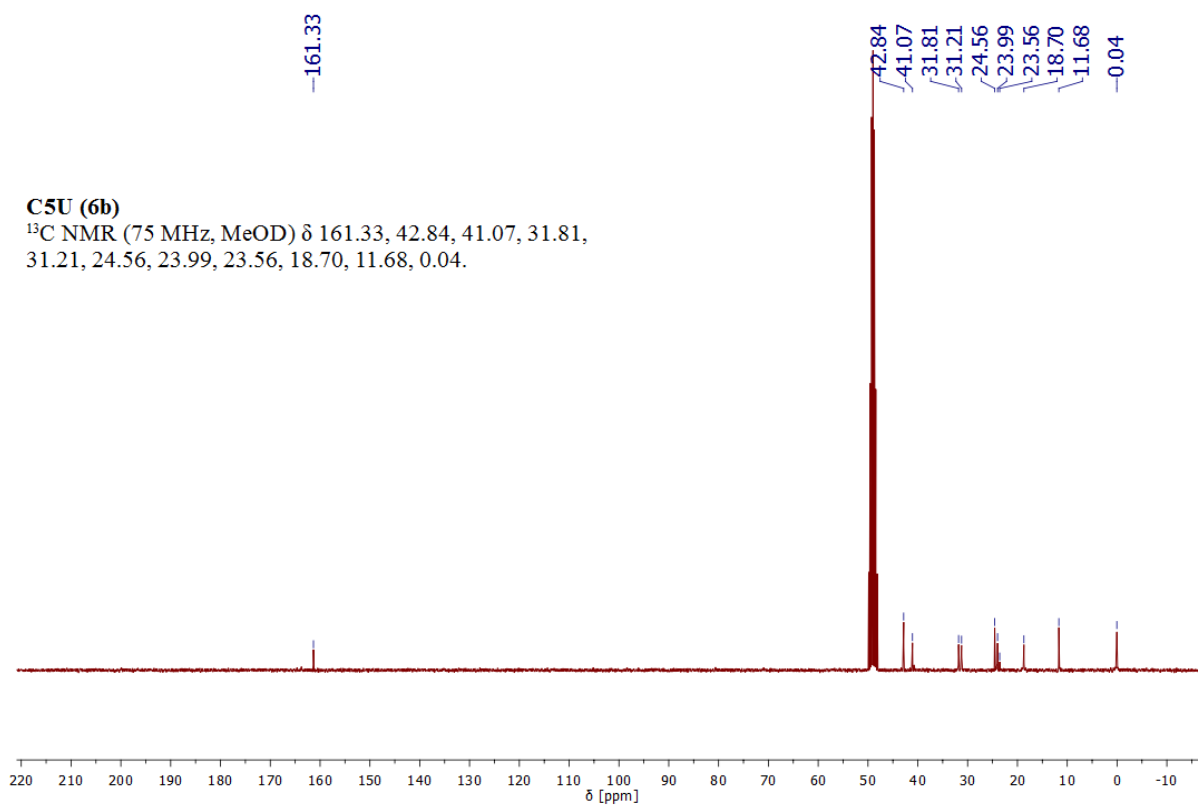
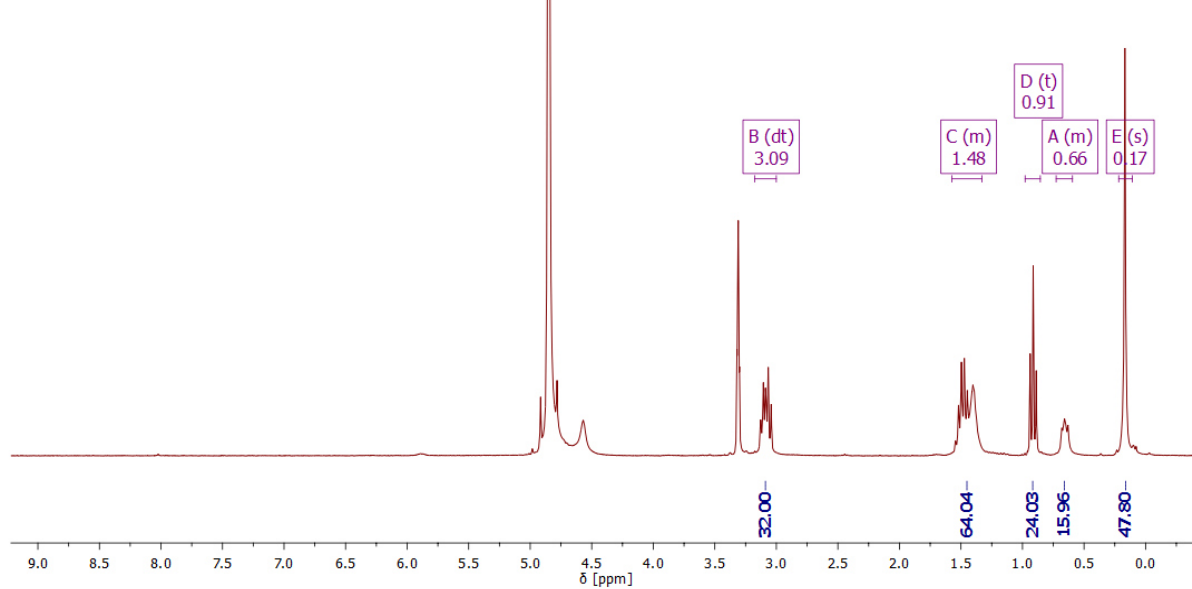


C11NH2 (5d)²⁹Si NMR (60 MHz, MeOD) δ 13.01, -108.63.**C4Urea (6a)****C4U (6a)**¹H NMR (300 MHz, MeOD) δ 3.20 – 3.01 (m, 32H), 1.49 (td, *J* = 14.6, 7.3 Hz, 48H), 0.91 (t, *J* = 7.4 Hz, 24H), 0.75 – 0.61 (m, 16H), 0.18 (s, 48H).

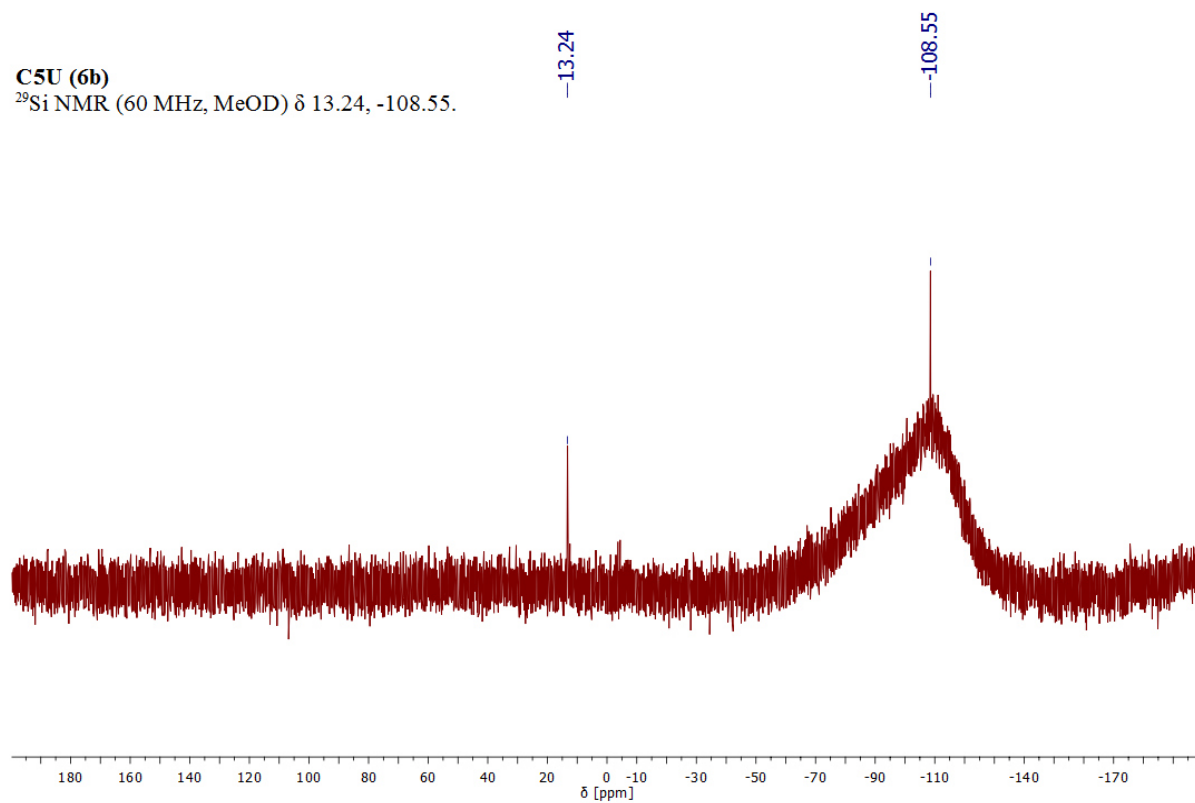
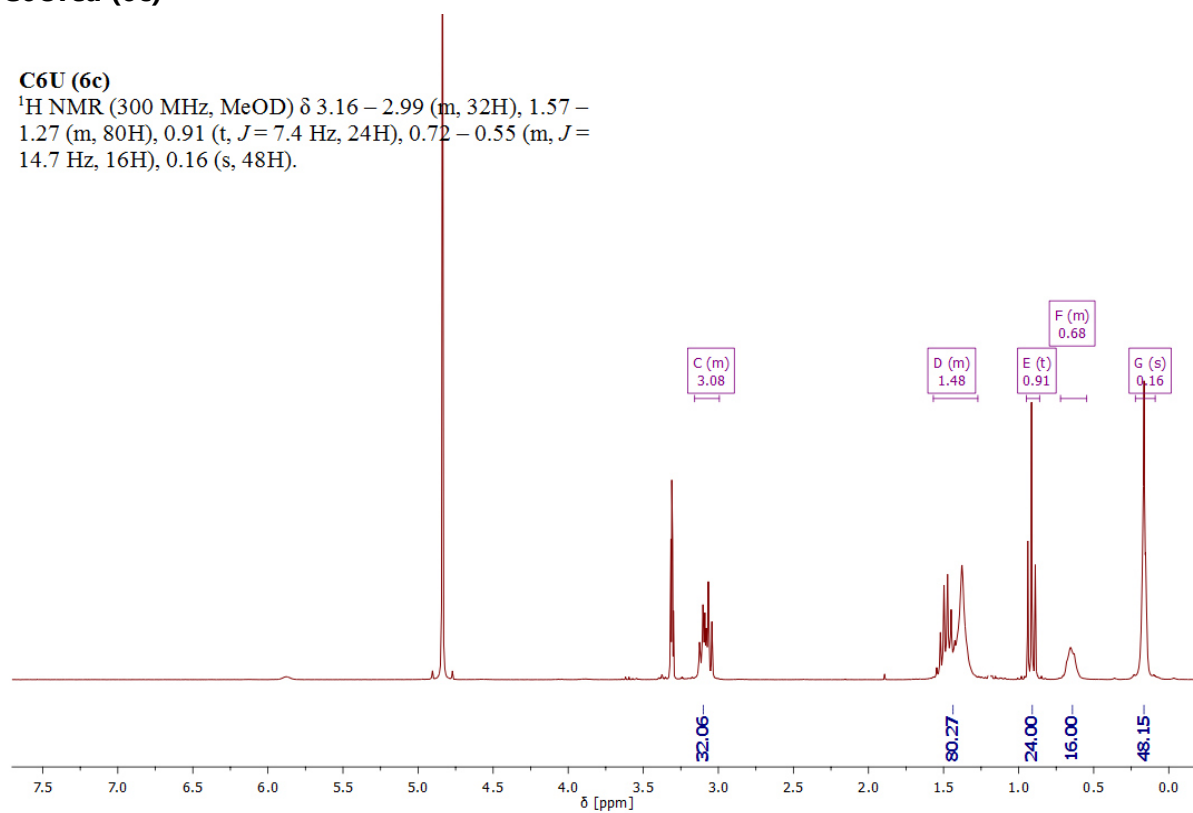


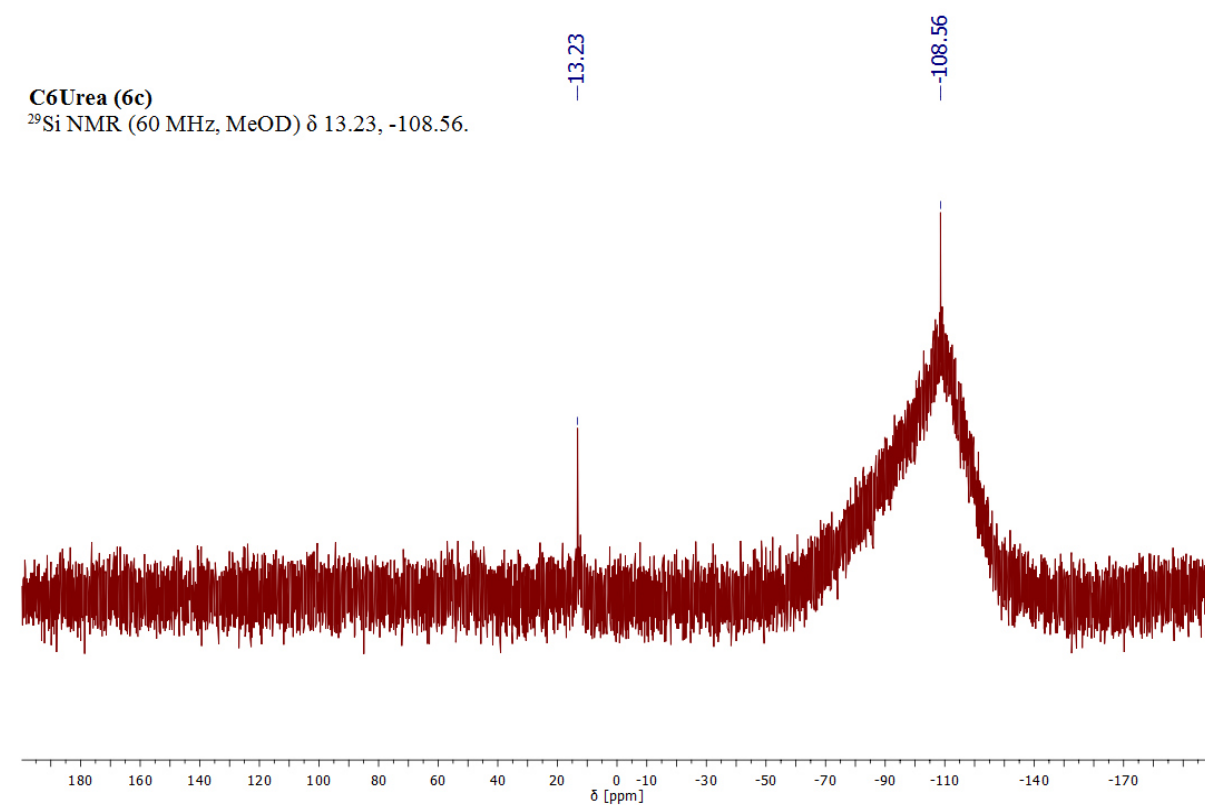
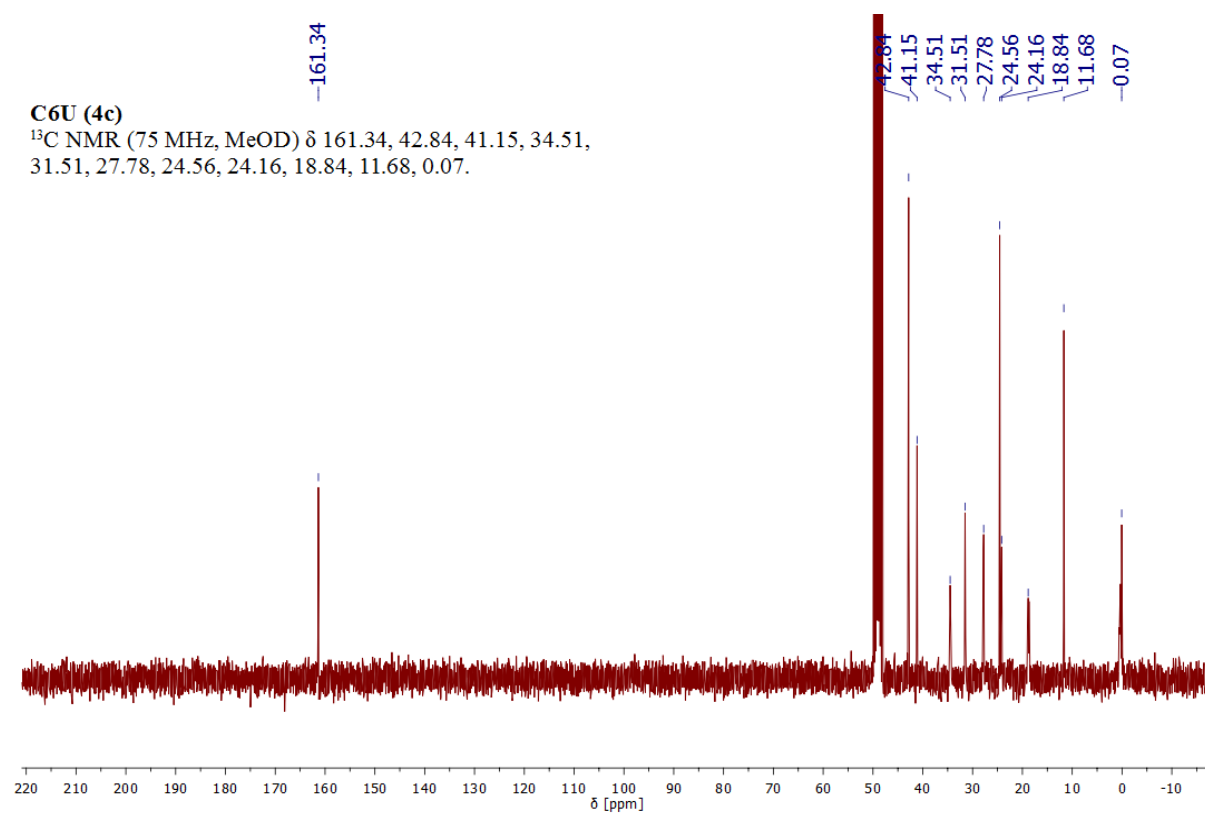
C5Urea (6b)**C5U (6b)**

^1H NMR (300 MHz, MeOD) δ 3.09 (dt, $J = 13.9, 6.9$ Hz, 32H), 1.57 – 1.33 (m, 64H), 0.91 (t, $J = 7.4$ Hz, 24H), 0.73 – 0.59 (m, 16H), 0.17 (s, 48H).

**C5U (6b)**

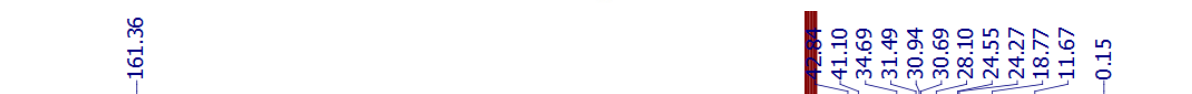
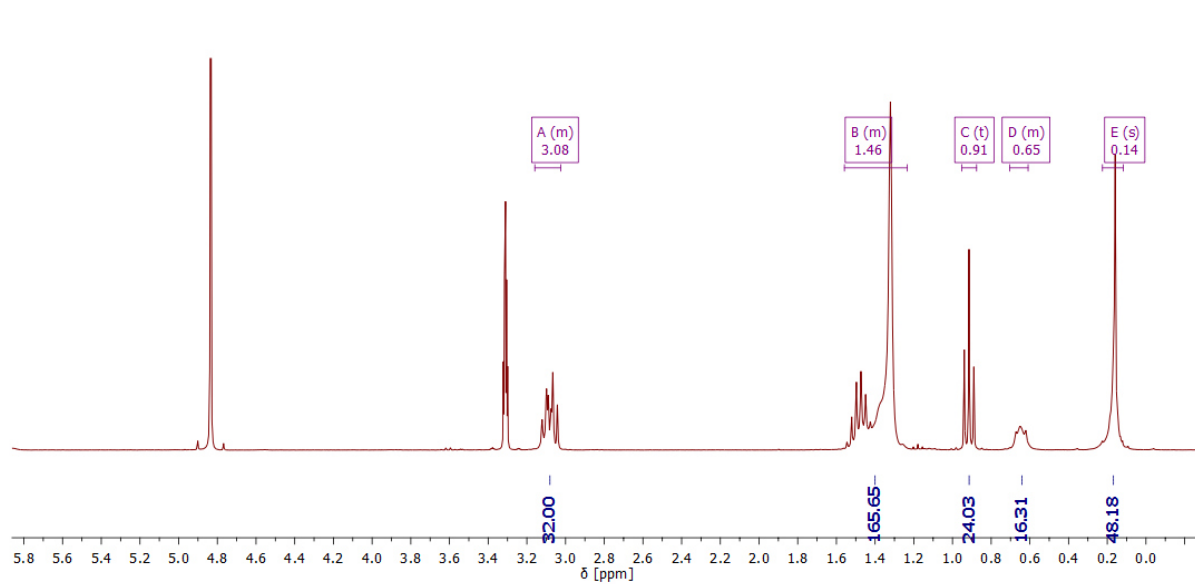
^{13}C NMR (75 MHz, MeOD) δ 161.33, 42.84, 41.07, 31.81, 31.21, 24.56, 23.99, 23.56, 18.70, 11.68, 0.04.

C5U (6b) ^{29}Si NMR (60 MHz, MeOD) δ 13.24, -108.55.**C6Urea (6c)****C6U (6c)** ^1H NMR (300 MHz, MeOD) δ 3.16 – 2.99 (m, 32H), 1.57 – 1.27 (m, 80H), 0.91 (t, $J = 7.4$ Hz, 24H), 0.72 – 0.55 (m, $J = 14.7$ Hz, 16H), 0.16 (s, 48H).

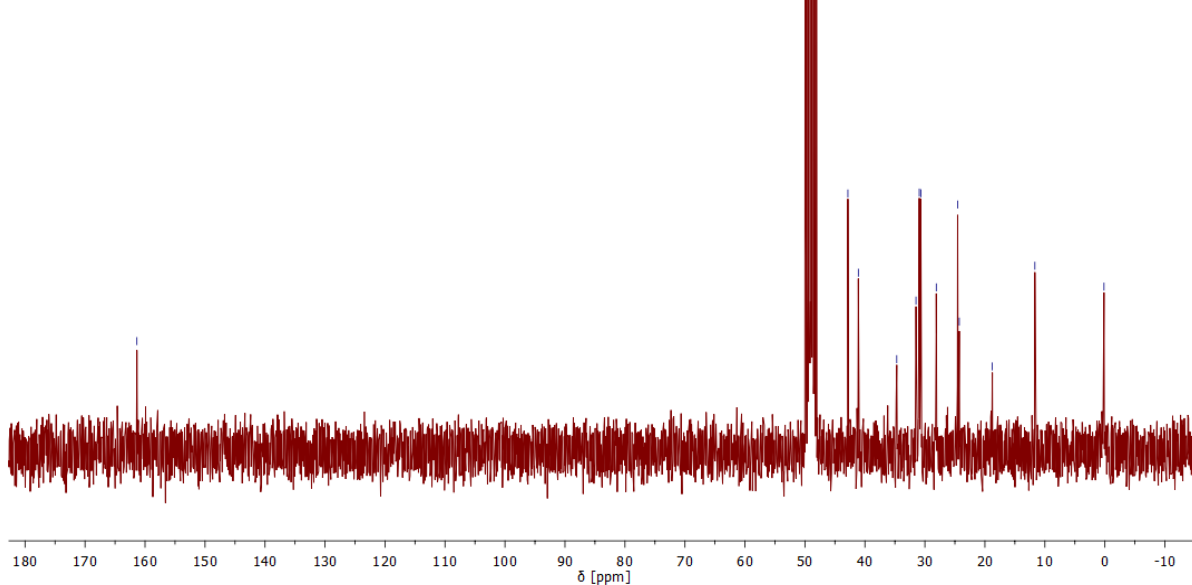


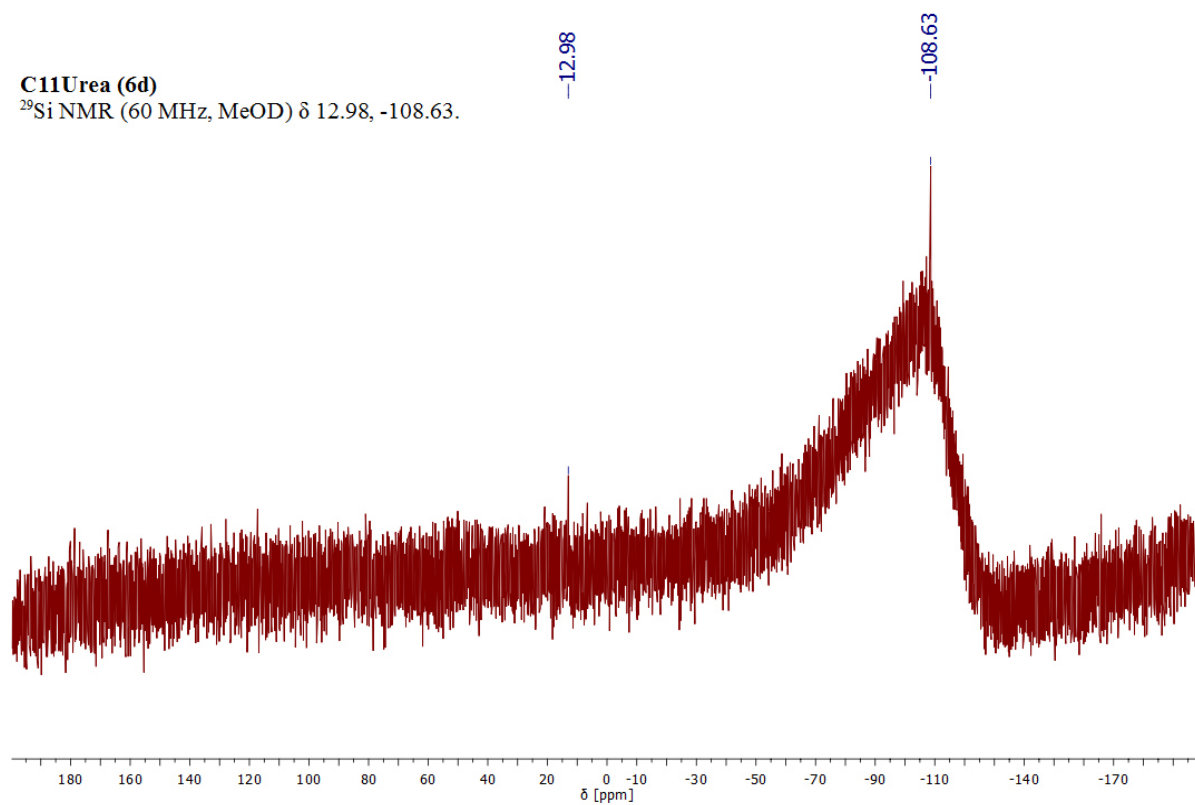
C11Urea (6d)**C11Urea (6d)**

^1H NMR (300 MHz, MeOD) δ 3.16 – 3.03 (m, $J=9.7, 7.0$ Hz, 32H), 1.56 – 1.23 (m, 160H), 0.91 (t, $J=7.4$ Hz, 24H), 0.70 – 0.61 (m, 16H), 0.14 (s, 48H).

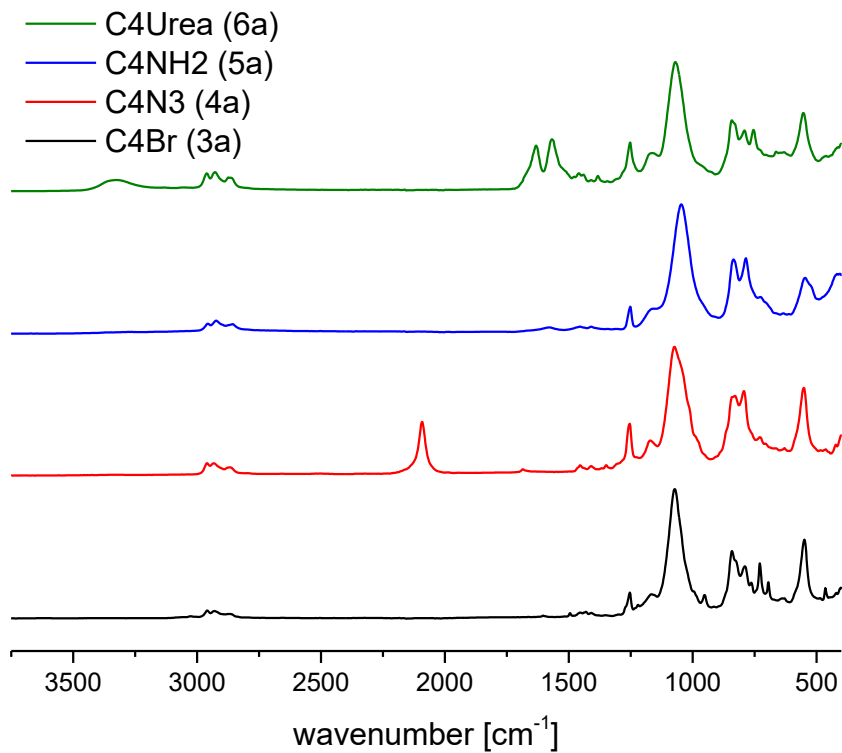
**C11Urea (6d)**

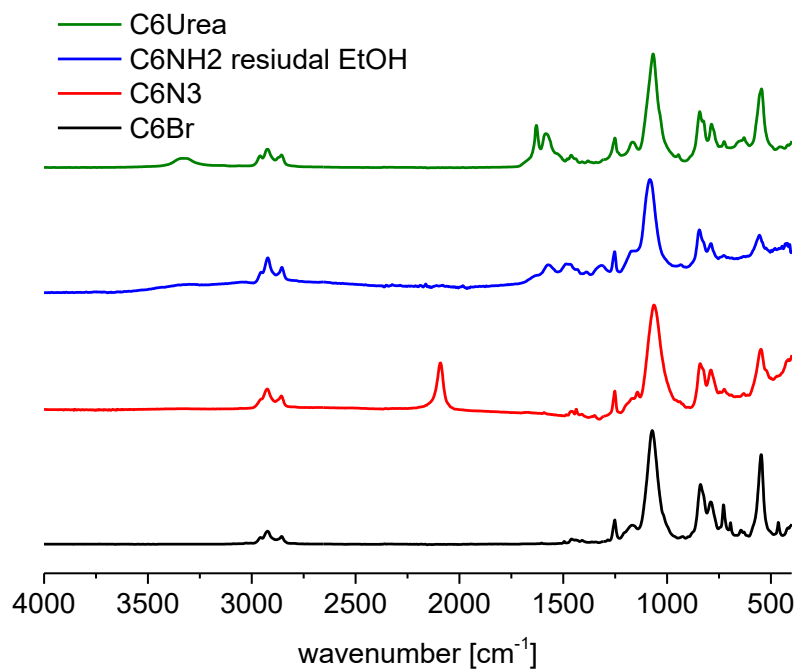
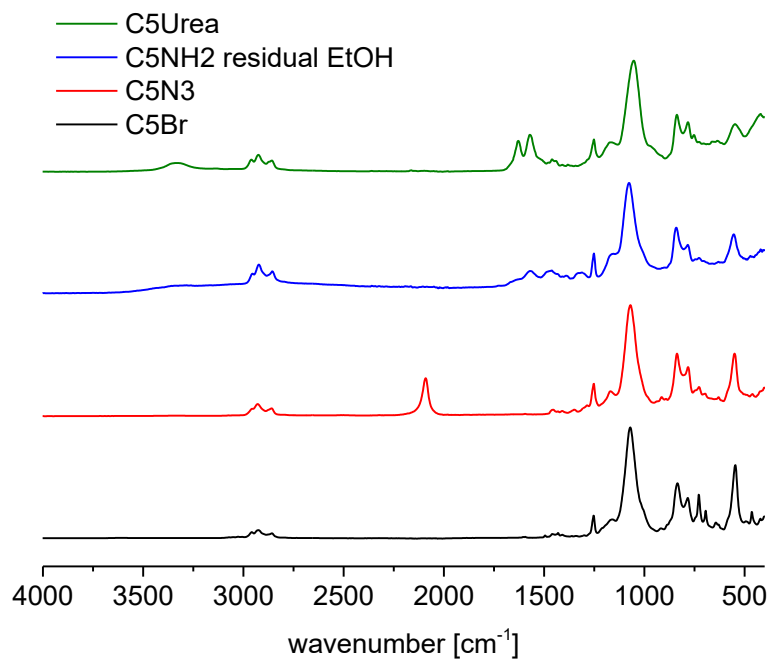
^{13}C NMR (75 MHz, MeOD) δ 161.36, 42.84, 41.10, 34.69, 31.49, 30.94, 30.69, 28.10, 24.55, 24.27, 18.77, 11.67, 0.15.



C11Urea (6d)²⁹Si NMR (60 MHz, MeOD) δ 12.98, -108.63.

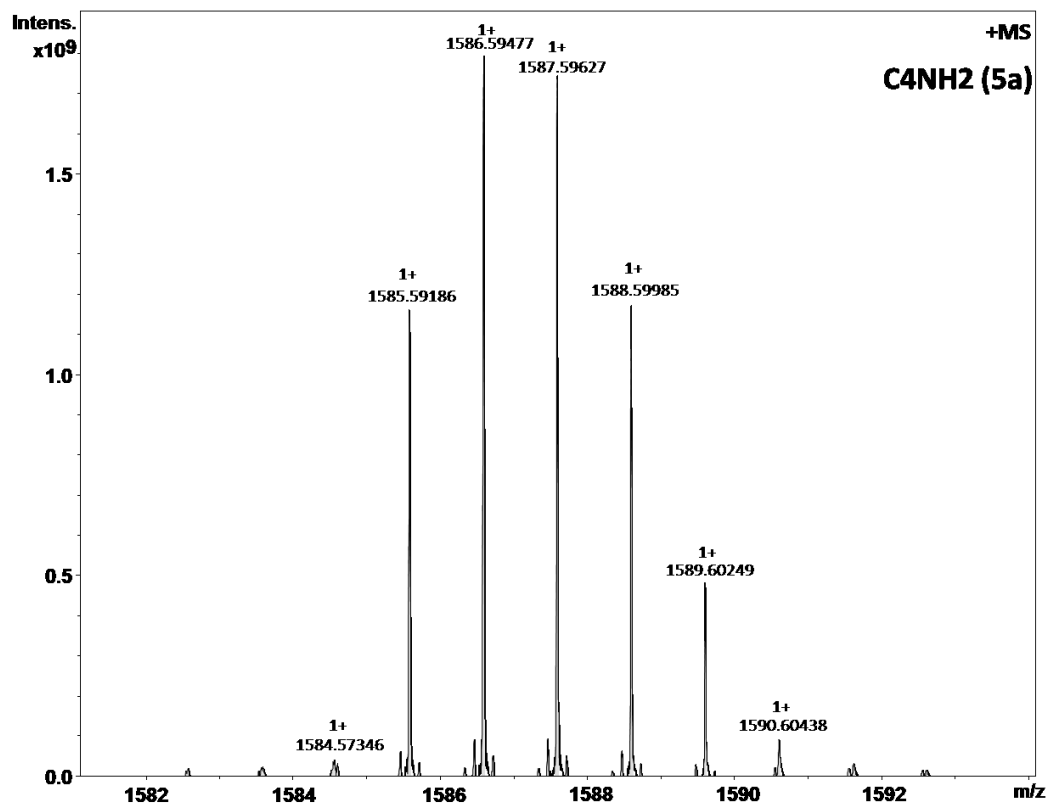
IR spectroscopy



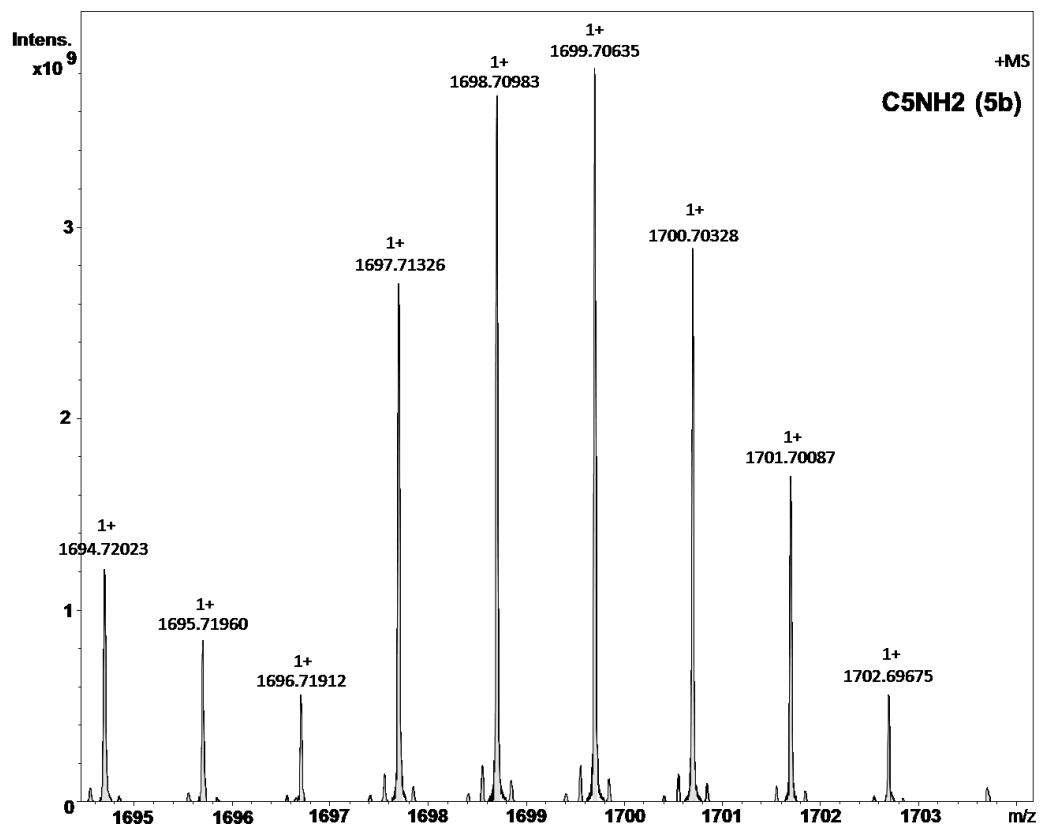


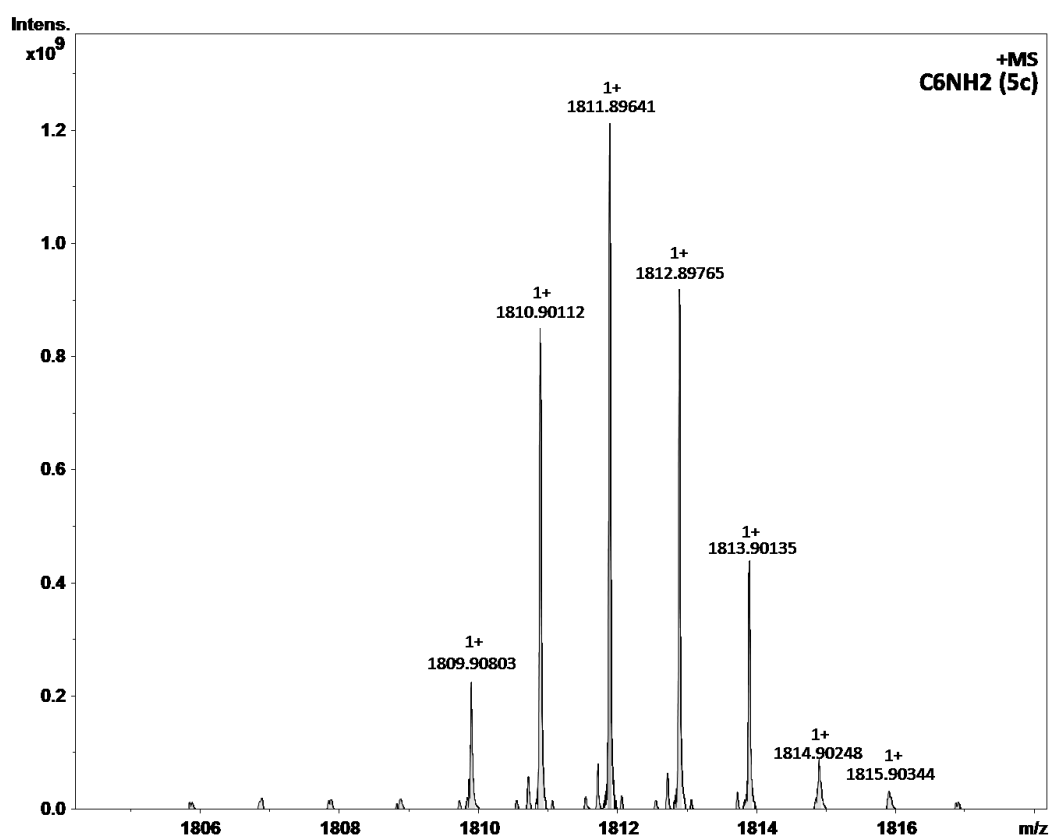
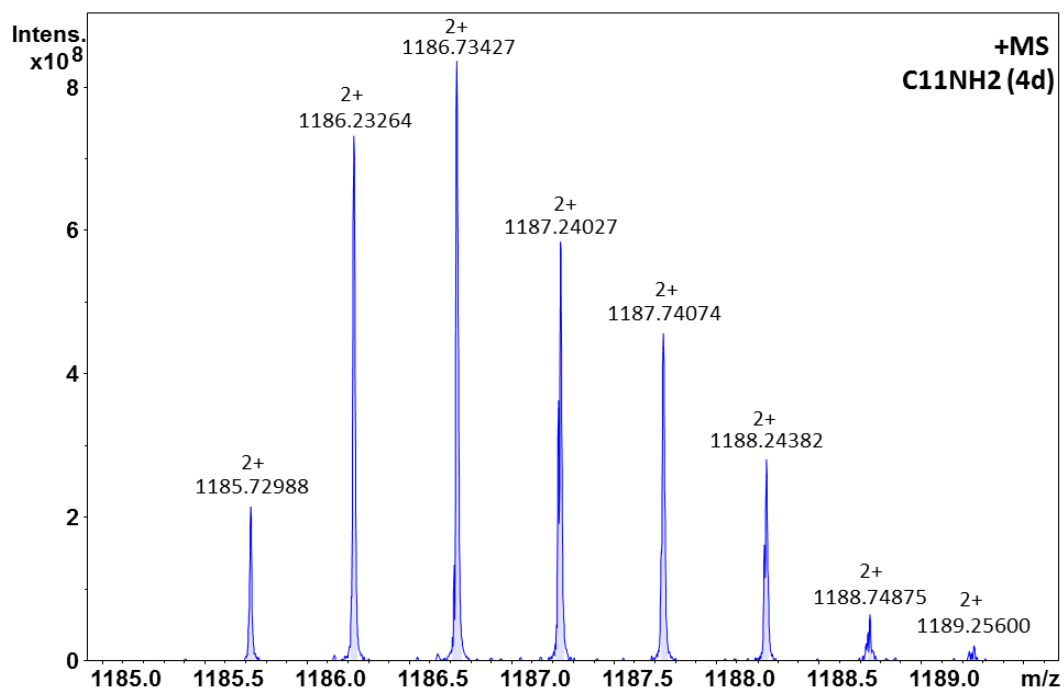
ESI- MS spectra

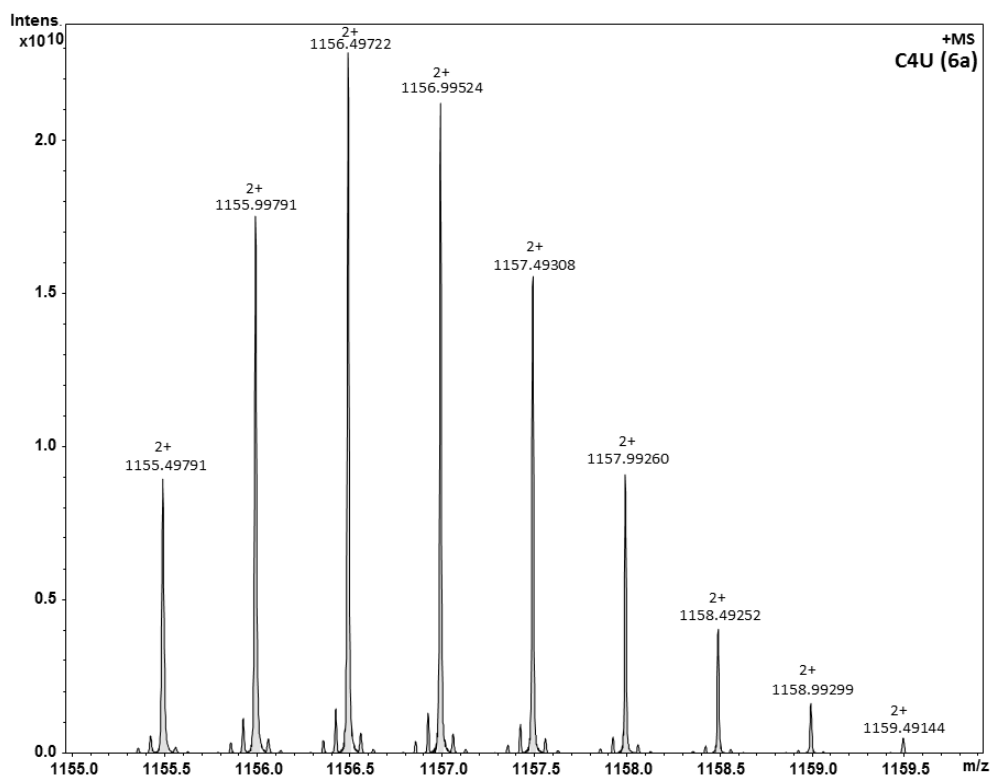
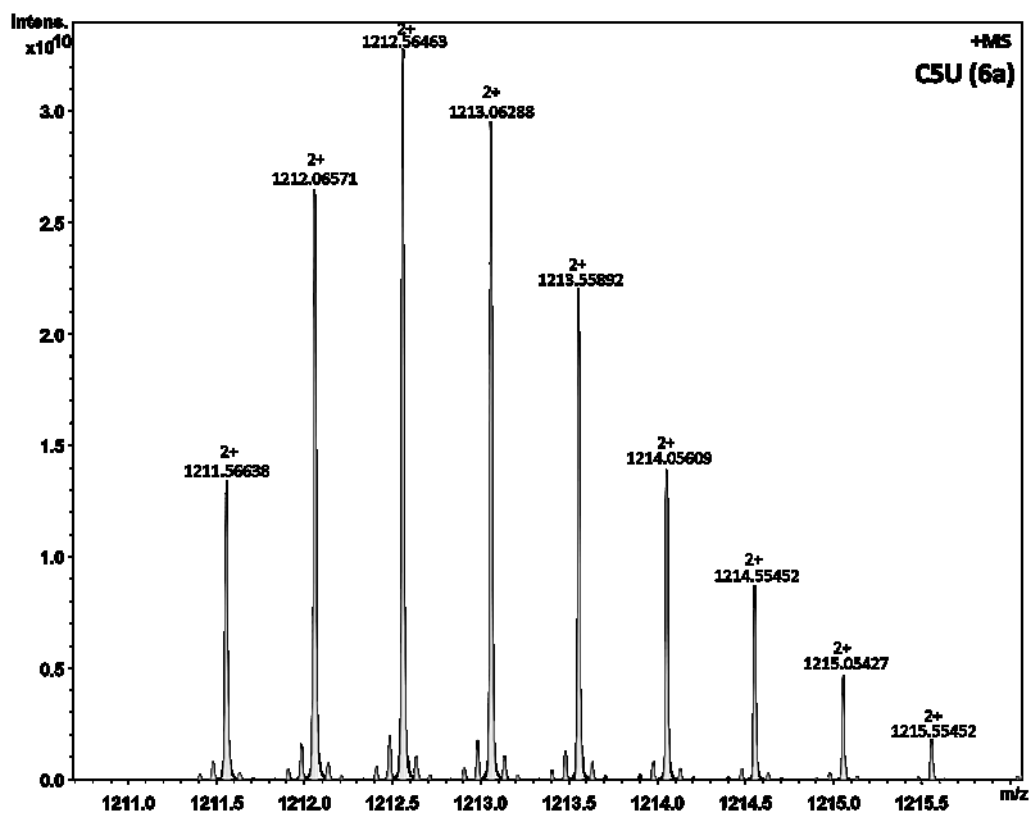
C4NH2 (5a)



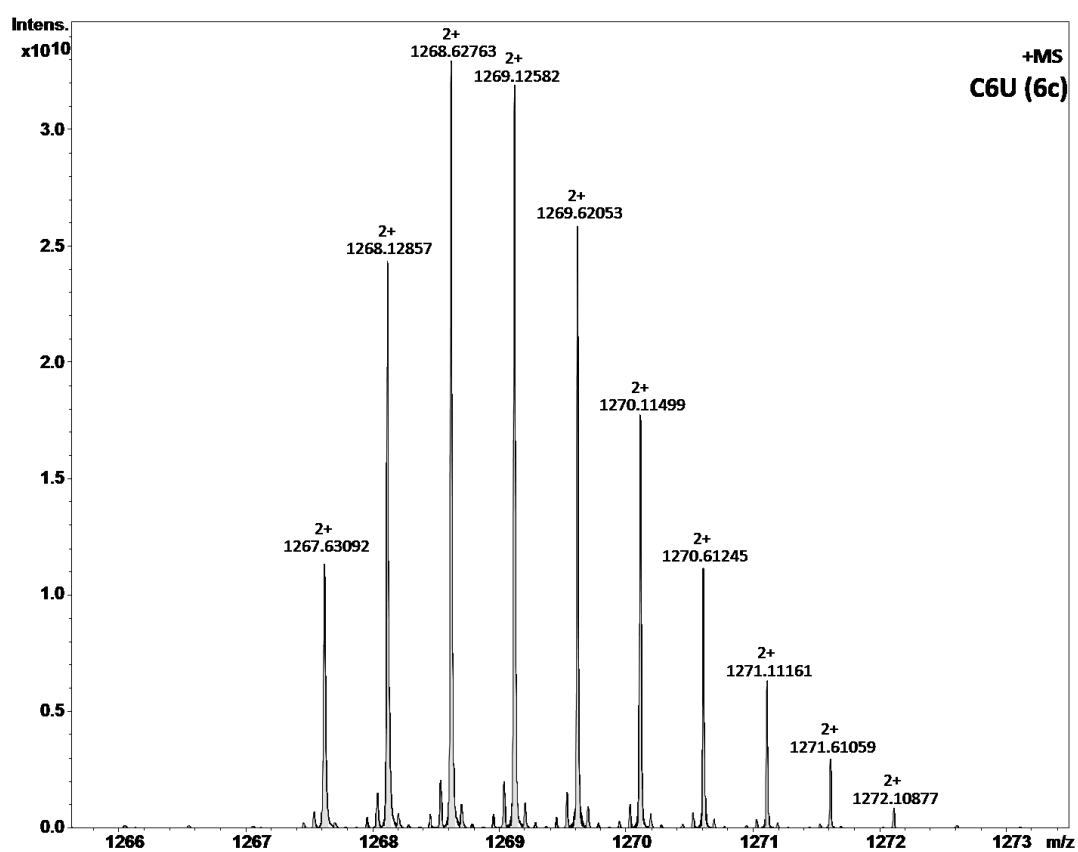
C5NH2 (5b)



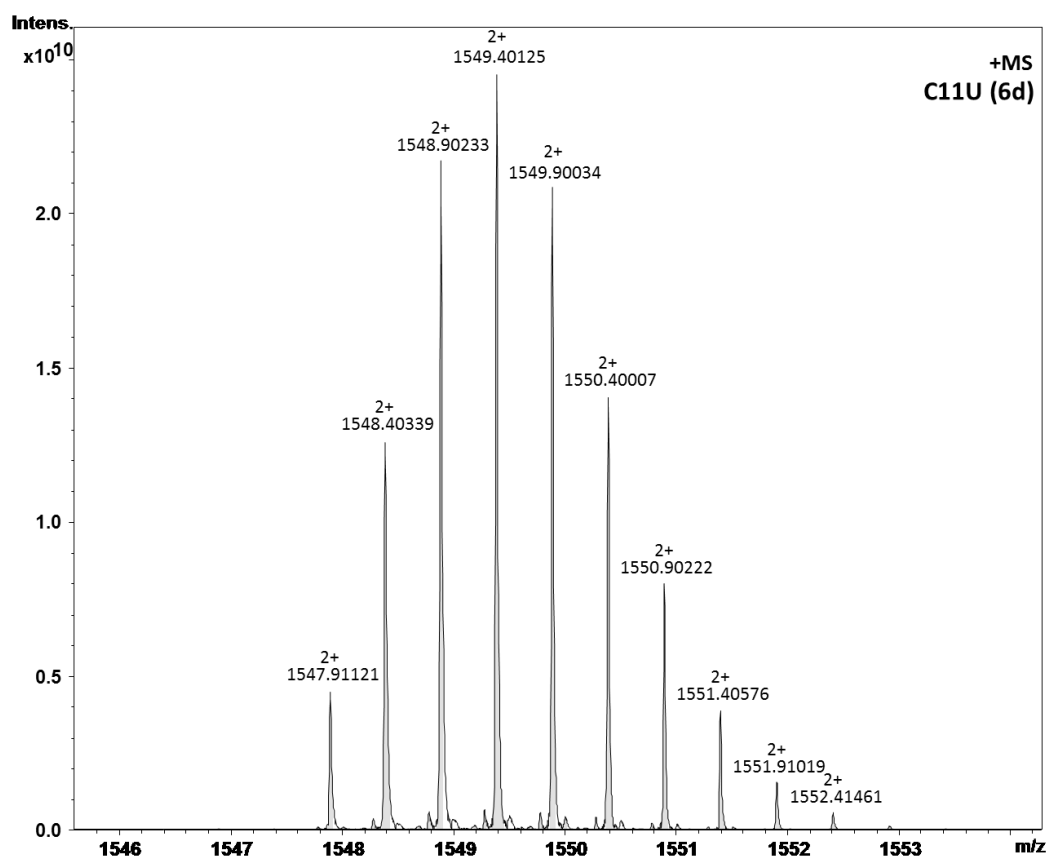
C6NH2 (5c)**C11 Amin**

C4 Urea (6a)**C5 Urea (6b)**

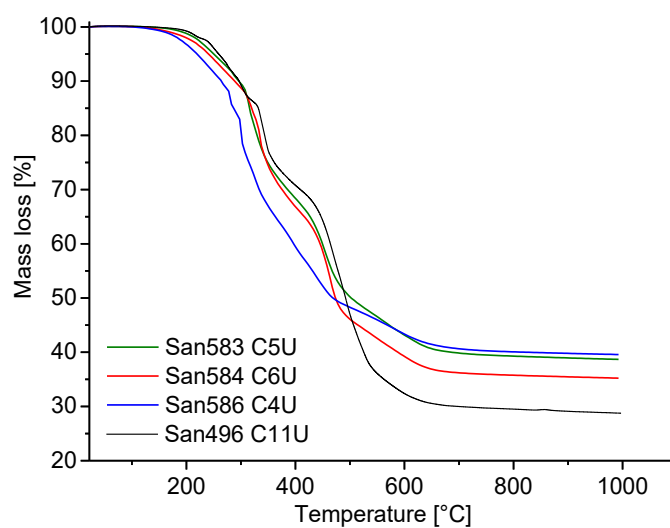
C6 Urea (6c)



C11 Urea (6d)



TG curves



	T_{5%} [°C]	Onset [°C]	m_{residual mass} [%]
C4	217	167	39.58
C5	247	181	38.69
C6	237	198	35.22
C11	259	204	28.76

Remark: Measurements were conducted under N₂, therefore the residual mass corresponds not to value of inorganic part. Measurements were conducted to determine thermal stability.

[i] Lübbe C., Dumrath A., Neumann H., Beller M., Kadyrov R., *ChemCatChem* **2014**, *6*, 105-108.

[ii] Kobayashi Y., Nakano M., Kumar G.B., Kishihara K., *J. Org. Chem.* **1998**, *63*, 7505-7515.

[iii] a) Dutkiewicz M., Maciejewski H., Marciniak B., Karasiewicz J., *Organomet.* **2011**, *30*, 2149-2153; b) Hasegawa I., Motojima S., *J. Organomet. Chem.* **1992**, *441*, 373-380.

Supporting Information

Double Reversible Network – Improvement of Self-Healing in Hybrid Materials via the Combination of Diels-Alder-Crosslinking and Hydrogen Bonds

Sandra Schäfer, Guido Kickelbick*

Inorganic Solid State Chemistry, Saarland University, Campus C4 1, 66123 Saarbrücken, Germany

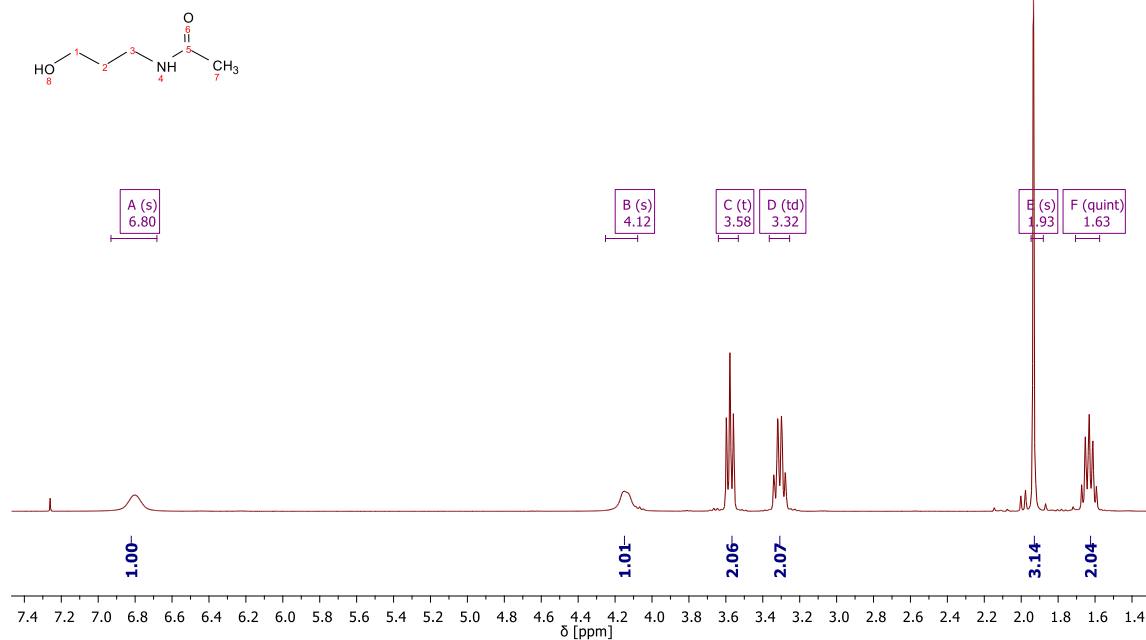
E-mail: guido.kickelbick@uni-saarland.de

CONTENT

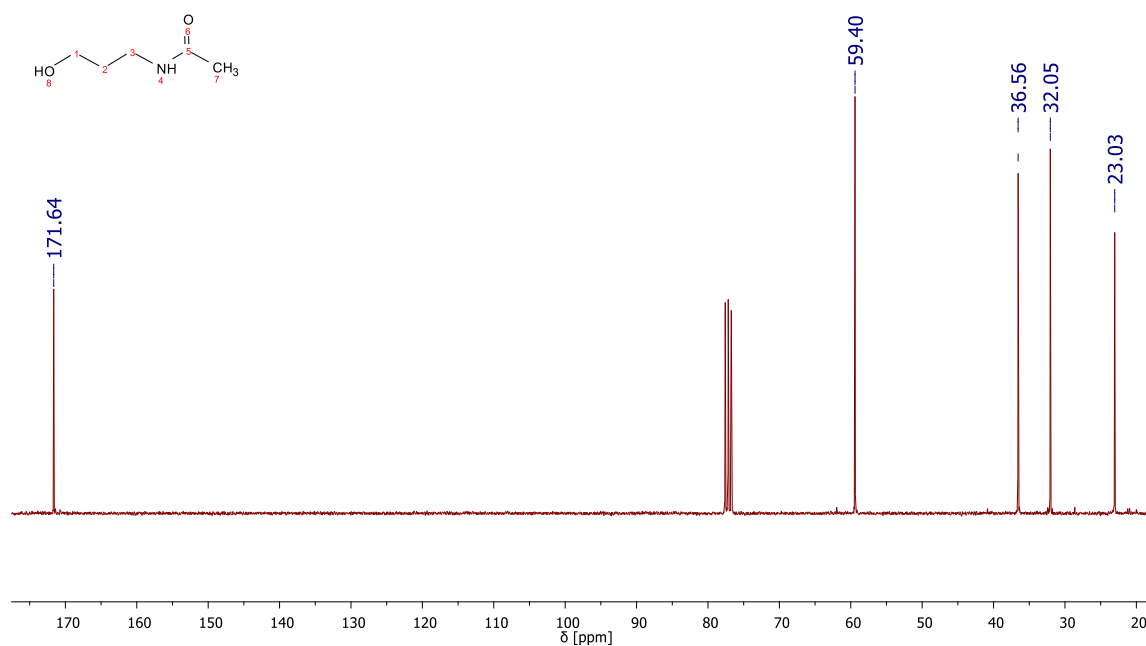
1. ^1H , & ^{13}C NMR spectra of synthesized molecules (**1-10**) and polymers (**P1-P10**)
2. FTIR spectra of synthesized molecules (**1-10**) and polymers (**P1-P10**)
3. DSC curves (2nd heating) of polymers **P6-P10**
4. IR spectra of composites **C1-C4**
5. DSC curves of **C1-C4**
6. Microscope Images of composites **C1-C3**
7. UV/Vis spectra and conversion over time for **P8**
8. Rheology measurement of **P8**
9. TEM images and EDX of **C3**

1. ^1H , & ^{13}C NMR spectra of synthesized molecules (1-10) and polymers (P1-P11)3-Acetylaminopropanol (1).ⁱ

^1H NMR (300 MHz, CDCl_3) δ 6.80 (s, 1H, H8 or H4), 4.12 (1H, H8 or H4), 3.58 (t, $J = 5.7$ Hz, 2H, H1), 3.32 (td, $J = 6.0$ Hz, 2H, H3), 1.93 (s, 3H, H7), 1.63 (quint, 2H, H2).

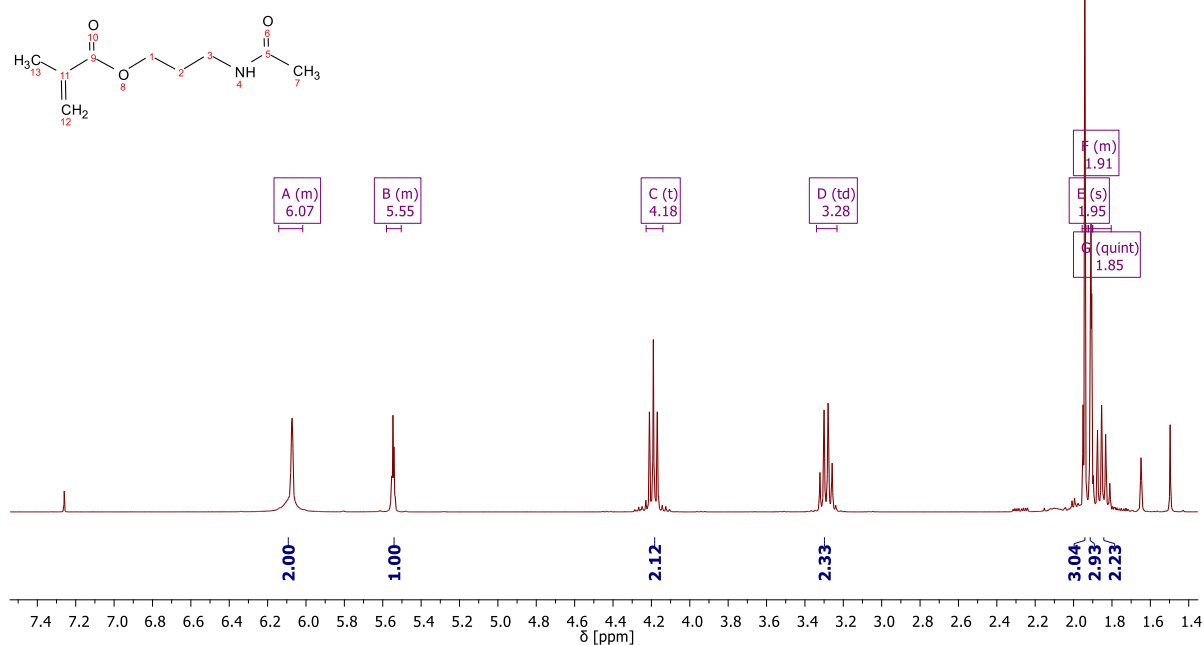
Figure S1: ^1H NMR of 3-Acetylaminopropanol (1).

^{13}C NMR (75 MHz, CDCl_3) δ 171.64 (C5), 59.40 (C1), 36.56 (C3), 32.05 (C2), 23.03 (C7).

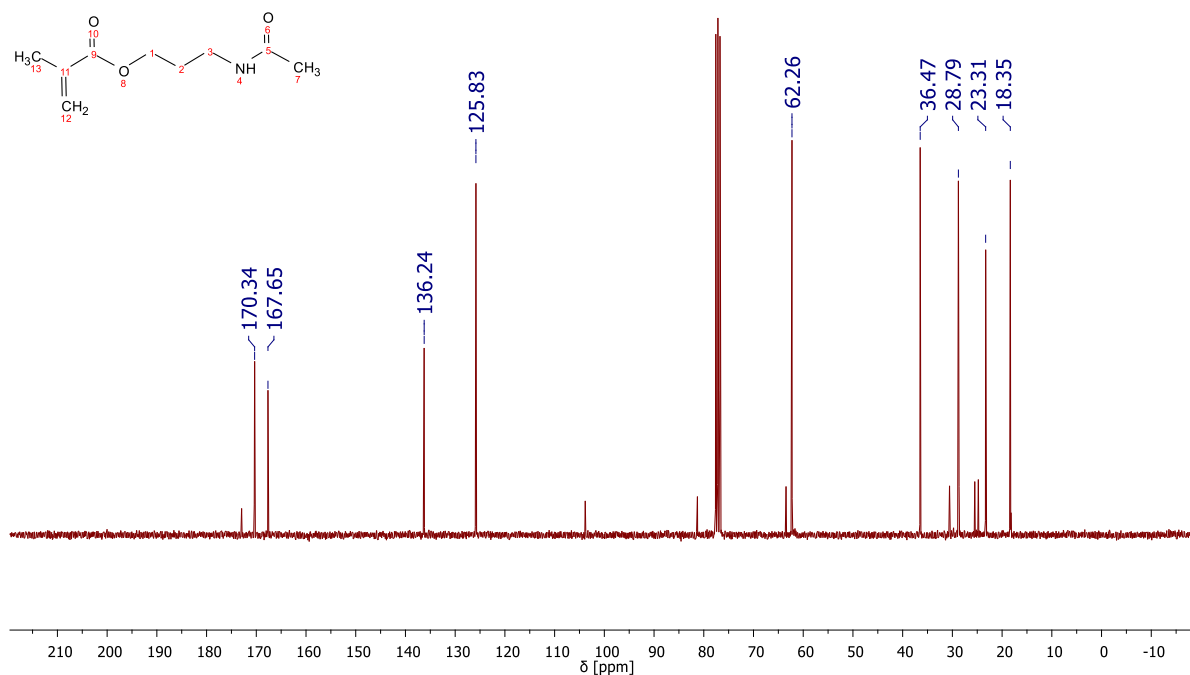
Figure S2: ^{13}C NMR of 3-Acetylaminopropanol (1).

3-Acetamidopropyl methacrylate (2).

^1H NMR (300 MHz, CDCl_3) δ 6.14 – 6.02 (m, $J = 1.5, 1.0$ Hz, 2H, H12 and H4), 5.58 – 5.50 (m, 1H, H12), 4.18 (d, $J = 6.0$ Hz, 2H, H1), 3.28 (td, $J = 6.0$ Hz, 2H, H3), 1.95 (s, 3H, H7), 1.92 – 1.90 (m, 3H, H13), 1.85 (quint, $J = 6.0$ Hz, 2H, H2).

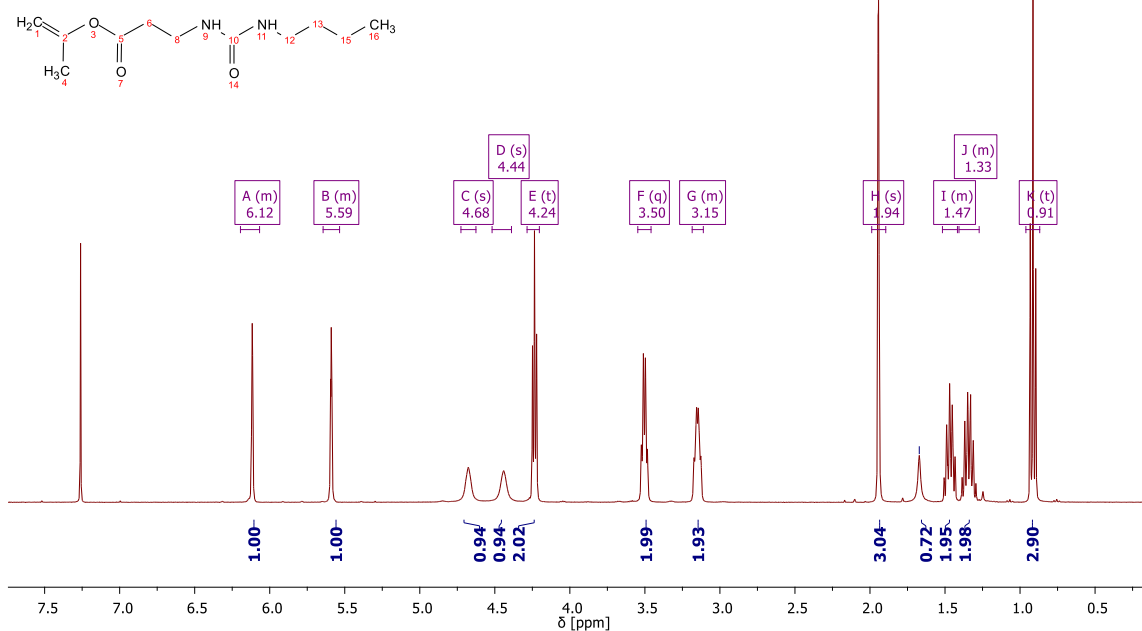
**Figure S3: ^1H NMR of 3-Acetamidopropyl methacrylate (2).**

^{13}C NMR (75 MHz, CDCl_3) δ 170.34 (C5), 167.65 (C9), 136.24 (C11), 125.83 (C12), 62.26 (C1), 36.47 (C3), 28.79 (C2), 23.31 (C7), 18.35 (C13).

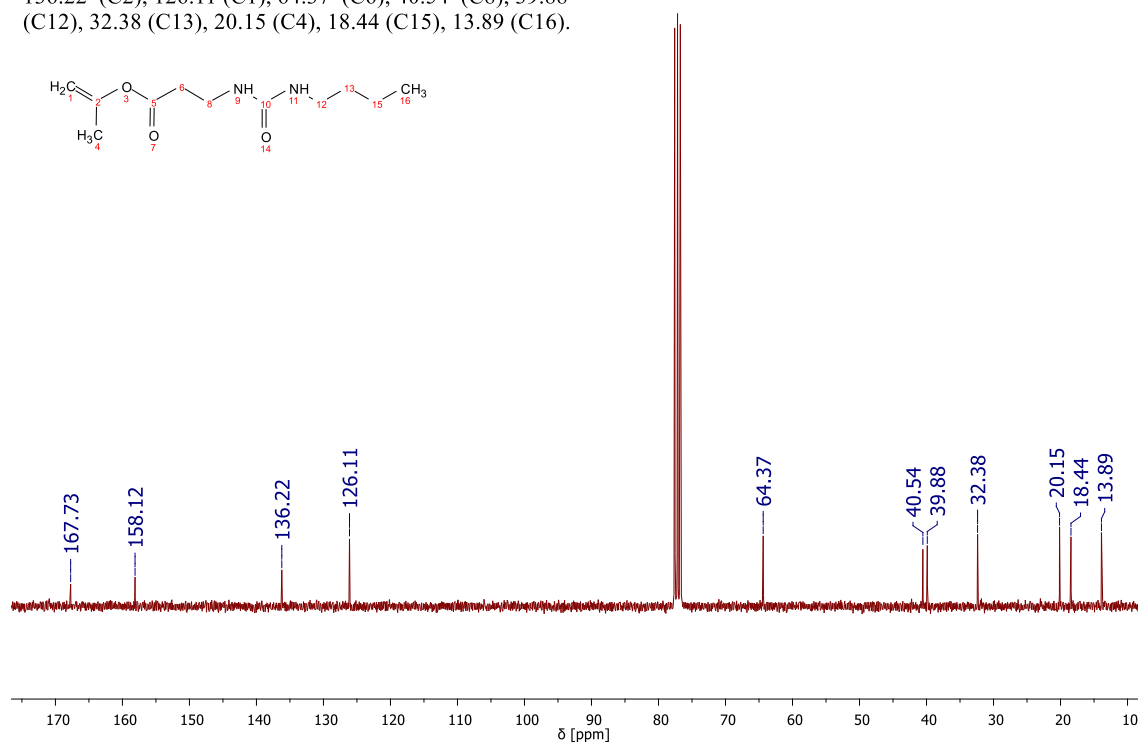
**Figure S4: ^{13}C NMR of 3-Acetamidopropyl methacrylate (2).**

2-(4-Butylureido) ethyl methacrylate (3).

^1H NMR (400 MHz, CDCl_3) δ 6.19 – 6.07 (m, 1H, H1), 5.64 – 5.53 (m, 1H, H1), 4.68 (s, 1H, H9 or H11), 4.44 (s, 1H, H1, H9 or H11), 4.24 (t, $J = 5.4$ Hz, 2H, H6), 3.50 (q, $J = 5.4$ Hz, 2H, H8), 3.18 – 3.11 (m, 2H, H12), 1.94 (s, 3H, H4), 1.52 – 1.42 (m, 2H, H13), 1.41 – 1.27 (m, 2H, H15), 0.91 (t, $J = 7.3$ Hz, 3H, H16).

Figure S5: ^1H NMR of 2-(4-Butylureido) ethyl methacrylate (3).

^{13}C NMR (75 MHz, CDCl_3) δ 167.73 (C5), 158.12 (C10), 136.22 (C2), 126.11 (C1), 64.37 (C6), 40.54 (C8), 39.88 (C12), 32.38 (C13), 20.15 (C4), 18.44 (C15), 13.89 (C16).

Figure S6: ^{13}C NMR of 2-(4-Butylureido) ethyl methacrylate (3).

2-(2-Hydroxyethyl)-3a,4,7,7a-tetrahydro-1H-4,7-epoxyisoindole-1,3(2H)-dione (4).

^1H NMR (300 MHz, CDCl_3) δ 6.53 – 6.48 (m, 2H, H1&2), 5.27 (t, $J = 0.9$ Hz, 2H, H3&6), 3.79 – 3.72 (m, 2H, H14), 3.71 – 3.63 (m, 2H, H13), 2.88 (s, 2H, H4&5), 2.37 (s, 1H, H15).

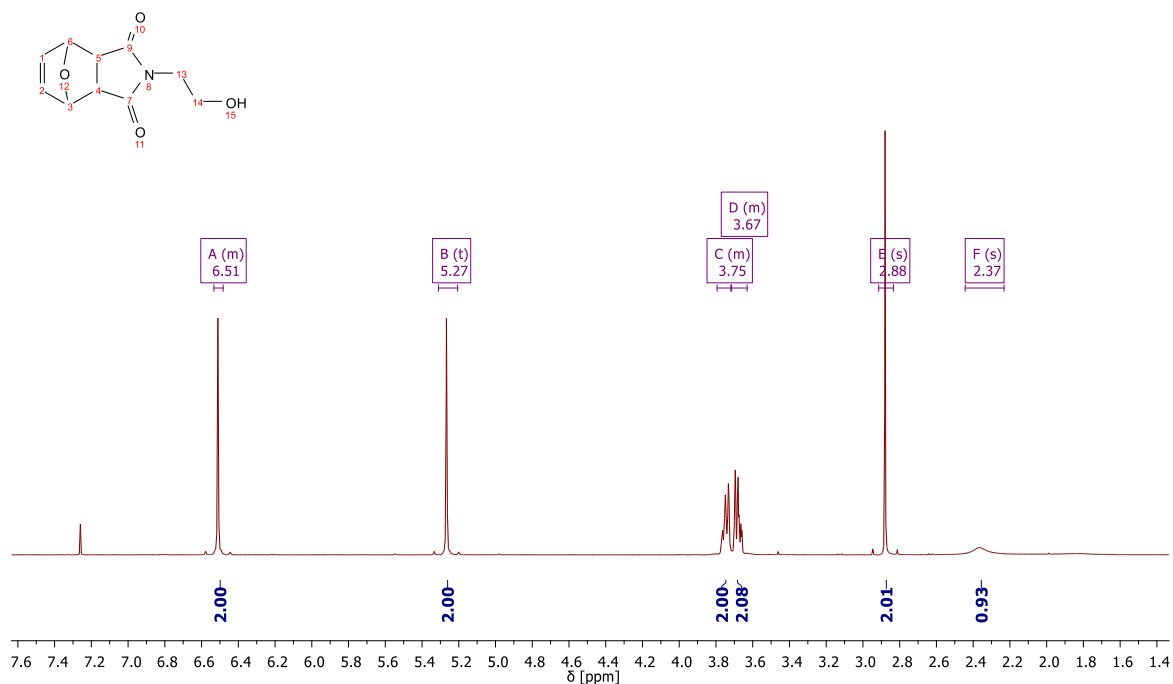


Figure S7: ^1H NMR of 2-(2-Hydroxyethyl)-3a,4,7,7a-tetrahydro-1H-4,7-epoxyisoindole-1,3(2H)-dione (4).

^{13}C NMR (75 MHz, CDCl_3) δ 176.92 (C7/9), 136.67 (C1/2), 81.15 (C3/6), 60.57 (C14), 47.65 (C4/5), 41.97 (C13).

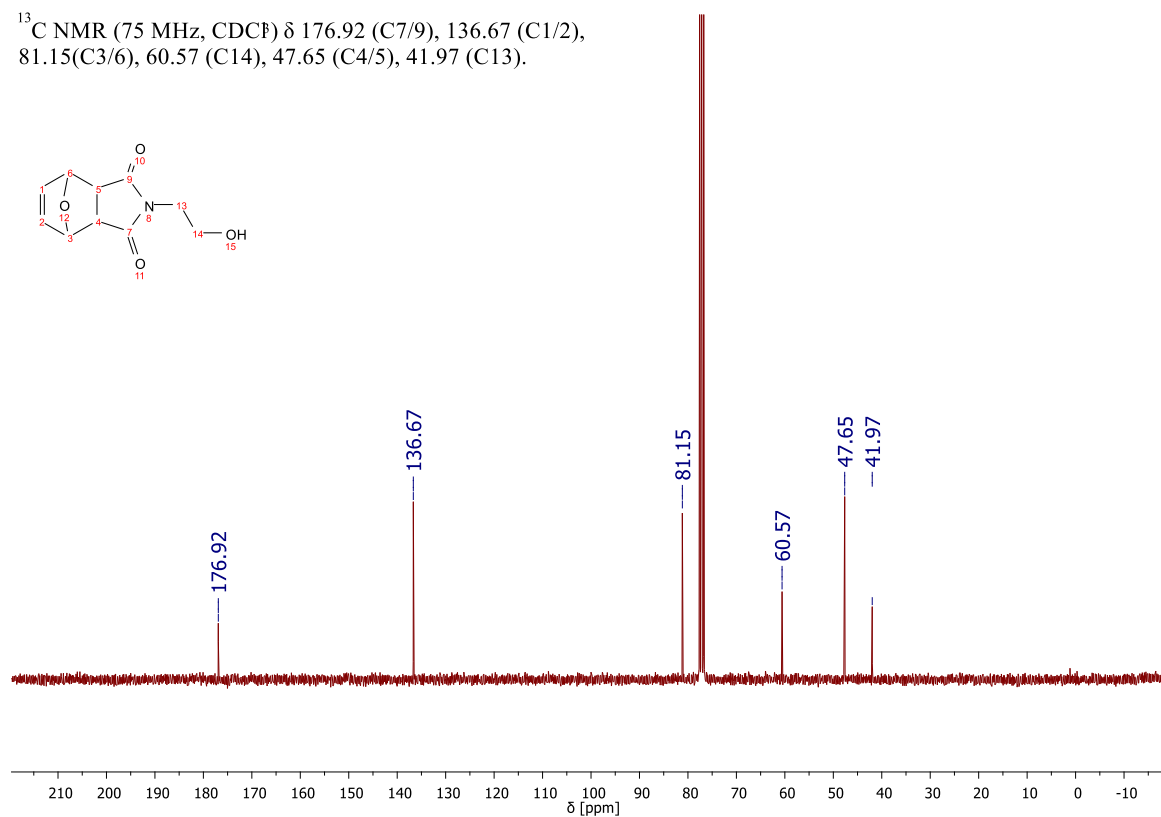
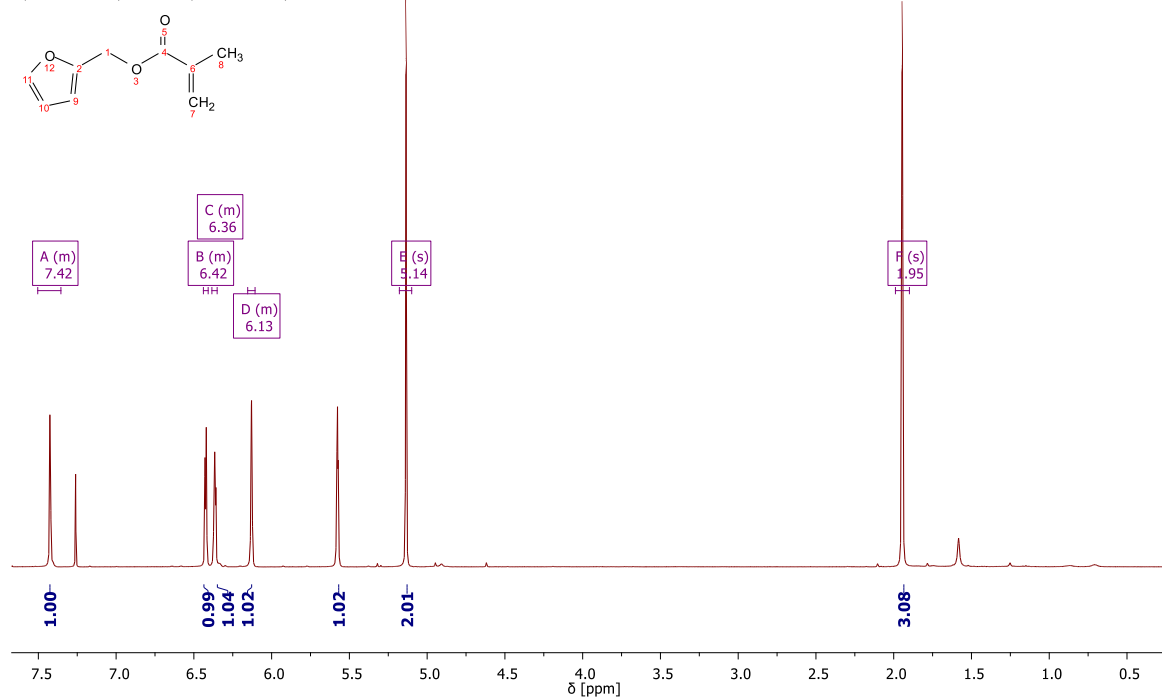


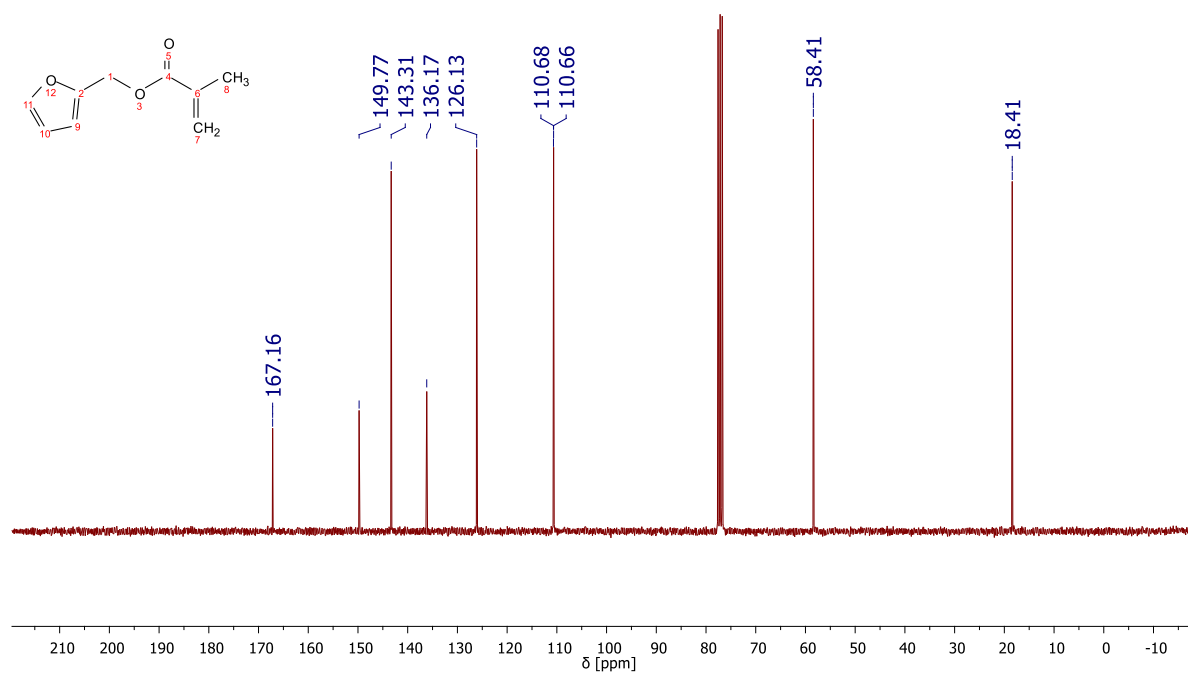
Figure S8: ^{13}C NMR of 2-(2-Hydroxyethyl)-3a,4,7,7a-tetrahydro-1H-4,7-epoxyisoindole-1,3(2H)-dione (4).

Furfuryl methacrylate (5).ⁱⁱ

¹H NMR (400 MHz, CDCl₃) δ 7.50 – 7.35 (m, *J* = 1.0 Hz, 1H, H11), 6.44 – 6.41 (m, *J* = 3.2 Hz, 1H, H9), 6.38 – 6.35 (m, *J* = 3.1, 1.9 Hz, 1H, H10), 6.15 – 6.11 (m, 1H, H7), 5.14 (s, 2H, H1), 1.95 (s, 3H, H8).

Figure S9: ¹H NMR of Furfuryl methacrylate (5).

¹³C NMR (75 MHz, CDCl₃) δ 167.16 (C4), 149.77 (C2), 143.31 (C11), 136.17 (C6), 126.13 (C7), 110.68 (C10), 110.66 (C9), 58.41 (C1), 18.41 (C8).

Figure S10 ¹³C NMR of Furfuryl methacrylate (5).

2-(1,3-Dioxo-3a,4,7,7-tetrahydro-1H-4,7-epoxyisoindol-2(3H)-yl)ethylmethacrylate (MIMA, 6)ⁱⁱⁱ

¹H NMR (400 MHz, CDCl₃) δ 6.50 (s, 2H, H1&H2), 6.06 (s, 1H, H20), 5.59 – 5.51 (m, 1H, H20), 5.25 (s, 2H, H3&H6), 4.27 (t, *J* = 5.4 Hz, 2H, H14), 3.80 (t, *J* = 5.3 Hz, 2H, H13), 2.86 (s, 2H, H4&H5), 1.89 (s, 3H, H19).

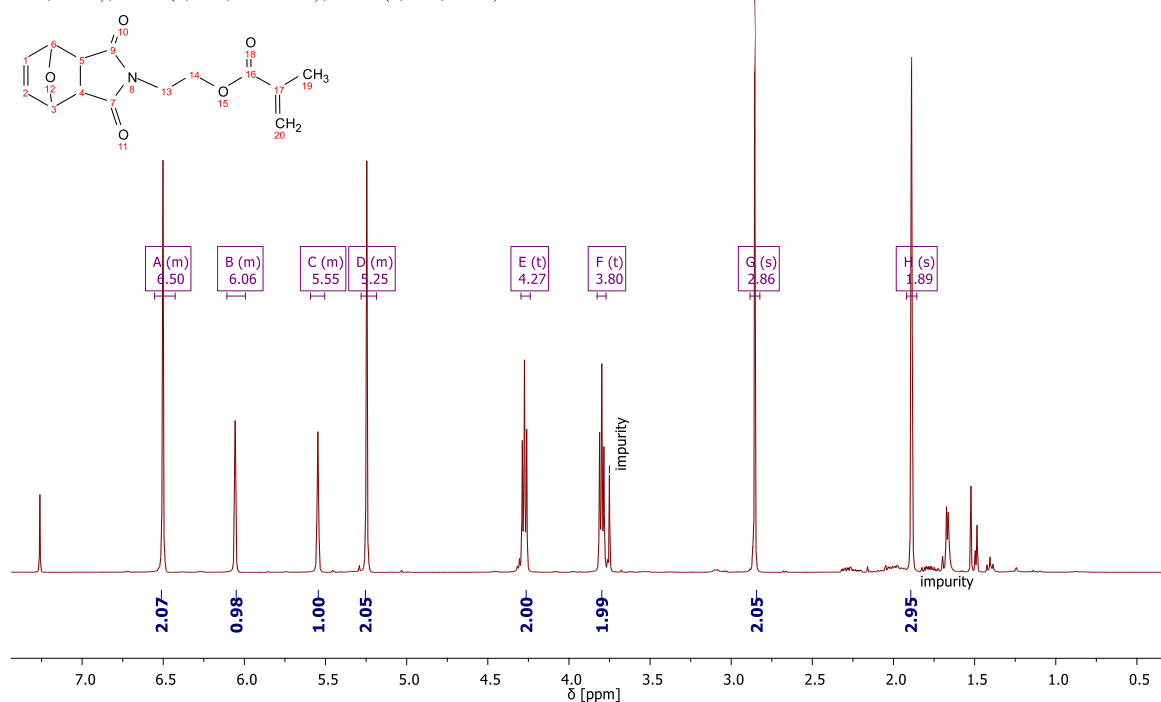


Figure S11: ¹H NMR of 2-(1,3-Dioxo-3a,4,7,7-tetrahydro-1H-4,7-epoxyisoindol-2(3H)-yl)ethylmethacrylate (MIMA, 6).

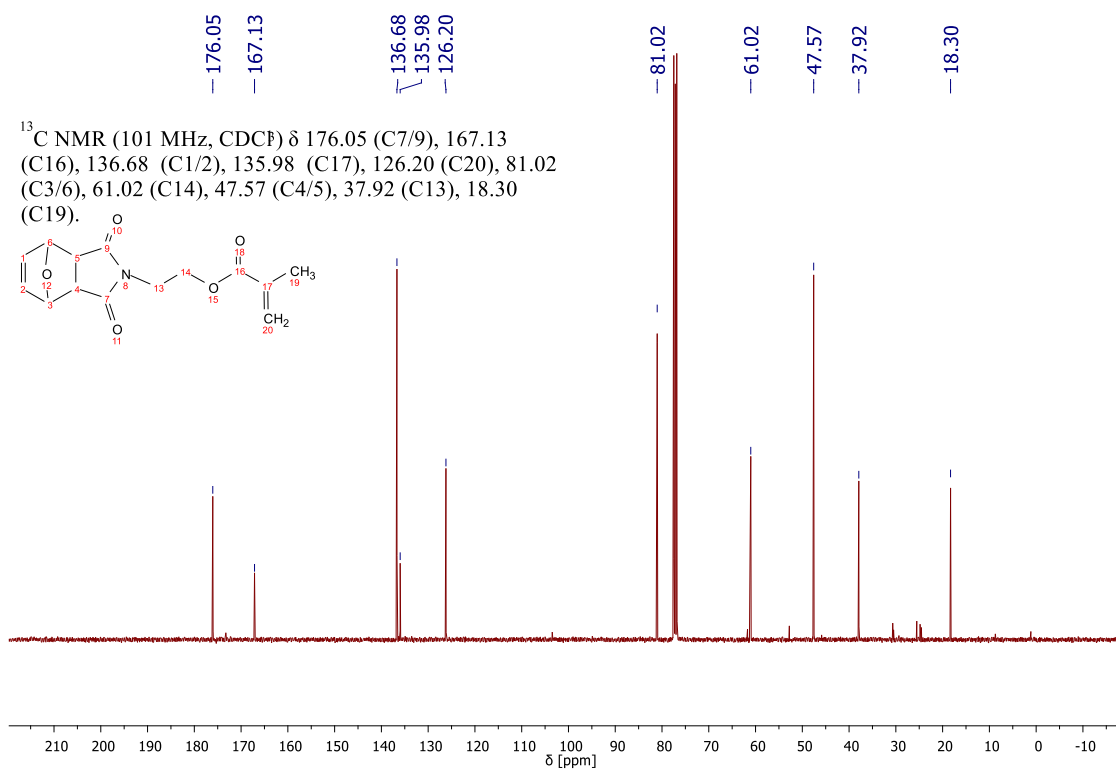


Figure S12: ¹³C NMR of 2-(1,3-Dioxo-3a,4,7,7-tetrahydro-1H-4,7-epoxyisoindol-2(3H)-yl)ethylmethacrylate (MIMA, 6).

^1H NMR (300 MHz, CDCl_3) δ 4.10 – 3.82 (m, 1H, OCH₂),
2.14 – 0.59 (m, 6H, pBMA backbone).

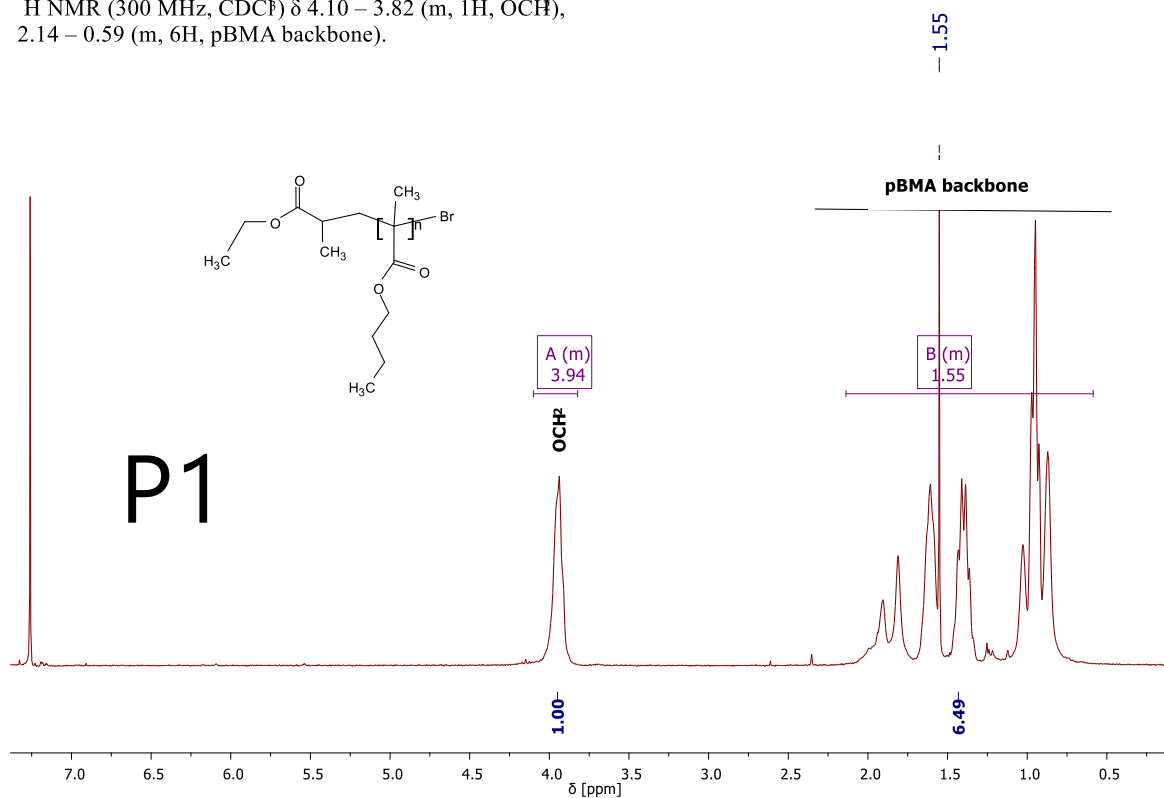


Figure S13: ^1H NMR of pBMA (P1).

^1H NMR (300 MHz, CDCl_3) δ 7.42 (s, 1H), 6.44 – 6.29 (m, 2H), 5.02 – 4.88 (m, 2H), 4.08 – 3.81 (m, 21H), 2.12 – 0.64 (m, 140H).

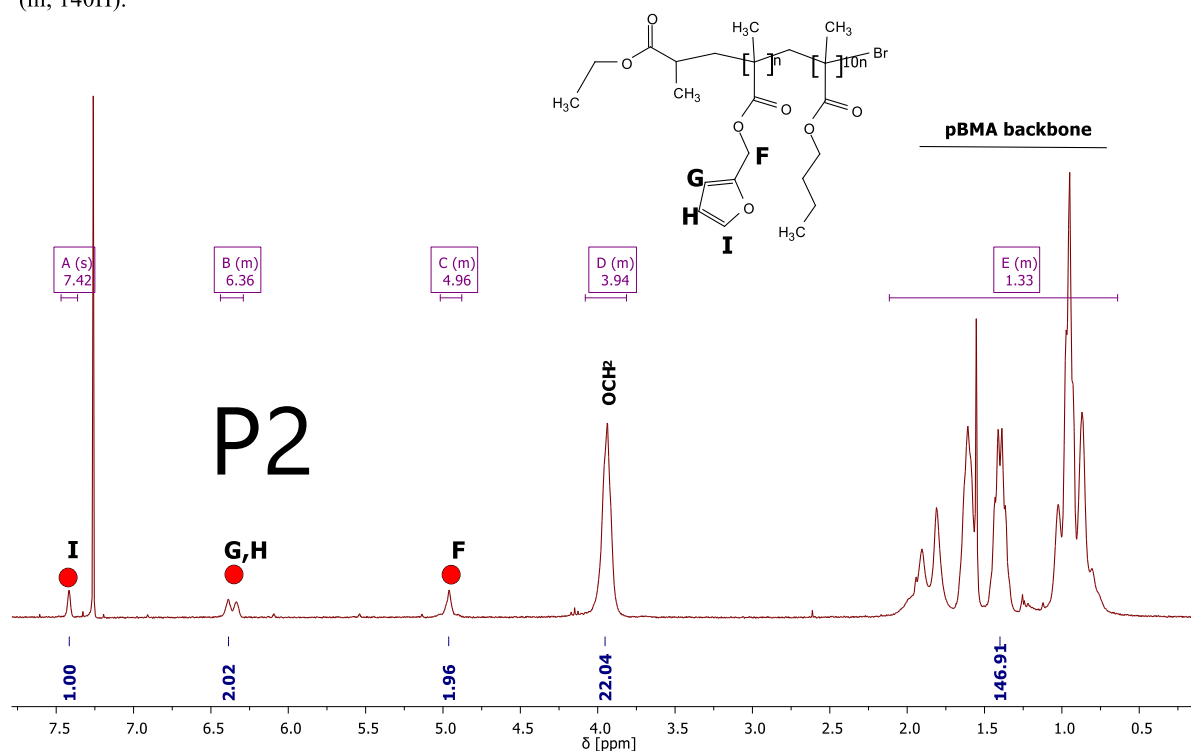


Figure S14: ^1H NMR of pBMAcoFMA (P2).

^1H NMR (300 MHz, CDCl_3) δ 6.58 – 6.45 (m, 1H), 5.32 – 5.15 (m, 1H), 4.13 – 3.81 (m, 24H), 3.68 – 3.48 (m, 1H), 2.91 – 2.79 (m, 1H), 2.14 – 0.62 (m, 149H).

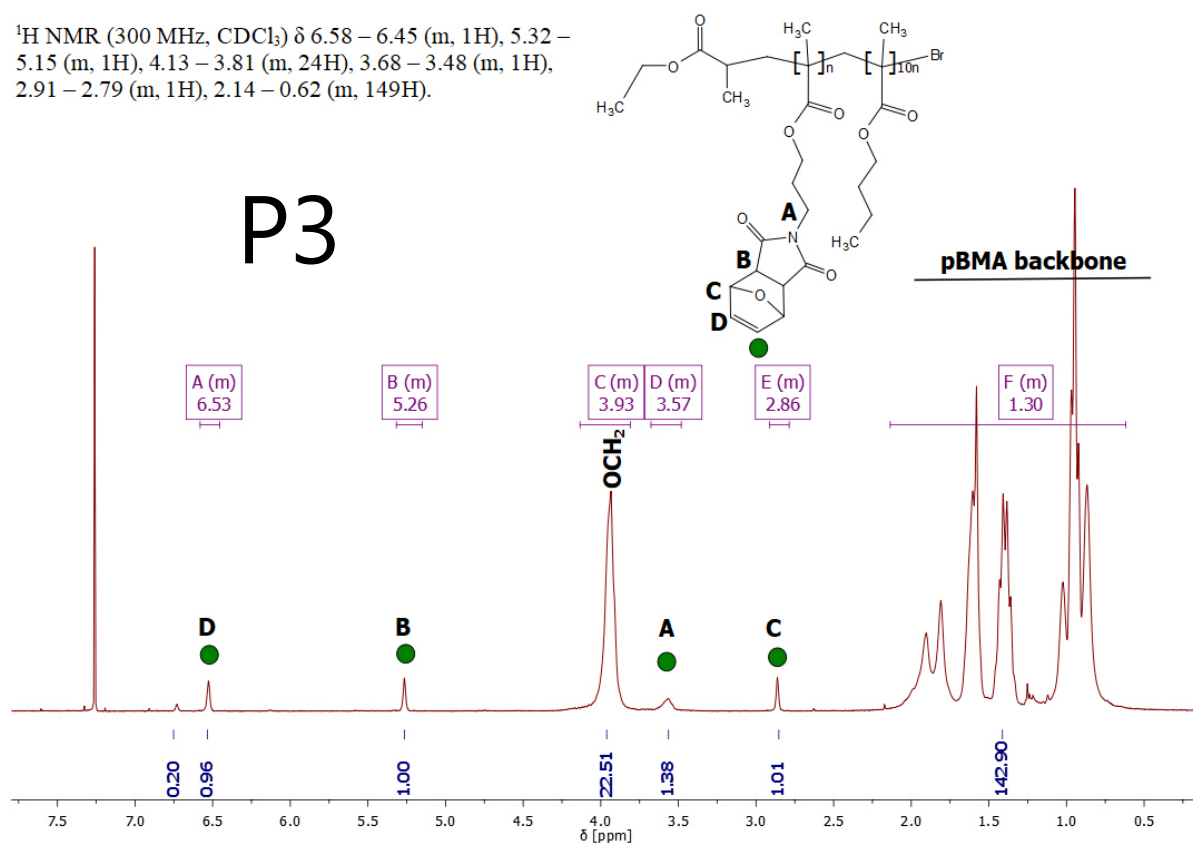


Figure S15: ^1H NMR of pBMAcoMiMA (P3).

^1H NMR (400 MHz, CDCl_3) δ 6.80 – 6.68 (m, 1H), 4.05 – 3.83 (m, 20H), 3.67 – 3.54 (m, 1H), 2.18 – 0.51 (m, 132H).

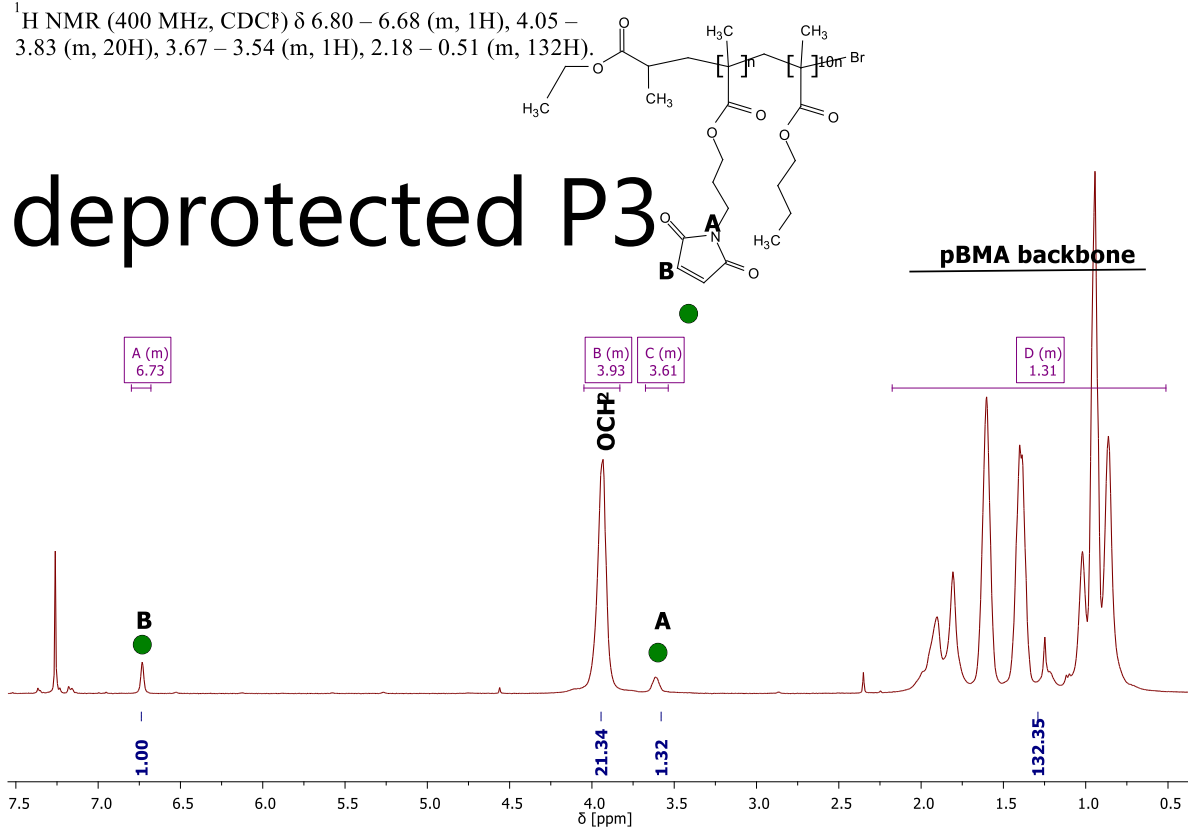


Figure S16: ^1H NMR of deprotected pBMAcoMiMA (dP3).

^1H NMR (300 MHz, CDCl_3) δ 4.08 – 3.85 (m, 15H), 3.44 – 3.25 (m, 1H), 2.11 – 0.63 (m, 100H).

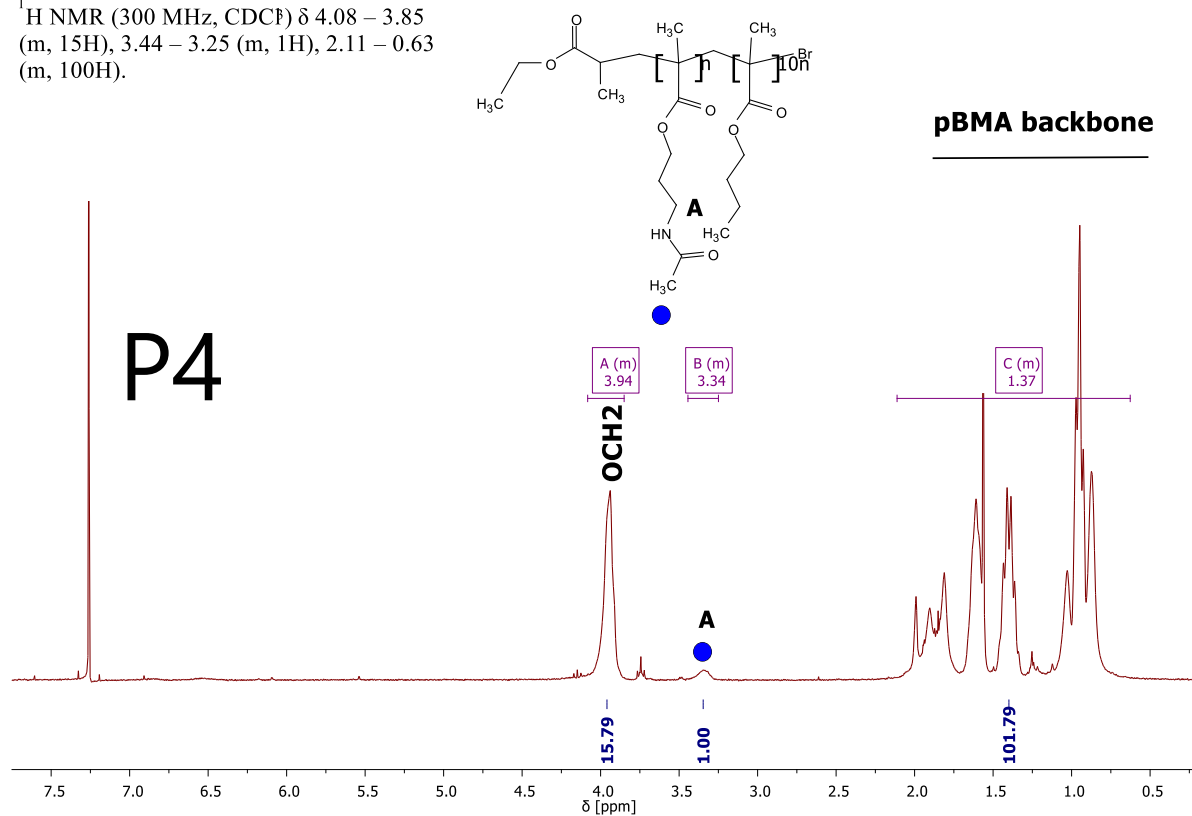


Figure S17: ^1H NMR of pBMAco'H1' (P4).

^1H NMR (400 MHz, CDCl_3) δ 7.51 – 7.34 (m, 1H), 6.64 – 6.48 (m, 2H), 6.48 – 6.29 (m, $J = 19.8$ Hz, 2H), 5.34 – 5.18 (m, 1H), 5.06 – 4.88 (m, 1H), 4.19 – 3.83 (m, 22H), 3.83 – 3.68 (m, 2H), 3.48 – 3.24 (m, 2H), 3.10 – 2.86 (m, 1H), 2.33 – 0.48 (m, 163H).

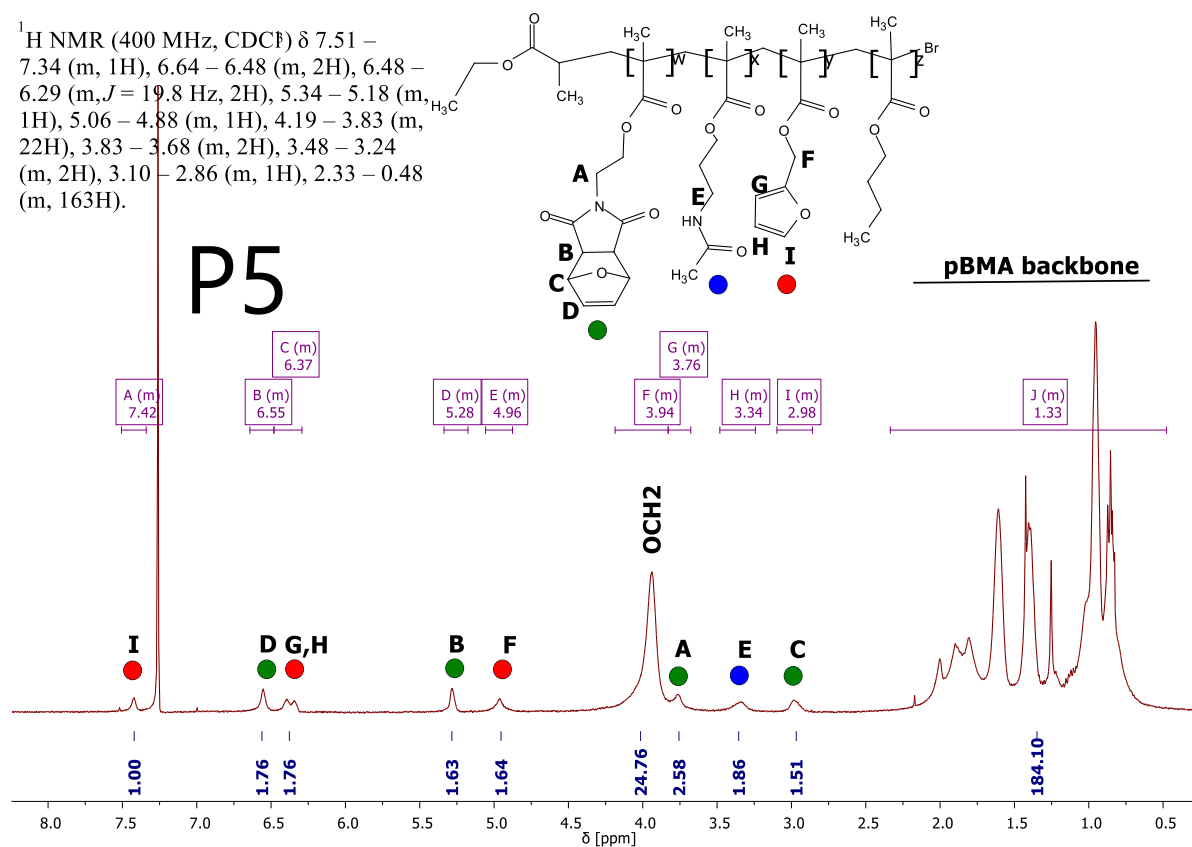


Figure S18: ^1H NMR of EKH1_A (P5).

^1H NMR (400 MHz, CDCl_3) δ 7.50 – 7.34 (m, 1H), 6.64 – 6.49 (m, 1H), 6.49 – 6.27 (m, $J = 19.1$ Hz, 2H), 5.33 – 5.21 (m, 2H), 5.06 – 4.85 (m, 2H), 4.16 – 3.84 (m, 24H), 3.84 – 3.65 (m, 2H), 3.61 – 3.36 (m, 3H), 3.31 – 3.11 (m, 3H), 3.06 – 2.89 (m, 1H), 2.13 – 0.57 (m, 169H).

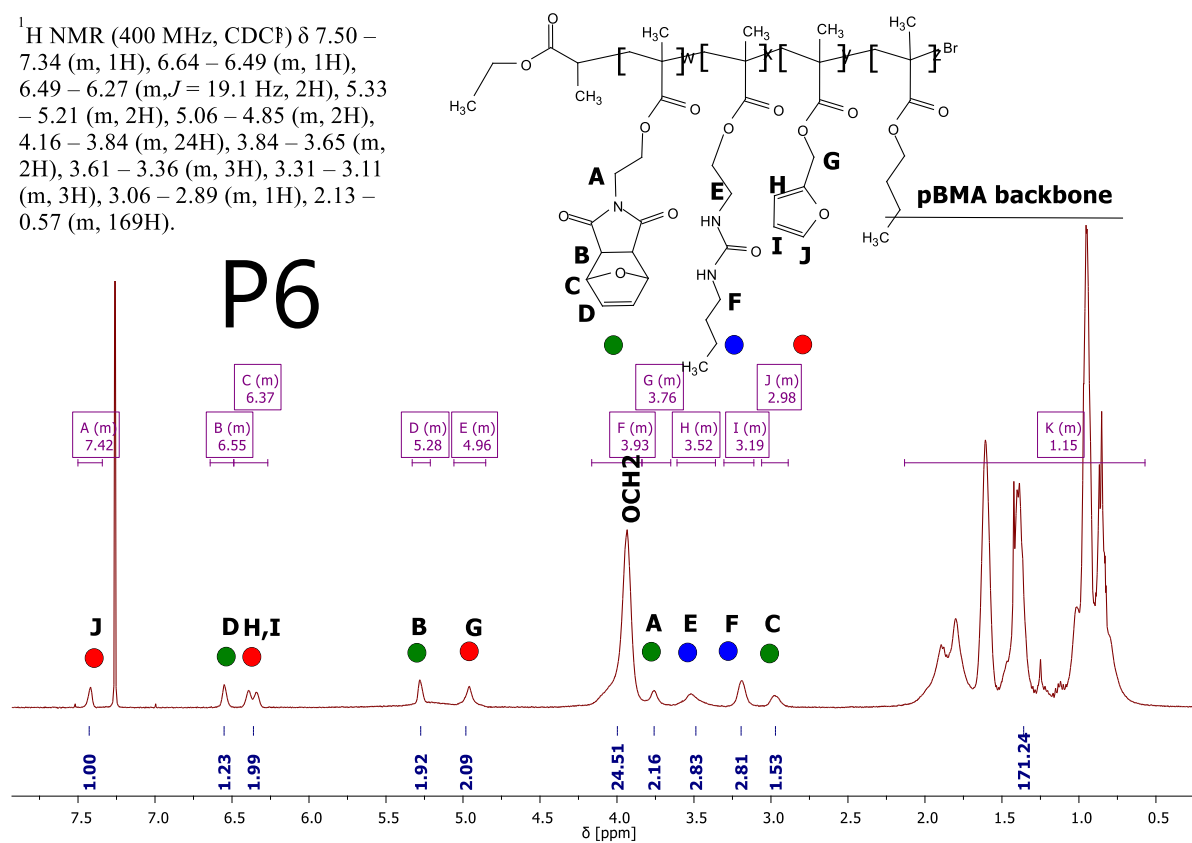


Figure S19: ^1H NMR of EKH2_A (P6).

^1H NMR (400 MHz, CDCl_3) δ 7.49 – 7.33 (m, 1H), 6.62 – 6.46 (m, 2H), 6.46 – 6.28 (m, $J = 21.6$ Hz, 2H), 5.35 – 5.24 (m, $J = 10.8$ Hz, 2H), 5.09 – 4.87 (m, 2H), 4.09 – 3.83 (m, 21H), 3.83 – 3.66 (m, $J = 6.7$ Hz, 3H), 3.04 – 2.90 (m, 1H), 2.78 – 2.60 (m, 2H), 2.13 – 0.55 (m, 153H).

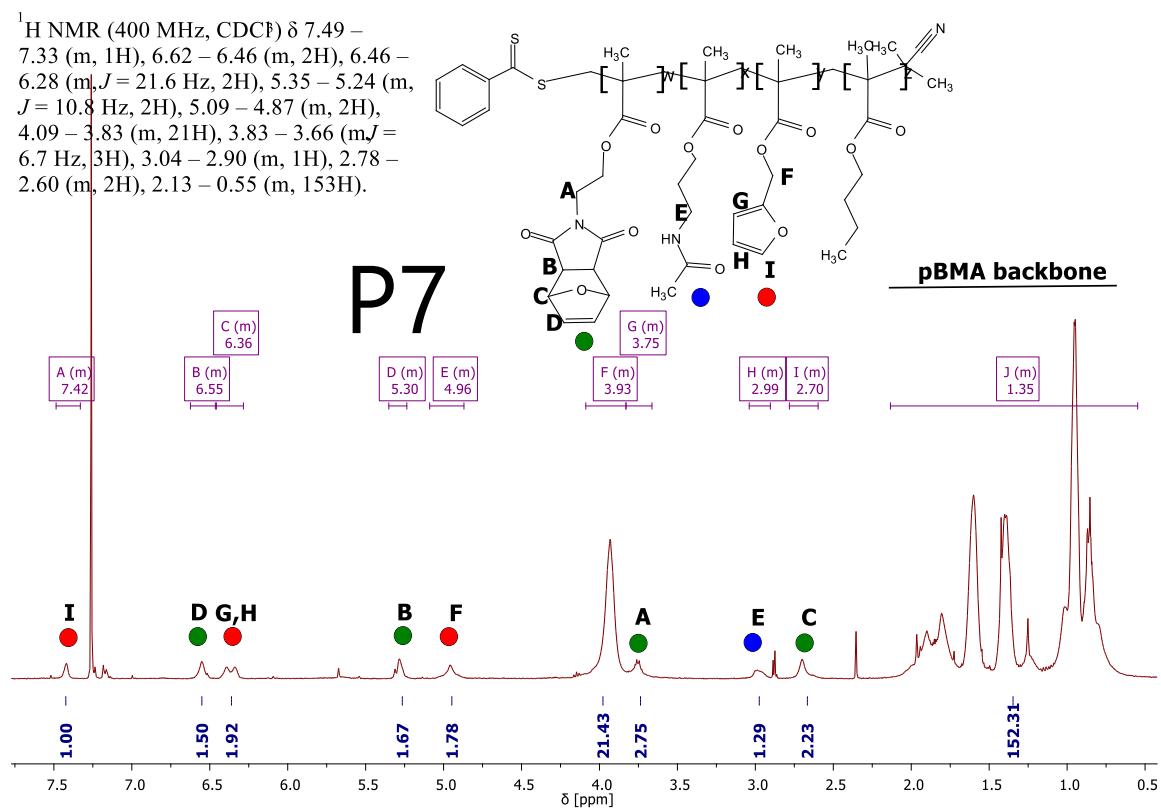
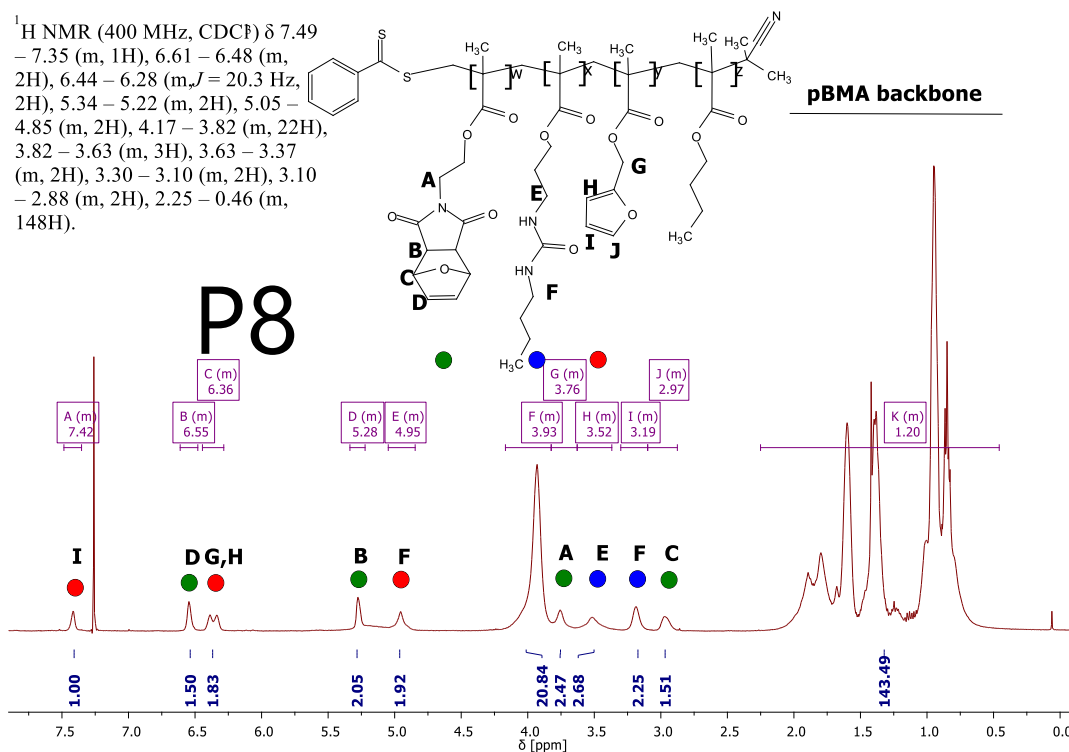
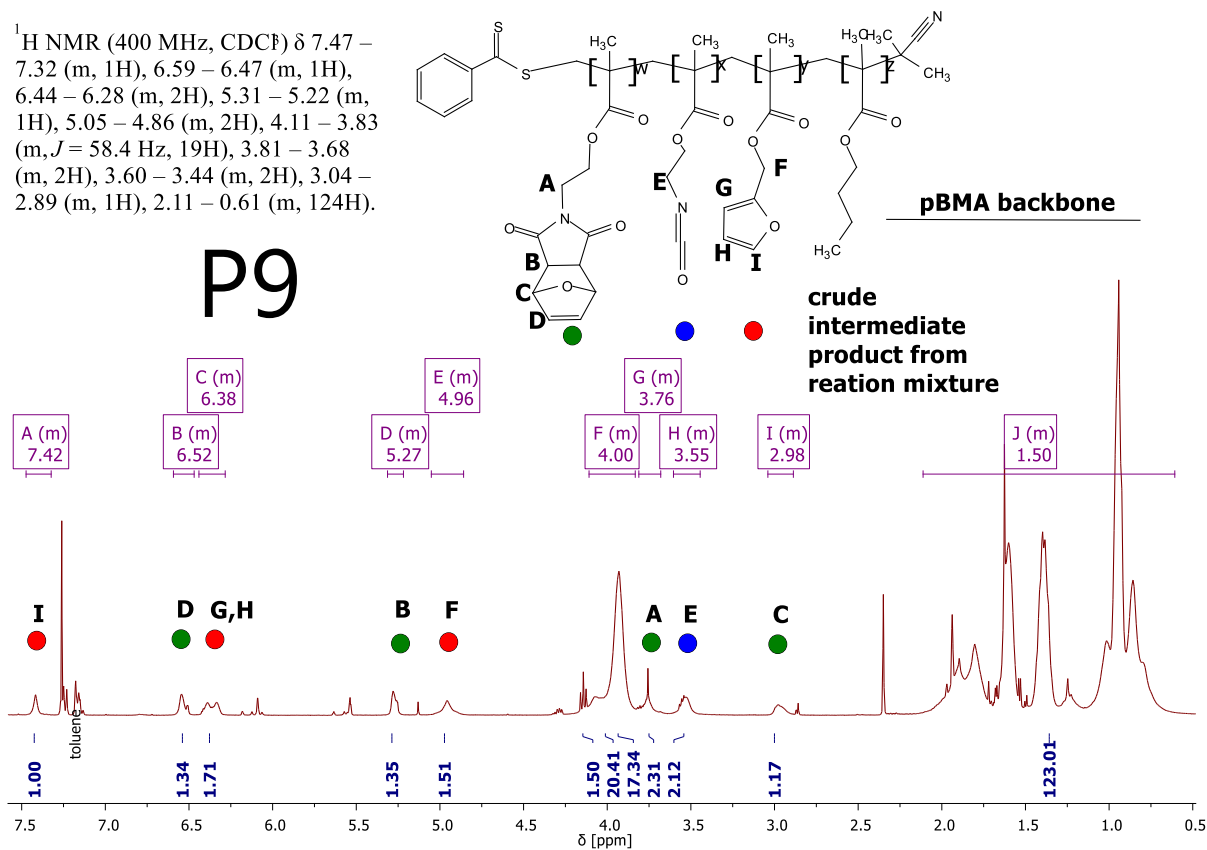


Figure S20: ^1H NMR of EKH1_R (P7).

Figure S21: ¹H NMR of EK₂R (P8).Figure S22: ¹H NMR of EK(OCN) (P9).

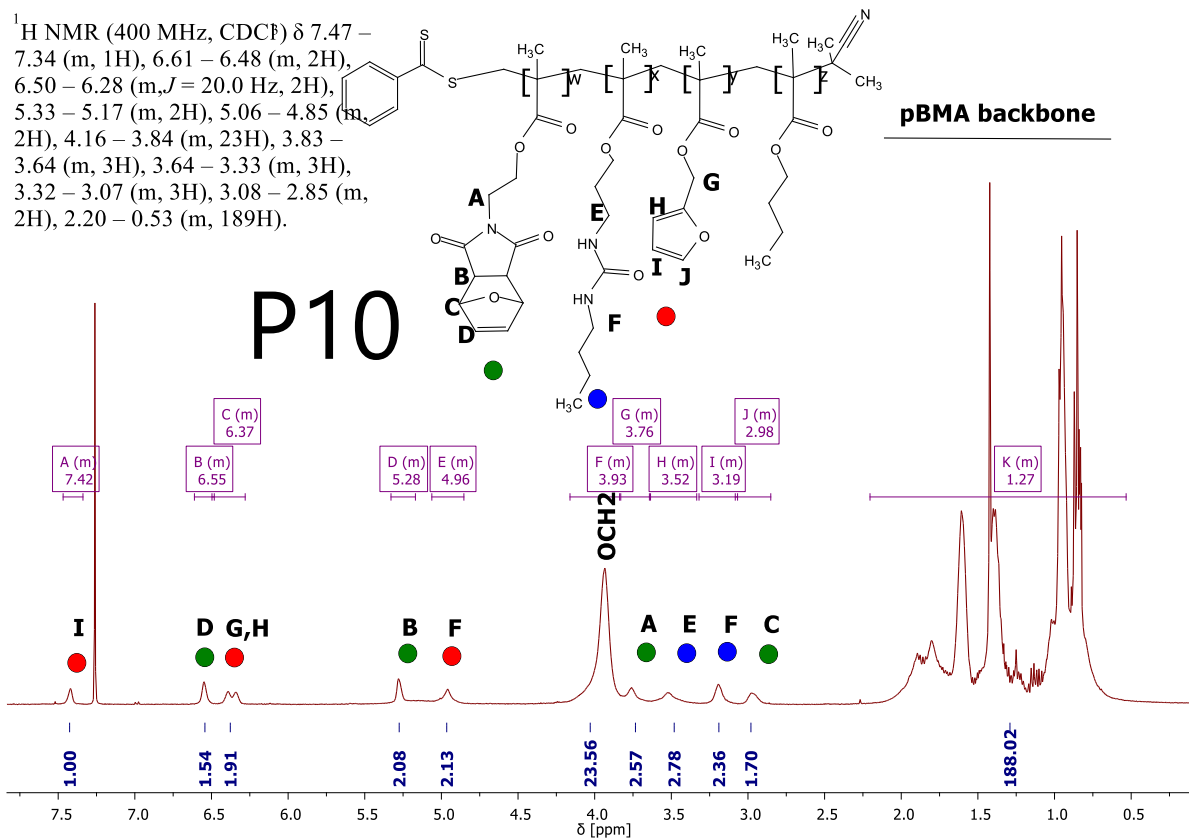


Figure S23: ¹H NMR of EK(OCN+amine)= EKH₂R (P10).

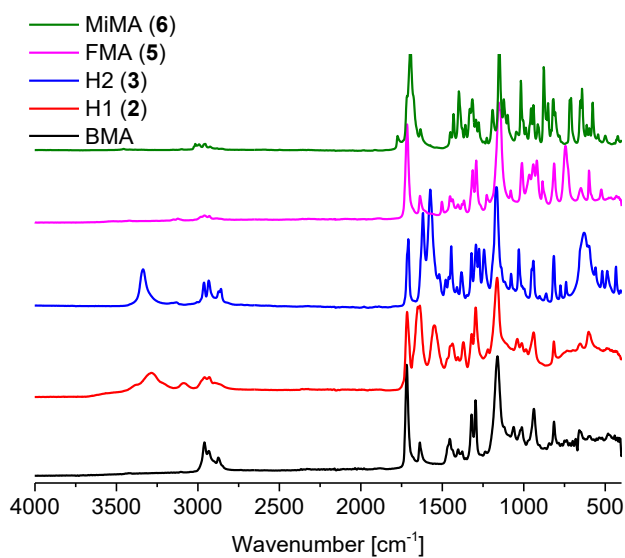


Figure S24: FTIR spectra of monomers: BMA, 2, 3, 5, 6.

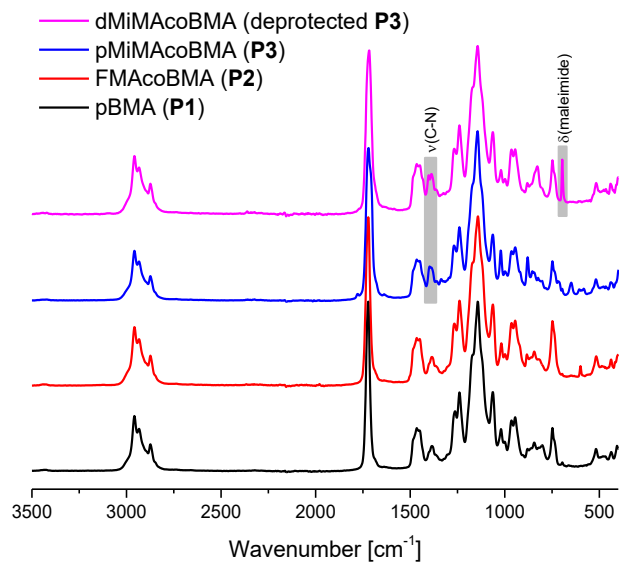


Figure S25: FTIR of polymers: P1, P2, P3 and deprotected dP3.

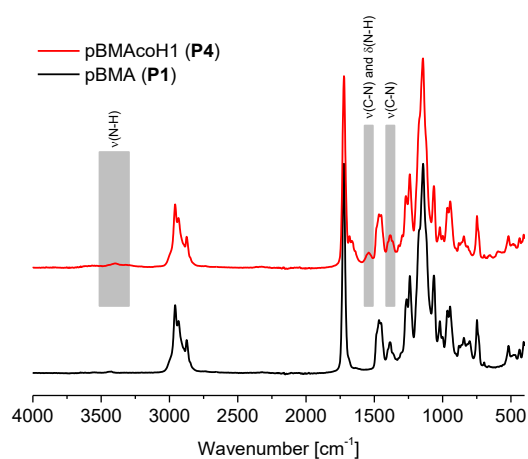


Figure S26: FTIR of polymers: P1 and P4.

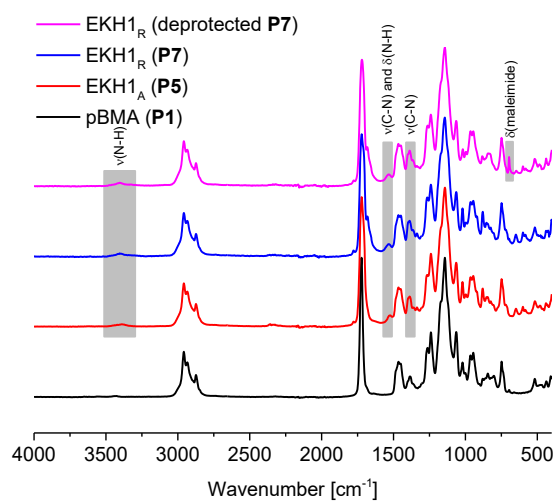


Figure S27: FTIR of polymers: P1, P5, P7 and deprotected dP7

3. DSC curves (2nd heating) of polymers P6-P10.

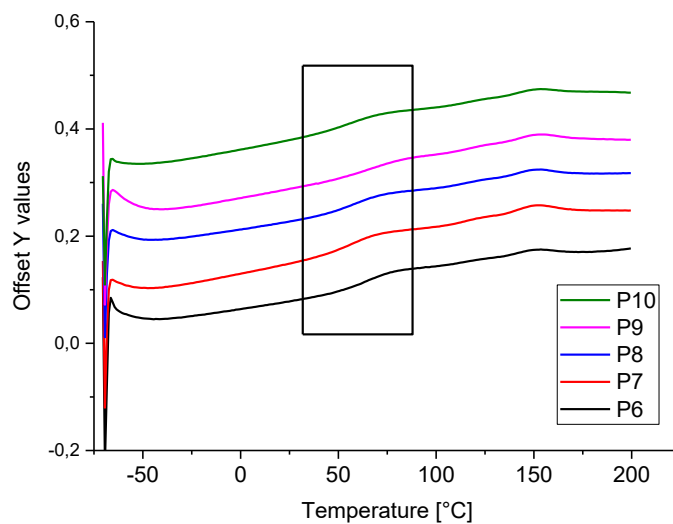


Figure S28: DSC curves (2nd heating) of P6-P10 for glass transition temperature. All curves show rDA signal.

4. IR spectra of composites C1-C4.

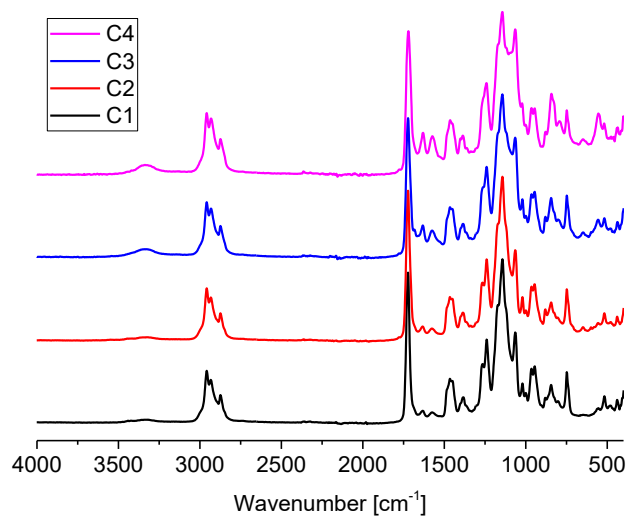


Figure S29: IR spectra of composites C1-C4.

5. DSC curves of C1-C4.

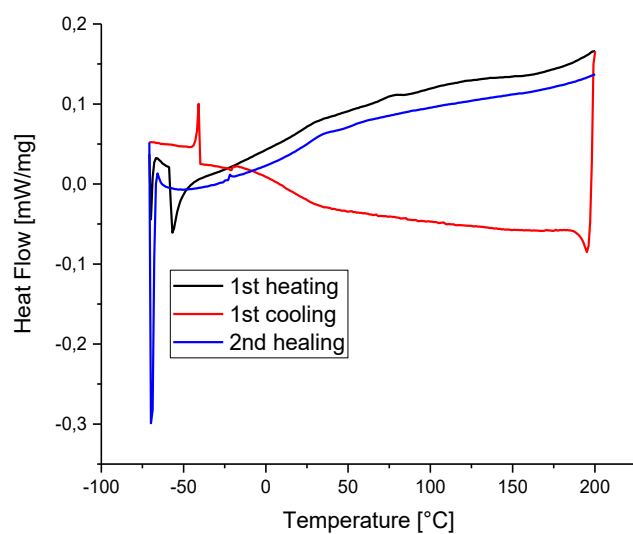


Figure S30: DSC curve of C1.

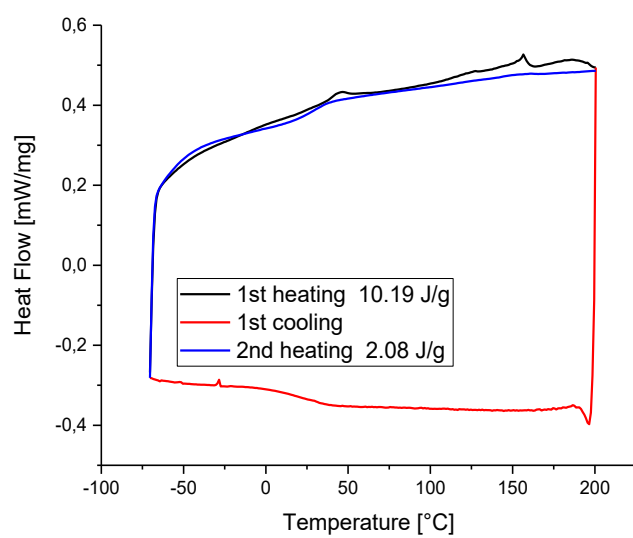


Figure S31: DSC curve of C2.

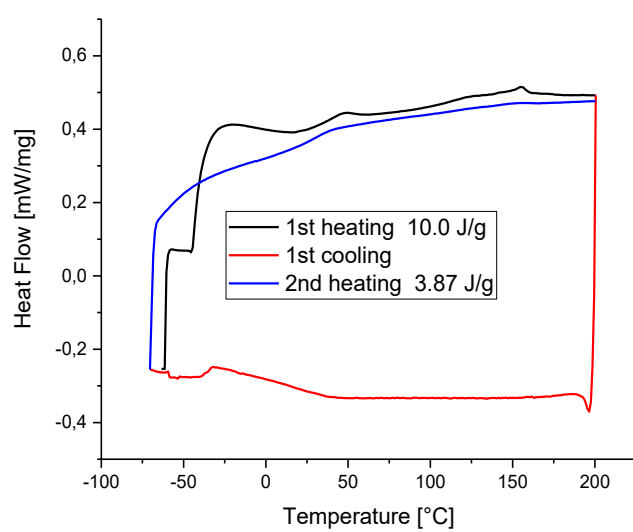


Figure S32: DSC curve of C3.

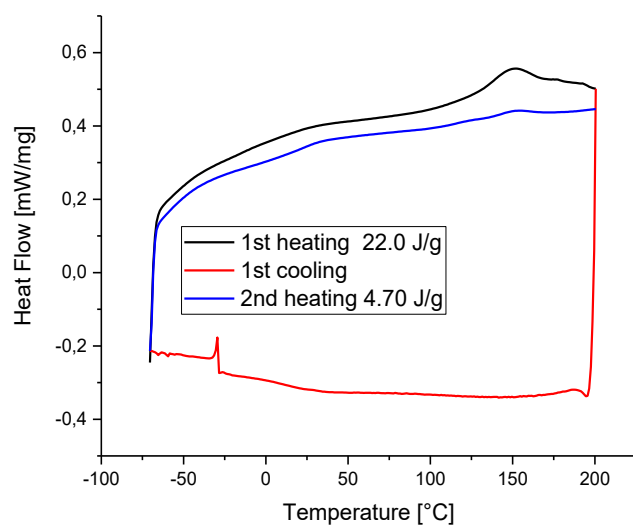


Figure S33: DSC curve of C4.

6. Microscope Images of composites C1-C3.

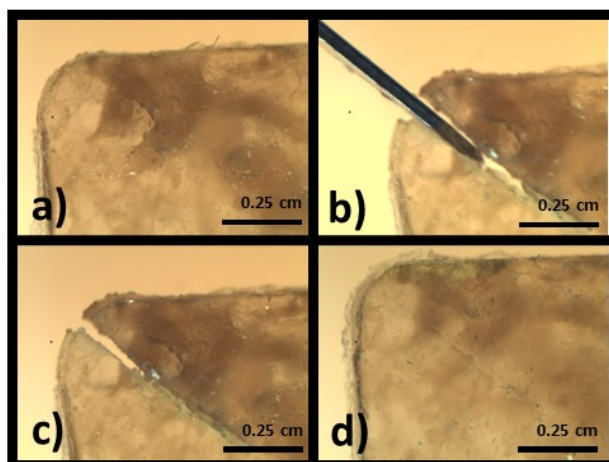


Figure S34: Microscope Images of self-healing experiment with C1:

a) cut through whole thickness; b-c) trying to reconnect at room temperature; d) “decrosslinked” (in this case = heated) at 120°C.

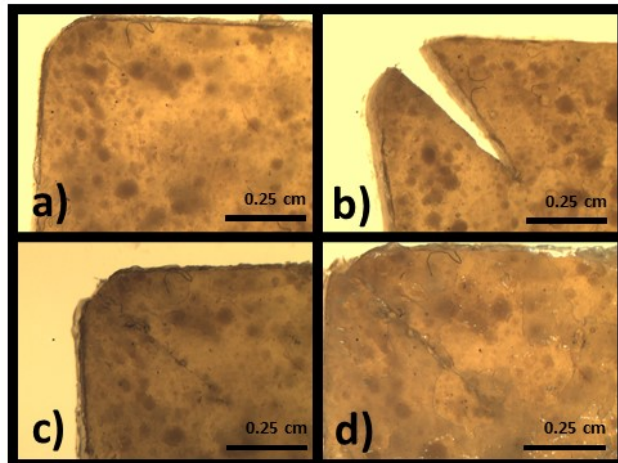


Figure S35: Microscope Images of self-healing control experiment with C2:

a) cut through whole thickness; b-c) trying to reconnect at room temperature; d) “decrosslinked” (in this case = heated) at 120°C.

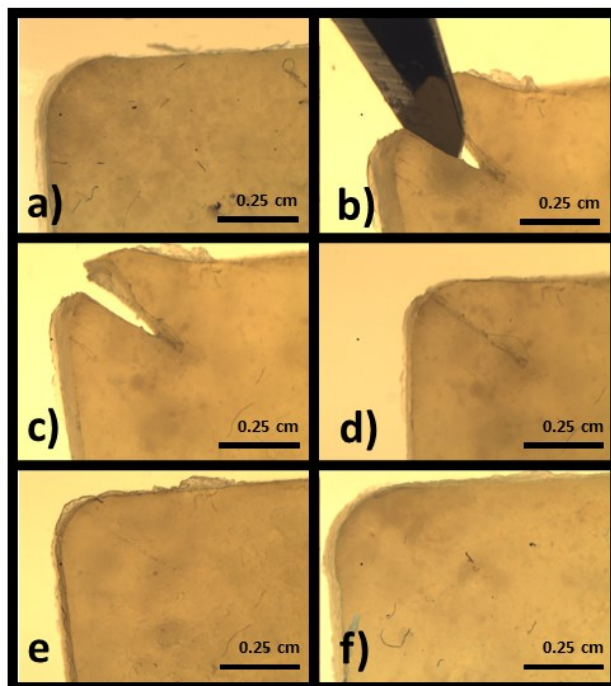


Figure S36: Microscope Images of self-healing control experiment with C3:

C4: a) cut through whole thickness; b-c) recombination of surfaces; d) gently pressed together interfaces at 30°C; e) decrosslinked at 120°C and f) crosslinked at 70°C.

7. UV/Vis spectra and conversion over time for P8.

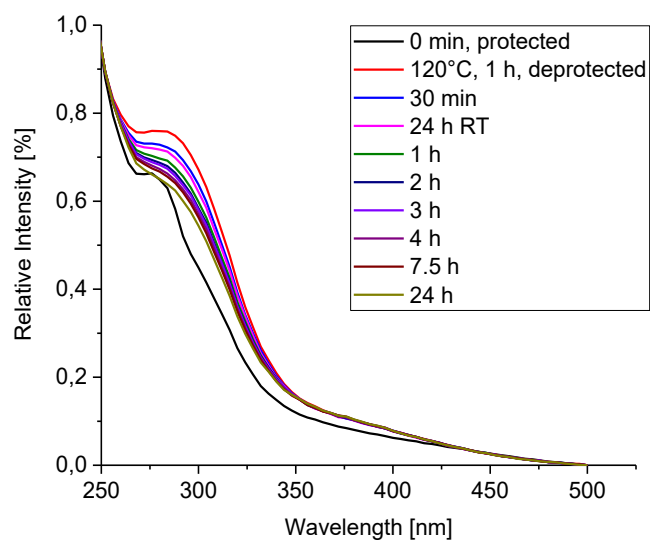


Figure S37: UV/ Vis spectra followed over time while crosslinking of P8 at 70°C.

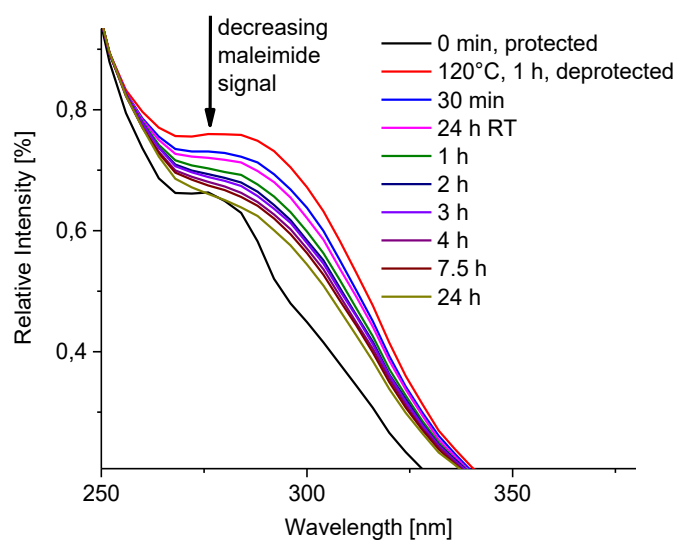


Figure S38: Zoomed UV/ Vis spectra followed over time while crosslinking of P8 at 70°C.

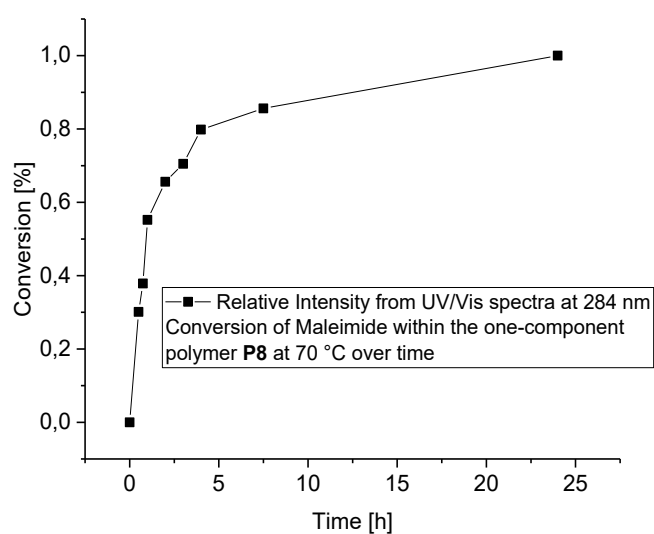


Figure S39: DA conversion over time of P8 determined from UV/Vis.

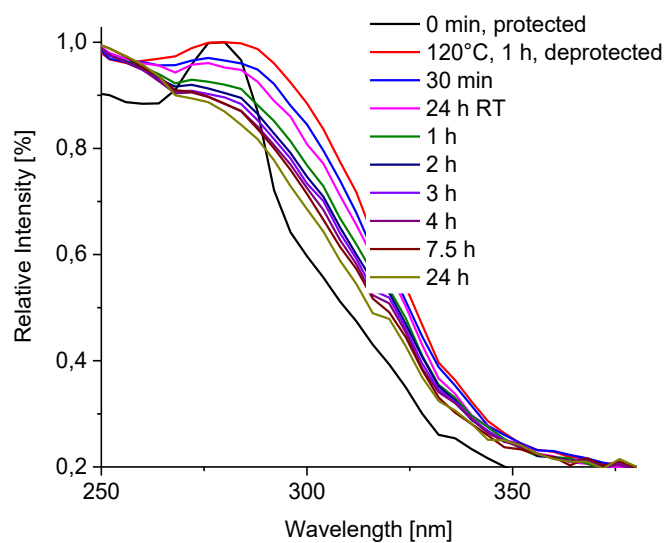


Figure S40: UV/ Vis spectra followed over time while crosslinking of C4 at 70°C.

8. Rheology measurement of P8.

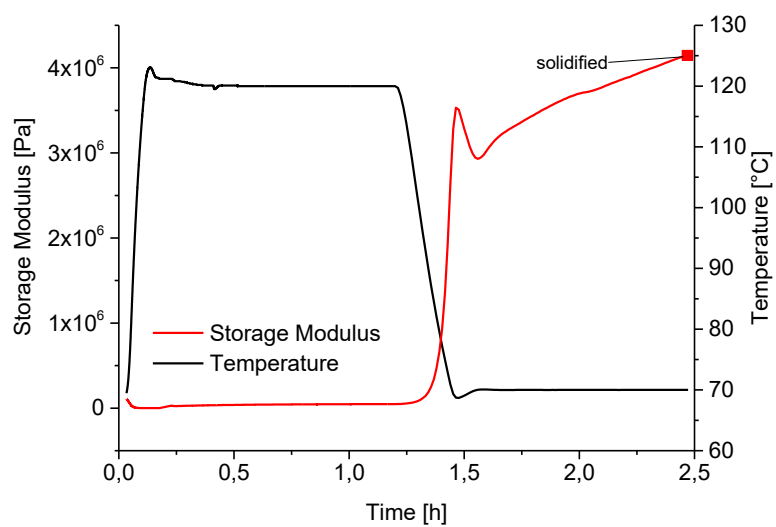


Figure S41: Rheology measurement of P8.

9. TEM images and EDX of C3

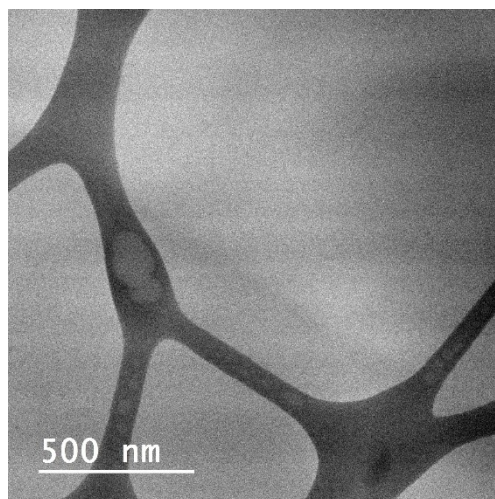


Figure S42: TEM image of microtome cutting slices (~ 20 nm depth) of C3.

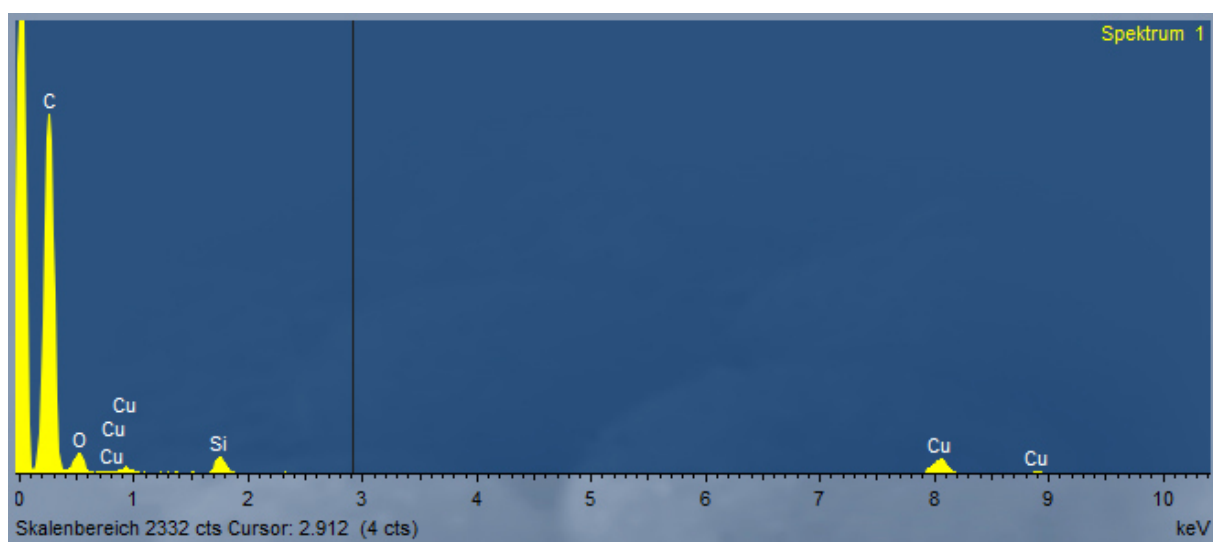


Figure S43: EDX spectrum of C3 determined from microtome cutting slice (~ 20 nm depth).

ⁱ R. Pelagalli, I. Chiarotto, M. Ferocia, S. Vecchioa *Green Chem.* **2012**, *14*, 2251-2255.

ⁱⁱ A.A. Kavitha, N.K. Singha *Macromol. Chem. Phys.* **2007**, *208*, 2569–2577.

ⁱⁱⁱ T. Dispinar, R. Sanyal, A. Sanyal, *J. Polym. Sci. A Polym. Chem.* **2007**, *45* 4545–4551.



**UNIVERSITÄT
DES
SAARLANDES**

Fachbereich Chemie
Universität des Saarlandes
Campus
66123 Saarbrücken
www.uni-saarland.de